Tampereen teknillinen yliopisto - Tampere University of Technology

Reijo Tuokko, Minna Lanz & Pasi Luostarinen (eds.)

International Workshop on MicroFactories (IWMF 2012)

17th-20th June 2012 Tampere Hall Tampere, Finland

Tampere University of Technology. Department of Production Engineering
Tampere 2012

ISBN 978-952-15-2936-8

Sequential Drive of Micro Piezo Actuator Stacks

Ping Guo[1,#], Kornel F. Ehmann[1]

1 Department of Mechanical Engineering, Northwestern University, Evanston, USA
Corresponding Author / E-mail: pingguo2009@u.northwestern.edu, TEL: +1 847-467-1851

KEYWORDS : Elliptical vibration texturing, Tertiary motion generator, Sequential drive, Piezo actuator

Elliptical vibration texturing is an innovative and fast method to generate micro-structures on engineered surfaces. The core part of the process is the tertiary motion generator (TMG) that can produce spatial trajectories at a high frequency. The non-resonant mode version of the TMG has the advantages of arbitrary operating frequencies, better control of the motion output, and generation of complex trajectories for complex micro-patterns; however, it requires special considerations in the driving technique to achieve large displacements at high frequencies. A sequential drive strategy for the piezo stacks is proposed to address the difficulties in driving the non-resonant TMG. Each piezo chip in the stack is excited in sequence, so that each of the chips works only intermittently a fraction of the total time. A special drive circuit is designed to distribute the excitation voltage to each of the chips. A one dimensional piezo actuator is developed to verify the principle of the proposed idea. Future work for the design of a three dimensional non-resonant mode TMG, based on the sequential drive technique, is also discussed.

1. Introduction

Micro-patterns and micro-structures on flat or curved surfaces are attracting more and more interest in different research and industrial applications. If one focuses on micro/meso-scale textures, there are many interesting applications. Micro-structures (e.g., gratings) on optical surfaces change their refractive and diffractive properties. Arrayed dimples on contact surfaces under lubrication help to establish hydrodynamic pressure and to decrease the friction force [1]. Micro-channels are widely adopted to accelerate heat exchange and mass flow. Carefully designed pillar arrays can create superhydrophobic (a.k.a, lotus effect) surfaces, which could lead to the development of self-cleaning surfaces. Other novel applications include surface texturing on biopsy needles to enhance their performance [2], etc.

The elliptical vibration texturing process is an innovative and fast method to generate micro-structures on engineered surfaces. It is an adaptation of the elliptical vibration cutting (EVC) process [3]. The cutting tool vibrates both in the cutting direction and in the depth-of-cut direction with respect to the workpiece surface to form an elliptical trajectory. This higher order motion (tertiary motion) of the cutting tool creates periodic dimples on the machined surface. The principle of the process is shown in Fig. 1.

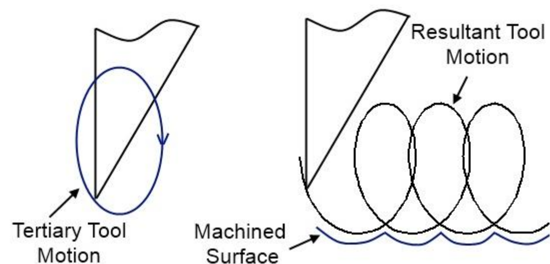

Fig. 1 Schematic of the elliptical vibration texturing process

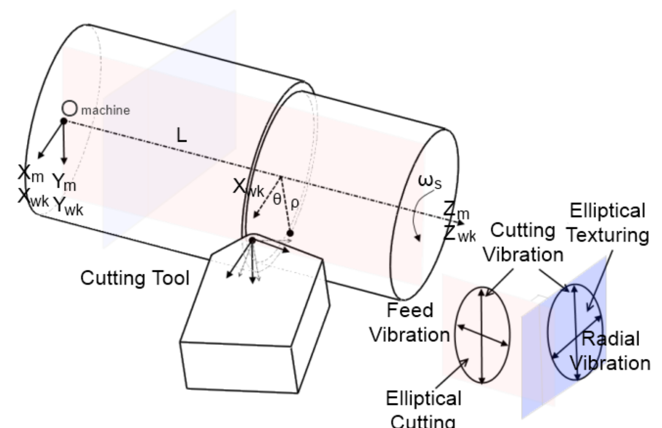

Fig. 2 Illustration of the elliptical vibration texturing process in cylindrical turning

The implementation of this new process is illustrated in Fig. 2 for the turning operation. The radial vibration of the cutting tool periodically changes the cutting depth, which generates peaks and valleys along the cutting direction. This motion is the key driving factor for the texturing process. The cutting direction vibration additionally brings the benefits of vibration assisted machining to the process. Moreover, it adds extended freedom to create more complicated micro-structures. The difference between the elliptical vibration cutting and texturing processes is also shown in the figure: the cutting tool vibrates in two different orthogonal planes in the two processes. One example surface of dimple arrays using this texturing technique is shown in Fig. 3.

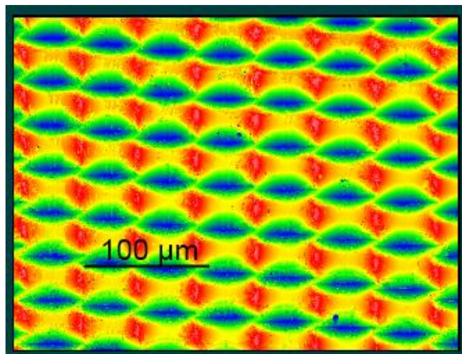

Fig. 3 Example surface produced by elliptical vibration texturing

The key technological problem of the process is to design a tertiary motion generator (TMG) that can produce spatial trajectories at high frequencies. This paper tackles the problems in driving a non-resonant TMG. The operational principles of non-resonant TMGs are introduced in Section 2 followed by the detailed description of the sequential drive strategy that alleviates excessive heat generation at high frequencies in Section 3. Section 4 outlines the design of a one dimensional non-resonant TMG whose performance is demonstrated in Section 5. A preliminary design of a 3D TMG, based on the proposed driving technique, is briefly discussed in Section 6 followed by conclusions in Section 7.

2. Non-resonant mode tertiary motion generator

There are two possible principles for the design of the TMG: the resonant mode and the non-resonant mode. The resonant TMG works at discrete natural frequencies of the system structure; while the non-resonant TMG operates in a continuous range of frequencies. The resonant TMG is able to achieve a higher operating frequency and is more energy efficient, but it is very hard to obtain precise control of the trajectory due to the nature of resonant vibration and the phase lag between the excitation and mechanical responses. The non-resonant TMG is not limited to a fixed operating frequency and has more precise control of the motion. It also has the potential to create an arbitrary motion trajectory for complex texture patterns. However, it is very difficult to achieve a high operating frequency due to various technical problems involved. The detailed design of the resonant vibrator for the texturing application is described in [4].

The non-resonant mode TMG usually utilizes “soft” PZT materials, since they have higher piezoelectric strain constants and a low mechanical quality factor, which leads to a larger displacement at off-resonance frequencies. It often has a mechanical amplification mechanism to boost the vibration amplitudes (Fig. 4) [5].

Non-resonant mode TMGs work at arbitrary working frequencies instead of a fixed frequency as the resonant mode TMGs do. Moreover, the geometry of its motion can be more precisely controlled. The trajectory only depends on the geometrical design of the transducer with a known magnification factor. While in the resonant mode, there’s unpredictable phase shift in the mechanical response; and the vibration frequency and amplitudes are very sensitive to the mass and geometrical configuration. It is very hard to analytically model the actual trajectory of the motion for the resonant mode TMG.

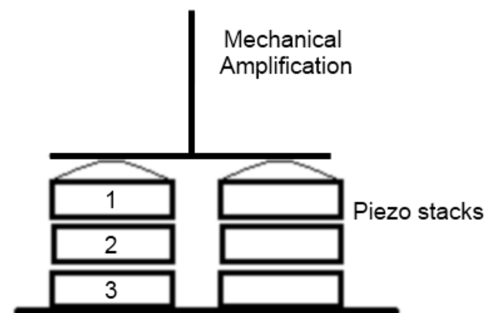

Fig. 4 Design schematic of a 2D non-resonant mode TMG

The non-resonant mode TMG, however, has its own technical problems. It requires a more powerful amplifier and is less energy efficient. Due to the dielectric loss and electromechanical loss, there are serious self-heating problems, especially when operating at a very high frequency. Although its operating frequency is in a continuous range, the upper bound is often limited by the first natural frequency of the mechanical structure, the capability of the power amplifier, and the self-heating issues.

The one dimensional design of a non-resonant motion generator is usually in the research field of fast tool servos (FTS). They could achieve several microns of stroke up to the operating frequency of 1 kHz [6]. In the EVC area, Overcash and Cuttino [7] developed a 1D non-resonant vibrator for vibration assisted cutting, which generates pulse motion up to 40 kHz. Negishi et al. [8] designed a 2D non-resonant vibrator for EVC, which generates an elliptical trajectory of 18 μm x 3 μm up to 4 kHz.

3. Sequential drive of micro piezo actuator stacks

In order to address the issues mentioned above, the idea of sequential drive of piezo actuators is adopted [7]. For example, three piezo chips are stacked vertically as a group. They are excited in sequence, so that each of the chips works only intermittently one third of the total time. This operating principle greatly alleviates the self-heating issues. An added

benefit is that a single high-power and high-voltage amplifier can be used to drive the three piezo chips. This, however, requires a special drive circuit that divides the amplified output signals (high voltage and high current).

3.1 Drive circuit design

The schematic of the developed drive circuit is shown in Fig. 5. The circuit takes inspiration from Chatterjee's work [9]. The piezo chips are connected in series mechanically and in parallel electronically. They are taken as capacitors in the schematic. There is a high-side switch for each piezo chip to control the connection to the amplifier output. If, for example, S1H is closed, piezo chip #1 will be charged through the solid route in the figure. The low-side switch for each piezo chip controls the discharge process. If then S1H is opened and S1L is closed, piezo chip #1 will be discharged through the dotted route in the figure. The PIC32 micro-controller interfaces with a function generator chip to provide sinusoidal signals to the amplifier and controls the drive circuit to open and close the switches at accurate time instances for precise durations. These switches are MOSFETs in essence, which have the capabilities to pass through several amperes of current and to open and close almost instantaneously (in less than 100 ns). The high-side MOSFET connects the output of the amplifier to the positive side of the piezo chip. The low-side MOSFET, unlike a normal low-side driver, connects the positive side of the piezo actuator to the ground. Two MOSFETs, operating in a group, are driven by a half bridge driver chip. The manufactured PCB of the circuit is shown in Fig. 6.

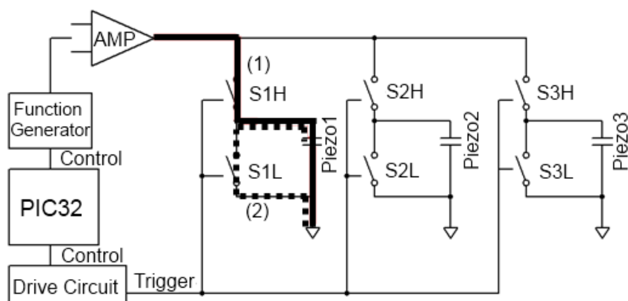

Fig. 5 Schematic diagram of the sequential drive circuit

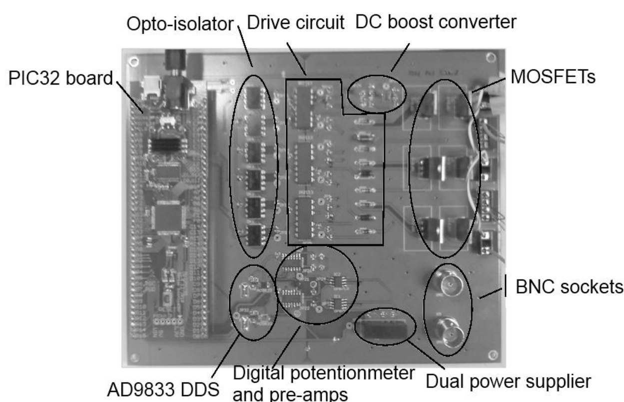

Fig. 6 PCB layout of the sequential drive circuit

3.2 Sequential drive strategy

The drive strategy is illustrated in Fig. 7. The sinusoidal signal is the output signal from a single output power amplifier. Piezo chip #1 is connected to the amplifier output at time t1, where the amplified signal begins to rise. The piezo chip #1 is then disconnected at time t2, where a full sine wave cycle ends. At time t3, piezo chip #2 is connected to the amplifier and disconnected at time t4. The small time gap between t2 and t3 is to ensure that only one piezo chip is connected to the amplifier at one time. Three piezo chips take turns to operate under sinusoidal excitation. The driver circuit acts like a rectangular window function. The key issue here is to keep precise control of the timing of the MOSFETs to synchronize a full 2π cycle starting from 0 V. This will provide minimum energy leakage and smoothness of the actuator motion. During each cycle, the piezo chip is charged to its maximal operating voltage and fully discharged. The low-side MOSFETs are used to keep the piezo chips grounded when discharging. For example, the low-side MOSFET for piezo chip #1 is turned on slightly after time t2 to assure only one of the high-side and low-side MOSFETs are in effect. This time instance is irrelevant to time t3 and does not interfere with the operation of the next piezo chip. The low-side MOSFET for piezo chip #1 is kept on until some time slightly before the next operation (time t7) to make sure that no charge builds up while it is not in operation.

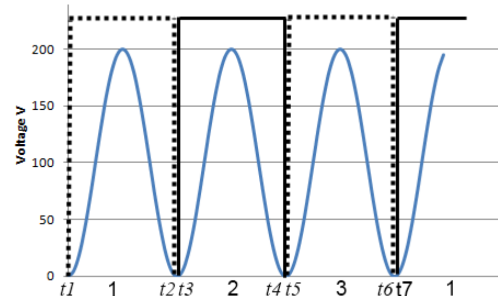

Fig. 7 Sequential drive scheme

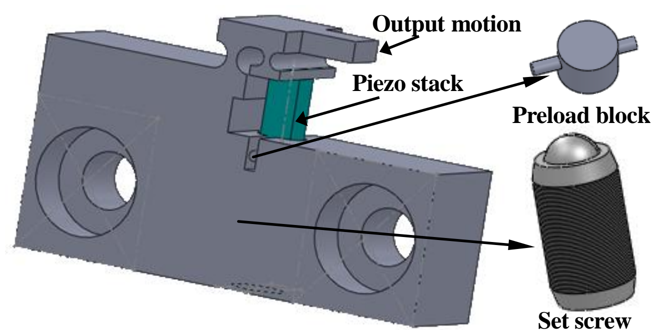

Fig. 8 CAD model of the 1D piezo actuator

4. Design of a 1D non-resonant transducer

4.1 Mechanical design

A 1D prototype of a non-resonant mode piezo actuator is designed to verify the idea of the proposed sequential drive method. The CAD model of the actuator is shown in Fig. 8. The three piezo chips are stacked in series. The output of the actuator is at the free end of the lever structure. When voltage is applied to the piezo chips, they expand in the thickness

direction, thus push the lever to generate one dimensional motion. The lever serves as a magnification mechanism. The lever is connected to the piezo chips via a flexure joint, which decouples the bending load to the piezo chips. There is a preload block and an ultra-fine set screw to provide enough preload to the piezo chips. The pin on the preload block constrains its movement only in the vertical direction by sliding in the slot on the main structure. The set screw has a 3/16-100 ultra-fine thread. It pushes the preload block up to provide a precise pre-tightening force. The existence of the preload block decouples the rotational movement of the set screw to the piezo chips. The ball head of the set screw decouples the bending load to the piezo stack.

4.2 Modal analysis

FEM simulation is carried out to study the characteristics of the actuator. The device is modeled as a monolithic structure in the simulation. From the frequency extraction analysis, the first natural frequency of the structure is at 23.2 kHz. The mode shape is in-plane bending, as shown in Fig. 9(a). The second natural frequency is at 24.5 kHz. The mode shape is out-of-plane bending, as shown in Fig. 9(b). The results are compared to the experimental data from sine sweep tests. The actual first natural frequency of the device is at 16 kHz. The difference comes from the increased stiffness of the monolithic model. Also, from the simulation results, the piezo actuator has a static stiffness of 10 N/μm; and the magnification factor of the lever structure is around 2.95.

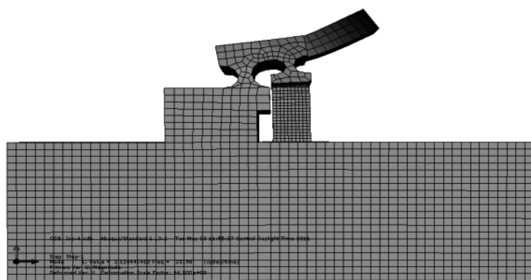

Fig. 9(a) 1st vibration mode: in-plane bending at 23.2 kHz

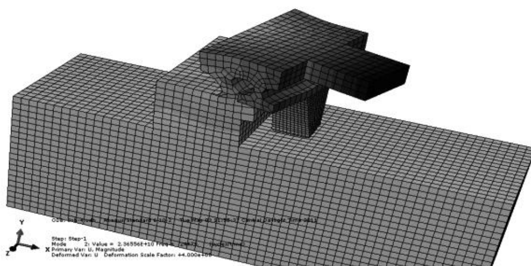

Fig. 9(b) 2nd vibration mode: out-of-plane bending at 24.5 kHz

5. Experimental verification

5.1 Static test

The experimental setup is shown in Fig. 10. The main piece of the piezo actuator is made by wire EDM. The testbed consists of the 1D piezo actuator and the capacitance sensor probe holder. The piezo actuator is attached horizontally to the base to eliminate gravity effects. There is a clearance between the lever and the base to assure free movement. The capacitance sensor points to the free end of the lever. The sensor has a range of 50 μm and a bandwidth up to 100 kHz.

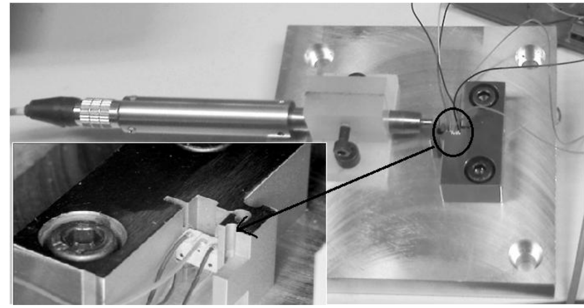

Fig. 10 Testbed and the piezo actuator

The piezo chip, closest to the lever, is labeled as the top chip. The one attached to the preload block is the bottom chip. The one in between is labeled as the middle chip. A DC voltage is applied to three piezo chips separately to test the static displacement of the actuator. The voltage outputs from the capacitance sensor are recorded and listed in Table 1.

Table 1 Static test results for the piezo actuator

Voltage	Top chip	Middle chip	Bottom chip
10V	-2.653 V	-2.554 V	-2.678 V
30V	-2.709 V	-2.612 V	-2.742 V
Δ20V	0.28 μm	0.29 μm	0.32 μm

5.2 Dynamic test

The frequency analysis results for the sine sweep tests on the top piezo chip are plotted in Fig. 11. The first natural frequency of the device is at 16 kHz. The second peak is at 19.5 kHz. In between these two peaks, there are two minor peaks at around 17.9 kHz and 18.5 kHz. The frequency responses are identical for all three piezo chips. All tested frequencies are denoted in the figure, including frequencies below, around and above the first natural frequency. The test conditions and results are summarized in Table 2.

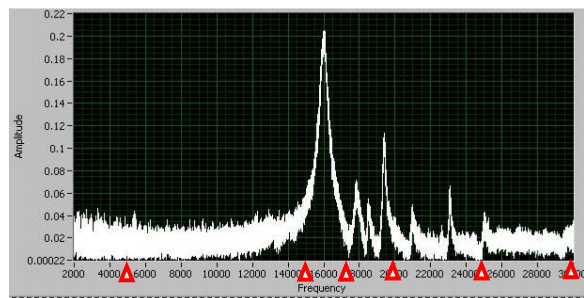

Fig. 11 Frequency analysis results for the piezo actuator

Table 2 Dynamic test results for the piezo actuator

Test case	1	2	3	4	5	6
Frequency (kHz)	5	15	17.5	20	25	30
Voltage (V_{pp})	60	40	40	40	40	40
Displacement amplitude (μm)	1.2	4.2	1.26	1.58	1.58	~

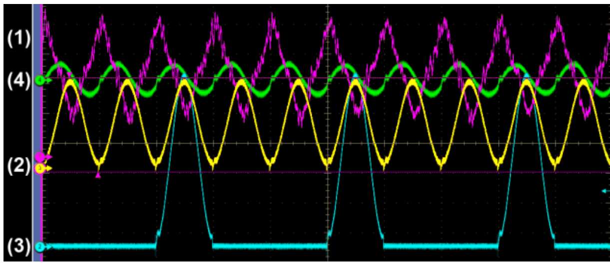

Fig. 12(a) Dynamic test result @ 5 kHz

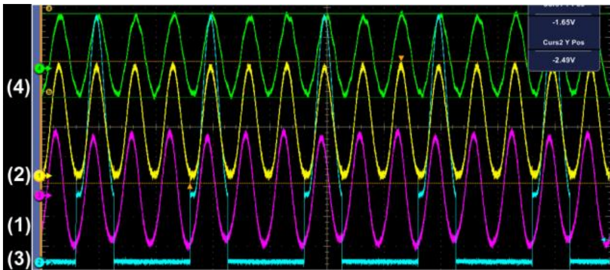

Fig. 12(b) Dynamic test result @ 15 kHz

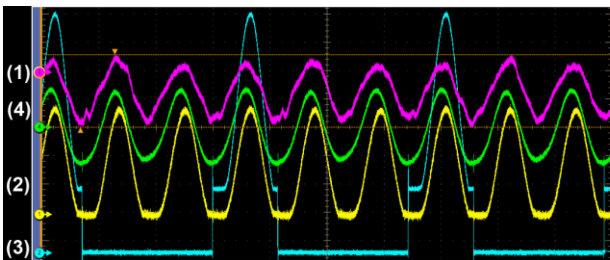

Fig. 12(c) Dynamic test result @ 17.5 kHz

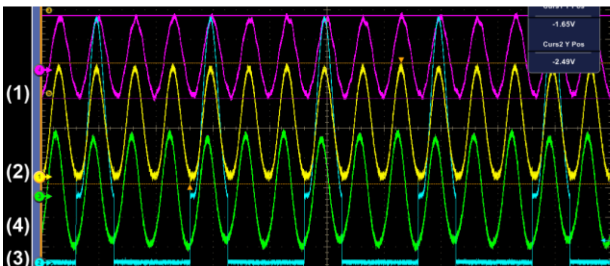

Fig. 12(d) Dynamic test result @ 20 kHz

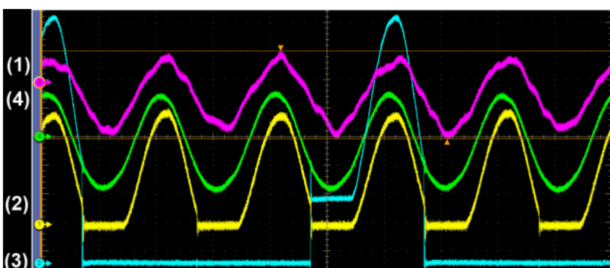

Fig. 12(e) Dynamic test result @ 25 kHz

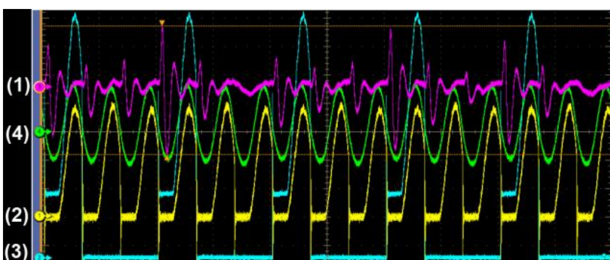

Fig. 12(f) Dynamic test result @ 30 kHz
(1) magenta: displacement (2) yellow: output voltage (3) cyan: gate voltage (4) green: output current

All test results with four channel information are plotted in Fig. 12(a)-(f). The signal labeled as (1) (in magenta) is the displacement output from the free end of the lever. The signal labeled as (2) (in yellow) denotes the output voltage from the amplifier. The cyan signal (3) is the gate voltage, or the control signal, over the top piezo chip. The green signal (4) is the output current from the amplifier.

The series of tests confirms the feasibility of the proposed idea of the sequential drive strategy. For example, in Fig. 12(a), the control signal for piezo chip #1 is turned on for one full cycle in every three cycles. Piezo chip #1 is charged to the amplifier output voltage in this cycle, while the other piezo chips are kept grounded. Three piezo chips take turns to operate under the sinusoidal excitation; and the displacement output of the actuator is continuous. The current and voltage signals have a 90 degree phase shift because the piezo materials act like capacitors in the circuit. The displacement output and voltage signals have no phase shift in the 5 kHz case (negatively related), which verifies the operation principle of the non-resonant actuator.

The result at 15 kHz, shown in Fig. 12(b), shows larger displacement outputs since the excitation frequency approaches the first natural frequency of the system. The phase shift between the driving voltage and the displacement outputs increases to around 180 degree, which also indicates the phase change at the natural frequency.

The rest of the test results show the operation conditions beyond the first natural frequency. The actuator performs as expected until reaching 30 kHz, where the displacement output fails to follow the excitation signal. It sets the upper bound of the operating frequency.

6. Future work

The ultimate goal is to design a non-resonant mode TMG, which is able to generate 3D space trajectories. Besides this unique 3D feature compared with the current state-of-the-art, this 3D TMG will be capable to operate near the ultrasonic frequency range using our newly developed sequential drive strategy. These two combined advances in the piezo actuator design will require special considerations in mechanical and electronic design.

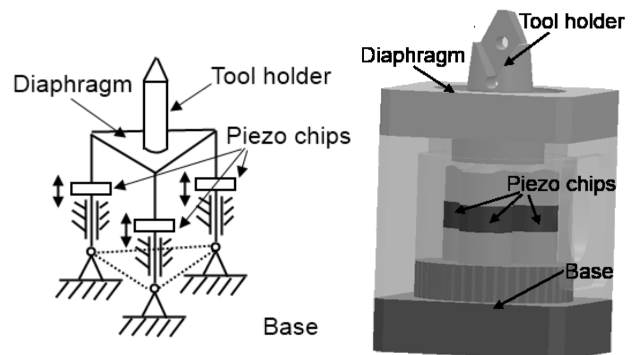

Fig. 13 Preliminary design of the 3D TMG

The mechanical structure of the 3D TMG has to minimize its mass to increase the first natural frequency, which sets the upper limit of the operating frequency. There is a trade-off for the mechanical amplification mechanism design to choose between a larger magnification factor and larger stiffness. Large mechanical amplification will decrease the stiffness of the system, which reduces the first natural frequency of the device and deteriorates its dynamic performance. The other trade-off is between a longer stroke and lower capacitance for the piezo actuator. Higher capacitance generates a longer stroke, but has higher power requirements. Other design considerations include precise preload mechanisms for the piezo actuator, piezo actuator alignment, piezo actuator load decoupling, etc. The preliminary design uses the tripod mechanism, which is shown in Fig. 13. The diaphragm acts as the mechanical amplifier.

7. Conclusion

In this paper, the sequential drive technique for the piezo stacks is proposed. Its application is for the operation of the non-resonant mode tertiary motion generator in the elliptical vibration texturing process. In the sequential drive scheme, each piezo chip in the stack is excited in sequence, so that each of the chips works only intermittently a fraction of the total time. A special drive circuit is designed to distribute the excitation voltage to each piezo chip. A one dimensional piezo actuator is developed to verify the principle of the proposed idea. Future work of the design of three dimensional non-resonant mode TMG based on the sequential drive technique is also discussed.

ACKNOWLEDGEMENT

This work was supported by the National Science Foundation under grant number DMI-0600175.

REFERENCES

1. A. Kovalchenko, O. Ajayi, A. Erdemir, G. Fenske, and I. Etsion, “The Effect of Laser Texturing of Steel Surfaces and Speed-Load Parameters on the Transition of Lubrication Regime from Boundary to Hydrodynamic,” Tribology Transactions, vol. 47, no. 2, 2004, pp. 299-307.
2. P. Han, K. Pallav, P. Guo, and K. F. Ehmann, "Medical Needle Insertion: Effects of Needle Tip and Surface Texturing," in Proceedings of the Internaltional Conference on Micromanufacturing Conference, 2011.
3. E. Shamoto, and T. Moriwaki, “Study on Elliptical Vibration Cutting,” CIRP Annals - Manufacturing Technology, vol. 43, no. 1, 1994, pp. 35-38.
4. P. Guo, and K. F. Ehmann, “Development of a New Vibrator for Elliptical Vibration Texturing,” ASME Conference Proceedings, vol. 2011, no. 44304, pp. 373-380.
5. M. Cerniway, “Elliptical diamond milling: kinematics, force, and tool wear,” MS thesis, North Carolina State University, 2001.
6. F. Kimura, K. Horio, D. L. Trumper, and X. Lu, "Fast Tool Servos: Advances in Precision, Acceleration, and Bandwidth," Towards Synthesis of Micro-/Nano-systems, pp. 11-19: Springer London, 2007.
7. J. L. Overcash, and J. F. Cuttino, “Design and experimental results of a tunable vibration turning device operating at ultrasonic frequencies,” Precision Engineering, vol. 33, no. 2, 2009, pp. 127-134.
8. N. Negishi, “Elliptical Vibration Assisted Machining with Single Crystal Diamond Tools,” MS thesis, Mechanical Engineering, North Carolina State University, Raleigh, 2003.
9. K. Chatterjee, M. C. Boyer, W. D. Wise, and E. W. Hudson, “An auxiliary capacitor based ultrafast drive circuit for shear piezoelectric motors,” Review of Scientific Instruments, vol. 80, no. 9, 2009, pp. 095110-095115.

Manufacture and Testing of an Aerostatic Lead Screw Actuator for High Performance Micro-Scale Machine Tools

James Zhu[1], Shiv G. Kapoor[1,#] and Richard E. DeVor[1]

1 Department of Mechanical Science and Engineering, University of Illinois: Urbana-Champaign, Urbana, Illinois, USA, 61801
Corresponding Author / E-mail: sgkapoor@illinois.edu, TEL: 217-333-3432, FAX: 217-244-9956

KEYWORDS : Aerostatic Lead Screw, Frictionless Motion, Micro-Scale Machine Tool, Porous Air Bearing, Precision Actuator, Sub-Micron Accuracy

The manufacturing process for a porous-restricted aerostatic lead screw actuator (ALSA) is presented. The ALSA provides near-frictionless motion with sub-micron accuracy, high stiffness at low inlet air pressures (<830 kPa), and a travel length of 50 mm. Porous graphite disk inserts are held in a helical pattern in an aerostatic nut housing against a lead screw thread to create multiple simultaneous air bearing surfaces. The manufacturing process developed herein aimed to achieve a uniform air gap across the entire helical thread surface. To do this, the following steps were employed, 1) Rough lapping operation to match graphite disks profile with the helical thread form; 2) Potting operation to secure the porous media in the aerostatic nut housing; 3) Application of a surface restriction layer to control permeability of the porous media; and 4) Final lapping operation to generate appropriate air gap. Experimental trials were performed to evaluate the performance of the manufactured ALSA. It was found that a stable nut with a per-thread stiffness of 9.7 N/µm was achievable with a 3.5 µm air gap and an overall permeability of 5.4e-15 m^2. Applications requiring higher stiffness may couple two or more single-threaded nuts to achieve the desired actuator stiffness.

1. Introduction

In a recent publication, Zhu et al. [1] proposed a design for a porous-restricted aerostatic lead screw actuator (ALSA). ALSAs have been found to be particularly suitable for the actuators used in high performance micro-scale machine tools (mMTs) due to their ability to achieve high accuracy as well as attain increased static/dynamic stiffness [2-4]. A nut housing is designed to hold porous graphite disk inserts in a helical pattern pressing against a lead screw to create multiple simultaneous air bearing surfaces. The simple geometry of the porous graphite disk inserts and the low tolerance on the nut housing reduce costs dramatically. The analyses performed on the design indicate that such an ALSA design is capable of providing sufficient actuator stiffness while maintaining stable operation. A preliminary manufacturing process was proposed, however, it was found that maintaining the precise air gap between the screw and the nut over the entire helical thread surface posed a major challenge.

Several manufacturing processes for the ALSA have been attempted [5-7], however, there have always been deficiencies in these past designs. These previous developments all struggled with precisely controlling the air gap, often resulting in either pneumatic hammering (instability/vibrations) of the nut [5] or inadequate stiffness characteristics [6-7]. Tachikawa et al. [6] was able to achieve a positioning accuracy of 10 nm, but only managed to obtain a stiffness of 30 N/µm while requiring the nut engagement with eight (8) lead screw revolutions.

The objective of this research is to expand upon the manufacturing process of the porous-restricted ALSA design proposed by Zhu et al. [1]. Specifically, improvements are made upon lapping procedures and the porous media configuration in the aerostatic nut. These developments have resulted in a manufacturing process that ensures a uniform air gap across the entire helical thread surface. Several experimental trials are performed to evaluate the performance of the ALSA as well as investigate the trade-offs between stiffness and stability.

The rest of this paper is organized as follows. Section 2 discusses the specific performance requirements for the ALSA followed by a review of the overall design. Section 3 explains the overall manufacturing process and describes each operation in detail. Section 4 details the experimental trials of the manufacturing process and the resulting ALSA

performance. Finally, conclusions are drawn from this work.

2. ALSA Design Overview

In this section, the ALSA design proposed by Zhu et al. [1] will be reviewed. The review will include a discussion of ALSA requirements, design parameters, and key components. A novel concept of pre-loading the porous media during manufacture with a wave spring flexure will also be introduced.

2.1 Porous-Restricted ALSA Configuration

ALSA performance requirements are similar to those described by Adair et al. [5]. The four key evaluation parameters for this ALSA include: 1) friction torque, 2) stiffness, 3) air supply pressure, and 4) travel length. The following requirements are needed to accommodate high dynamic cutting forces while maintaining sub-micron actuator accuracy. Typical air compressors in factory settings limit the inlet air pressure available to the ALSA.

Table 1 summarizes the requirements for the ALSA described herein.

Table 1 Actuator Requirements

	Requirement
Friction Torque	< 0.1 N-m
Stiffness	20 N/μm
Air Supply Pressure	830 kPa (120 PSI)
Travel Length	50mm

The porous-restricted air bearing configuration is illustrated in Fig. 1. Air enters into the plenum chamber that is connected to the porous graphite insert. The porous media is mechanically fixed in the housing and acts as a restrictor that controls the air flow. Air flow through the porous graphite will reach the critical air bearing surface and create a lift-off force, forming an air gap. Because of the porous nature of the graphite material, air flow is distributed evenly across the entire air bearing surface. The balance between the air flow lift-off force and the reaction force provided by the aerostatic nut will generate the air gap that provides the necessary stiffness for the ALSA.

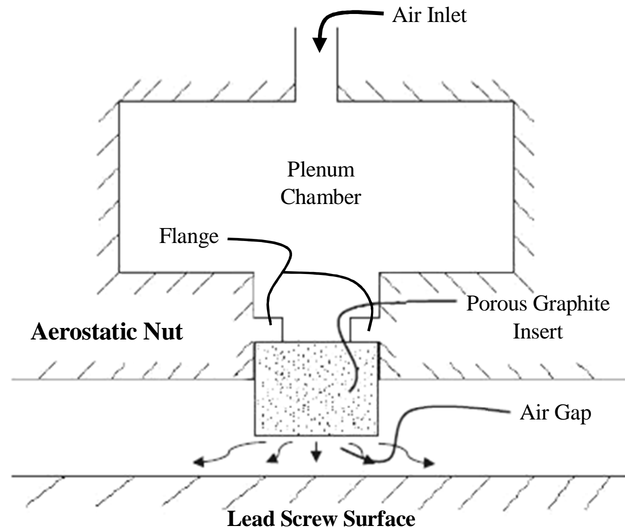

Fig. 1 Porous-Restricted Air Bearing Concept

Figure 2 depicts the approach taken by Zhu et al. [1] to incorporate porous graphite media into an aerostatic nut. In order to obtain bi-directional stiffness, disks on opposing faces in the aerostatic nut must be paired. These pairs of disks are held against the flanks of the lead screw thread and act as the medium for air to travel through to create an air gap. Each disk includes an O-ring that is used to center the disks within their locating holes. The porous disks are all interconnected by a helical plenum chamber that supplies the same inlet pressure to each porous disk.

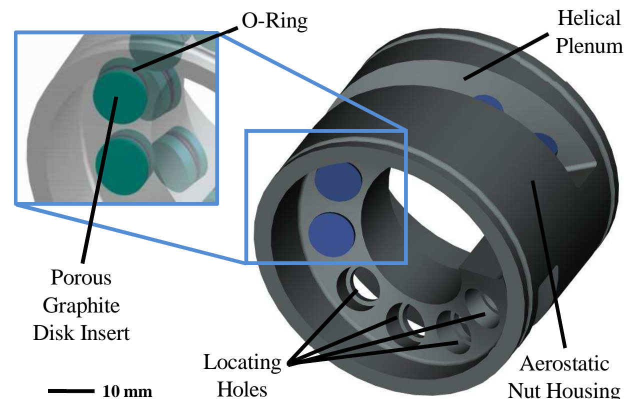

Fig. 2 Aerostatic Nut Housing

2.2 Porous Air Bearing Design Parameters

With the use of porous graphite as the air flow restriction media, there are two major parameters that can be controlled to influence the air bearing performance, viz., inlet pressure and permeability. The inlet pressure is the pressure applied to each of the porous graphite inserts. The permeability is a measure of the ability of a porous material to transmit fluids.

Figure 3 plots stiffness against air gap for several different configurations of inlet pressures and permeability constants. This plot was generated using a one-dimensional generalized flow method developed by Plante et al. [8] to analyze porous air bearing characteristics. Because stiffness is desired in the two directions along an axis, Fig. 3 provides the stiffness of a

pair of porous graphite disks. As seen in Fig. 3, tightening the manufacturing tolerance on the lead screw profile can provide higher stiffness since it reduces the range of available air gaps over the entire length of travel. A profile tolerance of ±4 µm was chosen based on the upper limit of traditional precision lead screw grinding techniques. On top of the profile variation of the lead screw, an air gap must be added to ensure no contact between the lead screw and the porous graphite disks during operation. For manufacturability purposes, a 4 µm air gap was chosen in this initial analysis. Assuming this limit on the profile variation and air gap, one option to increase stiffness in the ALSA involves increasing the total number of graphite disks, i.e., increasing the thread count through coupling multiple aerostatic nuts.

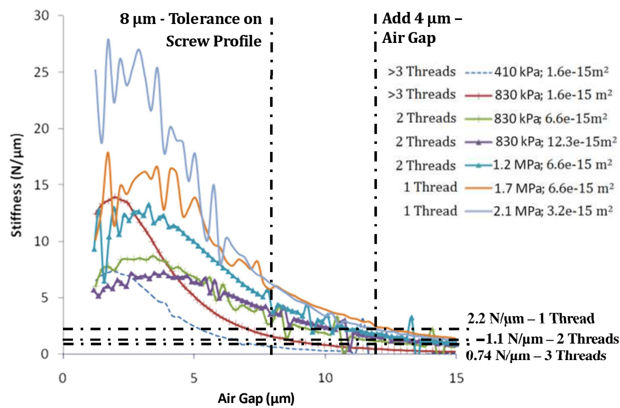

Fig. 3 Stiffness for a Pair of Air Bearing Disks with Increasing Thread Count

The aerostatic nut design described in Section 2.1 contains 18 graphite disks (nine pairs). From Fig. 3, for a single-threaded ALSA to achieve 20 N/µm of static stiffness, each pair of graphite disks must achieve at least 2.2 N/µm (i.e., 20 N/µm / 9 pairs of disks). For two coupled nuts (i.e., 20 N/µm / 18 pairs of disk), each pair of disks will only require stiffness of 1.1 N/µm to meet the initial stiffness requirement. By coupling multiple aerostatic nuts together, the inlet air pressure can be lowered to bring the supply pressure requirement more in line with common factory availability. According to Fig. 3, two coupled aerostatic nuts operating at 830 kPa with a permeability of either 6.6e-15 m^2 or 12.3e-15 m^2 appear capable of achieving the stiffness requirements for this ALSA configuration.

2.3 Key Components of ALSA Design

There are three (3) key components in the ALSA design. These include the aerostatic nut, the lead screw, and the lapping system platform, which supports the manufacturing process.

2.3.1 Aerostatic Nut

The presence of 18 separate air bearings in the aerostatic nut makes the creation of a uniform air flow essential to maintaining a consistent air gap. This is achieved by inserting wave spring flexures behind each disk to provide a pre-load, forcing contact between the disk and the lead screw thread. Wave spring flexures provide a pre-load of approximately 18 N and have over 380 microns of deflection. The use of the wave spring flexure provides a more robust design in the face of manufacturing variation when the 18 graphite disk surfaces must be precisely matched with the helical lead screw profile. This configuration is depicted in Fig. 4.

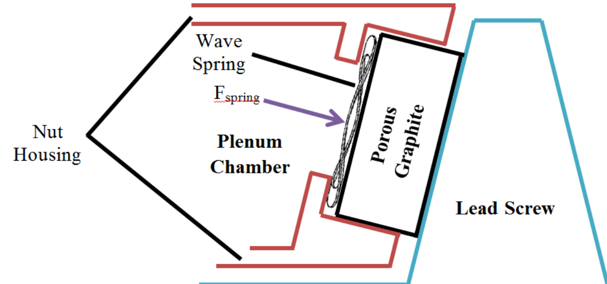

Fig. 4 Wave Spring Flexure Configuration

2.3.2 Precision Ground Lead Screw

The lead screw is made of a 440C stainless steel hardened to HRC 58. The profile tolerance of the thread geometry was set at ±4 µm. The geometry of the thread profile is depicted in Fig. 5. It must be noted that the threads are thinner than the standard trapezoidal thread. This is done in order to increase the spacing between the threads such that porous graphite disk inserts could be incorporated into the aerostatic nut housing.

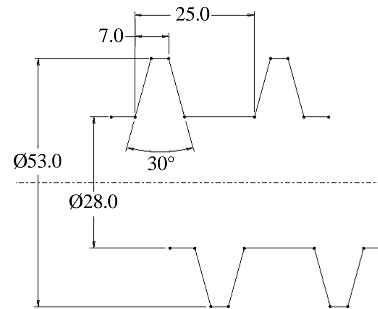

Fig. 5 Modified Trapezoidal Thread Profile (mm)

2.3.3 ALSA Lapping System Platform

The aerostatic nut design enables porous graphite inserts to be assembled to follow the contour of the thread profile. However, there must be a mechanism that enables the surfaces of the porous graphite inserts to mate with the helical surface of the lead screw such that the air gap is maintained in the range of several microns. This calls for a lapping system that is essential to the ALSA manufacture. Figure 6 depicts the design of such a system for the ALSA.

The integrated lapping system consists of a set of guide rails that are precisely offset from the lead screw such that the axes of the guide rails and that of the lead screw are on the same plane. Once aligned, the aerostatic nut can be attached to the guide rails through two outriggers. The guide rails serve two purposes. First, the guide rails constrain the rotational degrees of freedom of the aerostatic nut during manufacture. Second, the guide rails provide the greatest contribution to radial stiffness of the actuator and are therefore considered an

essential part of the ALSA system during operation.

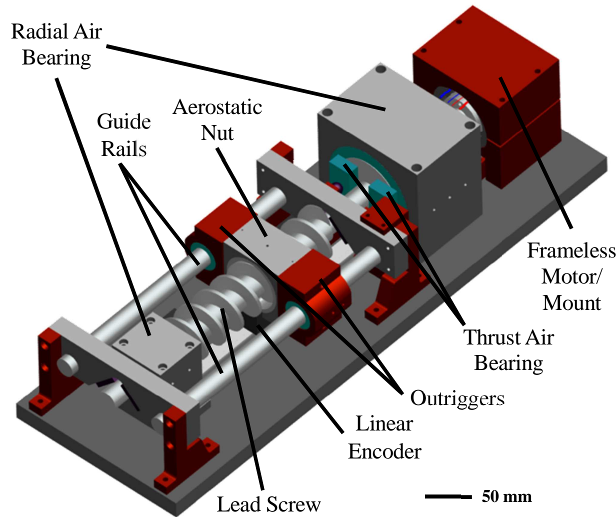

Fig. 6 ALSA with Precision Lapping System

3. ALSA Manufacturing Process

In [1], authors proposed a general ALSA manufacturing process. During experimental testing, however, several difficulties were found when attempting to achieve the target air gap specification. In this section, the steps of a modified general process are laid out followed by a description of proper manufacturing technique for each step.

3.1 Generalized Manufacturing Process

Given the design of the ALSA using porous air bearings, the generalized manufacturing process involves the following steps:

Step 1: Perform rough lapping operation on porous graphite material against lead screw to mate the graphite disks to helical thread form;

Step 2: Pot the graphite disks while wave spring flexures pre-load the graphite disks against the lead screw flank to ensure a consistent mate among all graphite disks;

Step 3: Apply surface restriction layer on roughly lapped graphite surfaces to control permeability;

Step 4: Perform final lapping operation to obtain proper air gap.

The basic components were manufactured and the ALSA platform is shown in Fig. 7.

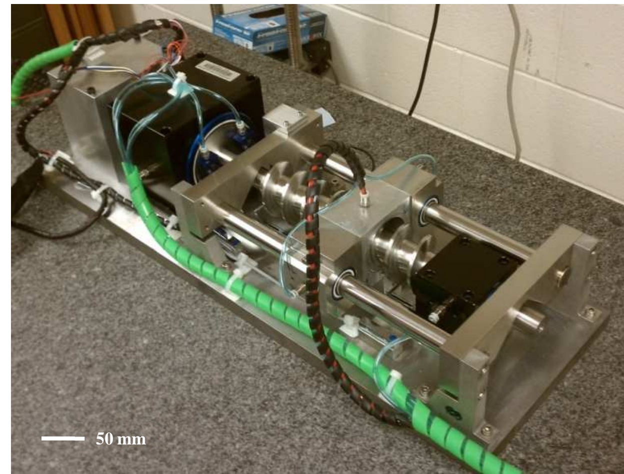

Fig. 7 ALSA Platform for Manufacturing and Testing Purposes

3.2 Rough Lapping Operation

A rough lapping operation on the graphite disks ensures that the critical air bearing surfaces roughly matches the geometric profile of the lead screw thread. Because the thread form follows a helical trajectory, the graphite surfaces must have some curvature, as seen in Fig. 8. During the rough lap, only one side of the nut is lapped at a time.

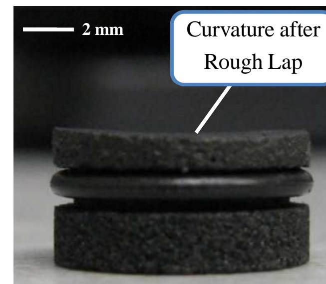

Fig. 8 Graphite Disk after Rough Lap

The disks are lapped until the nut can freely slide onto the lead screw with both sets of graphite disks assembled in the nut housing. At this point, the ALSA is reassembled with wave spring flexures placed behind each disk to provide a pre-load against the lead screw profile. Rough lapping is again performed with all graphite disks and wave spring flexures in place to ensure good contact between the lead screw thread and the disks. These wave spring flexures also guarantee that the angular orientation of the graphite disks are aligned with the curvature of the lead screw since the graphite disks will tend to rotate towards having a flush surface with the lead screw flank. Table 2 lists recommended abrasive compounds for lapping operations performed during ALSA manufacture.

Table 2 Recommended Lapping Compounds

Abrasive Particle Type	*Grit Size*	*Operation*
Garnet	4 µm	Rough Lapping
Iron Oxide	3 µm	Final Lapping
Red Rouge	1 µm	Final Lapping

3.3 Permanent Potting of Graphite Disks

The graphite disks must be permanently potted in the

locating holes of the aerostatic nut housing after the rough lapping operation. The ALSA is disassembled and each graphite disk is matched with its corresponding locating hole and roughly oriented using alignment markers. The graphite disks are potted in place using a slow-cure epoxy (Loctite Hysol E-120HP [9]) to provide ample time to reassemble the ALSA. The epoxy also acts as a sealant to block the pores on the side-walls of each graphite disk. While curing, wave spring flexure pre-loads the graphite disks against the lead screw, enabling each graphite disk to self-align itself into the correct orientation for a flush mate against the lead screw. Once cured, this epoxy provides enough strength to withstand the air pressures up to 1.4 MPa (200 PSI) inside the nut housing. Figure 9 shows the aerostatic nut during the permanent potting process.

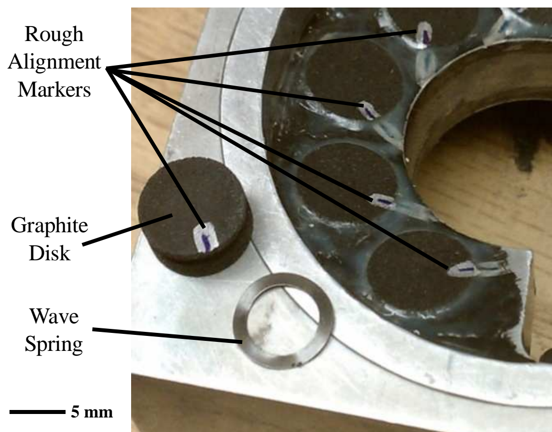

Fig. 9 Aerostatic Nut During Permanent Potting

3.4 Surface Layer Restriction Method.

Permeability of the porous graphite disks is an important parameter that affects the both the stiffness and stability of the ALSA. Permeability is controlled through a surface layer restriction technique [10] depicted in Fig. 10. In this technique, an acrylic resin dissolved in a solvent is applied to the critical air bearing surface and pulled into the pores through vacuum. The air flow is measured and depending on whether the measured value is greater than or less than the target air flow, either more resin is applied or a solvent (toluene or acetone) is used to wipe away some of the pre-existing lacquer already bonded to the surface. This method is repeated until the desired flow rate is achieved. By engineering this restriction, the porous material will provide the correct volumetric air flow to ensure stable air bearing operation.

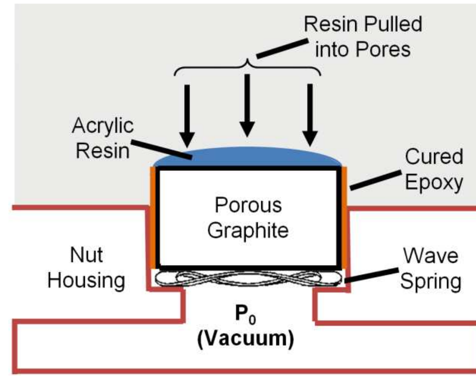

Fig. 10 Surface Restriction Layer Process

3.5 Final Lapping Operation

Final lapping ensures that both sides of the aerostatic nut have matching surface profiles with the correct air gap. From Fig. 11, the air gap in the ALSA can be calculated from the amount of backlash seen in the actuator. Backlash is measured from the linear encoder attached directly to the aerostatic nut. For instance, a backlash measurement of 5 μm would produce a calculated air gap of 4.83 μm. The assumption when making this kind of measurement is that all of the disks have the same air gap. With the use of wave spring flexures in previous steps in the manufacturing process, this is a reasonable assumption. Final lapping is complete once the friction torque requirement of 0.1 N-m is achieved with an appropriate air gap.

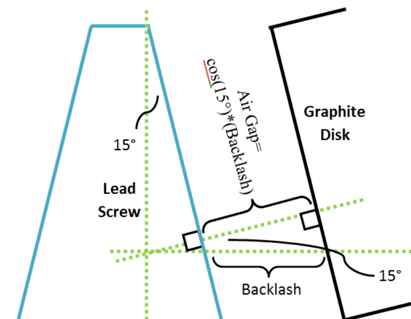

Fig. 11 Air Gap Calculation

Once final lapping is complete, ALSA components are sent through an ultrasonic cleaner to remove abrasive particles and then reassembled.

4. Evaluation of Manufactured ALSA

In this section, the ALSA evaluation procedure will first be described. From here, the experimental results from ALSA manufacturing trials will be examined.

4.1 Evaluation Procedure

Three trials of the manufacturing process were carried out to evaluate the ALSA performance. Stiffness was tested by first constraining all degrees of freedom of the aerostatic nut and outriggers while a constant torque was applied to the lead screw. Rotation of the lead screw caused by the applied torque was measured with a rotary encoder. Based on the pitch of the

lead screw, rotary deflection was correlated to linear deflection, i.e., 1° is equivalent to 1/360th of the pitch (25mm). Figure 12 shows the ALSA set-up for a stiffness test. Assuming perfect efficiency (due to the ALSA frictionless nature), the force was calculated according to Eq. 1,

$$F = \frac{2\pi T}{P}(Efficiency), \quad (1)$$

where F is the force, T is the torque, P is the lead screw pitch, and efficiency is assumed to be 1.

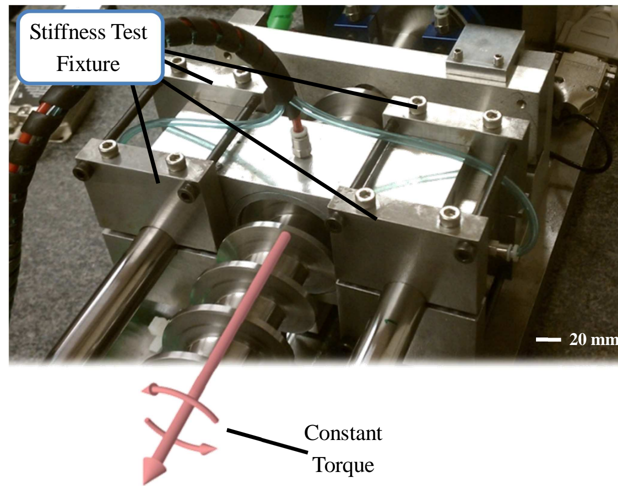

Fig. 12 Stiffness Measurement on ALSA

Stability was qualitatively determined by ramping up the inlet air pressure until the nut exhibited the pneumatic hammering effect. Stability must be maintained over the desired length of travel of the actuator.

4.2 Trial 1: Initial ALSA Evaluation

From Section 2.2, it was determined that in order to achieve adequate per-thread stiffness, a permeability in the range between 6.6e-15 m^2 and 12.3e-15 m^2 would be necessary with an air gap of 4 µm. A target permeability on the lower end of the range, 8.0e-15 m^2, was chosen to improve stability in this initial trial. Final lapping resulted in an air gap of 5 microns.

At inlet pressures of less than 550 kPa, the ALSA exhibited stable operation with a per-thread stiffness in the range of 3-5 N/µm. As inlet pressures were increased past 550 kPa, the nut began to vibrate due to the pneumatic hammering phenomenon.

When dealing with 18 separate air bearings, there will be some variation in permeability among all of the porous disks. After measuring the mass flow rate of each disk, the permeability can be calculated using Darcy's law, given in Eq. 1. Table 3 provides permeability data for Trial 1.

Table 3 Summary of Permeability of 18 Graphite Disks

Permeability Statistic	
N	18
Minimum (m^2)	6.50e-15
Average (m^2)	8.14e-15
Maximum (m^2)	1.18e-14
Std. Dev. (m^2)	1.37e-15
Coefficient of Variation	16.83%

To improve the stability of the ALSA, higher consistency of permeability among all 18 disks should be achieved. The coefficient of variation is used as a relative measure of variation in permeability. A coefficient of variation of less than 10% will be considered a target for the ALSA.

As permeability is increased, stability of the ALSA is jeopardized and there is an increased likelihood of vibration due to pneumatic hammering [11]. Therefore, to increase the stability of the aerostatic nut at higher pressures, the overall permeability may be reduced further. However, to obtain the high stiffness required by a precision actuator, the air gap must be decreased (See Section 2.2). To obtain the maximum stiffness for a given permeability and air gap, the aerostatic nut should operate at the highest supply pressure that still provides stability.

4.3 Trials 2 & 3: Further Testing to Improve Stiffness and Stability

In trial 2, improved stability was the primary goal. To achieve higher stability over a wider range of inlet pressures, the overall permeability was reduced and higher consistency of permeability among the 18 air bearings was targeted in this trial. The target permeability of the graphite disks was set at 5.0e-15 m^2. In attempting to increase the per-thread stiffness of the aerostatic nut in this trial, the target air gap was reduced to 3.5 microns. Table 4 provides the trial 2 ALSA performance results.

Table 4 Trial 2 ALSA Performance Results

ALSA Operating Parameters	
Pressure (kPa)	830
Air Gap (µm)	3.5
Average Permeability (m^2)	5.43e-15
Coefficient of Variation	7.73%
Floatation	Yes
Stable	Yes

In trial 2, the ALSA demonstrated stable floatation at high inlet pressures; trial 2 achieved stability over 50 mm of travel with inlet pressures greater than 1.4 MPa. In this trial, the ALSA exhibited a per-thread stiffness values on the range of 4-6 N/µm at an inlet pressure of 830 kPa.

To increase stiffness while maintaining stability up to 830 kPa, a third trial was conducted. In this trial, the overall permeability of the aerostatic nut was increased. Table 5 summarizes the trial 3 ALSA performance results. The average permeability measured was 9.54e-15 m^2 with a coefficient of variation of 2.93%. In this trial, the ALSA maintained both frictionless motion and stability over a 50 mm length of travel. The final per-thread stiffness attained was 9.7 N/µm. Therefore, to meet the pre-specified stiffness ALSA requirement, two single-threaded nuts may be coupled.

Table 5 Trial 3 ALSA Performance Results

ALSA Operating Parameters	
Pressure (kPa)	830
Air Gap (µm)	3.5
Average Permeability (m^2)	9.54e-15

Coefficient of Variation	2.93%
Floatation	Yes
Stable	Yes
Per-Thread Stiffness @ 830 kPa (N/µm)	9.7

5. Conclusions

Specific conclusions drawn from this work are:

1. The porous-restricted ALSA design features a unique nut design that consists of a set of porous-restricted air bearings backed by wave spring flexures and a helical plenum chamber. The wave spring flexures create a self-aligning method to consistently match all graphite disk insert surfaces to the helical profile of the lead screw thread.
2. A manufacturing process has been developed to ensure a uniform air gap across the entire helical thread surface to meet desired stiffness and stability criteria. Rough and final lapping are capable of producing air gaps as small as 3.5 µm.
3. The surface restriction layer technique has been implemented to achieve target permeability. Using this technique, the permeability values among all disks have a coefficient of variation of less than 3%.
4. Based on the results of several tests, a stable ALSA with a per-thread stiffness of 9.7 N/µm operating at 830 kPa over 50 mm of travel has been demonstrated.
5. This ALSA design is adaptable to accommodate applications requiring varying degrees of actuator stiffness by coupling two or more single-threaded nuts.

ACKNOWLEDGEMENT

The authors gratefully acknowledge the financial support of the Korean Institute of Machinery and Materials (KIMM) in the conduct of this research. This research was carried out in part in the Frederick Seitz Materials Research Laboratory Central Facilities, University of Illinois, which is partially supported by the U.S. Department of Energy under grants DE-FG02-07ER46453 and DE-FG02-07ER46471.

REFERENCES

1. Zhu, J., Kapoor, S.G., DeVor, R.E., Samuel, J., “Design and Manufacture of an Aerostatic Lead Screw Actuator for High Performance Micro-Scale Machine Tools,” Proceedings of IWMF, Daejon, Korea, October, 2010.
2. Aramcharoen, A., Mativenga, P.T., “Size Effect and Tool Geometry in Micromilling of Tool Steel,” Precision Engineering, Vol.33, No.4, pp. 402-407, 2009.
3. Cao, Z., Li, H., “Investigation of Micro-Milling Force Based on Miniature Machine Tool,” Applied Mechanics and Materials, Vols.29-32, pp. 1074-1078, 2010.
4. Ellicott, G.J., DeVor, R.E., and Kapoor, S.G., "Machinability Investigation of Micro-Scale Hard Turning of 52100 Steel," Transactions of NAMRI/SME, Vol.37, pp. 143-150, 2009.
5. Adair, K.g., “An Approach to the Economic Manufacture of an Aerostatic Lead Screw for Micro-scale Machine Tools,” Journal of Manufacturing Processes, Vol.13, No.1, pp. 16-23, 2011.
6. Tachikawa, H., Fukuda, M., Shinshi, T., Sato, K., and Shimokohbe, A., "Ultra Precision Positioning Using Air Bearing Lead Screw," Transactions of the Japan Society of Mechanical Engineers, Vol.66, No.645, pp. 1559-1566, 1997.
7. Slocum, A.H., System to Convert Rotary Motion to Linear Motion, USA, Patent 4,836,042, 1989.
8. Plante, J.S., Vogan, J., Aguizy, T.E., Slocum, A.H., “A Design Model for Circular Porous Air Bearings Using the 1D Generalized Flow Model,” Precision Engineering, Vol.29, No.3, pp. 336-346, 2005.
9. Loctite Hysol E-120HP Data Sheet, http://tds.loctite.com/tds5/docs/HYSAE-120HP-EN.PDF.
10. Rasnik, W.H., Arehart, T.A., Littleton, D.E., Steger, P.J., “Porous Graphite Air-Bearing Components as Applied to Machine Tools,” Society of Manufacturing Engineers, Technical Report MRR74-02, 1974.
11. Yoshimoto, S., Tozuka, H., Dambara, S., “Static Characteristics of Aerostatic Porous Journal Bearings with a Surface-Restricted Layer,” Proceedings of the Institution of Mechanical Engineers, Part J: Journal of Engineering Tribology, Vol.217, No.2, pp.125-132, 2003.

Integration of micro-EDM and EBL processes in silicon manufacturing

Gianluca D'Urso, Giancarlo Maccarini, Cristina Merla, Chiara Ravasio#
Department of Design and Technology, University of Bergamo, Italy
Corresponding Author / E-mail: chiara.ravasio@unibg.it, TEL: +39-035-2052330, FAX: +39-035-2052310

KEYWORDS : Micro-EDM, EBL, Micro features, Silicon machining

The current technological and productive scenario requires the fabrication of industrial components, characterized by dimensions and precision in the order of micron, in several sectors like manufacturing, optical, electronics, medical and biotechnological. Currently, various devices characterized by small dimensions, are fabricated using different processes; micro fluid, micro mechanical, micro optical and microelectronic functionalities are combined on very small areas of micro systems, which lead to new products in bio and medical technology, in information and communications technologies, in automotive engineering. Micro electro discharge machining (micro-EDM) is one of the recent and most promising micromachining techniques in the precision manufacturing field and it is used to fabricate products having geometrically complex profiles with high aspect ratio. Micro-EDM is an effective technology for machining any type of electrically conductive materials, regardless of the hardness, by means of rapid and repetitive spark discharges striking between a tool and a workpiece. The EBL technology consists in the electron irradiation of a surface covered with a resist which is sensitive to a focused electron beam. For this reason, EBL can generate arbitrary patterns without fabricating a mold first. Then, the very small structures in the resist can subsequently be transferred to the substrate material, often by etching. The use of the narrow electron beam, the same used also for the Scanned Electron Microscope (SEM), allows high resolution images and in the same way high resolution patterns.
Aim of this work is the integration of micro-EDM and EBL processes in silicon manufacturing. A Sarix SX200 micro EDM machine and an electron beam lithography system based on a SEM microscope Zeiss Evo 40 were used for this purpose. In particular, features having different dimension, were executed. As a first step, a set of engravings was performed using the EBL system. After development process, dissolving of the residual resist and transferring the engraved path on the silicon wafer, the EDM technology was applied to the same workpieces. Both geometrical and dimensional analyses were carried out on the produced features using a SEM microscope.

NOMENCLATURE

Ton = pulse on time
F = frequency of the discharges
I = peak current
U = voltage

1. Introduction

The trend towards the downsizing of mechanical parts is increasing in many fields. Several microfabrication technologies are available today and they are used to fabricate microcomponents and systems. The advances of modern process technology enable the access to many new research and product ideas, other than classical microelectronics. These activities are grouped under the label "micromechanics", "micromachining", "MEMS" (micro-electromechanical systems) or "MOEMS" integrating optics.

For the production of micro components, many possibilities based on different technologies are available: lithographic technologies (bulk and surface micromachining, LIGA, EBL), conventional technologies (micro drilling, micro turning and micro milling) and special technologies (micro-EDM, micro-laser, micro-ECM, micro-USM). The selection of the process or, in some cases, the combination of more processes, is a function of the technical and functional

specifications of the final components.

LIGA (German acronym for Lithographie, Galvanoformung and Abformung), plays an active role in emerging and competitive micro-technologies through the fabrication of high aspect ratio structures having very good quality and surface roughness. LIGA is now being evaluated for industrial applications and commercial exploitation. Several efforts are being made to standardize the process [1]. Some market segments like gear and watch industries are facing the technological barriers of their production methods (like punching, precision milling etc) to explore the potentiality of LIGA technology [2].

In LIGA the exposure phase can be made using X-ray, UV light, ion beam or electron beam. X-ray lithography offers extremely accurate patterning capabilities, but the high cost related to the exposure procedure (synchrotron radiation is needed) may represents a limit for the industrial applications. Another limit concerning X-ray process is the need for a mask containing the drawing to be engraved on the specimens. UV-Lithography, using UV light, is cheaper but it has a minimum feature size larger than 1 μm [3]. Ion beam lithography is a new technique for the 3D structuring of photoresist materials; it is a direct-write (maskless) technique that uses high energy (0.5–3.5 MeV) light ions (protons or helium ions) for the irradiation of photoresist materials [4]. Electron beam lithography (EBL) is a maskless technology which combines excellent resolution with high flexibility [5]. The electron beam can be highly focused and can produce very fine structures, (smaller than 100 nm). However the process is affected by electrons scatter (resulting in a loss of resolution), especially when high thickness resist is concerned.

Electrical Discharge Machining (EDM) is an effective technology for machining any type of electrically conductive materials, regardless of its hardness, by means of rapid and repetitive spark discharges striking between a tool and a workpiece. The workpiece and the electrode are submerged in a dielectric fluid and they are separated by a small gap known as sparking gap. The pulsed discharges remove the workpiece material through melting and evaporation processes. The melted and vaporized materials are transformed into tiny particles known as debris. These particles are removed from the machining zone by means of the dielectric fluid jet.

In EDM process there is no contact between tool and workpiece, so eliminating physical cutting forces, mechanical stresses and vibration problems [6]. For this reason, EDM is very effective in machining very hard and high strength materials, generally considered "difficult to be cut" using conventional technologies [7, 8]. Moreover, a contact less and "forceless" machining process is very desirable, or even essential, when miniaturized components are machined, so enabling the production of micro-parts without distortions due to physical forces. Micro-electrical discharge machining (micro-EDM) is the application of EDM on the micro-manufacturing field and it can be considered as one of the most promising machining technologies for the fabrication of micro-components. In recent years, machining of difficult-to-cut materials has become an important issue in the field of micro-EDM. Actually, hard materials show excellent mechanical properties which can be useful in many important applications. Besides, the promising applications of micro-EDM are not only limited to the machining of high hardness alloys for micro-molds or cutting tools, but also to the production of "difficult to make structures" (having complex three dimensional shape) or to machine micro-holes with high aspect ratio [9, 10, 11].

Although electrical discharge machining obviously relies on the electrical conductivity of the workpiece material, the range of machinable materials is not limited to metals and alloys, but includes semiconductors, as for instance, silicon [12]. The application of micro-EDM to the machining of silicon has some important advantages. The most important are the high material removal rate and the low electrode wear (in comparison with the machining of steel or tungsten carbide). Furthermore, the advantages given by the characteristics of the substrate (flatness, low surface roughness, low cost, etc…) are also noteworthy. Anyway, in silicon micro machining there are some problems that need to be solved. First of all, it may happen that no short circuit occurs, thus the machine is often unable to detect the contact between the electrode and the surface of the workpiece. This because of a lower conductivity of silicon, if compared to metals. Secondarily, the optimal settings for the process stability, strongly depend on the electrode diameter as well as on the desired surface roughness; in addition the accuracy of the machined structures relies on the accuracy of the dressed electrode diameter [13]. High flexibility, high accuracy and the possibility to generate three dimensional structures are relevant aspects of this technology, as compared to conventional methods used for the preparation of silicon masters. This means that silicon micro-EDM is suitable for the production of prototypes or small batches of products [14]. In fact a design change can be quickly implemented simply by modifying the CAM file. Furthermore, the process does not require to be operated in a clean room environment, with a consequent reduction of the manufacturing costs [13]. In the matter of silicon microstructure, it is demonstrated that the micro-EDM process is independent of the silicon crystal orientation. This means that a wafer can be machined in any direction with respect to the wafer's top plane. For all these reasons, silicon micro-EDM is not only feasible but it also represents an important and complementary technology to traditional silicon micro machining [14].

As regards micro-EDM, the dimension of the features depends on the diameter of the electrode. The modern micro-EDM manufacturing systems have a wire unit able to process the electrode in the spindle: it is possible to reduce the diameter of the electrode and, if necessary, at the same time to change its shape. Considering the process time of these operations not negligible, the manufacturing of a workpiece containing different features and having different dimensions, could not be advantageous.

Aim of this work is to study the integration of micro EDM and EBL processes in silicon manufacturing. A Sarix SX200 micro EDM machine and an electron beam lithography system based on a SEM microscope Zeiss Evo 40 were used for this purpose. The samples used for this study were composed by wafers of Si having a layer of SiO_2 and a PMMA resist, deposited on the wafer. In particular, features having different dimension, were executed. As a first step, a set of engravings was performed using the EBL system. After the development process, the dissolving of the residual resist and the transferring of the engraved path on the silicon wafer, the EDM technology was applied to the same workpieces. Both geometrical and dimensional analyses were carried out on the produced features using a SEM microscope.

2. The experimental research

2.1 The systems

The systems used in the experimental research are described here below.

2.1.1 EBL

The system built by the authors for this study is implemented on a Zeiss EVO 40 SEM and the control is based on a PCI-DAS (16-bit) board installed on a PC. The structure of the system is summarized in Figure 1a. The system acts by using four different signals:

- Analogical X signal used to control the X coordinate of the electron beam.
- Analogical Y signal used to control the Y coordinate of the electron beam.
- TTL control, digital signal adopted to take the SEM control.
- TTL beam blanker, digital signal adopted to blank the electron beam.

A basic aspect of the system is the use of a drawing in neutral (.dxf) format as input data, so giving a very high flexibility in path design. A software in java language was created for drawing analysis and optimization. The aim of this program is to load and analyze the input file, to extract all the information useful for the path generation and to sort all entities to optimize beam path. A software in C++ controls the microscope beam and the entire lithography process. The algorithms for movement control are optimized to make the most of board resolution. The solution for managing the electron beam speed is based on a layer approach and all the different entities of the drawing must belong to one layer. The layer number represents the inverse of the beam speed. This feature allows the engraving of any entity of a drawing by moving the beam with its own speed.

Several tests were already performed and the effects of the main process parameters were partially investigated. The samples used for this purpose were composed by wafers of Si having a layer of SiO_2 and a PMMA resist, deposited on the wafer. General good results were found, even though the reduction of the engraving area with increasing radial distance, connected to an inverse effect on eccentricity, is an evidence of an electron density different distribution. An example of the achieved results is reported in Figure 1b (logo of the University of Bergamo engraved on silicon) and in Figure 1c (detail of a very small etched part). It is important to remark that this system and the related technology are not significantly limited in engraving small parts; on the opposite, the lithography of large paths (tenth of millimeters) may give rise to some problems in terms of accuracy and high engraving time.

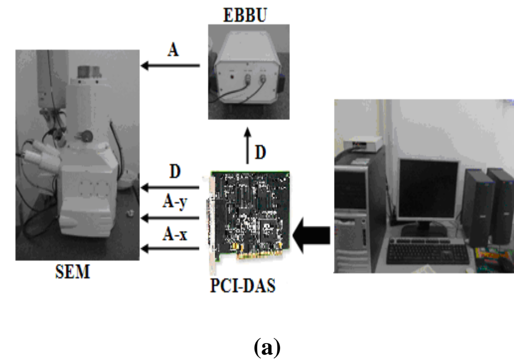

(a)

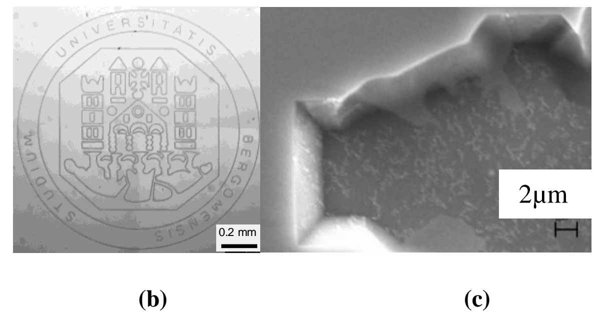

(b) (c)

Fig. 1(a) EBL system, (b) logo engraved on silicon and (c) details of an etched part

2.1.2 Micro-EDM

A Sarix SX-200 microEDM system is used for this research. Some details of the system are reported in Figure 2. A carbide cylindrical electrode having a diameter equal to 0.3mm was used as tool and oil as dielectric. The wire EDM unit is used to machine electrodes in order to reduce the diameter or to change the shape.

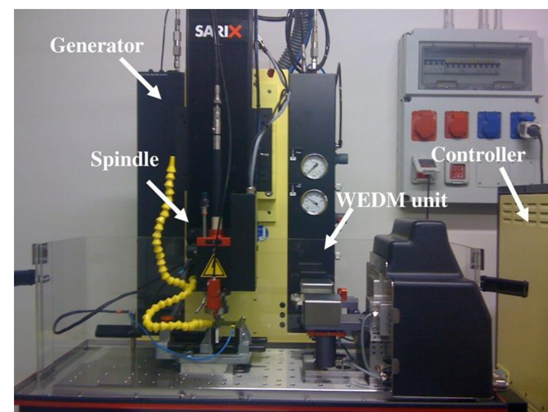

Fig. 2 Sarix SX200, details of the micro-EDM system

2.2 Samples and geometries

The samples used for EDM machining were wafers of Si having a resistivity in the range 0,001 - 0,002 Ohm cm. As regards the EBL tests, the samples were composed by the wafer of Si (thickness of 0.5 mm) having a layer of SiO_2 (3 μm) and a PMMA resist, deposited on the wafer through spin coating technique (thickness of 0.3 μm).

As regards the engravings executed using EBL system, once the engraving is achieved, the following steps are performed:

- development process carried out in a mixture of isopropyl alcohol and methyl isobutyl ketone; in this way, the PMMA layer impressed by electron beam is dissolved;
- bath in hydrofluoric acid solution in order to remove the silicon oxide layer;
- dissolving of the residual PMMA using acetone at 45°C;
- bath at 45°C in a potassium hydroxide in order to transfer the engraved path on the silicon wafer.

Concerning with the geometries, pockets having different dimensions and 0.1 mm depth were engraved.

3. Analyses of the results

3.1 EBL results

The following process parameters were used for the engraved pockets using EBL system: magnification 100X, voltage 20kV and probe current 4200 nA; the permanence time on each spot unit was equal to 10 ms. Table 1 reports the dimensional characteristics of the engraved pockets and the engraving time. It is important to remark that the reported engraving time does not include the time necessary to develop the sample.

Table 1 EBL pockets and engraving time

Test	Dimension [μm x μm]	Time [s]
1	300 x 300	11160
2	150 x 150	3000
3	75 x 75	840
4	37.5 x 37.5	300
5	18.8 x 18.8	120
6	9.4 x 9.4	60
7	4.7 x 4.7	30

The engraving time is directly proportional to the pocket area. Figure 3 shows some SEM photographs executed at different magnification of the engraved pockets after the development process and the etching.

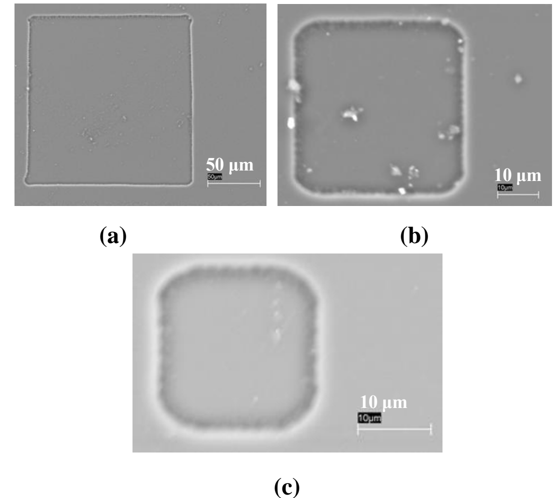

(a) (b) (c)

Fig. 3 EBL pockets: (a) 150 x 150 μm; (b) 37.5 x 37.5 μm; (c) 18.8 x 18.8 μm

3.2 EDM results

Table 2 shows the dimensions of the engraved pockets, the process parameters used and the machining time. In general, the machining time is directly proportional to the pocket area, except for Test 5. In fact, in this case the pocket was produced using a micro electrode (0.1 μm) and the energy parameter, that defines pulse shape and therefore the type of machining (roughing, finishing, etc.), is different. In particular, the Energy 206 is for roughing while the 13 one is for finishing.

It is important to remark that for the test 5, the reported time does not include the machining of the electrode using the wire unit.

Table 2 EDM process parameters and machining time

Test	1	2	3	4	5
Dimension [mm x mm]	5 x 5	2 x 2	1 x 1	0.5 x 0.5	0.25 x 0.25
Polarity	-	-	-	-	-
Ton [μs]	5	5	5	5	1
F [kHz]	130	130	130	130	160
I	50	50	50	50	80
U [V]	130	130	130	130	80
Gain	1500	1500	1500	1500	600
Gap [%]	65	65	65	65	72
Energy	206	206	206	206	13
Regulation	41-01	41-01	41-01	41-01	40-00
Spindle rotational speed	100%	100%	100%	100%	100%
Time [s]	599	93	30	9	609

Figure 4 shows some SEM photographs of engraved pockets having different dimensions.

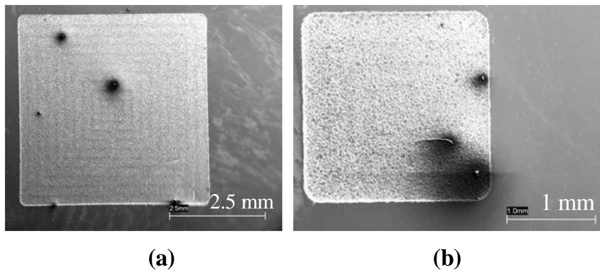

(a) (b)

Fig. 4 EDM pockets: (a) 5 x 5 mm; (b) 2 x 2 mm

Figure 5 reports a detail of the pocket having a size equal to 0.25 x 0.25 mm.

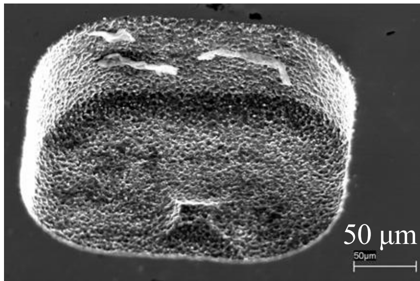

Fig. 5 Detail of a EDM pocket, 0.25 x 0.25 mm

The different dimensions of the craters on the surface are shown in Figure 6: in (a) (pocket 1 x 1 mm) the craters are larger than in (b) (pocket 0.25 x 0.25 mm). This is justified by the different energy used. In particular, to obtain a finishing surface, low energy has to be used but, in this case, the machining time remarkably increases. If the finishing surface is not necessary, high energy permits to produce pockets in short time.

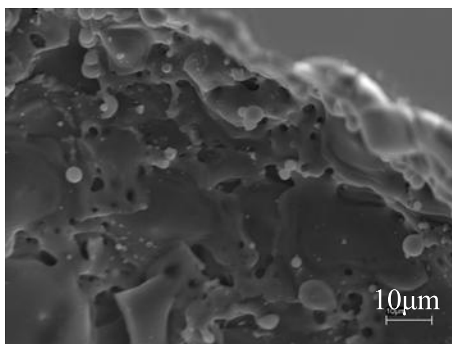

(a)

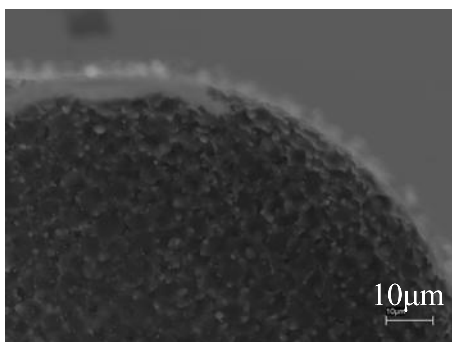

(b)

Fig. 6 Craters on the surface of pocket 1 x 1 mm (a) and 0.25 x 0.25 mm (b)

4. Conclusions

The integration of micro-EDM and EBL processes in silicon manufacturing was performed. In particular pockets having different dimension were engraved using both the manufacturing systems.

The conclusions that can be drawn are here summarized:

- EBL is able to make engravings having smaller dimensions than EDM;
- the process time is higher for EBL process and in general, it is directly proportional to the engraved area;
- the surface obtained using EDM system is characterized by the formation of craters. The dimension of these craters is a function of the process parameters used;
- the finishing surface of EBL pockets is better than EDM.

The results of this experiment may give some information about the optimal technological window as a function of the features dimension. Basing on this assumption, micro EDM can be used for the general manufacture of a microcomponents while EBL is useful for the engraving of very small details. Further studies will take into account the specific procedures for the combination of these technologies in a single component.

ACKNOWLEDGMENT

This work was carried out under the support of the "REMS – Rete Lombarda di Eccellenza per la Meccanica Strumentale e Laboratorio Esteso" project funded by Regione Lombardia.

REFERENCES

1. Lawes, Ron A., "Linewidth design rules for microstructures manufactured in PMMA resist using X-ray LIGA", Microsystem Technologies, Vol. 16, pp. 411–421, 2010.
2. Pascal Meyer, Joachim Schulz, Lothar Hahn and Volker Saile, "Why you will use the deep X-ray LIG(A) technology to produce MEMS?", Microsystem Technologies, Vol. 14, pp. 1491–1497, 2008.
3. Watt, F., Nuclear Instruments Methods B, pp. 158-165, 1999.
4. Munnik, F., Benninger, F., Mikhailov, S., Bertsch, A., Renaud, P., Lorenz and H., Gmuer, M., "High aspect ratio 3D structuring of photoresist materials by ion beam LIGA", Microelectronic Eng., pp. 67-68, 2003.
5. Hahmann, P. and Fortagne, O., "50 years of electron beam lithography: Contributions from Jena (Germany)", Microelectronic Engineering, Vol. 86, pp. 438–441, 2009.
6. Tak, H.S., Ha, C.S., Kim, D.H., Lee, H.J., Lee, H.J. and Kang, M.C., "Comparative study on discharge conditions in micro-hole electrical discharge machining of tungsten carbide (WC-Co) material", Transactions of Nonferrous Metals, Vol. 19, pp. 114-118, 2009.
7. Jahan, M.P., Wong, Y.S. and Rahman, M., "A comparative experimental investigation of deep-hole micro-EDM drilling capability for cemented carbide (WC-Co) against austenitic

stainless steel (SUS 304)", International Journal Advanced Manufacturing Technology, Vol. 46, pp. 1145-1160, 2010.

8. Liu, N.M., Chiang, K.T., Horng, J.T. and Chen, C.C, "Modeling and analysis of the edge disintegration in the EDM drilling cobalt-bonded tungsten carbide", International Journal Advanced Manufacturing Technology, Vol. 51, pp. 587-598, 2009.
9. Egashira, K., Morita, Y. and Hattori, Y., "Electrical discharge machining of submicron holes using ultrasmall-diameter electrodes", Precision Engineering, Vol. 34, pp. 139-144, 2010.
10. Liu, K., Lauwers, B. and Reynaerts, D., "Process capabilities of Micro-EDM and its applications", Int J Adv Manuf Technol, Vol. 47, pp. 11-19, 2010.
11. Allen, P. and Chen, X., "Process simulation of micro electro-discharge machining on molybdenum", Journal of Materials Processing Technology, Vol. 186, pp. 346-355, 2007.
12. Feng-Tsai, W., Chen-Siang, H. and Wen-Feng, L., "Fabrication of micro components to Silicon wafer using EDM process", Materials Science Forum, Progress on Advanced Manufacture for Micro/Nano Technology. Trans Tech Publ Switz 505–507:217–222, 2006.
13. Tosello, G., Bissacco G., Tang, P. T., Hansen, H. N. and Nielsen, P. C., "High aspect ratio micro tool manufacturing for polymer replication using EDM of silicon, selective etching and electroforming", Microsyst Technol, Vol.14, pp. 1757–1764, 2008.
14. Reynaerts, D., Meeusen, W. and Van Brussel, H., "Machining of three-dimensional microstructures in silicon by electrodischarge machining", Sensors and Actuators A, Vol. 67, pp. 159-165, 1998.

Concept of a programmable platform for micromanipulation with electrostatic forces

Panos Lazarou [1,#], Nikolaos Aspragathos [1] , Johan Dalin [2] and Jürgen Wilde [3]

1 Robotics Group, Department of Mechanical Engineering & Aeronautics, University of Patras, Rion, Patras, 26500, Greece
2 Inomed Medizintechnik GmbH, Im Hausgruen 29, 79312 Emmendingen, Germany
3 University of Freiburg – IMTEK, Department of Microsystems Engineering, Georges-Köhler Allee 103, 79110, Freiburg, Germany
Corresponding Author / E-mail: plazarou@freemail.gr, TEL: +302610996248

KEYWORDS : Micromanipulation, Electrostatic forces, Electrode platform, MEMS

In this paper, the concept of a programmable electrode platform for micromanipulation on a wafer using electrostatic forces is introduced. The motion mechanism consists of the successive activation of platform electrodes, which electrostatically attract complementary electrodes on the bottom surface of the parts. The dynamics modelling of motion is briefly presented and simulations are performed in order to investigate and assess the platform's basic manipulation capabilities. The electrode activation sequences for one and two dimensional translation are presented, showing successful positioning as well as successful part rotation taking place in several steps. These results as well as the limitations and the prospects of this concept are then discussed. With this approach for 3 degrees of freedom motion on the platform, a basis for the investigation of complex operations such as sorting and parallel manipulation can be established.

NOMENCLATURE

h = thickness of thin liquid film
U = difference of electric potential across complementary electrodes
R = radius of electrode
ε_0 = electric permittivity of vacuum
ε_r = relative electric permittivity of the liquid film
η_l = dynamic viscosity of liquid
w_p = width of the micropart
m_p = mass of the micropart
ω_p =rotational angle of the micropart
$S_p = \sqrt{(x^2+z^2)}$ planar distance of the part's COM from the origin of the global coordinate system {G}
d = distance between substrate and part complementary electrodes (misalignment)
F_{elec} =electrostatic force between complementary electrodes
F_{visc} = viscous damping force acting on the micropart
T_{elec} =electrostatic torque on the micropart due to F_{elec}
T_{visc} = viscous damping torque acting on the micropart

1. Introduction

Micropart manipulation is a very important stage of the overall MEMS assembly procedure. Most of the current microfabrication methods are able to produce hundreds or thousands of components; these components need to be properly distinguished, sorted and aligned for the assembly and packaging of the final MEMS products. Robotic micromanipulators and part-feeders used in industrial production lines are generally unable to simultaneously achieve most or all of the following desirable operational characteristics: low cost, flexibility, micron or submicron accuracy, fast manipulation and assembly cycles, parallel instead of serial/sequential handling of microparts.

An alternative approach to robotic handling is contact-free micromanipulation with force fields. A variety of theoretical artificial force fields – often called "programmable" force fields since they can be diffused/programmed on distributed manipulation systems or microactuator arrays for actual applications - has been presented in the literature. The use of such fields offers methodologies of mostly sensorless manipulation for a wide variety of microparts [1-2]. Many types of programmable force fields have been proposed, such as squeeze fields [3], elliptical fields [4], the combination of a radial and a gravity field [5], and fields formulated according to the shapes of the microparts to be manipulated [6] etc.

In addition to the programmable fields, various implementations that employ physical force fields have been introduced for micropart handling. Pneumatic fields created by platforms of inclined air jets can levitate and transport objects to desired positions, as evidenced in [7-8]. Precise micropart positioning based on superconducting magnetic levitation has been demonstrated [9]. In [10] fringe electric fields attract and position parts in structured orifices where the potential is minimum, while in [11-12] devices that utilize multiphase AC electric fields provide conveyance, smoothing, grouping, sorting, as well as two-dimensional handling of microparticles. The authors of this paper in their previous work [13-16] determined the electrostatic forces for alignment and self-assembly of microparts, verified by modelling, simulations as well as experimental results.

The present work follows the philosophy of contact-free handling with force fields and expands our previous work. Thus, the concept of a programmable electrode platform for micromanipulation on a wafer using electrostatic forces is introduced. The parts can be electrostatically manipulated, positioned and orientated on the substrate's plane by sequential activation of properly selected planar electrodes. Simulations of micropart motion are performed in order to verify the feasibility of electrostatic manipulation under this scheme; the target is to investigate and assess the proposed platform's basic capabilities of manipulation. The results are successful, proving that 1D, 2D translation as well as part rotation are feasible, thus setting the foundations for further investigation of more complex platform capabilities, such as part sorting, motion along defined trajectories and parallel handling of microparts.

2. Concept Description

The programmable platform for micromanipulation presented in this section is a continuation of the previous work [13-16] of the authors of the present paper. A schematic of this concept is shown in Fig. 1. An array of copper electrodes is fabricated on the upper surface of a PCB substrate; the spacing between the neighboring substrate electrodes should be small in order to achieve better resolution on the surface but also large enough to avoid current leakage. A detachable a thin layer of dielectric on top of the electrodes provides isolation as well as the plane where the microparts are manipulated. Between the dielectric and the parts lies a very thin film of liquid lubricant/photo-hardening adhesive in order to minimize friction during part motion but also to ensure the bonding of the parts on the wafer after the alignment phase is complete (for example through exposure to laser-lighting).

The manipulation principle lies in the successive activation of substrate electrodes, which cause surface charge reallocation on the parts' bottom conductive, interconnected electrodes. As a result, attractive electrostatic forces are exerted and thus "drag"/move the parts towards the desired locations. In this way, contactless micropart manipulation of 3 degrees of freedom (two translational, one rotational) can be achieved. From this point on, a substrate electrode that electrostatically interacts with a part electrode will be characterized as "complementary electrodes" or "complementary pair". It is possible for a substrate electrode to interact with more than one part electrodes simultaneously (depending on the part's position and orientation), thus there can be more than one complementary pairs equivalently.

An electric analogue of this manipulation mechanism is a system of a parallel-plate capacitor with the upper plate being horizontally misaligned. The upper plate moves horizontally to minimize the system's electrostatic energy, but before this minimization is achieved the bottom plate is translated further away. As a result, the upper plate is continuously "dragged"/attracted towards the moving bottom one.

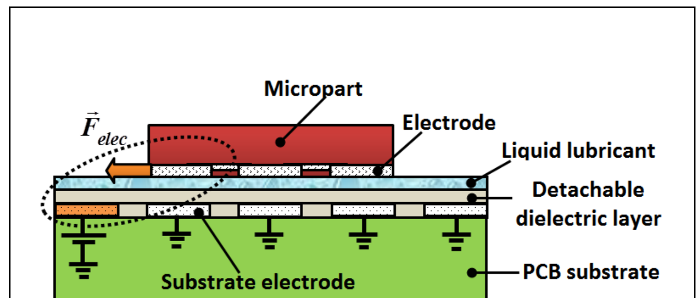

Fig. 1 Cross-cut of the platform concept (dimensions and thickness of the various layers and components are indicative)

3. Modeling and Simulations of Micromanipulation

This section investigates the basic manipulation capabilities of the proposed platform, i.e. 1D and 2D translation and rotation. In these first tests, only one micropart is used in order to assess the feasibility of manipulation. Firstly, the motion dynamics as well as the modelling details of the platform and micropart are given and subsequently the simulation results are presented.

3.1 Part dynamics

The dynamics of a part during the manipulation procedure are presented in this section. As already mentioned, the driving force is the total electrostatic force acting on the part due to the electrostatic interactions between the complementary pairs of electrodes. For each such pair, this force is given by a semi-empirical, fitted formula introduced in [15]:

$$F_{elec}(d) = \begin{cases} A\left[1-e^{-21.36\frac{d}{2R}}\right], 0 \le d \le 0.4(2R) \\ A\left[\dfrac{1}{1+e^{7.95(\frac{d}{2R}-0.91)}}\right], d \ge 0.4(2R) \end{cases} \qquad (1)$$

where A=0.38*(2R)*ε_0*ε_r*U^2/h. The main limitation of this force model is that the difference of potential U between the complementary electrodes of part and substrate is considered to be constant for all misalignments. According to the

proposed concept, all the electrodes of the part are interconnected and therefore constitute an equipotential area with a floating potential (it slightly varies, depending on the position, rotation and geometry). However, for small misalignments and due to symmetry, this potential is verified by simulations to remain nearly constant and equal to the potential of the nearby activated substrate electrodes [14-15]. For the purposes of manipulation and alignment of the part, the positions near the equilibrium have the highest significance (thus corresponding to small misalignments). Additionally, it must be noted that a dielectric layer was omitted (based on the afore-mentioned experimental results with a 0.1 μm thick dielectric layer) in order to simplify the derivation of Eq. (1).

The motion of the part is damped by a viscous drag force, whose measure depends on the velocity of the liquid medium near the part (assuming Couette flow) [15],[17]:

$$F_{visc} = \frac{\eta_l w_p^{\,2}}{m_p h} \dot{S}_p \tag{2}$$

Therefore the differential equation describing the planar motion of the micropart is:

$$\ddot{S}_p + \frac{\eta_l w_p^{\,2}}{m_p h} \dot{S}_p - \frac{F_{elec}^{tot}}{m_p} = 0 \tag{3}$$

where F_{elec}^{tot} is the sum of the components of the electrostatic forces between complementary electrodes along the direction of motion (example in Fig. 2, where motion only along the x axis is considered).

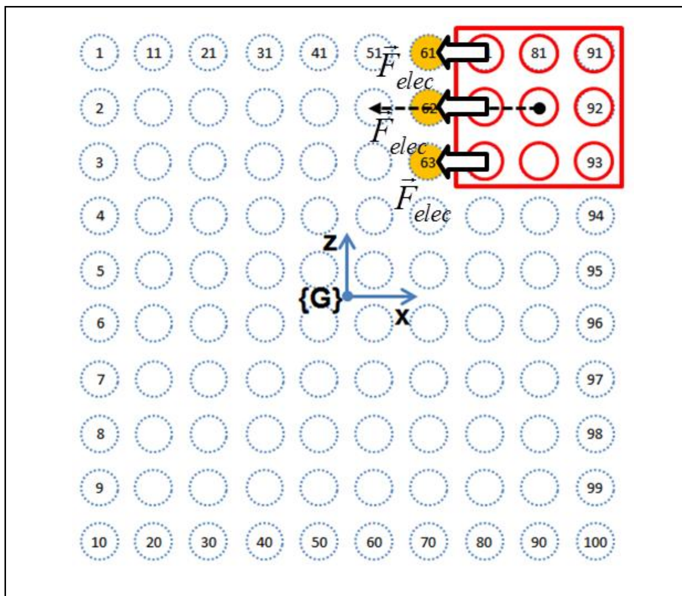

Fig. 2 Micropart and its electrodes (continuous lines and circles), substrate electrodes (dotted circles), neighboring electrodes for activation (color filled circles), desired horizontal trajectory of motion (thin arrow) and electrostatic forces between complementary electrodes (thick arrows)

The micropart rotation around the perpendicular axis to the x-z plane, is similarly affected by the driving total electrostatic torque as well as the viscous damping torque. The electrostatic torque for each pair of complementary electrodes is calculated as the cross product of the distance vector $\vec{r}'$ of the part electrode to its center of mass (local coordinate system {L}) with the electrostatic force vector acting on that electrode $\vec{F}_{elec}$. Obviously, only the perpendicular force components $\vec{F}_{elec}^{\perp}$ contribute to the part's torque and not the parallel ones $\vec{F}_{elec}^{\parallel}$. An example is seen in Fig. 3: in each of the four part electrodes an attractive electrostatic force is exerted towards the nearby complementary substrate electrodes. By analyzing the force vectors into parallel and perpendicular to $\vec{r}_i'$ components (where i=1…4), it is obvious that: a) due to symmetry, all the parallel force components negate each other and therefore no translational motion occurs, b) the perpendicular ones and rotate the part clockwise (clockwise torques) along the perpendicular to the plane axis of the local coordinate system {L} at the COM.

The viscous damping torque is calculated by the following formula [2]:

$$T_{visc} = -\frac{\eta_l \, I_{y'} \, w_p^2}{m_p h} \dot{\omega}_p \tag{4}$$

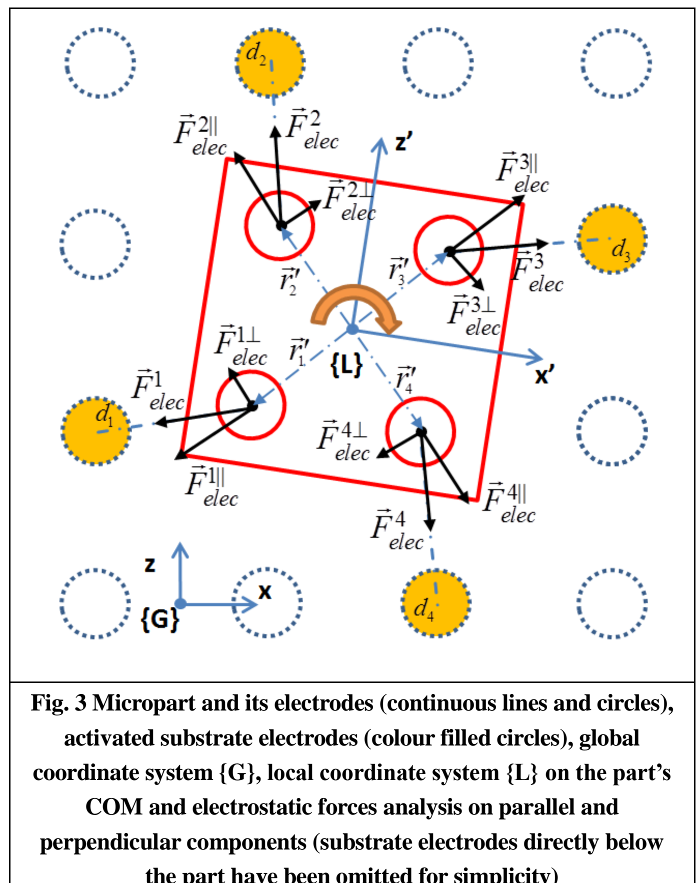

Fig. 3 Micropart and its electrodes (continuous lines and circles), activated substrate electrodes (colour filled circles), global coordinate system {G}, local coordinate system {L} on the part's COM and electrostatic forces analysis on parallel and perpendicular components (substrate electrodes directly below the part have been omitted for simplicity)

Therefore the differential equation describing the part's rotation around the axis y' of the local coordinate system {L}

is:

$$\ddot{\omega}_p + \frac{\eta_l \, w_p^2}{m_p h} \dot{\omega}_p - \frac{T_{elec}^{tot}}{I_{y'}} = 0 \quad (5)$$

Eq. (3) and Eq. (5) are used by the model of section 3.2 to calculate the translational and rotational motion of the part for each time-step of the simulations.

3.2 Modelling of the platform, electrodes and micropart

The modelling of a micropart of dimensions 1000x1000x180 μm made of glass is considered, carrying a 3x3 array of circular electrodes on its bottom surface. The thin film of fluidic medium has a relative electric permittivity ε_r =5, dynamic viscosity η_l =0.005 kg* m^{-1}*s^{-1} and a thickness of h=5 μm. The array of substrate circular electrodes is 10x10 and the diameter of all the electrodes is 2R=220 μm with vertical and horizontal spacing of approximately 100 μm. The choice of circular electrodes was made due to their symmetry, which greatly simplifies the calculations of the electrostatic force for planar motion [15].

The voltage applied is common to all the activated electrodes (200 V DC for planar motion and 400V DC for rotation). It must be noted that previous actual experiments of part alignment in [14],[16] were successfully performed with a very thin dielectric layer of a 0.1 μm thick Si_3N_4 and voltages of up to 200 V DC and 400 V AC. Based on these findings, it is understandable that the thickness of this dielectric layer is negligible compared to the thickness of the 5 μm of the fluidic medium and can therefore be ignored for simplicity in the simulations without significant error.

Fig. 4 shows the model of the platform and micropart in Simulink/Simmechanics, consisting of various blocks. The electrostatic block calculates the total electrostatic force of Eq. (3) between complementary electrodes as well as the torque of the part of Eq. (5) for each time step of the simulation, based on the current pose (position and orientation). The viscous drag block calculates the viscous damping force and torque acting on the part, based on the translational and rotational velocity respectively.

The actuation subsystem essentially defines the degrees of freedom and allows the planar motion and rotation of the part. The global coordinate system {G} lies at the center of the array of substrate electrodes, with the x and z axes defining the plane of motion and with the y axis being the perpendicular to the plane. For all the motion simulations presented below, it is assumed that at the micropart's initial pose is known in advance. At this pose, all the part's electrodes fully coincide/overlap with the electrodes of the substrate; additionally, the initial rotational angle is zero.

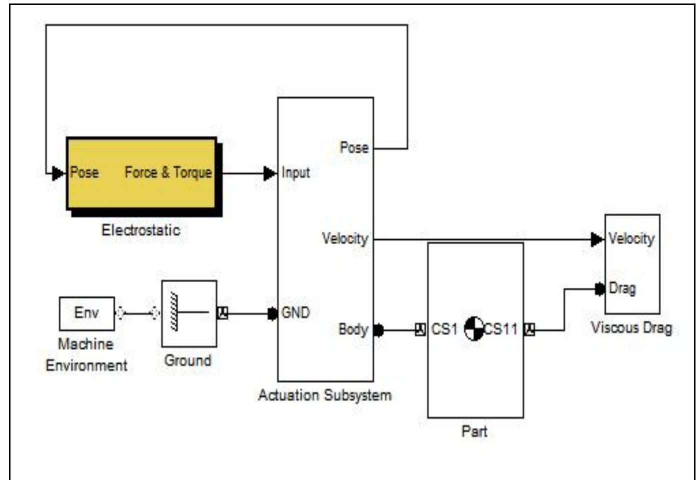

Fig. 4 The model of the platform and micropart in Simulink/Simmechanics

3.3 One and two dimensional translation

First, a simple motion of the micropart along the x axis is demonstrated. The initial position of its COM (center of mass) is set at the center of substrate electrode no. 82 and it will be translated three "electrode positions" leftwards, at electrode no. 52 (i.e. from 82, to 72, to 62 and 52). The global coordinate system, the micropart, the desired trajectory of its CG and the numbered substrate electrodes are shown in Fig. 2.

In order to perform the motion of the micropart leftwards, three triplets of neighboring substrate electrodes must be activated sequentially. The attractive electrostatic forces pull the part towards the activated electrodes. These triplets are the following: (61, 62, 63), (51, 52, 53) and (41, 42, 43). Each substrate electrode is activated for 0.05 s with a voltage of 200V. Fig. 5 shows the electrode activation signals of the last two triplets (the other is similar), whereas Fig. 6 presents the position of the part's COM, the total electrostatic and viscous damping force over time.

The trajectory is a straight line heading leftwards, as expected, and it can be observed that the COM oscillates briefly around the equilibrium at the centers of the electrodes 72, 62, 52, similarly to the findings in [14-15]. The horizontal distance travelled by the part is approximately 0.964 mm in less than 0.14 ms, while the maximum translational velocity and maximum electrostatic force are 88.7 mm/s and 1.125×10^{-4} N respectively.

Similar is the behavior of the micropart for two dimensional motion (diagonal). In this case, the desired motion is again translational, from electrode 82, to 73, to 64 and finally to 55. In order to implement the diagonal motion, groups of 5 electrodes are sequentially activated, essentially forming the shape of the head of an arrow (Fig. 7). The groups required are: (62, 63, 64, 74, 84), (53, 54, 55, 65, 75) and finally (44, 45, 46, 56. 66). Each substrate electrode is activated with a voltage of 200V, but this time for 0.1 s, as the diagonal distance the part's COM needs to travel is slightly bigger and therefore it requires slightly more time in order to reach the next equilibrium position. The longer distance, however, is offset with the increased total electrostatic force due to two more electrodes being activated.

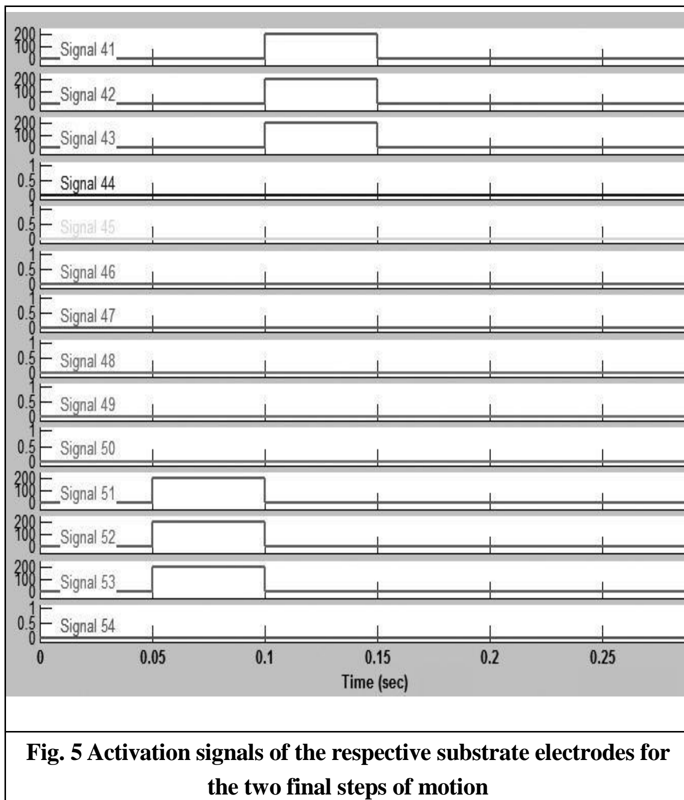

Fig. 5 Activation signals of the respective substrate electrodes for the two final steps of motion

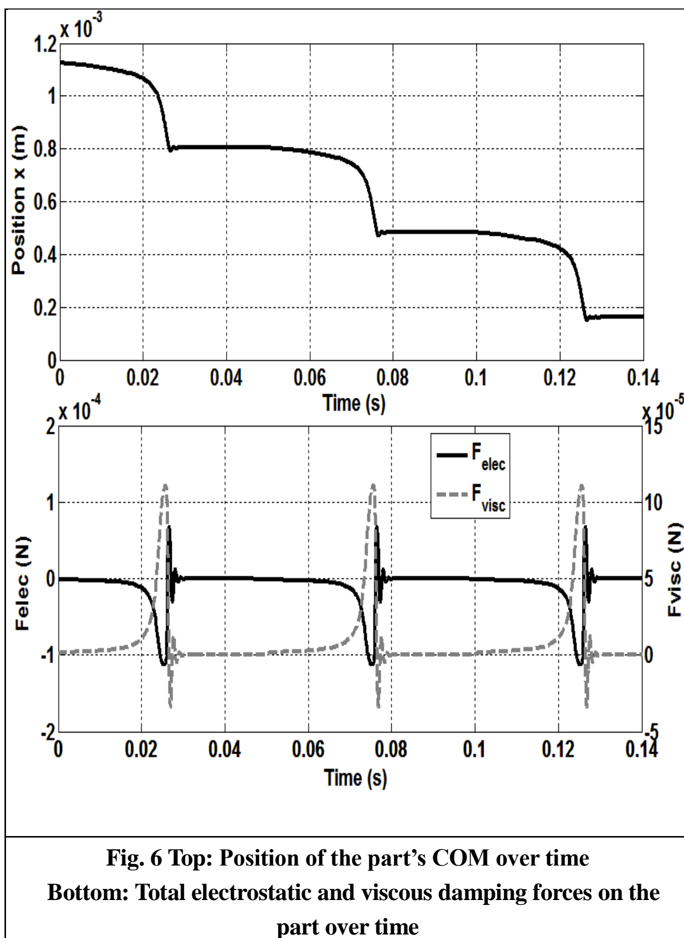

Fig. 6 Top: Position of the part's COM over time Bottom: Total electrostatic and viscous damping forces on the part over time

Fig. 8 shows the COM's position over time for both x and z coordinates as well as its actual trajectory on the plane. Due to symmetry, the resultant total electrostatic force has a diagonal direction and therefore the part moves diagonally. Its behavior is similar to the one dimensional translation, with brief oscillations when its electrodes overlap and align with the substrate electrodes. The diagonal distance travelled is approximately 1.4 mm in less than 0.3 s, the maximum translational velocity reaches 98.9 mm/s and, the maximum electrostatic force is 1.288×10^{-4} N along x and z axes.

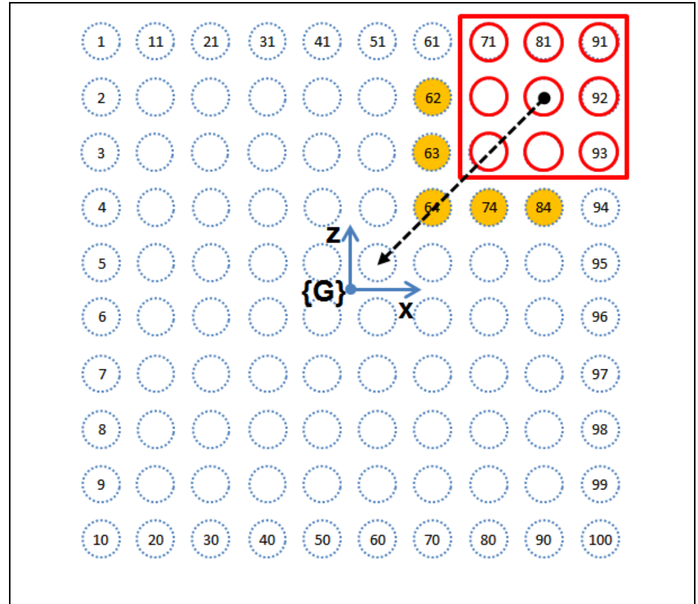

Fig. 7 Micropart and its electrodes (continuous lines and circles), substrate electrodes (dotted circles), neighboring electrodes for activation (color filled circles) and desired diagonal trajectory of motion (thin arrow)

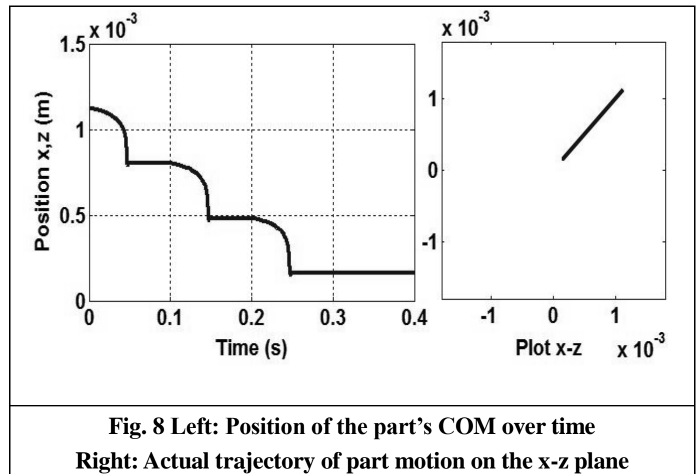

Fig. 8 Left: Position of the part's COM over time Right: Actual trajectory of part motion on the x-z plane

3.3 Rotation

Rotation of a micropart on the platform requires a slightly different manipulation approach. In this example, the part is rotated around the perpendicular to the plane axis at the center of electrode no. 65. In order to avoid any possible undesired translational motion of the part during its rotation (although due to symmetry as seen in section 3.2 the parallel force components negate each other), electrode 65 remains constantly activated. It essentially acts as an "anchor" to the substrate at the point of the rotation axis.

It has to be noted that the part is not automatically rotated

to a desired arbitrary angle. Instead, rotation takes place in several steps and in each of these the part is rotated by a specific angle. This is a limitation of the substrate electrodes' resolution as well as the way they are fabricated/placed on the array (equidistantly). The electrodes are activated with a voltage of 400V each for 1 or 2 s, depending on the rotation step, as seen in Table 1.

Table 1 Procedure steps, activation times of electrode groups and part's rotation angle (minus denotes clockwise rotation)

Step	Time (s)	Activated electrodes	Angle of rotation
1	0-1	46,53,65,77,84	-18.4°
2	1-2	45,63,65,67,85	-45° (-26.6°)
3	2-4	44,57,65,73,86	-71.56° (-26.5°)
4	4-5	54,56,65,74,76	-90° (-18.4°)

Fig. 9 shows the procedure for rotating a micropart by 90° in four steps, while Fig. 10 presents the rotation angle and the electrostatic torque acting on the part over time. The rotation sequences of Fig. 9 are based on the driving forces acting on the four corner electrodes. There are additional forces on the rest of the part's electrodes but they are always less significant than the four driving ones due to larger distances. For t=0, the four activated electrodes exert electrostatic forces to the nearby part electrodes, resulting in torque along the perpendicular axis at 65, rotating the part clockwise. Rotation stops at $t=1^-$ s at the angle of -18.4° (minus denotes clockwise rotation), when the electrodes 77, 65, 53 and the nearby part ones lie at the same straight line connecting them (similarly for the other group of electrodes). The driving electrostatic torque there becomes zero, as seen in Fig. 10 (no perpendicular force components).

At $t=1^+$ s the activation of the next set of electrodes takes place and the angle then decreases further to the value of -45° at $t=2^-$ s. By examining Fig. 10, one can see that there is an increase in the magnitude of the torque in this step compared to the previous one. This is due to the fact that there is a small overlapping of complementary pairs of electrodes, which significantly increases the electrostatic force and torque.

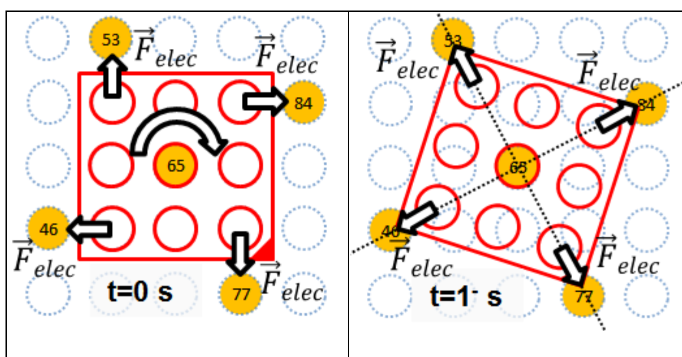

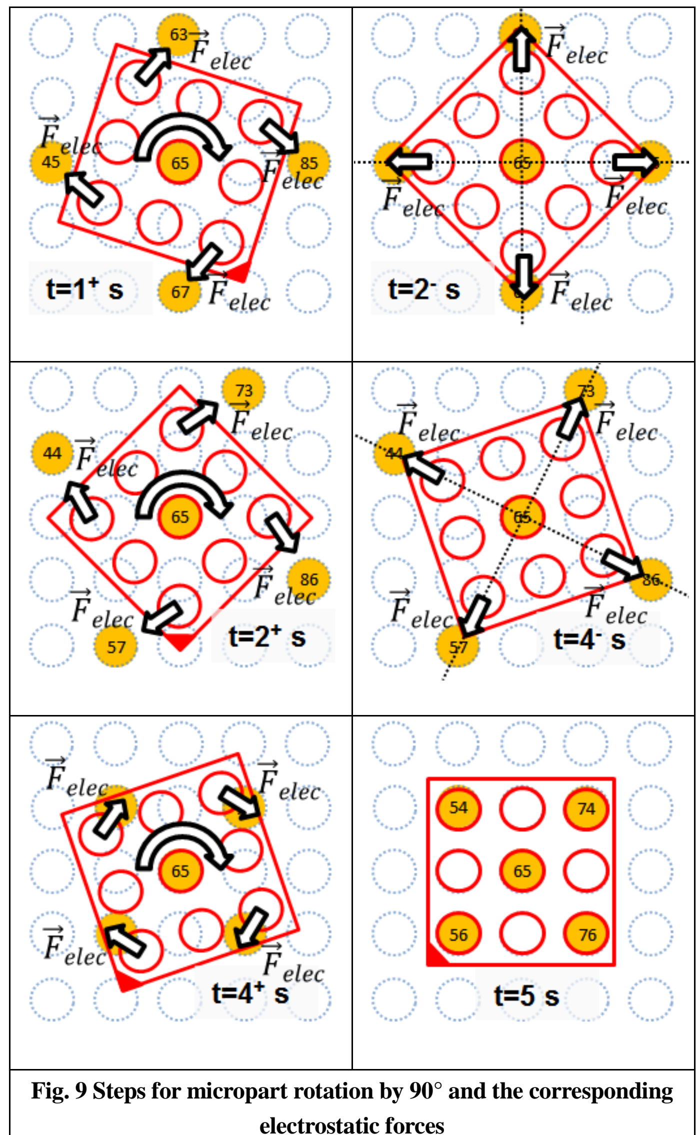

Fig. 9 Steps for micropart rotation by 90° and the corresponding electrostatic forces

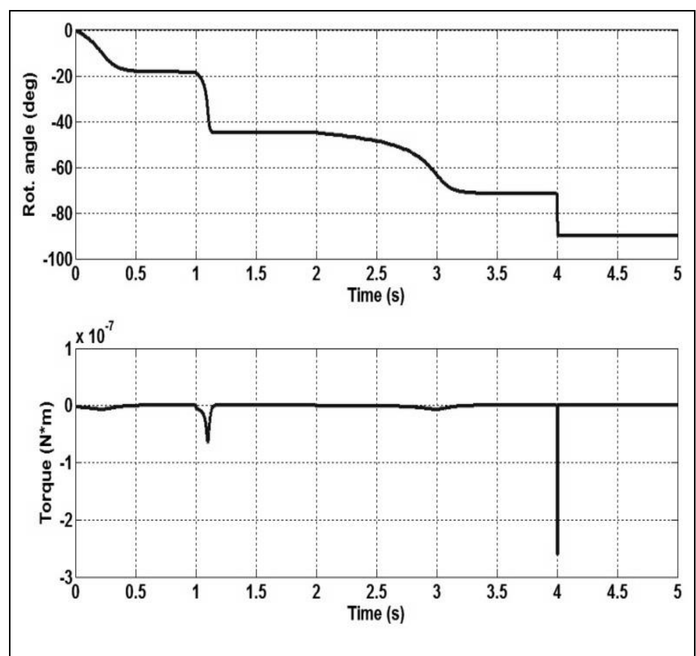

Fig. 10 Top: Rotation angle of the part over time
Bottom: Total electrostatic torque on the part over time

The third step lasts for two seconds, as the activated electrodes are "initially" relatively far from the part's nearby

electrodes and therefore it rotates with a slower rate (Fig 10). At the end of this step ($t=4^-$ s) the angle is set at -71.56°. At this pose, there is partial overlapping with the next set of electrodes that will be activated at the next time step ($t=4^+$ s). The electrostatic force and consequently the torque in this case are so strong (in combination with the high voltage) that they practically force an immediate alignment of the electrodes (t=5 s). This can be verified by the spike in the torque's magnitude and the abrupt change of the angle from -71.56° to -90° (Fig. 10). Obviously, the values of the angular velocity and torque are the maximum of all of the steps of the rotation: 2424 deg/s and 2.606×10^{-7} N*m respectively. For further rotation angles these activation signals can be repeated due to the symmetry of the electrodes.

4. Discussion

The results of the simulations previously presented show that 1D, 2D translation as well as part rotation are feasible with the programmable platform for micromanipulation. It must be reminded that all the simulations are performed without any optimization. In the cases of translation, due to the partial/full overlapping of the electrodes of part and substrate, the aligning electrostatic force is strong and thus the positional error of the part lies in the submicron scale.

For rotation, as mentioned earlier, the angle resolution achieved depends directly on the electrode array resolution and therefore completely arbitrary rotation angles are not feasible. A better electrode resolution would provide a better angle resolution and the possibility of finer and more precise translational motion, although the hardware complexity of the system would increase, so a compromise has to be made. Other combinations of electrode activation could possibly achieve smaller rotational angle steps without denser electrode resolution. In the stages where there is slight or partial overlapping of electrodes (2nd and 4th respectively of Table 1), the aligning torque is quite significant in measure and rapidly rotates and aligns the part with very good accuracy (two or three decimals of a degree). In the stages where there is no overlapping (1st and 3rd) the part rests at specific angles as soon as the electrostatic torque becomes zero and the viscous damping quickly retards the rotational motion. It must also be stated that in these stages (1st and 3rd) no significant rotation results were observed for applied voltages below 300V, hence the increased values of 400V.

Although the parts for industrial manipulation and assembly are usually of square or rectangular shape, in this platform a variety of part shapes can be used, as the manipulation procedure is affected by the electrodes of the substrate and the part (provided that the material the part is made of isn't highly conductive as well). Of course, different shapes have different dimensions and different part mass, affecting therefore its behavior during manipulation, but this can be rectified by properly adjusting the applied voltage.

For the simpler motions presented here, only the initial pose needs to be known in advance. Proper activation of substrate electrodes can drive the part towards the desired pose without the need for feedback during motion (similar to the 'dictated' motion of a roller-coaster moving on rails), assuming, however, sufficient voltage signals and timings. This signifies the necessity of a proper set of design constraints that take into account part mass, voltage and activation timings for proper, desired motion. For more complex operations, such as sorting, motion planning and parallel handling, feedback based on a vision or sensory system may be needed.

It should be emphasized that the focus of this work lies in the presentation of the concept of a micropart manipulation platform, with its function capabilities verified through simulations based on theoretical analysis with some approximations. The main actual application target for this platform is non-physical contact mass positioning and alignment of microparts on wafers (with subsequent wafer bonding for the production of the final microsystems). Additionally, integration for the fast feeding, sorting and positioning of microparts and microcomponents in an assembly line of a microfactory should also be considered, as it could contribute to faster assembly rates and increased production yield. However, for experimental and actual application purposes, further research is needed and all possible factors that may affect or complicate the electrostatic manipulation procedure should be taken into consideration (such as proper selection of materials for dielectic layer, lubricant, fabrication of uniform electrodes without imperfections).

5. Conclusions and Future Work

In this paper the concept of a programmable electrode platform for micromanipulation on a wafer using electrostatic forces is introduced. The parts are electrostatically manipulated, positioned and rotated on the substrate's plane by sequential activation of properly selected planar electrodes.

Simulations of micropart motion are performed in order to verify the feasibility of electrostatic manipulation and self-alignment, with the target being the investigation and assessment of the platform's basic manipulation capabilities. These first results are successful, proving that translation and rotation are possible with the proper electrode activation sequences, albeit not simultaneously. By establishing the platform's capability of driving three degrees of freedom micropart motion, the foundations for further investigation of more complex operations are set.

Future work will be targeted towards several goals. First of all, the electrostatic force formula introduced in [15] will be updated with the parameter of a dielectric layer (initially omitted for simplicity) for more accurate calculations, according to the presented concept. Additionally, optimization of the manipulation procedure based on factors such as minimum manipulation time and least energy consumption will be researched. Furthermore, the creation of design and operation constraints will be investigated, taking into account

part mass, voltage signals, timings and electrode dimensions that will potentially constitute the usage of vision feedback or sensory systems unnecessary for simple manipulation.

The ability of the proposed platform to handle more complex operations, such as sorting of parts, motion planning and parallel manipulation will also be examined, along with the search for sensorless manipulation sequences. The final desired objective is to properly mass align, sort, position and orient microparts of various materials (such as silicon, ceramics, polymers), shapes and dimensions on the detachable dielectric wafers, with minimum or no vision/sensor feedback. By subsequent bonding of such wafers with aligned parts, the packaging and heterogeneous integration of the final microdevices will be feasible.

ACKNOWLEDGEMENT

This work was carried out within the frame of the internal project "Microassembly Automation" of the University of Patras and the MNI-mst program from the German Federal Ministry of Education and Research–"Nanopad".

REFERENCES

1. Böhringer, K., Donald, B., MacDonald, N., "What programmable vector fields can (and cannot) do: force field algorithms for MEMS and vibratory plate parts feeders", IEEE ICRA, Vol. 1, pp. 822–829, 1996.
2. Luo, J. and Kavraki, L., "Part assembly using static and dynamic force fields", IEEE/RSJ (IROS), pp. 1468–1474.
3. Böhringer, K., Bhatt, V., Donald, B. and Goldberg, K., "Algorithms for sensorless manipulation using a vibrating surface", Algorithmica, pp. 389–429, 2000.
4. Kavraki, L., "Part orientation with programmable vector fields: two stable equilibria for most parts", IEEE ICRA, pp. 2446–52, 1997.
5. Böhringer, K., Donald, B., Kavraki, L. and Lamiraux, F., "Part orientation with one or two stable equilibria using programmable vector fields", IEEE Trans Robot Autom, Vol. 16, No. 2, pp. 157–170, 2000.
6. Lazarou, P. and Aspragathos, N., "An integrated mechatronic approach for the systematic design of force fields and programming of microactuator arrays for micropart manipulation", J. Mechatronics, Vol. 19, No. 3, pp. 287-303, 2009.
7. Delettre, A., Laurent, G. and Le Fort-Piat, N., "A new contactless conveyor system for handling clean and delicate products using induced air flows", IEEE/RSJ (IROS), pp. 2351–2356, 2010.
8. Zeggari, R., Yahiaoui, R., Malaperta, J. and Manceau, J., "Design and fabrication of a new two-dimensional pneumatic micro-conveyor", Sensors and Actuators A: Physical, Vol. 164, No. 1-2, pp. 125-130, 2010.
9. Iizuka, T. and Fujita, H., "Precise positioning of a micro conveyor based on superconducting magnetic levitation", Proc. Micromechatronics and Human Science, pp. 131-135, 1997.
10. Bohringer, K. et.al., "Parallel microassembly with electrostatic force fields", Proc. IEEE Int. Conf. on Robotics and Automation (ICRA), Vol.2, pp. 1204-1211, 1998.
11. Moesner, F. and Higuchi, T., "Traveling Electric Field Conveyor for Contactless Manipulation of Microparts", IEEE Industry Applications Society, Vol. 3, pp. 2004-2011, 1997.
12. Moesner, F. and Higuchi, T., "Electrostatic Devices for Particle Microhandling", IEEE Trans. Industry Applications, Vol. 35, No 3, pp. 530-536, 1999.
13. Dalin, J., Wilde, J., Zulfiqar, A., Lazarou, P., Synodinos, A. and Aspragathos, N., "Electrostatic Attraction and Surface-Tension-Driven Forces for accurate Self-Assembly of Microparts", J. of Microelectronics Engineering, Vol. 87, No. 2, pp. 159-162, 2010.
14. Dalin, J., Wilde, J., Lazarou, P. and Aspragathos, N., "Self-assembly of dies through electrostatic attraction: modelling of alignment forces and kinematics", J. of Micro-Nano Mechatronics, Vol. 6, No. 1-2, pp. 23-31, 2011.
15. Lazarou, P., Aspragathos, N. and Wilde, J., "Modelling, Simulation and Design Constraints of Electrostatic Self-Assembly of Microparts", CIRP J. of Manufacturing Science and Technology, Vol. 4, No. 4, pp. 401-407, 2011.
16. Dalin, J., Wilde, J., "Self-assembly of micro-structured parts using electrostatic forces and surface tension", Electronic Components and Technology Conference, pp 1517–1524, 2009.
17. Cho, Y. H. et al, "Slide film damping in laterally driven microstructures", Sensors and Actuators A: Physical, No. 40, pp 31–39, 1994.

Design Principles for a Tool Changing System for Flexible Micro Assembly in Desktop Factories

Christian Löchte[1, #] , Carsten Behring[1] , Arne Burisch[1] and Annika Raatz[1]
1 Institute of Machine Tools and Production Technology (IWF),
Technische Universität Braunschweig, Langer Kamp 19b, 38106 Braunschweig, Germany
Corresponding Author E-mail: c.loechte@tu-braunschweig.de, TEL: +49-531-391-7628, FAX: +49-531-391-5842
KEYWORDS: miniaturized tool changer, miniaturized robot, shape memory alloy (SMA), coupling system, micro assembly, desktop factory (DTF), design principles

This article describes the results of an extended design process of a coupling system for application in a miniaturized tool changer for a micro production scenario. After the introduction of a desktop factory production scenario with the "Parvus", a size adapted assembly robot, this article covers the following: the requirements for the design derived from this scenario, five concepts that were developed according to these requirements, implementation and test of these concepts and introduction of a new prototype, which is based on a shape memory alloy actuation. The scientific contribution of this article is the general discussion of design principles for miniaturized actuated coupling devices. This article discusses which principles are useful for a coupling device in a miniaturized environment of a desktop factory. The realization of a prototype based on one of these discussed design principles illustrates the applicability of the designs in a micro assembly scenario with a miniaturized handling system and tool changer.

1 Introduction

A desktop factory (DTF) is considered as a sophisticated, versatile and flexible production platform that is intended to implement an innovative energy efficient production of micro components. The potential offered by a DTF and the special requirements have encouraged many researchers to build suitable devices as parts of a DTF [15, 9, 16]. Up to now, the majority of these devices are rarely integrated into an overall automation platform with other devices. The "Parvus" designed at the IWF is such a device. It is a miniaturized handling system based on a hybrid parallel robot structure [3, 4]. Moreover, there are still many open issues to form a complete DTF. Many research projects concerning a flexible micro assembly showed that a further infrastructure to rebuild a whole production process in a DTF is still missing [13]. For example, to extend the skills of the "Parvus" or any other handling device within its work in a DTF it is desirable to change tools during the assembly sequence.

This triggered the development of the miniaturized tool changer "Cambio", which provides storage for up to six tools. "Cambio" was first introduced by Burisch et al. [2]. These tools can be mounted with a special designed coupling device to any robot hand axis. Practical experience with a first prototype of the "Cambio" have shown that a major challenge remains in the coupling device [2]. These challenges motivated the further development of this tool changer to come a step closer to a flexible DTF.

The following sections describe the results of the design process of a revised coupling device, which will operate in the tool changer "Cambio". The next section covers the main limitations of the first generation coupling device, as already presented in [2]. Chapter 3 gives a short overview of existing technologies for possible actuation of coupling devices. After this, chapter 4 introduces a DTF production scenario of the interaction of "Parvus" and "Cambio" , which allows to derive the requirements for the following design process. This chapter also describes five core concepts that were developed according to these requirements. The design process was followed by the implementation and test of these concepts. This leads to the set-up of a new prototype, which is based on a SMA (shape memory alloy) actuation, chapter 5.

2 First Generation Coupling System

The coupling device that was originally designed for the tool changer "Cambio" is based on a vacuum actuated ball coupling mechanism. Figure 2.1 shows a sectional view of the first design. Three metal spheres (A) can move through a bore hole in a guiding cylinder into a groove (C) in the robot axis. The re-

quired force that moves the spheres through the hole is provided by a bevel in the main coupling cylinder (D). This coupling cylinder forces the balls into the groove and thereby locks the axis into position. When not actuated, the cylinder is pressed onto the balls by a spring (E), which ensures a permanent locking. A partial vacuum applied through the opening (F) lifts the coupling cylinder against the spring force. The actuation takes place in the "Cambio" tool changer system. With applied vacuum the balls are released and drop out of the groove. This releases the axis that can now be withdrawn from the coupling system without applying further axial or radial force. A more detailed description of the working principle is presented in [2].

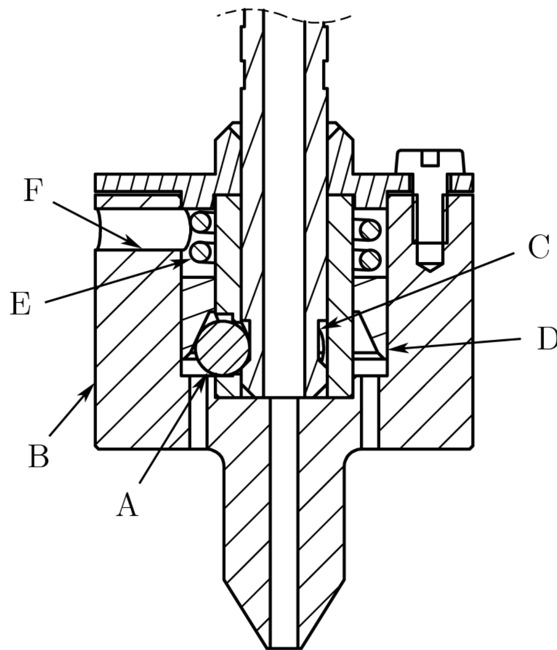

Figure 2.1: 1st Generation Coupling Device for the "Cambio" Tool Changer System

First tests with the described first generation prototype showed a severe lack in functionality and reliability. The vacuum required to move the cylinder cannot be established in a way that is suitable for an application in a size adapted system. The inner and outer air gaps cause a severe leak, which lets air stream into the cylinder chamber that compensates its evacuation. Thus, not enough force is generated to move the cylinder against the spring force. Using weaker springs results in insufficient reset force and an unstable locking effect. The inner friction of the coupling cylinder against the corpus exceeds the actuation capabilities of weaker springs. Another problem is caused by inaccurately manufactured parts. The ball bores and the bevel have to be extremely precise in shape, in order to achieve the required reliability of the system. Even slight tolerances can cause the balls to be tilted against the corpus or sit loosely inside the groove.

In short, the tests have shown that the current design of the coupling mechanism does not work. These negative aspects require a complete redesign, which is described in the following sections.

3 Overview - Coupling and Actuation

Most conventional tool changing systems for macro scale applications can be divided into two main groups: systems for only rotational tools and for more complex (non-rotating) tools. *Rotational tools* are used for a great variety of machining techniques, such as milling, turning, grinding and sawing. The tool is usually mounted on a cone-shaped socket. This unit is locked onto the main spindle, thus acting as an extension. The tool rotates at a set rate and is incapable of performing any other actions. *Non-rotating tools* for more complex tasks require platform tool changers with specific interfaces, e.g. industrial robots with manipulators for handling, spray guns, welding guns or measuring tools. The tool is mounted on a platform that provides the interfaces for all media that have to be transferred. The most common locking techniques are bayonet mounts or simple ball coupling mechanisms, similar to the one described in chapter 2. Both are highly efficient in large scale, but it is very difficult to realize any of them in a highly miniaturized design. The main aspect that does not allow a transition of these systems to a miniaturized scale is their actuation. Existing examples of a tool changer for micro assembly applications have been extensively discussed in [2]. The analysis showed that even the smallest commercially available systems (such as [8]) are inadequately dimensioned for a size adapted robot, such as "Parvus" or "APIS" [1, 4]. Thus, the overall goal is to develop a system that is highly optimized for the application in a size adapted environment, but still flexible within this application.

3.1 Actuation in Micro Applications

In the past, various materials and techniques have been identified to be particularly qualified for actuation of devices in the mini/micro-scale. Micro technological actuators usually depend on simple mechanisms. This covers electrostatic, magnetic and piezoelectric actuation. Further fluid based techniques include pneumatic and hydraulic actuation. Magneto- or electrorheological effects are also utilisable. Thermal actuation can be achieved by using bi-metal actuators or shape memory alloys (SMA) to provoke a material deformation through thermal variation. For example [6, 7] give an overview on materials and actuation mechanisms in a comprehensive field of microsystems.

3.2 Shape Memory Alloys and their Technological Effects

This section highlights the group of shape memory alloys that has great impact on the design process of the discussed coupling system. SMA summarize a number of materials with temperature-related shape changing properties. The most common material, a nickel-titanium alloy, has two stable states at room temperature. Its basic tension-free state is an austenite phase. When a certain stress is applied, it mechanically changes into a martensite structure, which is also stable at room temperature. By applying an electric current, the metal heats up and exceeds a critical transformation temperature. At this point, the martensite becomes unstable and the alloy reverts into its original austenite structure. After the current is switched-off and the material returns to room temperature, the process can be repeated. A SMA wire can be stretched by up to 8 % within this pseudo-elastic range [12]. Upon heating, this deformation is reversed and the wire contracts to its original length. The force generated by the heat induced phase change is greater than the force required to stretch the wire in its cool state. Hence, in

combination with a common coil spring, a simple two-way actuation mechanism can be realised. It is easy to control this mechanism via the electric current and generate much higher forces in comparison to magnetic or pneumatic mechanisms of the same size.

3.3 Proof of Concept - SMA in Small Grippers

An example of a successful implementation of this concept is a SMA actuated gripper developed at the IWF, see fig. 3.1 and [10, 11]. The parallel structure of the described gripper is equipped with two opposing SMA wires. Both wires can be heated individually by applying an electrical current. In case of actuation, the heated wire contracts and thus stretches the other wire. Heating the second wire reverses the mechanism into its original position. The wire movement is transferred onto the parallel gripper structure. This is an example for an extrinsic two-way actuation. Replacing the second wire by a spring would result in a self resetting mechanism. The experiences on such prototypes influenced the development of the coupling mechanism. Further examples of the capabilities of SMA actuated structures are summarized in the literature review by Sreekumar et al. [17, 5].

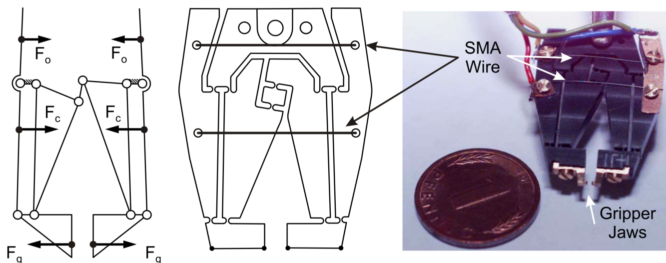

Figure 3.1: SMA actuated Gripper for Micro Assembly [10, 11]

4 Development and Design Process

This chapter describes the development process that was carried out to achieve the presented results. The requirements for an improved coupling device for the "Cambio" tool changer system are derived from a DTF scenario with a size adapted assembly robot.

4.1 DTF Scenario and Requirements

The considerations in the described design process are based on the following scenario: A size adapted assembly system, in this case the "Parvus" [4], is part of a DTF. To fulfill all its assigned tasks the tools (e.g. grippers) have to be exchangeable. The tool exchange is realized by the help of the size adapted tool changer "Cambio" [2]. It is placed within the workspace of the "Parvus". A tool coupling device is the interface between the two systems. Figure 4.1 illustrates this scenario. Since the design of the "Parvus" and the "Cambio" is fix, this scenario predetermines various parameters for the redesign of the used coupling system. These parameters are: the shape of the axis, maximum forces allowed, maximum dimensions. The shape and size of the tool holder are not yet predefined and will be adapted to the future design of the coupling device.

However, the new coupling device must not be limited to the specific application of this scenario. Moreover, there is the aim to design an universal tool changing system to work in any DTF. The most important aspect during the design process is the basic functionality and operation principle. This allows to reuse the presented design principles for any scenario.

To fulfill its purpose, the coupling system has to provide a stable and precise joint between the tool and the robot axis. This joint must persist without constant energy supply. It is desirable that the robot does not have to supply any sort of energy, besides the energy to control the tool (e.g. a partial vacuum, electric supply). The coupling has to withstand axial forces up to 1 N[1]. This maximum load may occur under usual circumstances considering the assembly of micro parts. In contrast to this, no radial force should be applied to the robot axis. This might damage the high precision drives of the robot structure. The coupling system must be able to establish a tool mounting in any position of the robot axis. After locking, the device has to withstand a minimal torque of 1 mNm to 3 mNm[2].

Besides these basic requirements, there are further aspects concerning the coupling device: a maximum weight of 3 g and a maximum size of up to 20x20x15 mm^3. The available energy sources that can be provided by the "Cambio" tool changer are limited to electricity and vacuum. Prior to the actual development process, these requirements are gathered in a product requirements document. All further design decisions are based on this compilation.

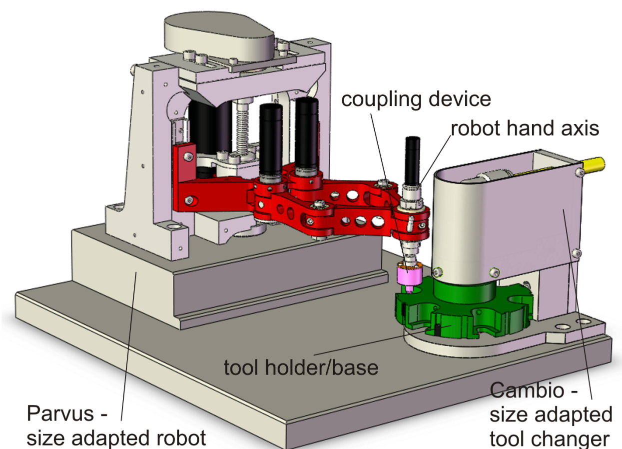

Figure 4.1: Scenario: "Parvus" interacting with "Cambio"

4.2 Concept Phase and Five Core Concepts

A morphological analysis led to several concepts meeting the above defined requirements. The five most promising concepts, in the following referred to as core concepts, are thoroughly investigated within the following section. These five core concepts are marked by their mechanical simplicity and innovative actuation principle. In the new coupling device the number of moving parts or active elements should be as low as possible. Each concept still incorporates a unique technological approach for the coupling task. All of them are discussed for the use in miniaturized machine design.

[1]The axis of the robot in the scenario does not withstand higher forces [4].
[2]3 mNm is the rated torque of the drive in the hand axis of the "Parvus" (MHD-8 IH 160:1, see [14]).

4.2.1 Direct Magnetic Coupling (DM-C)

Concept The tool is connected to the axis by a permanent magnet. To separate the tool from the robot, an electromagnet is activated in the tool changer base. Its magnetic field counteracts the permanent field, thus neutralizing the force holding the two parts together. The joint remains stable without any constant energy supply. Electric current controls the coupling process precisely.

Design The coupling device is separated into two parts, see fig. 4.2. The first part (A) contains the permanent magnets (B), e.g. neodymium magnets, and is fixed onto the robot axis. The second part (C) holds the tool and the electromagnets (D). The second part can be stored in the tool holder, from which it obtains the energy required for the un-coupling process. Axial pressure is not an issue, since the two parts bear on each other. Rotational and pull resistance is provided by the permanent magnets.

Concerns While the system is very simple and works without any moving parts, the coupling process must be controlled precisely. To avoid forces and displacement in an uncontrolled direction, the two opposing magnetic fields have to be specifically matched. Interferences may lead to uncontrolled movement and damage, especially at close proximity or in the transition phase from attraction to repulsion.

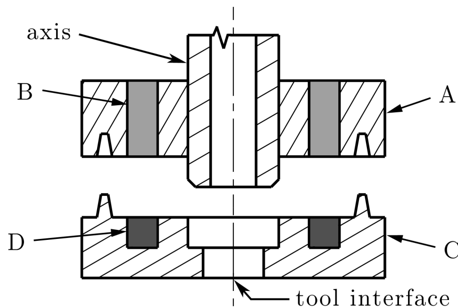

Figure 4.2: Direct Magnetic Coupling (DM-C)

4.2.2 Indirect Magnetic Coupling (IM-C)

Concept A magnetic field is used to actuate a mechanic joint, such as a positive locking. An electromagnet controls a spring-mounted lock. The spring holds the joint without energy supply. Furthermore, the configuration of the magnet is more simple than for the direct magnetic coupling due to the lack of a permanent counterpart.

Design Figure 4.3 shows the design of Indirect Magnetic Coupling. A steel wedge (A) on a steel sheet spring (B) generates a positive locking with a groove in the robot axis (C). The axis can be released by activating an electromagnet (D). This magnet attracts the wedge on the spring, thus pulling it out of the groove. Deactivating the magnet causes the sheet spring to push the wedge back into the groove, reestablishing the joint.

Concerns The magnet has to build up a strong field to attract the wedge in its initial position. This could require a magnet larger than feasible for this scale. The locking force of the spring might not be sufficient.

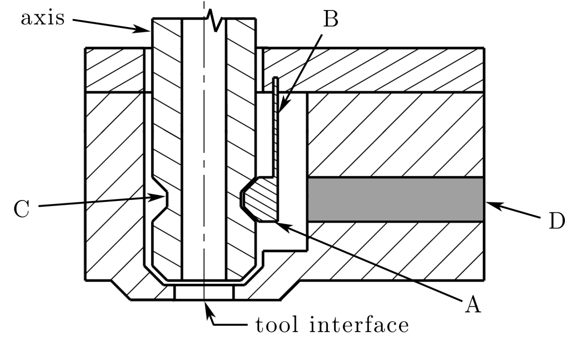

Figure 4.3: Indirect Magnetic Coupling (IM-C)

4.2.3 Vacuum Actuated Coupling (VA-C)

Concept A piston with a wedge or cone on top is retracted against a spring by a partial vacuum. In its non-activated state, the spring pushes the piston into a groove in the robot axis, establishing a positive locking. With applied vacuum, the retracted piston releases the axis.

Design The corpus (D) holds the tool and the coupling mechanism, see fig. 4.4. The working principle is related to the first generation design, chapter 2. To avoid the problems known from this mechanism, the moving parts are reduced to the piston (A) and the spring (B). The leaking problem is reduced by a better surface-to-gap ratio of the piston. The robot axis provides a groove (C) for the positive locking with the piston.

Concerns Despite the optimization, it remains unclear whether the precision achieved with conventional machining techniques is sufficient for a noncritical degree of leaking. The established retraction force by the vacuum might not be sufficient to overcome the spring force.

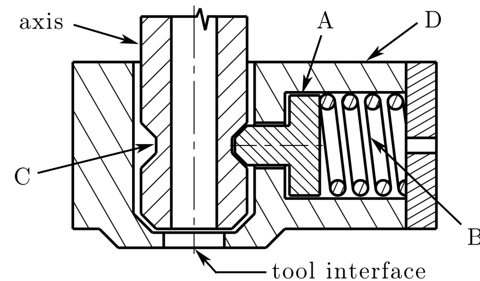

Figure 4.4: Vacuum Actuated Coupling (VA-C)

4.2.4 Coupling with Hotmelt Adhesives (HM-C)

Concept A hotmelt adhesive is stored in a heatable compartment in the coupling device. To insert or retract the axis, the adhesive is liquefied. After a cool down, a stable bond between the coupling system and the axis is established. The coupling device does not need a further energy supply.

Design In fig. 4.5 the corpus of the coupling device (A) contains an electric ring heater (B) around a hotmelt reservoir (C). The axis is coated to prevent the formation of adhesive residues. To ensure a stable connection, the axis is grooved to create undercuts (D).

Concerns If adhesives remain on the axis, despite a non-stick coating, the axis has to be heatable to remove these remains. Otherwise, the hotmelt on the axis would obstruct the precise mounting hole. The needed heat might harm the robot end effector. The coupling process might be too slow.

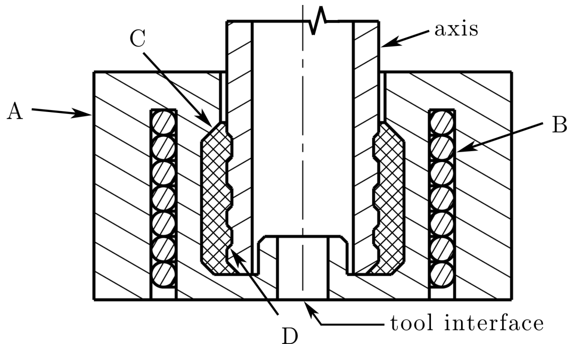

Figure 4.5: Coupling with Hotmelt Adhesives (HM-C)

4.2.5 SMA Actuated Coupling (SMA-C)

Concept A SMA wire is strained between a piston and the corpus of the coupling device. A spring alongside the wire stretches the alloy. In the stretched state, a cone on the piston is pushed into a groove in the axis and establishes a positive locking. This is similar to the idea of the concept in section 4.2.3. To release the axis, the wire is heated. This pulls the piston back against the spring force and removes the piston out of the groove. Cooling down the wire enables the spring to stretch the alloy into its original shape, see also section 3.2. Other examples already showed the high potential of SMA actuation in micro devices, see section 3.3.

Design The SMA wire (A) is heated electrically by applying a current, see fig. 4.6. The corpus is separated into two parts. The first part (B) contains the bore for the robot axis with a groove (C) and the guidance for the locking piston (D). The second part (E) insulates the wire from the corpus to allow the electric current to flow through the whole wire without creating a short-circuit.

Concerns The wire cannot be insulated by conventional means, so it may not touch the spring or the corpus. Moreover, the travel is limited. The mechanism therefore requires a certain wire length to operate reliably. This might result in a design which exceeds in size the maximum geometrical dimensions given by the scenario.

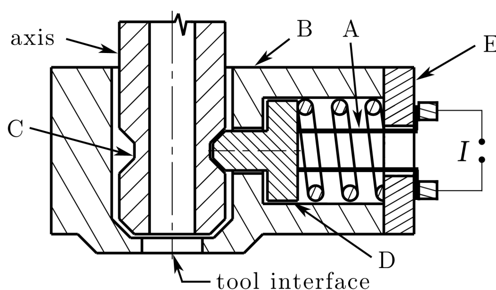

Figure 4.6: Coupling with SMA Actuators (SMA-C)

4.2.6 Summary of the Concept Phase

After the detailed discussion of five possible concepts for the assigned coupling task this section compares and evaluates these core concepts. Table 4.1 gives an overview of this comparison, using the following criteria: **1. moving parts** (m.parts): criterion for the amount of moving parts in the coupling mechanism - small amount of moving parts is positive for the overall performance of the concept, **2. functional density** (funct.): generally, a high density of function is appreciated, **3. scalability** (scal.): an indicator for the miniaturization of each concept, **4. reliability** (relia.): a high reliability (concerning e.g. the coupling force) during the use of the coupled tool is desired, **5. complexity** (compl.): criterion for the complexity of the bulid-up of the mechanism - here a low complexity is positive for an easy build-up, and **6. tolerance sensitivity** (toler.): indicates, how resistant the mechanism is concerning e.g. manufacturing tolerances.

The table shows the evaluation of each criteria in the following way: [+] marks a positive, [○] shows a neutral and [-] indicates a negative effect on the overall performance of the discussed concepts. Based on this table the following section describes the further testing of these concepts and leads finally to a prototype.

Table 4.1: Overview and Comparison of five Core Concepts

Concept	m. parts	funct.	scal.	relia.	compl.	toler.
DM-C	+	+	+	○	+	+
IM-C	○	-	-	-	-	○
VA-C	-	○	○	-	○	○
HM-C	+	○	○	-	○	+
SMA-C	-	○	○	+	-	+

4.3 Experimental Examination of the Core Concepts

After the concept phase, the developed mechanisms were tested with regard to their functionality. This requires the construction of an individual test rig for each concept. These rigs are scaled concerning the dimensions given by the scenario. This ensures testing in circumstances of the later use. Features relevant to the coupling mechanism are included. The energy interfaces are provisional and laid out for easy modification during the test phase. With these rigs, the functionality of each concept was tested and evaluated.

The concepts **IM-C**, section 4.2.2, and **HM-C**, section 4.2.4, failed the first functionality test. The magnetically actuated positive lock coupling is not operable, since the magnetic forces are not sufficient to withdraw the spring. The required magnets exceed the maximum dimensions. At the same time, the mechanism is too weak to properly lock the axis. This solution is not convenient for a size adapted application. Thus, the concept was dropped. The hotmelt adhesive coupling requires a heated robot axis to melt adhesive residues on the axis. Apart from this limitation, the concept itself still seems promising. Since an independent axis heating system is not an option in the scenario with the “Parvus” robot system, this concept was dropped as well.

The concept **VA-C**, section 4.2.3, still suffers from leaking problems during testing. These problems were reduced in

comparison to the first generation prototype, but still prevent the system from operating flawlessly. The main load and force requirements were fulfilled, but the coupling device lacked overall reliability (see table 4.2). In order to exploit the full potential of a size adapted fluid actuation, a different approach for the coupling mechanism would be required.

The tests with the concept **DM-C**, section 4.2.1, showed that the system is capable of meeting *all* requirements, as stated in section 4.1. It is reliable and sufficiently powerful (see table 4.2). However, the precise dimensioning of the magnetic system is crucial. The electromagnet and the neodymium magnet have to match precisely to achieve viable results for practical use. Micro-technological processes like magnetic or conductive coatings can help to optimize the mechanism. Moreover, a flux simulation would help to determine the most efficient magnet shape and arrangement. These analyses and developments exceeded the scope of this first examination. In summary this is a valid and promising solution, but it requires extensive optimization in future work.

The test of the concept **SMA-C**, section 4.2.5, showed the *best* overall results. It is very reliable and exceeds the load requirements by far, table 4.2. It can be employed in a wide range of applications with different load specifications. The only major drawback is its size. It meets the requirements of the scenario, but it cannot be scaled down at will. The SMA wire has a limited travel. To provide a reliable joint, a certain travel is required, thus dictating a minimum wire length.

Table 4.2: Test Results for the Best Performing Coupling Concepts

Concept	Force [N, avg]	Torque [mNm, avg]	Prototype
VA-C	**4.1**	**0.24**	**no**
DM-C	**0.7**	**1.1**	**no**
SMA-C	≥ 40	**1.4**	**yes**

Due to the results of the test phase, the SMA-C concept seem to be the most promising solution for the considered scenario. This concept shows superior results and an innovative, yet simple layout. A description of the developed prototype based on this concept is presented in the next section.

5 The Prototype

The final prototype is the consequent development of the SMA actuated coupling system, section 4.2.5. Figure 5.1 shows a sectional view of the realized prototype. Figure 5.2 compares the fully working prototype with a common match. The coupling system is composed of a main corpus (A), a wire holder (B), two contact pins (C), a piston (D), a spring coil (E) and the SMA wire (F).

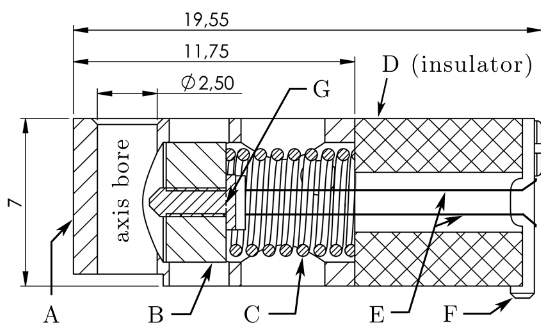

Figure 5.1: Sectional View of the Prototype, Dimensions in [mm]

The wire holder, electrical interface and insulation have been combined in one part. This provides a better space utilization and reduces the number of joints. The piston runs inside a bore in the corpus. The mid-point (G) of the wire is connected to the piston, while each end is screwed onto the backside of the wire holder. Two SMA wire halves running alongside each other duplicate the maximal force over a single strained wire from the holder to the piston. The spring rests on the wire holder, which is screwed onto the corpus.

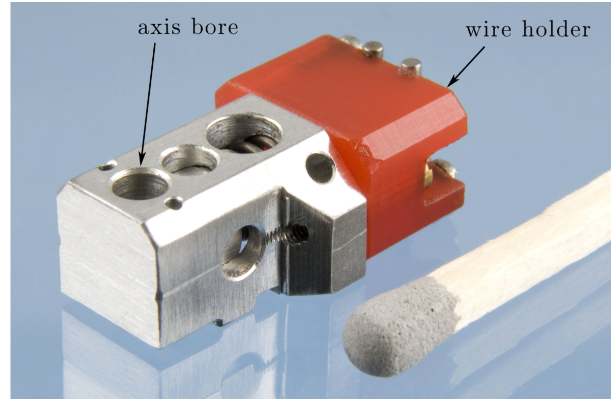

Figure 5.2: Prototype of a SMA Actuated Coupling Device

Due to the depth of the groove a travel of 0.15 mm is needed to release the robot axis. An effective wire length of 12.9 mm provides the needed travel. Improvement of the travel could be achieve by a pulley related design; but it is difficult to realize at miniaturized scale. Moreover, this would severely increase the complexity of the design, which should be avoided. Thus, the structure can be reduced in size without modifying the functional mechanism.

On the backside of the wire holder, the two contact pins are inlaid into corresponding grooves. The wire is then strained over those pins. They prevent the hot wire from touching the heat-sensitive insulation material and act as a simple electric interface, see fig. 5.3. The wire between the screw points and the contact pins remains passive, since no current flows through that section.

Apart from the SMA wire and the heat resistant parts that are in direct contact with the wire, the choice of material is not restricted by further requirements. The shown prototype is made from aluminium (corpus and piston), polyoxymethylen (wire holder) and steel (contact pins and screws).

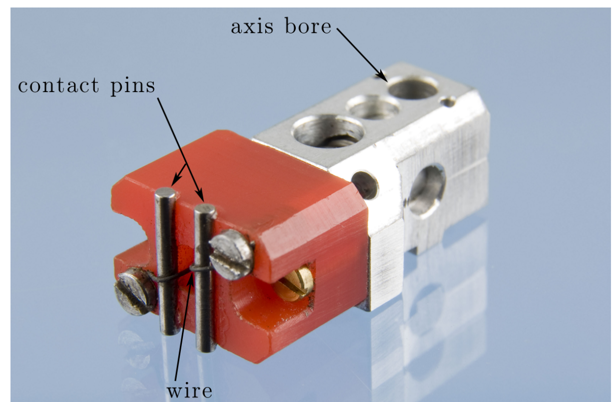

Figure 5.3: Electric Interface of the Prototype

The corpus of the coupling device is designed for various alignment and fixation methods within any tool holder. The “Cambio” tool changer base has yet to be redesigned according to the changed coupling device. Only the electric interface of the coupling device implies certain requirements for the integration of the coupling device into the base of the “Cambio” system or any other tool holder.

6 Conclusion and Outlook

The present article shows the need for devices that are capable of connecting size adapted production units within a DTF. A design process was carried out to find design principles that allow a tool coupling during micro assembly. A micro production scenario motivated the design process. During the design phase it was ensured that the possibility of reusing these design principles is given. Based on these principles five test rigs were build up. After the discussion of the test results this article describes a prototype derived from the findings.

In future work, tests on the actual prototype will be carried out. To work perfectly within a DTF the prototype of the coupling device will be integrated into an existing tool changing system. Further tests with a size adapted assembly system will show the potential of this tool changing system in a DTF.

REFERENCES

[1] Borchert, G., Burisch, A., Raatz, A.: Apis - a miniaturized robot for precision assembly with low-cost piezoelectric motors. International Journal of Precision Engineering and Manufacturing 12(4), 629–634 (August 2011), ISSN 1229-8557

[2] Burisch, A., Löchte, C., Raatz, A., Fabrizi, A.: Cambio - a miniaturized tool changer for desktop factory application. In: 2nd European Conference on Mechanism Science (EUCOMES 08). pp. 541–548. Springer, Cassino, Italien (2008), ISBN 978-1-4020-8914-5

[3] Burisch, A., Raatz, A.: Challenges of miniaturized robots and machine elements for desktop factory applications. In: 7th International Workshop on Microfactories (IWMF2010). pp. 100–105. Daejeon, South-Korea (2010)

[4] Burisch, A., Wrege, J., Raatz, A., Hesselbach, J.: Parvus - miniaturised robot for improved flexibility in micro production. Journal of Assembly Automation 27(1), 65–73 (2007), ISSN 0144-5154

[5] Carbone, G., Conghui, L., Hao, G., Ceccarelli, M., Burisch, A., Raatz, A.: Design and simulation of a binary actuated parallel micro-manipulator. In: 13th World Congress in Mechanism and Machine Science (IFToMM 2011). Guanajuato, Mexiko (2011)

[6] Gianchandani, Y.B., Tabata, O. (eds.): Comprehensive Microsystems - Vol. 1: Materials, Fabrication and Packaging, Electronics and Systems Design. Elsevier (2008), ISBN: 978-0-444-52191-0

[7] Gianchandani, Y.B., Tabata, O. (eds.): Comprehensive Microsystems - Vol. 2: Actuation Mechanism, Physical sensing, Chemical and Biological systems. Elsevier (2008), ISBN: 978-0-444-52192-7

[8] Haag, M., Härer, S., Hoch, A., Simons, F.: Standardised interface and construction kit for microassembly. In: Proceedings of Fourth International Precision Assembly Seminar (IPAS'2008). pp. 353–358. Chamonix, France (February 2008), ISBN 978-0-387-77402-2

[9] Heikkilä, R., Karjalainen, I., Uusitalo, J., Vuola, A., Tuokko, R.: Possibilities of a microfactory in the assembly of small parts and products - first results of the m4-project. In: Proceedings of International Symposium on Assembly and Manufacturing. pp. 166–171. Ann Arbor, Michigan, USA (2007), ISBN: 1-4244-0562-9

[10] Hesselbach, J., Pittschellis, R., Mertmann, M., Hornbogen, E.: Shape memory alloys for use in miniature grippers. In: Proceedings of Shape Memory and Superelastic Technologies. Pacific Grove, CA, USA (1997)

[11] Hesselbach, J., Thoben, R., Pittschellis, R.: Robots and gripper for microassembly. In: Proceedings of the 4th International Conference on Ultraprecision in Manufacturing Engineering. pp. 375–378. Braunschweig (1997)

[12] Janocha, H.: Adaptronics and Smart Structures. Springer-Verlag, New York (2007), `http://www.worldcat.org/oclc/318290592`, ISBN: 978-3540719656

[13] Jarvenpaa, E., Heikkilä, R., Tuokko, R.: Logistic and control aspects for flexible and reactive micro and desktop assembly at the factory level. In: Proceedings of International Symposium on Assembly and Manufacturing. pp. 171–176. Suwon,South-Korea (2009), ISBN: 978-1-4244-4627-8

[14] Micromotion GmbH: Think Smaller (2009), catalogue

[15] Okazaki, Y., Mishima, N., Ashida, K.: Microfactory - concept, history, and developments. Journal of Manufacturing Science and Engineering 126(4), 837–844 (2004), doi:10.1115/1.1823491

[16] Sitala, N., Heikkilä, R., Vuola, A., Tuokko, R.: Architectures and interfaces for a micro factory concept. In: 5th International Precision Assembly Seminar (IPAS 2010). pp. 293–300. Chamonix, France (2010), ISSN 1868-4238

[17] Sreekumar, M., Nagarajan, T., Singaperumal, M., Zoppi, M., Molfino, R.: Critical review of current trends in shape memory alloy actuators for intelligent robots. Industrial Robot: An International Journal 34(4), 285 – 294 (2007), ISSN: 0143-991X

Micro Machining Performance of Dual Piezoelectric-based Fast Tool Servo for Diamond Turning

Hong Lu[1], , S. M. Lee[1], M. R. Kim[1], S. J. Lee[3], S. C. Choi[2] , C. H. Park[2], and D. W. Lee[4,#]

1 Department of Nano Fusion Technology, Pusan National University, Miryang, South Korea
2 Korea Institute of Machinery & Materials, Daejeon, South Korea
3 Interdisciplinary Program in Innovative Manufacturing Engineering, Pusan, South Korea
4 Department of Nano Mechatronics Engineering, Pusan National University, Miryang, South Korea
Corresponding Author / E-mail: dwlee@pusan.ac.kr, TEL: +82-55-350-5281, FAX: +82-55-351-2982

KEYWORDS : Fast tool servo, Piezoelectric actuator, Frequency, Tracking precision, Precision machining

Piezoelectric materials are usually used in the form of a stack configuration acting as an actuator of a fast tool servo (FTS), for reducing undesired vibrations in manufacturing machinery, and in ultrasonic-assisted machining. This paper describes the design and evaluation of dual piezoelectric actuator-based FTS for sinusoidal microstructure fabrication. In machining processes, the FTS should be long travel, high frequency and high precision. In order to meet these requirements, a new lever-type flexure mechanism is designed to amplify the output displacement of piezoelectric actuator. Dual piezoelectric structures ensure that the flexure mechanism can transform the action of actuator effectively. According to compare the dynamic performance between single and dual piezoelectric actuator, dual actuator FTS shows better tracking precision and longer travel range than single actuator FTS, especially at the high frequency level. Furthermore, machining test results of the sinusoidal microstructure have also indicated the effectiveness of the designed FTS system.

NOMENCLATURE

K = leafspring constant
M = total mass of moving part
C = structural damping constant
(x) = tool distance
(u) = amplifier input
K_d = gain of digital to analog converter
s = sliding surface
G_a = amplifier gain
F_d = cutting force disturbance to actuator
K_{eff} = effective spring constant
M_{eff} = effective mass value
C_{eff} = effective damping constant

1. Introduction

Fast tool servo (FTS) was used widely in micro-machining applications as a fairly mature technology with some commercial realization. The machining process of FTS, described in this paper, is shown in Fig. 1. A copper alloy specimen is camped on the spindle. FTS is fixed on the feed guide of the machine which provides the feed rate at x-axis direction. Meanwhile, cutting tool is driven by the FTS cut into and out of the workpiece several times per revolution along y-axis direction.

There are two main applications of the FTS on a diamond turning machine. The one is to eliminate the repetitive errors of machine [1-2], the other is to produce complex geometries into a specimen [3-7]. In 1985, Patterson [5] designed first FTS system for diamond turning. Then, many other researchers developed various FTSs with different actuators and materials. Okazaki [8] reported on the “micro-positioning tool post” design for compensating the error motions of diamond turning machines and improving workpiece surface finish with high resolution. A 10 mm diameter by 6 mm long piezoelectric actuator was used and it produced a 9 mm free displacement under a maximum applied voltage of 400 V. When the piezoelectric actuator is inserted the FTS, the displacement of the FTS was reduced to 7 μm because of the

stiffness of the flexure., Two closed-loop control systems, including pole-zero cancellation with a notch filter and a proportional integral-derivative (PID) feedback control with a state observer, were applied to the tool post to eliminate the hysteresis in the piezoelectric actuator. The depth-of-cut resolution was reported to be smaller than 25 nm. The frequency bandwidth for this system was 200 Hz, which was limited by the resonance of the tool post. Crudele and Kurfess [9] published the design of integrating a piezo-based FTS servo with repetitive control for facing applications. The benefit of the repetitive controller was the tracking ability of surface waviness. A piezo-actuator with a nominal expansion of 60 μm was used, and a great reduction in waviness, up to 62 % was observed, while traditional polynomial control was somewhat detrimental to the waviness. The other application of the FTS on a diamond turning machine is to eliminate the repetitive errors that came from the resonances in the turning machine structure, spindle imbalance, bearing noise et al. For instance, Kim and Kim [10] developed a FTS to control depth of cut precisely and compensate the waviness of the machining surface. The results revealed that the peak-to-valley of the surface waviness profile has been decreased to 0.3 μm (from 3.3 μm) in one particular case.

However, for the FTS-based machining process with high driving frequency, some flexure mechanism could not follow the extension and contraction of the piezoelectric actuator very well due to the low stiffness of mechanism, deficient structure, material properties, etc. Finally, it leads to the tool displacement reduction at the high frequency level (> 800 Hz, <5 μm). In order to solve this problem, we designed a lever type flexure mechanism to amplify the output displacement of piezoelectric actuator. The dynamic performances experiments confirmed that the dual piezoelectric actuator FTS (DFTS) shows better tracking precision and longer travel range than single actuator FTS (SFTS), and can provide more travel range to the diamond tool. Furthermore, the machining test results point out that the profile of microstructure is a sinusoidal wave in the cutting direction with spatial wavelength of 100 μm and the peak-to-valley amplitude of about 5 μm. Actual fabrication results of the sinusoidal microstructure have indicated the effectiveness of the designed FTS system.

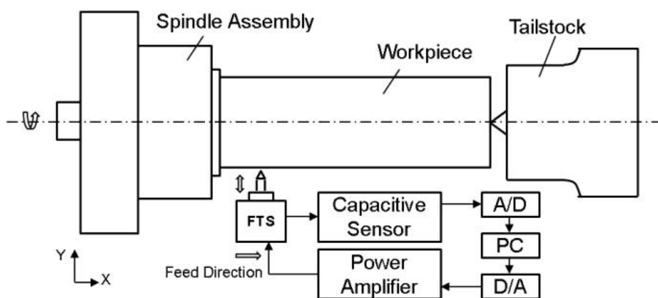

Fig. 1 Machining process of FTS

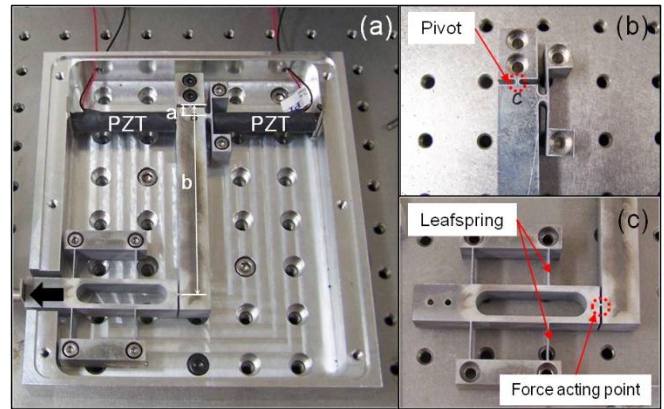

Fig. 2 Photograph of FTS (a) general view of flexure mechanism, (b) pivot of lever, (c) output part of lever

2. Flexure mechanism of fast tool servo system

2.1 Flexure mechanism

The details of the FTS mechanical flexure specially designed for machining micro structured surface in the diamond turning machine are shown in Fig. 2 (a). Dual piezoelectric actuators are of the stacked type, 70 mm in length and 10 mm in outer diameter. A diamond tool is fixed at the tool holder, which is connected with the mechanical main body through two sets of parallel leafspring, as shown in Fig. 2 (c). The symmetry structure in the design can inherently balance the flexure mechanism and avoid coupled interference motion.

The output motion can be amplified by the lever while the piezoelectric actuators oscillate at several kHz following the driving signals provided through a high voltage amplifier. For a lever with an arbitrary angle α (0≤α≤180˚) between its two arms where α is used to identify the configuration of a lever. Many classes of lever have a collective characteristic; the input effort is higher than the output load. Therefore, the distance moved by the resistance (load) is greater than the distance moved by the effort.

The lever whose arbitrary angle α is equal to 0˚ is used for this FTS flexure mechanism. In this class lever, effort is applied between the output loads on one end and the pivot on the opposite end. Hence the directions of the input effort and the output load are parallel to each other. The displacement at tool tip was magnified at the ratio of arm lengths "a" and "b" (1:10), because the mechanical lever is rotated through the pivot (shown in Fig. 2 (b)) while the right piezoelectric actuator is expanded, the left piezoelectric actuator that was applied a reverse signal is contracted, and the force acting point can be moved leftward.

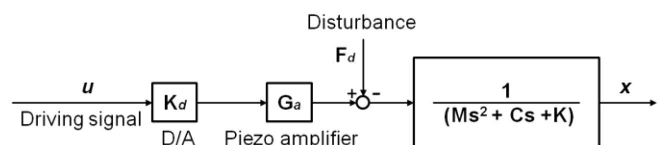

Fig. 3 Simplified model of flexure mechanism dynamics

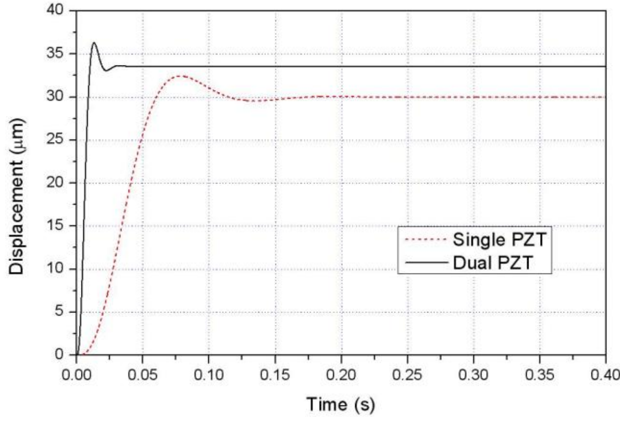

Fig. 4 Step response of open-loop control

Since the mechanical flexure acts as a spring, it can be modeled by a single degree of freedom system. The mass (M) is upper carriage which holds the tool, and structural damping constant is C. The spring constant, (K), is dominated by the set of leafspring. The structural dynamic parameters are identified from frequency response tests applied to the structure. Therefore, the tool holder and the actuator together are modeled as a second order dynamics as shown in Fig. 3. Open-loop transfer function between tool position (x) and amplifier input (u) in Laplace domain [11] is:

$$x(s) = \frac{K_d G_a}{Ms^2+Cs+K}\left[u(s) - \frac{1}{K_d G_a}F_d(s)\right] \quad (1)$$

Where K_d is the gain of digital to analog converter, Ga is the amplifier gain, and F_d is the cutting force disturbance to actuator. Expressing Eq. (1) as differential equation and rearranging

$$\frac{M}{K_d G_a}\ddot{x}(t) + \frac{C}{K_d G_a}\dot{x}(t) + \frac{K}{K_d G_a}x(t) = u(t) - \frac{1}{K_d G_a}F(t) \quad (2)$$

or

$$M_{eff}\ddot{x}(t) + C_{eff}\dot{x}(t) + K_{eff}x(t) = u(t) - d(t) \quad (3)$$

In order to reduce the mass of the moving part, the light diamond tool was used and the mass of tool holder was controlled at a lowest level, as shown in Fig. 2(c). Unnecessary mass was taken off from the output part.

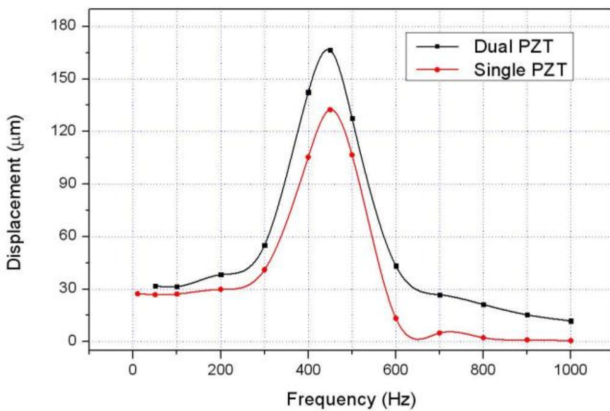

Fig. 5 Frequency response function of FTS

2.1.1 *Characteristics of the open loop system*

A series of tests are carried out to evaluate the performance of the FTS, a test system was built using a LabVIEW computer, a high voltage amplifier, a capacitive sensor, a high-speed data acquisition board and a function generator.

Capacitance displacement sensor is used for position measurement. Typically, the displacement signal ranges from -250 μm to +250 μm with a resolution of about 2.9 nm. Also, the bandwidth of the capacitive displacement sensor is set at 5 kHz, considering the maximum frequency required for fast tracking performance of the FTS. And the high voltage amplifier provides the complete voltage range from +3 to +1100 V with an average output power amounting to 110 W. It is capable of supplying a maximum peak output current of 500 mA for fast expansion of the piezoelectric actuator that behaves like a capacitive load.

The data acquisition board with their speeds set to 20 kHz for one cycle control of execution in the computer was used to obtain the signal from the capacitive displacement sensor and then transferred it to the LabVIEW computer. To reduce the external disturbance such as vibration, the experiments are carried out on a passive micro-vibration table. The environmental noise after the passive micro-vibration system is approximately 3 nm.

For the micro machining operation, the overshot of the flexure mechanism for dynamic positioning is undesirable, and will difficult to keep microstructure uniform. Therefore, the step responses of the flexure mechanism, actuated by single and dual actuator, were examined and compared carefully to guarantee the dynamic performance for micro machining. Fig. 2 (a) shows the piezoelectric actuators distribution of DFTS distinctly. When the SFTS operated, the left actuator will be dismantled. Fig. 4 shows the step responses of open-loop controlled DFTS and SFTS for a 50 V reference input, respectively. It is noted that the DFTS has a smaller overshoot and settling time than the SFTS. The DFTS takes very short periods of time (only about 0.03 s) to recover the final steady state value.

According to dynamic performance test, the frequency response function of the DFTS and SFTS are obtained respectively, as shown in Fig. 5. From the experiment data, it is noted that their primary natural frequencies are same due to the same flexure mechanism. The DFTS can provide larger travel range than the SFTS did. The displacement can reach 15.33 μm with an applied frequency of 900 Hz, which can satisfy the requirement of machining test well.

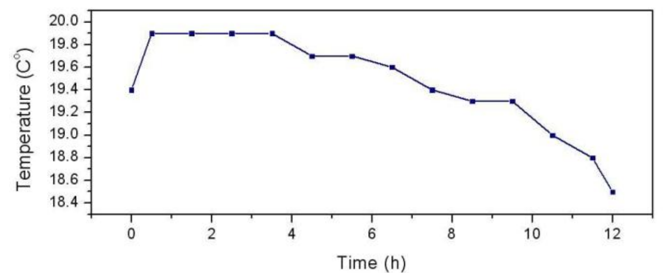

Fig. 6 Temperature variation of the FTS on operation (unloaded)

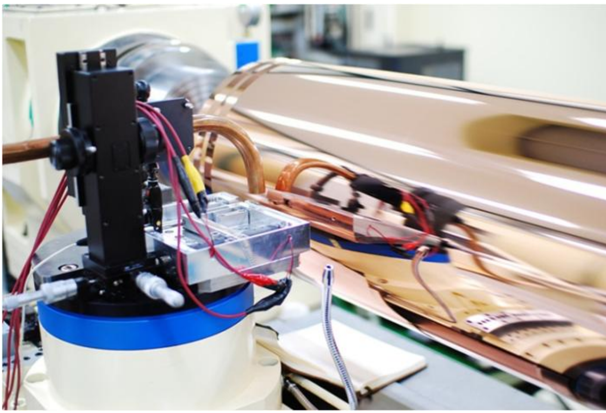

Fig. 7 Machining tests setup of FTS

Fig. 8 UV curing film of micro structures with different spindle speed

Thus the FTS is designed for the large area machining; it should be able to operate in a long time without interruption. The temperature rise of flexure mechanism will lead to alter the deformation value of the tool holder. It is unwanted for the precision machining. Therefore, the temperature variation of the flexure mechanism on operation is measured by a thermocouple during 12 hours, as shown in Fig. 6.

From the graph, it is found that the temperature of the flexure mechanism has not great change during operation. The maximum difference approximately reaches 1.4 °C. It is because the material is influenced by the background temperature. The results show that this flexure mechanism can provide precision output motion for the machining and small thermal expansion during actuation.

3. Machining test

Fig. 7 shows the photograph of the turning machine used for the fabrication of the microstructure machining test in this investigation. The workpiece is a brass roller with length of 2 meter and diameter of 200 mm. The machine is composed of three main parts: the aerostatic spindle and tailstock to rotate the roller, an X-axis linear servo to laterally move the diamond tool along the roller for providing the feed rate, and a Y-axis linear servo to translate the diamond tool for generating depth profile. The function generator produces the desired diamond tool motion trajectory that is sent to the amplifier as the reference input of the FTS. The quality of machined microstructures was evaluated by an optical microscopy and an AFM.

A UV casting technique was performed to replicate the profile of the microstructure on a plane. The UV casting provided a high degree of accuracy and could be achieved at the room temperature and low pressures [12]. A UV resin was poured in the liquid state between the workpiece and the plastic film. The profile of the microstructure was molded on the plastic film when the UV resin curing after the UV light irradiating, as shown in Fig. 8. This measured method was utilized widely in the large area machining. There are two groups of machining area in Fig. 8. The left three area have the same machining conditions with the right three area except the feed rate of 20 μm and 100 μm respectively.

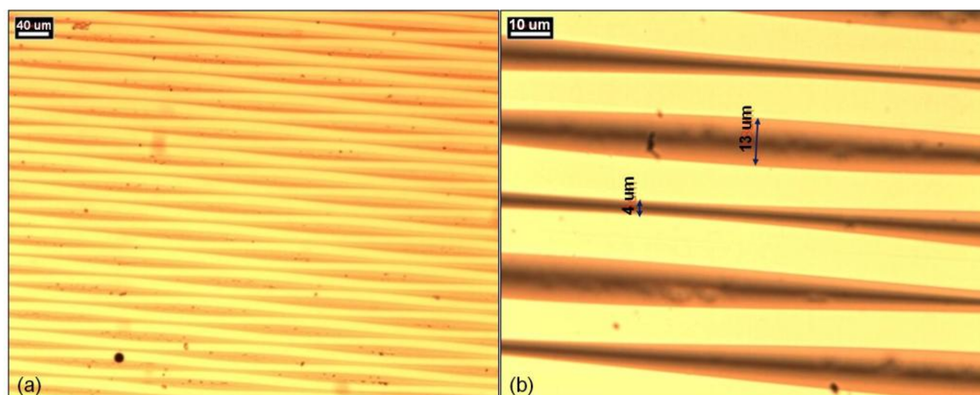

Fig. 9 Optical microscopy photographs of micro structure with spindle speed of 10 rpm, FTS driving frequency of 800 Hz (a) 100x magnification, (b) 500x magnification

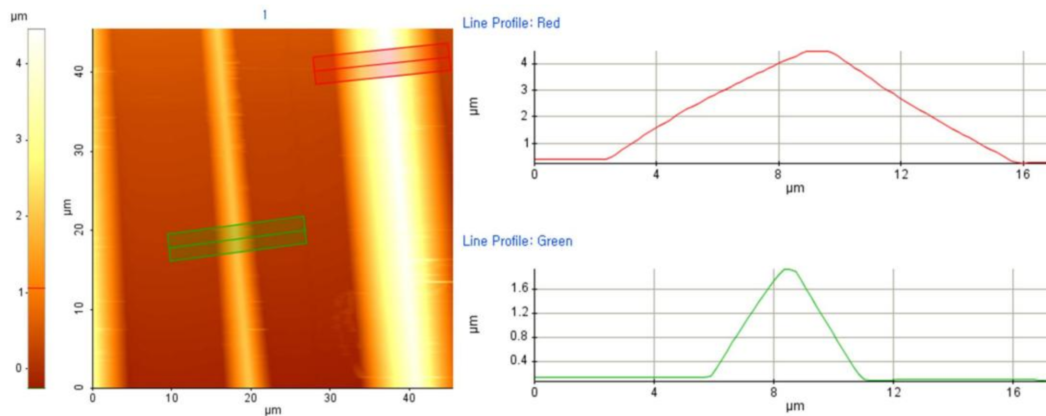

Fig. 10 AFM micrograph of microstructure

The microstructures, which machined with FTS frequency of 800 Hz feed rate of 20 µm and spindle speed of 10 rpm, were measured by optical microscopy, as shown in Fig. 9 and Fig. 10. In theory, the maximum groove width should be 10 µm when the cutting depth is 5 µm. It is because of the nose angle of diamond tool is 90°; the width is double of depth. We can found from the measured results that the maximum groove width is about 13 µm and the maximum depth is about 4.7 µm. The actual value is close to the theory value. It is has indicated the effectiveness of the designed FTS system.

4. Conclusions

This paper reported the machining evaluation of a dual piezoelectric actuator based FTS used to fabricate the microstructure. The methodology for design and control of lever-type magnified flexure mechanism used to the FTS system was described. The dynamic performances of the FTS were measured and the machining test results point out that the DFTS shows better tracking precision and longer travel range than the SFTS, and can provide more travel range to the diamond tool. Actual fabrication results of the sinusoidal microstructure point out that the profile of microstructure is a sinusoidal wave in the turning direction with profile wavelength of 100 µm and the peak-to-valley amplitude of about 4.7 µm and has indicated effectiveness of the designed FTS system.

ACKNOWLEDGEMENT

This work was supported by NCRC (National Core Research Center) program of the Ministry of Education, Science and Technology (2010-0008-277) and "Development of Micro Feature Machining System on Large Surface and Core Technologies for Measurement & Inspection" project of ministry of knowledge economy.

REFERENCES

1. Kim H.S., Kim E.J., “Feed-forward Control of Fast Tool Servo for Real-time Correction of Spindle Error in Diamond Turning of Flat Surface”, Int J Mach Tool Manu, Vol. 43, pp. 1177–1183, 2003.
2. Crudele M., Kurfess T.R., “Implementation of a Fast Tool Servo with Repetitive Control for Diamond Turning”, Mechatronics, Vol. 13, pp. 243–257, 2003.
3. LU X., TRUMPER D. L., “Spindle Rotary Position Estimation for Fast Tool Servo Trajection Generation”, International Journal of Machine Tool & Manufacture, Vol. 47, pp. 1362-1367, 2007.
4. Zhu W. H., Jun M. B., Altintas Y., “A Fast Tool Servo Design for Precision Turning of Shafts on Conventional CNC Iathes”, Int J Mach Tool Manu, Vol. 41, No. 6, pp. 953–965, 2001.
5. Patterson S. R., Magreb E. B., “Design and Testing of a Fast Tool Servo for Diamond Turning”, Precis Eng, Vol. 7 No. 3, pp. 123–128, 1985.
6. Gan S. W., Lim H. S., Rahman W.F., “A Fine Tool Servo System for Global Position Error Compensation for a Miniature Ultraprecision Lathe”, Int J Mach Tool Manu, Vol. 47, pp. 1302–1310, 2007.
7. Ku S., Larsen G., Cetinkunt S., “Fast Tool Servo Control for Ultra-precision Machining at Extremely Low Feed Rates. Mechatronics, Vol. 8, pp. 381–393, 1998.
8. Okazaki, Y., “A Micro-positioning Tool Post Using A Piezoelectric Actuator of Diamond Turning Machines,” Precision Engineering, Vol. 12, No. 3, pp. 151-156, 1990.
9. Crudele, M., Kurfess, T., “Implementation of a Fast tool Servo with Repetitive Control for Diamond Turning,” Mechatronics, Vol. 13, pp. 243-257, 2003.
10. Kim, J. D., Kim, D. S., “Waviness Compensation of Precision Machining by Piezoelectric Micro Cutting Device,” J. Machine Tool & Manufacture, Vol. 38, pp. 1305-1322, 1998.
11. Altintas, Y., “Manudacturing automation,” Cambridge University Press, Cambridge, 2000.
12. Kim, S and Kang, S., “Replication qualities and optical properties of UV-moulded microlens arrays,” J. Physics D: Applied Physics, Vol. 36, pp. 2451-2456, 2003.

A Tool to Design Industrial Service for Desktop Factories Gaining Flexibility

Hitoshi Komoto[1,#] **and Nozomu Mishima**[2]
1 Advanced Manufacturing Research Institute, National Institute of Advanced Industrial Science and Technology, Tsukuba, Japan
2 Graduate School of Engineering and Resource Science, Akita University, Akita, Japan
Corresponding Author / E-mail: h.komoto@aist.go.jp, TEL: +81-29-861-4139, FAX: +81-29-861-7201

KEYWORDS : Flexibility, Simulation, Service design

Flexibility is crucial for manufacturing systems to handle variations in manufacturing tasks and volumes as well as accidental malfunctions of system facilities. Portable and adjustable desktop machine tools in a manufacturing system can increase the flexibility by sharing manufacturing tasks with conventional less portable and adjustable machine tools. This paper presents a simulation tool to quantify the effect of introduction of a desktop machine tool to a manufacturing system with specific variations in manufacturing volumes and tasks. The tool is useful for manufacturers to select the type of desktop machine tools suitable to them.

1. Introduction

Miniaturization of industrial machines plays a crucial role in the realization of compact manufacturing systems with less energy and material consumption. It has been, and it still is, a challenging research topic in microfactory [1] to develop innovative compact machines as alternatives to conventional machines in terms of quality, productivity, and cost. Desktop machine tools, which are portable and adjustable machines equipped with a tool head for specific machining purposes (e.g., milling, coating, laser cutting, and polishing, etc.), are examples of such machines [2,3]. Some desktop machine tools are commercially available.

One of the recent research trends in the manufacturing industry is to study services offered in life cycles of industrial machines [4]. These services include maintenance and upgrade services that increase the life time of machines and satisfy the various needs and wishes of machine users. Following the trend, methods and tools to support service design have been proposed [5-7]. These methods and tools can be used for service design related with desktop machine tools.

Manufacturers of desktop machine tools offer various machine-related services to users of these tools in the use stage (Fig. 1), including maintenance and repair services through service engineers, monitoring services to diagnose these machines and schedule maintenance and repair services, and expert consultation regarding the operational planning of machine tools. These services are designed and offered to the users with consideration of their specific manufacturing environment characterized by the variety and intensity of the usage.

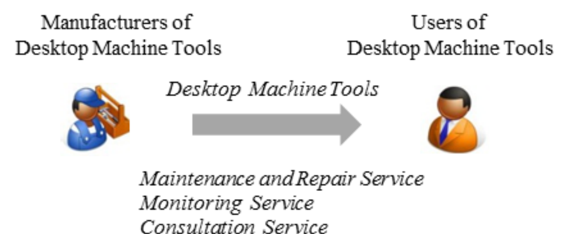

Fig. 1 Industrial Services in Machine Life Cycles

Flexibility is one of the major evaluation criteria of manufacturing systems. It is often regarded as the capability to quickly deal with variations in manufacturing tasks (e.g., micro-fabrication of electrical devices and repair of molding components) and their volumes as well as accidental malfunctions of system facilities. Manufacturers can gain the capability by the reconfiguration of their systems (i.e., production lines) at the operational levels such as allocation of manufacturing tasks to machines considering the availability (e.g., determined by maintenance schedule). However, such system-level reconfiguration is difficult with conventional machines regarding portability and adjustability. For instance, a breakdown of a conventional machine stops the operations

of the entire manufacturing system, and it takes hours to discharge, repair, and calibrate the machine and restart the pending operations. In comparison, portable and adjustable desktop machine tools are assumed to perform such reconfiguration with less effort by exchanging tool heads or replacing broken machines with spare machines.

In order to verify the superiority of desktop machine tools regarding such flexibility in comparison with conventional machines, the rigorous analysis of the operational behavior of desktop machine tools machine tools in a manufacturing system is necessary. However, there are several difficulties in analyzing the operational behavior. First, there are few cases in industry, in which desktop machine tools and conventional machines are comparable based on specific manufacturing tasks. Second, reproduction of the behavior of manufacturing systems under the identical manufacturing tasks is costly and hardly possible in practice. Therefore, the modeling and simulation of the behavior of manufacturing systems is inevitable for the evaluation of such flexibility. Related work [5-7] promoted the use of modeling and simulation techniques for design of manufacturing systems and service related with them (before manufacturing systems are actually built).

The objective of this research is to develop a tool to support service design for manufacturers and users of desktop machine tools with modeling and simulation technique. The tool simulates the operational behavior of desktop machine tools as well as conventional machines in a manufacturing system, which is used to evaluate its flexibility under variations in manufacturing tasks and volumes as well as accidental malfunction of system facilities.

In particular, this paper illustrates a usage of the tool to support the potential owners of desktop machine tools to quantify the impacts of introducing a desktop machine tool to a manufacturing system with conventional machines in terms of flexibility. With the tool, the potential owners can analyze and compare different configurations of system facilities with given specific manufacturing tasks and their volumes. Such support is crucial for manufacturers of desktop machine tools to deliver consultation services to the potential owners regarding operational planning before contracts are made between them.

The rest of the paper is organized as follows. Section 2 describes the model of a manufacturing system employed in the tool as well as the simulation mechanism. Section 3 shows the usage of the tool. Section 4 summarizes and concludes the paper.

2. Manufacturing System Configuration with Desktop Machine tools

This section describes a model of a manufacturing system with a focus on the characteristics of desktop machine tools regarding the aforementioned flexibility (i.e., variations in manufacturing volumes and tasks as well as accidental malfunctions of system facilities). A manufacturing system is modeled with relations among manufacturing *processes* such as cutting and polishing processes, *machines* in charge of processes, which includes both conventional machines and desktop machine tools, and *tasks* as the sequences of processes completed with these machines. The model represents the static configuration of a manufacturing system and it is described in Section 2.1. The assignment of manufacturing tasks to machines based on the condition and availability of machines is another type of the configuration, and it is described in Section 2.2.

2.1 Static Configuration of a Manufacturing System

This paper models the relation among processes, machines, and tasks of a manufacturing system as the static configuration with two bipartite graphs (see Fig. 2). The first bipartite graph consists of tasks, processes, and edges connecting tasks with processes. Each task is completed by a set of processes. An edge between a task and a process means that the process is necessary to complete the task. In order to represent the sequence of processes to complete a task, edges connecting processes with the task are numbered. For instance, in Fig. 2, Process I and Process II are performed in series to complete Task A. Edges include such information as process time, which is used for the simulation of the dynamic behavior of a manufacturing system (see Section 3).

The second bipartite graph consists of processes, machines, and relations between them. The graph shows the processing capability of machines. For instance, in Fig. 2, Machine 1 can only perform Process I, while Machine 3 can perform all processes. Edges include such information as cost and energy consumption per time as well as process speed relative to that of the other machines (e.g., Machine 1 is two times faster than Machine 3 to perform Process 1). The topology of the graph includes the capability of desktop machine tools to perform multiple processes by exchanging tool heads.

As described above, machines are indirectly connected with tasks through processes. The connections are dynamically assigned during the operation of manufacturing systems.

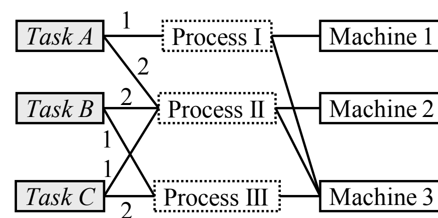

Fig. 2 Static Configuration of Manufacturing System

2.2 System Operational Behavior and Reconfiguration

The operational behavior of a manufacturing system is described with: (1) the operational behavior of individual machines triggered by external events during operations, (2) the scheduling procedure that generates events triggering the operation of individual machines, and (3) the placement of manufacturing tasks as input of the scheduling procedure.

The behavior of a manufacturing system is simulated based on these descriptions using discrete event simulation. It is simulated by executing a set of events, which generate and

dispose entities and assign (and change) the state of entities. In the model, machines and tasks are treated as entities. Manufacturing processes and other activities in the use stage of machines (such as setup, tool-exchange, discharge, and repair of machines) cause transitions of the state of tasks and machines. State transitions of tasks and machines triggered by events in life cycles are shown in Fig. 3 and Fig. 4 and explained in the following subsections.

2.2.1 State Transition of Tasks

Tasks are generated by order placement events. The number of tasks at an order placement event is defined by the volume of the order placement. A task consists of a process sequence, which is defined by an ordered list of a triplet (*process name*, *machine name*, *remaining time to complete the process*). Since machines assigned to processes are not known at the beginning, the second parameter of each triplet is empty. The third parameter of each triplet is also initially empty, because the remaining time to complete the process depends on the performance of the assigned machine.

The initial state of a task is *Placed*. It becomes *Assigned* when a process in the task is assigned to one of the machines in a manufacturing system. At this moment, the second and third parameters of the process (i.e., machine name and necessary process time) are determined. The state becomes *In-Process* at execution of the first process. During the execution, the corresponding process time decreases until it reaches 0, which indicates the completion of the process. At the completion, the triplet of the process is removed from the process sequence of the task.

While the state of a task is *In-Process*, the reassignment of processes to machines occurs at the occasion of breakdown of the machines in charge of the task's processes. The state finally becomes *Completed*, when the process sequence becomes an empty list (i.e., all processes of the task are executed).

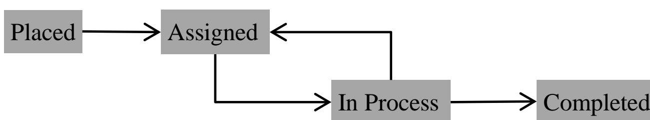

Fig. 3 State Transition of Tasks

2.2.2 State Transition of Machines

Generation and disposal of machines in a manufacturing system do not occur in the simulation, while tasks are generated and disposed (i.e., completed) during the operation of the system. Machines own a queue of orders (formulated below). An order is defined by a triplet (*process name*, *task name*, *remaining time to complete the process*).

The initial state of a machine is *Sleep*. The queue of orders is initially empty. The machine does not change the state, when a process is assigned to the machine. However, the state becomes *Prep*, when one of the assigned processes in the queue becomes executable (i.e., all prior processes of corresponding tasks have been already executed), and one of the executable process is selected. (It is assumed that machines cannot perform multiple processes at the same time.)

The state of the machine becomes *Busy*, when the machine start execution of the selected process. While the machine is performing the process, the remaining time to complete the process decreases incrementally. When the process time becomes zero, the corresponding triplet is removed from the queue, and another triplet is selected. In this way, the machine performs executable processes continuously in series.

When the machine starts performing different processes or the same process of different tasks, the state of the machine becomes *Prep*. In the model, the time interval necessary for the state transition from *Prep* to *Busy* depends on the type of the machine. In case of a desktop machine tool, the interval is shorter than that of conventional machines. When there are no executable processes, the state of the machine becomes *Sleep*. The state transition model includes probabilistic transitions representing breakdown and recovery of the machine. Variables determining the probability of occurrences of these events are defined with respect to each process.

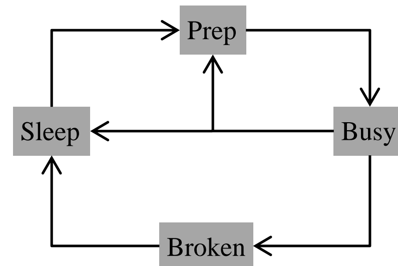

Fig. 4 State Transition of Machines

2.2.3 Scheduling Procedure

The scheduling procedure controls relations between tasks and machines. The procedure is triggered at the generation of tasks (i.e. order placements) and the breakdown of machines. At the generation of a task, for each process in the task, a machine with the minimal queue length is selected. At the breakdown of a machine, first, the queue of the machine becomes empty. Then, the elements of the process sequence of all tasks, which include the name of the broken machine in the second parameter (*process name*, <u>*broken machine name*</u>, *remaining time to complete the process*), are collected. The machine name of the collected elements becomes the name of a machine, which can execute the specified process and owns a queue with minimal length. If no other machines can execute the processes specified by the process name of each collected elements, the name of the machine name is not updated (i.e., the process is executed after the repair of the broken machine).

3. The Simulation Tool and Its Usage

3.1 Background of the tool

The model of a manufacturing system described in Section 2 has been implemented on the tool, which is an extension of the tool previously developed by the authors [5]. The tool is programed in Python and employs SimPy [8] as the discrete event simulation engine. Fig. 5 shows a screenshot of the tool.

The tool currently supports the evaluations of a manufacturing system with multiple criteria such as life cycle costs and productivity. Life cycle costs are calculated by a sum of machine prices, operational costs, and fee of industrial services such as repair and maintenance services. The productivity is measured by the average process time of all tasks (i.e., when the state of tasks is *In-Process*). The paper focuses on the evaluation of a manufacturing system in term of the productivity, because it is appropriate to evaluate flexibility during operations of the manufacturing system instead of its long-term performance such as life cycle costs.

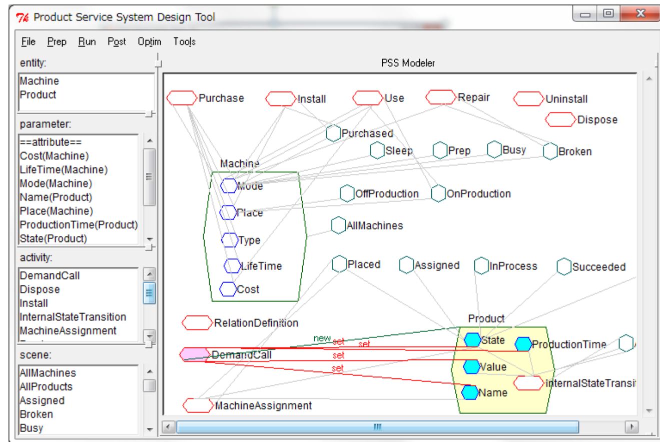

Fig. 5 Screenshot of the Simulation Tool

The generic usage of the tool is the design of services offered in life cycles of industrial machines (see Fig. 1). In particular, the model presented in Section 2 is necessary to characterize the properties of desktop machine tools in terms of flexibility. This section demonstrates a usage of the tool, in which potential users of desktop machine tools, who own a manufacturing system with conventional machines (the reference manufacturing system), considers installation of desktop machine tools to the system. As shown below, the tool can quantify the effect of a desktop machine tool (to be installed) on the flexibility of the manufacturing system considering specific variations in manufacturing tasks and demands.

This section first simulates the behavior of the reference manufacturing system. Then the performance of the reference manufacturing system is compared with that of alternative systems including a desktop machine tool.

3.2 Simulation of the Reference Manufacturing System

The reference manufacturing system consisted of four machines for single process (cutting, coating, polishing, and electrical discharge machining (EDM)) in Fig. 6. The system performs three types of tasks. The proportion of the tasks is given, while the quantity is specified at each simulation. The proportion and process sequence of each tasks, and the duration of processes in the process sequence are summarized in Fig. 6. For instance, 60% of all manufacturing tasks of the reference system is TaskA, in which cutting (requiring simulation 3 steps), polishing (1 step), and coating process (2 steps) should be performed in the given order.

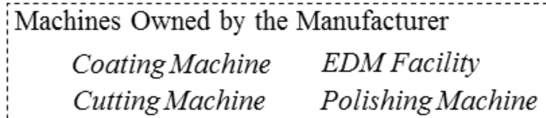

Fig. 6 The Reference Manufacturing System Model

3.2.1 Simulation Setting

In the initial simulation, 5 tasks were placed at every 25 steps during 1,000 steps. The type of tasks is determined by selecting one of TaskA, TaskB, and TaskC following the probability distribution defined by the proportion. In order to maintain the simplicity of the simulation, the probability of the occurrence of breakdown and recovery is same for all machines (the value is 0.005 [/step] and 0.1 [/step], respectively). An example of simulations of models with more detailed behavior (e.g., machine deterioration, multiple failure modes) is presented in the previous report [9].

3.2.2 Simulation Results

Fig. 7 shows the state of machines and the state of tasks in a simulation with respect to the progress of simulation (70 steps). Fig. 7(a) shows the number of *Busy* and *Broken* machines. Fig. 7(b) shows the number of *Assigned*, *In-Process* and *Completed* tasks and the generation of tasks at 0, 25, and 50 steps. After the generation, processes in the tasks were assigned to specific machines and they were processed when machines are available (tasks were *In-Process*). The number of *Completed* tasks gradually increased with the progress of simulation. A breakdown was occurred to the cutting machine at 30 steps. The other machines stopped operations because they could not perform any tasks. After the broken machine was repaired, other machines started operations again. Such behavior of machines influenced the state of tasks. During the breakdown the number of *Assigned* tasks did not decrease, because these tasks are on of Task A or Task B, which have to wait for the recovery of the broken cutting machine.

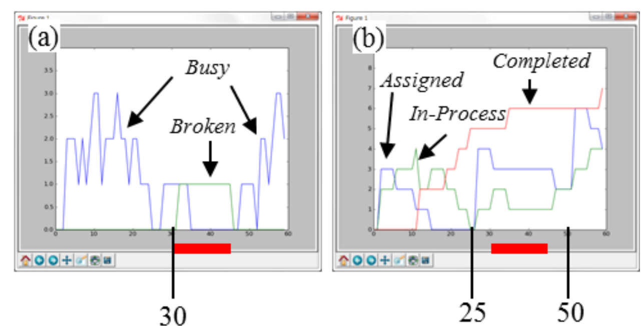

Fig. 7 Interpretation of simulation results

The simulated behavior of the reference system regarding the state of machines and the state of tasks is shown in Fig. 8. Fig. 8 shows (a) the number of *Broken* machines, (b) *Assigned*

tasks, (c) tasks with state *In-Process*, and the average of the process time of *Completed* tasks with respect to simulation steps. As shown in Fig. 8(a), there were concentrated occurrences of breakdown of machines around 800 steps. They temporally increased the number of tasks waiting for process executions (i.e., tasks with state *Assigned* in Fig. 8(b)) and the number of tasks *In-Process* with some delay (Fig. 8(c)). As a result, the average time to complete tasks increased (in Fig. 8(d)). It seems that the reference system model is flexible against such concentrated machine breakdowns with the given demand of tasks. The flexibility was analyzed in detail below.

Flexibility of the reference model was analyzed with variations in the probabilities of the event occurrences causing the breakdown of machines (0.000, 0.005, 0.010 [/step]) and the quantity of placement of tasks (5, 6, and 7 [tasks/25steps]). The average of the process time of *Completed* tasks with respect to simulation steps with the variations is shown in Fig. 8 (as same as Fig. 8 (d)).As shown in Fig. 9(a), the average process time temporally increases at the occurrences of breakdown of machines, while it decreases when all machines are functional. The result suggests that the reference manufacturing system possess flexibility in dealing with occasional breakdown of machines as far as the probability of the occurrences is under the critical value. The simulation is useful to find the critical probability (in this example, the value is between 0.005 and 0.010 [/step]).

As shown in Fig. 9(b), the simulation result was used to identify the capacity of the reference manufacturing system. In the example, the critical quantity of placement of tasks, which is below the capacity, is between 6 and 7 [tasks/25steps]. When breakdown of machines is assumed, the critical quantity decreases.

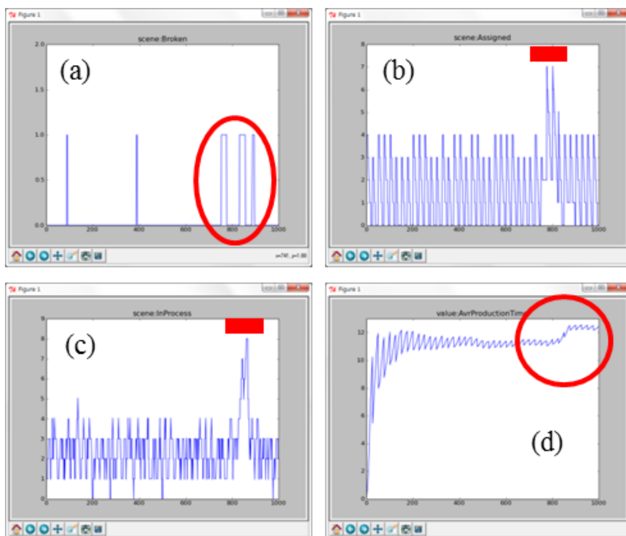

Fig. 8 Simulation Results

3.3 Replacing Machines with a Desktop Machine Tool

3.3.1 Replacement Strategy at a High Manufacturing Volume

In order to deal with a higher quantity of the placement of tasks, the coating machine was replaced with a desktop machine tool. The desktop machine tool can deal with one of the other three processes performed by the other three machines. The desktop machine tool is used to perform the other process, when it is not busy with coating processes.

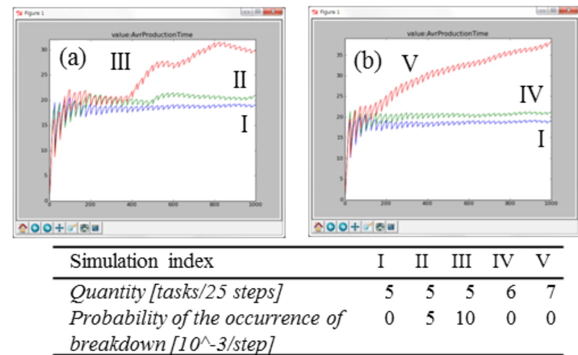

Simulation index	I	II	III	IV	V
Quantity [tasks/25 steps]	5	5	5	6	7
Probability of the occurrence of breakdown [10^-3/step]	0	5	10	0	0

Fig. 9 The Average Task Completion Time under Variations in Machine Breakdown Probabilities and Volumes of Tasks

Fig. 10 shows the simulation results of the reference system at a high manufacturing volume (7 [tasks/steps]) and those of manufacturing systems with a desk factory. Positive and negative signs in Fig. 10 indicate installed and removed machines. The horizontal broken lines show a reference value of the average process time in order to compare the results. As shown in Fig. 10(a), the capacity of the reference system was not sufficient to meet at the high manufacturing volume. Fig. 10(b) and 10(c) show that the introduction of a desktop machine tool to the manufacturing system is not always attractive, as the average process time of the systems still increases after the introduction. Fig. 10(d) shows that a desktop machine tool that can finally deal with both coating process and cutting process is sufficient to deal with the quantity of task placement.

3.3.2 Replacement Strategy at a Low Manufacturing Volume

Flexibility of manufacturing systems is also crucial at the occasion of decrease of manufacturing volumes (e.g., at the occurrence of economic depression). In this case, the number of facilities in a system may be decreased in order to decrease the capital costs.

Fig. 11 shows the simulation results of manufacturing systems with fewer machines at a lower manufacturing volume (5 [tasks/steps]). These systems are designed based on the reference manufacturing system. A desktop machine tool with multiple processing functions was installed on the reference system and two conventional machines performing the processes supported by the desktop machine tool (i.e., redundant machines) were removed. As Fig. 11 (a) shows, a desktop machine tool that could deal with coating and polishing processes was used as replacement of both the coating machine and the polishing machine without losing flexibility. However, as Fig. 11 (b) and (c) show, the systems with a desktop machine tool with different combinations of machining processes could not possess the capability to deal with flexibility at the manufacturing volume.

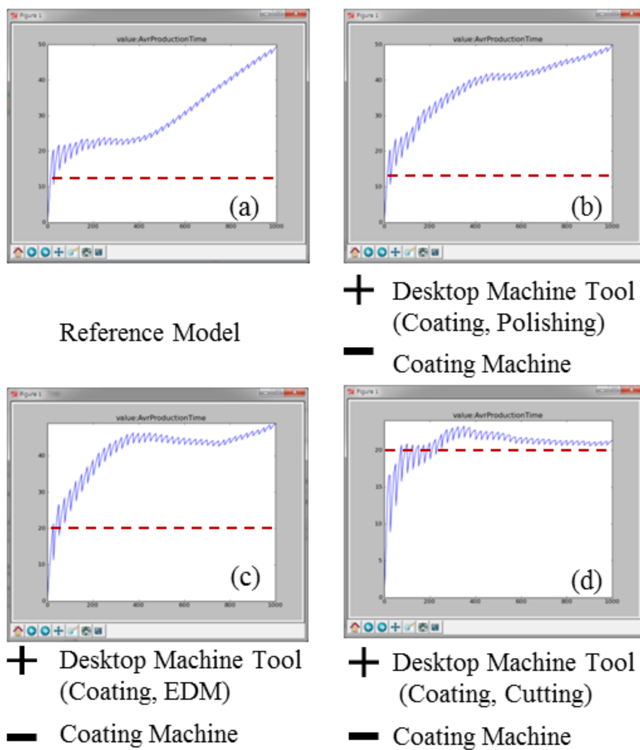

Fig. 10 The Average Task Completion Time with Desktop Machine tools

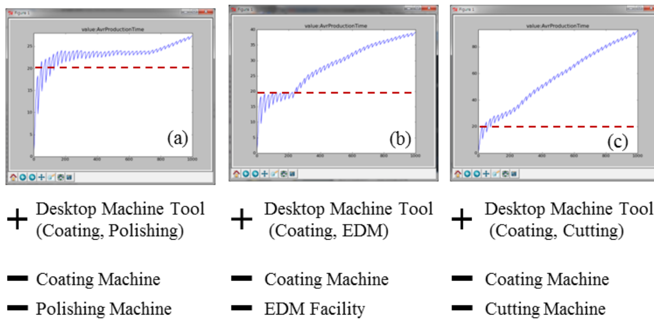

Fig. 11 The Average Task Completion Time at a Low Manufacturing Volumes with Fewer Machines

4. Summary and Conclusions

Flexibility is a crucial operational performance of manufacturing systems to handle variations in manufacturing tasks and volumes as well as accidental malfunctions of system facilities. Portable and adjustable desktop machine tools with exchangeable tool heads can become a part of flexible manufacturing systems in corporation with existing system facilities, which are less portable and adjustable.

This paper has presented a simulation tool to quantify the effect of desktop machine tools introduced to a manufacturing system with specific variations in manufacturing tasks and volumes. With an illustration of the usage, the paper has shown that the tool can be used for potential users of desktop machine tools to select appropriate machine types and related industrial services that effectively increase flexibility at different situations in terms of demands of tasks to be performed by the system.

The study found that there were wide configurations of a desktop machine tool to be introduced to a manufacturing system regarding machining capability. Appropriate configurations should be selected in order to increase the flexibility of the system with consideration of manufacturing tasks and volumes as well as the organization of existing system facilities. Therefore, modeling and simulation of the operational behavior of the entire manufacturing system is crucial for the selection of desktop machine tools introduced to the system.

REFERENCES

1. Okazaki, Y., Mishima, N. and Ashida, K., “Microfactory - Concept, History and Developments-,” Journal of Manufacturing Science and Engineering, Trans. ASME, Vol. 126, pp. 837 – 844, 2004.
2. Kurita, T. and Hattori, M., “Development of new-concept desk top size machine tool,” International Journal of Machine Tools and Manufacture, Vol. 45, No.7 – 8, pp. 959 – 965, 2005.
3. DTF Research Consortium, Technological Foundation of Nagano prefecture, Suwa Techno Lakeside Regional Center (http://www.dtf.ne.jp/en/), 2008.
4. Uhlmann, E., Gabriel, C., Raue, N. and Stelzer, C., “Influences of the IPS² Business Model on the Development of a Micro Milling Spindle,” Proceedings of the 3rd CIRP IPS² Conference, pp. 57 – 62, 2011.
5. Komoto, H. and Tomiyama, T., “Integration of a service CAD and a Life cycle simulator,” Annals of the CIRP, CIRP, Vol. 57 No.1, pp. 9-12, 2008.
6. Umeda, Y., Nonomura, A. and Tomiyama, T., “A Study on Life-Cycle Design for the Post Mass Production Paradigm,” Artificial Intelligence for Engineering Design, Analysis and Manufacturing, Cambridge University Press, Vol. 14, No. 2, pp. 149-161, 2000.
7. Meier, H., Roy, R. and Seeliger, G., “Industrial Product-Service Systems - IPS².” CIRP Annals Manufacturing Technology, Vol. 59, No. 2, pp. 607-627, 2010.
8. Simpy, an object-oriented, process-based, discrete-event-simulation language based on standard Python (http://simpy.sourceforge.net/).
9. Komoto, H. and Mishima N., “System Design of Maintenance Service for Distributed Production Facilities,” In: Proceedings of the 7th International Symposium on Environmentally Conscious Design and Inverse Manufacturing (EcoDesign 2011), pp. 367-372, 2011.

A Production Line with Flexible Unit Linkage -DTF Friendship Line-

Yuichi Okazaki[1#], Masahiko Hiraide[2], Chiaki Endo[3], Tsuyoshi Ogawa[4], Masumi Yanagisawa[5] and Koichi Ojima[6]

1 National Institute of Advanced Industrial Science and Technology, Tsukuba, Japan
2 Hiraide Precision Co. Ltd, Okaya, Japan
3 Takashima Sangyo Co. Ltd, Suwa, Japan
4 Toyo Seiki Co. Ltd., Chino, Japan
5 Engineering System Co. Ltd., Matsumoto, Japan
6 KEC Co., Toyama, Japan
Corresponding Author / E-mail: okazaki-u1@aist.go.jp, TEL: +81-29-861-7224, FAX: +81-29-861-7201

KEYWORDS : microfactory, desktop factory, production line, line construction, handling robot, milling machine, plating, nano-imprinting, wireless communication

The prototype of a compact production line based on the novel concept of a DTF® (Desktop Factory®) Friendship Line has been developed and evaluated. The production line is composed of four discrete units, dedicated to different processes, and of different sizes and forms. The units are linked by using compact handling robots attached to the individual units. In the demonstration production, all the processes, the workpiece handling, and the communication, were performed with no difficulty. A complete production line, with 1/7th the footprint and 1/10th the energy consumption of a similar line composed of conventional units, has been approved.

1. Introduction

The Desktop Factory® or DTF® philosophy enhances space/energy efficiency, flexibility, agility, reconfigurability, and economy in manufacturing, by means of downsizing manufacturing systems[1]. The conception is effectively identical to that of a microfactory. Though stand-alone miniaturized machines have the potential to enhance their specific fields of application[2),3)], several units combined into a line offer superior performance of tasks in industrial automated production, because a number of discrete processes are typically required in order to complete a given production procedure.

One methodology for building a compact production line involves introducing a strictly standardized modular policy to conform all units connected via standardized physical and informatics interfaces. Some successful developments based on this policy can be seen in academic trials and industrial applications[4)-8)].

However, this policy has the disadvantage that all the members of the system must comply with the strict standard of the design. When all the units are well designed and prepared according to this standard, the system may be easily constructed. Problems arise, however, when an existing processing unit is to be introduced: it is often inconvenient and impractical for the given unit to be redesigned and rebuilt to fit the standard. Some units may be provided by manufacturers without regard for the standard.

“DTF", “Desktop Factory", and their corresponding logos are trademarks or registered trademarks of NIDEC Sankyo Corporation., and their use is licensed to members of the DTF Research Consortium.

A more convenient and flexible means of system building, to cope with the contingent requirements of actual applications, consists in introducing minimum rules and methodologies required to connect the respective units to each other. In this case, every member of the system may differ from the others in character, size, form or even performance. A unit with a special function, for example, may be “invited" to become a member. Based on this conception, the prototype of such a compact production line—a “Friendship Line"—has been developed and evaluated.

2. System description

Outline of the system

The developed production line is composed of four units, with four different processes, from four different manufacturers. Each unit has different function, size and form. In order to accommodate these differences, the units are linked by using compact handling robots attached to the individual units. The system layout is illustrated in **Figs. 1** and **2**. In typical system configurations, the handling robots are located in between the respective units to which they are related and which they connect. As a result, in the system set-up, the allocation and relative positioning of the units and robots is complicated. In this prototype, on the other hand, a methodology has been developed to eliminate the precise relative positioning between the units and the respective handling devices, and the related physical wiring, so that an agile line reconfiguration is enabled (**Fig. 3**).

Milling unit-1

The first unit of the line is a column traverse type, heavy-duty vertical milling machine (**Fig. 4**), based on a commercial compact machining cell design[9]. By limiting the workspace and capacity, the

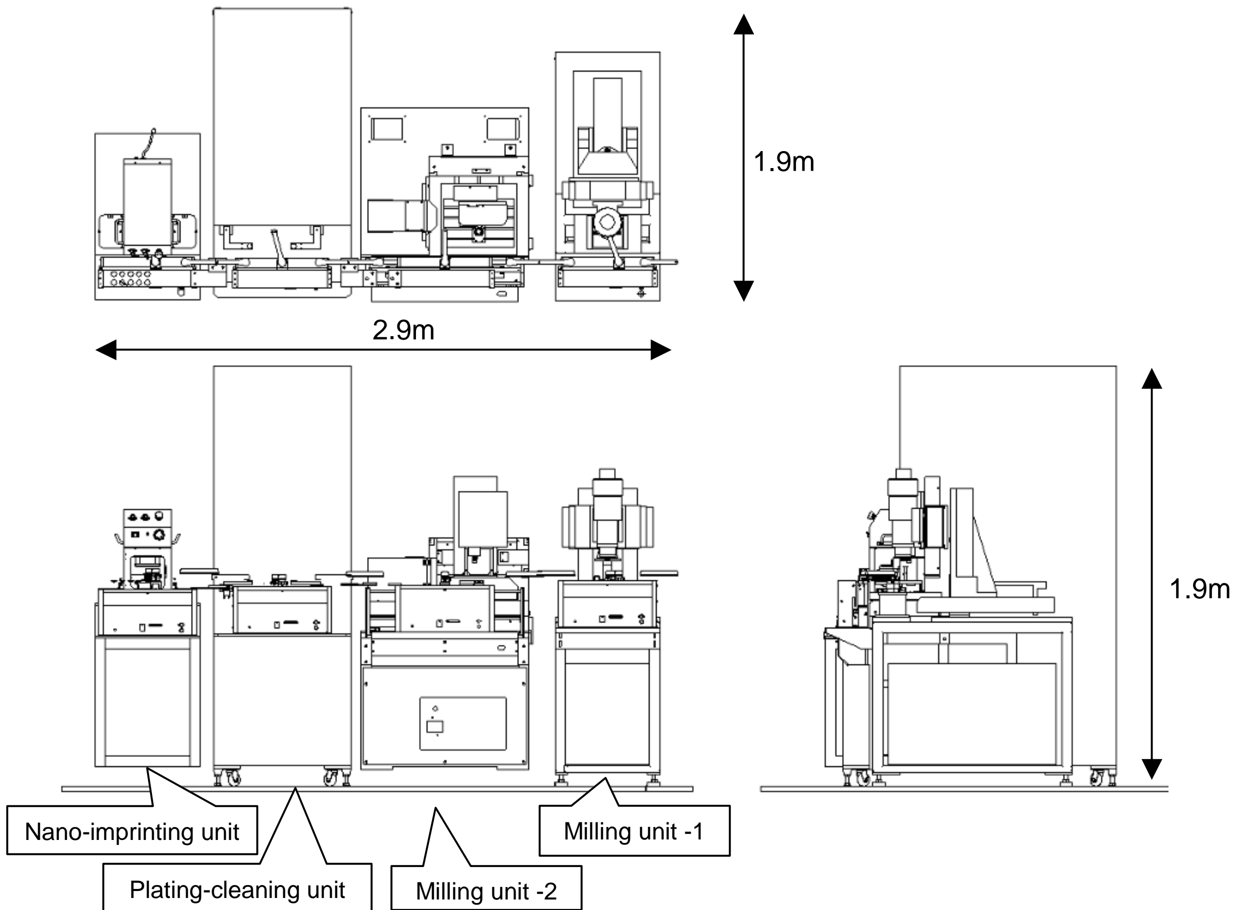

Fig. 1 System layout of the Friendship Line

mass of the moving members was reduced, and smaller actuators were employed. As a result, the volume and weight were greatly reduced, from the 1,750 x 2,910 x 2,425 mm (W x D x H) and 5,000 kg typical of conventional machines, to 500 x 984 x 1,698 mm and 400 kg—1/10th the conventional footprint and weight. An automatic tool changer (ATC) holds up to five tools. In the demonstration, rough milling and engraving were performed.

Milling unit-2

The second unit is also a milling machine equipped with an ATC (**Fig. 5**). It is smaller than the first unit, and performs precise and high accuracy machining with better than one micrometer of repeatability, due to its rugged structure employing a granite base and cast iron monolithic framework. In the demonstration, engraving and surface finishing (deburring) on the rear surface were performed.

Plating and cleaning unit

The third unit is an all-in-one plating and cleaning processing device, in a DTF form (**Fig. 6**). The sequential processes, of ultrasonic washing, acid cleaning, rinse, plating, rinse, and drying, which are normally done as batch processes, have been so designed that a piece-by-piece operation can be performed automatically using internal robots. The resulting footprint measures 650 x 1,400 mm. In addition, several kinds of plating processes are available simply by changing the plating bath. To synchronize the takt time with the other units, the plating bath is duplicated. The entire sequence is completed

Fig. 2 Photo of the Friendship Line

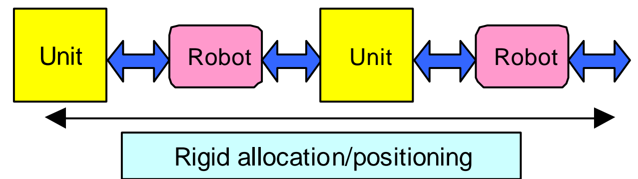

(a) Coventional in-line configuration

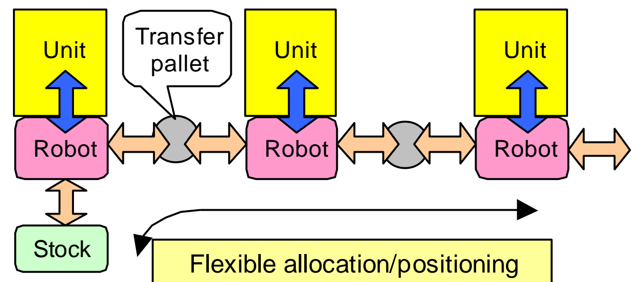

(b) Transfer configuration

Fig. 3 Processing units and handling robots

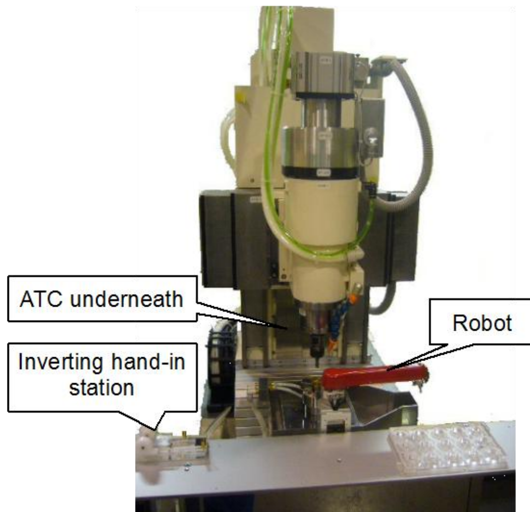

Fig. 4 Milling unit-1 and handling robot

Fig. 5 ATC of milling unit-2

within 210 seconds. The inner area of the enclosure is kept at negative pressure to prevent environmental contamination. In the demonstration, a sequence of electro-nickel plating was performed.

Nano-imprinting unit

The fourth unit is a desktop nano-imprinting device (**Fig. 7**), based on a commercial device for industrial manufacturing. Surface nano-patterning is performed by applying UV polymer, plying the mold, and then utilizing UV curing. Introducing UV-LED as the curing light source, instead of a metal halide lamp, enabled significant miniaturization and energy savings. In the demonstration, a hologram was printed on the workpieces.

Material handling and communication

Compact transfer robots, with a unique X-theta-Z-axis configuration, link the four units of the production line (**Fig. 8**). The robots have a smaller footprint and wider working range compared to conventional Cartesian robots and SCARA robots. In size, its footprint of 0.094 m^2 and volume of 0.02 m^3 are less than $1/6^{th}$ and $1/20^{th}$ of conventional robots, respectively. The robot arm can penetrate into the processing units without disrupting visibility or operability. Each processing unit is equipped with a robot on its reference surface.

In calibrating the relative position between each robot and its respective processing unit, the robot arm optically identifies the position of a target metal ball attached to the side of the processing unit (**Fig. 9**). Using this technique, better than 40 µm repeatability was achieved in the X, Y and Z directions.

The robot arm has a pneumatically operated chucking mechanism that holds various types of end effectors according to the given workpiece posture. A custom controller is embedded.

Workpieces are passed to another robot, of another processing unit, on a passive transfer pallet. Workpieces may be inverted on the pallet if necessary. The positioning on the transfer pallet requires less precision compared to that on the processing units, which enables easier alignment of the units.

In order to synchronize the motion of the handling robots and the processing units, both the robots and the processing units are equipped with wireless communication devices (**Fig. 10**). The wireless system uses weak radio wave in the 2.4 GHz band, based on the ARIB STD-T66 standard, with a transfer bit rate of 250 kbps. Each wireless unit communicates with adjoining units cyclically, without need of any master unit.

3. System integration and evaluation

As noted, the four processing units are equipped with compact handling robots and linked into a production line as a prototype. The four processing units, handling robots, and communication devices, are all supplied by different firms. Moreover, each unit is not completely developed, but based on existing equipment or technology. Therefore, the system integration itself was a challenging project. First, the interfacing standard for mechanical dimension and communication was negotiated. The resultant temporal standard was described as DTF Standard D0100 to D0300. Then, a target sample product was settled and processed through the line.

In the demonstration production, all the processes, workpiece handling, and communication, were performed without difficulty. **Fig. 12** shows photographs of the workpieces at each step. The

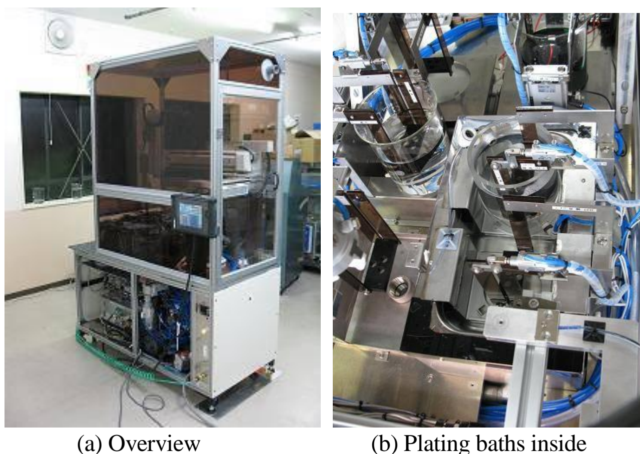

(a) Overview (b) Plating baths inside

Fig. 6 Plating and cleaning unit

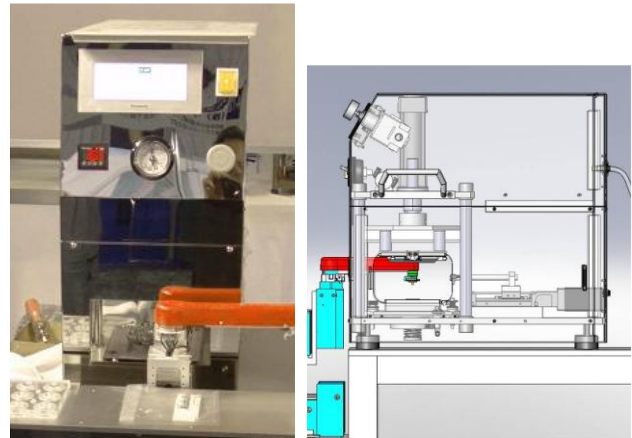

Fig.7 Nano-imprinting unit

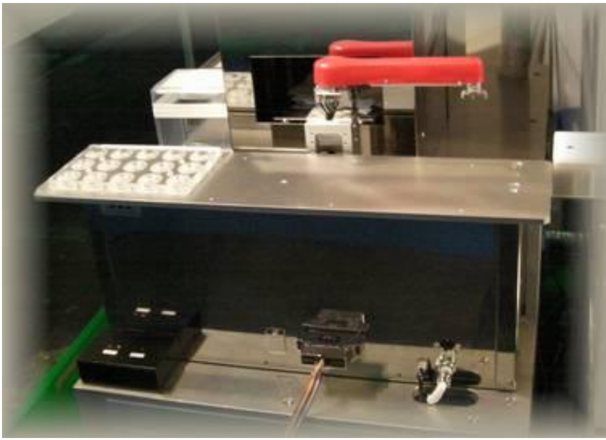

Fig.8 Handling robot attached to the individual unit

workpiece is shaped from a brass blank of 25 mm diameter. The total trial processing takt time was 16 minutes and 25 seconds per piece, which was not yet optimized.

The footprint and energy consumption of the entire production line have been approved for a maximum of 2 x 3 m and 11 kVA, respectively, which represent 1/7th and 1/10th the respective values of a similar line composed of conventional units.

As a result, a methodology for achieving compact and highly reconfigurable production lines has been presented.

ACKNOWLEDGEMENT

This project was conducted with the support of the Ministry of Economy, Trade and Industry, Japan, in FY 2009-2010.

REFERENCES

1) DTF Research Consortium: http://www.dtf.ne.jp/
2) Y. Okazaki, N. Mishima and K. Ashida: Microfactory – Concept, history and Developments, J. manufacturing Science and Engineering, Vol. 126, 2007, pp. 837-844
3) Y. Okazaki: Microfactories –A new methodology for sustainable manufacturing-, Int. J. Automation Technology, Vol. 4 No. 2, 2010, pp. 82-87
4) H. Tsuneda and K. Kobayashi: "Desk Top Factory" for the next generation manufacturing, Technical Review of Sankyo, Vol. 12, No. 1, 2003, pp. 42-46 (in Japanese)
5) K. Ashida, S. Nakano, J. Park and J. Akedo: On-demand MEMS device production system by module-build microfactory, Int. J. Automation Technology, Vol. 4 No. 2, 2010, pp. 110-116
6) T. Gaugel, et al.: Advanced modular production concept for miniaturized products, Proc. Second International Workshop on Microfactories, 2000, pp. 35-37
7) O. Klemd: Desktop Factory – New approaches for lean micro assembly-, Proc. 2007 IEEE Int. Sym. On Assembly and Manufacturing, 2007, pp. 161-165
8) S. Hara, H. Maekawa, S. Ikeda and S. Nakano: Concept of minimal fab and development of minimal equipments, J. of JSPE, Vol. 77 No. 3, 2011, pp. 249-253 (in Japanese)
9) T. Ogawa, Building of efficient, energy-saving lines with an extremely compact machining center and CNC lathe, Int. J. Automation Technology, Vol. 4 No. 2, 2010, pp. 150-154

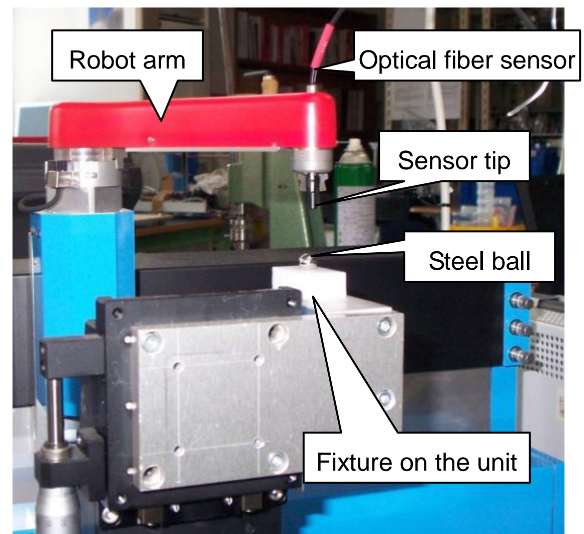

Fig. 9 Positioning calibration

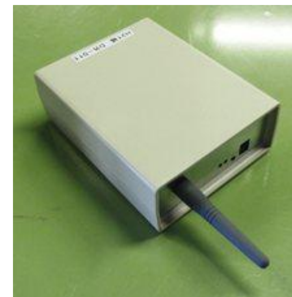

Fig. 10 Wireless communication unit

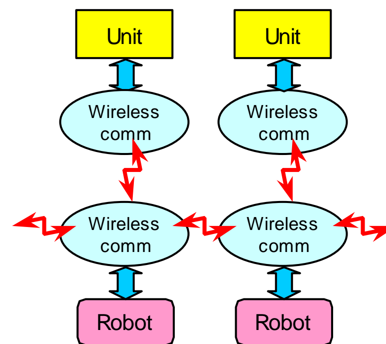

Fig. 11 Communication topology

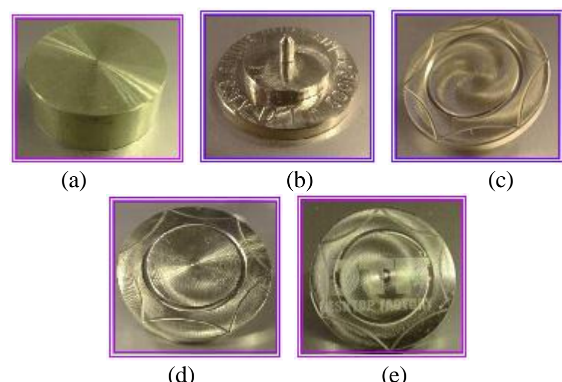

Fig. 12 Processed workpieces (ϕ25mm x t10mm)
(a) Blank, (b) Milled and engraved, (c) Ornamental milled, (d) Cleaned and plated, (e) Finished with nano-imprinting

FPGA-based high-speed object detection and classification inside optical microscopes

Claas Diederichs and Sergej Fatikow
Division Microrobotics and Control Engineering, University of Oldenburg, Germany
Corresponding Author E-mail: claas.diederichs@uni-oldenburg.de, TEL: +49-441-7984296, FAX: +49-441-4267
KEYWORDS: FPGA, Camera, Smart-Camera, Computer Vision, Visual Servoing, Neuronal Network, Connected component labeling

Object-detection and classification is a key task in micro- and nanohandling. The microscopy image is often the only available sensor to detect information about the positions and orientations of objects. FPGA-based image processing is superior to state of the art PC-based image processing in terms of achievable update rate, latency and jitter. The connected component labeling algorithm is presented and analyzed for its high speed object detection and classification feasibility. It is shown that an FPGA implementation of the algorithm can be used for high speed tool tracking as well as object classification.

1 Introduction

Image-based object-detection and classification is a key task in micro- and nanohandling, as the microscopy image is often the only available sensor in the system. The image information is used to detect and classify objects and specimen. It is also used to detect the position of the manipulator, if the used positioning system has no internal sensor or the internal sensor's resolution is not sufficient for the task. Vision-based tracking of the manipulator for the closed loop positioning is called visual servoing. State of the art is to use PC-based computer vision for both tasks. There are several algorithms available for for these tasks such as template matching or active contours ([1]).

PC-based image processing has several drawbacks for visual servoing, as discussed in [2]. The speed and quality of closed-loop control is directly connected to the speed and the quality of the connected sensors. Three main timing quality characteristics of an optical sensor are update rate, latency and jitter.

- The sensor's update rate is a limiting factor for the digital closed-loop control of a highly dynamic system. For vision-based sensor systems, the update rate is comparatively low, because a full image must be acquired and transferred. Common USB- or FireWire-cameras have update rates of 10 to 30 Hz.

- The latency of a sensor describes the age of a sensor value. With a high latency, the closed-loop control works with old data. Camera-based sensors have a high latency because an object position is calculated after a full image was captured from the camera. The latency of vision-based object tracking is usually at least one update interval.

- Jitter is time variation in a periodic signal (e.g. update rate), adding an uncertainty for closed-loop control. Jitter is a main problem in software-based object tracking on general purpose CPUs because of the unpredictable scheduling of the operating system.

One solution to overcome those drawbacks is to use hardware-based visual servoing. A Field-Programmable-Gate-Array (FPGA)-based solution was presented in [2] and further developed as shown in [3]. The presented approach uses an FPGA-based smart camera where the object detection is carried out during the image capture.

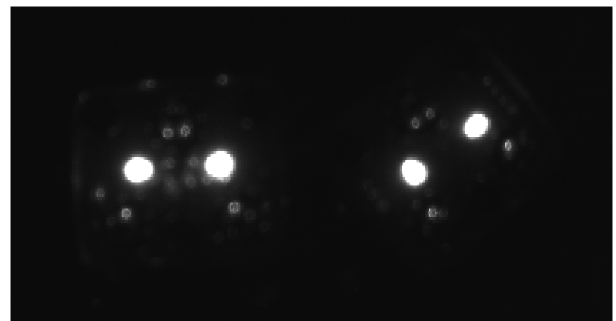

Figure 1.1: View from camera underneath mobile microrobots

The algorithm used in the described system is a special case of the binary large object (BLOB) extraction algorithm. It performs a single pass connected component labeling ([4]). The features of the objects are also detected during the single pass connected component labeling. The algorithm tracks

LEDs mounted at the bottom of the tracked microrobots, resulting in the image shown in Fig. 1.1.

The algorithm is designed for the presented special case and optimized for a small amount of regions. However, it shows gained improvement in terms of speed and accuracy for closed loop positioning. Other solutions for connected component labeling algorithms for FPGAs are presented in [5] and [6].

In this paper, the benefits of FPGA-based image processing for automated microhandling are discussed. The BLOB tracking algorithm is used as an example. It is used not only for visual servoing, but for specimen detection and classification as well. Firstly, the connected component labeling algorithm is described. Secondly, the features of objects that can be used for classification are discussed. Thirdly, different classification approaches are presented. Fourthly, experiments of closed-loop tool tracking and object classification are presented. Finally, a conclusion is drawn and an outlook stated.

2 Connected-component labeling

The connected component labeling algorithm is used to detect connected regions in a binary image ([4]). Classical approaches use a two-pass algorithm for component labeling.

The first-pass iterates through the data of the image and assigns a label to each foreground pixel. The label is assigned by taking the labels of the surrounding pixels into account. Only the pixel left of the current one and the above ones were processed earlier and have assigned labels. If one of the surrounding pixels has a valid label, the current foreground pixel gets the same label assigned. Otherwise, a new label is assigned. There a two ways of connectivity: four-connectivity (cross) and eight-connectivity (square). The pixels that are checked for label assignment are dependent on the connectivity as shown in figure 2.1.

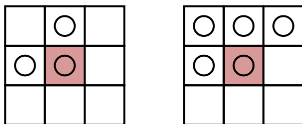

Figure 2.1: Pixels checked for label assignment: four-connectivity (left) and eight-connectivity (right).

If two of the surrounding pixels have distinct labels, these labels need to be merged in the second-pass. The algorithm stores the merge information in an appropriate datastructure.

The second-pass iterates through the result image of the first pass and relabels the elements by using the merge information. After the second-pass, all connected components have the same label.

After the components are labeled, features can be extracted for each object, using the label matrix as well as the original image.

2.1 FPGA-implementation

The above described two-pass algorithm is not suited for an efficient FPGA implementation. The label matrix as well as the image has to be stored in memory. The algorithm iterates through the image multiple times. Memory resources are limited on FPGAs. Therefore, stream processing is more suited for FPGA-based image processing ([6]). This gives an additional latency improvement as the algorithm does not need to capture the image before starting its calculation. In stream-mode, the algorithm works on the pixel-stream from the camera and can therefore start with the first pixel that arrives. Additionally, stream mode processing scales well in terms of speed and FPGA-resources if several algorithms are pipelined.

For stream-mode algorithms, a single pass connected component labeling algorithm can be used. In this type of algorithm, the merging of labels is done on the fly, often in parallel processing. Examples for stream-mode algorithms can be found in [2], [6] and [5]. Additionally, the features have to be detected during the single-pass connected component labeling.

3 Object features

Different features can be extracted for each BLOB. Examples of features are bounding box, center point and number of pixels in the BLOB.

Detecting object features during a single-pass connected component labeling without storing the image can be a challenging task. For each feature, there are several operations that have timing constraints. The feature must be *updated* with only the information of the current pixel available. The timing constraint for this operation is very strict (e.g. one cycle), as this happens frequently. If two ore more labels are merged, the features of two labels also have to be *merged*. After the merging, the feature has to be valid for the region composed of both labels. There are several features where these constraints can not be achieved, e.g. the average grayscale. It is not possible to update the average value if the size of the region is not known.

If features cannot be computed in the above described way, the have to be parted into features that can. The average grayscale can be described as follows:

$$\bar{v} = \frac{\sum_{i=0}^{n} v_i}{n} \tag{3.1}$$

The sum of all grayscales can be computed as described in the above passage, as well as the number of pixels. If the region is fully detected, a *post-processing* step can be executed to calculate the actually desired feature. The timing constraint for the post-processing is not as stringent as the others, because this step is done only once for each finished BLOB while the other operations are executed several times.

3.1 Number of pixels

The number of pixels is the easiest feature to calculate. It needs to be incremented on update and summed on merge:

$$\begin{aligned} update: n &= n' + 1 \\ merge: n &= n(a) + n(b) \end{aligned} \tag{3.2}$$

3.2 Average grayscale

The average grayscale can be computed by the sum of all grayscales and the number of pixels (see 3.1). The division is done in the post-processing step. The update and merge operations for the sum of grayscales are as follows:

$$\begin{aligned} update: v_{sum} &= v'_{sum} + v_i \\ merge: v_{sum} &= v_{sum}(a) + v_{sum}(b) \end{aligned} \quad (3.3)$$

3.3 Bounding box

The bounding box is the rectangle that encloses the found object. The bounding box consists of the four values *minX*, *maxX*, *minY* and *maxY*. Each of this values can easily be updated and merged:

$$\begin{aligned} update: x_{min} &= \min(x_i, x'_{min}) \\ merge: x_{min} &= \min(x_{min}(a), x_{min}(b)) \end{aligned} \quad (3.4)$$

The update and merge operations for *maxX*, *minY* and *maxY* are similar. The bounding box does not need a post-processing step.

3.4 Center of gravity

The center of gravity can be calculated by its parts analogous to the above described average grayscale value. The center of gravity is defined as follows:

$$\begin{aligned} x_{cog} &= \frac{\sum_{i=0}^{n} x_i}{n} \\ y_{cog} &= \frac{\sum_{i=0}^{n} y_i}{n} \end{aligned} \quad (3.5)$$

Both of these sums can be calculated analogously to Eq. 3.3.

A special case of the center of gravity is the weighted center of gravity. For this feature, a factor (the weight) is multiplied with the x and y values.

$$\begin{aligned} x_{wcog} &= \frac{\sum_{i=0}^{n} w_i \cdot x_i}{n} \\ y_{wcog} &= \frac{\sum_{i=0}^{n} w_i \cdot y_i}{n} \end{aligned} \quad (3.6)$$

For the weight w_i, the grayscale value v_i is often used. If the image is thresholded by a value v_t it is also common to use the value $v_i - v_t$.

3.5 Contour length

The contour length is the number of pixels that belong to the contour of an object. A pixel is defined as contour pixel if at least one of the surrounding pixels is not a foreground pixel.

The contour length update function needs a distinction of cases, the merge function is analogous to Eq. 3.2.

$$update: n_c = \begin{cases} n'_c + 1 & if\, p_i \in Contour \\ n'_c & else \end{cases} \quad (3.7)$$

3.6 Bounding Polygon

For a bounding octagon, the bounding rectangle feature is needed. Additionally, a 45°rotated rectangle is calculated. The rotated rectangle consists of four edges:

- $\min(x+y)$ (top left edge),
- $\max(x+y)$ (bottom right edge),
- $min(x-y)$ (bottom left edge) and
- $\max(x-y)$ (to right edge).

The minimum and maximum values of $x+y$ and $x-y$ can be updated and merged analogously to Eq. 3.4.

The rotated rectangle can be intersected with the bounding box in the post-processing step. The bounding octagon is a very rough approximation of the convex hull. The approximation can be improved by calculating finer structures, using more and differently rotated rectangles (e.g. hexadecagon).

3.7 Principal Component Analysis based features

The principal component analysis (PCA) is a method for data reduction and is well known in image processing. However, it can also be used to detect the main axis of an object ([7]). A factor PC_e which describes the relationship between the expansions of the main axis and its orthogonal axis can also be derived from the PCA ([8, 9]). For object classification, both of these features are of great interest. The computation of the PCA is a complex task and can not easily be parted into simple computations as the above features.

The PCA is computed from the covariance matrix of all points in one BLOB:

$$C = \begin{pmatrix} \mathrm{cov}(x,x) & \mathrm{cov}(x,y) \\ \mathrm{cov}(y,x) & \mathrm{cov}(y,y) \end{pmatrix} \quad (3.8)$$

Whereas the covariance is defined as follows:

$$\mathrm{cov}(x,y) = \mathrm{cov}(y,x) = \frac{\sum_{i=0}^{n} (x_i - \bar{x}) \cdot (y_i - \bar{y})}{n-1} \quad (3.9)$$

The main goal is to calculate the covariance during the update and merge process. The PCA calculation from the covariance matrix can be done in the post-processing step. In the Eq. 3.9, the local value of a pixel as well as the average value are inside the sum. This cannot be calculated like the other features, as $\bar{x}$ and $\bar{y}$ are not known during the *update* step. However, the above described constraints for the update and the merge processes can be achieved.

To be able to calculate the covariance matrix in the desired way, $\bar{x}$ and $\bar{y}$ are not allowed inside the sum. Starting from Eq. 3.9, a sequence of transformation steps will convert the equation into the desired form. The denominator of Eq. 3.9 is the number of pixels minus one. In the following, only the numerator will be transformed.

$$N = \sum_{i=0}^{n} ((x_i - \bar{x}) \cdot (y_i - \bar{y}))$$

$$
\begin{aligned}
&= \sum_{i=0}^{n}(x_i y_i - \bar{x} y_i - x_i \bar{y} + \bar{x}\bar{y}) \\
&= \sum_{i=0}^{n}(x_i y_i) - \sum_{i=0}^{n}(\bar{x} y_i) - \sum_{i=0}^{n}(x_i \bar{y}) + \sum_{i=0}^{n}(\bar{x}\bar{y}) \\
&= \sum_{i=0}^{n}(x_i y_i) - \bar{x}\sum_{i=0}^{n}(y_i) - \bar{y}\sum_{i=0}^{n}(x_i) + n\bar{x}\bar{y} \qquad (3.10) \\
&= a - b - c + d \qquad (3.11)
\end{aligned}
$$

In 3.10, $\bar{x}$ and $\bar{y}$ can be substituted with their actual computation:

$$
\begin{aligned}
\bar{x} &= \frac{\sum_{i=0}^{n} x_i}{n} \\
\bar{y} &= \frac{\sum_{i=0}^{n} y_i}{n} \qquad (3.12)
\end{aligned}
$$

Substituting $\bar{x}$ in the second term of Eq. 3.10 will result in the following equation:

$$
\begin{aligned}
b &= \frac{\sum_{i=0}^{n} x_i}{n}\sum_{i=0}^{n}(y_i) \\
b &= \frac{\sum_{i=0}^{n} x_i \sum_{i=0}^{n} y_i}{n} \qquad (3.13)
\end{aligned}
$$

Substituting $\bar{y}$ in the third term of Eq. 3.10 produces the same result. Substituting $\bar{x}$ and $\bar{y}$ in the fourth term of Eq. 3.10 results in a similar equation:

$$
\begin{aligned}
c &= n\frac{\sum_{i=0}^{n} x_i}{n}\frac{\sum_{i=0}^{n} y_i}{n} \\
c &= \frac{\sum_{i=0}^{n} x_i \sum_{i=0}^{n} y_i}{n} \qquad (3.14)
\end{aligned}
$$

Using the equations 3.13 and 3.14 the final equation from the transformed covariance computation can be created:

$$
\begin{aligned}
& b = c = d \\
N &= a - b \\
N &= \sum_{i=0}^{n}(x_i y_i) - \frac{1}{n}\sum_{i=0}^{n} x_i \sum_{i=0}^{n} y_i \\
\mathrm{cov}(x,y) &= \frac{\sum_{i=0}^{n}(x_i y_i) - \frac{1}{n}\sum_{i=0}^{n}(x_i)\sum_{i=0}^{n}(y_i)}{n-1} \qquad (3.15)
\end{aligned}
$$

In Eq. 3.15, there are three sums that can be updated and merged analogously to Eq. 3.3. The divisions and and subtractions of the sums are done in the post-processing step.

For all elements of the covariance matrix, five different sums have to be computed during the connected component labeling. In addition to the three sums shown in Eq. 3.15, two more sums have to be computed for $\mathrm{cov}(x,x)$ and $\mathrm{cov}(y,y)$. However, only the first term in the numerator of Eq. 3.15 introduces a new sum, the other sums can be reused for all covariance equations.

3.8 Feature summary

Connected component labeling extracts objects from an image. If the position of an object is known, its movement can be tracked. With all the features described above, it now becomes feasible to use connected labeling not only for object detection and tracking, but also for object classification.

4 Object classification

With a broad variation of object features, object classification based on those features becomes feasible.

One possibility is to classify the objects based on fixed, user defined bounds for features or their combinations. To detect e.g. a circle, the bounding box should be rectangular. Additionally, the PC_e energy should indicate that the shape has no significant main axis. The number of pixels in combination with the area enclosed by the bounding rectangle gives information whether the circle is filled or not. An additional indicator is the contour length. However, these bounds need to be found experimentally. Another solution is to use a self-training system.

A neuronal network is well suited to be used as a hardware-based solution. A small feed-forward neuronal network can be easily implemented for FPGA-use using a parallel pipelined approach [10]. Figure 4.1 shows a generic layout for such a neuronal network.

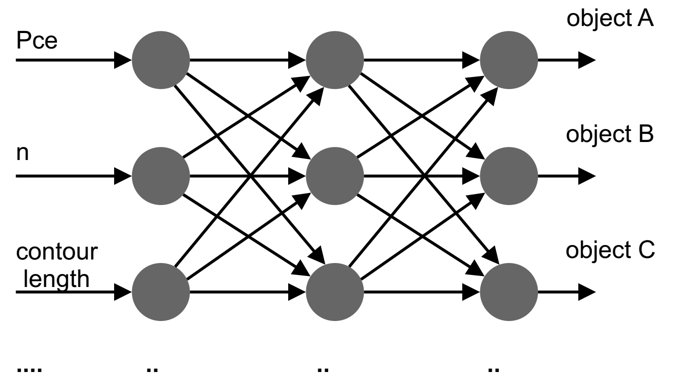

Figure 4.1: Generic layout of a feed-forward neuronal network for object classification.

Inputs to the neuronal network are the features of the BLOB extraction. As some features are not single values that can be used as input to the neuronal network, a deduction of the actual feature can be used. For a feature, several deductions can be possible. For the bounding rectangle, the enclosed area as well as the factor *height/width* are relevant sub-features for the classification. Other sub-features relevant for the classification are e.g. the length of an object in the main direction. To calculate this, a line can be drawn through the center of gravity in the direction of the main axis. This line than must be intersected with the bounding polygon, giving a close approximation of the object's length.

The outputs of the neuronal network are the different possible object types. As customary for neuronal networks used for classification, only one of the output neurons produces an output.

The training of the neuronal network is performed offline. The FPGA-based network uses the computed weights for the connections and the activation functions for the neurons.

5 Experiments

For the experiments, a microrobotic handling cell was used. The cell consists of two microrobots. The first microrobot has three degrees of freedom (x, y, ϕ). It is equipped with a specimen stub and acts as movable table. The second robot has four degrees of freedom(x, y, z, *phi*) and is equipped with a state of the art microgripper.

This cell was already used in earlier experiments regarding high speed positioning. In [11], the system was automated doing fast pick and place of microspheres using the algorithm presented in [2]; with the bottom tracking approach discussed in Sec. 1. For the experiments, a high-speed camera was mounted on top of the microscope (see Fig. 5.1).

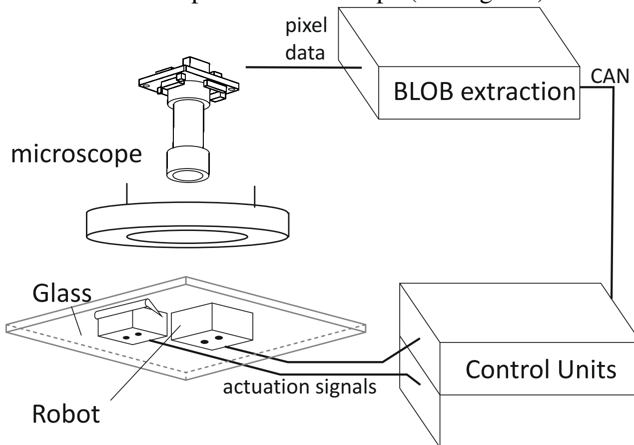

Figure 5.1: Setup of the handling cell.

The BLOB extraction hardware was tested for in tasks. Firstly, it was used as a tool tracking device to have higher placement accuracy than the bottom tracking approach ([3]). Secondly, it was used to extract and classify objects for pick and place handling.

5.1 Tool tracking

If connected component labeling is used to track a tool (e.g. a micro-gripper), the position must be determined from the above described features. There a two possibilities: track the gripper itself or track an applied marker.

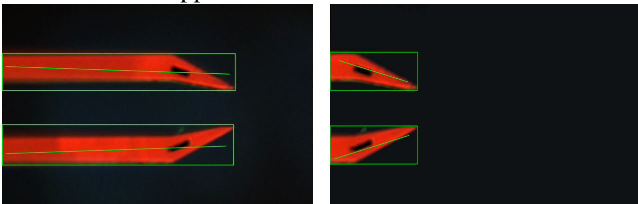

Figure 5.2: Bounding box and main axis of the gripper in two different positions.

If the gripper is tracked, the position of the gripper's tip can only be determined with prior knowledge of the gripper's orientation. While the gripper moves, the size of the gripper's region, the center of gravity and the contour length vary. Therefore, these features can not be used to find the tip position. The same limitation applies to the main axis, as the axis rotates dependent on the gripper's visibility as shown in Fig. 5.2. However, if the orientation of the gripper is known, the tip position can be taken from the bounding box. The position is not reliable if the background can be erroneously counted to the gripper. Additionally, a closed gripper is a special case that has to be treated differently, as the two regions may become one. All these limitations make the direct tracking of the gripper unfeasible.

To allow for a feasible tracking, a marker was applied to the gripper jaws. This was done using focused ion beam technology. Fig. 5.3 shows the microscopy image as well as an electron microscopy image of the applied marker.

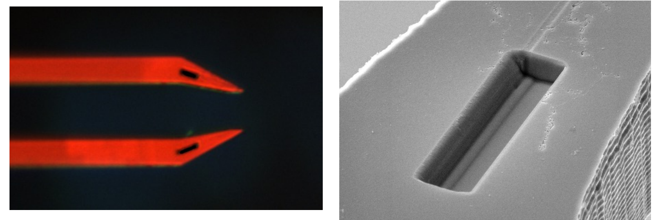

Figure 5.3: Left: Microscopy image of the gripper with applied markers. Right: Scanning electron microscope image of a single marker on the gripper jaw.

Tracking the applied marker overcomes the above described limitations. The region size of the marker does not vary significantly, nor does the center of gravity or the main axis. The main axis together with the (weighted) center of gravity can be used to locate the gripper's pick-up point. Fig. 5.4 illustrates how the point is found. The main axes of both markers are drawn through their center of gravity points. The gripper pick-up point is at the intersection of both lines. If the gripper is open, there is an offset in x direction. However, this offset can be calculated a priori. If the gripper is closed, the position is correct. As the intersection point and the two center of gravities form an isosceles triangle, the offset for the open gripper can be calculated independently of the grippers rotation using trigonometric functions.

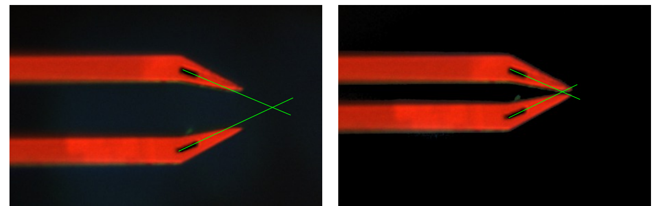

Figure 5.4: Tool placement point calculated by intersection of the main axes.

The visible scene of the microscopy image has a dimension of approx. 780×580 µm. The mounted camera has a resolution of 1024×768 px. A single pixel corresponds to approx. 0.75 µm. The resolution of the applied tracking is sub-pixel accurate. For a high accuracy, the weighted centers of gravity should be used as points for the triangle, as this has a better resolution and lower nose ([2]). The accuracy of this tracking is below 0.4 px, corresponding to less than 300 nm.

The update rate of the system is dependent on the used camera as well as the used connected-component implementation. However, with all cited implementations update rates above 200 Hz can be achieved for a one MPixel image. Additionally, the FPGA-based tracking approach is superior to software-based approaches in terms of latency and jitter as analyzed in [2].

5.2 Object detection and classification

Object detection based on static boundaries was tested. For this, microspheres of different type and material were placed

under the microscope. The goal was to classify each sphere to the correct size and material. Four different sphere types where used:

- 40 µm aluminum spheres
- 40 µm polystyrene spheres
- 53 µm polystyrene spheres
- 50 µm glass spheres

The different materials lead to different light reflections as shown in figure 5.5.

Figure 5.5: Different reflection of different materials. Left to right: aluminum, polystyrene and glass.

As the basic shape of all objects are the same, the main axis and the PC_e value have no impact on this special classification. The features with the best impact are number of pixels, bounding box area and contour length. The glass spheres additionally differ from the rest of the samples in the average grayscale.

100 samples of each object were used for classification testing. With experimentally found borders, over 95 % of the samples are classified correctly. The wrong classification was always between the polystyrene samples that only differ in size. The reasons for the misclassification are illumination and focus variations.

6 Conclusion and outlook

Image-based object-detection and classification is a key task in micro- and nanohandling, state of the art is to use PC-based systems. FPGA-based systems are superior regarding update-rate, jitter and latency.

A algorithm for hardware-based object detection is presented. The algorithm can extract several features of an object during the detection.

With new PCA-based features of regions, high-speed sub-pixel accurate tracking of a microgripper becomes feasible. Additionally, it was shown that high-speed object classification with static bounds is possible.

Future work will focus on experiments for object classification. Firstly, more different objects with different shapes and sizes will be used. Secondly, a neuronal network will be used for the object classification and compared to the static borders method. Thirdly, experiments will be performed with objects with high aspect ratio. To handle those objects with a microgripper, alignment of object and gripper has to be achieved.

REFERENCES

[1] T. Sievers and S. Fatikow, "Real-Time Object Tracking for the Robot-Based Nanohandling in a Scanning Electron Microscope," *Journal of Micromechatronics - Special Issue on Micro/Nanohandling*, vol. 3, no. 3-4, pp. 267–284(18), 2006.

[2] C. Diederichs, "Hardware-Software Co-Design Tracking System for Predictable High-Speed Mobile Microrobot Position Control," in *Proc. of IFAC Symposium on Mechatronic Systems*, 2010.

[3] ——, "Fast Visual Servoing of Multiple Microrobots using an FPGA-Based Smart Camera System," in *Proc. of the 18th IFAC World Congress*, 2011.

[4] M. B. Dillencourt, H. Samet, and M. Tamminen, "A general approach to connected-component labeling for arbitrary image representations," *J. ACM*, vol. 39, pp. 253–280, April 1992. [Online]. Available: http://doi.acm.org/10.1145/128749.128750

[5] K. Appiah, A. Hunter, P. Dickinson, and J. Owens, "A run-length based connected component algorithm for FPGA implementation," in *ICECE Technology, 2008. FPT 2008. International Conference on*, dec. 2008, pp. 177 –184.

[6] C. Johnston and D. Bailey, "FPGA implementation of a Single Pass Connected Components Algorithm," in *Electronic Design, Test and Applications, 2008. DELTA 2008. 4th IEEE International Symposium on*, jan. 2008, pp. 228 –231.

[7] Y.-S. Lee, H.-S. Koo, and C.-S. Jeong, "A straight line detection using principal component analysis," *Pattern Recogn. Lett.*, vol. 27, pp. 1744–1754, October 2006. [Online]. Available: http://dl.acm.org/citation.cfm?id=1195775.1195792

[8] T. Wortman and S. Fatikow, "Carbon Nanotube Detection by Scanning Electron Microscopy," in *Proc. of the Eleventh IAPR Conference on Machine Vision Applications (MVA)*, 2009.

[9] R. Rodrigo, W. Shi, and J. Samarabandu, "Energy Based Line Detection," in *Electrical and Computer Engineering, 2006. CCECE '06. Canadian Conference on*, may 2006, pp. 2061 –2064.

[10] V. Salapura, M. Gschwind, and O. Maischberger, "A fast fpga implementation of a general purpose neuron," in *Proceedings of the 4th International Workshop on Field-Programmable Logic and Applications: Field-Programmable Logic, Architectures, Synthesis and Applications*, ser. FPL '94. London, UK: Springer-Verlag, 1994, pp. 175–182. [Online]. Available: http://dl.acm.org/citation.cfm?id=647921.740703

[11] C. Edeler, D. Jasper, C. Diederichs, and S. Fatikow, "Fast and Accurate Pick-and-Place Automation with Nanorobots," in *Proc. of Intl. Conference on New Actuators*, Bremen, June 2010, pp. 397–400.

Fusion of Robotics and Capillary Self-assembly for Desktop Manufacturing

Veikko Sariola, Ville Liimatainen, Quan Zhou#

Department of Automation and Systems technology, School of Electrical Engineering, Aalto University, Helsinki, Finland
Corresponding Author / E-mail: quan.zhou@aalto.fi, TEL: +358-40-855-0311

KEYWORDS : Capillary self-assembly, Droplet self-alignment, Microassembly, Self-assembly, Wetting, Surface tension

Capillary self-assembly is an integration technology where the surface tension of a liquid droplet aligns parts to receptor sites. This self-alignment can used to correct the pick-and-place errors of microrobotic handling platforms. This paper summarizes our studies in capillary self-assembly, and proposes design rules based on theoretical and experimental analysis. Finally, the integration of capillary self-assembly into desktop manufacturing is discussed.

NOMENCLATURE

f	Fraction of solid surface area wet by the liquid
F_γ	Capillary force
F_μ	Viscous force
h	Liquid droplet film thickness
l	Part length
m	Part mass
r	Surface roughness
w	Part width
x	x-bias, the difference between the initial position and the equilibrium position of a part during self-alignment

Greek symbols

γ	Surface energy
θ	Contact angle
θ_0	Contact angle of a perfectly smooth surface
θ_1, θ_2	Contact angles of surface patterns 1 and 2, respectively
μ	liquid viscosity
ϕ	pad edge angle

1. Introduction

Manufacturing of high-precision microproducts traditionally often requires high-precision mechatronics and measurement systems capable of better precision than the desired results, which make the system either bulky or very expensive. On the other hand, the trend towards desktop manufacturing requires smaller system size and decreased costs, which is at odds with the requirements on assembly precision and capabilities. Thus, high-precision manufacturing becomes a challenge especially when the required throughput is high and the system size is small. Therefore, a solution to achieve high precision at high throughput with the constraint of low cost and low precision mechatronics is desired.

Capillary self-assembly process is an integration technology which achieves that performance, by correcting the pick-and-place errors of robotics using surface-tension driven self-alignment. Solder self-alignment [1] has long been used in surface-mount soldering and flip-chip assembly. Unfortunately, solders usually require high temperature processing. Furthermore, the metallic composition can have dramatic effects on the melting and wetting behavior of the solders, making it hard to apply the solders in low temperature conditions.

Our research group has done extensive studies in capillary self-assembly using water and oil-like liquids, such as low-temperature or UV-curable adhesives. This paper summarizes the results our findings, proposes design rules for practical applications of capillary self-assembly in robotic microassembly, and discusses the applicability of capillary self-assembly into desktop manufacturing.

2. Capillary self-assembly

When a droplet of liquid is placed between a part and a receptor site, the droplet forms a meniscus and aligns the part to the substrate. This is called **capillary self-assembly**[1] (Fig. 1). The phenomenon is a consequence of the surface energy of the droplet: the energy is minimized when the surface area of the droplet is minimized, i.e. when the part is aligned to the receptor site.

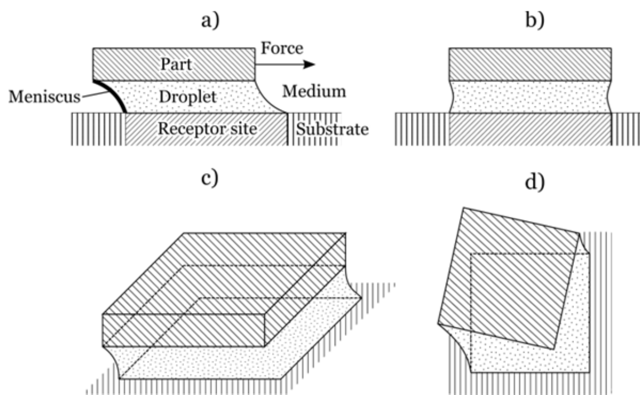

Figure 1. Illustration of the capillary self-assembly principle: a) A droplet forms a meniscus between a part and a receptor site. b) The surface tension of the droplet self-aligns the part to the receptor site. c) Perspective view of the phenomenon. d) View from the top: droplet self-alignment can correct both position and orientation of the part.

2.1 Inhibiting liquid spreading

The key to capillary self-assembly is to confine the wetting of the droplet between the part and the receptor site. The wetting properties of the surfaces depend on the surface materials, the droplet liquid, addition of surfactants, medium (air, water, vacuum etc.), temperature, surface charge etc. Two general approaches for inhibiting liquid spreading can be identified: **high wettability pad**s on a **low wettability background**, as done in the receptor site of Fig. 1, and **sharp edges**, as done with the part in Fig. 1. The approaches are illustrated in Fig. 2.

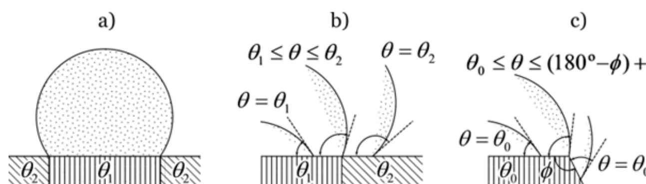

Figure 2. Inhibiting liquid spreading. a) When a droplet is placed on a pad with high wettability (contact angle θ_1) on a low wettability background (contact angle θ_2), the droplet assumes the shape of the pad. b) When there is too little liquid, the pad is not fully wetted. If there is too much liquid, the liquid overflows and wets the background. c) Liquid spreading can also be inhibited by a sharp edge

[1] Capillary self-assembly has also been called droplet self-alignment, surface tension driven self-assembly or solder self-alignment (if the liquid is solder)

High wettability is usually taken to mean contact angles less than 90º, while low wettability means contact angles more than 90º. However, this division is rather arbitrary, and for the purposes of capillary self-assembly, the **difference** between **wettability** of the areas is the important, not only the absolute values.

Many high wettability materials exist e.g. silicon dioxide [2] exhibits this omniphilic (wetted by all solvents, water contact angles around 0 – 30º) behavior. However, finding low wettability materials for low surface tension liquids (e.g. oils, adhesives) is more of a problem. The key in achieving ultra-low wettability materials is a combination of re-entrant surface curvature with low surface energy material [3].

Fluorocarbons. Fluorocarbons have the lowest surface energies known for materials [4]. Teflon-like fluorocarbons have long been known for their water and dirt repellent properties. Fluorocarbons suitable for droplet self-alignment have been deposited e.g. in a plasma process using CHF_3 [5] as the source gas. Alternatively, fluorocarbon coatings can be chemically deposited as self-assembled monolayers [6,7], based on silane or thiol chemistry. Fig. 3 shows square-shaped silicon dioxide pads on plasma-deposited fluorocarbon background. The droplets have clearly taken the shape of the pad. The wetting is incomplete only in the corners, which are rounded.

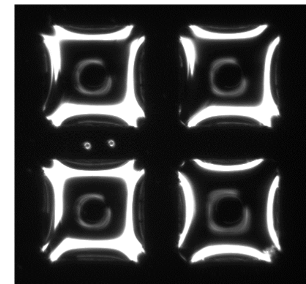

Figure 3. Water droplets on silicon oxide pads on CHF_3 plasma-deposited fluorocarbon background.

Porous structures. Porosity and re-entrant surface curvature can alter the effective contact angle on a surface [3,8]. Pockets of gas may become trapped under the liquid reducing the contact area with the droplet. Cassie-Baxter [8] equation describes the effect of the porosity and surface roughness on the apparent contact angle

$$\cos\theta = fr\cos\theta_0 + f - 1 \quad (1)$$

where θ is the apparent contact angle, θ_0 is the contact angle for a perfectly smooth surface, $r \ge 1$ is the roughness factor (ratio of the surface area to the projected surface area) and f is the fraction of the droplet area that is in contact with the surface.

Many natural and artificial materials have such a microstructure [9] e.g. lotus leaves [10] and fabrics. Several artificial methods for creating rough surfaces with reduced wettability have been proposed [11]; however, self-alignment needs not only microstructure, but also receptor site patterns on it, and not all materials are suitable for further processing

without losing their low wettability properties.

We have shown self-alignment on several different types of patterns on low wettability background based on a combination of nano-rough texture and fluorocarbon coating e.g. silicon dioxide on black silicon "nanograss" background [5] or gold patterns on fluorocarbon coated nanoporous ORMOCER [12].

Sharp edges. Pads with sharp edges can also inhibit liquid spreading [11]. The Gibbs condition for liquid confinement is

$$\theta_0 \leq \theta \leq (180^{\circ} - \phi) + \theta_0 \qquad (2)$$

where ϕ is the angle of the pad corner (see Fig. 2c). The liquid behavior is quite similar as having two wettability regions with a theoretical contact angle difference of $(180^{\circ} - \phi)$. The advantage of using sharp edges is in its simplicity: no chemical methods are needed. The disadvantage is that once the liquid spills over the edge, nothing is stopping it or dewetting it back to the pattern edge, and the self-alignment will most likely fail.

We have used SU-8 photoresist to define protruding patterns and shown self-alignment on these patterns [13]. The contact angle of our SU-8 pads is normally around 50º, but about 90º angle at the pad edge can inhibit liquid spreading until the contact angle goes past 140º.

2.2 Dynamic modeling

In the following Section, a simplified dynamic model of the capillary self-assembly is developed, which will later on be used as a basis for the design rules.

For square shaped pads (Fig. 4), by assuming a) perfect wetting of the chip and the pad; and b) parallelepiped-shaped droplet; and c) small displacement, the restoring force F_γ ("spring force") from the surface tension is given by [14,15]

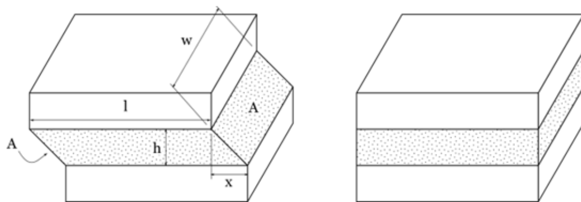

Figure 4. Approximating droplet shape with a right parallelepiped.

$$F_\gamma = -2\gamma wx / \sqrt{x^2 + h^2} \overset{x<<h}{\approx} -2\gamma wx / h \qquad (3)$$

where γ is the surface tension, *w* is the width of the chip, *x* is the displacement of the chip from equilibrium and *h* is the height of the liquid meniscus (see Fig. 4). Furthermore, assuming linear velocity profile inside the liquid, the viscous force can be written as [1]

$$F_\mu = -\frac{\mu l w}{h}\frac{dx}{dt} \qquad (4)$$

where μ is the liquid viscosity, *l* is the length of the chip and *dx*/*dt* is the velocity of the chip. Combining the two with Newton's law, we get the second order dynamics

$$m\frac{d^2x}{dt^2} + \frac{\mu wl}{h}\frac{dx}{dt} + \frac{2\gamma wx}{h} = 0 \qquad (5)$$

where m is the mass of the chip. The characteristic polynomial of the dynamic system has two poles $s_{1,2}$ at

$$s_{1,2} = -\frac{1}{2hm}\left(l\mu w \pm \sqrt{l^2\mu^2w^2 - 8\gamma hmw}\right) \qquad (6)$$

None of the assumptions of this model are entirely justified in practice, but the model already gives good understanding on the behavior of the process. For full derivation of the equation and discussion on the validity of the assumptions, interested reader should see references [16–19].

3. Design rules for droplet self-alignment

3.1 High surface tension helps liquid confinement

The surface tension of the liquid plays a role in finding suitable materials for making the patterns. Many oil-like liquids (e.g. adhesives) have a small surface tension (~ 20 – 40 mN / m) compared to the surface energy of all known materials, which means they will have a small contact angle on the solid and therefore wet the solid easily. For small surface tension liquids it is difficult to find solids with low enough energy to inhibit liquid spreading. This can be partly overcome by using a combination of porous material and fluorocarbons, but one simple solution for finding low wettability materials is to simply choose a high surface tension liquid as the self-alignment liquid in the first place.

This is partly the reason why many early self-alignment experiments in air were done using high surface tension liquids such as water [20]. When adhesives have been used, the liquid confinement is usually achieved using sharp edges instead [17,21].

3.2 Liquid volume is critical

The fluidic film height is set by the fluid volume. The restoring force (eq. 3) near the equilibrium scales as F ~ 1/h. This suggests that smaller droplets should be beneficial, due to increased forces acting on the chip. However, too small a droplet will hinder the self-alignment due to tilting of the chip and dry friction hindering the self-alignment.

If the liquid used does not evaporate (e.g. many adhesives in room temperature or solders during reflow), the liquid height is fixed and it is expected either too large or too small liquid amount to fail. We have confirmed this parabolic dependence of the success rate on the liquid volume using adhesives on oleophilic/oleophobic patterns [12]. Using parts of the size 200 µm × 200 µm, we found that the assembly was most successful with the droplet size around 0.5 nL – 1.5 nL.

Significantly smaller or larger amounts failed.

The situation is different with droplets that evaporate e.g. water in room temperature. Due to the evaporation, the droplet gets progressively smaller during self-alignment, which increases the force. There is a possibility that the increased force corrects initial alignment errors. While excessive amounts of liquid will still deteriorate the self-alignment, larger droplets are less critical for success rate. We have measured the yield of water droplet self-alignment as a function of droplet volume experimentally; the optimum water droplet volume for 300 µm × 300 µm was 1.8 nL and 98% yield was achieved when droplet volume was between 0.97 and 3.07 nL, if other parameters are kept optimal. For 100 µm × 100 µm the optimum volume was 0.7 nL [13].

For practical applications of capillary self-assembly with part sizes close to these, these values offer a reasonable starting point. However, as of yet, we have not fully confirmed how the optimum droplet volume scales as a function of pad size.

3.3 Release height is the most critical positioning dimension,

With too high releasing position, the wetting is not complete (see Fig. 5a). When the chip is released, the wetting will continue (Fig. 5b), but the progression depends largely on the initial state of the meniscus. There is a risk that the chip tilts before the wetting is complete and dry contact is created, preventing the self-alignment. Similarly, if there is meniscus at all and the chip is released, the chip can still fall due to gravity and/or speed upon release into contact with the liquid, but the wetting may not be even or fast enough to prevent dry contact failure.

If the chip is lowered too low, the liquid will bulge from the sides (see Fig. 5c). If sharp edges are used for inhibiting liquid spreading, there is a critical contact angle after which there will be catastrophic overflow of the liquid, preventing self-alignment altogether (Fig. 5d). In the case of patterns with wettability contrast, the receding contact angle of the background can still be too large for the liquid to spontaneously recede back to the pattern, and the alignment fails again.

For 300 µm × 300 µm parts we have measured the optimum release height as 47 µm and 98% yield was achieved when the release height was between 25 and 69 µm [13].

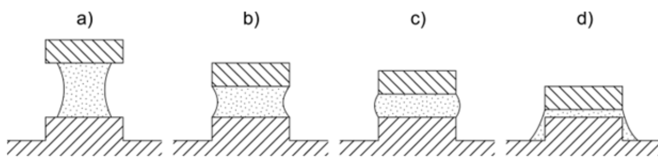

Figure 5. Effect of releasing height on self-alignment. a) Too high releasing position. The wetting is incomplete and there is a risk of failure when the chip is released. b-c) Good releasing positions. d) Too low release position. The chip was pushed too low and the liquid overflows the patterns. In the case of geometric pinning effect, there is no force to pull the liquid back, and the self-alignment most likely fails.

3.4 Low viscosity, high surface tension and smaller chip size speed up the process

In eq. 5, when the system is very damped (damping coefficient $l\mu w / \sqrt{8\gamma mwh} >> 1$), the dynamics will be slow and the self-alignment will take a long time. The dynamics are dominated by the pole s_2, which is closer to zero and it can be approximated by

$$s_2 = -\frac{1}{2hm}\left(l\mu w - \sqrt{l^2\mu^2 w^2 - 8\gamma hmw}\right) \approx -\frac{2\gamma}{l\mu} \quad (7)$$

and the associated time constant $\tau \equiv -1/s_2 = l\mu/(2\gamma)$. Larger viscosity gives slower dynamics. Larger surface tension gives faster dynamics. This is a direct consequence of the fact that liquid viscosity increases the damping force and surface tension increases the capillary force.

With high enough surface tension or low enough viscosity, the system will have two significant poles, and ultimately it will be under damped and exhibit oscillatory behavior.

Eq. 4 underestimates the viscous force and therefore the oscillatory behavior is not often observed in practice, even with low viscous and high surface tension liquids such as water. However, oscillatory behavior has been reported in very high surface tension liquids, such as solders [1].

Eq. 7 gives good rule of thumb for the scaling of the self-alignment time. The self-alignment time is expected to scale as $\sim l\mu/\gamma$, a result which can be also be derived using simple dimensional analysis. With water ($\gamma = 72mN/m$), we have measured self-alignment times of about 90 ms [13] for 300 µm × 300 µm parts in room temperature ($\mu \approx 1mPa \cdot s$). For low viscosity adhesives ($\gamma = 53.7N/m$, $\mu \approx 400mPa \cdot s$), we measured self-alignment time of 500 ms [12] for 200 µm × 200 µm parts in room temperature. When designing droplet self-alignment, these values can be used as a starting point and scaled accordingly to give an estimate of the expected self-alignment time.

3.5 High wettability contrast is beneficial

When using wettability contrast for confining the wetting, it is beneficial to have as high wettability possible for the pads and as low wettability as possible for the background so that the liquid takes exactly shape of the patterns, but does not overflow. Fig. 6a illustrates this situation.

In Fig. 6a, continuing with the parallelepiped approximation, the maximum contact angle at the pad edge is $\theta = \theta_2$ and at that moment, the displacement x is given by

$$x/h = \tan(\theta_2 - 90^\circ) \quad (8)$$

This does not mean that the self-alignment will always fail when x is larger than the limit of eq. 8, but beyond this point, there is a risk of overflowing the pattern and the dewetting characteristics of the background material need to be considered also.

When using sharp edges (Fig. 6b), the situation is slightly

different. Inserting the upper limit of eq. 2 into eq. 8 gives

$$x/h = \tan(90^{\circ} - \phi + \theta_0) \quad (9)$$

and when x is larger than given by eq. 9, the left edge overflows and the self-alignment likely fail. In reality, the meniscus is curved and the receptor site and chips are not fully wetted, so that eq. 8 and 9 give only rough estimates for the magnitude of positioning errors that can be corrected using the receptor sites and patterns.

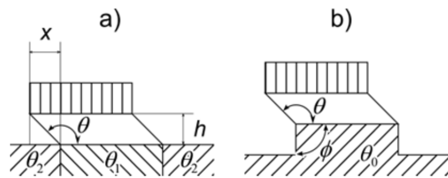

Figure 6. Maximum displacement before liquid overflow when trying to pull the chip over the pad edge when using a) surface patterns; and b) sharp edges.

4. Integrating droplet self-alignment into a desktop factory

In order to apply droplet self-alignment in a desktop factory, several steps need to be considered, including: a) how to integrated capillary self-assembly with robotic pick-and-place systems; b) how to fabricate the alignment pads? c) how to dispense liquid? and d) how to achieve final bonding. In the following subsections, we discuss potential solutions to these problems.

4.1 Integration with robotic pick-and-place systems

Capillary self-assembly can be used to correct the pick-and-place errors of robotic systems. We have previously discussed this concept of **hybrid microhandling** [22]. In hybrid microhandling, first a microrobotic handling platform picks a component, and brings it close to the assembly site. Liquid is dispensed on the assembly site, and the part is brought into contact with the liquid. Finally, the capillary self-assembly aligns the part to the assembly site.

The accuracy of the robotic systems can be very low, because the capillary self-assembly defines the final accuracy. For lateral accuracy, an estimate of the required precision can be calculated using eqs. 8 and 9. We have experimentally verified that the yield was over 98% even when the lateral positioning errors were less than 80 µm for 300 µm × 300 µm parts.

The most critical positioning dimension is the release height (see Section 3.3), so that most accurate positioning systems should be in this direction.

4.2 Alignment pad fabrication

Two major approaches for alignment pad fabrication were identified: a) creating high wettability areas on low wettability background using a combination of surface topography and surface chemistry; and b) using a pad with sharp edges for inhibiting liquid spreading.

Considering a desktop factory where all fabrication and assembly steps are carried out, the integration of chemical reactors for surface energy modification seems unlikely. Therefore, the surface energy can only be affected by the choice of the base material, and, in the case of working on single material, the choice of material affects the surface energies of both the pad and the background. Surface topography can be controlled using abrasive methods, but surface topography alone may not be enough for reliable droplet confinement.

Using sharp edges for inhibiting liquid spreading has several attractive properties considering desktop factories: it can be implemented using one material and it can naturally confine even oil-like adhesives. In practice, the sharp edges can be created using material removal methods e.g. using laser micromachining [23].

4.3 Liquid dispensing

Liquid dispensing methods can be divided into three major categories: a) non-contact methods; b) contact methods; and c) parallel, stochastic dispensing methods (Fig. 7). In non-contact methods, a droplet is shot from a nozzle to the assembly site. In contact methods, the droplet is formed into a nozzle of a needle and dispensed by bringing it into in contact with the pad. In parallel methods, liquid is delivered randomly to the substrate e.g. by condensation from vapor phase or by water mist droplets impacting on the surface. We have successfully applied all three dispensing methods in droplet self-alignment [12,13,24].

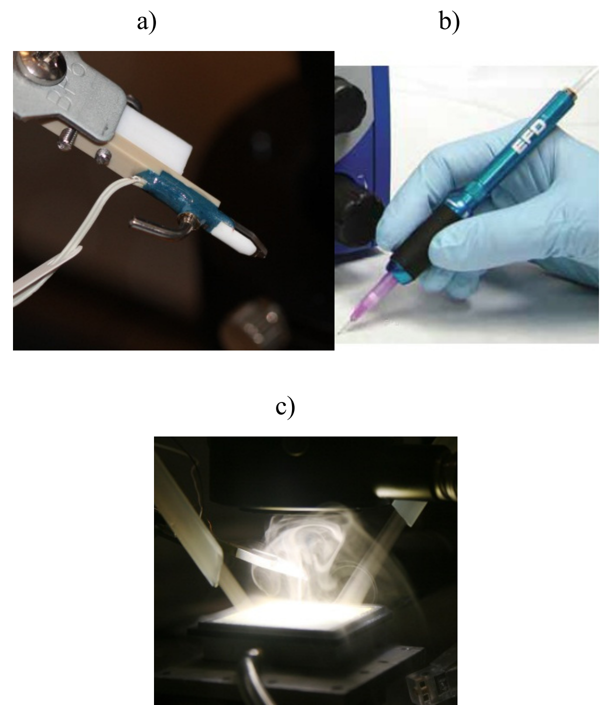

Figure 7. Liquid dispensing using a) non-contact dispenser, where the droplet is shot from the nozzle of the dispenser; b) contact dispenser, where the dispenser touches the assembly site using a needle; and c) parallel spraying using water mist.

Considering integration into a desktop factory, the most suitable dispensing method depends on the chosen liquid. In

the particular case of water, parallel dispensing from water mist has the benefit of being able to work without direct contact with the assembly operation, so that the dispensing system can be kept far away from the actual assembly operation.

4.4 Bonding

Final bonding can be achieved using a) post-bonding methods after the self-alignment e.g. part-matching, soldering or welding; or b) using bonding liquid e.g. an adhesive as the self-alignment liquid.

If post-bonding is used, then the self-alignment process is only used for the pre-alignment of the parts to the receptor sites. The main improvement is that no high accuracy robots or vision systems is required. Post-bonding using part-matching seems viable in the context of desktop factories, as the same manufacturing method used for geometric pad fabrication can be used for making the part-matching joints (e.g. pegs and holes).

Curable adhesives have the added benefit that no further bonding is required. However, adhesives have usually low surface tension and high viscosity, which complicates the self-alignment process, so that this choice is not independent from the rest of the process design. High viscosity of the adhesives requires contact dispensing, as discussed previously, and low surface tension complicates the wetting pad confinement.

Considering a desktop factory and adhesives, the curing method has to be considered also. UV-curing and temperature curing are popular alternatives. Some adhesives can be cured in room temperature, but this process is typically slower than UV- or heat-induced curing. For a desktop factory, all the methods seem viable: the integration of UV-light or heating element should not pose a too large of a problem. Fig. 8a shows UV-curing being applied in situ in a microassembly station after a capillary self-assembly operation. Fig. 8b shows results of a heat-cured adhesive after self-alignment, inspected under scanning electron microscope (SEM).

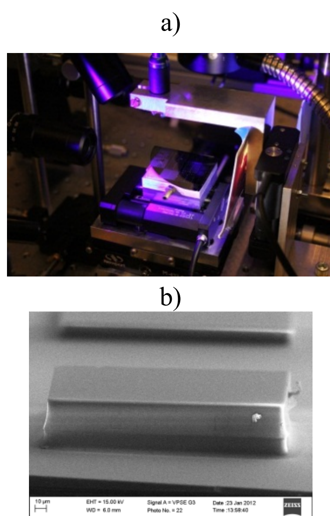

Figure 8. a) UV-curing being applied in situ, after adhesive droplet self-alignment of 200 µm x 200 µm SU-8 parts; b) Results of the self-alignment, inspected in SEM. The top chip is aligned to the bottom pattern even after curing of the adhesive.

There are adhesives with various viscosities and surface tensions with all different types of curing methods (albeit, in general, the surface tension of the adhesives tends to be low and the viscosity high). Therefore, the choice of the curing method is less restrictive in terms of the process design.

5. Conclusions

We have proposed general design rules for droplet self-alignment processes. **High surface tension** helps liquid confinement on patterns. **High surface tension, low viscosity** and **small size** speed up the process, and the self-alignment time is expected to scale as $\sim l\mu/\gamma$. The critical parameters that should be in acceptable ranges are **liquid volume** and **release height**. Finally, the liquid should be confined inside the patterns using topographical and chemical surface modification methods or by using sharp edges.

Based on previous experience and theoretical analysis of the process, we discussed the applicability of capillary self-assembly into desktop manufacturing.

ACKNOWLEDGEMENTS

This work has been supported by the Academy of Finland under Grant 134206 Programmable and Spatially Multi-scale Self-assembly of Microcomponents, MUSA (2010-2013), and the Graduate School in Electronics, Telecommunication and Automation (GETA).

REFERENCES

1. Patra, S.K. and Lee, Y.C., "Modeling of Self-Alignment Mechanism in Flip-Chip Soldering - Part II: Multichip Solder Joints," Proc. 41st Electronic Components and Technology Conference, pp. 783-788, 1991.
2. Williams, R. and Goodman, A.M., "Wetting of thin layers of SiO2 by water," Applied Physics Letters, Vol. 25, pp. 531, 1974.
3. Tuteja, A. *et al.*, "Designing superoleophobic surfaces.," Science (New York, N.Y.), Vol. 318, pp. 1618-22, 2007.
4. Drummond, C.J., Georgaklis, G. and Chan, D.Y.C., "Fluorocarbons: Surface Free Energies and van der Waals Interaction," Langmuir, Vol. 12, pp. 2617-2621, 1996.
5. Jokinen, V., Sainiemi, L. and Franssila, S., "Complex droplets on chemically modified silicon nanograss," Advanced Materials, Vol. 20, pp. 3453-3456, 2008.
6. Sabatani, E. and Rubinstein, I., "Organized self-assembling monolayers on electrodes. 2. Monolayer-based ultramicroelectrodes for the study of very rapid electrode

kinetics," J. Physical Chemistry, Vol. 91, pp. 6663-6669, 1987.

7. Barriet, D. and Lee, T.R., "Fluorinated self-assembled monolayers: composition , structure and interfacial properties," Current Opinion in Colloid and Interface Science, Vol. 8, pp. 236-242, 2003.

8. Cassie, A.B.D. and Baxter, S., "Wettability of Porous Surfaces," Trans. Faraday Society, pp. 546-551, 1944.

9. Feng, L. *et al.*, "Super-Hydrophobic Surfaces: From Natural to Artificial," Advanced Materials, Vol. 14, pp. 1857-1860, 2002.

10. Barthlott, W. and Neinhuis, C., "Purity of the sacred lotus, or escape from contamination in biological surfaces," Planta, Vol. 202, pp. 1–8, 1997.

11. Guo, Z., Liu, W. and Su, B.-L., "Superhydrophobic surfaces: from natural to biomimetic to functional.," Journal of colloid and interface science, Vol. 353, pp. 335-55, 2011.

12. Chang, B. *et al.*, "Capillary-driven self-assembly of microchips on oleophilic/oleophobic patterned surface using adhesive droplet in ambient air," Applied Physics Letters, Vol. 99, pp. 034104, 2011.

13. Sariola, V., Jääskeläinen, M. and Zhou, Q., "Hybrid microassembly combining robotics and water droplet self-alignment," IEEE Trans. Robotics, Vol. 26, pp. 965-977, 2010.

14. Tsai, C.G., Hsieh, C.M. and Yeh, J.A., "Self-alignment of microchips using surface tension and solid edge," Sensors and Actuators A: Physical, Vol. 139, pp. 343-349, 2007.

15. Lambert, P., Mastrangeli, M., Valsamis, J.-B. and Degrez, G., "Spectral analysis and experimental study of lateral capillary dynamics for flip-chip applications," Microfluidics and Nanofluidics, Vol. 9, pp. 797-807, 2010.

16. Patra, S.K. and Lee, Y.C., "Design of solder joints for self-aligned optoelectronic assemblies," IEEE Transactions on Components, Packaging, and Manufacturing Technology: Part B, Vol. 18, pp. 543-551, 1995.

17. Kim, J., Shin, Y. and Fujimoto, K., "Dynamic modeling for resin self-alignment mechanism," Microelectronics Reliability, Vol. 44, pp. 983-992, 2004.

18. Lua, H. and Bailey, C., "Dynamic analysis of flip-chip self-alignment," IEEE Trans. Advanced Packaging, Vol. 28, pp. 475-480, 2005.

19. Mastrangeli, M., Valsamis, J.-B., Hoof, C.V., Celis, J.-P. and Lambert, P., "Lateral capillary forces of cylindrical fluid menisci: a comprehensive quasi-static study," J. Micromechanics and Microengineering, Vol. 20, pp. 75041, 2010.

20. Sato, K., Ito, K., Hata, S. and Shimokohbe, A., "Self-alignment of microparts using liquid surface tension—behavior of micropart and alignment characteristics," Precision Engineering, Vol. 27, pp. 42-50, 2003.

21. Corral, C. del *et al.*, "Droplet based self-assembly of SU-8 microparts," Proc. 2nd VDE World Microtechnology Congr., pp. 293–298, 2003.

22. Sariola, V., Zhou, Q. and Koivo, H.N., "Hybrid microhandling: a unified view of robotic handling and self-assembly," Journal of Micro-Nano Mechatronics, Vol. 4, pp. 5-16, 2008.

23. Römer, G.-willem *et al.*, "Laser micro-machining of hydrophobic-hydrophilic patterns for fluid driven self-alignment in micro-assembly," The 12th International Symposium on Laser Precision Microfabrication (LPM2011), Takamatsu, Kagawa, Japan, June 7-10, 2011, 2011.

24. Chang, B., Sariola, V., Jääskeläinen, M. and Zhou, Q., "Self-alignment in the stacking of microchips with mist-induced water droplets," Journal of Micromechanics and Microengineering, Vol. 21, pp. 015016, 2011.

Optimal design of a pad type air-bearing for LCD panel inspection

S.M. Lee[1], Hong. Lu[1], M.N.Seo[1], S.C. Choi[2], J.H. Hwang[3] and D.W. Lee[4,#]

1 Department of Nano Fusion Technology, Pusan National University, Miryang, South Korea
2 Nano Convergence and Manufacturing Systems Research Division, Korea Institute of Machinery and Materials, Daejeon, South Korea
3 Department of Ultra Precision Machine and Systems, Korea Institute of Machinery and Materials, Daejeon, South Korea
4 Department of Nano Mechatronics Engineering, Pusan National University, Miryang, South Korea
Corresponding Author / E-mail: dwoolee@pusan.ac.kr, TEL: +82-55-350-5281, FAX: +82-55-351-2982

KEYWORDS : Air bearing, Air pad, Air guide, Inspection system, Glass fluctuation

LCD production is comprised of various complicated processes. A defect in LCD panel has an enormous impact on the performance of LCD so the inspection of the product is one of the very important processes. LCD inspection system can be classified into macro, micro, macro-micro composition types. Micro examination equipment is capable of precise inspection, however, takes a long time as it conducts examinations locally and macro-micro equipment is usually expensive. For this reason, macro examination equipment combined roller for in-process is used commonly. This roller method can reduce inspection time but can also cause scratches on the glass or excessive fluctuation of the glass, and such scratches can lead to LCD product defect and excessive fluctuation of glass can cause going out of the view range of the CCD camera. This study suggests the use of air pad in replacement of the roller to eliminate scratches or excessive fluctuation, the problems of roller inspection device while minimizing the inspection time.

NOMENCLATURE

AIH = Air Injection Hole
ASH = Air Suction Hole
AIP = Air Injection Pressure (P)
ASP = Air Suction Pressure (V)
Fluctuation = Glass deflection

1. Introduction

LCD is an abbreviation for 'Liquid Crystal Display' and it is widely used. LCD production is comprised of various complicated processes such as PECVD (Plasma Enhanced Vapor Deposition) → Sputtering → Photo-lithography → Dry etch. [1] After these processes, the LCD product is examined in the final inspection.

A defect in LCD panel has an enormous impact on the performance. The inspection process on the LCD is one of the very important processes, and recently companies are more emphasis on the inspection stage in order to find and resolve defect for its quality.

LCD is examined by eyes (macro), microscopic (micro) and combines (macro-micro). Micro examination equipment is precise inspection, however, it takes a long time for examinations and macro-micro equipment is usually expensive. For this reason, macro examination equipment is used commonly [2].

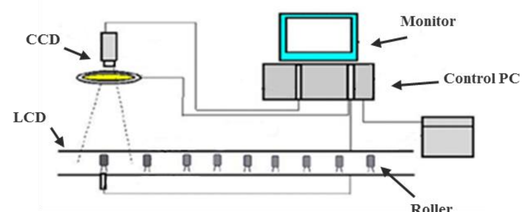

Fig. 1 Process of macro LCD inspection system [3]

Generally, the roller is applied to macro inspection system for reducing the inspection time through continuous inspection. This roller method can reduce inspection time but can also cause scratches on the glass or excessive glass fluctuation glass, and such scratches induce defects and excessive LCD fluctuation can cause the glass to go out of the view range of

the CCD camera under 30 ㎛.

This study suggests the use of air pad in replacement of the roller to eliminate scratches or excessive fluctuation, the problems of roller inspection device while minimizing the inspection time.

In the air pad inspection system, the bed comprised with inlet part, inspection area, and outlet parts is attached to the LCD glass through vacuum suction with air injection for equilibrium of air pressure while it is conveyed in the system. The inspection is conducted through the CCD camera which mounted to the inspection device. However, the pressure generated while supplying air into the air pad caused the fluctuation of the LCD glass that lead to problems such as going out of the view range of the camera (under 30 ㎛) during the inspection process. [4][5] The air pad is a device of applied the air pressure. It is generated by the air emitted through microscopic holes to act as the sliding bearing for the conveyed object [6]. Its performance is depended on the air gap between pad and glass, air suction and injection pressure, shape and size and the arrangement of the air emitting holes. For this reason, this study intends to optimize the air pad design to minimize the fluctuation of glass while conveying for satisfaction on the view range of the CCD camera.

2. Analysis of air pad used FEM

2.1 Distribution of AIH and ASH

More than the required holes will make long time and great cost. This study intended to make appropriate number of holes with the direction of progress under the influence of pressure distribution. First of all, ASH was ignored and only the effect of the AIH was taken into consideration in the FEM analysis.

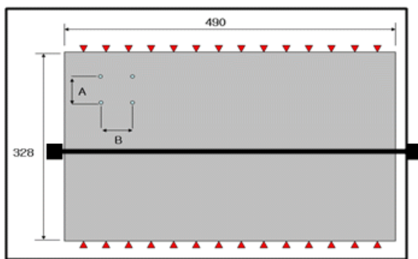

Fig. 2 Distance of each AIH

Fig. 2, A is the longitudinal direction of the air pad and B is the crosswise direction. The black line is the section of detection for the glass deflects. Analysis process is that A or B is fixed and increased for adjusting to reduce the number of holes, AIP condition is 94kPa with AIH size is ø0.3mm.

Table 1 Principal mechanical properties of LCD glass and

Thickness of LCD glass [mm]	0.7
Density of LCD glass [kg/m^3]	2600
Poisson's ratio	0.29
Young's modulus of LCD glass [GPa]	72

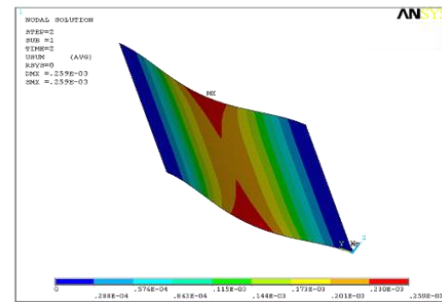

(a) Self-load

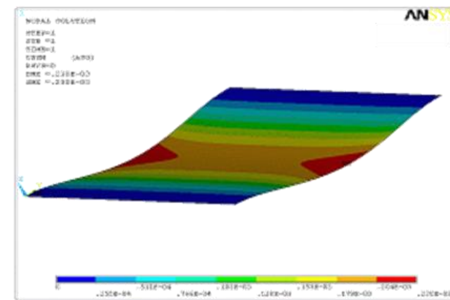

(b) 40×43mm (A×B) with air injection

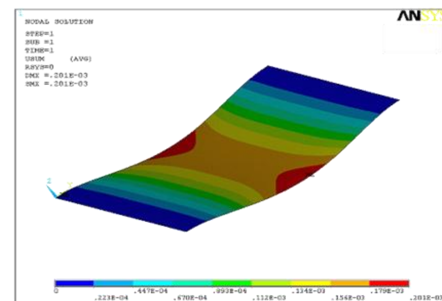

(c) 80×43mm (A×B) with air injection

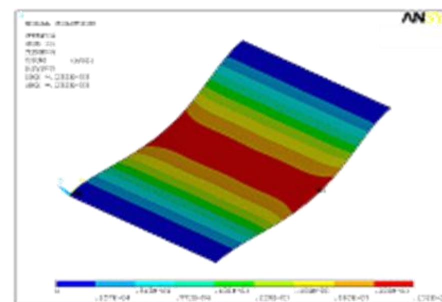

(d) 120×43mm (A×B) with air injection

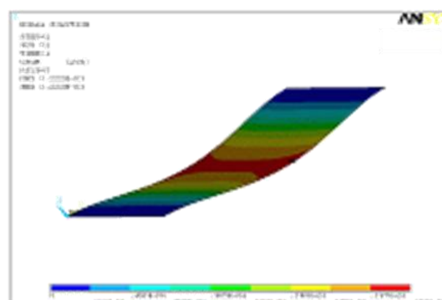

(e) 40×86mm (A×B) with air injection

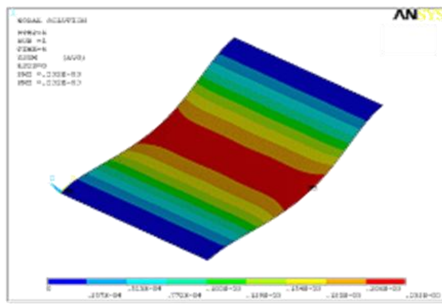

(f) 40×129mm (A×B) with air injection

Fig. 3 Glass deflection by air injection with self-load

The analysis of glass deflection by self-load with air injection is shown in Fig. 3, the difference between the deflection on both ends of the glass and the center is over 100um. When adjusting the gap in the direction B (as there are more AIH in direction B), the overall flatness of the glass increases. But it goes out of the view range within the CCD camera under 30 ㎛ as mentioned.

It was impossible to eliminate the deflection of the LCD glass by self-load only with the application of the AIH. It was assumed that the glass has to be supported with consistent force through the balance between AIP and ASP in order to eliminate deflection in the center of the glass or the lifting on both ends.

The ASH is applied to control the pressure balance and analyzed the deflection of the glass. The application of AIH, AIP conditions are 94kPa and ASP condition is 84kPa with AIH size is ø0.3mm, ASH size is ø0.5mm.

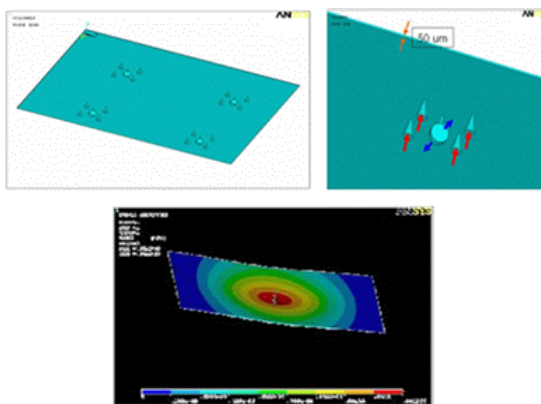

Fig. 4 Pressure distribution on the pad surface with AIP, ASP

When four AIH (14×14mm) and one ASH are applied, the deflection in the local pad was calculated to be a few nm as in Fig. 4. It is considered that there is no deflection near the air supply hole.

2.2 Equilibrium between AIP and ASP

If the ASP is applied, the glass can be stable state when the ASP distribution equals with AIP. In other words, the pressure has to be relatively equalized in order for reducing the fluctuation of the glass.

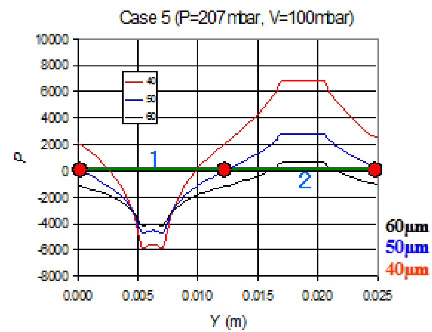

Fig. 5 Equilibrium of AIP with ASP [7]

The parallel between AIP and ASP at 50 ㎛ from the pad is shown in Fig. 5. The areas of x axis are similar to each other. Section 1 is the ASP and section 2 is the AIP. It can be applied to design the pad and the application pressure.

For analyzing equilibrium between AIP and ASP, each holes distance is 15×15mm and arranged likes checkerboard. For control the low pressure in a high pressure area, orifice or chamber must be applied to pressure dropping [8].

Pressure dropping effect by orifice is shown in Fig. 6. With ø4mm AIH and ø1mm orifice, approximately 1/3 or more pressure dropping can be achieved. In other words, low pressure can be controlled.

Analyzing conditions of orifice transformation are the AIH and ASH is ø4mm and the orifice hole is ø0.3mm. AIH and ASH are placed in the checkerboard arrangement. The AIP is 50kPa and ASP is 40kPa are applied. The pressure was formed around 50 um distance from the pad and it was constrained.

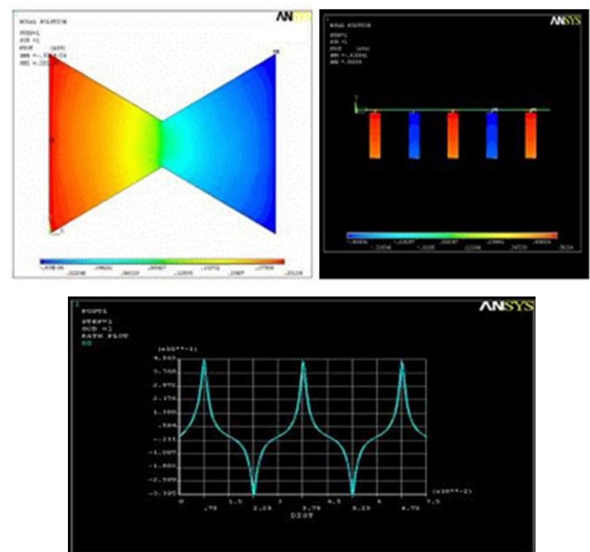

Fig. 6 Orifice effect and transformation profile

As shown in Fig. 6, the pressure profile appears symmetrically because the AIH and ASH are the same size. Also, air injection and suction are almost parallel.

3. Design of air pad on system

The air pad is divided into three types: self-compensation,

surface-compensation and porous-compensation type. Self-compensating type is easy to produce, but the repetitive error and exhausting vibration are problem. The surface-compensation type has the advantage of a great diversity and minimizing the gap to the bearing. The porous-compensation type has the multiple layer structure for preventing air hammer and can use various materials but it is relatively difficult to process and produce [9].

Self-compensation type air pad is applied in this system. It is designed such as dimensionless load capacity, dimensionless strength, and dimensionless flow. Particular it determined by MTI Chart and equations as in Fig. 7.

$$\Gamma=\frac{6\mu n d^2\sqrt{gRT_0}}{p_s h^2} \qquad W=A\overline{W} \qquad k_s=\frac{1}{h}A(p_s-p_a)\overline{k_s}$$

Γ : Coefficient of Air Supply
μ: Coefficient of Viscosity
n : Number of Micropores for Air Supply
d : Diameter of Micropores
g : Gravity Acceleration
R : Gas Constant
T_0 : Gas Temperature
p_s: Air Supply Pressure
p_a : Atmospheric Pressure
h : Bearing Clearance
A : Area of Bearing
$\overline{W}$: Dimensionless Load Capacity
$\overline{k_s}$: Dimensionless Bearing Strength

Fig. 7 Equations for air bearing design [10]

Self-compensation type air pad is designed that holes are arranged the checkerboard for the force equilibrium [11], the AIH and ASH are manufactured by FEM analysis basically. Also, it is applied to orifice.

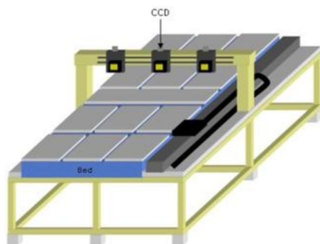

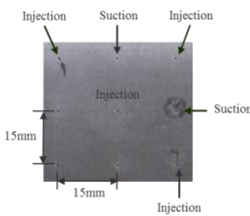

Fig. 8 Designed and manufactured inspection system with air pad

Fig. 8 is the manufactured air pad device and inspection system. The conveyer unit of the LCD glass is mounted to the air guide to control pitching, tilting, and rolling. A stepping motor was mounted under the air guide to enable precise conveyance (1/1000mm). Also, a control program was developed to control position and obtain data. For air injection and suction, separate tanks are installed to maintain the air injection and suction volume delivered from outside constantly.

4. Air pad evaluation on inspection system

Inspection device is divided into 3 paths which along carried glass direction, as shown in Fig. 9; carry in part, inspection area, carry out part, and 3 laser displacement sensors are placed in the inspection area to measure the fluctuation when conveyed the glass. The fluctuation condition by feed rate and air supply, it does not have enormous impact on the decrease or trend of the glass fluctuation [12].

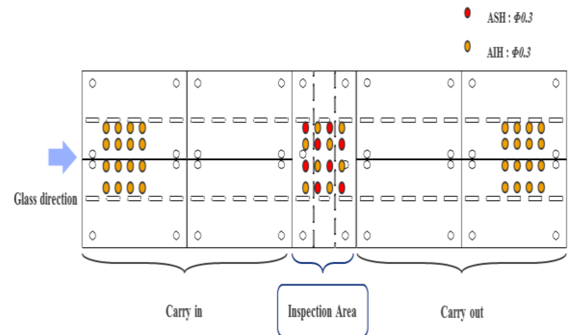

(a) Air pad of all areas on inspection system

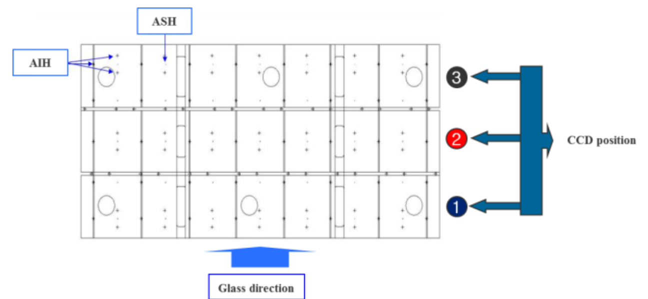

(b) Air pad of inspection area

Fig. 9 Design of air pad on inspection stem

For measure the fluctuation of glass, sensor is moved to ①, ② and ③ as shown in Fig. 9(b) while the glass is conveyed. Fluctuation is appeared differently at measurement points, as shown in Fig. 10. The glass is unstable at the beginning area of ①, fluctuation is less than 20 ㎛ at ②, and unstable again at ③. This indicates that the fluctuation of the glass decreased by the load supporting capacity increased. The AIP at the carry in and carry out part are 101kPa, and inspection area pressure is 50kPa. The AIH and ASH are arranged in the same interval (L ×L mm) in the inspection pad.

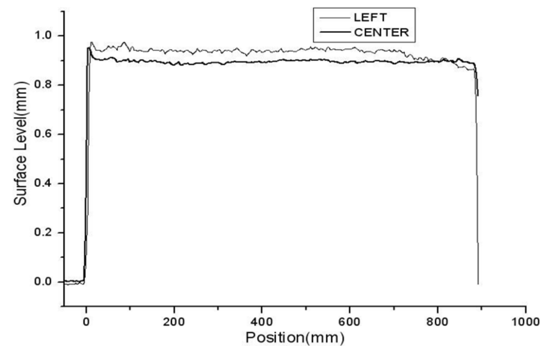

(a) Sensor position ①

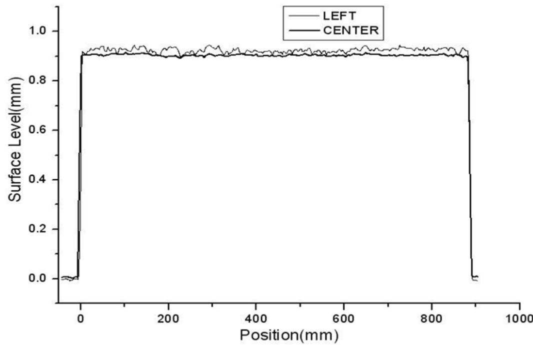

(b) Sensor position ②

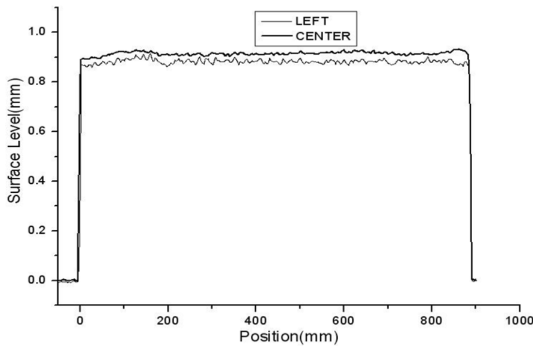

(c) Sensor position ③

Fig. 10 Fluctuation at inspection area depends on sensor positions

The AIP for the carry in and carry out part is fixed to 101kPa, the ASP of the inspection area is 50kPa, and the arrangement of holes in the all pad are changed to 2L×2L mm. Fig. 11 shows relatively unstable state compared with L×L mm arrangement and it is difficult to control the fluctuation under 30 ㎛.

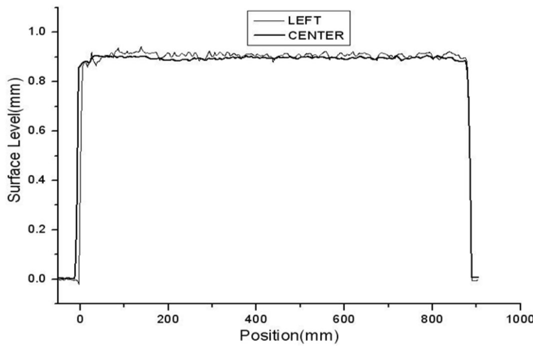

(a) Inspection part pad P = 25kPa

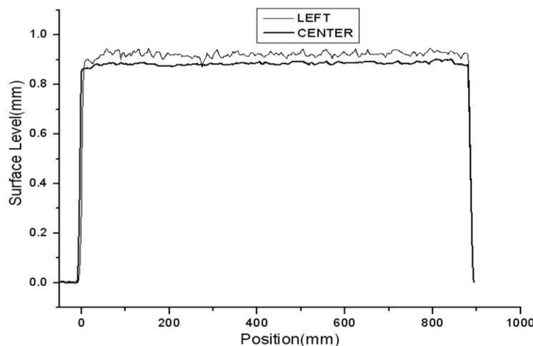

(b) Inspection part pad P = 30kPa

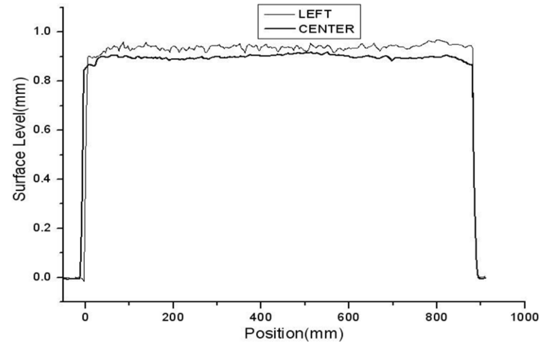

(c) Inspection part pad P = 35kPa

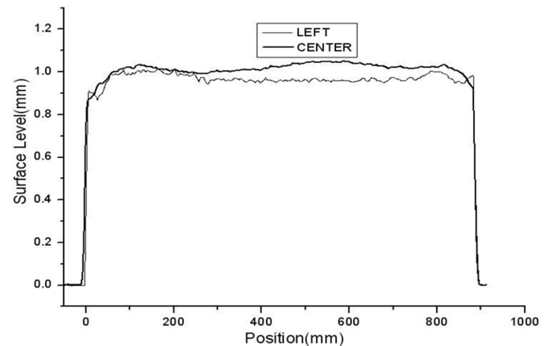

(d) Inspection part pad P = 40kPa

Fig. 11 Fluctuation at inspection area depends on gap of each hole

As shown in Fig. 11(b), the fluctuation of the glass is measured at approximately 20 ㎛ or less. This means that there is a section of stable section while maintaining glass fluctuation under 20 ㎛. For this reason, this study intended to find stable section and also check the section for the glass to be stabilized.

For measuring fluctuation of glass depended on different points at the inspection area, it is divided by L/12, inspection area length is 300mm through beginning of the inspection area to the end of the inspection area as shown in Fig. 12. CCD camera is moved to separated position and check the fluctuation of glass.

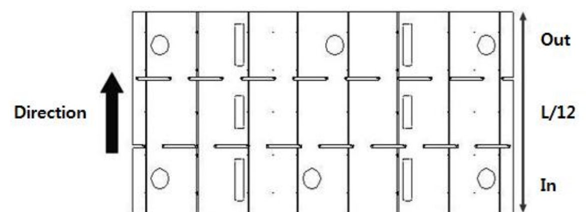

Fig. 12 Measurements of fluctuation by direction

Conditions are 101kPa of carry in and carry out parts and 38kPa of AIP and 50kPa of ASP for the inspection unit. As shown in Fig. 13(a~b), the increase of the ASP became relatively greater compared with the AIP after the glass enters the inspection area which lead to unstable area at the beginning. As shown in Fig. 13(c~d), approximately 20 ㎛ fluctuation of glass is occurred from 150mm to 250mm after

the glass entered the inspection area. This is satisfied with the ability range of the CCD camera under 30 ㎛. As shown in Fig. 12(e~f), indicate that the glass becomes increase fluctuation again in the inspection area which passed 250mm.

For this, CCD camera must be installed after the stabilizing distance and approximately 1L/2(in this system 150mm) which are applied AIH and ASH in the inspection area for stable inspection of the glass.

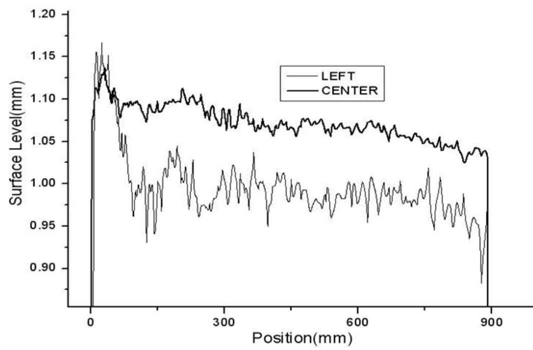

(a) Glass position = -25mm (-1L/12)

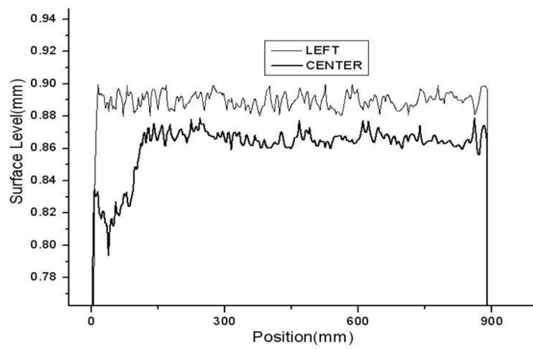

(b) Glass position = 125mm (5L/12)

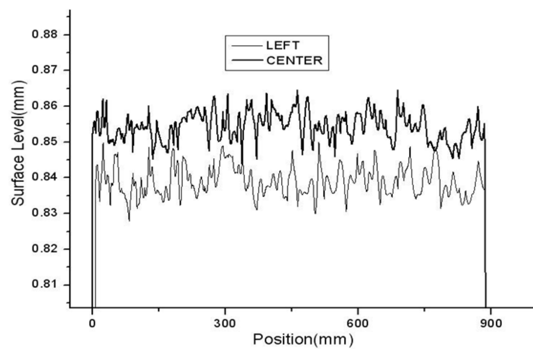

(c) Glass position = 150mm (6L/12)

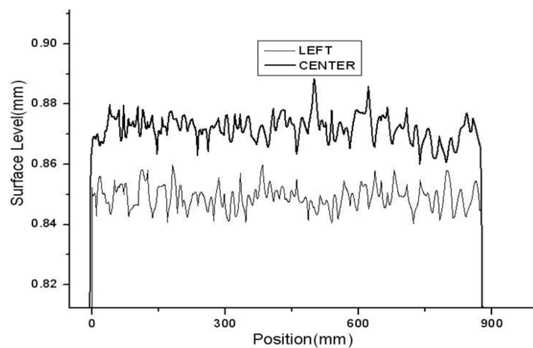

(d) Glass position = 225mm (9L/12)

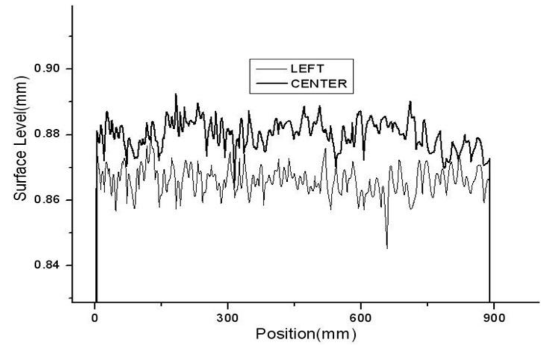

(e) Glass position = 275mm (11L/12)

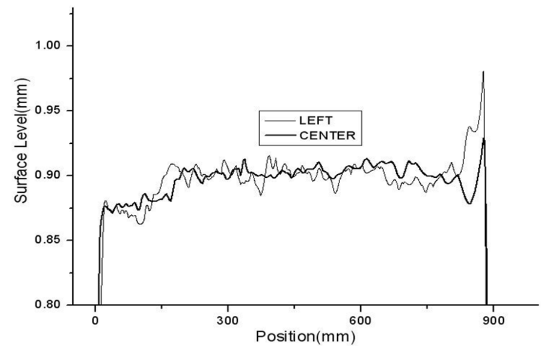

(f) Glass position = 300mm (12L/12)

Fig. 13 Fluctuation at inspection area depends on glass position

5. Conclusions

This study designed pad type air bearing and applied for LCD glass inspection system, and it is evaluated the performance. The glass is moved to inspection area in the section of 0~125mm and then after 150mm the glass is kept the stable by the AIP and ASP. But the glass is lost pressure equilibrium because of the influence of the AIP when it is out of 275mm. Finally, this paper comes to following conclusions.

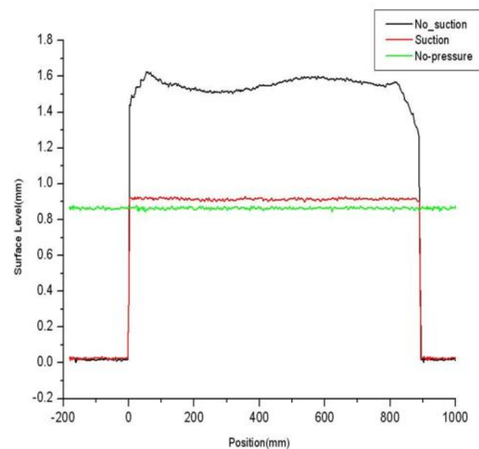

Fig. 14 Comparison with fluctuation applied for suction and non-suction at the air pad

①The air pad for the LCD glass inspection system is divided into carry in, inspection area, and carry out part, and the each part have different impact on the conveyance the

glass.

②The fluctuation of glass is approximately 100 ㎛ or greater when the air is just applied to the inspection area. This exceeds the view range of the CCD camera that the ASH becomes an essential element.

③The gap between holes and their arrangement become important factors for applying AIH and ASH at the inspection area, and narrower gap between holes and checkerboard arrangement appeared to be the most adequate. L×L mm of hole gap and checkerboard arrangement could achieve approximately 20 ㎛ or less fluctuation, and this satisfied with the range of the CCD camera for inspection.

④The inspection area is divided into L/12 to measure the fluctuation of the glass in each position. Glass stabilized gradually while it entered the inspection area and passed 0L/12mm~5L/12mm, finally continued to stabilize up to 6L/12mm~10L/12mm. Therefore, at least 1L/2mm of stabilization section is required after the glass enters inspection pad.

ACKNOWLEDGEMENT

This work was supported by NCRC (National Core Research Center) program of the Ministry of Education, Science and Technology (2010-0008-277) and "Development of accuracy simulator for rotary motion units" project of ministry of knowledge economy.

REFERENCES

1. http://www.lgphilips-lcd.com/ko/recruitment/rec01.html (LG Philips LCD)
2. http://www.kwangwo.co.kr/2002/k_lcd_detail.htm
3. Hagen. K., Ulrich. M., Peuker, Harald. P.,“Method and device for optically measuring the surface shape and for the optical surface inspection of moving strips in rolling and processing installations”, Korea Patent, App. 2004-7012273, August 2004
4. Michael Harke, Martin Stelzle and Hubert R. Motschmann, “ Microscopic ellipsometry: imaging monolayer on arbitrary reflecting supports”, Thin Solid Films, Volumes 284-285, Pages 412-416, 15 September 1996
5. G. Häusler, “ Optical preprocessing for automated inspection”, Optics and Lasers in Engineering, Volume 10, Issues 3-4, Pages 251-263, 1989
6. P. L. Holster and J. A. H. Jacobs, "Theoretical analysis and experimental verification on the static properties of externally pressurized air-bearing pads with load compensation", Tribology International, Volume 20, Issue 5, Pages 276-289, October 1987
7. Dr. Daniel Levin, "Glass handling for gen. 5 and beyond: A novel non-contact air float technology as used on Orbotech AOI", Coreflow Ltd.
8. L. Peksa, T. Gronych, J. Tesa, "Uncertainty analysis of the high vacuum part of the orifice-flow-type pressure standard", Vacuum, n Press, Corrected Proof, Available online 25 July 2004
9. Mohamed Fourka, Marc Bonis, "Comparison between externally pressurized gas thrust bearing with different orifice and porous systems", Wear, Vol. 210, pp. 311-317, September 1997
10. D. F. Wilcock, G. N. Sandor, H. Sneck, N. F. Rieger, “Notes supplemental to the RPI-MTI course on gas bearing design”, August 14-18, 1976
11. NEWS, "Small vacuum pump for precision applications", World Pumps, Vol. 2004, Issue 453, pp. 11, June 2004
12. Y.W. Kim, S.M. Lee, J.W. Park, H.S. Kim, Y.H. Moon, D.W. Lee, “Design of air bearing for CCD inspection of the flexible patterned plates”, The 2nd international conference on positioning technology (2006), pp. 112−115

Desktop factory for Micro Assembly or Lab Automation

Christoph Hanisch[1], Johannes Hoos[2]

1 Festo AG & Co. KG, Germany
2 Festo AG & Co. KG, Germany
1 E-mail: dha@de.festo.com
2 E-mail: hojo@de.festo.com

KEYWORDS : Mechatronic systems, Evolvable production systems, Adaptive manufacturing, Agent Technology

Abstract: Basic thinking in automation is purely technical oriented: how to make a certain procedure in assembly more quickly, cost efficient, avoiding if at all possible human interference. For dedicated systems, that is systems that produce large volumes of a very low variety of devices, this theory has worked well and profitable in the past. As technology is advancing and as customers' wishes get more sophisticated there is a drive towards the request of producing low or lower volumes of small devices with a high variety of product features. This is of course not new and widely discussed. The organizational answer to this bouquet of requirements often is outsourcing to so called low cost labour countries. Technology can give a differentiated response to this situation. Research in the past few years has shown that decentralized systems can be designed in a way that on the one hand human – machine cooperation allows for producing smaller volumes in a very flexible way and on the other hand the modularity of such decentralized systems enable the production (e.g. the assembly) of a large variety of products in a very economical way. This paper will present the latest results of our agentified desktop factory which allows modules for different applications to be put into operation via a real plug and produce approach and due to its control architecture will lead in the near future to a completely new way of engineering such systems.

1. Introduction

The situation of manufacturing in industrial enterprises in Europe has undergone severe changes over the last two decades. This change was mainly triggered in the beginning by saving costs in immediate production processes, later it was understood that outsourcing to low cost countries especially in Asia is not considering the overall economic picture as it might be a strategic mistake for a company to give core knowledge "out of hand". The picture changed to consider two very interesting questions:

- the local production process as a process for the local market
- how to organize manufacturing economically viable for smaller batch sizes and fast changing product variants in so called high cost labour countries.

Here we take a short cut bypassing the complex discussion of the interdependencies of the different factors influencing this area of operations of an (e.g. globally operating) enterprise by recurring to the fact that manufacturing cannot any longer really rely on cheap labour or cheap ressources at some other place in the world. The gaps of labour costs at different location in the world are closing notably. On top of this people living in 2012 have experienced unforeseen and drastic effects of natural hazards like the burst of Islantic vulcanoes as well as the yet not fully understood effects of the financial world economy. This forces to ask for some marked measures of change in running production in companies.

Why would such basically not technical argument be included in the here presented discussion on desktop factories? It is because the ongoing research under this topic and the results so far available show the potential to provide very effective answers to underlying economic problems by:

- reducing the footprint of the factory which means to reduce initial investment and running costs
- reducing the size and the weight of equipment (even if it was not supported by suitable modularity)

minimizes times of changes in the line or relocation of parts of the equipment ("put it on another desktop")

Research and development of desktop factories or mini factories has be carried out for a number of years. The technical promising possibilities that can be provided by this work to manufacturing enterprises shall be explained in detail when we address the technical requirements in the next section.

2. Problem to be tackled

Research on reconfigurable manufacturing systems has been introduced to explore technological solutions to make an otherwise rather static and product fixed production facility more flexible. Change to variants or change to new products should be faster and not so intensive on investment [1]. Flexibility is one of the keywords of this discussion [2]. The concepts of flexibility and reconfigurability were introduced as technical answers to an urgent economic problem: factory automation that is compatible even for rising product variety.

The work on flexibility in the 90ties showed the need [3] [4]to progress to adaptive systems, system that have the intrinsic capacity to adapt to change whenever new equipment or software is added. Fig.1 illustrates that this change in focus needed to reconsider the interdependency of hardware and software in mechatronic devices. Adaptabiliy increased the demand on control and software.

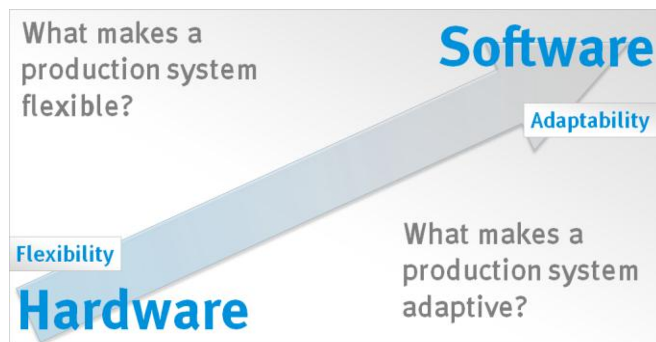

Fig. 1 Changing from Flexibility to Adaptability

Studying such systems it becomes clear that the software architecture and software content of adaptive hardware is completely different from the former generation of reconfigurable or flexible systems. As the desktop factory requires not only smaller devices but also fast reconfigurable and relocatable set ups we consider adaptability a key requirement for such installation.

3. Evolvable systems

Speed, size, software architecture and control power enable new technological solutions when it comes to the question of downsizing manufacturing equipment, integrating of additional functionality and the question of reducing ramp-up or change over times. Inspired by the mathematical theory of Mandelbrot sets the concept of evolvable assembly systems [5] [6] has been developed. Based on software agent architecture as it is used in Internet technology a software architecture for mechatronic agents has been put forth that links the mechanisms of agent technology down to actual automation hardware with IOs and mechanical motion and processes on shop floor level. Fig. 2 shows a set of mechatronic components as they could be realized with components from Festo. The appended "A" at each component indicates that the control of the component is carried out by an (decentralized) agent. The industrial component and it's functionality implemented in the agent code is now merged. A new basic building block of automation systems has been formed – the mechatronic agent.

Fig. 2 Illustration of mechatronic devices that are equipped with agent architecture

Thus a production process can be dealt with on the basis of completely new procedures. Plugging in a new module is comparable to plugging in a USB stick into a computer. The mechanical procedure of putting the stick into the plug triggers the negotiation of the new device into the system automatically without any further manual interference by the operator.

4. Point of departure

The concept of evolvable systems is especially interesting for the desktop factory application. Desktop Factories have been a research topic for some time [7] and they also have reached some industrial application [8]. Why is it such a interesting industrial topic?

For the automation of a process at subsystem level or for a complete line a system integrator's effort is devided into roughly two equal blocks of costs: project management, hardware and control plus installation, ramp-up, debugging. The second block installation, ramp-up and debugging is the one in which a modular system approach, new ways of coding, self-diagnostics, automatic code generation are very effective levers for reducing system integration costs. This is of course not limited to the desktop factory application but it is very interesting for such a field as the changing of modules "on a desk" for the next type of product within "no time" is the goal. Theoretical work [9][10] shows that these consideration are in line of system development.

5. New applications

Before entering the details of the technical work presented here we would like to discuss another important aspect such systems can provide. Traditionally we think of automation as a means to apply machine precision to a process that without such support implies lower process speed, unstable cycle times and being susceptible to many forms of human faults. This automation works as long the process under consideration is designed for high volume or may be extreme process conditions if the volume is lower. In all other cases costs for automation are considered to be too high which in turn results in seeking means to produce at lower costs someplace else.

The technology discussed here has the potential to reverse this trend to some degree as the automated line is not any longer a static installation the change of which requires huge effort. At the same time the underlying system architecture opens new ways for condition and process monitoring and supports the human personnel in a very effective way [11]. Thus new ways of running shop floor processes can emerge. The equipment is not only designed to support the human work force, but it can be used to challenge his capacities and qualities because a decentralized system can be more fault tolerant than its historic counterpart and switching between the automatic, the semi-automatic or the manual mode is achieved almost effortlessly.

6. The developed system(s)

In a road mapping exercise for the European Commission a consortium of research institutes, universities and industry described the problems that are connected with producing (or to be precise in assembling) miniaturized products for smaller and medium volumes as manual assembly is not possible due to size restrictions [12]. This study made it clear that modular, self-adaptive equipment is needed in order to assembly a variance of products cost effectively.

Fig. 3 The original MiniProd system

In a first attempt to provide equipment that can be used by many different stake holders, that can easily be supplemented with extra modules for e.g. a new technological step in the process, a national research project (MiniProd; ref.: BMBF 02PD2370) a consortium including Festo AG. & Co. KG. designed a desktop factory process on the basis of carriers driven by planar motors that can move independently to process modules (devices for different assembly tasks; clipped to edges of the table).

At the edge of the table one can see different modules like a stacker, a dispensing unit or a a mechanical unit for pressing a mechanical hub onto a device [13]. The table is equipped with a set of standardised interfaces where the modules can be “clicked” to it’s working position. These interfaces supply the modules with power, air pressure and network communication. Additionaly, a precise fixation of the units is solved by these interfaces. This first prototype was to produce a laser diode and – after change over – dispense biological liquids unto different substrates on a carrier.

The carriers can be moved freely in the plane of the table therefore it is not difficult to change the series of process steps, or use the time while one operation is carried out a specific module to exchange a module at another place. In this sense the MiniProd has to be conceived more as a tool used by intelligent humans to quickly perform a given task than a machinery of automation.

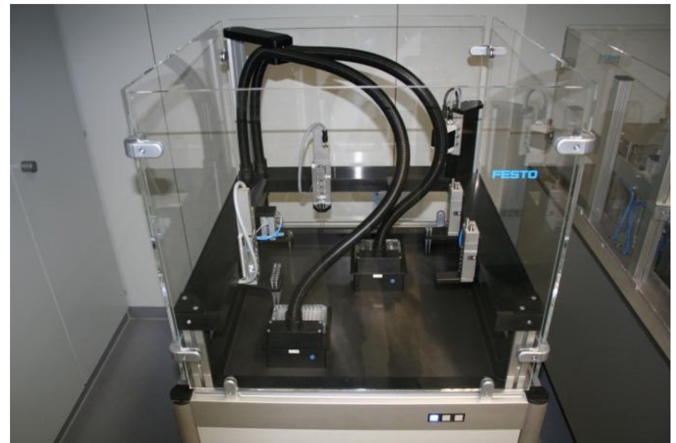

Fig. 4 A desktop set up for a biological lab applications

Clearly for the prototype concept and practice still diverge. But it is also clear that it approaches the concept for desktop manufacturing in a very nice way. In the meantime this work has continued. In the next generation of devices a smaller unit was built which aims clearly at the biological application only.

The process has a high potential for Med Lab applications. The following figure shows a device that is built according to industrial standards. The easy to change module is documented. A new module “clicked” into a specific module position is recognized and the process organized in such a way that an optimum of performance is achieved.

The fascination connected to work on desktop factories has clearly the origin of being able to move equipment quickly to new sites and / or to rearrange equipment in very small time intervals.

As described in the section on evolvability our development led to a changed system architecture compared to the first installation of the MiniProd. Such an agent based system not only meets the requirements of being able to exchange quickly modules or rearrange processes but it enters a new dimension of the desktop application.

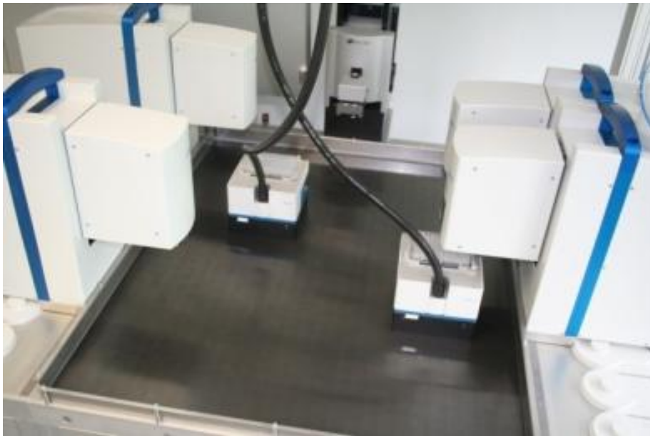

Fig. 5 Laboratory automation system (LabFab)

A product that is to be produced is entered into the system as a product agent negotiating all necessary process steps with the mechatronic equipment of the system as it proceeds through processing. This equipment includes the transportation system represented by transport agents and all kind of mechatronic process modules represented by resource agents.

Fig. 6 A module of the LabFab system

Adding a new module – because e.g. a new technology is needed – is working according to the “click trick”. The new module is connected to its position and the process is informed at the same time of the arrival of the new device and its skills. The product agent directing a new product through the process can access this new resource very quickly. One can see that this leads to new ways of process planning and programming.

7. Conclusion and outlook

So far, the concept has been tested in industrial applications. It was shown, that a dedicated software architecture combined with industrial mechatronic equipment leads to a new form of mechatronic equipment and a new control architecture for desktop factories.

The next step of development has to be an even higher degree of technology ready level. Industrial engineers need tool, that enable them to develop such kinds of systems. To achieve this, a new way of engineering has to be developed and established in industry. The product becomes a reference point. More software tools will be needed to bring laboratory set up implementation to industrial safety. This work is ongoing and it will include software that allows to compose the process without actual line coding. We see this as a bright chance for desktop applications.

REFERENCES

1. Manufuture High Level Group and Support Group, *Strategic Research Agenda-assuring the future of manufacturing in Europe*, Manufuture Platform-Executive Summary, EC, 2005.
2. Koren, Y., Jovane, F., Heisel, U., Moriwaki, T., Pritschow G., Ulsoy G., and VanBrussel, H..: *Reconfigurable Manufacturing Systems*. A Keynote paper. CIRP Annals, Vol. 48, No. 2, pp. 6-12, November 1999
3. H.A.Elmaraghy, *Flexible and reconfigurable manufacturing systems paradigms*, International Journal of Flexible Manufacturing Systems, 17, 261-276, 2006
4. Koren, Y., *The Global Manufacturing Revolution: Product-Process-Business Integration and Reconfigurable Systems*, John Wiley & Sons, Inc., ISBN: 978-0-470-58377-7, 2010
5. Onori, M., Barata, J.: *Evolvable Production Systems: mechatronic production equipment with process-based distributed control*, Proceedings of the IFAC/SYROCO Conference, Gifu, Japan, 2009.
6. Onori, M., Barata, J.: *Evolvable Production Systems: New domains within mechatronic production equipment*, in: 2010 IEEE International Symposium on Industrial Electronics (ISIE), pp. 2653-2657, Bari, Italy, 2010
7. Gendreau, D., Gauthier, M., Hériban, D., Lutz, P.: *Modular architecture of the microfactories for automatic micro-assembly*, Journal of Robotics and Computer Integrated Manufacturing, Vol. 26, No. 4 (2010), pp 354-360
8. Tuokko, R.: *Desktop Factories – Actual Knowledge Status and Experiences from Far East*, ManuFuture Conference 2011, Wroclaw, Poland, 24 October, 2011

9. Järvenpää, E., Luostarinen, P., Lanz, M. & Tuokko, R.: *Presenting capabilities of resources and resource combinations to support production system adaptation*. International Symposium of Assembly and Manufacturing (ISAM), Tampere, Finland, 25-27 May 2011
10. Nylund, H., Salminen, K., Andersson, PH., 2011, *Framework for Distributed Manufacturing Systems*, The 4th International Conference on Changeable, Agile, Reconfigurable and Virtual Production (CARV 2011),Montreal, Canada, 2-5 October, 2011
11. Hanisch, C., Munz, G.: *Evolvability and the Intangibles* , Assembly Automation, Vol. 28, Iss: 3, pp.194 – 199, 2008
12. Onori, M., Barata, J., Lastra, J., Tichem, M. *European Precision Assembly Roadmap 2010*, Document Ref.No.: D02c-2003-09-15-KTH, September 2003
13. Gaugel,T., Kegeler, J. and Munz, G.: *Miniaturized reconfigurable micro-assembly system*, International Precision Assembly Seminar - IPAS 2004, Badhofgastein - Austria, 2004

Study of the Deformation of the SMA Tool Clamping Device

Sungcheul Lee[1,#], Seung-Kook Ro[1] and Jong-Kweon Park[1]

1 Department of Ultra-Precision Machines and Systems, Korea Institute of Machinery and Materials, Daejeon, Republic of Korea
Corresponding Author / E-mail: sclee@kimm.re.kr, TEL: +82-42-868-7896, FAX: +82-42-868-7180

KEYWORDS : SMA(Shape Memory Alloy), Tool Clamping Device, Deformation Analysis

Recently small precision parts such as medical implants and mobile devices have been developed increasingly. In addition, high-precision miniature machine tool market to meet the demand for the parts of high-tech industry is growing. As a machine tools being smaller, many small key components have been actively developing.

To date, tapered collet-chuck is used device mostly at small-spindle system of machine tools in the tool holder. The usage of the scaling down tool holder system for commercial spindle such as collet-chuck is limited by their inherently complicated structural and operational mechanisms. To overcome these shortcomings, SMA tool clamping devices are suggested, which have simple structural mechanisms and enough holding forces. In this paper, the analytical deformation analysis of the tool holder is executed to estimate the characteristics of SMA tool clamping systems.

NOMENCLATURE

M_a = Moment at position A
R_a = Reaction force at A
M_b = Moment at position B
R_b = Reaction force at B
M_c = Moment at position C
R_c = Reaction force at C
I_1 = Momentum of inertia of section 1)
I_2 = Momentum of inertia of section 2)
L = Total length
a = Length of section 1)
b = Length of section 2)
a = Length of section 1)
E = Young's modulus

1. Introduction

Recently small precision parts such as medical implants and mobile devices have been developed increasingly. In addition, high-precision miniature machine tool market to meet the demand for the parts of high-tech industry is growing. As a machine tools being smaller, many small key components have been actively developing.[1-5]

To date, tapered collet-chuck is used mostly at small-spindle system of machine tools in the tool holder. However, the accumulated errors caused by the additional device, have a bad effect on the tool clamping accuracy and drop the holding forces.

We developed new conceptual tool clamping devices made by the Shape Memory Alloy (SMA) ring in order to compensate for these shortcomings. This device uses the restoring forces between the Shape Memory Alloy ring and tool holder. The restoring forces are affected by the deformation of SMA ring and the tool holder. At this point, it is important to predict the deformation of the tool holder. So, by formulating the equation of the deformation between SMA ring and tool holder, tool clamping force, such as grip strength, can be predicted.

In this paper, we define the shape of the SMA tool clamping device and represent a schematic diagram. Using a mathematical relationship, the deformation between the SMA ring and the tool holder are predicted and is compared with the result of the commercial FEA tool.

2. Schematic of the Tool Clamping Devices

2.1 Configuration of tool holder

SMA tool clamping device is composed of tool holder part and SMA ring. SMA ring stage is fixed at tight fit at the tool

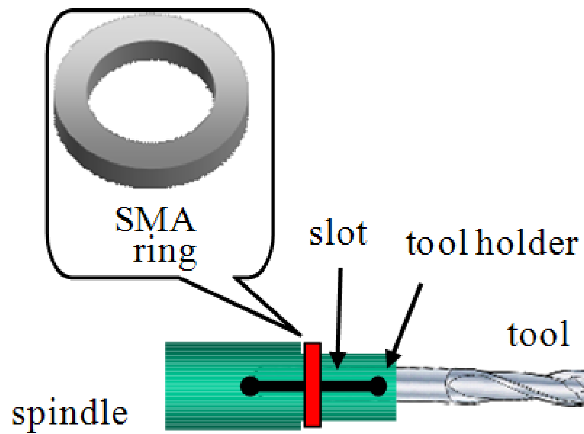

Fig. 1 Block diagram of multi-modal chatter model of a high speed machining center

holder outside. Tool holder is made up the spindle part to implement of the rotational motion of the tool holder, and the slots which increase the deformation of the holder. The diameter and the size of the hole at the tool holder are determined by considering the fit tolerance of the tool sank. At the low-temperature(martensitic phase), the hole is larger than the size of the tool, but at the high temperature(austenitic phase), is smaller than that to hold tools by contraction. This method uses the characteristics that the stiffness of Shape Memory Alloy ring changes in the condition of the temperature. Once, a tool holder and SMA rings are assembled at low temperatures, integral components are not easily separated. So the tolerance between tool holder and SMA ring is important. Thus, four slots are made on the side of tool holder unit by 90 degrees, and the slots help the elastic deformation of the radial direction when clamping and unclamping work. These slots effect greatly on the contraction of the radial deflection of the four beams.

The shape memory effect is the characteristics that Shape Memory Alloy deformed in the low temperature martensite phase, where it restored the original shape at high temperatures austenite phase. When the restoration of the SMA shape is restricted by contacting with the external structures, the restoring stress occurs. This restoration stress is used to develop the various clamping mechanisms.

At clamping device tool for machining, unlike the common clamping device, unclamping operation is important, as well as clamping work. Different kinds of tools are used at rough machining and finish machining, and especially it needs to hold drilling tool in multi-process machining. The clamping and unclamping processes are important to change these tools properly. So bidirectional shape memory effect can also be used at tool holder. However, the commonly used Shape Memory Alloy has a single-directional shape memory effect, because bi-directional one requires a special training course, and it is not fit for commercial one. In this paper, the appropriate mechanism is suggested to realize clamping and unclamping with the typical single-directional SMA ring.

The main concept is interference fit between the structural holder and SMA ring. In low temperature, the Young's Modulus of SMA ring is so low that the internal diameter is larger, and tool can be unclamped. However, maintained at room temperature, tool holder is shrunk due to the stress caused by SMA ring at austenite condition. Young's Modulus increased, then internal diameter of tool holder diminished and can clamp the tool. That is to say, it is a key technology to determine the holder diameter larger than tool diameter at low temperatures, and smaller than that to clamp the tool at room

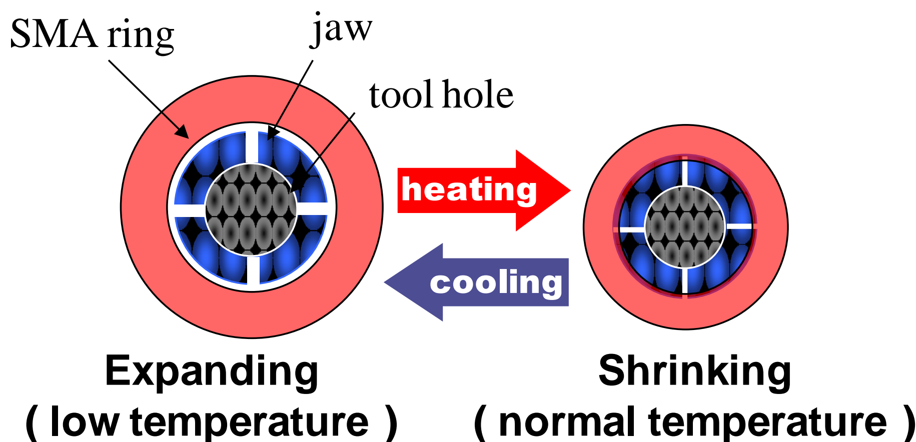

Fig. 2 The schematic diagram of clamping and unclamping of tool holder

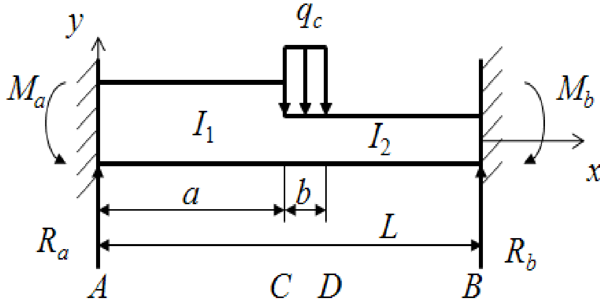

Fig. 3 Schematic diagram of simulation

temperature.

3. Analysis

3.1 Schematic diagram of analysis

In order to obtain the deformation of the tool holder portion, the other ends with the moment of inertia of the system was defined as a form of built-in beam. In addition forces, q_c, by SMA rings act in the middle part of the beam. By using force equilibrium equation, moment equilibrium equation, and displacement and angle relations, the governing equations can be calculated. And also simulation result can be compared with the result of the commercial FEA tool.

Equation is as follows.

- Force equilibrium equation

$$R_a + R_b - q_c b = 0 \tag{1}$$

- A momentum equilibrium equation at the point A.

$$M_a + M_b + R_b L - q_c b\left(a + \frac{b}{2}\right) = 0 \tag{2}$$

3.2 Displacement curve equations by the interval

The whole bar is divided by three sections and the curve equation is available in the specified interval. The displacement curve equation by the interval is as follows.

1) $0 \le x \le a$

$$v_1 = \frac{1}{EI_1}\left(\frac{R_a}{6}x^3 - \frac{M_a}{2}x^2 + C_0 x + C_1\right) \tag{3}$$

2) $a < x \le a + b$

$$v_2 = \frac{1}{EI_2}\left\{-\frac{R_b}{6}(x-L)^3 + \frac{M_b}{2}x^2 - \frac{q_c}{24}\{x-(a+b)\}^4 + C_2 x + C_3\right\} \tag{4}$$

3) $a + b < x \le L$

$$v_3 = \frac{1}{EI_2}\left\{-\frac{R_b}{6}(x-L)^3 + \frac{M_b}{2}x^2 + C_4 x + C_5\right\} \tag{5}$$

3.3 Constraint equation

Boundary equation is expressed as follows.

Force equilibrium equation:

$$R_a + R_b - q_c b = 0 \tag{6}$$

Momentum equilibrium equation:

$$M_a + M_b + R_b L - q_c b\left(a + \frac{b}{2}\right) = 0 \tag{7}$$

At point A, the slope angle is zero,

$$C_0 = 0 \tag{7}$$

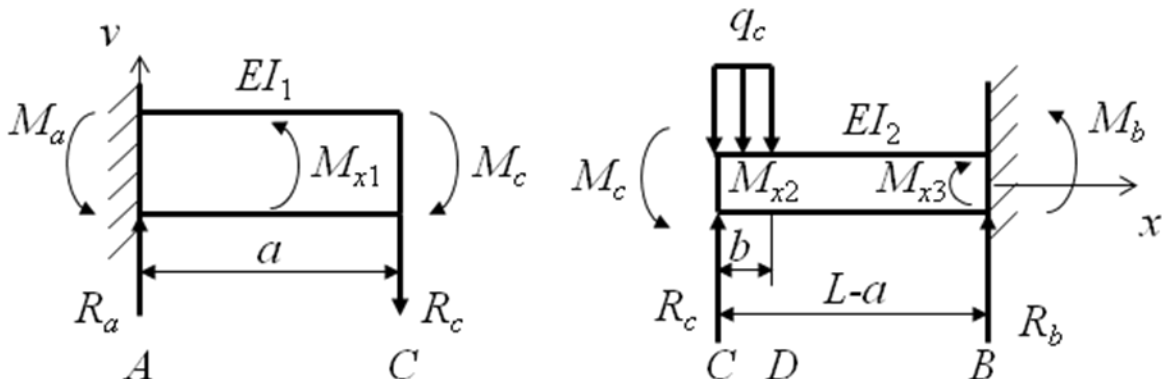

Fig. 4 The schematic diagram by the sections

Table. 1 Input parameters simulation result

I_1 (mm^4)	5.008	I_2 (mm^4)	0.406
Dia. of SMA ring (mm)	5.0	Dia. of Tool holder (mm)	5.2
q_c (Mpa-mm)	3,615	L (mm)	6
a (mm)	2	b (mm)	2
Ma (Nmm)	12,067	Mb (Nmm)	2,587
Ra (N)	5,195	Rb (N)	2,035

Displacement at point A is zero,

$$C_1 = 0 \tag{8}$$

The slope angles are same between left and right sections at point C

$$\frac{1}{EI_1}\left(\frac{R_a}{2}a^2 - M_a a + C_0\right) = \frac{1}{EI_2}\left\{-\frac{R_b}{2}(a-L)^2 + M_b a - \frac{q_c}{6}(-b)^3 + C_2\right\} \tag{9}$$

The displacements are same between left and right sections at point C

$$\frac{1}{EI_1}\left(\frac{R_a}{6}a^3 - \frac{M_a}{2}a^2\right) = \frac{1}{EI_2}\left\{-\frac{R_b}{6}(a-L)^3 + \frac{M_b}{2}x^2 - \frac{q_c}{24}(-b)^4 + C_2 a + C_3\right\} \tag{10}$$

The slope angles are same between left and right sections at point D,

$$C_2 = C_4 \tag{11}$$

The displacements are same between left and right sections at point D,

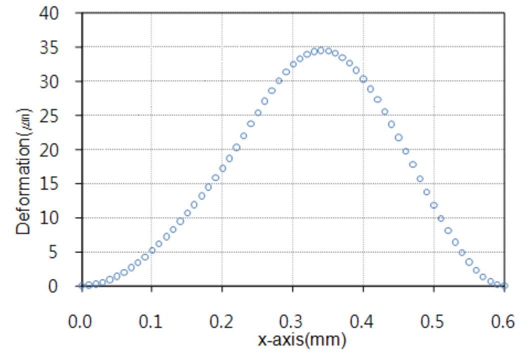

Fig. 5 The estimated result by Matlab

$$C_3 = C_5 \tag{12}$$

Angle is zero at the point B,

$$M_b L + C_4 = 0 \tag{13}$$

Displacement is zero at point B,

$$\frac{M_b}{2}L^2 + C_4 L + C_5 = 0 \tag{14}$$

Ten equations can be obtained and also, the number of variable is ten, $R_a, R_b, M_a, M_b, C_0, C_1, C_2, C_3, C_4, C_5$. The corresponding values can be obtained for each variable.

Numerical analysis is executed by using MATLAB and implementation results are summarized as follows. The results of a calculation of the governing equations are as follows: analysis shows that the maximum displacement is 34.5 ㎛ at 0.34mm from the original position. In particular, the position of the maximum displacement is not the center of the beam but the right side by 0.04mm at the center point.

3.4 Simulation by commercial FEA tool

The shrinkage deformation according to the direction of

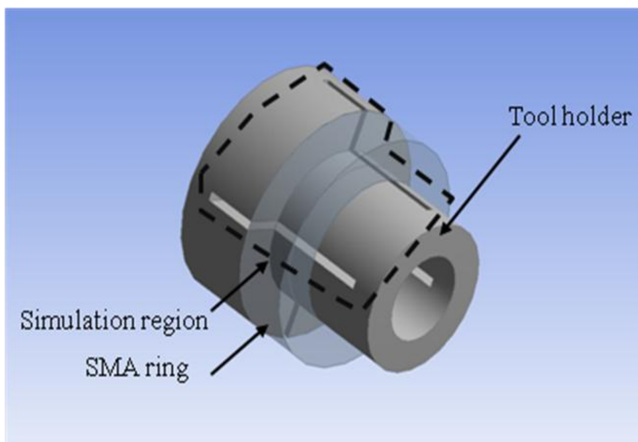

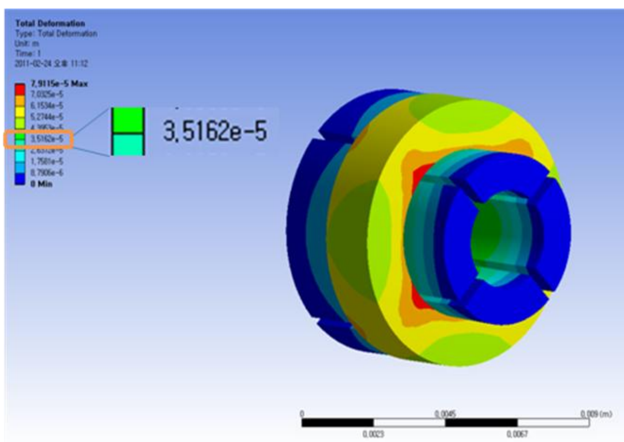

Fig. 6 The FEA result by ANSYS

the diameter of tool holder was studied by using commercial finite element program (ANSYS). Organization of the initial condition is equivalent to the Matlab simulation conditions and SMA ring is assumed austenite phase. The calculated results were compared with the ANSYS simulation ones by comparing the displacement at the maximum displacement point.

ANSYS simulation results showed 35.2 ㎛ as maximum displacement value. Estimated simulation result is different from the ANSYS result by 2 percent.

4. Conclusion

The deformation analysis of SMA tool clamping device is performed. To obtain the deformation of the tool holder the governing equations are solved and the simulation was performed. The estimated result was compared with the result of commercial FEA tool, and the difference between them is 2 percent.

ACKNOWLEDGEMENT

This work was financially supported by the grant from the Industrial Source Technology Development Program of the Ministry of Knowledge Economy(MKE) of South Korea.

REFERENCES

1. Chung, J.M., Shin, W.C., Park, J.K., and Lee, D.J., "implementation of the rotating tool clamping device using a shape memory alloy," Transaction of the korea society of machine tool engineers, Vol. 17, No. 1, pp. 16-20, 2008
2. Rivin, E. I., “Tooling Structure: Interface between Cutting Edge and Machine Tool,” Annals of the CIRP, Vol. 49, pp. 591~634, 2000.
3. Kim, S. J., Bae, M. I., Kim, H. C., and Kim, K. S., “A study on the design, manufacturing and performance evaluation of air bearing spindle for PCB drilling,” Journal of the Korea Society of Precision Engineering, Vol. 23, No. 4, pp. 29~36, 2006.
4. Shin, W. C., Ro, S. K., Park, J. K., Lee, D. W., and Chung, J. M., “Investigation for Clamping Properties of the Tool Clamping Devices based on the Shape Memory Alloy for Application of a Micro Spindle System,” Transaction of the KSMTE, Vol. 16, No. 6, pp. 9~14, 2007.
5. GSI Group, Inc., PCB spindles, August 2007, http://www.westwind-airbearings.com/pcb/index.html
6. Choi, C.-H., “High Speed Machining & Technology of Tooling for Die and Mold Making,” Journal of the Korean Society of Precision Engineering, Vol.18, No.8, pp.18~23, 2001.
7. Rivin, E.I., “Tooling Structure: Interface between Cutting Edge and Machine Tool,” Annals of the CIRP, Vol.49, pp.591~634, 2000.
8. Park, C.-W., Kwon, K.-S., Kim, W.-B., Min, B.-K., Park, S.-J., Sung, I.-H., Yoon, Y.S., Lee, K.-S., Lee, J.-H. and Seok, J., “Energy Consumption Reduction Technology in Manufacturing - A Selective Review of Policies, Standards, and Research,” Internationa Journal of Precision Engineering and Manufacturing, Vol.10, No.5, pp.151~173, 2009.
9. Shin, W. C., Ro, S. K., and Park, J. K., “Shrink Fit Tool Holder Using Shape Memory Alloy: Feasibility Test,” Proceeding of the KSMTE Spring Conference 2010, p.36, 2010.
10. Lee, D. J., Shin, W. C., Park, H. W., Ro, S. K., Park, J. K. and Chung, J. M., “Design of Tool Clamping Device Based on a Shape Memory Alloy,” Transaction of the korea society of machine tool engineers, Vol.17, No.5, pp.70~75, 2008.
11. Otsuka, K., and Wayman, C. M., Shape Memory Materials, Cambridge University Press, New York, pp.49~96, 1998.
12. Lee, H.U., Cho, D.W., Ehmann, K.F., Ko, T.J. and Yun, W.-S., “Prediction of Cutting Forces in Micro-End-Milling Using the Cutting-Condition- Independent Cutting Force Coefficients,” Transactions of NAMRI/SME, Vol.34, pp.453~459, 2006.

Micro-parts handling system for micro assembly with manual operation

Kensuke Tsuchiya [1,#], Masamitsu Nakaminami[2], Kiyokazu Saito[3], Yonezo Nakajima [3] and Takeshi Kawaguchi [4]

1 Institute of Industrial Science, The university of Tokyo, Tokyo, Japan
2 MORI SEIKI Co., Ltd., Nara, Japan
3 IRISO SEIMITSU Co., Ltd., Saitama, Japan
4 Honda R&D, Saitama, Japan
Corresponding Author / E-mail: tsu@iis.u-tokyo.ac.jp, TEL: +81-3-5841-6229, FAX: +81-3-5452-6228

KEYWORDS : Micro parts, Assembly, Manual operation, Manipulator

The authors have been developed a handling system for micro parts. Recently general cutting machine tools have realized 0.1mm micro parts with sub-micrometer accuracy. However there have been no enough assembly tools for such micro parts.
We newly designed a micro parts handling system, and developed a prototype. It has two microscopes, two arms and a table. We can observe top view and side view of the workspace. Each arm has 8 degrees of freedom. All rotation centers are adjusted at the tip end of the arm by R-guide in order to rotate micro parts without moving the position. The table has 4 degrees of freedom. The system has totally 20 degrees of freedom, which allowed us any assembly task. Micro grippers are installed on the tip ends of the arms, however they can be changed to other tools according as the assembly task. We suppose that the system is located machining, and used for assembly of micro parts of 0.1mm size. It means the system is desired to be inexpensive, compact and lightweight, strong against dusty environment. For this reason, the system has minimal resolution, minimal accuracy, no feedback control, a lot of mechanical drive mechanisms.
In order to evaluate the prototype system, we executed several demonstration tasks. At first we inserted 0.05mm shaft into 0.06mm hole. We achieved the task in 1 minute with the system, while we could not complete it without the system. Nextly, we arranged 0.3mm precise dices on the substrate with curved surface such as rice grains. The operator did it for the first time, however the task was completed in 10 minutes. Then he repeated the same task, it was completed 5minutes in second trial, 3 minutes in third trial downward. This result indicates that it is easy to learn system operation. Through these evaluation, it has been confirmed that the our system is useful for assembly of micro parts..

1. Introduction

Information equipment, optical devices, and medical equipment have been increasingly miniaturized and highly integrated. This trend is a result of the advances in lithography and nanoimprinting technologies. These technologies can be used for fabricating two-and-a-half-dimensional shapes on the surface of objects, but not for fabricating three-dimensional objects with small overall dimensions.

Recently, the performance of machine tools and cutting tools has improved, which has enabled the microcutting of parts with submillimeter overall dimensions and a dimensional accuracy of approximately 1 μm. However, methods of repeatedly and stably performing the processes conventionally carried out manually, such as handling, assembly, jointing, and adjustment, before and after fabrication have not been established. The setting and attachment/detachment of work, which are part of the submillimeter-order microcutting process, require much time and effort and are very difficult to perform because the work are so small that they cannot be identified by visual observation.

Although handling systems that can support cutting tasks are required to solve the above problem, the functions of most of the existing handling systems have been designed to transfe r and sort small granular objects. Moreover, such systems ha ve not been widely used as a tool to support microcutting beca use (1) they cannot freely perform tasks as they have few degr

ees of freedom, (2) their portability is low because of their large structure, and (3) the cost is high owing to an excessively high positioning accuracy.[1,2]

In this study, we develop a practical handling system to support the fabrication of micro-parts by cutting.

2. Development of system

2.1 Design of system

In this study, we targeted micro-parts with dimensions of 0.1 mm order that can be fabricated using current state-of-the-art machining technology.

We first focused on the processes of transferring and assembling micro-parts to develop the system. From the viewpoint of engineering, the function required for these processes is for multiple micro-parts to settle into predetermined positions through their relative motion. These processes include the insertion, fitting, and sliding insertion of two micro-parts as well as the switching of planes to be processed during six-side fabrication, tightening of screws and bolts, and connection of wires to connectors.

First, magnified observation is required for handling micro-parts. At this time, micro-parts should be observed from multiple directions rather than a single direction, because three-dimensional spatial information is required for three-dimensional handling. In addition, the workspace should be lit from multiple directions, which will help when checking the surface roughness and the contact state of the objects, owing to the shade and contrast with the background.

Next, at least six degrees of freedom, i.e., three translational degrees of freedom and three rotational degrees of freedom, are necessary for a manipulator to freely control the position and angle of micro-parts. In this study, we added two more degrees of freedom; one is a translational degree of freedom in the arm direction and the other is a degree of freedom to open or close a gripper at the end of the arm, as shown in Fig. 1. These degrees of freedom were determined by considering the operation of inserting a micro-part while rotating it, similar to the tightening of screws.

Moreover, two arms with the above eight degrees of freedom are incorporated into the system considering operations such as passing micro-parts, pinching and inserting them, and positioning and jointing two micro-parts at once. The table to hold micro-parts is also given a total of four degrees of freedom, i.e., three translational degrees of freedom and a rotational degree of freedom.

Micro-parts handling systems cannot necessarily be downsized although they handle fine targets. Therefore, microscopes used for observation and working mechanisms such as arms must be arranged to surround target micro-parts[3], as shown in Fig. 2. Also, the micro-parts, the focal point of the microscope, the end of the arms, and all the rotational centers of the arms in the manipulator must be directed to one point. Otherwise, the operator may lose micro-parts during operation, or the end of the arm may go out of the field of view, making the operation difficult to continue.

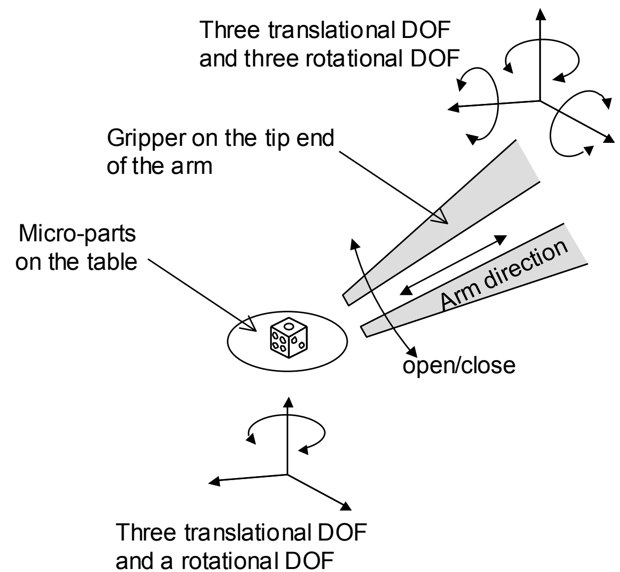

Fig. 1 Required degrees of freedom for the handling system. The arm is given four translational degrees of freedom and three rotational degrees of freedom and one open/close degree of freedom. The table is also given three translational degrees of freedom and a rotational degree of freedom.

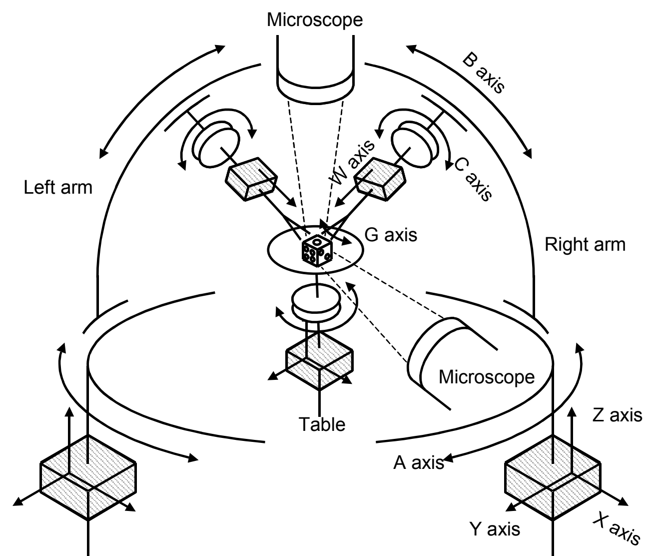

Fig. 2 Configuration of the handling system which consist of two arms and two microscope and a table. All the components are arranged to surround target micro-parts.

Commercially available handling systems have few degrees of freedom but excessively high performance for each degree of freedom, exceeding that required to handle machined parts; for example, they are equipped with coarse-motion and fine-motion mechanisms at a resolution of 10 nm. In addition, some handling systems are equipped with a high-resolution optical or electron microscope for observation. In this study, the positioning accuracy and observation resolution of the system are suppressed to the minimum necessary levels (2-10 μm) because the system targets 0.1-mm-order machined parts. Thus, we minimize the cost of the entire system

with the aim of realizing its practical application.

2.2 Development of prototype system

Fig. 3 shows the outline of the prototype system developed. Two charge-coupled device (CCD) cameras with a DFK61AUC02 lens (The Imaging Source Co., Ltd.) were placed above and in front of the work space to obtain three-dimensional visual information. The observation area is 5 × 5 mm2 and the observation resolution is approximately 5 μm. Zooming is digitally performed. Images are displayed on the monitor next to the system.

There is another method of conveying the stereoscopic effect to the operator using images taken from two different angles (right and left), similar to human eyes, which is referred to as the stereoscopic view. However, quantitative depth information (positional relationship in the viewing direction) obtained by the stereoscopic view is not accurate although it is easy to instinctively understand the shape and positional relationship of micro-parts from a single image. This is similar to the fact that it is difficult to visually measure the distance between micro-parts that are lined up along the viewing direction. In contrast, the multiview method adopted in this study can accurately convey three-dimensional information to the operator because the object can be viewed from the side to obtain depth information. However, individual images do not provide the stereoscopic effect owing to a lack of information for one dimension, and the operator must understand the three-dimensional information cognitively rather than intuitively. Thus, each method has both advantages and disadvantages, and we adopt the multiview method to ensure the accuracy of operation.

A mechanism with which a slider moves on an arc guide was adopted to match all the rotational centers of the arm to its tip end. A structure with dovetail grooves on both sides of the guiding plane of the rotation axis was used to save space and realize highly accurate and rigid operation. We fabricated the arc guide and slider by cutting, instead of using commercial products, to facilitate their transport to the site of system development and reduce the cost (Fig. 4). The three translational degrees of freedom were realized by screw-type feeding mechanisms and manually controlled with a handle. Although vibration and structural deformation may occur when these mechanisms are manually driven, they were given a rigidity sufficient to neglect such problems. The arms and the table have a total of 20 degrees of freedom, among which, 10 are controlled by manual operation and the remaining 10 are driven by stepping motors connected to reducers. Table 1 summarizes the movable range and the minimum motion of the arms.

The end of two arms is exchangeable in accordance with the task. A grip tool was attached to the end of the arm in this study. The end of this tool was machined to 0.15 mm, and spring steel was used as the material to suppress the deformation when the tool comes in contact with a micro-part. A certain level of grasping force of the grip can be attained by the use of the built-in spring.

The system was designed to have a compact overall

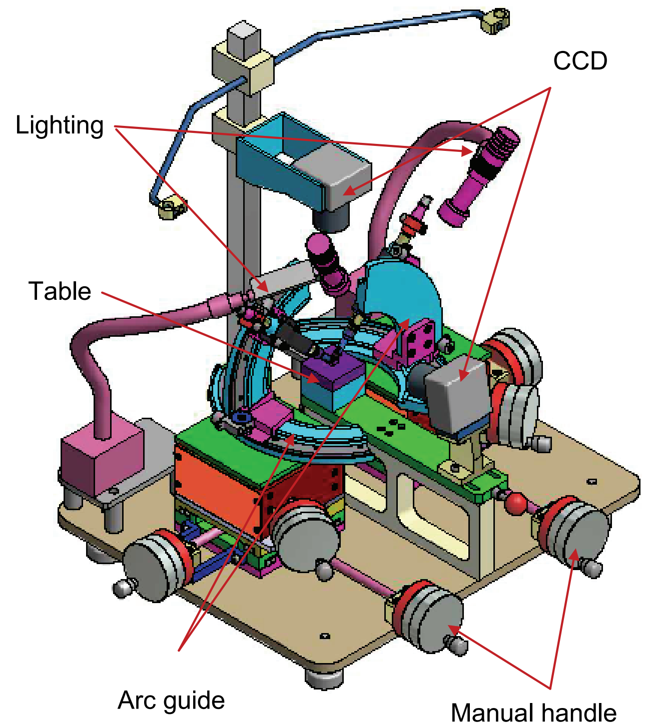

Fig. 3 the outline of the prototype system developed.

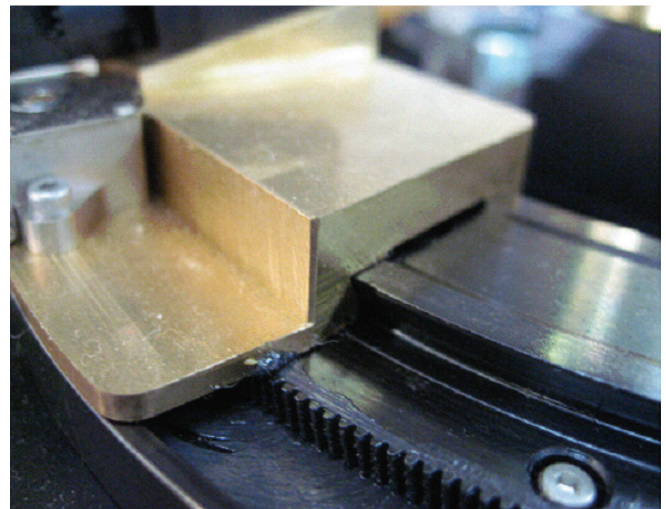

Fig. 4 the arc guide and slider by cutting fabricated by cutting.

Table 1 The specification of the arm motion.

	Working range	Minimum motion
Translation X	40mm	5μm
Translation Y	40mm	5μm
Translation Z	14mm	5μm
Translation W	10mm	5μm
Rotation A	100°	0.025^{o}
Rotation B	70°	0.025^{o}
Rotation C	360°	1.8^{o}
Open/close G	3.3mm	50μm

structure within the dimensions of 500 × 500 × 500 mm3 and a weight of 13 kg so that it can be placed next to machine tools. Fig. 5 shows a photograph of the entire system.

3. Evaluation Experiments

3.1 System operation

The basic operation of the prototype system was checked. All the translational degrees of freedom were controlled by the mechanical driving method using feed screws, and there were no errors in their movement with respect to the rotation of the handle. The rotation axes operated as designed, as shown in Fig. 6. Fig. 7 shows the sequential photographs of the rotational movement of the arm at this time. The angle of the arm was changed around the part as the rotational center.

3.2 Comprehensive experiment

The performance of the system was comprehensively evaluated through the following three tasks. All the tasks require accurate angle control of micro-parts using the two arms and must be observed from multiple directions.

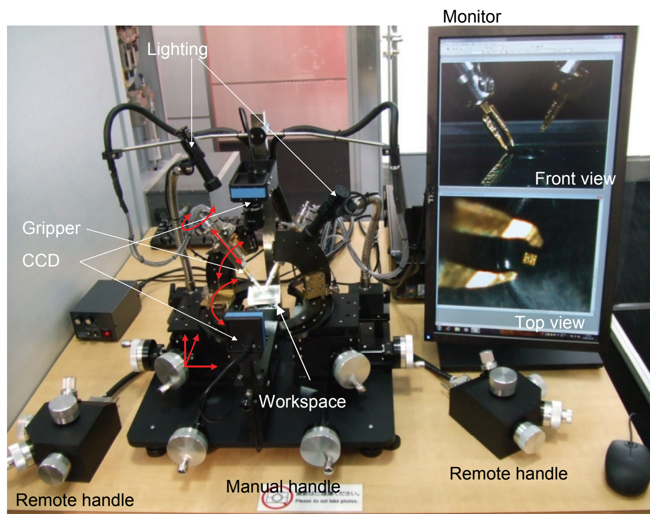

Fig. 5 Photograph of the entire system.

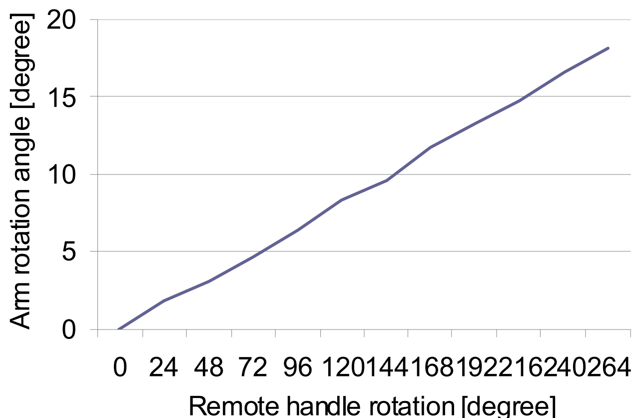

Fig. 6 The relation between the handle rotation and the arm rotation.

(a) Insertion of thin wire into fine hole

A thin wire was inserted into a fine hole using the prototype system. The wire was 50 μm in diameter and made of SUS304 stainless steel. The fine hole was a drilled hole with a diameter of 60 μm and had a rough inner surface. Therefore, the wire cannot be inserted if its end comes into contact with the inner surface of the hole. For reference, the wire was manually inserted into the hole, which required six hours. However, it took only two minutes when the system was used because the wire was inserted accurately in parallel to the hole. Fig. 8 shows a photograph taken during the task.

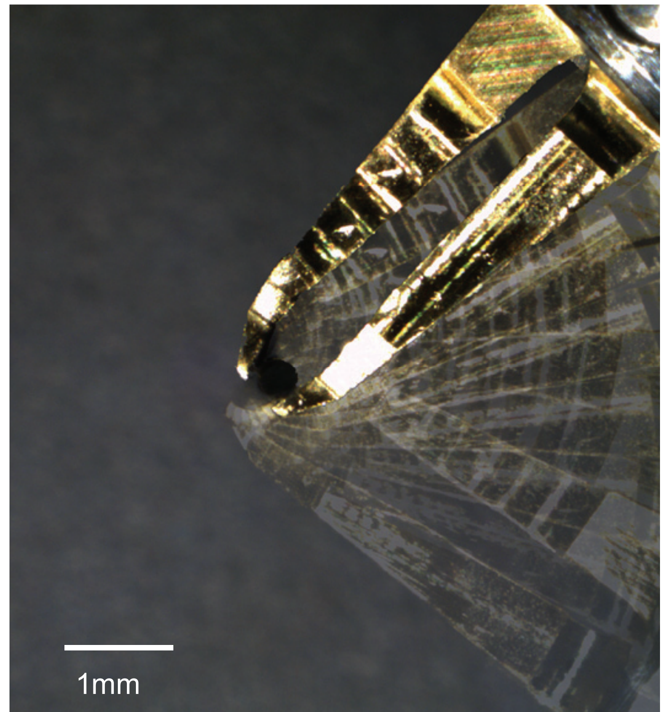

Fig. 7 The sequential photographs of the rotational movement of the arm.

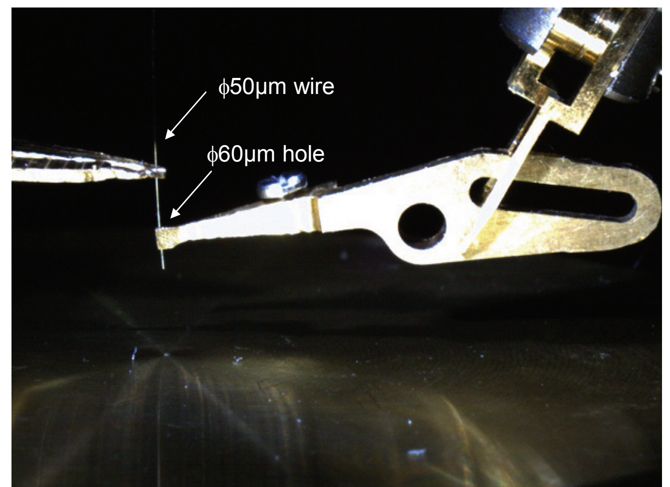

Fig. 8 The demonstration of a 50 micrometers wire insertion into a 60 micrometers hole.

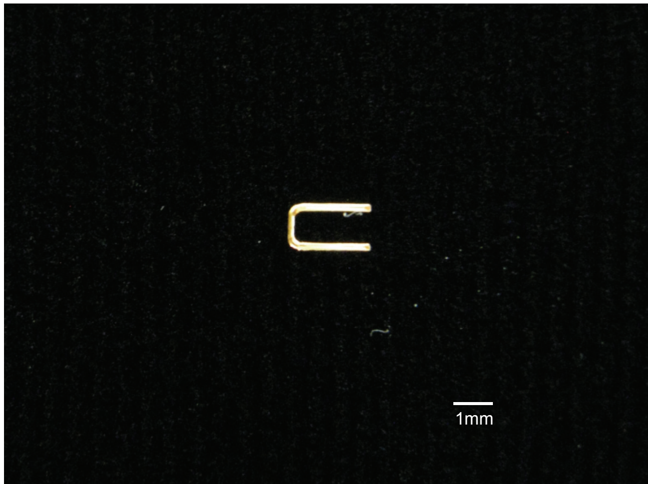

Fig. 9 The machined micro-part with two needle tips.

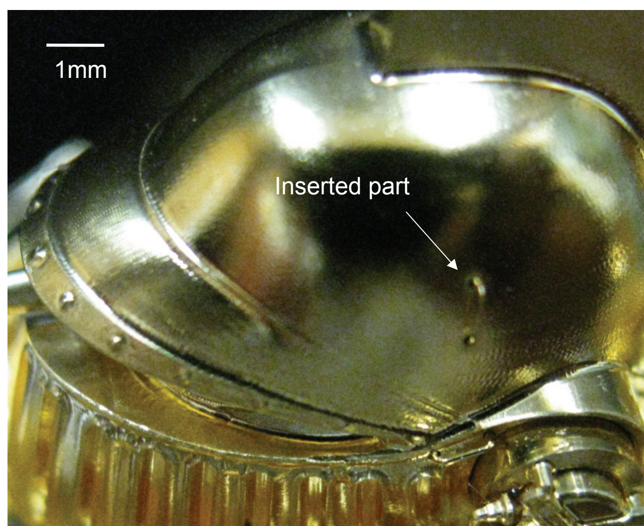

Fig. 10 The inserted micro-part into the hole.

(b) Simultaneous insertion of two axes

Next, a machined micro-part with two needle tips shown in Fig. 9 were inserted into the corresponding holes simultaneously. The diameters of the axes and the holes were 200 and 230 μm, respectively. This task was impossible by manual handling but was completed in one minute when the system was used. Figure 10 shows a photograph taken during the task.

(c) Stacking 300 μm dice in three tiers

Finally, multiple micro-parts randomly placed on the table were grasped, moved, and accurately arranged at predetermined positions one by one. More specifically, 300 μm dice were stacked in three tiers on a rice grain. This task was impossible by manual handling but was completed within ten minutes when the system was used (Fig. 11).

In addition, the stacking task was repeated five times and the time taken to complete the task was measured (Fig. 12). It took ten minutes the first time, seven minutes the second time, and three minutes for the third and subsequent times. This revealed that operators can acquire skill in manipulating the system after approximately three trials.

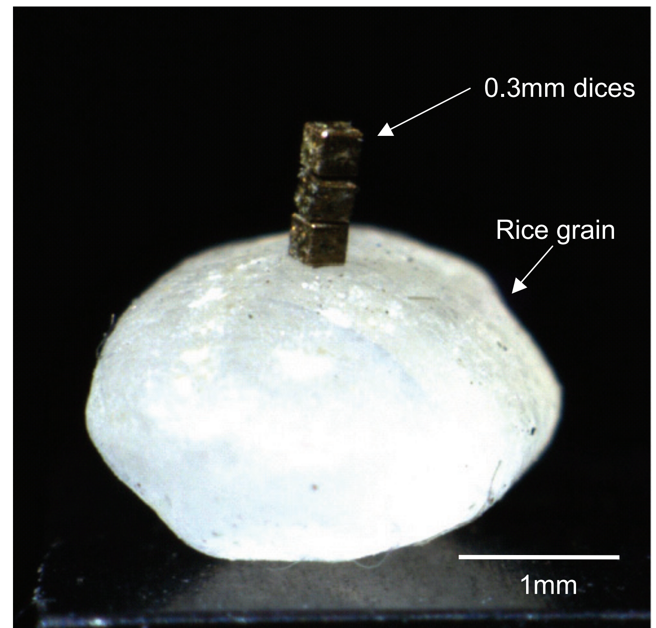

Fig. 11 The demonstration of stacking 300 μm dice in three tiers.

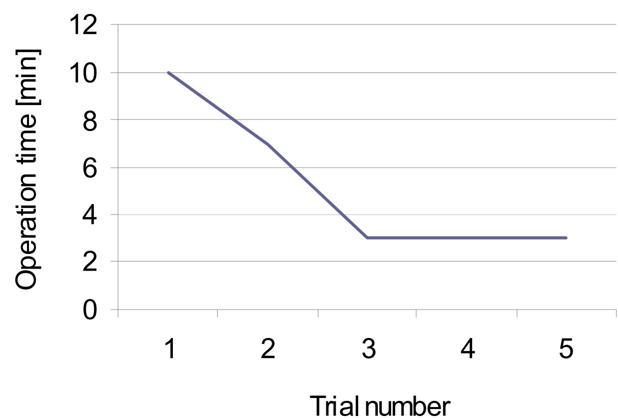

Fig. 12 The operation time taken to complete the task.

The results of these tasks confirmed that the efficiency of handling the micro-parts can be markedly increased using the developed system.

4. Conclusions

In this study, we developed a practical handling system with the aim of supporting the fabrication of 0.1-mm-order machined parts. The work space was observed from multiple directions to obtain accurate three-dimensional information. Moreover, a total of 20 translational and rotational degrees of freedom were given to two arms and a table to allow the system to freely perform tasks. The observation resolution and operation accuracy were suppressed to the minimum necessary levels to develop the system at a low cost.

We handled actual micro-parts using the developed system and confirmed that the system can perform tasks that are difficult by manual handling and can markedly shorten the working time. It was also demonstrated that operators can

acquire skill in manipulating the system after several trials.

REFERENCES

1. Kamiya, D., Gozu, T. and Horie M., “Design and manufacturing of micromechanism elements of 2-DOF micromanipulator”, J. of Microsystem Techonologies, 11(8-10) 1013-1019, 2005.
2. Zhou, L., Nishida, K., Qiu, Z., Shimizu J., Eda, H. and T. Ishikawa, “Development of Micro Manipulation System for Bio-applications”, Proc. of the 4th euspen, pp.166-165. 2004.
3. Nakao, M., Tsuchiya, K., Matsumoto, K. and Hatamura, Y., “ Micro handling with rotational needle-type tools under realtime observation”, Annals of the CIRP , Vol. 50/1, pp. 9-12, 2001.

Micro holes on different materials: a comparison between micro EDM and micro LASER technologies

Gianluca D'Urso[1], Enrico Gallus[2], Giancarlo Maccarini[1], Cristina Merla[1], Chiara Ravasio[1,#]
1 Department of Design and Technology, University of Bergamo, Italy
2 RTM-Spa, Micromachining Division, Torino, Italy
Corresponding Author / E-mail: chiara.ravasio@unibg.it, TEL: +39-035-2052330, FAX: +39-035-2052310

KEYWORDS : Micro holes, Micro EDM, Micro Laser

The miniaturization of parts and components plays an important role in today's economy, enabling the design and the production of new and highly sophisticated components in various industrial fields, such as medical, bio-chemistry, automotive and telecommunications. Micro holes are widely used in micro-electromechanical systems (MEMS) serving as channels or nozzle to connect two micro-features. There are many micromachining technologies available to obtain micro holes such as photo-etching, micro-ultrasonic machining, laser, micro electrical chemical machining, micro electrical discharge machining. However, each process may have different limitations in cost, machining efficiency, properties of the workpiece and aspect ratio of micro hole.
Micro Electrical Discharge Machining (micro-EDM) and micro laser ablation are both thermal processes used to realize micro holes. As regard micro-EDM technology, material is removed by a series of rapid electric spark discharges between the cutting tool (electrode) and the workpiece. It is able to machine complex micro parts of only conductive materials that traditional processes are unable to create. In fact, being a contact-less process, there are very small machining forces between the electrode and the workpiece. This makes it easy to produce micro parts without distortion due to physical forces. EDM is an ideal process for obtaining burr-free micro-size machined parts with high aspect ratio using different materials. Laser is a flexible tool for the material processing. Materials removal can be achieved by laser ablation through physical process. Due to their short wavelength (up to UV regime), short pulse-length (nanosecond regime) and excellent beam quality (TEM00 mode), the innovative laser technology is a competitive solution for applications such as micro drilling, cutting, milling and texturing. Depending on the chosen wavelength and configuration, laser sources are capable of directly machining a wide range of micron scale features in a large range of materials, including metals, semiconductors, ceramics, hard materials, polymers and glasses.
Aim of this work is to carry out a comparison between micro EDM and micro laser technologies in order to balance the pros and cons of both technologies on the execution of micro holes on different industrial materials. Stainless steel, titanium and brass plates, having a thickness equal to 1mm and 0.5mm, were taken into account. The diameter of micro holes was varied from 0.3mm to 0.1mm. Since in both technologies there are many process parameters affecting the results in term of process time, electrode wear rate (only for the EDM technology) and the machining accuracy, several tests were carried out in order to optimize all these aspects. Geometrical and dimensional analyses were performed using both optical and scanning electron microscopes to evaluate both the over cut and the taper rate.

NOMENCLATURE

DOC = diameteral overcut
TR = taper rate
D_{top} = diameter at the top
D_{bottom} = diameter at the bottom
D_{tool} = diameter of the tool electrode
h = thickness of the plate
T = machining time
TWR = tool wear rate
MR_{tool} = material removed from the electrode

$MR_{workpiece}$ = material removed from the workpiece
$Ø_{el}$ = diameter of the electrode
$Ø_{nom}$ = nominal diameter
I = peak current
V = voltage
F = frequency
E = energy
SC_{cyl} = special carbide cylindrical
SC_{tub} = special carbide tubular
B_{cyl} = brass cylindrical

1. Introduction

Micro technologies can be considered the most promising issue in different fields of application, such as biotechnology, microelectronics, optics, telecommunications, sensor technologies and micromechanics. Therefore, due to the advantages of micro technological solutions (such as small dimensions, low weight and simultaneous functions integration), the product miniaturization is worldwide considered as the new key technology for the future years [1-4]. However, the fast growing of product miniaturization, requires a very precise and reliable manufacturing technology. This because micro machining is not an easy machining process, for example because of the difficulty in finding an accurate positioning, the poor stiffness of the tool or the difficult burr removal. Anyway, in the field of micro technologies, micro drilling can still be considered as one of the most popular micro machining process. The main technologies used for micro drilling are micro-EDM (Electrical Discharge Machining), laser ablation, ion beam etching and other conventional micro machining [5]. The selection of an appropriate micromachining technique mainly depends on size and shape of the feature, the aspect ratio achievable (in the case of a micro hole) and the material properties. Technologies like micro-EDM and laser ablation are both suitable for a non-contact material removal process and thus they allow a material removal without any process forces [7]. Micro-EDM for example is able to drill burr-free micro holes with high precision, regardless of the hardness of the workpiece. Current production techniques based on micro-EDM drilling, are continuously facing new challenges, because as the holes get smaller, frequent breakage of electrodes occurs and moreover tooling cost gets higher [6-9]. Focusing on micro-EDM and laser ablation, it is possible to enumerate specific advantages and disadvantages of each technology, which mainly depend on the specific characteristics of each process. About the advantages, micro EDM ensures high aspect ratios and relatively high removal rates with large electrode diameters; on the other hand laser ablation gives no tool wear, the possibility to machine all materials (not only the conductive ones) and the smallest structures achievable. Concerning the disadvantages of micro-EDM, the tool (electrode) wear, the possibility to machine only conductive materials and the smallest tool diameter achievable (about 10 μm), are the most important. On the other hand, the disadvantages of laser ablation are mainly the low removal rates for high surface qualities, the low aspect ratios achievable and the time consuming in machining perpendicular walls [7]. By combining laser ablation and micro-EDM specific advantages of the respective technology can be exploited while drawbacks can partially be eliminated [7]. The present work carries out a comparison between micro EDM and micro laser ablation in order to balance the pros and cons of both technologies on the execution of micro holes. A short description of both technologies is reported below.

1.1 Micro EDM

Micro-EDM is one of the most promising micromachining techniques in precision manufacturing field. In micro-EDM process the material is removed by a series of rapid electric spark discharges between the cutting tool (electrode) and the workpiece. During the machining the workpiece is submerged in a dielectric fluid and a voltage is applied between the tool electrode and the workpiece. The pulsed discharges remove the material through melting and evaporation processes and the melted and vaporized materials are transformed into tiny particles known as debris. These particles are removed from the machining zone by means of the dielectric fluid jet. Finally, the movement of the tool determines the shape of the cavity created in the workpiece. The micro-EDM technology can be used for the processing of any type of electrically conductive material regardless of the workpiece hardness because it is a contactless technique, so it is possible to eliminate physical cutting forces, mechanical stresses and vibration problems [10]. For these reasons, EDM is very effective in machining high strength and very hard materials, generally considered "difficult to be cut" with conventional technologies [11-12]. Hard materials show excellent mechanical properties which can be useful in many important applications; a contact less and "forceless" machining process is worthwhile or even essential in micro machining, to avoid any type of distortions due to physical forces. The promising applications of micro-EDM are not only limited to the machining of high hardness alloys for micro molds or cutting tools, but also to the production of "difficult to make structures" (having complex three dimensional shape) or to machine micro holes with high aspect ratio [13-15]. In micro-EDM many factors can affect the performance of process; these factors can be related to the process parameters (such as voltage, peak current, pulse duration, spark gap, etc.) or to the system (such as type of dielectric fluid, tool properties, chemical and physical material properties). Unfortunately the effect of micro-EDM process parameters on the final output is partially unknown. Furthermore, it is important to remark that optimal EDM process parameters depend on the material of the workpiece [2] since they are influenced by the thermal and electrical properties of the material itself. Finally, in order to become efficient for industrial purpose, Micro-EDM needs to combine high material removal rate, low values of tool wear, and excellent surface quality [15].

1.2 Micro Laser

Laser microdrilling is the process of removing material from a solid surface by irradiating it with a laser beam focused in very small spot able to melt and vaporize the material. Laser ablation strongly depends on laser characteristics and on the target properties. The laser pulse duration and irradiance are the most important factors for defining ablation conditions. Reducing pulse duration has the effect of reducing thermal penetration depth and increasing irradiance. The removal process is so dominated by vaporization rather than melting and accuracy increases. Another important parameter in laser ablation process is the laser wavelength. Shorter wavelengths offer a best laser-material coupling, particularly with dielectrics, but also with metals (reflectivity of most metals decreases at shorter wavelengths). In addition to the mentioned factors some other important parameters are the beam profile and the repetition rate.

Due to its flexibility and versatility, innovative laser technology has gained recognition by industry as competitive solution for micromachining techniques. Novel laser sources are capable of directly machining with high accuracy and speed a wide range of micron scale features in a large range of industrial materials, including metals, semiconductors, ceramics, hard materials, composites, polymers and glasses.

2. Experimental campaign

2.1 Experimental plan

The micro holes carried out to compare the performance of micro EDM and micro laser technologies were executed on different materials, having two different thickness. The diameters of micro holes were equal to 0.3mm and 0.1mm. Table 1 shows all the tested conditions.

Table 1 Experimental tested conditions

Material	Thickness	Diameter
AISI 304 Stainless Steel	1mm, 0.5mm	0.1mm, 0.3mm
Titanium ASTM Grade 2	1mm, 0.5mm	0.1mm, 0.3mm
CuZn35 Brass	1mm, 0.5mm	0.1mm, 0.3mm

The characterization of the micro holes was made considering both qualitative aspects and the process performance.

2.2 Geometrical characterization

Diametral overcut (DOC) and taper rate (T) were taken into account as geometrical parameters. Considering that the diameter of the drilled hole is larger at the top, it decreases along the depth and it is minimum at the bottom, the diameter was measured at both the top (D_{top}) and the bottom (D_{bottom}) of each hole through an optical measuring microscope at the magnification of 100X. Diametral Overcut was calculated by subtracting the diameter of the tool electrode (D_{tool}) from the top diameter of the machined micro-hole as given in Equation 1:

$$DOC = D_{top} - D_{tool} \tag{1}$$

The taper rate (TR) of the machined micro-holes was calculated as follows:

$$TR = \frac{D_{top} - D_{bottom}}{2h} \tag{2}$$

where h is the thickness of the plate.

Qualitative aspects of the top and bottom size of micro holes, in terms of burr, sharpness of outline and circularity, were also taken into account.

2.3 Process performance

The evaluation of the process performance was carried out considering the machining time (T) of micro hole. Moreover, considering that in EDM process the electrode wears out, tool wear rate (TWR) was measured. Tool wear rate was calculated as ratio between the material removed from the electrode and the material removed from the workpiece as given in Equation (3):

$$TWR = \frac{MR_{tool}}{MR_{workpiece}} \tag{3}$$

2.4 EDM tests

The experimental campaign was carried out using a micro-EDM machine Sarix SX-200. Some details of the EDM system are reported in Figure 1.

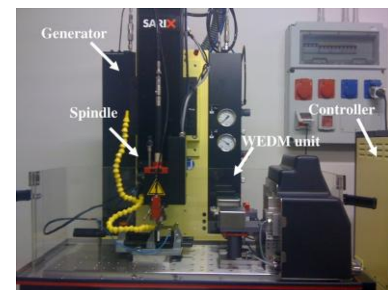

Fig. 1 Sarix SX200, details of the micro-EDM system

In electrical-discharge machining, many factors can affect the performance of the process. These factors can be related to the process parameters (i.e. voltage, peak current, spark gap, etc.) or to the system (i.e. type of electrode, type of dielectric fluid). In this paper, different conditions were tested in order to optimize at first the machining time (affecting the electrode wear) and then to minimize the electrode wear (increasing therefore the machining time). Peak current, voltage and type of electrode (material and shape) were varied for each tested experimental condition (workpiece, thickness and hole diameter) in order to optimize machining time and electrode wear. It is important to remark that machining accuracy was taken into account for all the experiments. Table 2 summarizes the technologies used for every experimental condition. For the holes having a diameter equal to 0.1mm, the electrode has always a diameter equal to 0.3mm and the wire unit of the EDM system is used to reduce its diameter.

Table 2 EDM process parameters

Material	h [mm]	$Ø_{el}$ [mm]	Electrode	E	I	V [V]	Polarity	F [kHz]	Width [µs]	Gain	Gap	Regulation
Stainless Steel	1	0.3	SC_{cyl}	201	50	105	-	125	3.5	30	60	01-01
	1	0.3	B_{cyl}	365	50	120	-	150	4	80	15	03-01
	0.5	0.3	SC_{cyl}	201	50	105	-	125	3.5	30	60	01-01
	0.5	0.3	B_{cyl}	365	50	120	-	150	4	80	15	03-01
	1	0.08	SC_{cyl}	103	70	140	-	140	3	10	60	03-00
	0.5	0.1	SC_{cyl}	103	70	140	-	140	3	10	60	03-00
Titanium	1	0.3	SC_{tub}	201	50	105	-	125	3.5	30	60	01-01
	1	0.3	B_{cyl}	365	50	120	-	150	4	80	15	03-01
	0.5	0.3	SC_{tub}	201	50	105	-	125	3.5	30	60	01-01
	0.5	0.3	B_{cyl}	365	50	120	-	150	4	80	15	03-01
	1	0.08	SC_{cyl}	103	70	140	-	140	3	10	60	03-00
	0.5	0.1	SC_{cyl}	103	70	140	-	140	3	10	60	03-00
Brass	1	0.3	SC_{cyl}	365	50	120	-	100	6	10	40	03-01
	1	0.3	SC_{tub}	365	50	120	-	100	6	10	40	03-01
	0.5	0.3	SC_{cyl}	365	50	120	-	100	6	10	40	03-01
	0.5	0.3	SC_{tub}	365	50	120	-	100	6	10	40	03-01
	1	0.1	SC_{cyl}	103	70	140	-	140	3	10	60	03-00
	0.5	0.1	SC_{cyl}	103	70	140	-	140	3	10	60	03-00

2.5 Laser tests

The Nd:YAG laser used for tests was a Diode-Pumped Solid State laser (DPSS laser), with a wavelength of 532 nm (SHG) and a typical pulselength of 70 ns at 5 kHz. The laser exhibited a Gaussian spatial intensity profile (M^2 < 1.3) and were focused on the target surface using a galvanometer scanner (Raylase MiniScan, 14 mm aperture), equipped with a flat-field lens (f = 100 mm). Finally, laser could be practically operated between 1-50 kHz.

3. Analyses of the results

3.1 EDM

The results obtained in the EDM experimental campaign are reported in Table 3. It is important to remark that several repetitions for every experimental conditions were made and the shown values are mean value. The measured parameters were the diametral overcut (DOC), the taper rate (TR), the machining time (T) and the tool wear rate (TWR); the column "Quality top/bottom," reports a general evaluation of the micro hole quality in terms of burr, sharpness of outline and circularity. The following main observations can be made:

- as regards the electrode material for the 0.3mm holes, for both stainless steel and titanium, there is a remarkable difference in terms of T and TWR: using a special carbide electrode the machining time is higher than brass electrode while the wear is lower. The DOC value is comparable and the taper rate is always lower using the brass electrode. This observation is not true for the combination stainless steel, 0.5mm thickness and brass electrode where there is an anomalous result in term of tool wear rate;
- the type of electrode (cylindrical or tubular) when 0.3mm holes are executed on brass, has negligible effects on the measured parameters;
- comparing the workpiece materials, the material removal rate for the brass is higher than the other materials and the electrode wear is lower. Nevertheless, brass machining is not suitable for using brass electrode;
- the micro holes having a diameter equal to 0.1mm on brass shown no difficulties. This observation is also true for stainless steel and titanium having 0.5mm thickness. Some difficulties were observed for the last mentioned materials of 1mm thickness. In fact, in these cases, the removal of bubbles and debris in working area is difficult, resulting in frequent formation of abnormal discharge, causing high machining time, high value of wear of the electrode and poor data repeatability. To overcome this limit, the planetary movement of the electrode is used;
- for every experimental conditions the qualitative aspect of the top and bottom of micro holes, in terms of burr, sharpness of outline and circularity, is excellent; in EDM micro holes process there is no burr formation.

Table 3 EDM results

Material	h [mm]	Øel [mm]	Electrode	DOC [mm]	TR [-]	T [s]	TWR [-]	Quality top/bottom
Stainless Steel	1	0.3	SC_{cyl}	0.05	0.04	163.54	0.747	Good
	1	0.3	B_{cyl}	0.06	0.013	18.37	1.588	Good
	0.5	0.3	SC_{cyl}	0.05	0.07	77.23	0.797	Good
	0.5	0.3	B_{cyl}	0.06	0.011	9.02	0.538	Good
	1	0.08	SC_{cyl}	0.05	0.002	333	0.361	Good
	0.5	0.1	SC_{cyl}	0.02	0.008	62	0.369	Good
Titanium	1	0.3	SC_{tub}	0.04	0.026	197.08	0.513	Good
	1	0.3	B_{cyl}	0.06	0.005	16.75	0.813	Good
	0.5	0.3	SC_{tub}	0.03	0.021	181.4	0.212	Good
	0.5	0.3	B_{cyl}	0.06	0.004	9.55	0.979	Good
	1	0.08	SC_{cyl}	0.02	0.002	268.5	0.51	Good
	0.5	0.1	SC_{cyl}	0.02	0.002	125.5	0.582	Good
Brass	1	0.3	SC_{cyl}	0.07	0.010	70.48	0.049	Good
	1	0.3	SC_{tub}	0.07	0.008	70.96	0.048	Good
	0.5	0.3	SC_{cyl}	0.06	0.017	43.50	0.063	Good
	0.5	0.3	SC_{tub}	0.06	0.011	43.80	0.06	Good
	1	0.1	SC_{cyl}	0.05	0.012	106.5	0.086	Good
	0.5	0.1	SC_{cyl}	0.08	0.021	27	0.038	Good

Some photographs obtained using optical microscope are reported in Figure 2 and 3.

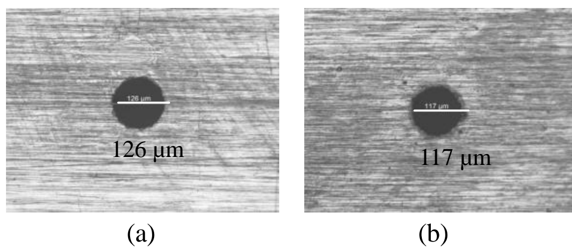

(a) (b)

Fig. 2 Stainless steel, 0.5mm thickness, brass electrode, 0.1mm diameter, at top (a) and bottom (b)

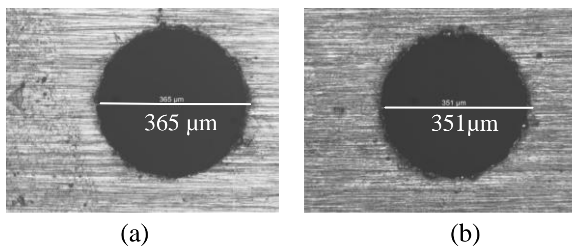

(a) (b)

Fig. 3 Stainless steel, 0.5mm thickness, brass electrode, 0.3mm diameter, at top (a) and bottom (b)

Figures 4-6 shows some photographs obtained using a scanning electron microscope (SEM).

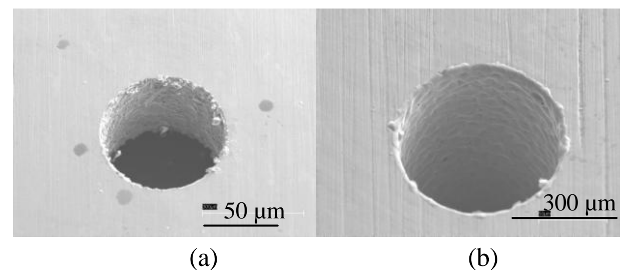

(a) (b)

Fig. 4 Stainless steel, 0.5mm thickness, brass electrode, at top, 0.1mm (a) and 0.3mm (b) diameter

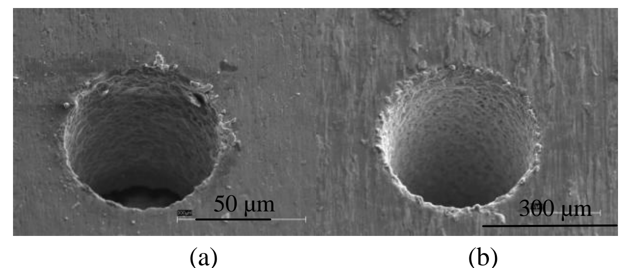

(a) (b)

Fig. 5 Titanium, 0.5mm thickness, brass electrode, at top, 0.1mm (a) and 0.3mm (b) diameter

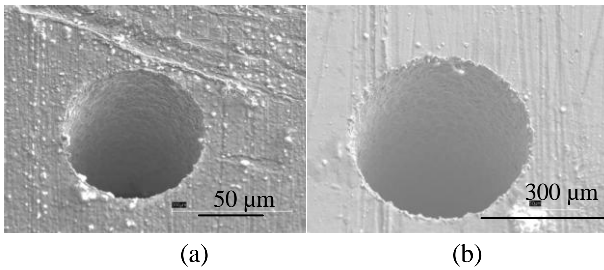

(a) (b)

Fig. 6 Brass, 0.5mm thickness, cylindrical metal carbide electrode, at top, 0.1mm (a) and 0.3mm (b) diameter

3.2 Laser

Table 4 reports the results obtained in the experimental campaign using laser system.

Table 4 Laser results

Material	h [mm]	∅ $_{nom}$ [mm]	D_{top} [mm]	D_{bottom} [mm]	DOC [mm]	TR [-]	T [s]
Stainless Steel	1	0.3	0.375	0.300	0.075	0.037	40
	1	0.1	0.140	0.105	0.04	0.017	10
	1	<0.1	0.070	0.035		0.017	< 1
	0.5	0.3	0.360	0.330	0.06	0.015	15
	0.5	0.1	0.130	0.110	0.03	0.01	4
Titanium	1	0.3	0.370	0.300	0.07	0.03	20
	1	0.1	0.160	0.125	0.06	0.017	8
	0.5	0.3	0.360	0.325	0.06	0.017	15
	0.5	0.1	0.150	0.115	0.05	0.017	6
Brass	1	0.3	0.360	0.260	0.06	0.05	30
	1	0.1	0.135	0.075	0.035	0.03	15
	1	<0.1	0.050	0.040		0.005	8

Laser microdrilling of AISI 304 is characterized by a large production of molten material due to low thermal diffusivity of this metal. During the ablation process, the heat is confined and facilitates melt formation. As regard titanium, the drilling process was dominated by a strong reaction with atmospheric O_2. The exothermic heat significantly enhances the total energy available and leads to a higher dimension of top diameter. Finally, brass shows a behavior quite different from the previous metals. At first, brass is a high reflectivity material. Moreover, the drilling process of brass is characterized by a strong plasma plume which shields the laser beam. This phenomenon explains slow process time respect to other metals, above all in percussion drilling where laser beam must penetrate a dense plasma plume of one-dimensional vapor expansion. As post processing cleaning procedure to remove debris and burr, micro fine abrasive paper was used, followed by an acetone ultrasonic bath.

Some photographs of micro holes obtained in different conditions are here reported (Figures 7-11).

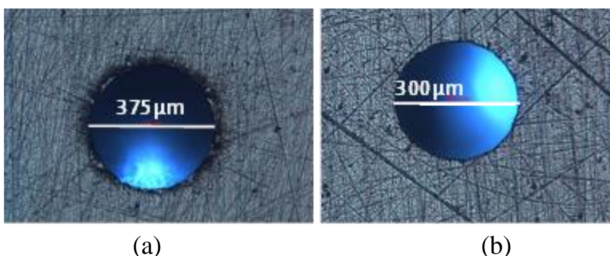

(a) (b)

Fig. 7 Stainless steel, 1mm thickness, 0.3mm diameter, at top (a) and bottom (b)

(a) (b)

Fig. 8 Titanium, 1mm thickness, 0.1mm diameter, at top (a) and bottom (b)

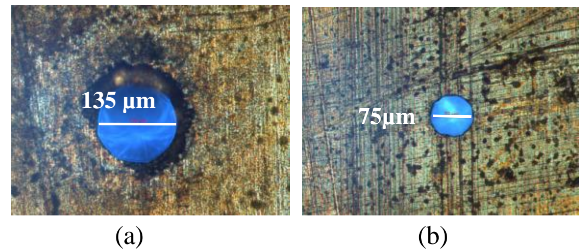

(a) (b)

Fig. 9 Brass, 1mm thickness, 0.1mm diameter, at top (a) and bottom (b)

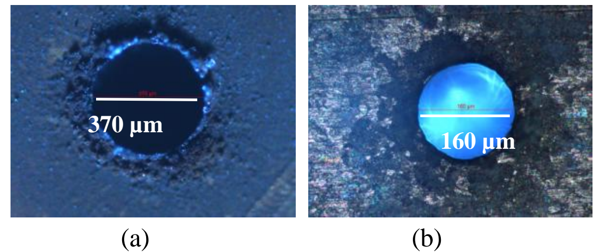

(a) (b)

Fig. 10 Stainless steel (a) and titanium (b) before cleaning

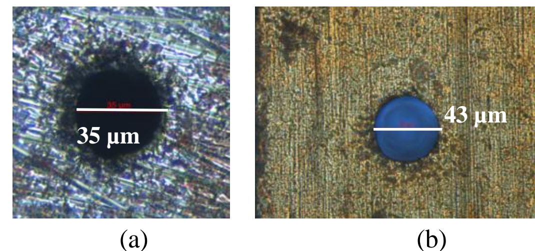

(a) (b)

Fig. 11 Stainless steel (a) and brass (b) having a diameter less than 0.1mm

4. Conclusions

A comparison between micro EDM and micro laser process was carried out in order to balance the pros and cons of both technologies on drilling of micro holes. The experimental campaign took into account the region where the two technologies can have a matching point. In particular, metals of industrial interests (stainless steel, titanium, brass), having different thickness (0.5 and 1mm), were processed to obtain holes with medium aspect ratio. The conclusions that can be drawn are here summarized:

- micro holes obtained using EDM system show an excellent quality in terms of burr, sharpness of outline and circularity. The taper rate of holes is limited;
- micro holes obtained using laser system show a lower quality than EDM. In fact, laser process is

characterized by top burr formation (the exit hole is generally clean) due to the deposition of molten material (in particular for some materials) and therefore a following cleaning of hole is necessary in some applications;

- in general, when in EDM process the brass electrode is used for holes having a "big" diameter (0.3mm), the machining times are lower than laser. Decreasing the diameter (0.1mm), the performance of laser process improves (machining time of holes having a diameter smaller than 50 µm is very short).

REFERENCES

1. Klocke, F., Gerschwiler, K. and Abouridouane, M., "Size effects of micro drilling in steel", Prod. Eng. Res. Devel., Vol. 3, pp. 69-72, 2009.
2. Alting, L., Kimura, F., Hansen, H.N. and Bissacco, G., "Micro engineering", Annals of the CIRP, Vol. 52, No. 2, pp. 635–657, 2003.
3. De Chiffre, L., Kunzmann, H., Peggs, GN. and Lucca, D.A., "Surfaces in precision engineering", Microengineering and Nanotechnology, Annals of the CIRP Vol. 52, No. 2, pp. 561–577, 2003.
4. Weule, H., et al. "International state of the art of micro production technology", Prod Eng Res Dev Vol. XI, No. 1, pp. 29–36, 2004.
5. Muhammad, A., Osamu, O. and Hiromichi, O., "Novel micro deep drilling using micro long flat drill with ultrasonic vibration", Precision Engineering, Vol. 36, pp. 168– 174, 2012.
6. Lin, Li, Diver, C., Atkinson, J., Giedl-Wagner, R. and Helml, H. J., "Sequential Laser and EDM Micro-drilling for Next Generation Fuel Injection Nozzles Manufacture", Annals of the CIRP, Vol. 55, No. 1, 2006.
7. Fleischer, J., Schmidt, J. and Haupt, S., "Combination of electric discharge machining and laser ablation in microstructuring of hardened steels", Microsyst Technol, Vol. 12, pp. 697–701, 2006.
8. Yu, Z.Y., Rajurkar, K. P. and Shen, H., "High Aspect Ratio and Complex Shaped Blind Micro Holes by Micro EDM", CIRP Annals - Manufacturing Technology, Vol. 51, No. 1, pp. 359-362, 2002.
9. Pham, D.-T., Dimov, S.-S., Bigot, S., Ivanov, A. and Popov, K., "Micro-EDM – Recent Developments and Research Issues", Journal of Materials Processing Technology, Vol. 149, pp. 50-57, 2004.
10. Tak, H.S., Ha, C.S., Kim, D.H., Lee, H.J., Lee, H.J., Kang, M.C., "Comparative study on discharge conditions in micro-hole electrical discharge machining of tungsten carbide (WC-Co) material", Transactions of Nonferrous Metals, Vol. 19, pp. 114-118, 2009.
11. Jahan, M.P., Wong, Y.S., Rahman, M., "A comparative experimental investigation of deephole micro-EDM drilling capability for cemented carbide (WC-Co) against austenitic stainless steel (SUS 304)", International Journal Advanced Manufacturing Technology, Vol. 46, pp. 1145-1160, 2010.
12. Liu, N.M., Chiang, K.T., Horng, J.T., Chen, C.C, "Modeling and analysis of the edge disintegration in the EDM drilling cobalt-bonded tungsten carbide", International Journal Advanced Manufacturing Technology, Vol. 51, pp. 587-598, 2009.
13. Egashira, K., Morita, Y., Hattori, Y., "Electrical discharge machining of submicron holes using ultrasmall-diameter electrodes", Precision Engineering, Vol. 34, pp. 139-144, 2010.
14. Liu, K., Lauwers, B., Reynaerts, D., "Process capabilities of Micro-EDM and its applications", Int J Adv Manuf Technol, Vol. 47, pp. 11-19, 2010.
15. Allen, P., Chen, X., "Process simulation of micro electro-discharge machining on molybdenum", Journal of Materials Processing Technology, Vol. 186, pp. 346-355, 2007.

Scheduling Approach for Microfactories with Setup Times

Mathias Coqblin, Dominique Gendreau, Philippe Lutz, Jean-Marc Nicod, Laurent Philippe and Veronika Rehn-Sonigo
FEMTO-ST Institute, UMR CNRS / UFC / ENSMM / UTBM, Besancon, France
Corresponding Author E-mail: mathias.coqblin@femto-st.fr, TEL: +33-3-8166-2065, FAX: +33-3-8166-6450
KEYWORDS: Multicell Microfactory, Scheduling, Setup Time, Buffer

In this paper we consider microfactories for manipulation and assembly. These microfactories are composed of several cells containing microrobotic systems capable of a high level of repeatability. The assembly plan of the production is a pipeline of tasks that are performed by the cells. Our aim is to manage the production flow in the case where the cells can be reconfigured to perform different task types. Each cell is in charge of several consecutive tasks. A setup time is necessary to switch from the processing of one task type to another, and multiple intermediate results may be stored temporarily in storage areas to avoid switching the task type after the processing of each product. In this context we assess the optimized use of these storage areas, called buffers, and its impact on the production throughput.

1 Introduction

Microfactories are small production systems designed to manufacture microproducts [11]. In our work, we focus on the microfactories for manipulation and assembly. The manipulation or assembly tasks are performed by systems which have to be adapted to the microworld context. The considered systems are microrobotic systems whose architecture and control system permit to obtain high performance as high level of repeatability, resolution or even speed [7]. To perform complex manipulation and assembly tasks, the microrobots are grouped inside cells. Microrobotic cells often have a great number of degree of freedom (more than 10 for example). A microfactory could be a unique cell (most of the time in case of semi-automatic microfactories) but has to consist in several associated cells to allow a good management of a workflow. This flow has to be optimized to obtain the best global performance characterized by the throughput, the reliability, and the setup time.

Among the different properties that can be those of microfactories, we consider that we are able to reconfigure the cells. Different task types can be performed by the same cell. Moreover, the number of available cells is generally small compared to the number of tasks. Consequently, we assume that each cell in charge of several consecutive tasks as defined in an assembly plan. Switching from a task type to another requires to reconfigure the system, i.e. to change the associated tools, which induces an unavailability time called setup time [1]. Hence the whole production time for one piece includes the process time of each task as well as the setup times needed for cell reconfiguration. To organize the production flow, the storage areas described by their size and position are of great importance to define the cell organization of a microfactory. We name "buffers" the storage areas which can be containers or wafers.

Our work is motivated by the high cost – and the low availability – of reconfigurable cells in microfactories. The targeted production process is defined as a pipeline composed of several tasks, or steps. So before being completed a product has to undergo each of the tasks of the pipeline, as illustrated on Figure 3.1. Our goal is to maximize the overall throughput of the production. We consider that, due to their cost, the number of available stations is much lower than the number of tasks to be performed in the pipeline, hence the need to assign multiple tasks to a single production cell. As the number of machines is limited and the reconfiguration times are significant, using buffers is needed to greatly improve the throughput. If for instance setup times are at least the same as processing times, we are able to almost half the average period. On standard factories and assembly lines however, the use of buffers would not be as easy because the costs of keeping intermediate results usually exceed the benefits of using buffers.

The problem can be split in two sub-problems: first, find the correct allocation of tasks to production cells then find the optimal schedule of tasks within a cell (inner schedule). For the first problem we use an assignment called Interval Mapping, which means that a subset of consecutive tasks is assigned to the same cell [9]. We then concentrate on the second problem.

The scheduling issue is here to find a schedule (i.e. de-

fine an order to perform the tasks) inside a cell in the case where cells require a setup time to change from one task to another and where we consider the production of a batch of the *same* product. As stated before, we assume that intermediate productions can be temporarily stored in a dedicated space called buffer. Using buffers allow to perform several times the same task on different products and thus avoid to reconfigure the cell each time a new product arrives. In this context, as the goal of our work is to maximize the production throughput, this implies to minimize the cell unavailability and thus making the maximum use of the buffers is the key to reduce setup times and maximize the overall throughput. So the issues related to the global problem depend on the properties of the microfactory, in particular their buffer sizes, and on the properties of the tasks, their execution times and their setup times.

Considering that buffers may be of different sizes and differently used also involves scheduling and configuration issues. We must carefully choose the sizes of the buffers, which must be of reasonable size to avoid spending a long time filling them up or to meet a deadline condition. They also have to be consistent with each other to avoid unnecessary space allocation, and ensure the correct execution of any scheduling algorithm applied on the cells. Using buffers does not guarantee the overall optimization of the schedule: the schedule may be optimal for on a given machine, but outputting pieces by batches may delay the work of the next machine, hence reduce the overall throughput.

In the paper we tackle the problem of mapping tasks on cells taking setup times into account. The presented contribution is theoretical results on the complexity of mapping algorithms. For homogeneous production cells – cells with the same performance and storage capability – we propose a greedy scheduling algorithm that computes an optimal schedule. Then, for the case where the storage capacity differs from one cell to another, we show that the problem becomes considerably more difficult, indeed the mapping problem is strongly NP-Hard. On homogeneous platforms, when setup times are sequence-dependent [1] – they depend on the current task as well as on the previous one – the problem is also NP-Hard, but can be modeled as a Traveling Salesman Problem (TSP) [8].

The organization of the paper is as follows: first, we present the framework model in Section 3. In Section 4 we present our solution for single machine scheduling and interval mapping. In Section 5 we show the resulting execution of our solution on an example application. Then we conclude our work in Section 6.

2 Related work

Most of the research works involving reconfigurations focus on the ability of machines to process batches of pieces from a specific family, then to be reconfigured – or recalibrated – to process batches from another family. In other words, a single machine or a series of machines follow an assembly plan to create a product, then have to be reconfigured to follow another assembly plan that is totally unrelated, or at least require a recalibration. In this context, the problem of reducing the impact of setup times has been covered several times, mainly in semiconductor manufacturing. For instance, Zhang and Goldberg [12] focus on wafer-handling robots and propose a solution of eliminate costly manual re-calibration during component replacements. Li et al. [5, 6] study the problem of batch processing of incompatible lot families by reducing the total weighted tardiness. Jing and Li [4] provide a linear programming solution to minimize the total completion time in semiconductor factories.

Becker and Scholl [2] covered the problem of mapping tasks on machines in form of assembly line balancing problems (ALBP). In these kinds of problems typically one or more types of models have to be produced, and thus a precedence graph is mapped onto a linear assembly line. The setup part of the problems, however, focuses on the decision which type of piece has to be produced at a time, and when to reconfigure for another type of piece. The specific Interval Mapping problem has also been studied [3], and solutions are offered to map sequences of tasks on a lesser number of machines. These works however do not involve any reconfiguration in the process.

3 Framework model

Our study includes a theoretical contribution on task mapping algorithms. So before explaining how these algorithms are designed we first formally set the context of the work that will define its range. The production model relays on tasks that are performed by cells. We consider that a batch of the same product has to be realized, i.e., the same set of tasks is performed on each product in the same order. So when a product enters the production line it has to be processed by the whole set of tasks before being completed.

As the tasks are performed one after the other, always in the same order, their set can be modeled as a pipeline (Figure 3.1). A pipeline is made of a set $\mathcal{T}$ of n **tasks**: $\mathcal{T} = \{T_1, \dots, T_n\}$. The output of task T_i is the input of the next task T_{i+1}. Each task T_i requires an operating time w_i to be performed on the current product. As the aim of this production line is to output a huge amount of products out of the pipeline we concentrate on the steady state behavior of the line.

To perform tasks we use a multi-cell microfactory. We assume that these cells are interconnected by a transport system that can convey the products from one cell to every other cell. So we just take processing times into account and we do not take any transporting issue into consideration as the transport time can be neglected compared to the processing times. So the target platform is modeled as a set $\mathcal{M}$ of p machines: $\mathcal{M} = \{M_1, \dots, M_p\}$ interconnected as a clique. A processing speed v_u is associated to each cell M_u.

To execute a given application pipeline on a given platform, tasks are mapped onto machines considering consecutive tasks, then a inner schedule has to be planned. Each machine is indeed able to perform sequentially its allocated tasks. However, to switch from the processing of one task T_i to another task P_j $(i \neq j)$, the machine M_u has to be reconfigured. This induces a setup time of $st_{i,j,u}$ time units. On the other hand it is possible to perform several times the same task on multiple input pieces without setup. This allows eventually to save setup times. However, the number of task repetitions is limited; each task T_i mapped onto M_u has an input buffer B_i, where the output parts from the previous task are stocked. Given this context, different versions of the model may be considered depending on the framework's heterogeneity in terms of setup times and buffers.

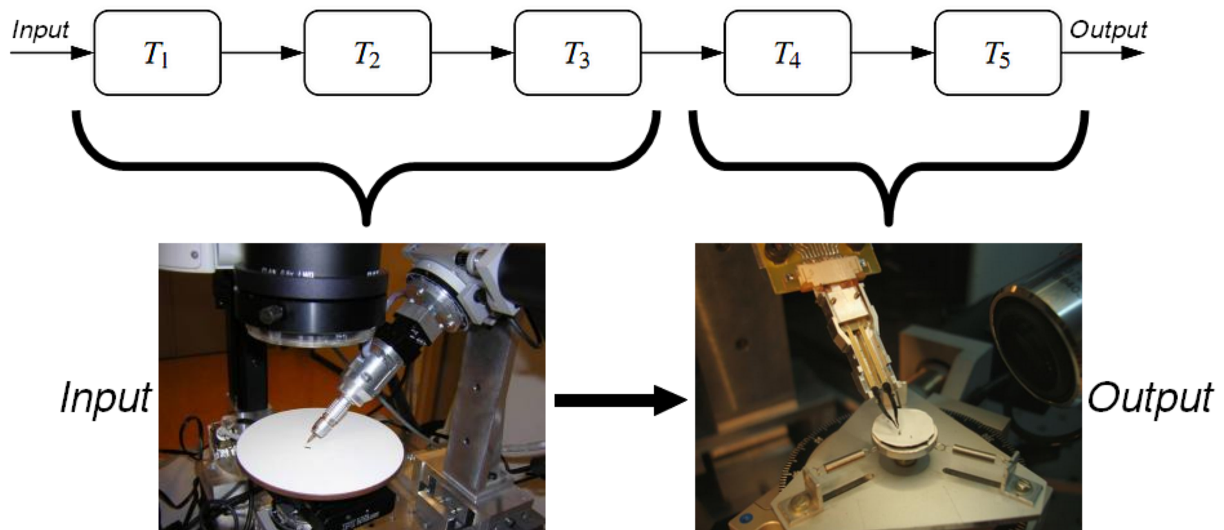

Figure 3.1: Example of tasks mapping on a microfactory: tasks 1 to 3 are mapped on the first cell, while tasks 4 and 5 are performed on the second cell

Setup times Considering the setup times, if the application is fully homogeneous, the setup times may be the same on every machine, and for every task. This will be referred to as **st**. On the other hand, on most applications, setup times will depend on the task we want to setup to. These times may be *sequence-independent* ($\mathbf{st_i}$), or *sequence-dependent* ($\mathbf{st_{i,j}}$). Sequence-dependent setup times mean that the setup time depends on both the task the machine is already configured for and the next task to be performed. Sequence-independent setup times usually occur where changeovers have minor influence, such as gripper calibration, or when both tasks are from the same type. Sequence-dependent setup times occur when there is a diversity amongst the tasks, such as going from handling and assembling parts to gluing them together.

The schedule problem with sequence-dependent setup times is NP-Hard and can be modeled as a Traveling Salesman Problem (TSP). It is not studied in the scope of this paper.

Buffers The problem of allocating available space into buffers may result in four variants:
• **B** All space is allocated evenly, so that every single task's buffer has the same capacity.
• $\mathbf{B_u}$ Likewise, if the available space is linked to a machine, buffers may be allocated to have the same capacity within a machine, but not the same amongst machines.
• $\mathbf{B_i}$ **(fixed sizes)** If the available space is not related to any machine, buffer sizes may have been fixed before any mapping is done. This is the most constrained variant we have to deal with.
• **(allocable sizes)** The most general problem, where the whole space is available within a machine, and we may freely choose the capacity of each buffer.

In the rest of this paper, we use the notation B_i to denote the name of the input buffer of task T_i, while b_i is the capacity of buffer B_i. When we are under the context of homogeneous buffer capacities (**B** and $\mathbf{B_u}$), it is implied that for all tasks b_i has the same value b (respectively b_u).

In this context, our objective function is to maximize the throughput of the production line: $\mathscr{T} = \frac{1}{\mathscr{P}}$ where $\mathscr{P}$ is the average period of time between two outputted products.

4 Scheduling with setup times and buffers

Our contributions cover several problems. First, since there are less cells available than there are tasks to perform, cells will have to perform several tasks. To find a solution that maximizes the throughput of the assembly line, we have to perform load balancing when assigning tasks on machines, so that we minimize the impact of the bottleneck cell.

Each machine then has a set of consecutive tasks to perform, which must be scheduled to avoid any unnecessary setup time involved. The latter is done by using buffers to stock intermediate productions at each step before treating them, allowing batch processing of the pieces.

Thus, our study will focus on three main operations:

- For a given machine with a given set of tasks to perform, finding an optimal schedule on a machine to maximize its throughput.
- Mapping tasks on machines as interval mapping – each machine has a set of consecutive tasks to perform. Assuming that on each machine a schedule is found that maximizes the throughput, the mapping has to be done in a way that allows to maximize the throughput of the machine with the lowest throughput - the bottleneck cell.
- Allocating the available space as input buffers for each task.

The combination of these three operations will allow to determine if our solution is optimal. The solution is optimal if:

- The schedule within a machine, as well as buffers allocation, perform the lowest period possible (or highest throughput).

- The bottleneck station on the pipeline – the one with the highest period – has no idle time while in steady state.

  Thus the whole pipeline has the same period as this bottleneck machine.

As a result, assuming we found an optimal solution, we know that the slowest machine will have a throughput as high as possible, and is never slowed down within the process. Since the overall execution of the pipeline is limited by the bottleneck station, we will be able to assess that the throughput of the application is maximum. However, even if the slowest machine has idle times, the solution may still be optimal if there is no way to meet this "no idle time" criteria.

We split this contribution section in two parts: the *single machine scheduling* section is dedicated to the schedule within a single given machine, and the *multi machine scheduling* section treats the mapping of tasks on the machines. We will not cover the buffer allocation part in the scope of this article, as most of the time the space can be evenly distributed amongst buffers, and other specific situations (such as a remainder of space that could be used to raise the size of some buffers only) are to be studied on a case-by-case basis. Thus, in the following sections we assume that the capacities of buffers are already fixed. That is, in regard to our framework model, only buffer models $\mathbf{B}$, $\mathbf{B_u}$ and $\mathbf{B_i}$ are considered, while *allocable sizes* are not.

4.1 Single Machine Scheduling

The approach for inner schedules is not directly linked to model variants. At machine level, the problem with buffers $\mathbf{B_u}$ is the same as $\mathbf{B}$, as they are both homogeneous buffer capacities within a machine; for all task T_i, the value of b_i is b. The problem with heterogeneous buffer capacities ($\mathbf{B_i}$) is a little more complex. Likewise, the heterogeneity of setup times (st or st_i) has absolutely no influence: some setups may take longer than others, but our algorithms will minimize the amount of setups the machine has to perform for each task, regardless of the time each will take.

Homogeneous buffer capacities We developed a greedy scheduling algorithm – GREEDY-B – that minimizes the period for homogeneous buffer capacities. The schedule is as follow: for buffers of size b, perform the first task all available pieces, that is b pieces. This will empty the first buffer and fill the next. Then we setup to the next task, where its input buffer is now full. The algorithm will continue to treat as many pieces as it can on each task before performing a setup to the next task. Since all buffers are the same, the progression is linear and after the last task the machine will setup back to the first task.

Heterogeneous buffer capacities Handling different buffer capacities is harder. This cannot be done the same way we did it with homogeneous buffers, except if set the limit of pieces processed on each task to the lowest buffer. The would however not be optimal, as better solution exist, that make better use of all buffers.

It is not possible to express a specific period for any random buffer sizes. However, it is possible to have a control over the behavior of the algorithm if all adjacent buffers are multiples to each others. More formally: $\forall i \in [1,..,n], \min(b_i, b_{i+1}) | \max(b_i, b_{i+1})$. In this configuration, we know that any buffer will be either x times larger or smaller than its predecessor, or its successor.

Based on that knowledge, we improved our GREEDY-B algorithm into GREEDY-BI. The idea is that once the cell is reconfigured for a specific task, the maximum amount of pieces that can be processed before a new setup is needed is limited by either the input buffer (the amount of pieces available) or the next buffer (the space available to store them). The minimum of both will be a hard limit; to stay active the cell will have to reconfigure to perform another task.

Keep in mind that by processing as many pieces as possible on a single task T_i, we minimize the impact of the setup time st_i on that task, as the ratio of st_i and the time needed to process all pieces on T_i is the lowest possible. Thus, when selecting the next task the cell will reconfigure to, we restrain this choice to maximize the use of buffers on the task. On GREEDY-BI, a reconfiguration for task T_i is done on task when on of the following conditions holds true:

- $b_i \geq b_{i+1}$, b_{i+1} is empty, and we can process enough pieces to totally fill b_{i+1}.
- $b_i \leq b_{i+1}$, b_i is full, and we can process enough pieces to totally empty b_i.

The conditions of the algorithm allow to fill perfectly the buffers when they are multiple to each others. If this is not the case, the behavior of the algorithm is undefined and depends on the actual implementation. We are then unable to work out an expression for the period, and cannot consider GREEDY-BI optimal for all configurations other than buffers to each others.

We however developed heuristics that aim to truncate the size of some buffers in order to have them multiple to each other. The resulting pipeline is a pipeline on which the execution of GREEDY-BI is well defined and optimal. However since we truncated some buffer, we may have lost setup time reduction potential.

4.2 Multi Machine Scheduling

Subhlok and Vondran [9, 10] addressed the problem of Interval Mapping on fully homogeneous platforms *without* setup times. They developed a dynamic programming algorithm to find an optimal mapping solution in polynomial time. This algorithm was later slightly adapted by Benoit and Robert [3] to find the optimal period.

The aim of the algorithm is to find a mapping that will eventually maximize the throughput of the application, of minimize its period, when running a schedule on each machine. Remind also that the period is determined by the period of the bottleneck machine. Through binary search, the algorithm will try to find a mapping that minimizes the period of the slowest machine; that is to say, it will try to minimize the value of the maximum period amongst the period of all machines. Every time the algorithm has a mapping to test on a machine, it will calculate its period and determine if it is better than the previous one.

We proceeded to adapt this algorithm to take setup times into account. The solution is the same algorithm as before, but

the period calculation on a machine has been. This period is calculated according to the execution of the scheduling algorithm we would use.

Assuming an optimal inner schedule is found for each machine, this mapping solution has been proved optimal for any setup times (**st**, $\mathbf{st_i}$), and for **B** and $\mathbf{B_u}$. However, experimentations has shown that idle times may appear on the slowest machine when fully heterogeneous buffers capacities ($\mathbf{B_i}$) are used. This is due to the behavior of the schedule: before any new batch of n pieces is outputted, the machine must go through the process of all its tasks for n pieces. When buffers are heterogeneous, the size of those batches do not reflect the period of the machine – a faster machine may take too much time to output by small batches, while the slowest machine is waiting for its first big buffer to be filled before proceeding.

5 Results

In order to test the behavior of all our algorithms and heuristics, we have simulated them using the distributed system simulation tool SimGrid. With the simulator, we are able to test on platforms that reflect several real case scenarios, and compare the results with other (worse) solutions we come up with. We can also assess the execution behavior and the performance of the algorithms on different configurations.

In the following we give an example of execution for a system consisting of eight tasks and four cells, as shown on Figure 4.1. A total of 100 pieces are processed in the simulation. The configuration of the application is as follows:

- Tasks are mapped according to Figure 4.1, namely they are distributed evenly: two tasks per machine.
- Homogeneous setup times, fixed at $st = 2$ time units.
- Homogeneous buffers within machines ($\mathbf{B_u}$). As show on the figure, the buffer capacities are $b_1 = b_2 = 4$ on M_1, $b_3 = b_4 = 5$ on M_2, $b_5 = b_6 = 3$ on M_3, and $b_7 = b_8 = 5$ on M_4.
- All tasks take the same time to process a piece: 2 time units.

On this configuration, the slowest machine is M_3: as all machines have to perform the same amount of tasks and the process times are homogeneous, having buffer capacities lower than the other machines implies that the total time spent on reconfiguration is higher.

Figures 5.1 and 5.2 show two extracts from the Gantt chart obtained executing this configuration. The times are given in time units (compatible with any unit and coefficient that may suit a problem). The first sample – on Figure 5.1 – goes from $t = 219$ to $t = 309$, and the second sample – on Figure 5.2 – goes from $t = 441$ to $t = 531$. Each of the four lines corresponds to the activity of a machine (going from M_1 to M_4). Each black rectangle represents a setup while colored rectangles are the processing of a piece. The colors on the chart identify a single piece to track its location (colors are looped every 40 pieces to keep them distinguishable), and the values inside rectangles are the name of the task being processed. For instance, as illustrated on Figure 5.1, on M_1 (line 1) a yellow piece being processed on T_1 (a yellow rectangle marked as T_1) will later be found, after a setup, as a yellow rectangle marked as T_2 on the same line. It will then be found on the second line still as a yellow rectangle, marked as T_3 then T_4, and so on.

The output of the execution shows that, once the system has reached a steady state, the slowest machine M_3 has no idle time. On the Gantt chart the line corresponding to M_3 always shows a full activity, while other lines have time slots with no activity.

Both samples from the chart show that M_4 regularly has idle times. The machine is periodically in a state of starvation, as M_3 cannot deliver new pieces fast enough (for instance, on Figure 5.1 it is waiting for purple then red pieces to arrive from M_3). On Figure 5.2, we can observe that both M_1 and M_2 have inactivity. As the machines are located before M_3 on the pipeline, this is a case of saturation: M_3 cannot process pieces from its buffers fast enough, therefore M_2 has to wait for some space available on M_3 before proceeding. Then, by propagation, as M_2 is slowed down by M_3, M_1 is also slowed down by waiting for M_2 to empty its buffers.

As we can see, the throughput of the application is limited and thus determined by the throughput of M_3, the slowest machine. Assuming the mapping on which this execution is tested is optimal, M_3 has the highest throughput possible and we maximize the throughput of the application.

6 Conclusion

In this paper we have presented theoretical results on the problem of mapping tasks on the cells of a microfactory. These tasks are organized as a pipeline in the production process and in the case where several tasks can be mapped on the same cell our work relays on interval mapping which assumes that two consecutive tasks are mapped on the same cell. In this context we tackle the optimization of the production throughput depending on setup times, i.e. the time needed to switch from a task to another. We define a global model for the problem and propose some polynomial time heuristic to solve the problem.

As shown in Section 4 several problems are identified depending on the buffers and setup times properties. Most of them seems to be NP-Hard. So in our future works will concentrate on giving proofs for their complexities and defining efficient heuristics.

Acknowledgments

This work is part of the MUSINE2 project, supported by the Région de Franche-Comté.

Bibliography

[1] A. Allahverdi, C. Ng, T. Cheng, and M. Kovalyov. A survey of scheduling problems with setup times or costs. *European Journal of Operational Research*, 187(3):985–1032, 2008.

[2] C. Becker and A. Scholl. A survey on problems and methods in generalized assembly line balancing. *European Journal of Operational Research*, 168(3):694 – 715, 2006. ISSN 0377-2217. doi: 10.1016/j.ejor.2004.07.023. URL `http://www.sciencedirect.com/science/article/`

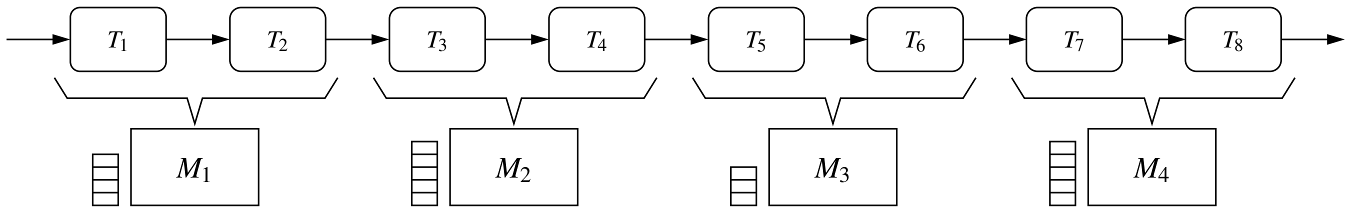

Figure 4.1: Example of execution configuration

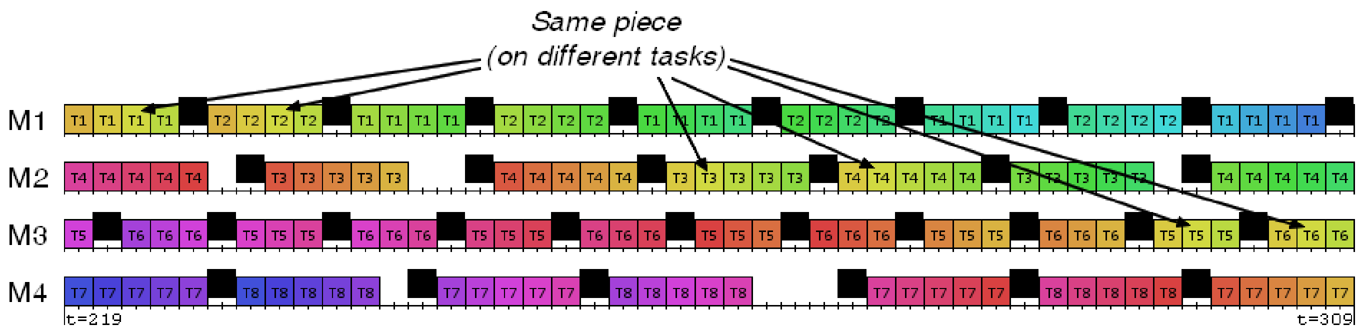

Figure 5.1: Example of execution (sample 1)

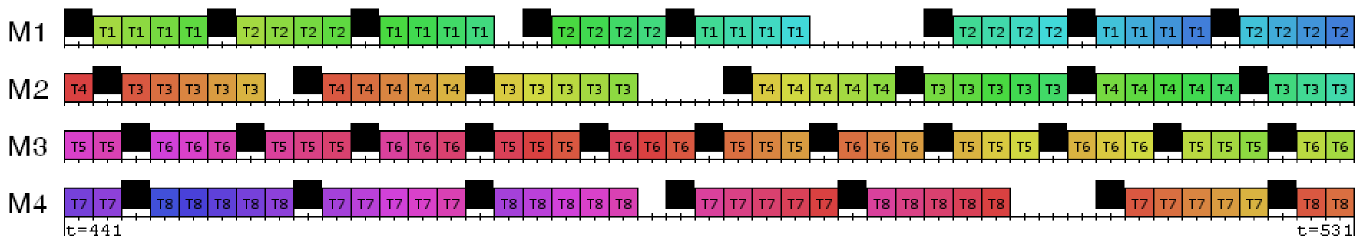

Figure 5.2: Example of execution (sample 2)

pii/S0377221704004801. <ce:title>Balancing Assembly and Transfer lines</ce:title>.

[3] A. Benoit and Y. Robert. Mapping pipeline skeletons onto heterogeneous platforms. *J. Parallel and Distributed Computing*, 68(6):790–808, 2008.

[4] X. Jing and Z. Li. A milp-based batch scheduling for two-stage hybrid flowshop with sequence-dependent setups in semiconductor assembly and test manufacturing. In *Automation Science and Engineering (CASE), 2010 IEEE Conference on*, pages 87–92. IEEE, 2010.

[5] L. Li and F. Qiao. Aco-based scheduling for a single batch processing machine in semiconductor manufacturing. In *Automation Science and Engineering, 2008. CASE 2008. IEEE International Conference on*, pages 85–90. IEEE, 2008.

[6] L. Li, F. Qiao, and Q. Wu. Aco-based scheduling of parallel batch processing machines to minimize the total weighted tardiness. In *Automation Science and Engineering, 2009. CASE 2009. IEEE International Conference on*, pages 280–285. IEEE, 2009.

[7] M. Rakotondrabe, Y. Haddab, and P. Lutz. Development, modelling and control of micro/nano positioning 2 dof stick-slip device. *IEEE/ASME Transactions on Mechatronics, IEEE/ASME TMech/ *14* (6)*, pages 733–745, 2009.

[8] B. Srikar and S. Ghosh. A milp model for the n-job, m-stage flowshop with sequence dependent set-up times. *International Journal of Production Research*, 24(6):1459–1474, 1986.

[9] J. Subhlok and G. Vondran. Optimal mapping of sequences of data parallel tasks. In *ACM SIGPLAN Notices*, volume 30, pages 134–143. ACM, 1995.

[10] J. Subhlok and G. Vondran. Optimal latency-throughput tradeoffs for data parallel pipelines. In *Proceedings of the eighth annual ACM symposium on Parallel algorithms and architectures*, page 71. ACM, 1996.

[11] M. Tanaka. Development of desktop machining microfactory. *Journal RIKEN Rev*, 34:46–49, April 2001. ISSN:0919-3405.

[12] M. Zhang and K. Goldberg. Calibration of wafer handling robots: A fixturing approach. In *Automation Science and Engineering, 2007. CASE 2007. IEEE International Conference on*, pages 255–260. IEEE, 2007.

Calibration strategies for a micromanipulation work-cell

Gianmauro Fontana[1,#], Serena Ruggeri[1], Irene Fassi[1] and Giovanni Legnani[2]

1 Institute of Industrial Technologies and Automation, National Research Council, Italy
2 Department of Mechanical Engineering, University of Brescia, Italy
Corresponding Author / E-mail: gianmauro.fontana@itia.cnr.it, TEL: +39-02-2369-9920, FAX: +39-02-2369-9915

KEYWORDS : Calibration, Micromanipulation, 2D vision systems

The paper presents and compares some calibration procedures used to calibrate a work-cell for micromanipulation of sub-millimetric objects by means of a variety of grippers.
The experimental setup is based on a 4-degree-of-freedom robot, a vacuum gripping system and a two-camera vision system.
Since the robot and the vision system have to cooperate within the same working area, a robot calibration, a camera calibration and a robot-camera georeferencing are required. Standard calibration methods result in a very onerous process at the microscale, thus non-conventional calibration strategies have been developed and implemented in the work-cell. This paper discusses the results obtained with the different approaches, analyzing performance and limitations.
Moreover, since the microgripper can be affected by misalignment and orientation errors with respect to vertical rotational axis of the manipulator, a simple and agile kinematic calibration of the robot end-effector has been developed. The paper describes the method and shows the achieved improvements.

1. Introduction

A robot is generally only one of the components of a robotic work-cell. This can contain other robots and other devices performing different operations, depending on the application the work-cell is supposed to execute. Some examples are: rotating tables, conveyor belts, orientation platforms, tool stores. Nowadays, also vision systems are progressively integrated in the robotic work-cells, exploiting many functions, such as object identification and recognition, measurements, quality control, supervision.

Each component introduces errors and presents inaccuracies, but, in any case, all the devices constituting the work-cell have to cooperate in a suitable way. This is especially relevant when high-precision operations have to be executed automatically, as in the case of manipulation and assembly of small products constituted by components with sub-millimetric dimensions. Therefore, the whole work-cell needs to be calibrated. The stand-alone devices have to be calibrated and their relative location has to be univocally determined [1].

1.1 Calibration issues

When a robot and a vision system have to cooperate within the same working area, a robot calibration, a camera calibration and a robot-camera georeferencing (also called registration) are required. In Fig. 1 the main reference systems involved during a general calibration process are reported: the subscripts g, r, c and i represent the ground, the robot base, the camera and the image respectively. The 3D space coordinates are indicated by x, y, z expressed in millimeters while u and v are the image coordinates in pixels.

Considering the simple case in which the manipulator must grasp and release objects on a planar area under the supervision of a camera, a 2D camera calibration can be considered suitable.

The calibration of the camera has to be performed to compute image pixel to real-world unit transformation and to compensate for perspective, distortion and spatial referencing errors [2]. Perspective errors occur when the camera axis is not perpendicular to the component under inspection. To reduce this error one can try to position the camera the most perpendicular possible to the plane, but in any case, this error has to be compensated to achieve higher quality images. Moreover, distortion errors are introduced by lens

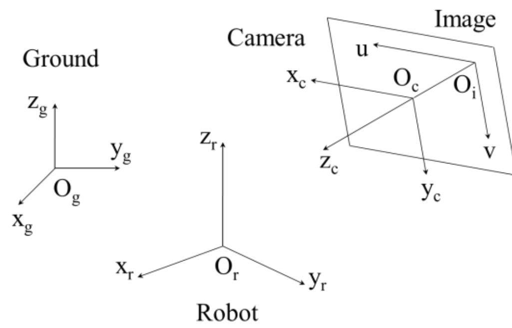

Fig. 1 Representation of the main reference frames involved in the calibration processes.

imperfections. Typically, camera lens introduces radial distortion, that is the image information is misplaced relatively to the optical center of the lens [3].

1.2 The standard calibration strategy

The camera calibration is usually performed by taking a picture of an object of known shape and size and comparing the position of some image features measured in image pixels with the known actual position expressed in millimeters or other suitable units. This procedure is generally based on a model of the camera, the perspective transformation, and the distortion model. When a 2D calibration is required, the calibration object is usually a grid traced on a flat non-deformable surface, invariant with respect to temperature, humidity and other external agents. For example, standard grids may be obtained by printing a set of circles in predefined positions on a glass or ceramic substrate. The quality of the grid, and the final calibration accuracy, depend on the number and on the precision of the position of the circles as well as on the precision of their shape. The mentioned characteristics should be optimized also depending on the dimension of the field of view of the camera.

In order to perform a 2D camera calibration, the pattern has to be placed to be seen in focus. As no information is given about the displacement along the optical axis, the focal plane is assumed to be parallel to the robot *x*-*y* plane. The camera frame has the origin located at the barycenter of a chosen dot of the grid; the *x*-axis is usually identified as the line passing through the origin and the barycenter of a chosen dot belonging to the row including the origin dot, while the *y*-axis is perpendicular to the first one. The georeferencing between the robot base frame and the camera frame is performed by means of a calibration tool mounted on the robot end-effector (usually a pin) which is moved to a minimum of two specific points whose absolute coordinates are known in the robot working space (3D georeferencing requires at least three non-aligned points). The position of the pin is measured by the camera using its reference system and the corresponding transformation between the two systems is easily computed.

The perspective transformation is performed by the pin-hole camera model [4] which results in the system of equations:

$$\begin{cases} u = \dfrac{ax+by+c}{gx+hy+1} \\ v = \dfrac{dx+ey+f}{gx+hy+1} \end{cases}$$

where u and v are the image coordinates in pixels of one feature whose position in the real world is represented by x and y, and a, b, c, d, e, f, g, h are suitable constants to be determined by calibration.

The distortion is represented by a model in which the distance D of each point from the center of the distortion (x_{0D}, y_{0D}) is affected by an error proportional to a quadratic form $\Delta D = k_1 + k_2 D^2$ where k_1 and k_2 are constants to be experimentally determined.

The above described calibration procedures, commonly used at the macroscale, result in a very onerous process at the microscale, where the tolerances are very strict. First of all, due to the high resolution required by the vision system, the dot spacing tolerance has to be very accurate (in the micrometric range), increasing the fabrication costs of the calibration grid. In addition, the calibration pin has to be accurately manufactured and manually positioned, which is an onerous and time-consuming operation. Moreover, due to its small dimensions, its manufacturing could be challenging and the final pin very fragile. For these reasons, non-conventional calibration strategies were conceived and implemented for our work-cell prototype, which is described in the following section.

2. The work-cell for microassembly

A suitable experimental setup (Fig. 2) able to move the parts to be manipulated and measure their position in the working area was designed.

The work-cell is equipped with a Mitsubishi Electric [5] RP-1AH robot (1). It presents a 5-joint closed link structure and 4 degrees of freedom with Schönflies motion [6]: 2 revolute joints for the positioning in the *x*-*y* working area, a third revolute joint for the rotation and a prismatic joint for the *z* vertical end-effector motion. The operating limits are 150x105 [mm^2] with a vertical stroke of 30 [mm]. The repeatability is ±5 [μm] in the *x*-*y* plane, ±10 [μm] for the vertical motion, and ±0.02° for the end-effector rotation.

A smart and standard mechanical interface (2) was realized in order to facilitate the tool change. It was directly connected to the bottom part of the hollow screw constituting the third and fourth axis of the robot.

The vacuum generation system is a critical part of the setup, mainly during the releasing phase. It consisted of an air compressor, a FRL (Filter Regulator Lubricator) group, and a piCOMPACT10 vacuum ejector (3). This ejector integrates a vacuum sensor and two normally closed solenoid valves, one for the supply and one for the release. This generation system was chosen to assist the release with a positive pressure. By modifying the throttling, the entity of the blow in the release phase can be set and optimized for the specific component and application.

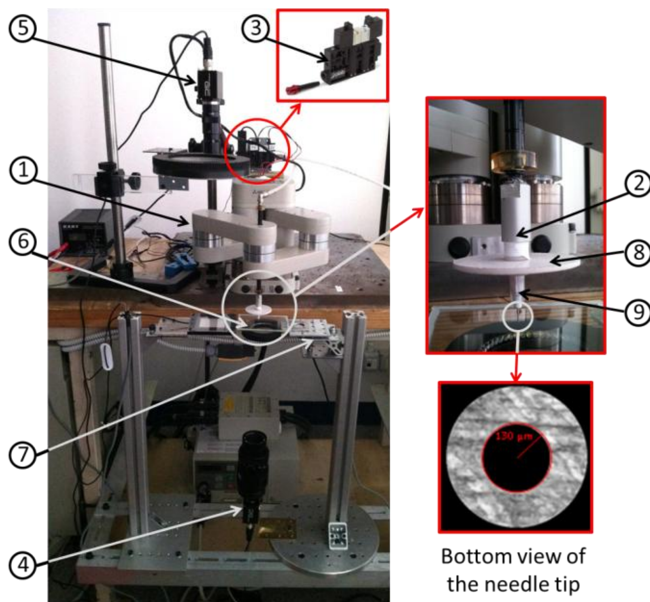

Fig. 2 The prototype of the work-cell.

The measurements of the position of the parts in the focal plane were performed using a suitable vision system, consisting of a first camera (4) with field of view (FoV) 16.3x13.5 [mm^2] and spatial resolution 6.6 [μm] and a second camera (5) with FoV 32.70x24.59 [mm^2] and spatial resolution 24 [μm]. The parts to be manipulated lied on a transparent glass substrate (6) so that the first camera, fixed on a rigid structure below the robot working area, detects from the bottom their position and orientation. The second camera allows instead a top view of the assembly area. The glass substrate, as well as the assembly area, was mounted on an adjustable orientation platform (7) in order to assure its planarity and avoid the influence of the substrate inclination. Moreover, thanks to the compliance this system provides, it is intrinsically more safe against accidental impacts of the gripper on the substrate. An opportune lighting system is essential for the detection, robust recognition and reliable measurement, thus a diffuse illumination of the scene was adopted, making the disturbance of the environment light negligible. In order to obtain better images, the end-effector was also equipped with a contrast panel (8) on the top of the gripping tool (9). The gripping tools are standard vacuum microgrippers (commercially available needles for dispensing). Many sizes are available, ranging from a cannula with internal diameter of 1.60 [mm] down to 0.10 [mm]. A SEM (Scanning Electron Microscope) bottom image of the needle with an internal diameter of 0.260 [mm] is displayed in Fig. 2.

3. The non-conventional calibration strategies

In the specific case, the manipulator must grasp and release objects in two separate planar zones (hereafter called area1 and area2) under the supervision of two cameras, one for each zone, as shown in Fig. 2. Thus, as said above, the robot has to be calibrated, as well as both the cameras, then a georeferencing is needed. The aim of the robot calibration is the improvement of its accuracy [7] and was performed measuring its actual motion [8, 9] to estimate its geometrical parameters [10, 11]. In this work, it is assumed that the robot was already calibrated and exhibited a suitable accuracy; thus this step is not discussed. In any case, the calibration of the vision system was necessary and a 2D calibration was considered appropriate. Two different calibration strategies are proposed: the former represents an adjustment of the standard method, thus called *hybrid strategy*, while the latter is a fully non-traditional method, named *virtual grid strategy*.

3.1 Hybrid calibration strategy

The camera calibration is performed by means of an actual grid of dots printed on a substrate. The grid is placed on the camera focal plane and the camera takes a picture of the grid. The developed vision algorithms provide for the calculus of the set of barycenters of the dots in pixels that, together with the corresponding set in millimeters, is processed by the camera calibration algorithm. Then, the georeferencing between the robot base frame and the camera frame is needed.

As said above, in the work-cell two separate 2D vision systems are integrated and must be calibrated: one camera looking from below up to the robot end-effector, and another one having a top view of the assembly area.

Performing a georeferencing in the standard way is a big challenge at the microscale, due to the high-demanding positioning of the pin mounted on the end-effector on the points of the grid. Thus, depending on the configuration of the camera to be calibrated, two alternative automatic approaches have been adopted.

Concerning area1, the referencing is obtained by moving a sphere gripped by the robot end-effector in the field of view of the camera in n known positions ($n \geq 2$). Similarly, in area2 the georeferencing of the second camera frame with respect to the robot frame is obtained by commanding the robot to place n spheres in the FoV of the camera in known positions. In both cases, the positions of the spheres are measured by the related camera using its reference system and the corresponding transformation between the two systems is computed.

3.2 Virtual grid calibration strategy

The novel calibration strategy allows to simultaneously calibrate the camera and georeference the camera with respect to the robot without using external tools (as the calibration pattern or the calibration pin).

For the first camera, the calibration procedure was based on the use of a “virtual grid” with the same characteristics of the standard calibration pattern, created by moving a sphere gripped by the robot end-effector in several known positions inside the field of view of the camera. A similar procedure was presented in [12]. The robot, already calibrated, grasped a sphere and moved it to a series of known positions in the x-y plane. At each position, the camera took an image and measured the sphere position in pixel units. The collection of the two sets of the sphere position in millimeters and in pixels

was processed with the same algorithms used for an ordinary grid.

Also for the second camera looking at area2, a similar procedure was adopted. The manipulator grasped one sphere at each time and placed it to a known position in the field of view of the second, non-calibrated, camera, thus building a sort of virtual calibration grid. Also in this case, the set of position in millimeters and pixels (measured by the camera) was processed by the calibration algorithm.

Thereby, the camera calibration and its georeferencing with respect to the robot were performed simultaneously and automatically and it was not necessary to use a calibration object. In this way the accuracy of the calibration was influenced by the spatial resolution of the vision system and the robot encoder resolution affecting the robot feedback position reading, and not by the fabrication quality of the calibration object.

Some considerations have to be done. First of all, the downwards end-effector movement to pick the sphere was fully automated. Indeed, no manually taught vertical information was provided to the robot controller. An interrupt sent by the vacuum switch to the robot controller when a part has been picked is exploited in order to aim at the maximum system flexibility. Moreover, in order to avoid the influence of the release performance of the mounted gripper, the sphere was released on an adhesive substrate. In this way the sphere was glued to the substrate, increasing the accuracy of the whole grid and avoiding undesired part rolling. Finally, a sort of passive compliance control was assured by the presence of the adjustable orientation platform supporting the working area2. In this way, even if the height of the part release, that is the distance from the substrate, was accidentally lower than the sphere diameter, thus pressing excessively on the substrate, neither the system could be damaged nor the calibration process fail. Note that glass spheres with a diameter of 1 [mm] and a diameter tolerance of ±0.2 [mm] were adopted. This type of object has been chosen to benefit from the gripping auto-centering capability of the vacuum needle. A pre-selection of the spheres has been done by means of the vision system to assure their roundness (to exclude those with the poorest roundness).

To evaluate the performance of these calibration strategies, depending on the camera, the robot was asked to move the end-effector gripping a sphere in some *x*-*y* positions in the first camera FoV or to place them in the assembly area supervised by the second camera. Points different from those used for the georeferencing in the hybrid strategy or for the construction of the virtual grid were chosen. The positions of the sphere were measured by the vision system. This time the calibration information previously computed was used to convert the positions of the sphere from pixels to millimeters. The calculus of the deviation between the reference and calculated end-effector positions was then possible. For the sake of completeness, this calculus has been computed also for the points used for the georeferencing in the hybrid process and for the virtual grid construction in the second process. The chosen performance index was the position error *e* defined as:

$$e = \sqrt{(x_a - x_d)^2 + (y_a - y_d)^2}$$

where x_a , y_a are the reference coordinates of the center of the sphere, that is the end-effector coordinates expressed in the robot base reference system, and x_d , y_d are the coordinates measured by the calibrated camera.

4. Implemented calibration strategies

4.1 Calibration of the area1

In the sequel, the implementation of the two different approaches to the calibration of the first camera and its georeferencing with respect to the robot base frame are presented.

4.1.1 Hybrid strategy

As prefaced in §3, the camera calibration is performed by means of an actual grid. In this case, a grid of 8x7 black dots printed on a white substrate with a diameter of 1 [mm], a dot spacing of 2 [mm] and a dot spacing tolerance of 5 [μm] has been adopted. The grid was fixed on the glass substrate and placed to be seen in focus. The camera took a picture of the grid and the developed vision algorithm provided for the identification of the dots and the calculus of their barycenters.

The origin of the coordinate system of the calibration grid was set to coincide with the barycenter of the top left dot, the *x*-axis was aligned with the topmost row of dots and the *y*-axis was perpendicular and directed downwards in the image. In this way the two sets of barycenter positions expressed in millimeters and pixels could be processed by the calibration algorithm. Then, the algorithm performed the transformation and compensated for perspective and non-linear errors. In the present work, all the vision algorithms have been developed in LabView™, whose vision libraries make a "calibration block" available to the user, with the possibility to choose the type of error compensation. In this case, aiming at the highest vision system performance, a calibration taking into account both perspective and distortion errors was chosen.

To perform the georeferencing, the robot grasped a sphere and moved it to n ($n \geq 2$) known positions in the *x*-*y* plane. For all these positions, the *z* height has been kept constant and chosen in order to make the sphere to be seen in focus: in this way, the offset between the georeferencing and calibration planes falls into the camera depth of field, which has the order of magnitude of 1 [mm] for the first camera. At each position, the robot stopped, the feedback position was sent from the robot controller to the master personal computer and the camera took an image. The developed vision algorithm provided for the identification of the sphere in the field of view. Then, the algorithm performed the calculus of its barycenter in pixels and, since the camera was already calibrated, in millimeters too. Thus, the corresponding transformation between the camera and the robot systems can be computed estimating the parameters (ϑ, x_0, y_0) of the planar rototranslation matrix between the two reference systems,

represented by the following relation:

$$\begin{bmatrix} x_r \\ y_r \end{bmatrix} = \begin{bmatrix} \cos(\vartheta) & -\sin(\vartheta) \\ \sin(\vartheta) & \cos(\vartheta) \end{bmatrix} \begin{bmatrix} x_c \\ y_c \end{bmatrix} + \begin{bmatrix} x_0 \\ y_0 \end{bmatrix}$$

Linearizing it in the neighborhood of $\vartheta = \vartheta_e$, where ϑ_e is a first estimation of the angle ϑ, one obtains:

$$\begin{bmatrix} x_r \\ y_r \end{bmatrix} = \begin{bmatrix} (-\sin(\vartheta_e)x_c - \cos(\vartheta_e)y_c) & 1 & 0 \\ (\cos(\vartheta_e)x_c - \sin(\vartheta_e)y_c) & 0 & 1 \end{bmatrix} \begin{bmatrix} \Delta\vartheta \\ x_0 \\ y_0 \end{bmatrix} + \begin{bmatrix} \cos(\vartheta_e)x_c - \sin(\vartheta_e)y_c \\ \sin(\vartheta_e)x_c + \cos(\vartheta_e)y_c \end{bmatrix}$$

Then, applying the Least Square Method to the collected data, it is possible to derive the estimated values of the vector parameters $L = [\Delta\vartheta, x_0, y_0]^T$ from equation:

$$L = A^+ B$$

where A^+ is the pseudoinverse matrix of the coefficient matrix A ($2n$ x 3) and B is the ($2n$ x 1) vector of the known terms. Therefore, we get $\vartheta = \vartheta_e + \Delta\vartheta$.

Since the linearization introduces errors, the estimation of $\Delta\vartheta$, x_0, y_0 can be reiterated to improve the calibration.

Note that, in order to avoid the effects of the geometrical errors at the end-effector, its orientation has been kept constant to an angle $\alpha = \alpha_{cal}$ during this phase. The geometric errors at the end-effector will be considered in §5.

The results obtained with this approach are reported in Table 1, which shows the absolute values of the mean and maximum errors and the standard deviation.

Table 1 Results of the hybrid calibration applied to the area1 (number of georeferencing points n=4 and grid of verification points of 56 positions).

Error in georeferencing points [µm]			Error in non-georeferencing points [µm]		
Mean error	Max error	Standard deviation	Mean error	Max error	Standard deviation
15.2	43.2	10.5	14.2	50.4	11.9

4.1.2 Virtual grid strategy

As described above, the procedure was based on the use of a virtual grid. Practically, as a first step, the robot grasped a sphere with a known diameter. Then, it was commanded to move in order to position the sphere to be seen in focus by the camera. After that, the cycle of movements and images captures started, until the grid was complete. Again, a grid of 8x7 sphere positions has been used and the end-effector orientation has been kept constant.

As for the hybrid strategy, the positions of the barycenters of the sphere are identified and, again, the origin of the coordinate system of the calibration grid was set to coincide with the barycenter of the top left dot. However, in this case, such point corresponds to a specific position achieved by the robot, thus the georeferencing between the robot and camera reference frames is simultaneously provided.

The statistical information of mean and maximum errors and standard deviation calculated for a single complete grid is reported in Table 2. Both the results in the case of the points used for the calibration and in that of different points are reported.

Table 2 Results of the virtual grid calibration applied to the area1 (in all, two grids of 56 positions each have been considered).

Error in calibration points [µm]			Error in non-calibration points [µm]		
Mean error	Max error	Standard deviation	Mean error	Max error	Standard deviation
3.9	8.8	1.7	6.3	19.0	3.1

4.2 Calibration of the area2

Hereby, the hybrid and "virtual grid" strategies are addressed for the calibration and referencing of the camera providing a top view of the assembly area.

4.2.1 Hybrid strategy

The same physical standard grid used for the first camera was adopted. The camera takes a picture of the 16x12 black dots grid which is processed by the vision algorithm.

The georeferencing of the camera frame with respect to the robot frame is then obtained by commanding the robot to place n ($n \geq 2$) spheres in the FoV of the camera in non-aligned positions.

To accomplish this task, the first already calibrated camera was exploited. It allows to calculate the x-y coordinates in the robot reference system of some spheres lying in the substrate in area1 and to send them to the robot controller.

The robot then picks by vacuum and places the spheres in the specified positions of the FoV of the second camera. The spheres barycenters are then calculated in the camera reference frame and the transformation with respect to the robot frame can be computed.

The procedure for the evaluation of the calibration error for the second camera was identical to the previous one. The calibration quality was checked by placing some spheres to some points different from those used for the georeferencing and the measuring error was evaluated.

Table 3 reports the obtained results.

Table 3 Results of the hybrid calibration applied to the area2 (number of georeferencing n=4 and grid of verification points of 12 positions).

Error in georeferencing points [µm]			Error in non-georeferencing points [µm]		
Mean error	Max error	Standard deviation	Mean error	Max error	Standard deviation
67.5	128.3	36.0	62.7	103.1	31.5

4.2.2 Virtual grid strategy

Operatively, the process for the grid of spheres construction was similar to the approach used for the first camera georeferencing. A grid of 4x3 dots was considered suitable, since it provided a more than sufficient amount of data and an execution time relatively low, which is an

important aspect if a re-calibration of the system is needed frequently. The robot picks and places, one by one, the spheres in the FoV of the camera to be calibrated. For each sphere deposition, the camera takes a picture of the under-construction grid. This last placed sphere is detected and its pixel barycenter is calculated. The data are then used to calibrate the second camera using the same mathematical approach used for the first camera. The position errors obtained with this approach are reported in Table 4.

Table 4 Results of the virtual grid calibration applied to the area2 (in all, two grids of 12 positions each have been considered).

Error in calibration points [μm]			Error in non-calibration points [μm]		
Mean error	Max error	Standard deviation	Mean error	Max error	Standard deviation
6.8	20.8	4.8	19.5	46.2	12.3

5. The end-effector calibration

When commanding the robot to move over a part to pick it with an angle different from that used during the camera-robot calibration, a position error was observed.

It was verified that the error was due to a geometrical error of the gripper (Fig. 3). Thus, a simple and agile kinematic calibration of the robot end-effector has also been conceived to obtain higher accuracy. This calibration exploited the setup available in area1 able to provide a bottom view of the microgripper. Indeed, the already calibrated and georeferenced camera 1 has been considered a suitable measurement system of the robot end-effector position. The following describes the method and shows the achieved improvements.

5.1 The error model

The microgripper can be affected by misalignment and orientation errors with respect to vertical rotational axis of the manipulator which can lead to imprecise grasping and releasing of the microparts. A simple schematization of the comparison between the ideal and the actual situation is reported in Fig. 3. In the ideal case, a commanded rotation α about the fourth robot axis results in a pure rotation of the microgripper, thus no displacement in the x-y plane occurs. In case (b), since the center of the gripper is not located on the rotation axis, the gripper rotation produces a displacement of the grasped part.

An analysis of the system suggested the adoption of a rigid model to describe the gripper deformation. If we consider to command a set of angular displacement keeping constant the position x, y and z of the end-effector, the sphere barycenters detected by the vision system should lay on a circumference about the vertical axis. The reference model can thus be derived and its representation is reported in Fig. 4. It can be considered as the bottom view of the robot end-effector by the camera looking at area1.

Let's denote with α_{cal} the end-effector rotation angle used during the camera calibration process and with $P = [x, y]$ the corresponding planar position of the end-effector, lying on the

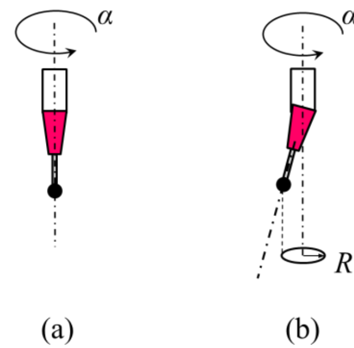

Fig. 3 Schematization of the end-effector error: (a) ideal model; (b) error affected model.

circumference of radius R and center $P_o = [x_o, y_o]$ belonging to the rotation vertical axis:

$$\begin{bmatrix} x \\ y \end{bmatrix} = \begin{bmatrix} x_o \\ y_o \end{bmatrix} + \begin{bmatrix} \Delta x \\ \Delta y \end{bmatrix}$$

where Δx and Δy represent the misalignment of the microgripper with respect to P_o when $\alpha = \alpha_{cal}$.

Now consider to rotate the end-effector of the angle α_j relative to α_{cal}; it will achieve the new position $P_j = [x_j, y_j]$:

$$\begin{bmatrix} x_j \\ y_j \end{bmatrix} = \begin{bmatrix} x_o \\ y_o \end{bmatrix} + \begin{bmatrix} \cos(\alpha_j) & -\sin(\alpha_j) \\ \sin(\alpha_j) & \cos(\alpha_j) \end{bmatrix} \begin{bmatrix} \Delta x \\ \Delta y \end{bmatrix}$$

Thus, the position error ΔP_j due to the misalignment results:

$$P_j - P = \begin{bmatrix} \Delta x_j \\ \Delta y_j \end{bmatrix} = \begin{bmatrix} \cos(\alpha_j) - 1 & -\sin(\alpha_j) \\ \sin(\alpha_j) & \cos(\alpha_j) - 1 \end{bmatrix} \begin{bmatrix} \Delta x \\ \Delta y \end{bmatrix}$$

In this model, Δx and Δy are two unknown constant parameters. Their estimation is fundamental, since it allows to compensate for the described error without hardware intervention and increase the overall system accuracy. In order to find the actual values of the parameters, the Least Square Method has been applied to a set of different achieved positions on the circumference.

It is worth to note that increasing the number of rotations, a better estimation could be obtained.

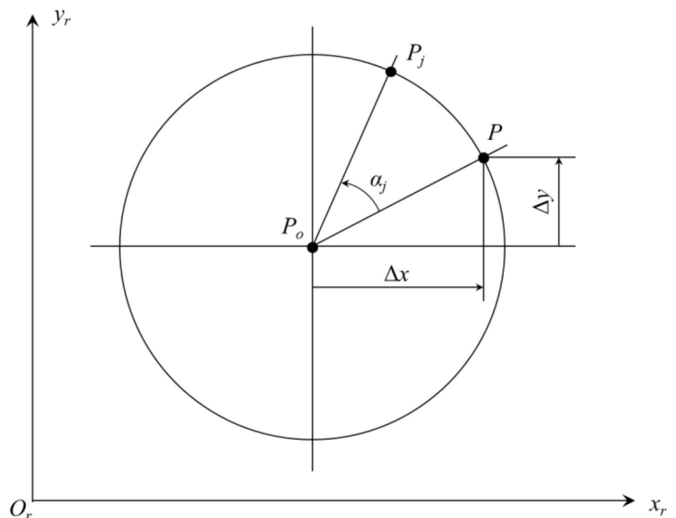

Fig. 4 Reference model for the end-effector calibration.

5.2 Experimental procedure and results

It was decided to make the end-effector rotate over 360° with a step of 20°, thus 18 rotations about the vertical axis were executed. Since the previous camera calibration could not totally eliminate errors in the image acquired by the camera, the series of rotations were repeated in many different positions in the field of view, aiming to maximize the performance of the calibration process. Therefore, a grid of 30 positions (6x5) was considered suitable. The process develops as follows:

1. the robot end-effector, while grasping a sphere, is commanded to the first position of the grid with the same angle used during the camera calibration process;
2. the camera takes a picture of the sphere, calculates its position and stores it in memory;
3. the end-effector rotates of the chosen step angle (20°);
4. steps (2) and (3) are repeated until the span of 360°;
5. the robot is commanded to move in the second (or the following) position of the grid with the calibration angle;
6. steps (2) to (5) are repeated until the last rotation in the last position of the grid has been performed.

An over-constrained system of equations is obtained rewriting the equation of ΔP_j for all the considered gripper poses. The system is linear in the unknowns Δx and Δy, thus they can be easily estimated by the Least Mean Square method (see Table 5). This makes the compensation of their effect possible by means of a geometrical model.

To evaluate the benefit of this calibration process, the final mean and maximum position errors and the standard deviation values have been measured before and after the correction in 30 positions different from those used during the calibration process and scattered in the working area. The results are reported in Table 6: in particular, the first three columns in table report the errors that would be obtained if a position were achieved with different orientations ignoring the correction. As one can see, the errors without the use of end-effector calibration are an order of magnitude higher than those with the end-effector calibration. Thus, a dramatic improvement has been obtained.

Table 5 Estimated values of the end-effector calibration parameters.

Δx [µm]	Δy [µm]
-68.7	137.2

Table 6 Results of the end-effector calibration (in all, two grids of 30 positions each and 18 rotations per position have been considered).

Error before calibration [µm]			Error after calibration [µm]		
Mean error	Max error	Standard deviation	Mean error	Max error	Standard deviation
188.8	309.3	109.7	11.8	30.0	6.2

6. Discussion

In the previous sections, the developed strategies for the complete work-cell calibration have been addressed. Concerning the non-conventional calibration methods applied to the different areas, consider the obtained results reported in Table 1, 2, 3, 4. As one can notice, the virtual grid strategy appears more efficient than the hybrid one, both in terms of mean and maximum errors and standard deviation.

An analysis of the two calibration strategies leads to the evaluation of the different sources of errors. With reference to the hybrid calibration, the total error is given by the combination of errors deriving both from the camera calibration and from its georeferencing. In particular, the camera calibration is affected by the dot spacing tolerance of the grid and by the error committed by the vision algorithm which detects the dot barycenters. In the georeferencing, a considerable error arises since there is an offset between the georeferencing and the calibration planes, which cannot be neglected without the use of high-precision devices. This causes the mean and maximum errors in the georeferencing points to be comparable with those in non-georeferencing points, oppositely to what happens in the case of the virtual grid strategy. Moreover, the use of the robot to move the spheres involves a further error due to the encoder resolution. Again, an error associated to the barycenter identification by the vision algorithm occurs. In the specific case of the first camera, a small error in the auto-centering of the sphere gripped by the robot end-effector can affect the process. In the case of the second camera, this error adds to the error in positioning the sphere on the adhesive substrate caused by the subtle collision between the gripper and the substrate itself.

On the other side, since in the virtual grid calibration strategy the camera calibration and its georeferencing are performed simultaneously, less sources of error than in the previous strategy arise. In this case, errors due to the encoder resolution and to the vision algorithm performance occur. The error associated to the auto-centering of the sphere adds when the first camera is calibrated, and, for the second camera, the additional error in positioning the spheres arises.

To support the calibration of the area2, it has been decided to exploit the already calibrated camera 1: on the other hand, a mechanically fixed reference place where spheres are picked up could also be adopted. This choice has been done to neglect the use of external devices.

Concerning the end-effector calibration, an important aspect is represented by the need of a calibrated vision system to support its actual implementation. Thus, both from the conceptual and operational point of views, the end-effector calibration has been addressed subsequent to the calibration of the area1. For this reason, the main error source is the area1 calibration error, which adds to the errors due to the encoder resolution, the vision algorithm performance and the auto-centering of the sphere.

It is worth to note that the sphere diameter is not an influential parameter as long as it does not involve mechanical interference among the placed spheres. Moreover, it does not need to be precisely known in advance.

To conclude the discussion about the different calibration strategies, besides a performance analysis in terms of precision,

an investigation on the feasibility of the calibrations execution is fundamental. Comparing the two calibration strategies in terms of execution time, the virtual grid approach is slower than the other one, since the grid construction takes time: indeed, with reference to the calibration of area1, while the execution of the hybrid strategy takes some seconds (8 seconds in the case of 4 georeferencing points), the construction of a 8x7 virtual grid takes about 2 minutes. This difference is due to the definitely fewer positions needed for the georeferencing than for the virtual grid calibration strategy, since the time needed for taking an image of the physical grid of dots is negligible. Furthermore, the time necessary to calibrate the area2 is always much higher than that needed to calibrate the area1, regardless of the adopted method, since both the virtual grid construction and the georeferencing derive from a pick and place operation. For example, in the case of a 4x3 virtual grid construction in area2, the execution time is about 3 minutes (note that, compared to the virtual grid of area1, 50% more time is necessary to build a grid of one-fifth of positions). As to the hybrid strategy, the georeferencing of the second area using 4 positions takes about one minute, that is eight times more than that of the first one. Concerning the end-effector calibration, the execution time can take several minutes: for example, a 6x5 grid with 18 rotations for each position can be executed in 12-13 minutes. Obviously, as the number of points in the calibration grid or the step in the series of the end-effector rotations increases, the time will increase proportionally. In all cases, note that the time can vary depending on how fast the vision system recognizes the spheres.

The economic aspect is also relevant: in fact, an accurate actual grid can be very expensive, thus the hybrid approach requires higher costs than the virtual grid strategy. Indeed, the price of a commercial grid can be two orders of magnitude higher than that of some glass spheres.

7. Conclusions

This paper presented different calibration strategies applied to a micromanipulation work-cell. Two methods for the camera calibration and the camera-robot georeferencing have been compared and critically analyzed. The virtual grid approach demonstrated its effectiveness and higher efficiency than the hybrid calibration strategy, both from the performance and economic points of view. Moreover, the developed kinematic end-effector calibration procedure allowed a significant improvement of the overall system accuracy, fundamental when manipulating parts with sub-millimetric dimensions.

ACKNOWLEDGEMENT

The work has been developed within the research project PRIN 2009 - MM&A “Micro Manipulation and Assembly”, supported by the Italian Ministry for University and Research (MIUR).

REFERENCES

1. Schröer, K., “Precision and calibration”, in “Handbook of Industrial Robotics”, 2nd edition, Wiley & Sons Inc., New York. Edited by Shimon Y. Nof, 1999.
2. Zhang, Z., “A flexible new technique for camera calibration”, IEEE Transactions on Pattern Analysis and Machine Intelligence, Vol. 22, No. 11, pp. 1330-1334, 2000.
3. Fryer, J. G. and Brown, D. C., “Lens distortion for close-range photogrammetry”, Photogrammetric Engineering and Remote Sensing, Vol. 52, pp. 51–58, 1986.
4. Shapiro, L. G. and Stockman, G. C., “Computer Vision”, Englewood Cliff s, NJ: Prentice-Hall, 2002.
5. Mitsubishi website: http://www.mitsubishi-automation.co.uk/
6. Bottema, O. and Roth, B., “Theoretical kinematics”, Dover Publications Inc., New York, pp. 312–315, 1979.
7. ISO 9283:1998 Manipulating industrial robots - Performance criteria and related test methods, 1998.
8. ISO/TR 13309:1995 Manipulating industrial robots - Informative guide on test equipment and metrology methods of operation for robot performance evaluation in accordance with ISO 9283, 1995.
9. Legnani, G., Mina, C., and Trevelyan, J., “Static calibration of industrial manipulators: Design of an optical instrumentation and application to SCARA robots”, Journal of Robotic Systems, Vol. 13, No. 7, pp. 445-460, July 1996.
10. Mooring, B. W., Roth, Z. S. and Driels, M. R., “Fundamentals of manipulator calibration”, John Wiley & Sons Inc., New York, 1991.
11. Omodei, A., Legnani, G. and Adamini, R., “Calibration of a measuring robot: Experimental results on a 5 DOF structure”, Journal of Robotic Systems, Vol. 18, No. 5, pp. 237-250, May 2001.
12. Tamadazte, B., Dembélé, S., Le Fort-Piat, N., “A Multiscale Calibration of a Photon Videomicroscope for Visual Servo Control: Application to MEMS Micromanipulation and Microassembly”, Sensors & Transducers Journal, Vol. 5, Special Issue, pp. 37-52, March 2009.

Micro Oscillation Milling System with Magnetically Suspended Micro-Spindle and a 3DOF Wedge Stage

Seung-Kook Ro[1,#], Gyungho Khim[1], Soo-Chang Choi[1] and Jong-Kweon Park[1]

1 Department of Ultra-Precision Machines and Systems, Korea Institute of Machinery and Materials, Daejeon, Korea
Corresponding Author / E-mail: cniz@kimm.re.kr, TEL: +82-43-868-7115, FAX: +82-42-868-7180

KEYWORDS : Oscillation milling, Magnetic bearings, Tool orbit control, Micro-milling

This paper introduces a system to machine micro-sized patterns effectively on surface based on micro-milling process using tools with rotation and oscillation. A spindle supported by active magnetic bearings in radial directions were developed and implemented for proposed system. The rotating axis of the tool can be moved faster than stage system up to 500 Hz of within air gap as amplitude. This can be applied for repeated patterns without movement of stages carrying workpiece or spindle which have usually slower response time. To review the effectiveness of proposed concept, we integrated the proposed micro-spindle with active magnetic bearings with a precision 3-axis air bearing stage using double-wedge mechanism, and tested this oscillation milling. A flat end mill with 0.8 mm diameter rotating 100 krpm was induced to workpiece with 35 degrees of inclination angle while oscillated 200 Hz in radial direction. The results show machined pattern spacing 20 μm and 40 μm due to feeding speed of the workpiece 4 mm/sec and 8 mm/sec.

1. Introduction

Recently, the Micro-factory system technology covers more area in manufacturing industries for mobile electronics, automobile and biomedical area with various processes such as cutting, forming, joining and more. For the micro-machining system with minimized size, it is regarded as beneficial to reach high precision easily during less usage of resources and energy. In this manner, we developed some micro-machining system such as desktop milling machine, 5-axis milling machine, desktop turning machine and reconfigurable multi-axis machines. The developed systems were demonstrated for machining of complex mechanical parts less than 5 mm with accuracy of few μm.
There are various researches and developments on going for manufacturing micro-patterns on surfaces for special functionalities such as reduction of friction, biomedical absorption or desorption and optical performances. The required features have size of 0.1~100 microns with repeatable or arbitral patterns. Many methods of the machining were introduced so far, such as laser-based micro machining, chemical process and coatings, forming and molding on surface or film, and mechanical machining directly on surfaces of metal or other materials.
For machining of micro-patterns in metal, micro turning, fly cutting and grinding can be implemented. The micro-milling with small flat or ball end mills can provide accurate machining features less than 10 μm with precision micro-machining systems. But the features must be created by movement of machines, stages or feed-drives, and the speed of the process is limited by the response time of the drive system. So, one possible solution for increasing productivity is making machining system react faster, so the miniaturization of machine system can be a solution as the Micro-factory concept. This limits the productivity especially when the features should be machined on large area. Hence, micro-machining with very fast moving tools such as fast tool servo (FTS) or fly-cutting were considered so far. In this paper, we propose a method of machining micro features using oscillating milling, oscillation of rotating axis of the tool with high speed micro milling spindle. To do this, a magnetically suspended micro-spindle was developed and tested for its control bandwidth of the oscillation. The micromachining set-up was built with desktop 3-DOF double wedge platform with air bearing stages, and preliminary oscillation machining was performed.

2. Proposed System

2.1 Concepts

The Fig. 1 shows the concept of the proposed method as an example. If a micro milling tool rotates with 100,000 rpm, and also rotating center is oscillating simultaneously with 200 Hz

and amplitude of 10 μm while a workpiece is moving with speed of 1 mm/sec, the result will be a pattern of 10 μm wave with wave length of 5 μm. Considering this uses rotating tools, the cutting mechanism will be similar to the micro milling with low cutting forces. If this is tried with conventional micro-milling, the stage carrying spindle or the workpiece should move as 200 Hz, and this is usually higher than servo bandwidth of the stage system. To realize this concept, some mechanisms that can oscillate rotating tools directly are needed, so a spindle supported by magnetic bearings was applied. For the movement of the workpieces, a 3-DOF stage with double wedge stage was implemented.

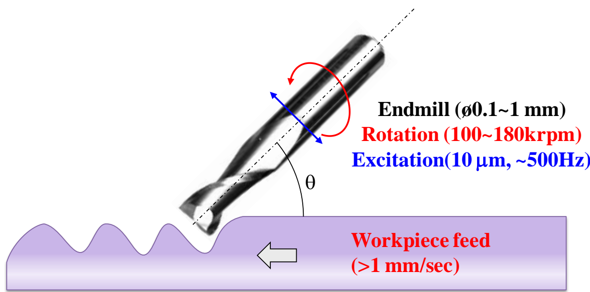

Fig. 1 Example of the concept of micro oscillation milling

2.2 Spindle with magnetic bearings

Fig 2 shows the micro-spindle proposed by the authors. The 4-axis active magnetic bearings with permanent and electromagnets were designed for high speed rotation and active control of the tool position. The size of the spindle is 62 mm of diameter including housing and 94 mm long. The shape memory based tool clamping system is located front end for tools with 3-mm shank diameter. This spindle can be run up to 200,000 rpm with air turbine in the middle of the shaft. The desirable operating range is 80,000 ~ 180,000 rpm for stable rotational response. The control bandwidth for the radial motion of the spindle is about 1 kHz, and the radial auxiliary air bearing gap is 15 μm. So, the shaft can be oscillated up to 20 μm within the air gap of the auxiliary bearings.

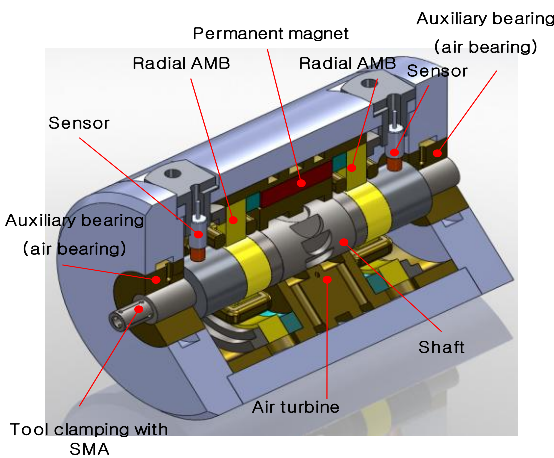

Fig. 2 Micro spindle with active magnetic bearings and air bearings

Fig. 3 shows measured orbit result of tool position obtained from magnetic bearing sensors while spindle is rotating 110,000 rpm (1.8 kHz) and excited 50~500 Hz in radial direction by injecting external signal to the reference signal of the magnetic bearing controller. It can be noticed that runout measured at the front and rear sensors were less than 10 μm, and about 10 μm of additional oscillations were possible up to 500 Hz. Fig. 4 shows measured displacement at the shaft front end with a capacitive sensor with 50~500 Hz of excitation. Considering the outer envelope will be the machining trajectory, it can be noticed that about 10 μm of shape can be machined if there is no deflection of the tool.

Table1 Specifications of the active micro spindle

Radial bearings	Active magnetic bearings / air bearings
Thrust bearings	Air bearings
Motor	Air turbine
Maximum speed (rpm)	200,000
Static stiffness (N/μm)	0.6
Tool shank	3 mm (SMA clamping)
Air gap of magnetic bearings, g_0 (mm)	0.05
Radial clearance of air bearings (μm)	15

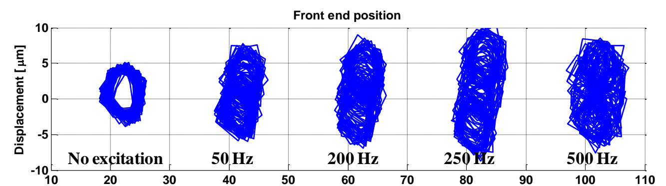

Fig. 3 Tool orbit measured by front sensors with excitations

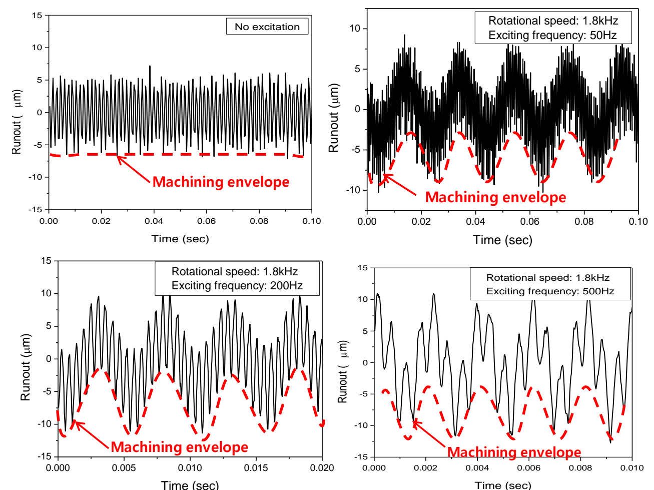

Fig. 4 Radial displacement of tool measured with a capacitive sensor while rotating 110 krpm with 0, 50, 200 and 500 Hz of oscillation.

2.3 3-axis wedge stage

For the large long area of machining with high precision, a 3-axis double wedge stage is used for work piece carriage. The wedge stage consists of two side wedges and a center wedge. The two side wedges are responsible for x-axis motion (horizontal) and z-axis motion (vertical). The movement direction (pure x-axis motion, pure z-axis motion, simultaneous motion of x and z-axis) of the wedge stage depends on a relative velocity of the two wedges. An independent y-axis slide is installed on the center wedge. So the wedge stage can move in the direction of three axes. A

pneumatic counterbalance system between the two side wedges is installed for counteracting the weight of the center wedge and the y-axis slide to achieve a better control ability of the z-axis motion. A pressurized air is supplied in the pneumatic cylinder in order to support the weight of the center wedge and the y-axis slide.
Fig. 5 shows the diagram of the stage, and Fig. 6 shows working principle of wedge stage. If the two side wedges move in the same velocity “a” and same direction, the center wedge also moves in the same direction with a velocity of “a”. On the other hand, if the two side wedges move in the same velocity “a” and opposite direction, the center wedge moves in the only z-axis direction with a velocity of “b”. The relation between “a” and “b” depends on the angle (θ).

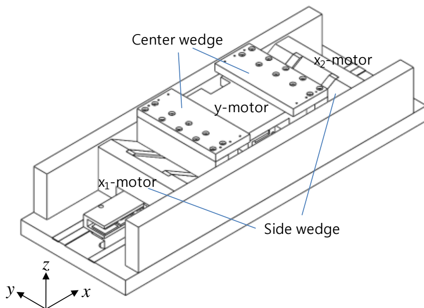

Fig. 5 XYZ stage system with air bearings and linear motors

Table2 Specifications of the double wedge XYZ stage

Bearing type	Air bearings with magnetic preloads
Motors	Linear motors (108 N peak)
Positioning resolution (μm)	0.05
Moving range (X, Y, Z) (mm)	180, 25, 25
Positioning accuracy (μm)	0.85
Straightness (vertical, horizontal) (μm)	0.22, 0.29

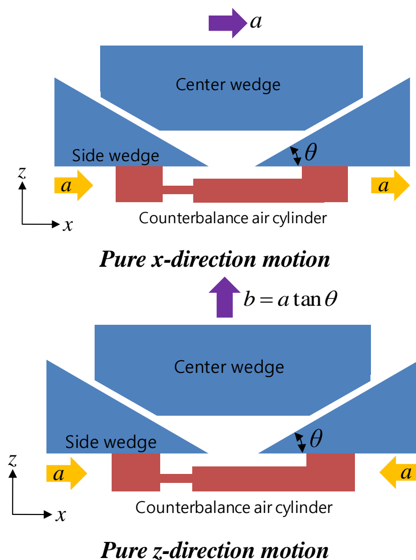

Fig. 6 Principle of a double-wedge stage

The prototype was built with a numerical controller (Delta-Tau UMAC system), and the angle of the wedge was measured as 30.157°. The positioning accuracy and motion errors were measured and compensated by on-line compensation. After using conventional pitch error compensation method , 0.85 μm for positioning accuracy reduced from 8.96 μm, and 0.22 μm and 0.29 μm for vertical and horizontal straightness errors were obtained for 180 mm of movement range for x direction. These results are satisfactory for precision machining where relatively long stroke in one direction is required.

3. Oscillation milling test

3.1 Desktop machining set-up

Fig. 7 shows the machining test system proposed in this research. The active magnetic bearing (AMB) spindle was attached on a rotary table horizontally to change tool incidence angle. The XYZ stage was used to carry a workpiece in three directions. As the moving range of the X axis of the stage covers enough space, the tool end point should not be near to the center of the rotary table.

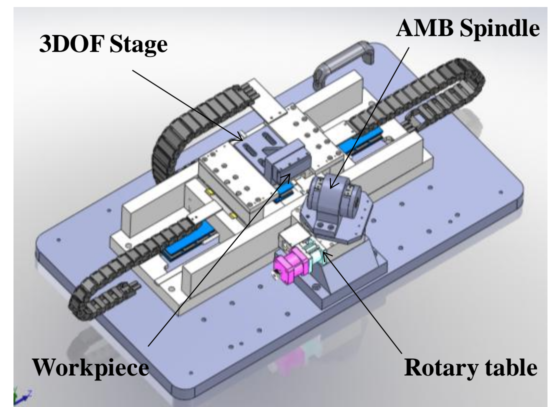

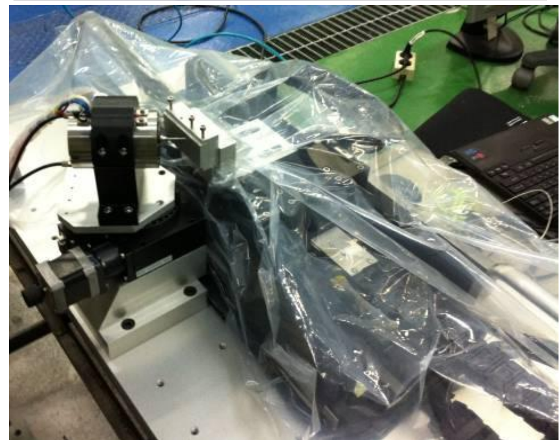

Fig. 7 Experimental set-ups for oscillation micro milling

3.2 Oscillation micro milling results

To verify proposed concept, we performed primitive machining test with a flat end mill with 0.8 mm diameter as shown in Fig. 8. The angle between tool and workpiece was 35°, and rotating speed of the spindle is 100,000 rpm. During with rotation of the spindle horizontal oscillation of the shaft was applied from the controller of the magnetic bearing controller. 200 Hz of sine signal of the injected, and the resultant displacement of the tool was expected as shown in Fig. 4. The workpiece was fed x direction with two speeds, 4 mm/sec and 8 mm/sec. Fig. 8 shows the machining set-up.

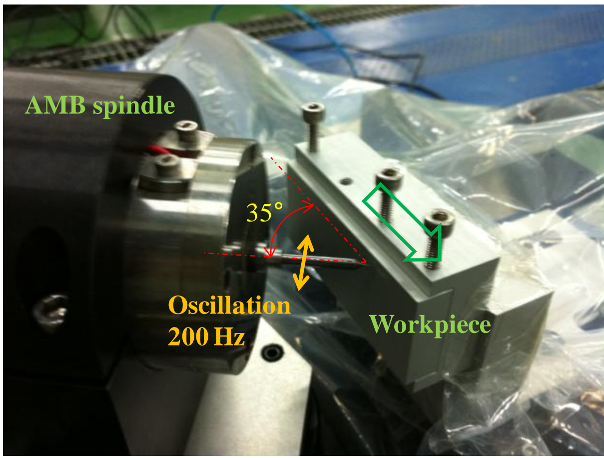

Fig. 8 Oscillation micro-milling set-up

Fig. 9 shows the picture of the machined surface with and without oscillation at to feeding speed, 4 mm/sec and 8 mm/sec. Four sections were machined. The area 1 is surface without oscillation, and the area 2 is machined surface with 200 Hz of oscillation at 4 mm/sec. It can be observed that there is clear patterns with oscillation. For the area 3 and 4, which are fed at 8 mm/sec with different vertical feed step. the size of groove became bigger than those at area 2. These result can be also confirmed from the measured surface profile with con-focal microscope image shown on Fig. 10. At 8 mm/sec feed rate with oscillation of 200 Hz, pattern with 8 μm period and 10 μm of amplitude could be obtained. So, it can be concluded that period can be controlled by choice of oscillation frequency and feeding speed. However, future improvement of spindle reducing runout may be needed to improve surface quality.

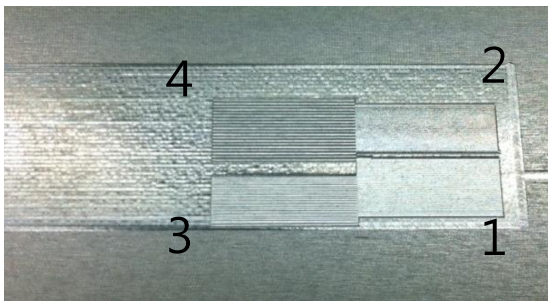

a. Machined surfaces

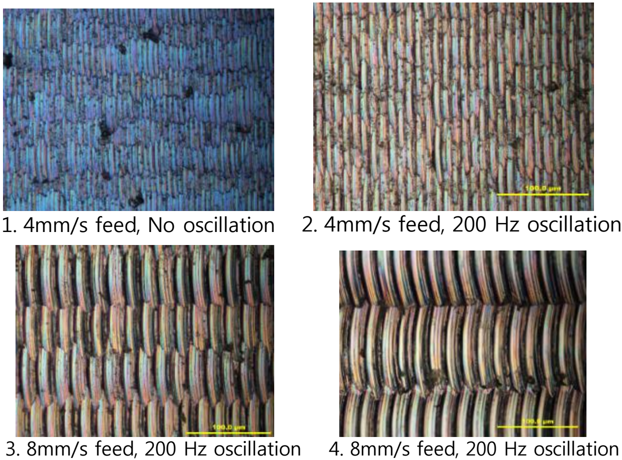

b. microscope images of the 4 sections

Fig. 9 Photo and optical microscope image (50x) of machined surfaces with oscillation milling

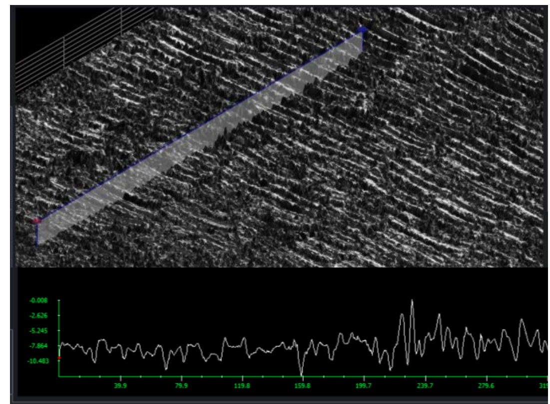

a. section 1, no oscillation

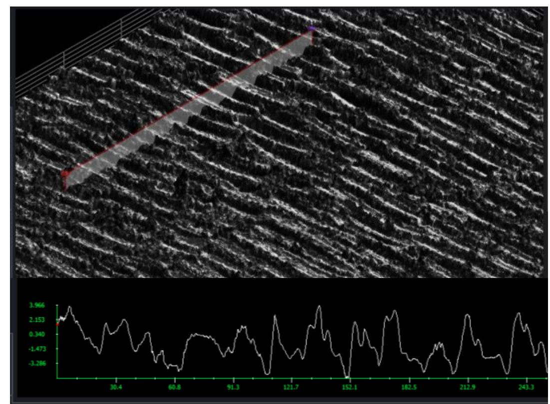

b. section 2, 200 Hz, 4 mm/sec

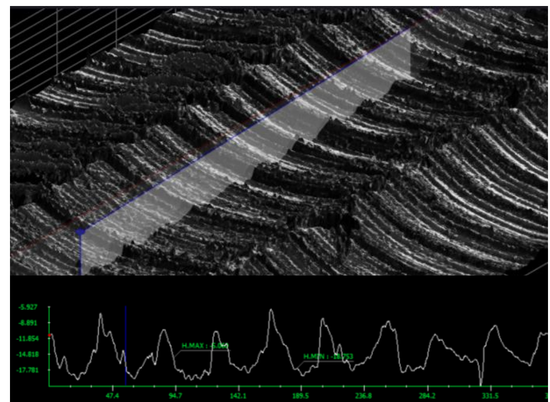

c. section 4, 200 Hz, 8 mm/sec

Fig. 10 Surface machined with oscillation milling measured by a con-focal microscope

4. Conclusion

In this paper, we proposed a micro-machining with a magnetic bearing spindle with oscillation while rotating high speed over 100,000 rpm with conventional micro-end mills. The desktop machining set up was built with a 3-axis wedge stage with long travel in one direction and a rotary table to change incidence angle of tool to surface. The machining test was performed with rotating and oscillating end mill with 100,000 rpm and 200 Hz, and the regular forms of the machined surface were observed to reveal the feasibility of the proposed concept.

ACKNOWLEDGEMENT

The works described in this paper were supported by the Industrial Source Technology Development Programs funded by the Ministry of the Knowledge Economy, MKE, And the authors specially thanks to the Technorise Co. Ldt, Daekon Cooperation and Prof. Kornel Ehmann of Northwestern University for collaboration on prototype developments.

REFERENCES

1. Denkena, B., Kaestner, J. and Wang, B., "Advanced Microstructures and Its Production Through Cutting and Grinding," CIRP Annals - Manufacturing Technology, Vol. 59, No. 1, pp. 67-72, 2010.
2. Ro, S.-K., Jang, S.-K., Kim, B.-S. and Park, J.-K. "Development of a Miniature Vertical Milling Machine for Automation Used in a Microfactory," Proc. Of ICSMA, pp. 186-189, 2008.
3. Kuroki, J., Shinshi, T., Li, L. and Shimokohbe, A. "A Micro-Magnetic Bearing Using Capacitive Axial Displacement Sensing," Precision Engineering, Vol. 30, pp. 54-62, 2006.
4. Ro, S.-K., Shin, W.-C., Kyung, J.-H. and Park, J.-K., "A Miniature High-Speed Spindle with Permanent Magnet-Biased Magnetic Bearings," Proc. Of the 8th IFToMM Int. Conf. on Rotor Dynamics, pp. 676-680, 2010.
5. Khim, G., Ro, S.-K., Park, J.-K. and Ehmann, K. F., "Motion Error Compensation of the 3-Axis Wedge Stage," Proc. Of 7th Int. Workshop on Microfactories, 2010.
6. Park, J.-K., Ro, S.-K., Kim, B.-S., Shin, W.-C. and Lee, H.-H, "Precision Component Technologies for Microfactory Systems Developed at KIMM," International Journal of Automation Technology, Vol. 2, No. 2, pp 127-137, 2010.

Proposal of a position sensor for the spherical motor

Tomoaki Yano[1], **Nagayoshi Kasashima**[1] and **Kiwamu Ashida**[1,#]
1 Advanced Manufacturing Research Institute, National Institute of Advanced Industrial Science and Technology,1-2-1 Namiki, Tsukuba, Ibaraki, Japan,
Corresponding Author / E-mail: ashida.k@aist.go.jp, TEL: +81-29-861-7155, FAX: +81-29-861-7201

KEYWORDS : Position sensor, Spherical motor, Image sensor

A Spherical motor is an actuator with multi degrees of freedom and the rotation centers coincide. As three conventional motors are replaced by a spherical motor, the spherical motor will make the multi DOF system compact. Therefore, it will be one of the key components of the small multi DOF systems like micro handling system. But there are no good sensors which measure the position of the spherical rotor in the spherical motor. This paper proposes a rotor position sensor for the spherical motor with two mouse sensors, which measure 2DOF circumferential speed.

At first, several ideas of the position sensors for the spherical motor are reviewed and discussed. Select a position sensor with two mouse sensors. The basic ideas for getting the position from the data of two mouse sensors are presented. The mouse sensors which satisfy the specifications of the position sensor for the developed spherical motor are selected. Two mouse sensors are set on the manufactured rotor holder and the performances of rotor position measurement are tested. The problems of the developed position sensor and the future works are also discussed.

NOMENCLATURE

basis of the stator coordinate system

= $\mathrm{S} =< \mathbf{s}_1, \mathbf{s}_2, \mathbf{s}_3 >$

sequence of bases of the rotor coordinate system

= $\left\{ \mathrm{R}^{(i)} =< \mathbf{r}_1^{(i)}, \mathbf{r}_2^{(i)}, \mathbf{r}_3^{(i)} > \right\}$

basis of the sensor coordinate system

= $\mathrm{M} =< \mathbf{m}_1, \mathbf{m}_2, \mathbf{m}_3 >$

basis transformation matrix from $\mathrm{R}^{(i)}$ to $\mathrm{R}^{(i+1)}$ = $\mathbf{K}_{\mathrm{R}_i}$

basis transformation matrix from S to M = $\mathbf{K}_{\mathrm{M}}$

rotor angular velocity vector on S = $\boldsymbol{\omega}_{\mathrm{S}}$

unit vector of the rotational axis on S = $\mathbf{n}_{\mathrm{S}}$

angle of rotation around $\mathbf{n}_{\mathrm{S}}$ = θ

position vector of the mouse sensor j on S = $\left(\mathbf{p}_j\right)_{\mathrm{S}}$

unit vectors of sensing direction of mouse sensor j on S

= $\left(\mathbf{u}_{j1}, \mathbf{u}_{j2}\right)_{\mathrm{S}}$

reading data of mouse sensor j = $\left(v_{j1}, v_{j2}\right)$

a set of reading data of mouse sensors = $\boldsymbol{\upsilon}$

sequence of sensing time interval = $\{\Delta\tau_i\}$

1. Introduction

From humanoid robots to automobiles, the number of degrees of freedom of mechanical systems continues to grow. There has also been a proportional increase in the number of motors used in the mechanical systems. On the other hand, the human joints like the shoulder joints have at least three degrees of freedom (lateral direction, anteroposterior direction, and arm rotation). When a spherical motor with multi degrees of freedom like a human shoulder joint is in practical use, a lot of systems with multi degrees of freedom will be compact, lightweight, and high performance.

Therefore, various kinds of spherical motors have been developed and tested [1-7]. The authors also proposed the structures of the spherical motors based on the polyhedrons [8,9]. The performances of the proposed spherical motors are expected to be the same in any rotational direction by their spherical symmetric structures. The experimental results of developed spherical motors are shown in the previous papers [10,11]. However, the motors are controlled by open-loop, as there are no good rotor position sensors.

The performances of the developed motors are limited without position sensor.

There are several reports for the position sensors of the sphere. The most popular sensing system uses gimbal mechanism fixed on the rotor output shaft [12]. Three rotational angle sensors are put on the pivots of the gimbal. The rotary encoders are usually used to measure the rotational angles. The absolute position is calculated from the measured three angles, which are roll, pitch, and yaw. However, the gimbal mechanism has several problems. It will make the motor large and heavy and limit the working area of the rotor.

Wada, Y. and Gofuku, A. developed an absolute rotor posture sensor with 64 Hall devices [13]. The sensor can measure the absolute position of the 100mm diameter rotor with 32 permanent magnets. However, the position measurement error is around 5deg. As the radius of a Hall device's sensing area is around 8mm, a lot of Hall devices should be needed for the precise position sensing.

Aoyagi, M. et.al. developed an absolute rotor position sensor with CCD camera [14]. Two luminescence devices are fixed on the rotor surface. The rotor position is calculated from the two luminescence device coordinates on the graphic image of the CCD camera. The sensor resolution is 0.57 deg and the measurement area is 70 x 70 x 360deg^3. This sensor system needs a wide opening in the stator for taking the graphic image.

Stain, D. et.al. developed an absolute spherical encoder [15]. The rotor surface is colored in black and white Voronoi diagram. 192 one bit black and white detect devices are put on a ring. The sensor can measure the position of the rotor within 1 deg error by reference to the prepared position map. This sensor needs a lot of black and white detect devices for the precise position measurement.

Lee, K. M. developed an incremental rotor orientation sensor with a vision sensing device [16]. A grid pattern and an origin marker are painted on the rotor. The orientation of the rotor is calculated from the vision.

Hama, N. et.al. developed an absolute rotor position sensor with a full color sensing device [17]. The rotor surface is colored in Hue, Lightness, and Saturation graduating color. Hue changes around z axis, Lightness changes around x axis, and Saturation changes around y axis. However, the sensing error is several deg.

Kumagai, M. et.al. developed an incremental ball rotating sensing system with three mouse sensors [18]. The diameter of the ball is 200 mm. The sensing error is less than 3.6 deg for each rotational axis after rotating the rotor 360 deg around the rotational axis at 100 deg/s.

This paper proposed a position sensor with two mouse sensors. The sensing method is similar to the previous work [18]. Although the previous work uses three rotational angles to obtain the rotation matrix, our work uses the basis transformation matrix to obtain the rotor position.

2. Sensing Method

2.1 Representation of the rotor position

The basis of the coordinate matrix system $\mathrm{R}^{(0)} =< \mathbf{r}_1^{(0)}, \mathbf{r}_2^{(0)}, \mathbf{r}_3^{(0)} >$ is fixed on the rotor and the basis of the coordinate matrix system $\mathrm{S} =< \mathbf{s}_1, \mathbf{s}_2, \mathbf{s}_3 >$ is fixed on the stator as shown in Fig.1.

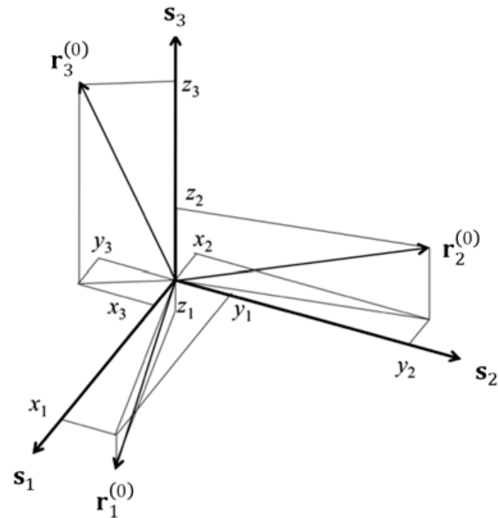

Fig. 1 Rotor coordinate system and stator coordinate system

Matrix $\mathbf{K}_{\mathrm{R}_i}$ is referred to as the "basis transformation matrix from S to $\mathrm{R}^{(i)}$", and can be used for transforming any vector $\mathbf{a}$ from S representation to $\mathrm{R}^{(i)}$ representation, according to the following theorem:

$$\mathbf{a}_{\mathrm{R}i} = {}^t\mathbf{K}_{\mathrm{R}_i}\mathbf{a}_{\mathrm{S}} \tag{1}$$

Therefore, when the basis vectors $\left(\mathbf{r}_1^{(i)}, \mathbf{r}_2^{(i)}\mathbf{r}_3^{(i)}\right)$ are measured on the stator basis such as equation (2) (Fig.1), $\mathbf{K}_{\mathrm{R}i}$ is simply represented by equation (3).

$$\begin{aligned} \mathbf{r}_1^{(i)} &= x_1^{(i)}\mathbf{s}_1 + y_1^{(i)}\mathbf{s}_2 + z_1^{(i)}\mathbf{s}_3 \\ \mathbf{r}_2^{(i)} &= x_2^{(i)}\mathbf{s}_1 + y_2^{(i)}\mathbf{s}_2 + z_2^{(i)}\mathbf{s}_3 \\ \mathbf{r}_3^{(i)} &= x_3^{(i)}\mathbf{s}_1 + y_3^{(i)}\mathbf{s}_2 + z_3^{(i)}\mathbf{s}_3 \end{aligned} \tag{2}$$

$$\mathbf{K}_{\mathrm{R}i} = \begin{bmatrix} x_1^{(i)} & x_2^{(i)} & x_3^{(i)} \\ y_1^{(i)} & y_2^{(i)} & y_3^{(i)} \\ z_1^{(i)} & z_2^{(i)} & z_3^{(i)} \end{bmatrix} \tag{3}$$

The rotor position is represented by $\mathbf{K}_{\mathrm{R}i}$. As $\mathbf{K}_{\mathrm{R}i}$ is the orthogonal matrix, the inverse matrix $(\mathbf{K}_{\mathrm{R}i})^{-1}$ is the transposed matrix ${}^t\mathbf{K}_{\mathrm{R}i}$. Therefore, from the theorem of $\mathbf{K}_{\mathrm{R}i}$, equation (4) are derived for any vector $\mathbf{a}$.

$$\mathbf{a}_{\mathrm{S}} = \mathbf{K}_{\mathrm{R}i}\mathbf{a}_{\mathrm{R}i} \tag{4}$$

This is a very important transformation equation. For transforming any vector $\mathbf{a}$ from $\mathrm{R}^{(0)}$ representation to S representation, only multiply ${}^t\mathbf{K}_{\mathrm{R}i}$ to vector $\mathbf{a}$

$\mathbf{K}_{\mathrm{R}i}$ is also calculated from $\mathbf{n}_{\mathrm{S}} = {}^t(n_1, n_2, n_3)_{\mathrm{S}}$ and θ by equation (5), where $\mathbf{n}_{\mathrm{S}}$ is a unit vector of the rotational axes and θ is an angle of rotation of the basis transformation from S to $\mathrm{R}^{(i)}$.

$$\mathbf{K}_{Ri} = \begin{bmatrix} n_1^2(1-\cos\theta)+\cos\theta & n_1n_2(1-\cos\theta)-n_3\sin\theta & n_3n_1(1-\cos\theta)+n_2\sin\theta \\ n_1n_2(1-\cos\theta)+n_3\sin\theta & n_2^2(1-\cos\theta)+\cos\theta & n_2n_3(1-\cos\theta)-n_1\sin\theta \\ n_3n_1(1-\cos\theta)-n_2\sin\theta & n_2n_3(1-\cos\theta)+n_1\sin\theta & n_3^2(1-\cos\theta)+\cos\theta \end{bmatrix} \quad (5)$$

Equation (5) is derived from Rodrigues' rotation formula (6).

$$\mathbf{K}_{Ri} = \mathbf{I} + \mathbf{N}^2(1-\cos\theta) + \mathbf{N}\sin\theta \quad (6)$$

where

$$\mathbf{N} = \begin{bmatrix} 0 & -n_3 & n_2 \\ n_3 & 0 & -n_1 \\ -n_2 & n_1 & 0 \end{bmatrix} \quad (7)$$

$$\mathbf{N}^2 = \begin{bmatrix} -n_2^2-n_3^2 & n_1n_2 & n_3n_1 \\ n_1n_2 & -n_3^2-n_1^2 & n_2n_3 \\ n_3n_1 & n_2n_3 & -n_1^2-n_2^2 \end{bmatrix} \quad (8)$$

2.2 Sensor coordinate system

Two mouse sensors are arranged at the arbitrary positions on a stator $(\mathbf{p}_1)_\mathrm{S}$ and $(\mathbf{p}_2)_\mathrm{S}$. Each mouse sensor measures two circumferential speed (v_{j1}, v_{j2}) along the unit vectors of sensing directions $(\mathbf{u}_{j1}, \mathbf{u}_{j2})_\mathrm{S}$.

The basis of the sensor coordinate system $\mathrm{M} =< \mathbf{m}_1, \mathbf{m}_2, \mathbf{m}_3 >$ is introduced. $\mathbf{m}_1$, $\mathbf{m}_2$, and $\mathbf{m}_3$ are determined by equations (9) to (11).

$$\mathbf{m}_1 = \frac{(\mathbf{p}_1)_\mathrm{S}}{|(\mathbf{p}_1)_\mathrm{S}|} \quad (9)$$

$$\boldsymbol{m}_3 = \frac{(\mathbf{p}_1)_\mathrm{S} \times (\mathbf{p}_2)_\mathrm{S}}{|(\mathbf{p}_1)_\mathrm{S} \times (\mathbf{p}_2)_\mathrm{S}|} \quad (10)$$

$$\mathbf{m}_2 = \mathbf{m}_3 \times \mathbf{m}_1 \quad (11)$$

Then, $\mathbf{K}_\mathrm{M}$, which is the basis transformation matrix from S to M, is $[\mathbf{m}_1, \mathbf{m}_2, \mathbf{m}_3]$. As the mouse sensors are fixed on the stator, $\mathbf{K}_\mathrm{M}$ can be calculated previously.

$(\mathbf{p}_1)_\mathrm{M}$ and $(\mathbf{p}_2)_\mathrm{M}$, which are the position vectors of the mouse sensors on M, are easily derived as $\mathbf{K}_\mathrm{M}(\mathbf{p}_1)_\mathrm{S}$ and $\mathbf{K}_\mathrm{M}(\mathbf{p}_2)_\mathrm{S}$. $(\mathbf{u}_{j1}, \mathbf{u}_{j2})_\mathrm{M}$,which are the unit vectors of sensing direction of mouse sensor j on M, are represented as $(\mathbf{K}_\mathrm{M}\mathbf{u}_{j1}, \mathbf{K}_\mathrm{M}\mathbf{u}_{j2})_\mathrm{S}$. Fig.2 shows the sensor coordinate system M.

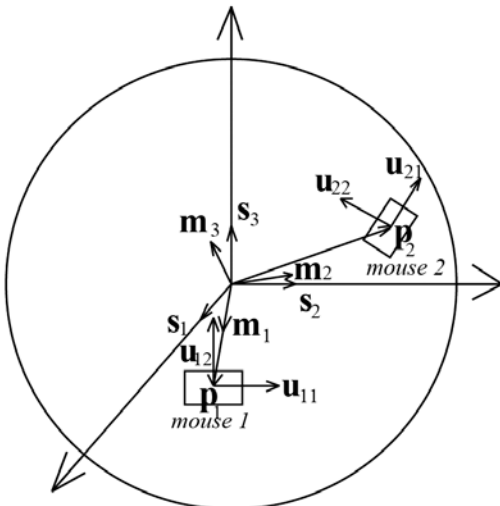

Fig. 2 Sensor coordinate system and mouse sensors

2.3 Obtain current position of the rotor from the sequence of the basis transformation matrices

At first, the rotor coordinate system $\mathrm{R}^{(0)}$ is set equal to the stator coordinate system, and at every sensing time interval $\Delta\tau_i$, the rotor coordinate system $\mathrm{R}^{(i)}$ is set to equal to the stator coordinate system after rotation. In other words, the rotor coordinate system $\mathrm{R}^{(i-1)}$ is equal to the stator coordinate system S before rotation.

Therefore, the basis vectors $\mathbf{r}_1^{(i)}, \mathbf{r}_2^{(i)}\mathbf{r}_3^{(i)}$ of the rotor coordinate system after rotation is represented by equation (12). Equation (13) is obtained from equation (12).

$$\left[\mathbf{r}_1^{(i)}, \mathbf{r}_2^{(i)}\mathbf{r}_3^{(i)}\right] = \left[\mathbf{r}_1^{(i-1)}, \mathbf{r}_2^{(i-1)}\mathbf{r}_3^{(i-1)}\right]^t\mathbf{K}_{\mathrm{R}i} \quad (12)$$

$$\left[\mathbf{r}_1^{(i-1)}, \mathbf{r}_2^{(i-1)}\mathbf{r}_3^{(i-1)}\right] = \left[\mathbf{r}_1^{(i)}, \mathbf{r}_2^{(i)}\mathbf{r}_3^{(i)}\right]\mathbf{K}_{\mathrm{R}i} \quad (13)$$

After the rotor rotates h times from the initial position, the basis vectors of the initial position of the rotor $\mathbf{r}_1^{(0)}, \mathbf{r}_2^{(0)}\mathbf{r}_3^{(0)}$ are represented by equation (14).

$$\begin{aligned} \left[\mathbf{r}_1^{(0)}, \mathbf{r}_2^{(0)}\mathbf{r}_3^{(0)}\right] &= \left[\mathbf{r}_1^{(1)}, \mathbf{r}_2^{(1)}\mathbf{r}_3^{(1)}\right]\mathbf{K}_{\mathrm{R}1} \\ &= \left[\mathbf{r}_1^{(2)}, \mathbf{r}_2^{(2)}\mathbf{r}_3^{(2)}\right]\mathbf{K}_{\mathrm{R}1}\mathbf{K}_{\mathrm{R}2} \\ &= \left[\mathbf{r}_1^{(h)}, \mathbf{r}_2^{(h)}\mathbf{r}_3^{(h)}\right]\mathbf{K}_{\mathrm{R}1}\mathbf{K}_{\mathrm{R}2} \cdots\cdots \mathbf{K}_{\mathrm{R}h} \end{aligned} \quad (14)$$

By introducing matrix $\mathbf{K}_\mathrm{R}$ defined by equation (15), equation (14) is simplified to equation (16).

$$\mathbf{K}_\mathrm{R} = \mathbf{K}_{\mathrm{R}1}\mathbf{K}_{\mathrm{R}2} \cdots\cdots \mathbf{K}_{\mathrm{R}h} \quad (15)$$

$$\left[\mathbf{r}_1^{(0)}, \mathbf{r}_2^{(0)}\mathbf{r}_3^{(0)}\right] = \left[\mathbf{r}_1^{(h)}, \mathbf{r}_2^{(h)}\mathbf{r}_3^{(h)}\right]\mathbf{K}_\mathrm{R} \quad (16)$$

As $\mathrm{R}^{(h)}$ is equal to the stator coordinate system after h time rotation, equation (17) is obtained.

$$\left[\mathbf{r}_1^{(0)}, \mathbf{r}_2^{(0)}\mathbf{r}_3^{(0)}\right] = [\mathbf{s}_1, \mathbf{s}_2, \mathbf{s}_3]\mathbf{K}_\mathrm{R} \quad (17)$$

$\mathbf{K}_\mathrm{R}$ is the basis transformation matrix from S to $\mathrm{R}^{(0)}$ after h rotation. Therefore, the current position of the rotor is represented by $\mathbf{K}_\mathrm{R}$.

2.4 Calculation of the basis transformation matrix

In this section, a basis transformation matrix $\mathbf{K}_{\mathbf{R}i}$ is calculated.

Three circumferential speeds among four measured circumferential speeds $(v_{11}, v_{12}, v_{21}, v_{22})$ are chosen such that three corresponding unit vectors of sensing direction are not in parallel.

Assume that (v_{11}, v_{12}, v_{21}) are selected. Then, $\boldsymbol{\omega}_\mathrm{M}$ is obtained by solving equation (18) [18].

$$\boldsymbol{\upsilon} = \mathbf{A}\boldsymbol{\omega}_\mathrm{M} \quad (18)$$

where

$$\boldsymbol{\upsilon} = \begin{bmatrix} v_{11} \\ v_{12} \\ v_{21} \end{bmatrix}, \qquad \mathbf{A} = \begin{bmatrix} (\mathbf{p}_1)_\mathrm{M} \times (\mathbf{u}_{11})_\mathrm{M} \\ (\mathbf{p}_1)_\mathrm{M} \times (\mathbf{u}_{12})_\mathrm{M} \\ (\mathbf{p}_2)_\mathrm{M} \times (\mathbf{u}_{21})_\mathrm{M} \end{bmatrix} \quad (19)$$

Rotor angular velocity vector on M is transformed on S by equation (20)

$$\boldsymbol{\omega}_S = {}^t\mathbf{K}_M \boldsymbol{\omega}_M \quad (20)$$

Rotation angle θ and $\mathbf{n}_S$ are calculated by equations (21) and (22).

$$\mathbf{n}_S = \frac{\boldsymbol{\omega}_S}{|\boldsymbol{\omega}_S|} \quad (21)$$

$$\theta = |\boldsymbol{\omega}_S| \quad (22)$$

$\mathbf{K}_{Ri}$ is obtained by calculate equation (5), and $\mathbf{K}_R$ is obtained from equation (15).

The flowchart for calculate $\mathbf{K}_R$ is shown in Fig.3.

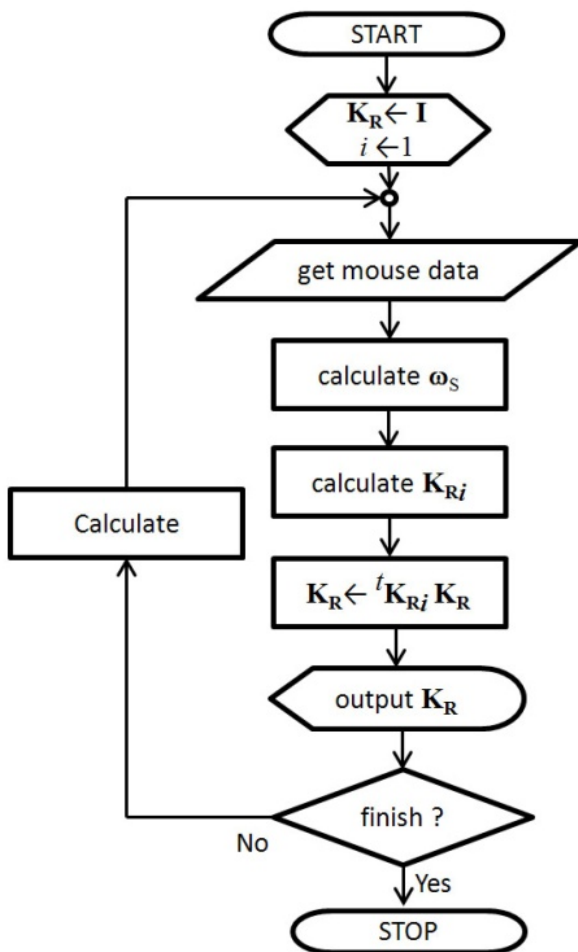

Fig. 3 Flowchart of calculate the current position

3. Experimental Results

3.1 Selection of mouse sensor

Fig.4 shows the developed spherical motor. Eight permanent magnets are attached on the rotor such as the North poles and South poles appear alternatively at the vertexes of the hexahedron subscribed in the rotor. Twenty-five coils are attached on the stator at the vertexes, center of edges, and center of planes of the octahedron subscribed in the rotor. The rotor can be driven in any direction by the control currents of the coils. The rotor is sphere and the diameter d is 78mm. For position feedback control of the developed motor, the mouse sensor should read the data at 300 rpm rotational speed and the angle resolution should be less than 0.01 deg.

The calculation results of the rotor speed of the developed spherical motor to the tracking speed of the mouse sensor is shown in Fig.5, and the angle resolution of the developed spherical motor to the XY resolution of the mouse sensor is shown in Fig.6.

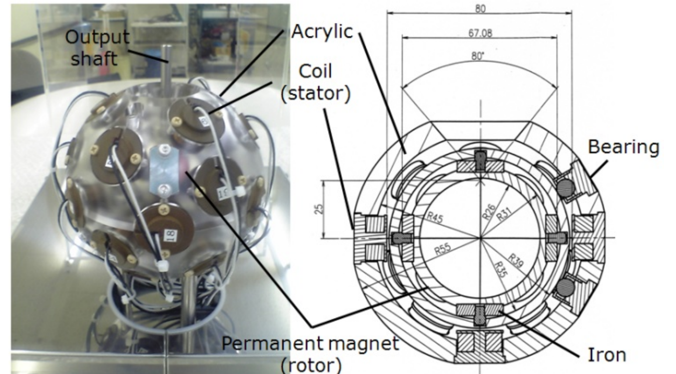

Fig. 4 Developed spherical motor

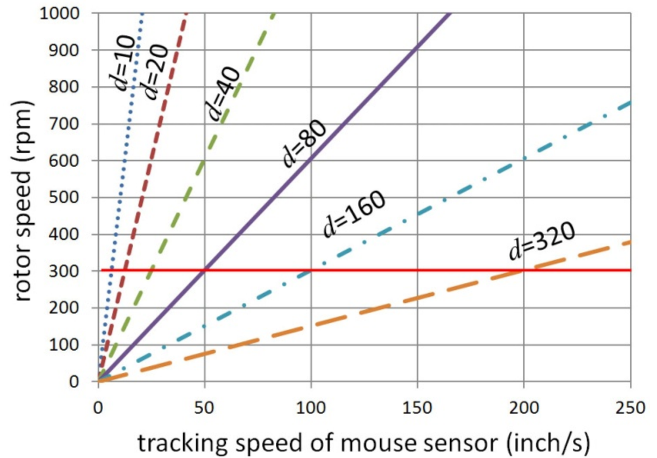

Fig. 5 rotor speed to tracking speed

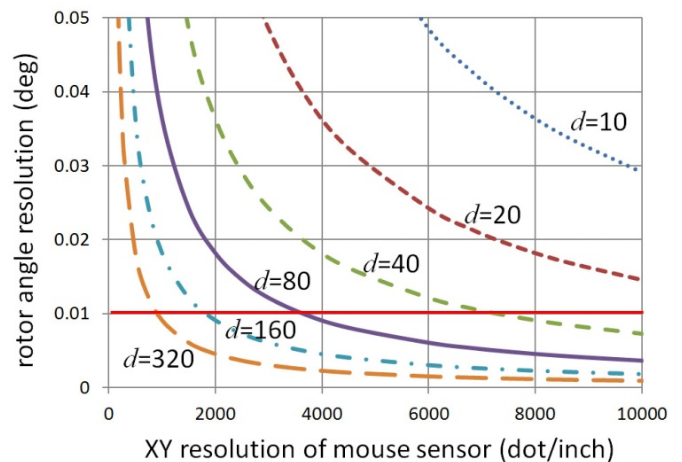

Fig. 6 angle resolution to XY resolution

The mouse sensors are connected at the USB ports. The data is obtained through Windows 7 OS. Therefore, the data acquirement interval is not controlled. So, for checking the reliability of the obtained mouse data, the resolution of the mouse data is tested to put a mouse sensor on the XY

precision linear stage. Fig.8 shows the test results. The upper graph shows the large movement and the lower graph shows the small movement.

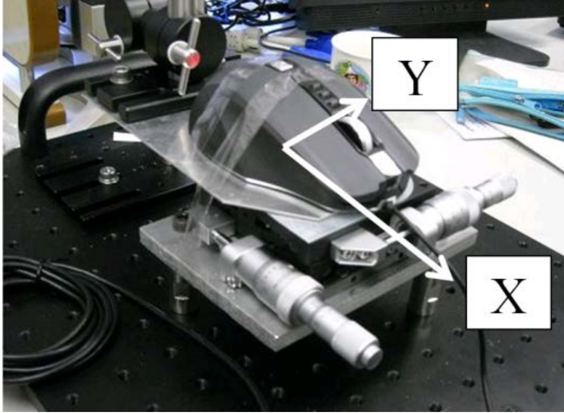

Fig. 7 mouse sensor on XY precision linear stage

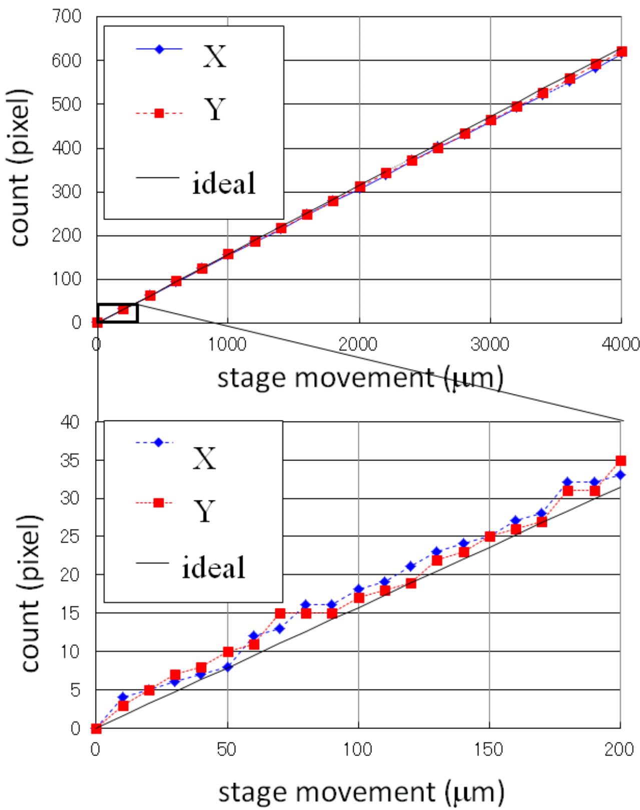

Fig. 8 mouse count to the stage movement

The mouse counts are 15 pixels short for 620 pixels at X direction and 9 pixels short at Y direction, which are 2.41% and 1.13% of the 620 pixels. For the small movement, the mouse counts are within 4 pixels from the ideal count line. The test results show that the mouse sensor is useful for the sensing device of the spherical position sensor.

3.2 Experimental setup

A rotor holder with two mouse sensor holders is manufactured and two sensing parts of the mouse sensors are picked up and mounted on the holder. Fig.9 shows the holder. The mouse sensors are set at the position vectors $(\mathbf{p}_1)_S$ and $(\mathbf{p}_2)_S$ in equation (23).

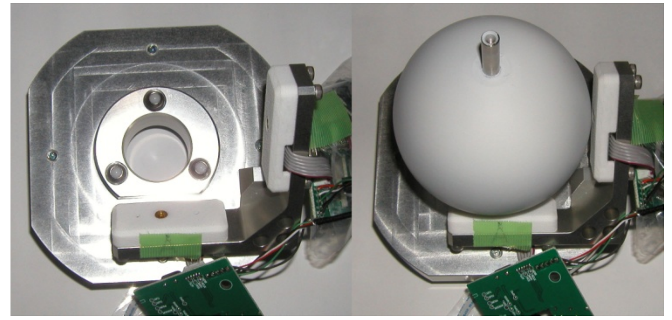

(a) without rotor (b) with rotor

Fig. 9 manufactured rotor holder with mouse sensors

$$(\mathbf{p}_1)_S = \begin{bmatrix} \cos\frac{\pi}{4} \\ 0 \\ -\sin\frac{\pi}{4} \end{bmatrix}, \quad (\mathbf{p}_2)_S = \begin{bmatrix} 0 \\ 1 \\ 0 \end{bmatrix} \tag{23}$$

Therefore, the basis vectors of the sensor coordinate system are represented by equation (24).

$$[\mathbf{m}_1 \quad \mathbf{m}_2 \quad \mathbf{m}_3] = \begin{bmatrix} \cos\frac{\pi}{4} & 0 & \sin\frac{\pi}{4} \\ 0 & 1 & 0 \\ -\sin\frac{\pi}{4} & 0 & \cos\frac{\pi}{4} \end{bmatrix} \tag{24}$$

$(\mathbf{u}_{11}, \mathbf{u}_{12}, \mathbf{u}_{21}, \mathbf{u}_{22})_M$, the unit vectors of sensing direction on the sensor coordinate, are set as equation (25).

$$(\mathbf{u}_{11}, \mathbf{u}_{12}, \mathbf{u}_{21}, \mathbf{u}_{22})_M = \left(\begin{bmatrix} 0 \\ 1 \\ 0 \end{bmatrix}, \begin{bmatrix} 0 \\ 0 \\ 1 \end{bmatrix}, \begin{bmatrix} -1 \\ 0 \\ 0 \end{bmatrix}, \begin{bmatrix} 0 \\ 0 \\ 1 \end{bmatrix} \right)_M \tag{25}$$

3.3 Experimental results

A position calculation program is developed. Visual C++ language is used to develop the program. The display part of the position sensing program is shown in Fig.10. The 3D rotor position is graphically displayed at the lower right.

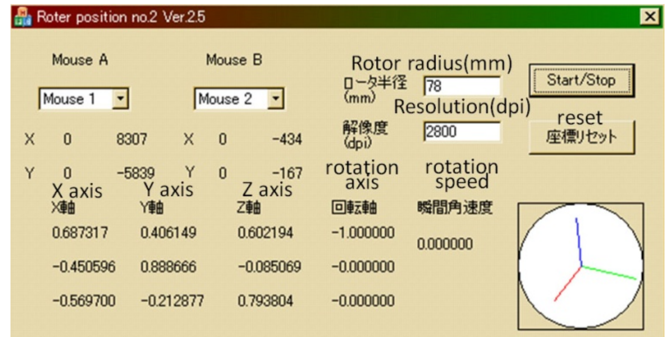

Fig. 10 display of the rotor position measurement program

The measurement error of the rotor position is evaluated by rotating the rotor around X, Y, and Z axis by hand.

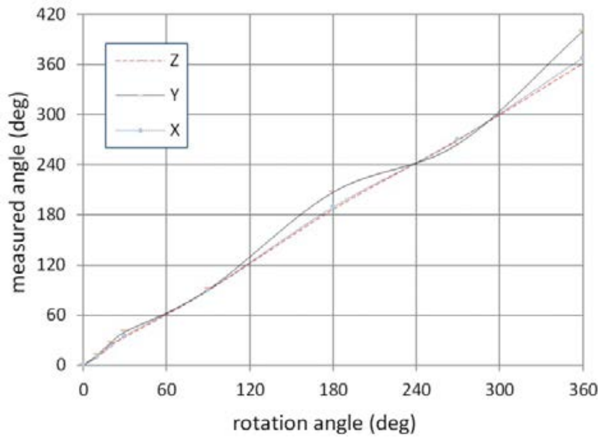

Fig. 11 sensing test around vertical axes

The measurement rotational angles are shown in Fig.11. The measurement error increased gradually according to the measurement time. For avoiding the long term measurement error, the reference position marker which resets the measurement error or an absolute position sensor should be used in parallel.

4. Conclusion

Several ideas of the position sensors for the spherical motor are reviewed and discussed. Among them, a position sensor with two mouse sensors is selected. The basic ideas for getting the position from the data of two mouse sensors are presented. Two mouse sensors are set on the manufactured rotor holder and the basic performance of the rotor position measurement is evaluated. As the mouse sensor is an incremental sensor, the measurement error increases during sensing. The reference position marker to reset the error or some absolute position sensor should be used with the developed sensor in parallel.

In the near future, an automatic rotor position evaluate stage will be developed and more precise data are obtaoned. The reference position marker will be also added in this sensor to reset the error.

The developed spherical motor is also controlled by position feedback with the developed rotor position sensor.

REFERENCES

1. Kaneko, K., Yamada, I., and Itao, K., "A spherical DC servo motor with three degrees of freedom," Trans.ASME J. of Dynamic Systems, Measurement, and Control, pp398/402, 1989.
2. Anders, M., Andresen, E. C., and Binder, A., "A novel spherical linear PM motor for direct driving infrared optical telescope", IEEE Trans. on International Conference on Electric Machines and Drives (IEMD), pp.528-530, 1999.
3. Stein, D., and Chirikjian, G. S., "Experiments in the communication and motion planning of a spherical stepper motor," ASME paper DET00/MECH-14115, pp.1-7, 2000.
4. Dehez, B., Grenier, D. and Raucent, B., "Two-degree-of freedom spherical actuator for omnimobile robot," Proc. IEEE International Conference on Robotics and Automation, pp2381-2386, 2002.
5. Lee, K.M., Son, H., Joni, L., et.al., "Concept development and design of a spherical wheel motor (SWM)," Proc. of IEEE International Conference on Robotics and Automation, pp. 3652-3657, 2005.
6. Onillon, E., et.al. "Reaction sphere for attitude control", Proc. of 13th European Space Mechanisms and Tribology Symposium, pp.1-6, 2009.
7. Ikeshita, S., Gofuku, K., Kamegawa, T., Nagai, T., et.al., "Development of a spherical motor driven by electro-magnets," J. Mechanical Science and Technology, Vol.24, pp.43-46, 2009.
8. Yano, T., "Design of a hexahedron-octahedron based spherical stepping motor", Proc. of IEEE International Symposium on Micromechatronics and Human Science, pp.519-524, 2008.
9. Gofuku, A., Sasaki, R., Yano, T., Wada, Y., and Shibata, M., "Development of a spherical stepping motor rotating around six axes," Proc. of International Symposium on Applied Electromagnetics and Mechanics, pp.1/6, 2011.
10. Um, Y., and Yano, T., "Characteristic of torque on spherical stepping motor based on hexahedron-octahedron structure", Proc. of IEEE International Conference on Mechatronics and Automation, pp.170-175, 2009.
11. Yano, T., "Spherically symmetric characteristics of a hexahedron and octahedron based spherical stepping motor," Proc. of International Symposium on Linear Drives for Industrial Applications, No.LS2, pp.1/4, 2011.
12. Yano, T., Kaneko, M., and Sonoda, M., "Position control of a developed synchronous motor with three degree of freedom", Proc. of France-Japan Congress & 1st Europe-Asia Congress on Mechatronics, pp.127/132, 1996.
13. Wada, Y., and Gofuku, A., "Measurement of rotor posture of spherical motor by Hall devices," The papers of Technical Meeting on Linear Drives, IEE Japan, Vol. LD-11, No. 66, pp. 63-68, 2011.(in Japanese)
14. Aoyagi, M., Fujita, T., Takano, T., Tamura, H. and Tomikawa, Y., "A detection and control of rotary position of a disk-type spherical ultrasonic motor by image processing," J. of IEICE Japan, Vol.J93-A, No.8, pp.501-509, 2010.
15. Stain, D., Scheinerman, E. R., Chirikjian, G. S., "Mathematical models of binary spherical-motion encoders," Trans. on Mechatronics, Vol.8, No.2, pp.234-244, 2003.
16. Lee, K. M., "Orientation sensing system and methods for a spherical body," US Patent 5319577, 1994.
17. Hama, N., Yokohama, T. and Kudoh, T., "Development of an absolute-encoder using a full-color sensor," Tamagawa seiki technical report, Vol.24, No.1, pp.23-25, 2007. (in Japanese)
18. Kumagai, M., and Hollis, R. L., "Development of a three-dimensional ball rotation sensing system using optical mouse sensors," Proc. IEEE ICRA, pp. 5038-5043, 2011.

Proposal of Industrial Services for Microfactories

Nozomu Mishima[1#], Eckart Uhlmann[2], Christian Stelzer[2], Hitoshi Komoto[1], Niels Raue[2], Christian Gabriel[2]

1 Advanced Manufacturing Research Institute, AIST, Ibaraki, Japan
2 Department of Machine Tools and Factory Management, Technical University of Berlin, Berlin,Germany
Nozomu Mishima / E-mail: n-mishima@aist.go.jp TEL: +81-29-861-7227, FAX: +81-29-861-7227

KEYWORDS : Microfactory, Industrial Services, Industrial Product-Service Systems, Lifecycle

The Microfactory developed by AIST is the origin of modern compact and distributed manufacturing systems, which ensure a flexible combination of different manufacturing, assembly and measuring tasks. Since its introduction 12 years ago, various machine tools to fulfill the different tasks covered by the Microfactory have been developed. However, promoting system-level innovation of the businesses utilizing Microfactory features is insufficient.
The paper first identifies relevant services considering three exemplary Industrial Product-Service Systems (IPS²) business models and a lifecycle in the manufacturing industry in general, which potentially motivates provider of the Microfactory toward the servicification of their businesses. Although tradional business models with conventional manufacturing systems are not unique, the service can be distinguished in case of the Microfactory regarding its on-demand, on-site, and on-time-delivery properties. It can also enhance the energy and the resource efficiency of the manufacturing industries. In order to clarify the advantage, the paper analyzes the process using the Microfactory and combines identified industrial services with the lifecycle stages of IPS². Finally, the paper concludes that a manufacturing service featuring the Microfactory is one of the promising areas in future production.

1. Introduction

The Microfactory [1] is developed by AIST as a modern compact and distributed manufacturing system. This system allows a flexible combination of different manufacturing, assembly and measuring tasks. It was introduced 12 years ago. Various machine tools and production equipment to fulfill the different tasks covered by the Microfactory have been developed and introduced in the market. One of the remarkable characteristics of the system is the high level of modularity. The modularity allows the minimization as individual products by employing particular downsizing technologies and the fulfillment of customer-specific solutions [2]. There have been some significant approaches [3] to cover industrial practicalities by utilizing high modularity of the microfactories. However, sometimes the modularity has also prevented the provider of the Microfactory from promoting the system-level innovation of their business, since it is difficult to develop a new business model beyond combining the provided modules. This is the reason why there is no common strategy or framework to make the provider's business successful. Facing the recent serious economic situation, on top of severe global competition and environmental legislation, service engineering and especially industrial product-service systems (IPS²) can be a key to overcome the underlying challenges by creating more innovative businesses and sustainable, customer individual combinations of product and service shares [2, 4]. Different

business models, which are coupled with the customer requirements, are available for such a provider [5]. One important aspect of market acceptance and therefore success of an industrial solution is the integration of product and service shares over a continuous lifecycle [2, 4]. In addition to this, emerging environmental concern is another reason to consider Microfactories as sustainable solutions in industries. A main goal of downsizing is reducing the environmental impact of production and operation of systems. Therefore it is a good strategy to consider how far a system can be downsized. However, since the production systems should be productive enough to make the business successful, a balance between productivity and environmental impact is needed. So-called eco-efficiency [6, 7] can be the key performance index in this aspect. Remaining questions are how the eco-efficiency can be applied to practical use-cases and what the strategies to plan, develop and use production systems eco-efficiently are. Especially, since it is said that “de-materialization” is one of the keys towards sustainability [8], a proper combination of product and service shares in a Microfactory should be discussed not only because of the enhancement of business feasibility but also for increasing sustainability. Thus, the objective of this paper is to clarify the framework of a service-oriented business for the Microfactory by consideration of three exemplary IPS² business models; function-, availability- and result-oriented [4, 5]. Additionally, a concrete case of how IPS² product and service shares can be combined and managed properly will be introduced. The cases will be carried out by using a newly introduced desktop production system as an example, corresponding to the different lifecycle phases of the Microfactory.

2. Product shares and characteristics of Microfactories

2.1 The Microfactory

The Microfactory combines different product shares, which are realized by machine tools, measuring systems and other production equipments. In the first prototype of the Microfactory [1], the total system was composed of five components. Thus, at the first look, the five micro production machine tools correspond to the basic product shares in the system.

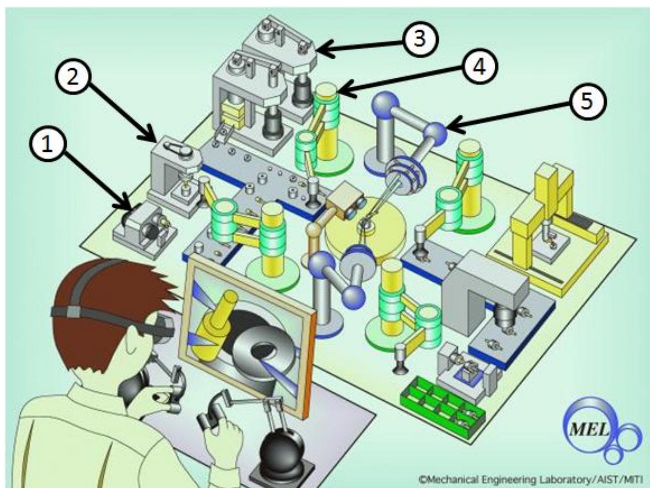

Figure 1: Schematic view of the first Microfactory [9]

The product shares, indicated from 1 to 5, measuring systems and other production equipments are integrated in the concept of the Microfactory (Figure 1):

1. Micro-lathe,
2. Micro-milling machine,
3. Micro-press machine,
4. Micro-transfer arm and
5. Micro-manipulator (two-fingered micro hand).

2.2 Definition and potential merits of the Microfactory

The Microfactory is a compact production system for precise microproducts [1]. However, a concrete definition has not been discussed thoroughly. Thus, the authors, hereby, define Microfactory by the following sentences:

> “A production system which is composed of properly downsized machine tools and other production equipment and realize at least one feature of a workpiece, such as tolerances, dimensions etc., with a `micron order´ requirement.”

Based on an existing definition [4], it has been stated that a lifecycle of an IPS² can be divided into five stages. Those are IPS²-planning, IPS²-development, IPS²-realization (or IPS²-implementation), IPS²-use and IPS²-reuse (or IPS²-end-of-life management). In Table 1 the potential merits of a Microfactory are related to the different IPS²-lifecycle stages. In addition to Table 1, for the different product shares of the Microfactory, potential merits are listed in Table 2.

Because of the smallness of the machine tools and other production equipment, it might be possible to use more unified components and a simple design technique without any necessary critical simulation. By this aspect it is also possible to easily change the factory layout and add new components to the production line. Thus, time for the development process can be reduced (see Table 2). For the design aspect the degree of material use and parts use is usually small. Thus, if the machine tools and other production equipment are composed of commercially available components, the costs are lower. Since the machine tools and other production equipment sizes are small and work-loads are small, a low degree of secondary processes such as providing coolants, lubrication and spare parts is necessary (see Table 2). As an existing study [10] shows, modularized compact production systems can be energy efficient e. g. by designing process time of each modular unit consistently. Corresponding to the flexibility in the factory layout and modularity of the machines, it is possible to increase or decrease the number of machine tools and other production equipment and change production line configurations. Due to the smallness of the machine tools and other production equipment, it is possible to move the whole or the part of the production lines to where demands exist. Because of the size effects of various error factors in machine tools and other production equipment, a downsized machine tool has clear advantages, e. g. in the aspect of theoretical positioning errors [11]. The smallness of the machine tools and other production equipment leads to the characteristic that

some error factors may decrease its' effect on the overall positioning error.

Table 1: Potential merits of Microfactory and allocation to corresponding IPS² lifecycle stages

Potential merits	Related IPS²-lifecycle stages			
	IPS²-planning	IPS²-development	IPS²-realization	IPS²-use
Fast design	X	X		
Low-cost design	X	X	X	
Flexibility	X	X	X	
Energy efficiency	X	X	X	X
On-demand capability	X	X	X	X
On-site / mobility	X	X	X	X
Low-cost operation		X	X	X
Precision		X	X	X
Robustness against error sources		X	X	X
Fast production			X	X
Safety				X

Table 2: Potential merits of the Microfactory product shares

No.	Product shares	Potential merits
1	Micro-lathe	On-site, Precision (decreasing absolute error), Robustness against vibration, Safety
2	Micro-milling machine	Precision, Low-cost operation, Safety
3	Micro-press machine	Fast design, Energy efficiency, Precision, Low-cost operation, Safety
4	Micro-transfer arm	Precision, Low-cost operation
5	Micro-manipulator (two-fingered micro	Precision

The smallness can also realize reduced process time such as e. g. warming up, heat treatment and cooling down. Because of the smallness of the machine tools and other production equipment, moving components of the machine tools and other production equipment may not hurt operators accidently (see Table 2).

2.3 Specification of product shares of the Microfaytory

For a specification of the different product shares of the Microfactory, different questions have to be answered. With this, a special data specification can be generated for the product shares of the Microfactory (Figure 2).

Therefore the following seven questions should be answered to build up a suitable specification of the used product shares.

1. Which production price does the product share have?
2. How long is the process time of product share in the production process?
3. Is the product share automated?
4. Is the product share programmable?
5. Is there a user interaction?
6. Are there special requirements that have to be taken into account, e. g. clean booth?
7. Which are the input media, e. g. electricity, air, water, oil or internet?

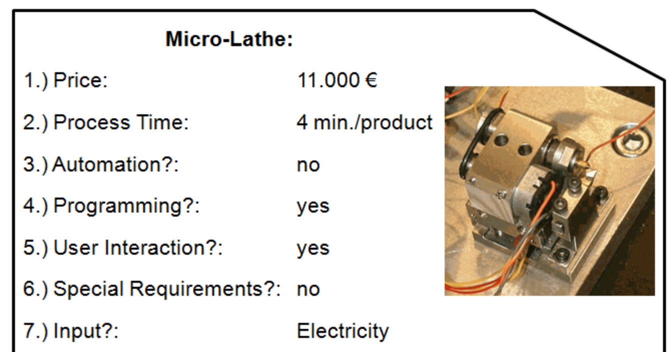

Figure 2: Example answer-set of product share

3. Lifecycle process model of Microfactory

Based on the process modeling [10] of the test production carried out by the Microfactory, Figure 3 is the schematic illustration of general processes that service shares are composed of, focusing on the tasks and organization levels, in various stages of the lifecycle of an IPS². The *level* dimension of the Figure helps to allocate the roles that are relevant in the provision of a service share. On the network level, the IPS²-provider and his network partners are involved in the process steps. On the system, machine tool and component level, the IPS²-provider, who e. g. is responsible for the IPS² development, is needed.

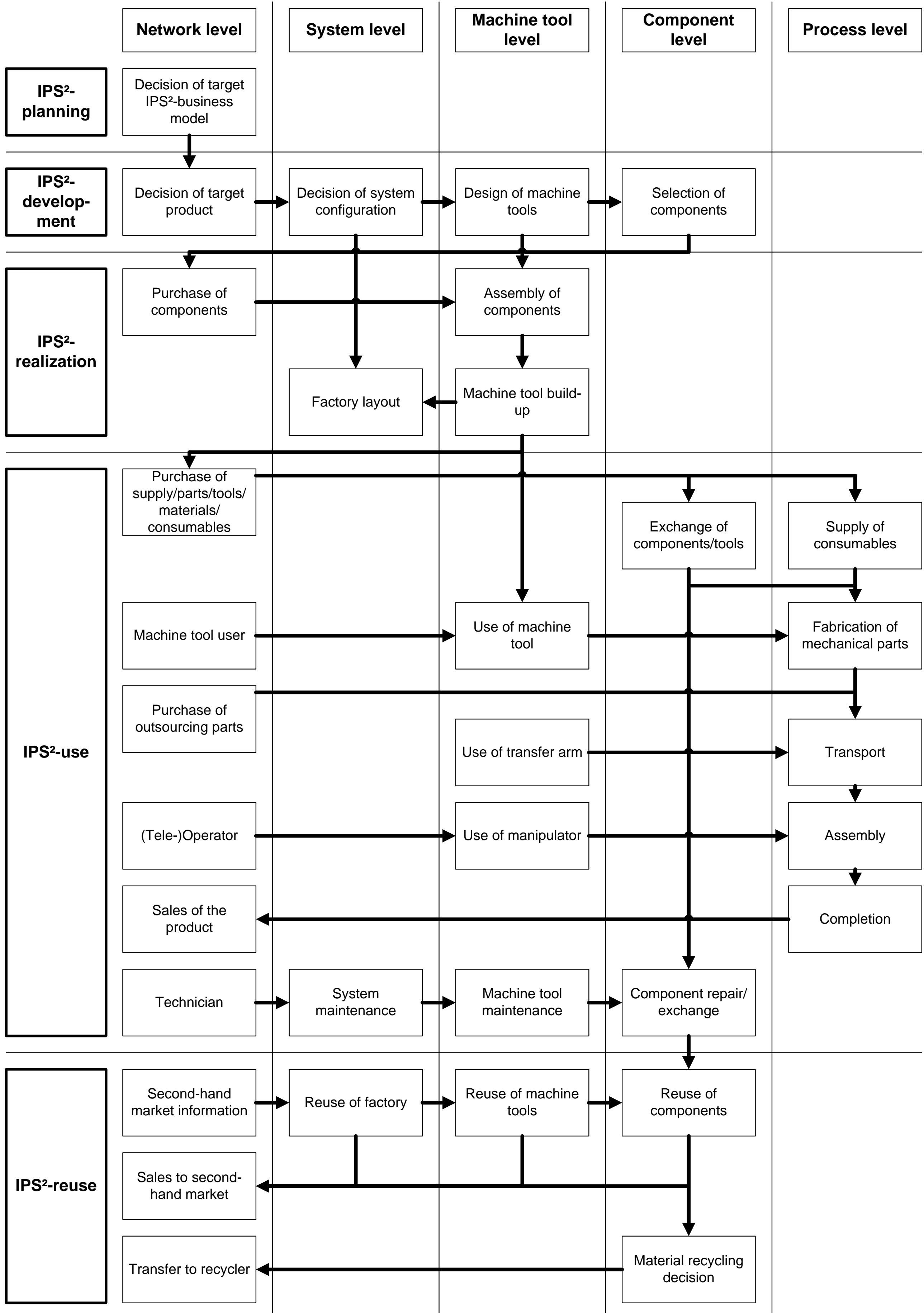

Figure 3: Structure of potential service shares in the lifecycle of IPS²

4. Service shares of Microfactory

By the identified characterization of the different product shares (Table 2) and the process view (Figure 3), the potential service shares at the different levels can be addressed. The proposed service share framework (Figure 3) can now be utilized to further characterize specific service shares listed in Table 3. Two detailed examples will be given.

The service share *factory layout planning* can be localized on system level in the IPS² realization phase (see Figure 3). The results *decision of system configuration* as well as the concrete *machine tool build-up* serve as input parameters for the planning (see Figure 3). This implies that these two steps have to be performed, either on customer or IPS²-provider side, before the service share can be provided. Due to the minimized size of the manufacturing equipment of the Microfactory, their arrangement is highly flexible and enables quick layout changes. Therefore the factory planning becomes more important. Some tasks concerning the factory planning will be delivered by the IPS²-provider. Usually a factory planning consists of tasks which concretize the factory layout and control the execution of the planning afterwards.

According to the literature these tasks can be arranged into the phases preparation, structural planning, detailed planning, execution planning and execution [12]. In the structural planning the IPS²-provider offers the transformation of a concrete production program into the ideal layout of the Microfactory under consideration of the necessary manufacturing technology; technology consulting; an optimized work piece flow or CAD-CAM can be offered. The workpiece flow is very specific in the field of Microfactory because of the miniaturized workpieces, machine tools and their components, like clamping systems. In a next step the existing boundary conditions on customer's site have to be taken into account. This circumstance requires an information flow between IPS²-provider and customer. The IPS²-provider has to identify important boundary conditions at the customer side to ensure that the Microfactory can be used in an adequate way (see Figure 3). Subsequently the IPS²-provider customizes the ideal planning into a real factory layout plan and implements the Microfactory at the customer's site.

As a second example, the location of the service share Tool provision and management indicates that, during the use phase of a Microfactory, service shares on network as well as process level are required (see Figure 3 and Table 3). Because of the smallness of the Microfactory the needed resources have according dimensions, are fragile and very specific in their e. g. cutting conditions.

Table 3: List of potential service shares of the Microfactory

Service share	Network level	System level	Machine Tool Level	Component Level	Process Level	Phase
Training (e. g. for machine operation)		x	x	x		
Controlling	x	x	x			
Marketing	x	x	x			IPS²-planning
Financing	x	x	x			
Marketing (second-hand)	x	x	x			
Sustainability	x	x	x	x	x	
Environment (analysis, ensuring)	x	x	x	x	x	
Factory layout planning		x	x			
Ramp-up (Implementation)	x	x	x	x		IPS²-development
Planning, development and realization IPS²	x	x	x	x	x	
Product development	x	x	x	x	x	
CAD/CAM		x	x	x	x	IPS²-realization
Integration of parts inspection			x	x	x	
Process modeling		x	x	x		
Technology consulting			x	x	x	
Condition monitoring			x	x	x	
Spare parts/unit exchange			x	x	x	
Measuring tasks			x	x	x	
Tool**/consumables **provision and management	◇			x	x	
Production (fabrication, logistics, assembly)	x	x	x	x	x	
Quality control		x	x	x	x	IPS²-use
Certification	x	x	x	x	x	
Condition-based maintenance	x	x	x	x		
Ensure/enable operation	x	x	x	x	x	
Maintenance	x	x	x	x		
On-site pay-per-production	x	x	x	x	x	
Process optimization			x	x	x	
End-of-life management	x	x	x	x		IPS²-reuse

Adequate resources have to be delivered by qualified network partners whom the IPS²-provider has to identify, since the market for e. g. micro cutting tools is not as large as the market for conventional cutting tools. Besides the search of the IPS²-provider for an adequate network partner for delivery, the support of customized process data to use these special cutting tools is necessary. This will be realized via technology consulting in the use phase (see Figure 3 and Table 3). For very specific manufacturing tasks appropriate cutting tools may not be available. In this case the IPS²-provider will cooperate with a company to deliver the needed resources. Additionally, a clamping system, due to the increased handling requirements in the micro production context, can be taken into account.

The identified service shares have different influences in the level dimensions, as shown exemplarily (see Table 3). The *factory layout planning* is relevant for the early stages of the lifecycle and secures the flexibility of the Microfactory for manufacturing a wide range of workpieces. This service share has influences in the system level and the machine tool level (Table 3). The second service share *Tool provision and management* is coupled with the use of the Microfactory. The realized process, which constitutes the service share, influences the quality, productivity and availability of machine tools. The network level, component level and the process level should be changed for and by this service share (Table 3).

Such a holistic view and the identified combination of the mentioned product and service shares lead to a customer individual solution and a long term customer provider relationship with a benefit for all involved partners.

5. Summary

In this paper, one of the first ideas to apply service shares to a compact modular manufacturing set-up called the Microfactory is discussed. The paper first identified the general merits of the Microfactory, and listed basic product shares featuring those merits. Furthermore the manufacturing processes using the Microfactory were analyzed, by categorizing the processes to five levels from network level to process level. It also categorized the processes to five lifecycle stages of an IPS², from the planning stage to the reuse stage. This categorization can be helpful to allocate service shares to corresponding lifecycle stages and structural levels of the Microfactory. By examining this categorization shown in Figure 3 and Table 3, the classification of service shares of the Microfactory can be possible. As a primitive step of this, two exemplary service shares were shown and discussed.

As a future work the identified service shares have to be adopted for the Microfactory in detail by verification, e. g. if the mentioned requirements are relevant or not. After this step a wider variety of service shares should be discussed to design business models of IPS² utilizing the Microfactory. With the designed processes constituting the service shares, it is possible to increase the customization of the Microfactory and to generate more input for future modifications of the Microfactory.

At last, the paper concluded that IPS² featuring the Microfactory can be a promising area, since the production system can be optimized by manual processes, which are part of many typical service shares in manufacturing industries.

6. Acknowledgement

We express our sincere thanks to the Deutsche Forschungsgemeinschaft (DFG) for funding this research within the Collaborative Research Project SFB/TR 29 on Industrial Product-Service Systems – dynamic interdependency of products and services in the production area.

REFERENCES

[1] Y. Okazaki, N. Mishima and K. Ashida, Microfactory - Concept, History and Developments-, Journal of Manufacturing Science and Engineering, Trans. ASME, Vol. 126, 2004, pp. 837 - 844.

[2] E. Uhlmann, C. Gabriel, N. Raue, C. Stelzer, Influences of the IPS² Business Model on the Development of a Micro Milling Spindle, Proceedings of the 3rd CIRP IPS² Conference 2011, pp. 57 - 62.

[3] R. Heikilla, E. Jarvenpaa and R. Tuokko, Advances in TUT Microfactory Concept Development, International Journal of Automation Technology, Vol. 4, No. 2, 2010, pp.117-126.

[4] H. Meier, R. Roy, G. Seliger, Industrial Product-Service Systems - IPS². CIRP Annals Manufacturing Technology 2010, Vol. 59, No. 2, pp. 607 - 627.

[5] U. Tukker, U. Tischner, New Business for old Europe, Final report of suspronet, 2004.

[6] L. DeSimone, F. Popoff, Eco-Efficiency - the Business Link to Sustainable Development, Cambridge, MA: MIT Press, 1997.

[7] WBCSD (World Business Council on Sustainable Development), Eco-efficiency: Creating more value with less impact. Geneva: WBCSD, 2000.

[8] A. Lelah, F. Mathieux, D. Brissaud, Building a Network of SME for a Global PSS Infrastructure in Complex High-Tech Systems: Example of Urban Applications, Proceedings of the 3rd CIRP IPS² Conference 2011, pp. 344 - 349.

[9] N. Mishima, T. Tanikawa, K. Ashida, H, Maekawa, Proc. of DETC2002:7th Design for Manufacturing Conference, Sept., 2002, Montreal, Canada, DETC2002/DFM-34164.

[10] N. Mishima, S. Kondoh, K. Masui, Proposal of An Efficiency Evaluation Index for Micro Manufacturing Systems, Proc. of IEEE ICMA 2007, Harbin, China, Aug. 2007, pp. 51 - 56.

[11] N. Mishima, Design evaluation method for miniature machine tools utilizing form-shaping theory, Proc. of ASME/DETC 2003, Chicago, IL, Sept. 2003, DAC-48787.

[12] C.-G. Grundig, Fabrikplanung. Planungssystematik – Methoden – Anwendung, München, 2006.

Towards reconfigurable and modular microfactory based on the TRING-module stick-slip microrobot

Dominique GENDREAU, Micky RAKOTONDRABE and Philippe LUTZ

Department of Automatic Control and Micro-Mechatronic Systems (AS2M)
FEMTO-ST Institute, UMR CNRS / UFC / ENSMM / UTBM, Besancon, France
Corresponding Author E-mail: dominique.gendreau@univ-fcomte.fr, TEL: +33-381-402-810 FAX:+33-381-402-809

KEYWORDS : microfactory, reconfigurability, modularity, stick-slip microrobot, TRING-module, station and cell, pick-and-place

Abstract – This paper deals with the presentation of a reconfigurable and modular microfactory based on a stick-slip microrobot called TRING-module and that can performs 2-degrees of freedom. The main advantage of the presented approach is that the microfactory can be quickly reconfigured in order to match with the requirements of the microproducts to be fabricated or to be assembled. This high reconfigurability is obtained thanks to the modularity imposed at the microrobot level. In particular, we demonstrate in this paper that based on only one duplicable microrobot (the TRING-module), several configurations of the microfactory are possible. The paper ends with an example of configuration based on two TRING-module microrobots followed by their characterization that can be further used for a controller design for pick-and-place tasks.

1. Introduction

A microfactory is a highly compact micromanufacturing system composed of micromachines and microrobots with very high precision. A microfactory transforms or assembles microparts in order to result microproducts. The resulting microproducts are often expensive due to the high complexity of assembly and fabrication of the microparts as their sizes are reduced and as the required precision of assembly is very severe (micrometric or sub-micrometric). In order to reduce the cost fabrication of microproducts and the cost of the microfactory itself, we present in this paper an approach for the design of a microfactory. Based on the concept of modularity of the elements (micromachines and microrobots) that compose the microfactory, this latter presents a high level of re-configurability and then can be easily used for a broad types of products to be fabricated.. The paper is particularly focused on the use of a 2-degrees of freedom (dof) microrobot named TRING-module microrobot developed in our previous works [1] as modular elements. Different configurations of the microfactory are therefore possible according to the combination and the structure of the different TRING-modules used.
The paper is organized as follows. In section-2, we present the TRING-module microrobot and its performances. Section-3 is devoted to a non exhaustive list of possible configurations of the microfactory based on the TRING-module. Finally, in section-4 we present a case example of configuration that is afterwards used for pick-and-place tasks commonly utilized in micro-assembly applications.

2. Presentation of the TRING-module microrobot

In this section, we present the microrobot TRING-module which will be used as modular element of the reconfigurable microfactory.

2.1 Kinematic and principle of motion

The TRING-module is a microrobot that has 2-degrees of freedom (2 dof): a linear motion along the x-axis (Tx) and an angular motion about the same axis (Rx) (Fig.1). The axis that supports the microrobot is a cylindrical glass. A cantilever is placed at the extremity of the TRING-module and used as end-effector that facilitates the handling of the manipulated objects. Developed in the previous work [1], the principle of movement of the TRING-module is based on the stick-slip functioning and uses piezoelectric micro-actuators described in [2]. The main features of the TRING-module are its

theoretical unlimited stroke both in rotation and in translation, the high resolution that it can offer and its good dexterity (rotation and translation).

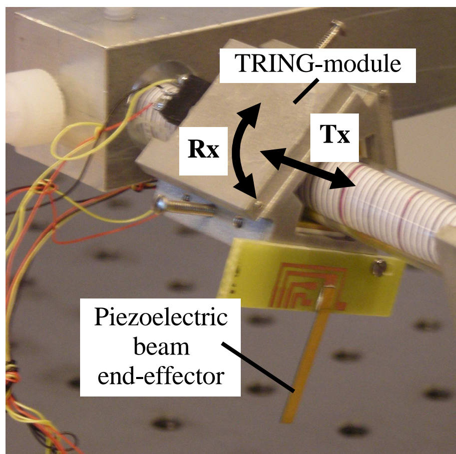

Fig. 1 A photography of the TRING-module.

2.2 Performances of the TRING-module

As a stick-slip microrobot, the TRING-module can perform the high stroke motion thanks to the step-by-step principle. This is obtained by applying a saw tooth voltage to the piezoelectric micro-actuators. The speed of the microrobot is proportional to both the frequency f and the amplitude U of the voltage, while the step-magnitude depends principally on the amplitude [3]. The high stroke motion is usually employed for a coarse positioning in a large distance. It is also possible to work within a step (sub-step). This sub-step motion, usually employed for fine positioning, is obtained by applying a voltage with limited slope to the micro-actuators. In sub-step motion, the resolution of the TRING-module is greatly amplified. The step-by-step motion and the sub-step motion can be managed and automatically switched by using the closed-loop control law developed in [3]. The principal advantage of the latter control law is the obtaining of high speed and high precision at the same time without manual reconfiguration of the controller. Tab.1 summarizes the performances of the TRING-module alone without closed-loop control [1][3][4]. It clearly shows the high performances of the microrobot in term of resolution and stroke and that are well suited to the requirements in microfactory in general.

Motion	Step (=resolution)	Max Speed	Stroke
Linear	70nm → 200nm	2mm/s	unlimited
Angular	17µrad → 44µrad	3.4rpm	unlimited

Table 1 Performances of the TRING-module microrobot [1][3][4]

2.3 Modules and modular element

The TRING-module itself is considered as a module in the proposed reconfigurable microfactory. Its principal functionality is the positioning. The end-effector of the TRING-module can also be considered as an active module if it has a function. For instance if a piezoelectric cantilever is used as end-effector, it can be used as manipulation force sensor at the same time, etc.

3. Reconfigurable microfactory based on the TRING-module

By using one or more TRING-modules and by conveniently adapting their emplacement, it is possible to obtain various configurations of cell, station or microfactory. A configuration is generally used such that it corresponds to the optimal production of a given microproduct, in terms of yield, reliability, rate, or other criteria. In this section, we give some example of configurations based on the TRING-module.

The configuration in Fig.2 represents one TRING-module with an end-effector. This configuration can be used in pick-transport-and-place tasks of objects by using only the cantilever (end-effector). The task is possible if the objects are small enough such that they can stick on the end-effector.

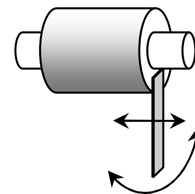

Fig. 2 Configuration with one TRING-module for pick-and-place tasks and for manipulation.

In Fig.3, the TRING-module is immobilized on the basis and the cylindrical glass that was initially the support is now the movable part. Hence, a platform placed at the extremity of the cylinder can rotate about or moves along the vertical axis Rz. This configuration can be used as a table to precisely place, orientate and position an object to be manipulated.

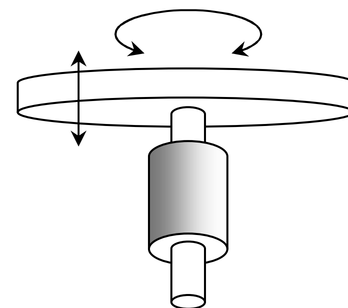

Fig. 3 Configuration with one TRING-module for linear and angular motions of a table.

To tilt the table, the configuration of Fig.3 is extended as shown in Fig.4. In this latter configuration three TRING-modules are used. According to the motion of the different TRING-modules, the table can be oriented in two directions: about Rx and about Ry axis. A vertical linear motion can also be made by moving in the same direction the three TRING-modules.

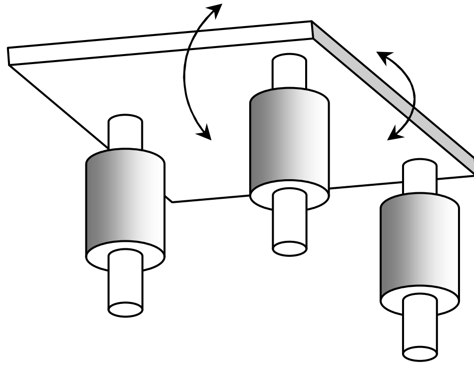

Fig. 4 Configuration with three TRING-modules for a tilt table.

In Fig.5 two independent TRING-modules are used for pick-and-place applications. The main advantage of this configuration is that the microgripper has a variable gap and therefore can manipulate various types and sizes of objects. The objects can be positioned along and about the axis of support of the microrobots. In addition to that, if the two TRING-modules rotate in opposite direction, the object can be oriented.

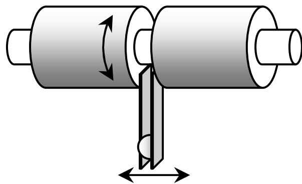

Fig. 5 Configuration with two TRING-modules for pick-and-place tasks.

In Fig.6, we present a configuration where the two TRING-modules are immobilized on the basis and where a belt is moved by the two cylindrical glasses and can position in the plane any object. As the strokes of the microrobots are theoretically unlimited, the strokes obtained with the final conveyor are only limited by the length of the belt and the length of the movable cylindrical glasses.

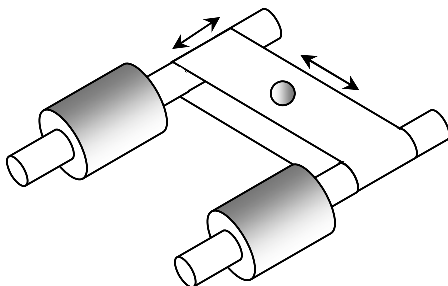

Fig. 6 Configuration with two TRING-modules for xy-positioning.

The different configurations presented so far can also be mixed in order to obtain a more complex configuration of microfactory. For instance, in Fig.7, the configurations in Fig.5 and Fig.6 are combined. The advantage is that the cell, station or microfactory becomes more dexterous.

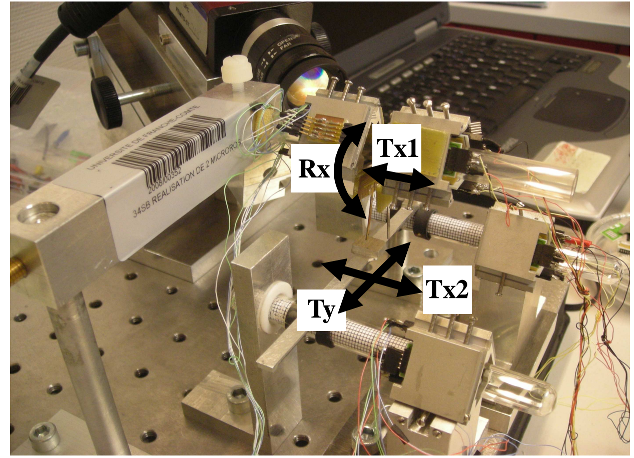

Fig. 7 A configuration that combines Fig.5 and Fig.6.

4. Study of a case of configuration

We consider the configuration of Fig.5 in this example. Experimental tests were successfully carried out and reported in this paper.

4.1 Presentation of the setup

The two TRING-modules used for the setup is pictured in Fig.8. The end-effectors (also called fingers) are based on piezoelectric materials. If necessary, they can be used to measure and control the force applied to the manipulated object thanks to the direct piezoelectric effect [5].

The challenge is to coordinate the movements of the two TRING-modules that carry an object between their end-effectors such that the object is still maintained during the transport. A first solution is to control the force additionally to the position. In such solution, one of the TRING-module is closed-loop or open-loop controlled in position while the other one is closed-loop controlled in force. This solution requires a force sensor put on the end-effector which increases the complexity of the design. The second solution consists to control the two devices in an open loop manner. During the linear motion for instance, one of the TRING-module functions as a pulling module while the another one as a pushing module. In this second solution, the control law consists in conveniently giving a speed reference to each TRING-module.

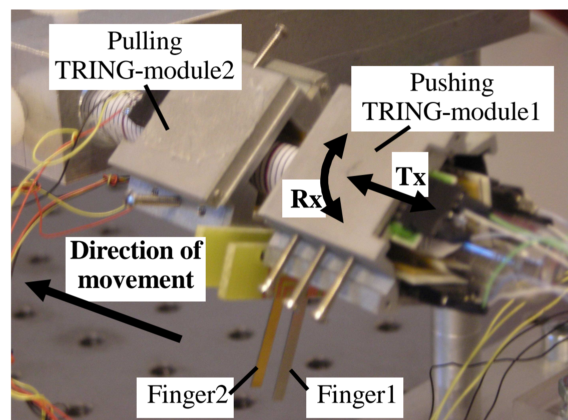

Fig. 8 The setup.

4.2 Precise characterization of one TRING-module

In order to open-loop control the two devices, it is essential to characterize their behaviors as precise as possible. Behind the characteristics listed in Tab.1, the velocity characteristics of each TRING-module are essential here.

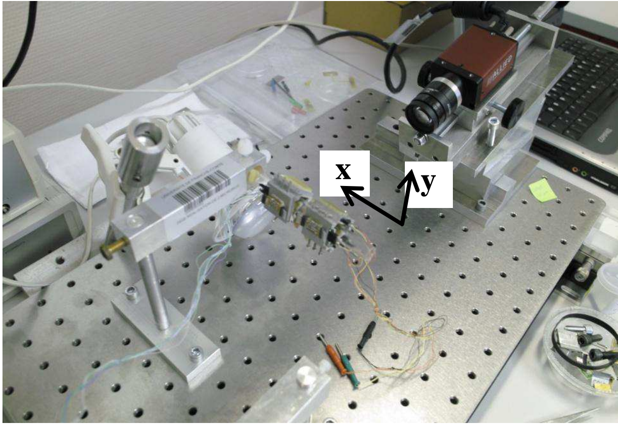

Fig. 9 Identification of the displacement with a camera.

The setup used for characterization is pictured in Fig.9. A camera records the successive positions of the end-effector of one TRING-module microrobot. A program developed with Matlab-Simulink® acquires the images of the end-effector, provides the contour plot with the Canny algorithm [6] and finally calculates its coordinates. Fig.10 gives the calculated position versus the time of the TRING-module.

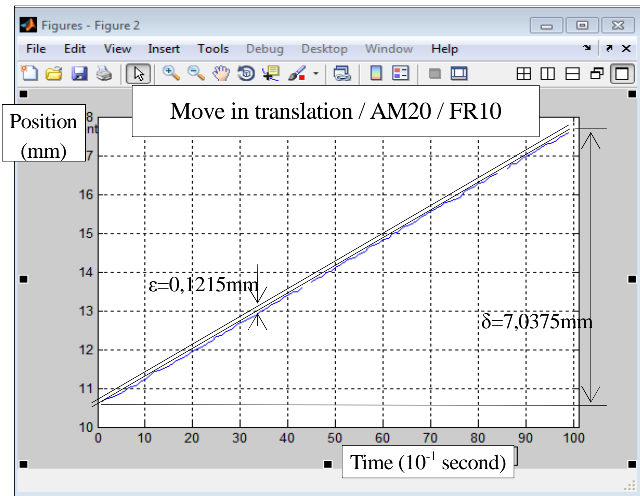

Fig. 10 Linear motions of one TRING-module.

From Fig.10, an average speed of S_1=0,704 mm/s is obtained with the following parameters: AM20 (Amplitude=157,8 V), FR10 (Frequency=4261 Hz). As we can see, a very low displacement variance is seen. Indeed the displacement variance is bounded by 0.1215mm

4.3 Precise characterization of two TRING-modules

The sequence of transfer is said successful if the two fingers move at two equivalent speeds. It is therefore necessary to characterize the two TRING-modules. In particular it is of important to determine what are the input frequencies and input amplitudes to be applied and with which the two microrobots have the same speed. Indeed, they do not necessarily have the same speed for the same input voltage. This is due to small difference in design, etc. Several experiments were carried out for that (Fig.11) and we found that the with AM20 (Amplitude=157.8V) and FR14 (Frequency=3125 Hz) applied to both TRING-modules, they have the same speed.

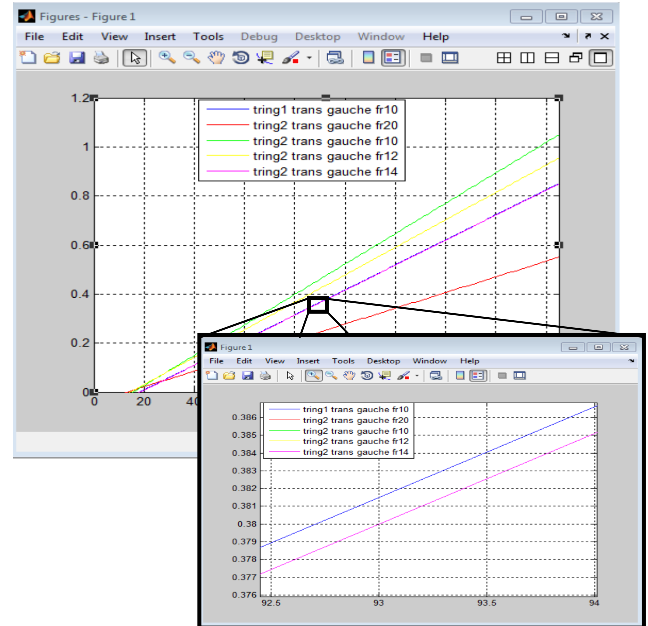

Fig. 11 Velocity characteristics of the two TRING-modules.

5. Discussion

5.1 TRING-module principle

With the increasing need of precise tools for micro/nano-manipulation, the microgripper structure based on two TRING-module we presented in this paper is new face to the existing industrial manipulators [7][8][9][10][11]. It has two main advantages: 1) the structure combines translation and rotation with the same microrobot which opens increases the possibilities of configurations of the microfactory; 2) different sizes and shapes of micro-objects can be manipulated thanks to the variable gap of the microgripper based on the two TRING-modules. The sizes of the micro-objects can vary from few tens of microns to some millimeters.

The slip-stick motion principle used allows a precise and high stroke displacement of the TRING-modules. During the rotation however, the weight of the TRING-modules can affects the displacement variance. Feature works include the design of new versions of the TRING-modules that account this aspect.

5.2 Design of microrobotic stations based on TRING-modules

We have presented some possible configurations of microfactory based on the TRING-module and we have focused on one of them as a case example. A feature work is now to provide a design method of the station itself. For

instance, according to the microparts to be assembled, to the microproducts to be fabricated and to the scenario of assembly/fabrication, the design method will provide the optimal configuration of the station/microfactory knowing that the modular elements are one or several TRING-modules. For that we will start with the DFμA technique (Design for Micro-Assembly) [12].

5.3 Control of the TRING-modules

As we saw in Tab.1, the performances in term of resolution and range of motion of a TRING-module are very interesting and convenient for the expected applications. In order to obtain the required precision during the pick-and-place tasks, the two TRING-modules that compose the station with the particular configuration in Fig.8 should be controlled. Two schemes of control exist: open-loop and closed-loop schemes.
Closed-loop control techniques, for instance that presented in the previous work [3], allow the stick-slip TRING-module microrobot to be robust face to external disturbances and to any model uncertainties. These disturbances include for instance the interaction force between the microrobot and the manipulated object. However closed-loop control techniques are mainly limited to the lack of convenient sensors in micro/nano scale applications. Indeed precise enough sensors are bulky and expensive (e.g. interferometry, triangulation based optical sensors, etc.) while embeddable sensors (for instance strain gage) are fragile, with limited range and do not often provide the required resolution. This is why open-loop control techniques are recognized in micro/nano applications [13].
The control technique of the two TRING-modules used in this paper was an open-loop technique. The velocity is the output signal and the reference signal as well for each module. The success of the control mainly depends on the precision of the model to be used [14]. The characterization of the TRING-modules as detailed in Section-4 is to allow the obtaining of such precise model. Open-loop technique can be assumed to be efficient in our applications as long as the interaction force (manipulation force) between the end-effector and the objects to pick-transport-place is weak, which is the case when the objects are small [15].

5.4 Application to micro-assembly

In the case of more complex task such as micro-assembly, a visual feedback may be required (Fig.12). This visual feedback is used to track the assembly operation between the transported object and the second (receptacle) object. To summarize, open-loop control techniques are used during the pic-transport of the object while a visual feedback technique is used during the release assembly. The main advantage is that a high speed is gained from the open-loop transportation while a high precision of assembly is obtained from the visual feedback. This application of micro-assembly will be implemented and tested in future works.

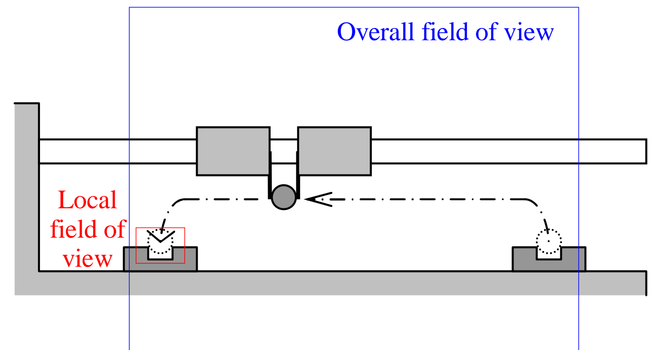

Fig. 12 Pick and place sequence.

6. Conclusion

This paper presented an approach to develop microfactory, cells or stations that can be reconfigured easily according to the requirement. Based on the modularity of the elements that compose the microfactory, we use a stick-slip microrobot called TRING-module as modular element. Several possible configurations were presented and one of them has been developed as a case example for a pick-and-place task. The experimental results showed the interest of the modularity aspect in this example, in particular the simplicity of control. Indeed, as the modules are similar (TRING-modules), the same control law can be applied to each of them. Future works include the experimental tests on other configuration of the microfactory and the realization of more complex tasks.

ACKNOWLEDGEMENT

This work is supported by the μUSINE-II-project.

REFERENCES

1. M. Rakotondrabe, Y. Haddab and P. Lutz, "Development, Modeling, and Control of a Micro-/Nanopositioning 2-DOF Stick–Slip Device", IEEE/ASME - Transactions on Mechatronics (T-mech), 14(6), pp. 733-745, Dec 2009.
2. A. Bergander, W. Driesen, T. Varidel and J.M. Breguet, "Monolithic piezoelectric push-pull actuators for inertial drives", IEEE International Symposium Micro-mechatronics and Human Science, pp. 309-316, 2003.
3. M. Rakotondrabe, Y. Haddab and P. Lutz, "Voltage /frequency proportional control of stick-slip microsystems", IEEE - Transactions on Control Systems Technology (T-CST), 16(6), pp. 1316-1322, Nov 2008.
4. Li Ang, "Mise en œuvre d'une station de micro-manipulation", MSc thesis, University of Franche-Comte in Besançon (UFC), 2011.
5. M. Rakotondrabe and Y. Le Gorrec, "Force control in piezoelectric microactuators using self scheduled H_inf technique", IFAC - Mech, (Symposium on Mechatronic Systems), pp. 417-422, Cambridge Massachusetts USA, Sept 2010.

6. WANG Zhi, HE Sai-xian "An Adaptive Edge-detection Method Based on Canny Algorithm", Journal of Image and Graphics, 2004-2008.
7. "Kleindiek Nanotechnik MM3A" http://www.nanotechnik.com/.
8. "Zyvex Nanomanipulator" http://www.zyvex.com/.
9. "Imina Techonologies miBot" http://www.imina.ch/.
10. "Attocube Nanopositioners" http://www.attocube.com/.
11. "Percipio Robotics" http://www.percipio-robotics.com/.
12. L.Benmayor, "Dimensional Analyse and Similitude in Microsystem Design and Assembly", PhThesis N°2232, EPFL, Lausanne, Switzerland, 2000.
13. B Borovic et al., "Open-loop versus closed-loop control of MEMS devices: choices and issues", Journal of Micromechanics and Microengineering, Vol.15, N°10, 2005.
14. A.N. Das and D.O. Popa, "Precision Evaluation of Modular Multiscale Robots for Peg-in-Hole Microassembly Tasks", 2011 IEEE/RSJ International Conference on Intelligent Robots and Systems, San Francisco, CA, USA, Sept 25-30, 2011.
15. Manikantan Nambi, Aayush Damani, and Jake J. Abbott, "Toward Intuitive Teleoperation of Micro/Nano-Manipulators with Piezoelectric Stick-Slip Actuators", 2011 IEEE/RSJ International Conference on Intelligent Robots and Systems, San Francisco, CA, USA, September 25-30, 2011.

Applications and business models for micro and desktop production systems

Anssi Nurmi[1], **Riku Heikkilä**[1,#] and **Reijo Tuokko**[1]

1 Department of Production Engineering, Tampere University of Technology, Tampere, Finland
Corresponding Author / E-mail: riku.heikkila@tut.fi, TEL: +358-408490272, FAX: +358-3-31152753

KEYWORDS : Microfactory, Desktop factory, Miniature production systems, Commercialization, Industrial practice, Applications, Business models

Micro and desktop factories are small-size production systems suitable for the manufacture of small products with micro and/or macro size features. The development originates in Japan. Small machines were developed in order to save resources when producing small products. In the late 1990's, the research spread around the world. Multiple miniaturized production systems have been developed. However, level of commercialization is still low and the breakthrough remains unseen.

This paper discusses how micro and desktop factories could be used profitably in the industry, and what the real benefits for users and equipment providers are. The research includes 18 semi-structured interviews in Europe. The interviewees are both from academic and industry, including equipment and component providers, as well as users and potential users.

Within the academics, miniaturization links to a general philosophy to match the products in size. In the industry, the small size is still only a secondary sales argument. It appears that the main factors preventing breakthrough are lack of examples, lack of subsystems and engineers' attitudes.

Based on interviews, the systems are used currently as semi-automatic tools for component manufacturing and assembly. In the future, educational and laboratory use as well as prototyping are promising. Local cleanrooms interest but questions arise. In addition, retail level personalization and home fabrication include problems. For providers, the technology offers two promising customer segments (Lean manufacturers and fully loaded factories), few additional segments (e.g. education, laboratories and offices) and it eases some alternative charging models (e.g. and capacity sales).

1. Introduction

Today's industrial production is rather different than a couple decades ago. Products are becoming smaller, more complex and they have more variations. The cost advantage of mass production disappears with a high rate of product variation. Consequently, new production paradigms for more flexible production have been introduced, e.g. Lean manufacturing. In addition, ecologic and ethical issues affect the business. Companies have to think more about energy consumption, use of recourses and recycling, among others.

New production technologies have been developed to meet the flexibility and ecological requirements of modern production and the new production paradigms. Miniaturization of production equipment has been suggested as one solution.

The term microfactory originates from research conducted in Japan in the 1990's. Research institutions, national universities and corporations developed smaller machines in order to produce micro parts and machines. Energy saving and economizing were some of the primary goals. [1]

In the late 1990's, the research spread around the world, and multiple miniaturized production systems were introduced. In addition, new topics, such as modularity [2], virtual models [3] and cleanrooms [4], embedded into the research.

However, the level of commercialization remains relative low. The discipline lacks of empirical cases and industrial practice on microfactory-related business.

1.1 Concept and equipment development

Under terms "microfactory" and "desktop factory", at least four types of concepts have been developed [5]: microfactories as a set of small-size equipment (e.g.[6][7][8]), modular microfactory platforms (e.g.[2][4][9]), miniaturized machining units (e.g.[10][11][12]), and robotic cells (e.g.[13][14][15]).

So far, only few commercial desktop factories have been developed (e.g.[16][17][18]). Multiple small-size machining units exist (e.g.[19][20][21]). Desktop-size stand-alone automation units have been developed for different purposes (e.g.[22][23][24]). In addition, desktop-size rapid prototyping units are appearing on the market (e.g.[25][26][27]).

1.2 Scope and structure

Within the discipline, the terminology alternates considerably. Terms used to describe highly miniaturized production equipment include: "desktop factory", "microfactory", "mini factory", "modular microfactory", "factory-in-a-suitcase", "palm-top factory" and "portable microfactory". In addition, the definitions tend to vary.

In this paper, micro and desktop production systems refers to micro and desktop factories, as well as miniaturized production equipment in general, including e.g. desktop-size machining units, robotic cells and rapid prototyping units.

In the chapter 2, research objectives and methods are presented. In the chapter 3, six industrial cases are introduced. The applications are discussed in the chapter 4. The business models are discussed in the chapter 5. The chapter 6 concludes the paper. In the chapter 7, the findings are discussed and research recommendations are given.

2. Objectives and method

The aim of this research was to examine how micro and desktop factories are used in the industry, how they could be used business-wise in the future, and what the real benefits for both users and equipment providers are. In addition, commercialization of the research was examined. The research is a mixed-method research, and it has an inductive approach.

Besides the literature, the research includes 18 semi-structured interviews in Finland, Germany, Switzerland and France. The interviewees are both from academic and industry, including equipment and component providers, as well as users and potential users. In addition, one interview focused on product personalization processes, and another on 3D printing and home fabrication aspects.

The interviews were used, because the literature lacks of empirical cases and industrial practice. In addition, they brought up different viewpoints to the topic, apart from the standard arguments within the discipline. For instance, current use, benefits, sales arguments and investment calculations, relating to micro and desktop factories, were discussed.

3. Industrial cases

In this chapter, six industrial cases are presented. All the cases are based on the interviews. Four principal cases relates to commercialization of microfactory research. Two following cases relate to use of micro and desktop production systems.

3.1 Development of commercial systems based on research

In this section, the four cases present different ways how industrial products can arise from the microfactory research.

Percibio Robotics represents a traditional academic spin-off. It further developed an academic micromanipulation system and made a product out of it. Asyril commercialized a miniaturized delta robot. However, the commercialization was achieved by an adaption of another company. µFemos and microFLEX represent cases where products have been developed based on direct funding and cooperation between the industry and academics. Finally, MAG Lean is an example on how research can encourage product development.

3.1.1 Percibio Robotics – an academic spin-off

Percibio Robotics is a young French spin-off based on the research conducted at FEMTO-ST (*Franche-Comté Electronique, Mécanique, Thermique et Optique - Sciences et Technologies*). The start-up designs and prototypes robotic systems for micro handling. The core product is a precise electrostatic gripper based on two piezo electric beams (see the previous gripper in [15]). Currently, the core business is to build specific solutions for the high-tech industry, e.g. electronics, biomedical and clockwork industries. [28]

In addition, Percibio Robotics designs standard desktop robotic systems for clockwork assembly. A tele-operated desktop system is under development (see the previous system in [15]). The new system consists of two grippers, robotic arms, a planary table, 2-3 cameras and control software. It is designed to work as a tool in the clockwork industry, for applications beyond capabilities of human hand. [28]

3.1.2 Asyril – commercialization through adaption

Asyril is a Swiss company focussed on miniaturized mechatronic devices for automation. The product line includes delta robots, flexible feeder systems and robotic cells [24]. Asyril was set up based on the small delta robot, PocketDelta.

PocketDelta is a result of a common microfactory project at HTI-Biel (*Hochschule für Technik und Informatik*), EPFL (*École Polytechnique Fédérale de Lausanne*) and CSEM (*Centre Suisse d'Electronique et de Microtechnique*).[29]

Alain Codourey searched funding to establish a company based on the robot. CP Automation (CPA) wanted to widen the engineering know-how. In the beginning, Codourey worked at CPA. The first task was to establish a new company. Asyril was established in 2007. It was not sure whether or not the miniaturized robot would sell. Therefore, a larger delta robot was launched as well. However, suitable applications in the watchmaking industry were found, and the robot started to sell. The start-up worked out well, but it is a relative risky strategy. Nowadays, Asyril focuses on developing equipment based on the customer needs, without forgetting innovativeness. [29]

Together with CPA, the products can be sold for end users and system integrators. Asyril sells desktop cells for the end customers, as well as robots and feeders for system integrators. In addition, CPA integrates the systems for applications. [29]

3.1.3 µFemos and microFLEX – cooperation between the academics and the industry

IEF Werner is a German component and automation provider. Two concepts, µFemos and microFLEX, have been developed in cooperation between IEF Werner, Karlsruhe Institute of Technology (KIT) and few other companies [30].

The µFemos project lasted from 2002 to 2005. A German company had developed a high precision optical distant sensor. A research project was proposed for the assembly process. As a result, the µFemos machine was developed (see [31]). IEF Werner never sold the machine with the same layout. However,

Fig. 1 JOT Automation – JOT Lean cell [22]

Fig. 2 JOT Automation – Final assembly jig [37]

based on the knowledge, multiple commercial products were developed, e.g. positioning systems and piezo driven axis. [30]

The funded microFLEX project lasted from 2009 to 2011, in cooperation between IEF Werner, KIT and an industrial partner (customer). The target was more or less to have a finished product in a catalogue. As a result, microFLEX was created (see [17]). It is compatible with manual, semi-automatic and fully automatic production. Dimensions of the unit respond to the manual assembly table in the industry. [30]

KIT developed tools, interfaces and logistics in the project. Now the system is handed to the customer. IEF Werner has further developed and sold it to other customers as well. [30]

3.1.4 MAG Lean – research as forerunner

Master Automation Group (MAG) is a Finnish automation provider for telecom, marine and aerospace industries. MAG has participated the TUT (Tampere University of Technology) Microfactory projects since 2007 and launched two generations of commercial microfactories.

The first miniaturized cells were mostly for the telecom industry. A 500mm wide floor standing cell was developed for assembly and packing. The cells performed well but they were still not competitive with low-cost manual production. [32]

In the second phase, the desktop cells were developed. Targets included an A4 paper size footprint and cheaper price. The in-house component development was inspired by the TUT Microfactory projects. In the third phase, desktop cells were built out of commercial components. As a result, the first generation of MAG Lean cells was launched in 2010. [32] In 2011, the second generation of Lean cells was launched [16]. Again, MAG acted as an auditor of TUT in the beginning.

Lately, based on merging of MAG and JOT Automation, new JOT Lean cells have been launched (see Figure 1). The system is built for Lean and scalability of automation. For example, the Poka-Yoke assembly jigs can be used to increase efficiency and quality of manual assembly (see Figure 2). Secondly, a JOT Lean cell can be used as semi-automatic tool. Finally, an automation line can be built of multiple cells.

3.2 Users and potential users

In this section, two industrial cases, a user and a potential user of miniature production systems, are presented. Nokia is using desktop automation cells in production, and the use has evolved interestingly during the past years. Biohit instead, would like to use desktops for certain stand-alone processes.

3.2.1 Nokia

Nokia's production is mainly assembly of subcomponents, including only little automation. The production is divided into high-end and mobile phone factories. [33]

The mobile phone factories are based on mass production. Products do not vary much. In the high-end factories, small quantities of versatile products are produced based on orders. The production is organized into Lean production cells, each having 2-3 employees and semi-automatic tools. Desktop automation cells are used in the high-end production. [33]

First, small assembly lines were designed out of desktop cells. The main motivation was floor-space reduction. The lines were abandoned because flexibility requirements. If technology is flexible enough, it becomes too expensive. [34]

Currently, the desktop cells are used as tools for repetitive assembly steps, or for processes which cannot be conducted by humans. The processes include screwing, gluing and precision assembly. An operator loads a cell and the cell conducts a specialized task. Manual assembly is extremely flexible and thus always needed. For example, the Desktop cells can help to place components precisely. However, flex cables have to be attached manually. The approach suites also better to Lean, which is contradictory to automation. [33][34]

In the future, one option is to combine manual assembly to low-level and high-level automation (see Figure 3). The desktop cells, i.e. the high-level automation, would provide quality improvements to manual assembly. In addition, a larger safety robot, i.e. the low-level automation, is tested for automated assisted assembly. It could operate next to operators to replace repetitive tasks, e.g. pick-and-place from trays and loading/unloading the desktop cells. The system might be in use within couple years. [34]

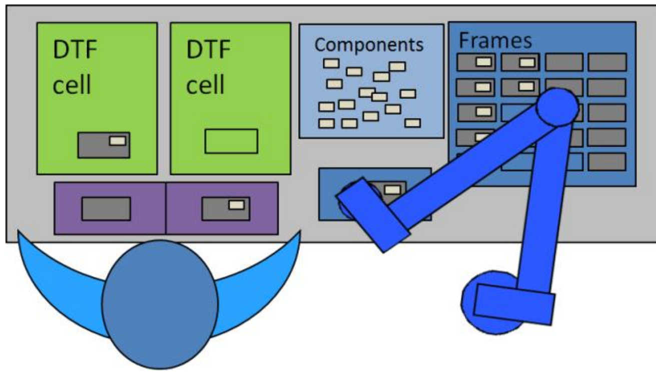

Fig. 3 Combining low-level and high-level automation

3.2.2 Biohit

Biohit is a Finnish company focused on liquid handling products, diagnostic tests and analysis systems. The products are mostly handheld devices, including micromechanics, electronics and plastic parts.

Excluding the disposable pipette tips, the production is mainly Lean assembly. For instance, the production process of high-end electronic pipette includes seven steps: 1. Fabrication and purchase of component; 2. Assembly of subassemblies 3. Assembly of the engine and gears; 4. Testing; 5. Marking serial numbers; 6. Final liquid testing; 7. Packing. [35]

There is a need for desktop cells in the first and the second assembly steps. First, they could be used for machining of injection moulded components during the assembly. For instance, two current pipettes include a very similar plastic component, but other requires machining. Because of small batches, machining is difficult to outsource. Thus, the injection moulded components are machined once a year, including large stocks. Instead, the components could be machined on the spot. Process time is not highly critical, because takt time planning and *kanban* provide tools for scheduling. [35]

Secondly, desktop automation could be used for flexible co-operation between humans and machines, eliminating repetitive working phases. Currently the Lean assembly includes flexible tools, e.g. electric screw drivers. Workers and the desktop robot(s) could work in as small area. In addition, a dust-free ISO 8 class environment is needed for the new products. Local cleanrooms could be one solution. [35]

In addition, some other assembly phases, e.g. final liquid testing and packing, could have applications for desktop production systems. The production of disposable pipette tips has too large volumes. However, a small-size and stand-alone test device could be usable to test the tips on-line. [35]

4. Applications

In this chapter, the applications are discussed. In the section 4.1, the level of automation is discussed. There are a broad range of speculated applications in the literature. In the section 4.2, the applications are categorized by a supply chain. In the section 4.3, the current industrial practice is discussed.

4.1 Scalability of automation

Highly miniaturized products, which are too small to be assembled by human operators, require different automation strategy than traditional products. The adaption of automation includes usually different phases (see list below). [36]

Levels of automation (based on [36])

1. Manual
2. Semi-automatic
    - A. Automatic Alignment
    - B. Automatic Process
    - C. Automated Batches
3. Automatic
    - A. Robotic material handling
    - B. Automated Inter-Cell Transfer
        - i. Offline ‘lines’
        - ii. Automated logistic system

The classification above applies not only for MEMS products and fiber optic components, but also for any small products. Because of the small size, micro and desktop factories can be used for flexible human-machine cooperation.

First of all, small products can be produced manually by simple and flexible electronic tools. Efficiency and quality of manual production can be enhanced e.g. by assembly jigs [37]. Production is still manual, but the jigs prevent human errors.

To improve efficiency and quality further, tele-operated desktop factory units can be used. Even though the manipulation is semi-automatic, automation of simple and repetitive tasks can save up to 90% of time [28].

Secondly, a whole process can be automated. An operator feeds products and components and the desktop cell conducts a given process, as in the Nokia case above.

Thirdly, automation can be applied for batches as well. Here, the operator feeds multiple products and/or components and the desktop cell applies the process for a batch (see 2C & 3A above). However, part feeding, e.g. large trays, can be a problem. Nokia is trying to round the problem by using large-scale safety robots to complement the desktop automation [34].

Finally, automated inter-cell transfer can be applied to few cells or to complete factory logistics system. In the former case, the operator is using the cells as an offline process. The process is just divided into few cells (e.g. optical lamination). The latter represent a fully automated factory system, build on microfactory modules. It should be noted that e.g. flexibility requirements in some industries may prevent such systems.

4.2 Applications within and beyond production chain

In this section, the use of microfactories is categorized into three scenarios: *I* miniaturization of production equipment in a traditional production chain, *II* relocating production further into the downstream and *III* production on the spot.

If microfactories were used just to replace the large-scale production equipment, it is the scenario *I*. If microfactories were used to at the place of use, it is the scenario *III*. Everything else between the factories and consumption, including the point of purchase, is the scenario *II*.

4.2.1 Replacing the large-scale machinery I

The first scenario takes place in a traditional production chain. In general, micro or desktop factories could be applied to all products and processes, which fit into the reduced working space. However, it does not mean that the miniaturization was feasible. There is usually large-scale machinery for any given process. Desktop machinery is bought if it is better for the application. However, if the large-scale machinery is replaced with the small machines in order to cut costs, the investment has to yield e.g. 15% annually.

By definition, micro and desktop factories are small and they can save space. Thus, they are expected to cut costs of facilities, e.g. rents or capital costs, as well as costs of energy, material, heating, air conditioning, illumination, waste and recycling. Similarly, local cleanrooms can cut cleanroom investments and maintenance costs. In addition, desktop solution might suite better for Lean and manual production in general, enhancing quality of products. The benefit might be difficult to quantize. However, it reflects to e.g. costs of poor quality. Finally, microfactories are expected to be more flexible, having shorter set up times. The flexibility reflects to capital costs as less stock, of products and semi-finished products, is needed. The cost reduction factors have been discussed in the literature (e.g. [38][39][40]). Furthermore, some product characteristics might be enabled. E.g. small-size machinery and grippers might prevent fragile products.

4.2.2 Relocating production downstream II

The second scenario relates to relocating production further into the downstream. Because of the small size, microfactories could be used for e.g. production on the way or personalization at wholesaling and/or retailing level.

On one hand, a small and mobile production system could be integrated e.g. into a car, truck, train, ship or aeroplane. The process could shorten delivery and enable production of perishable products on the way. [41] The shorter delivery could gain add-on sales. In addition, capital costs decrease, as delivery is faster and stocks of finished products decrease. Suitable products would be small and perishable products having a long time of delivery and a stabile demand.

On the other hand some production phases could be placed at wholesaling and/or retailing level. At wholesaling level, the model would suite well for personalization of small products having modular design and an intermediate level of personalization. At retail level, microfactories could be used to personalize small and highly personalized products e.g. contact lenses, watches, jewellery, cosmetics, small sport equipment, pharmaceutics and other medical products. Potential processes include coating and UV-printing (e.g. electronics), marking (e.g. jewellery), final assembly (e.g. optics), machining (e.g. custom-fit sport equipment) and sorting (e.g. drug dosage and encapsulation). The process relate mostly to add-on sales. Customers might choose the product because it is more personalized. In addition, decentralize production hubs are expected increase dynamics of the supply chain, adapting more easily to a fluctuating demand and decreasing costs of logistics. Goldsmiths, opticians, and orthotics are examples of current businesses, relating to retail level personalization. Miniature production systems could enable more processes to be automated.

However, a lot of uncertainty relates to the advantages. For instance, the production on the way might not shorten much the delivery time. Production is usually only a small fraction of the delivery time. The total delivery time might not decrease a lot by producing the products on the way. Therefore, the capital costs would not decrease much either. In addition, the equipment and handling require space. More products can be packed e.g. in a ship in a normal way.

In addition, the impact of personalization on costs of logistics depends highly on the processes. If assembling process is personalized, the components have to be transported to many locations instead of one factory. As a result, the costs of logistics might even increase. Subtractive manufacturing, coating and marking and are more potential instead.

Furthermore, the retail level customization should relate to some products which can be bought on impulse. If a customer wants to buy a highly personalized product, he or she can usually wait few days to get the product from a factory.

Finally, the number of personalizing retailers includes a compromise as well. Multiple retailers can serve many customers but it increases costs. Companies might choose to personalize only in large flagship stores for marketing purposes, and centralize the service for other customers.

4.2.3 Production on the spot III

As microfactories are small, they could be used to produce products on-the-spot, if time of delivery is critical and there is no space for traditional factory and/or machinery. Battlefields, trouble spots and the Third World as well as city centres and researchers' special conditions are examples of situations where logistics can be problematic. Exchange part fabrication is one potential application. Medicament is another specific application area. Microfactories could be used in the field for fabrication of custom implants [42] or dental products [21], as well as for sterilization and drug fabrication and dosage.

The U.S. Army has Mobile Parts Hospital containers (MPHs) for replacement part fabrication. For example, the MPH made a rotor brake seal for an Apache helicopter. Instead of waiting two months, the helicopter could be used within days, and $393,000 was saved. [43] In addition, the U.S. Army has Mobile Army Surgical Hospital (MASH) container hospitals. MASHs are used to for lifesaving surgical care. [44] Respectively, micro and desktop production systems could be used in containers for distinct processes. Because of the small size, more machines can be fitted into a container.

In addition, in some occasions, ordering is not a direct substitute but it would be beneficial to use a machine locally. The most potential applications are prototyping (e.g. in engineering, design, or architecture offices) and educational use. In addition, small automation could be used in laboratories [23], and for processes inside of industrial and laboratory equipment [45]. The small size is a benefit because non-manufacturing facilities are usually not built for heavy and large-scale machinery. Ordering is not a direct substitute,

because the process is the product (education). Similarly, the process provides information for prototyping. In laboratories instead, logistics might be a problem. Samples cannot always be transported elsewhere. The processes are conducted on the spot, either manually or automated by machines which fit into the space. Finally, small machinery could be used even for personal fabrication at home or communities [46].

4.3 Current practice

The current use of microfactories relates mainly to the first scenario (q.v. 4.2.1). According to the interviews, they are used in the industry mainly as stand-alone tools for component manufacturing and assembly processes.

MAG Lean cells are used mostly in the electronic and life science industries as well as within component manufacturers (e.g. in the automotive industry). Processes include e.g. screw insertion, precision assembly, plasma treatments, dispensing, marking and cleanroom processes. In addition some special processes and assembly are combined into one cell. [47]

Similarly at Nokia, the desktop cells are used currently as tools for repetitive assembly steps, or for processes which cannot be conducted by humans. The processes include screwing, gluing and precision assembly. For example, components might have small gaps at joints. If a component is placed exactly in the middle, the human eye does not see the difference. However, an operator would not be able to place it precise enough. [33]

In addition, two companies had manual Lean assembly. The production is divided into Lean cells and products are assembled with simple tools, e.g. electronics screwdrivers. Similar to Nokia, microfactories could be used as stand-alone processes to enhance quality and efficiency.

The watchmaking industry is the largest industry for all the products of Asyril. In addition, the medical and semiconductor industry have some applications. Applications include e.g. pick and place, feeding, palletizing and other standard applications. PocketDelta and Asycube are used together as a feeder, substituting e.g. vibrating bowls. The customers prefer individual machines instead of lines. In addition, CPA integrates Asyril's products for special applications, e.g. systems with multiple manufacturing steps or gluing. [29]

The watchmaking industry is also important for Percibio Robotics. The applications include e.g. placing small stones in the encore of the motion and placing axis for gears in as small holes. Swiss clockwork industry is currently under revolution. The monopolistic production of the movements will stop in 2012. More companies need to set up their own production. The situation is highly favorable for equipment providers. [28]

At Biohit, desktop cells could be used for machining of injection moulded components during the assembly. Secondly, desktop automation could be used for flexible co-operation between humans and machines, eliminating repetitive working phases. Finally, some other assembly phases, e.g. final liquid testing and packing, could have applications. [35]

In addition, challenges relating to few industries and applications were brought up. For example, Percibio Robotics aimed for the MEMS industry in the beginning, as it was often referred within the academics. However, it turned out that the industry has already up to 20-year technology roadmaps. The companies preferred to develop the old processes instead. [28]

Health care and laboratory work were cited as potential applications. However, medical industry is highly regulated and it can be challenging for traditional automation providers. It is vital to understand the industry and the application area. In addition, desktops might have more potential in research and laboratory use. Pharmacy requires too high volumes. Same applies for micro cultivation. [48]

For example, local cleanrooms interest companies in the bio industry. However, practical issues, relating to e.g. maintenance, raised questions. They require still development and standardization. For instance, traditional cleanroom standards are still applied for local cleanrooms. A specific ISO standard is currently under development [49].

On-the-spot medical applications were also brought up. Instead of having all the different variations of an implant, a hospital could buy bulk implants and specific machine to personalize them. Especially specific operations e.g. face and scull surgery, would benefit of the personalized implants, if the amount of surgeries could be decreased or they would shorten dangerous operations. In case of average fracture, the surgeon has enough time to modify the implants. Metallic implants might be the first applications. The processes of biodegradable implants are still under development. [50]

A Finnish retailer of home electronics is personalizing products with a laser carver, a UV-printers and a vinyl printer. For them, automated microfactories include two problems. First, the process is currently manual. An employee picks the product up and opens the box. After personalization, the products are packed manually. Small bulk batches would be more expensive and they do not want to change the business model. Secondly, larger equipment, instead of smaller, is needed for home electronics. Smaller equipment could be used parallel e.g. for MP3 players and phones. However, the specific machines, e.g. UV printers, are already small. [51]

5. Business models

In this chapter, the business models for equipment providers are discussed. By definition, micro and desktop production systems are small and portable. In addition, they represent a new production technology on the market. The main question relates: how do these factors benefit the equipment providers?

The section 5.1 discusses business models for providers of small-size automation cells. Similarly, the section 5.2 discusses the business models for providers of small-size machining units. The section 5.3 discusses the characteristics of non-manufacturing users as a customer segment. Finally, the section 5.4 discusses the technology for subcontractors.

5.1 Small-size automation cells

For equipment providers, the technology offers two promising customer segments: Lean manufacturers and manufacturers with fully loaded factories.

Lean is much more than a set of tools [52][35][53]. However, it appears that Western companies tend to adapt primary only the Lean tools and method invented by Toyota [53]. As a result, production is often divided into Lean cells (islands of excellence), one-piece-flow is favoured and the production is mainly manual [am]. Therefore, Lean is contradictory to traditional automation [34]. Process equipment has been one of the least covered topics in the key Lean literature [ak, p.131]. In addition, according to Lean, robots and automation must remain as tools for men, not the other way around [am]. Automated desktop cells can improve quality and enhance efficiency of certain processes because they fit into the Lean production cells, and they can be used as tools [48][33].

It appears that the compatibility to Lean production might be actually one of the primary benefits. The CEO of JOT Automation, cites the "next coming of lean assembly" as one of the major trend for automaton as well [54].

However, Lean is not an easy segment for the automation providers. On one hand, the reliability is important for traditional mass production as the production volumes are usually huge. On the other hand, Lean tends to favour robust and thoroughly tested technologies by offset. In case of a breakdown, there are no (or small) safety stocks. In addition, *Jidoka* and *andon* stop the process [55].

The manufacturers with fully loaded factories relate to the fact that the floor space is relative cheap (€/m^2), even with all the fixed costs. However, acquiring new space includes huge step costs [34]. It can be a major competitive advantage for a provider of miniaturized production system. Even if the smaller option is more expensive, it might be selected because it fits well into the factory layout.

5.2 Small-size machining units

For providers of machining units, the small size of machines might enable new business and charging models, e.g. leasing, tie-up sales and capacity sales. Small machines can be carried in, e.g. with a pallet jack, and the space at customer's premises does not require any preparations. As the technology is new, customers are more likely to accept the new models.

A company could provide free or inexpensive machines and charge the use. It is kind of leasing but it enables the company to move the machine elsewhere if needed. Charging is only a matter of a contract, e.g. €/hours, €/working hours or €/produce. Depending on a customer and a contract, an employee could be provided as well. [48] It decreases the buying decision as investments include always risk. In addition, many small and medium size companies do not evaluate the investments broadly enough. It is therefore easier to justify cash flow financing. Furthermore, buyer's shifting costs increase. The machine at customer's premises binds the customer. Changing provider becomes more difficult.

In addition, the small size enables capacity sales, i.e. the machines lay at provider's premises and only capacity is sold. As the machines are small, more machines fit into the same space. Wegera, a Finnish subcontractor for metal industry, has developed a miniaturized 5DOF CNC machine Kolibri [55]. They are providing already such service. Customer can order instant machining services for monthly payment. [56]

Finally, a provider could have multiple machines on stock and provide a service of capacity scaling. In this case, the provider would adjust the amount of machines, either in customer's or provider's premises, based on how much capacity the customer needs. However, both the business models, tie up sales and capacity sales, increases capital requirements, and thus marginal utilities have to be evaluated.

5.3 Small-size equipment for non-manufacturing use

In the non-manufacturing market segment, the small size of machinery can be a major competitive advantage. Three primary scenarios came up in the interviews: prototyping on the spot, laboratory automation and education. Prototyping relates mostly to machining and rapid prototyping units. Laboratories relates mostly to desktop automation. For education, there are different small-size machines on the market. Prototyping and education will be probably important applications for Wegera's Kolibri as well [56].

At KIT, there is an interesting research project going on, relating to laboratory automation. Small machine-vision based robotic cells have been developed for sorting and analysing of zebrafishes. Currently the process, of breeding, pipetting, and analysing, is mainly manual. It takes approximately 14 minutes for a researcher to sort manually 384 chambers. In addition to saving in time, the system can maintain a constant temperature of 28°C. [57]

The size is a benefit because facilities (offices, laboratories and classrooms) are not built for heavy and large-scale machinery. If, for example, an engineering company wants to buy a CNC machine to prototype metal parts in an office, a traditional machine is not a reasonable option. In addition, there are usually no direct substitutes for the use.

In addition, retail level product customization has been suggested as one application. However, it includes a different setting. For a retailer, it is important to customize locally only if the products which can be bought on impulse. If a customer wants to buy a highly personalized product, he or she can usually wait few days to get the product from a factory. Therefore, ordering substitutes the customization on the spot.

Similarly, personal fabrication includes a different setting. If the machine is used as a hobby, it is not substituted easily. However, if a consumer produces utility articles for itself, there is always an option to buy the articles elsewhere. The desktop-size hobby 3D printers have gained popularity. The industry seems to have a strong network effect and the critical mass might be already obtained. It is possible that desktop-size hobby machining units will gain more popularity in the future.

5.4 Subcontracting with small-size machines

Finally the small size and modularity of microfactories might enable some new business models for subcontractors.

For example, a subcontractor or a contract manufacturer can acquire a stock of small-size process modules. Based on orders, different production lines can be built out of the modules and more customers can be served. Because of the

small size, more modules fit into the space. The subcontractor can be the equipment provider but they can be separate companies as well. Apparently, the Japanese manufacturers have used microfactories for this purpose [58].

Subcontracting is also good counterbalance for machine development. Subcontracting can provide parts for the machines, and the machines can be tested in production. [56]

On the other hand, the small of machinery can enable portable maintenance service. The examples of MPH and MASH are presented above (q.v. 4.2.3). Similar model can be expanded into other industries as well. A company could provide spare parts locally for factories and other machines.

6. Conclusions

In this paper, applications and business models as well as commercialization relating to micro and desktop production systems were discussed. In the literature, there are a broad range of speculated applications for the systems relating to different advantages. The MEMS industry is stated as a potential industry. In many cases, the research aims for integrated desktop production systems and high level of automation, including e.g. intelligent conveyors.

The applications were categorized into three scenarios, relating to different benefits and what substitutes the use The first scenario is to replace the traditional large-scale machinery by miniature production systems. The expected benefits relate mainly to different costs. However, because of the small size, the desktop solution might suite better for Lean and manual production in general. The second scenario relates to relocating production further into the downstream, e.g. production on the way or personalization at wholesaling and/or retailing level. The benefits relate mainly to add-on sales. The third scenario is to produce products on the spot by small machines. Here, the small equipment might enable the production and the whole business.

The current use of microfactories relates to the first scenario. According to the interviews, they are used in the industry mainly as stand-alone tools for component manufacturing and assembly processes. In many cases, flexibility requirements are too high for desktop lines. Conveyors are against new production paradigms, e.g. Lean. Industries include e.g. watchmaking, telecom, medical and semiconductors. Processes include e.g. precise pick and place, screwing, dispensing, palletizing and marking, as well as laser and plasma treatment. The miniature machining systems suite for versatile materials and applications, for example metal (e.g. micro mechanics, jewellery and watches), glass (e.g. micro-optics), plastic (e.g. hearing aids), ceramics (dental applications) and biodegradables (implants).

However, the small size of equipment is usually only a secondary sales argument. There is no urgency to replace the large-scale machinery. In general, a customer buys a specific process, impact or working phase. The most important factor is whether or not the machine does what it is supposed to do. Price and size are secondary arguments if there are equal products on the market. Although, one real benefit for companies that desktop systems can be used as tools. One employee can operate multiple small-size machines.

In the future, non-manufacturing applications, e.g. educational and laboratory use as well as prototyping are promising. Within manufacturing industry, local cleanrooms interest companies, especially in the bio industry. However, practical issues, relating to e.g. maintenance, raise questions. The MEMS industry might not be the first industry having specific processes. Retail level personalization includes problems relating to logistics and business models. Home fabrication will be likely relative small niche in the near future.

For equipment providers, the technology offers two promising customer segments (Lean manufacturers and manufacturers with fully loaded factories), few additional segments and it eases some alternative charging models. Lean manufacturers are a promising segment because Lean is contradictory to traditional automation. Currently, based on Lean production principles, the production is mainly manual. Automated desktop cells can improve quality and enhance efficiency. The fully loaded factories relate to the fact that the floor space is relative cheap, even with all the fixed costs. However, acquiring new space includes huge step costs.

The additional customer segments can be reached because the small machines fit well into non-manufacturing environments, e.g. offices (prototyping), classrooms (education) and laboratories (e.g. automatic pipetting).

The alternative charging models are enabled because the small machines can be carried easily in, and the space does not require any preparations. A company can provide cheap or free equipment, and make the profits out of net billing, easing buying decision and increasing buyer’s shifting costs. On the other hand, provider can to store multiple small-size machines and sell only the capacity. Similarly, subcontractors, focusing on small batches, can have multiple modules on the stock and build versatile production lines can out of the modules.

7. Discussion

As discussed in the section 3.1, industrial products already arise from the microfactory research. However, introduction of new production technology takes time. Companies and engineers prefer not to use new production technologies as there are few examples. Consequently, few examples arise.

To bring microfactories faster into the industry, more cooperation is needed between academics and the industry. More precisely, academics should continue on searching the limit of downscaling. In addition, they should inform the industry and the new engineers about the technology. A large scale production demonstration is needed, so that the industry would understand the potential. The equipment providers are already modifying and commercializing the concepts. In addition, the users of automation should inform the academics which miniaturized applications and processes are needed.

More attention should be directed towards industrial and business aspects. As noted, the academics and the industry

have slightly different viewpoint to the miniaturization. It should be explored, what the feasible applications in various industries are and what the real benefits for companies are. Cases and demonstrations should be selected respectively.

In addition, combination of Lean and miniature production systems requires more examination. It should be identified how, in practice, companies tend to combine Lean production practices and desktop automation and/or production machines.

ACKNOWLEDGEMENT

The authors would like to acknowledge the constructive comments by the TUT Microfactory team and Professor Petri Suomala. In addition, we wish to acknowledge all the interviewees who provided valuable insight for the research.

REFERENCES

1. Okazaki, Y., Mishima, N. and Ashida, K., "Microfactory - Concept, History, and Developments," J. of MSE, Vol. 126, No. 4, pp. 837-844, 2004.
2. Gaugel, T. and Dobler, H., "Advanced modular microproduction system (AMMS)," In SPIE, 29-30 October 2001. Newton, USA, pp. 278-285, 2001.
3. Rizzi, A.A., Gowdy, J. and Hollis, R.L., "Distributed coordination in modular precision assembly systems," The International Journal of Robotics Research, Vpl. 20, No. 10, pp. 819-838, 2001.
4. Verettas, I., Clavel, R. and Codourey, A., ""Pocket Factory": Concept of miniaturized modular cleanrooms," Mechanical Engineering, 2005.
5. Nurmi, A., "Business models and applications for micro and desktop production systems," MSc thesis, 120 p., 2012
6. Ataka, T., "The Experimental Microfactory System in Japanese National R&D project," 1999.
7. Kitahara, T., Ashida, K., Tanaka, M., Ishikawa, Y., Oyama, N., and Nakazawa, Y., "Microfactory and Microlathe," International Workshop on Microfactories, pp. 1–8., 1998.
8. Park, J.-K., Lee, N.-K., Lee, D.W. and Song, J.-Y., "Development of Microfactory Systems for the Next Generation - 3rd Year Report," 3th International Workshop on Microfactory Technology, pp. 5-12., 2007.
9. Heikkila, R.H., Karjalainen, I.T., Uusitalo, J.J., Vuola, A.S. and Tuokko, Reijo O., "Possibilities of a Microfactory in the Assembly of Small Parts and Products - First Results of the M4-project," *International Symposium on Assembly and Manufacturing,* pp. 166-171, 2007
10. Kurita, T., Watanabe, S. and Hattori, M., "Development of hybrid micro machine tool," 2nd International Symposium on Environmentally Conscious Design and Inverse Manufacturing, pp. 797-802, 2001
11. Okazaki, Y., Mori, T. and Morita, N., "Desk-top NC milling machine with 200 krpm spindle," In ASPE 16th Annual Meeting, pp. 192-195, 2001
12. Okazaki, Y., "Development of a desk-top milling machine with a 300 krpm spindle and a linear motor stage," 4th IWMF 2004, pp. 29-33, 2004
13. Koelemeijer Chollet, S., Bourgeois, F., Benmayor, L., Moll, B., Wulliens, C. and Jacot, J., "A Flexible Microassembly Cell for Small and Medium Sized Batches," International Symposium on Robotics, 6 p., 2002
14. Kunt, E.D., Naskali, A. T., Cakir, K. and Sabanovic, A. "A Versatile and Reconfigurable Microassembly Workstation," *6th IWMF 2008,* pp. 37-41, 2008
15. Clévy, C., Hubert, A. and Chaillet, N., "Flexible micro-assembly system equipped with an automated tool changer," Journal of Micro - Nano Mechatronics, Vol. 4, No. 1, pp.59-72, 2008
16. MAG, "MAG Lean: Solutions for industry," Available at: http://www.mag.fi/products_and_services/electronics/mag_lean [Accessed December 10, 2011], 2010
17. Hofmann, A., Hummel, B., Firat, O., Bretthauer, G., Bär, M. and Meyer, M., "microFLEX - A New Concept to Address the Needs for Adaptable Meso and Micro Assembly Lines," ISAM, 5 p., 2011
18. JOT Automation, "JOT Automation Lean Solutions – Datasheet," 2 p. Available at: http://www.jotautomation.com/media/datasheets/final-assembly/a4_and_a3_datasheet_1_2_0_print.pdf, 2011
19. Iijima, D., Ito, S., Hayashi, A., Aoyama, H. and Yamanaka, M., "Micro Turning System: A Super Small CNC Precision Lathe for Microfactories," 3rd IWMF, pp. 37-40, 2002
20. Lin, W., Ohmori, H., Uehara, Y., Asami, M. and Ohmori, M., "Development and Characteristic on the Desk-top 4-Axes Machine "TRIDER-X" for Micro-fabrication,". 4th IWMF, pp. 74-79, 2004
21. vhf camfacture, "Impression Line," Available at: http://www.vhf.eu/en/Machines/BasicSystems/Impression Line [Accessed December 10, 2011], 2010
22. JOT Automation, "Desktop Screw Inserting Cell - Datasheet," 2 p. Available at: http://www.jotautomation.com/media/datasheets/final-assembly/j505-62_datasheet_1_0_0_screen.pdf, 2010
23. Biohit, "Biohit Roboline™ - your automate," Available at: http://www.biohit.com/resource/files/media/brochures/liquid-handling/all/roboline-brochure-490100en-screen.pdf, 2011
24. Asyril, "Rethink Micromanipulation," Available at: http://www.asyril.ch/media/PDF/Asyril_Products_E.pdf, 2010
25. Dimension, "BRING YOUR IDEAS TO LIFE WITH A uPRINT® PERSONAL 3D PRINTER," Available at: http://www.dimensionprinting.com/pdfs/up-prodspecs/up-prodspecs.pdf, 2010
26. 2BOT physical Modeling Technologies, "Classroom ModelMaker™ ...enhancing cognition through subtraction," Available at: http://www.2bot.com/images/stories/DOWNLOADS/85-0601-001RA_BRO_EDU_CUT_Sheet.pdf, 2010
27. Objet, "Objet24 Personal 3D Printer," 2p. Available at: http://www.objet.com/Portals/0/docs2/Objet24_A4_New_IL_low.pdf, 2010
28. Hériban, D., Interview at Percibio Robotics, Bensançon, France, 23 September, 9:00-10:30, 2011
29. Codourey, A., Interview at Asyril, Villaz-St-Pierre, Switzerland, 22 September, 9:00-11:30, 2011
30. Hofmann, A., Interview at KIT, Karlsruhe, Germany, 21 September, 09:00-11:00, 2011
31. Bär, M., "Modulare Montagemaschine – Tischfabrik. In M. Bär, ed. μFEMOS - Mikro-Fertigungstechniken für hybride mikrooptische Sensoren," 2006
32. Laitinen, M., Interview at Fastems, Tampere, Finland, 10 August, 12:15-13:30, 2011
33. Luotonen, J., Interview at Nokia. Salo, Finland, 2 September, 10:15-12:00, 2011
34. Zott, A., Interview at Nokia, Ulm, Germany, 19 September, 10:00-12:00, 2011

35. Spear, S. and Bowen, H.K., "Decoding the DNA of the Toyota Production System," Harvard Business Review, pp. 96-106, 1999
36. Duncheon, C., "Product miniaturization requires automation – but with a strategy," Assembly Automation, Vol. 22, No. 1, pp. 16-20, 2002
37. JOT Automation, " Final Assembly Jigs and Tools," Available at: http://www.jotautomation.com/en/front-page/production-solutions/final-assembly/final-assembly-jigs-and-tools.html [Accessed December 13, 2011], 2010
38. Koelemeijer Chollet, S., Benmayor, L., Uehlinger, J.-M. and Jacot, J. "Cost effective micro-system assembly automation," In 7th International Conference on Emerging Technologies and Factory Automation, pp. 359-366, 1999
39. Koelemeijer Chollet, S., Bourgeois, F. and Jacot, J., "Economical justification of flexible microassembly cells," International Symposium on Assembly and Task Planning, 2003.
40. Koelemeijer Chollet, S., Bourgeois, F., Wulliens, C. and Jacot, J., "Cost modelling of microassembly," 2nd International Workshop on Microfactories, 6 p., 2003
41. Kawahara, N., Suto, T., Hirano, T., Ishikawa, Y., Kitahara, T., Ooyama, N., Ataka, T., "Microfactories; new applications of micromachine technology to the manufacture of small products," Microsystem Technologies, 3(2), pp.37-41, 1997
42. Heikkilä, R., Uusitalo, J., Heikkilä, R. and Tuokko, R., "A Microfactory Concept for Laser-Assisted Manufacturing of Personalized Implants," IWMF, pp. 77-80, 2008
43. Barkley, S., "Mobile parts hospitals resuscitate broken gear," Available at: http://www.army.mil/article/21502/mobile-parts-hospitals-resuscitate-broken-gear/ [Accessed July 22, 2011], 2009
44. King, B. and Jatoi, I., "The mobile Army surgical hospital (MASH): a military and surgical legacy," Journal of the National Medical Association, Vol. 97, No. 5, pp. 648-656, 2005
45. Eichhorn, V., Fatikow, S., Dahmen, C., Edeler, C., Stolle, C. and Jasper, D., 2008. "Automated Microfactory inside a Scanning Electron Microscope," IWMF, pp. 207-212, 2008
46. Rolanda DG Co., "iM-01 Brochure," Available at: http://www.rolanddg.com/PDF/im-01.pdf, 2011
47. Hirvonen, V., Interview at Master Automation Group, Vantaa, Finland, 26 August, 10:00-11:30, 2011
48. Härkönen, K., Interview at Biohit, Helsinki, Finland, 25 August, 13:00-14:30, 2011
49. Kobel, P., Interview at EPFL/LSRO, Lausanne, Switzerland, 21 September, 10:00-12:00, 2011
50. Heino, H., Interview at Bioretec, Tampere, Finland, 16 August, 09:00-10:15, 2011
51. Tirkkonen, P., Interview at Verkkokauppa.com, Helsinki, Finland, 6 September, 13:00-14:30, 2011
52. Womack, J.P., Jones, D.T. and Roos, D., "The Machine that Changed the World," Macmillan Publishing Company, 323 p., 1990
53. Liker, J.K., "The Toyota Way: 14 Management Principles from the World's Greatest Manufacturer," McGraw-Hill, 330 p., 2004
54. Hines, P., Holweg, M. and Rich, N., " Learning to evolve: A review of contemporary lean thinking," International Journal of Operations & Production Management, Vol. 24, No. 10, pp. 994-1011, 2004
55. Sipilä, M., "Visions for Visions for Production Automation," Presentation in Tampere Finland December 13, 18 p., 2011
56. Wegera, "Compact CNC module Variations: KOLIBRI CNC System basic data," Available at: http://www.wegera.com/images/kolibri_englanti.pdf, 2011
57. Kauppi, S., Interview at Wegera, Oulu, Finland, 19 August, 2011, 08:00-10:30, 2011
58. Pfriem, A., Schulz, S., Pylatiuk, C., Alshut, R. and Bretthauer, G., "Robotersysteme für Hochdurchsatzverfahren in der Bioanalysis," Automatisierungstechnik, Vol. 59, No. 2, pp.134-140, 2011
59. Endo, C., 2010. "Small Processing Machinery Effectiveness in Micropart Processing and Factory Construction with Desktop Production Equipment," IJAT, Vol. 4, No. 2, pp. 155-159, 2010

Development of micro transfer hand system for micro transfer press

Ichiro Ogura[1#], Kiwamu Ashida[1], and Tetsuo Koga[2]
1 Advanced Manufacturing Research Institute, National Institute of Advanced Industrial Science and Technology (AIST), Japan
2 Shotoku Zerotech co. ltd., Japan
Corresponding Author / E-mail: ogura.i@aist.go.jp, TEL: +81-29-861-7221, FAX: +81-29-861-7201

KEYWORDS : micro press, transfer press, handling, grasp sensor

AIST has developed the micro press system, which uses micro dies and strip materials, to produce small and complicated profiles. This type of micro press system can machine sub-millimeter order profiles in 60 spm using a series of in-line press machines. Although this system is one of the effective micro factories, there is a disadvantage from the point of view of saving material consumption. B ecause of the strip material feeding system, many materials become scraps to throw away after machining. To reduce the waste of materials, the technique of transfer press processing, which machines the pre-cut materials of product size and transfer them between press machines, is effective. The transfer press machining is already realized in large scales. But still there is no case of applying the transfer press to the micro press machining. Therefore in this study, we developed new micro transfer hand system for the micro transfer press. Two types of grasp sensors for the transfer hand were selected and we had a series of experiments to evaluate these sensors. The developed transfer system also has a function to transfer the material in reverse or half rotate for value added press machining. A test bench for transfer experiment was developed to check the micro transfer and reverse setting. The transfer experiments were performed and not less than 99% of micro transfer was achieved by this system without the mistake.

1. Introduction

About micro metal forming, the micro press or micro punching has outstanding advantages, which are simple process, high production rate and machining accuracy. Consequently, toward realizing advanced micro fabrication, this machining method is able to compete with other precise machining methods, such as laser forming, etching or micro-EDM.

AIST has developed the desktop size micro press system [1] for the desktop machining factory [2-3]. And there are many other studies about development for the micro press by universities, research institutes, and companies in the world. Many of them are stand-alone press systems for challenging the possibility of new micro forming [4-8], and the others are rather practical forming systems with micro progressive die [9] or micro transfer system [10].

Not only in [1], AIST also developed the micro press which uses micro progressive dies, to produce micro mechanical parts with millimeter size in 60 shots per minute [11]. In this system, four in-lined press machines press the material one after another, and the products are machined gradually.

This micro progressive press uses strip material-feeding system, which is thin rolled metal belt with sub-millimeter thickness. The circumference area of the product in strip material is used for positioning and sending for press machining. This area is finally removed and disposed as waste in the last press machine to get the product.

Because the strip or coil material-feeding system [12] is able to send materials stably and continuously, progressive press style is usually selected for multi-in-lined press machines. However, the strip material-feeding system has two disadvantages shown below.

(1) Disadvantage of yield rate: As mentioned, many part of strip materials are only used for positioning and sending for press machining and become waste. The ratio of waste to product becomes higher when the product is smaller. The cost of materials is important issue. Therefore, the efficient technique for material feeding is demanded.

(2) Disadvantage of difficulty for high value-added machining: During multi-in-lined press machining, the high value-added machining, such as changing the direction of work material between in-lined press machining, is sometimes

needed. Sending and turning upside down materials between two dies is one of the typical example. Directions of burs become reverse with press direction for material. Opposite direction bur may be suitable for smooth connecting when those parts are assembled by screw. And turning materials to lateral direction realizes a press machining for lateral side. Thus the application of press processing spreads further. The strip material feeding system cannot realize such sending and turning of materials.

To overcome these disadvantages, transfer press [13] technique is proposed. The transfer-press uses the transfer bars, which make reciprocating motion synchronizing with press motion. The transfer hands are attached to the transfer bar, and transfer the pre-cut materials between the adjacent dies. Since the materials are cut within almost same size of products, the yield rate becomes higher than the strip material-feeding system. Moreover, if the transfer hands turn over the materials during sending, the high value-added machining with different press directions is realized.

The transfer press machining has been used for automobile parts or electric motors shells with size of several ten to hundred millimeters. But there are no examples of micro transfer press system for minute parts with size of millimeters order. The micro transfer press has own problems on account of its small size, such as grasp error or setting space for transfer system.

Therefore, our final goal of this study is to establish the micro transfer press system, which includes multi-in-lined press machines and multi-transfer systems with synchronizing reciprocation to press motion. This paper reports about the basic study for the final goal of this study.

To realize the micro transfer press system, repeatable and fast workings of transfer machine are needed. The transfer workings should be, 1) approaching grasp finger to the material from stand-by position, 2) grasping the material, 3) picking-up the material from machining position to transfer position, 4) sending the material to the next press position with material turning, 5) putting-down the material to the next machining position, 6) releasing the material, 7) going back to the stand-by position.

For 1) 2) 6), we developed micro finger with grasp sensors for detecting hold position of materials to realize stable transfer. And for 3) 4) 5) and 7), we also developed a test bench, which is able to turn the materials by a few actuators for high value-added press machining.

2. Development of micro finger with grasp sensors

2.1 Overview of the micro finger

We selected a desired value for developing the transfer system as 60 rpm transfer working with more than 99% strike rate. A prototype of micro finger with grasp sensor was developed to accomplish the aim as shown in Fig. 1.

This system has tweezers type fingers to grasp plate materials. A liner actuator’s slider moves ball rollers and the rollers exchange the linear slider motion to open and close motion of the fingers. Sliding amount of the actuator changes

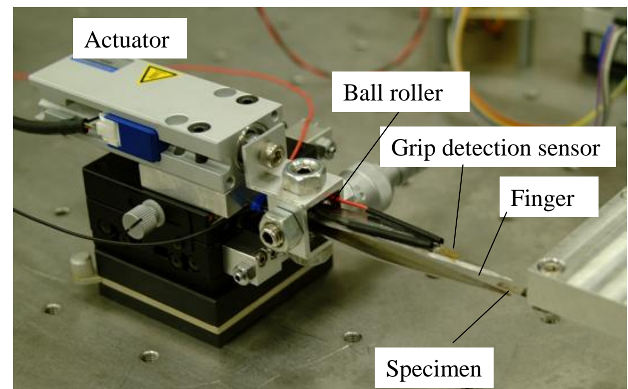

Fig. 1 Overview of a prototype micro finger

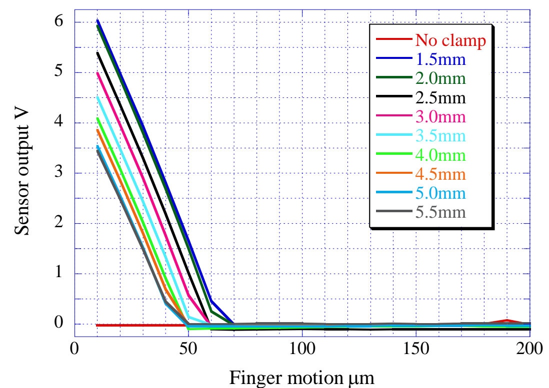

Fig. 2 Outputs of strain gauge type grasp sensor

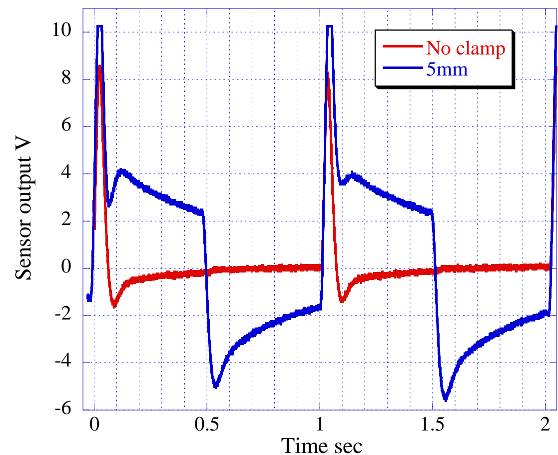

Fig. 3 Typical output of repeatable grasping and releasing

grasping force of the fingers. From actual measured value, the maximum grasping force of the fingers is approximately 2N. Since the weight of the materials to transfer is about 150mg, this finger system has enough force to grasp.

For the first-step to control a contact state of finger to materials, we developed two types of grasp sensors as follow sections.

2.2 Strain gauge type

The first type of grasp sensor uses a strain gauge sensor to detect flexure of the fingers when the fingers grasp the material to transfer. This method realizes grasp detection easily with simple principle and structures.

We tested relationship between positions of grasping points and outputs of strain gauge. The strain gauge was

attached at 25 mm position from the tip of the finger. Fig. 2 shows the results. In this experiment, the material was set to the each position, which are 1.5mm to 5.5mm from the chip of the finger. And the output voltage of the strain gauge was plotted respectively when a finger was closed gradually. No clamping result is also shown in this figure. From these results, we can see that the output of sensor is stable when fingers do not grasp the material, and the outputs vary with the setting positions at same finger closing position when fingers grasp the material. From 2.0mm to 5.0mm positions, this sensor is able to detect the setting positions at least 0.5mm resolution.

Repeatable grasping and releasing tests for material by the finger system in Fig. 1 was conducted, and Fig. 3 shows the typical results. This figure shows the no clamping case and clamping case at 5mm from the chip of the finger. The speed of grasping motion was set to 60rmp to satisfy the transfer working speed.

From this result, the differences of outputs are easily confirmed between no-clamping and clamping. Consequently, even in repeatable motion, we can detect the error of grasp by this sensor type.

2.3 Electric contact detection type

Although the strain gauge can detect grasp position of the materials well, there is some problem about stability of output. Gradual change of sensor output with progress of time, what is called drift, occurs and to confirm a stable detection, we need frequent zero-adjustment of sensor.

The second sensor, the electric contact detection type was developed to overcome this problem.

Fig. 4 shows the principle model of the sensor and the actual model for attaching to the finger. This type of sensor has a series of electrodes, and detects conductivity of the electrodes and material to pick-up when the finger closes.

The output of this sensor is shown in Fig. 5. In this experiment, we set an electrode for applying voltage to upper finger, and set a series of electrode patterns for detecting conductivity to lower finger. Fig. 5 (a) shows no-clamping state and (b) shows full-clamping state that means a tip of picked material was set at 9mm position from the tip of the sensor. In (a), the conductivities of electrodes are not detected at 0 micron position, which is a standard close position of finger. And at –400 microns position, the conductivities of all electrodes are detected because upper finger contacts to lower finger. On the other hand, in (b), conductivities of all electrodes are confirmed at the standard close position. Both (a) and (b), unevenness between conductivities detecting position is observed. The reason is that there is some variation in height of electrodes. When we distinguish the grasping at 200 microns position for example, even in (b), some grasping error should be detected. Therefore, we decided to distinguish the grasping at 0 micron position as a standard close position of finger.

This electric contact detection type does not need zero-adjustment of sensors and have an advantage of stability of output compare with the strain gauge type. But there is some disadvantage in possibility of miss detection caused by the variety in height of electrode. Moreover, contamination by oil of press machine may bring a miss-conductivity and make a detection error. Consequently, to select which sensor should be selected, it is necessary to observe actual finger style and the hardware requirement.

3. Test bench for micro transfer system

3.1 Overview of the test bench and development of the finger and arm system

To develop a transfer press machining system, a series of repeatable transfer motions as sown in section 1 should be required. For the high value-added machining, a procedure of changing the direction of work material is applied to sending motion.

In this study, we developed a finger and arm system for test bench of the micro-transfer system to realize repeatable motions between two places. We selected distance of two places as 100mm, which is approximately same as our developed in-lined press machines. This test bench has a transfer arm with finger to change the direction of work material while arm moves. If we use five actuators -- 1) approaching 2) grasping 3) picking up or putting down 4)

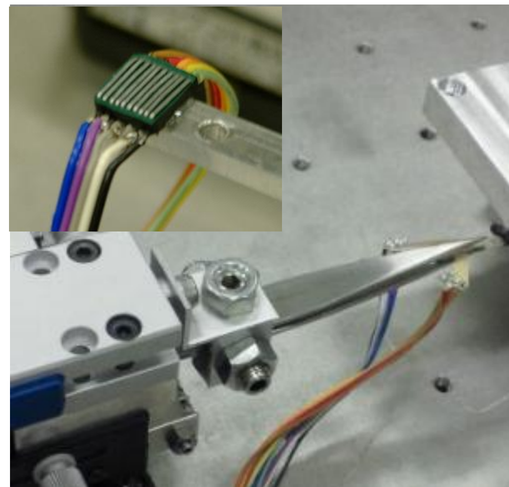

Fig. 4 Principle and actual model of electric contact detection sensor

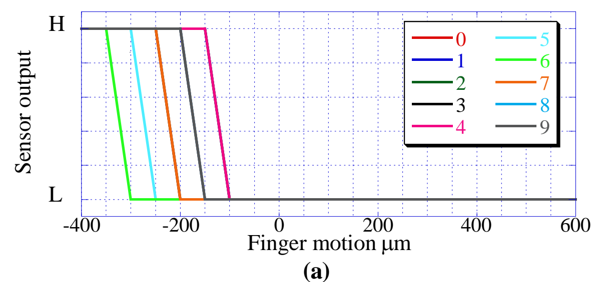

(a)

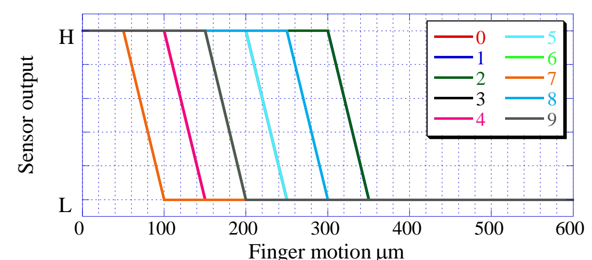

(b)

Fig. 5 Output of contact detection sensor

transfer 5) rotate, this system can be realized. But when the multi transfer systems for multiple press system are built, we need many actuators. It causes complication of transfer system and rising of price for the system.

Therefore, we applied a kind of link system for picking and rotating material to reduce actuators.

Fig. 6 shows a schematic diagram of the test bench. A linear actuator set behind the finger pushes and pulls the finger, and a link system for finger exchanges the linear motion to finger closing and opening motion. The finger closes after approaching to the material by this link system. Fig. 7 shows the actual motion photographed by high-speed camera which the finger grasps material. The material to grasp is set on a pseudo-die and a plunger is holding the material. This plunger rolls a pushpin of real press machine. In the upper figure, the finger is in stand-by position. The finger approaches to the material in the middle figure. And in the bottom figure, the finger grasps the material. After these sequences, the plunger moves to upper direction to release, and the finger picks up and moves the material.

A pinion in Fig. 6 meshes with a rack by the picking up actuator and rotates the finger with the motion of transfer actuator. There is a slip clutch between the finger and pinion as shown in Fig. 8. The finger stops to rotate when a latch hits to a stopper and a holding system of the stopper holds the latch. Then after the latch hitting, although the pinion continues to rotate, finger keeps same direction of rotation while transfer actuator is moving. In going back motion after the finger puts the material, the pinion meshes with the rack again and finger rotates opposite direction until the latch hit to the stopper in another side. If the position of stoppers is changed, the angle of finger rotation changes optionally. When we set the stoppers to 90 degree, the finger can put the material in lateral direction, that realize lateral press machining of material.

Fig. 9 shows the actual rotating motion of the finger while the arm is moving. In this figure, the acceleration of the actuator for transfer was 1G and the maximum stage speed was set as 500 mm/s. Selected rotation angle of finger was 180 degrees that means the turn over putting of material. We took these photographs at middle point of the transfer distance. In the upper figure, the material is already rotated in 90 degrees and in the middle figure, the finger finished to turn over the materials. Since the slip clutch keeps the direction of the finger, the material is moved in turned position as shown in the

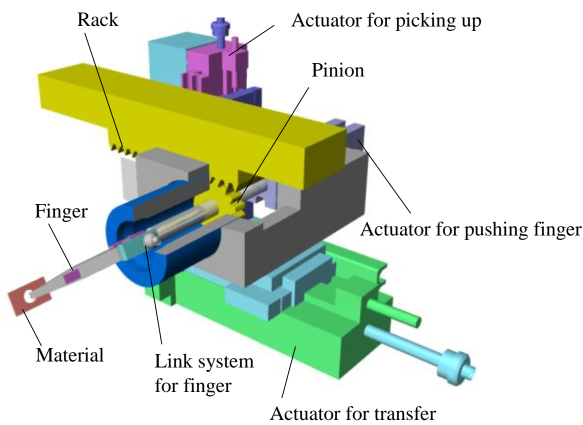

Fig. 6 Schematic diagram of the test bench

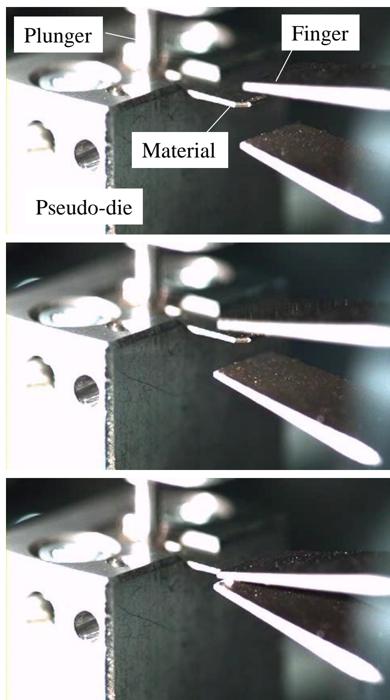

Fig. 7 Photograph of the finger grasping material

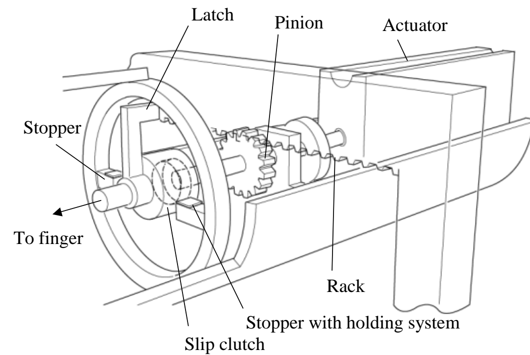

Fig. 8 Slip clutch and stopper of the system

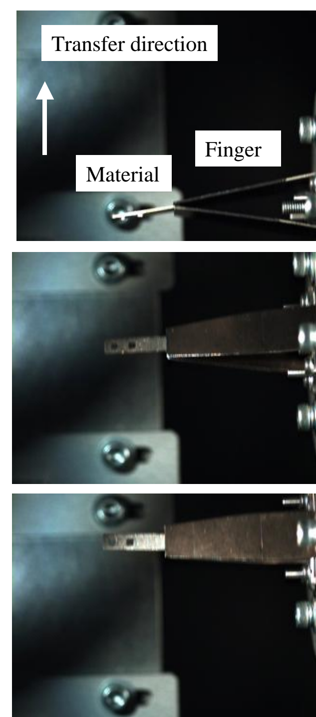

Fig. 9 Photograph of the finger rotating material

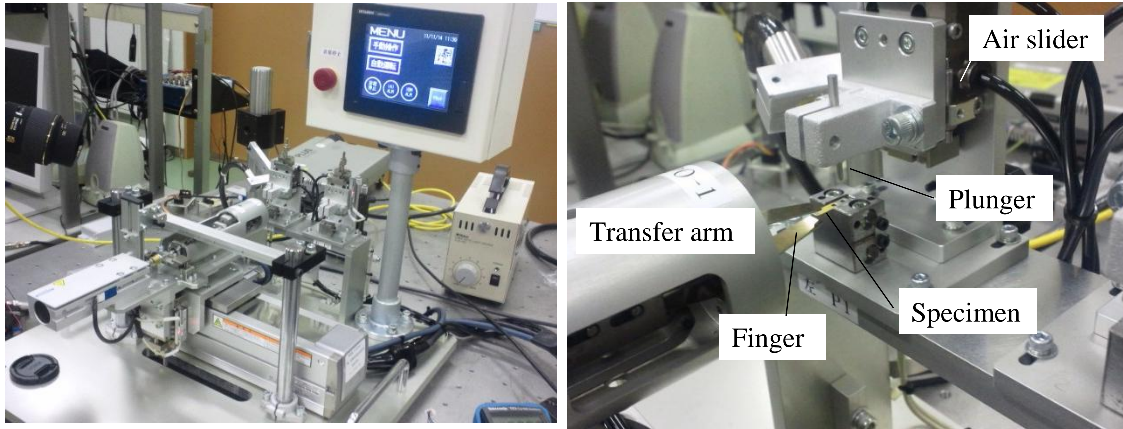

Fig. 10 Set-up of developed test bench

bottom figure.

3.2 Repeatable transfer experiment by the test bench

We integrated the arm and finger system to develop the test bench shown in Fig. 10. This is an actual set-up of Fig. 6. There are two points to picking up and putting down the materials, and the transfer arm moves between these two points repeatedly. Two air sliders in each point move each plunger as shown in Fig. 7.

A sequencer controls the finger, arm and assisting systems as procedure. In this system, we did not prepare a parts feeding system for repeated transfer motions. Then only one time material transfer can be realized after the material is set on the first point.

The system has an emergency stop circuit which acts when the external personal computer sends TTL signal. If we attach the grasp sensor mentioned in section 2 to the finger, and detect the grasp miss by the personal computer, this test bench is able to stop to avoid the transfer miss when the grasp miss of the finger occurs.

We had a transfer experiment by using this test bench. The timings of the stage, liner actuator, and air slider are adjusted to realize 60 transfer numbers for one minute. A series of photographs when the hand is putting material on the die continuously are shown in Fig. 11. In this figure, we can see the sequence as follows: the finger is approaching to the die, positioning to putting point, putting the material, the plunger is holding the material, the finger is releasing, and leaving from the die. 100 times repeatable transfer experiment was performed. In this experiment, there was no case, which failed in transfer the material. From this result, we can say that not less than 99% of micro transfer was achieved by this system without the mistake.

4. Future works

To realize the practical system set-up of transfer hand for in-lined press machine, we have a plan for the system as shown in Fig. 12. This figure stands for the four in-lined transfer system. There are four transfer fingers to move the materials between adjacent dies. Because of the mechanical system for grasping and rotating materials as mentioned in 3.1, basically, we need only three actuators to realize this system. Ordinal material to cut is a kind of strip material, and the 1st die cuts the material to the same size of the final products. 2nd die makes bending machining, 3rd die makes hole to the material, and 4th die also makes bending machining to a part of material. In this example, we need 180 degrees rotation between 2nd and 3rd dies, and 90 degrees rotation between

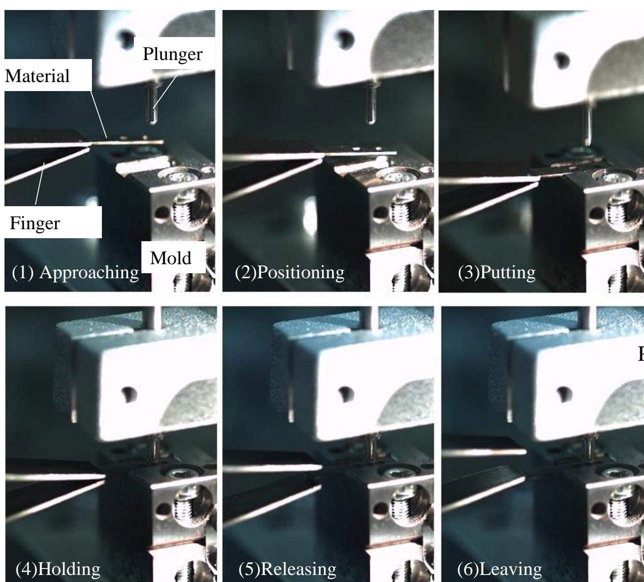

Fig. 11 Sequence of putting material on the die

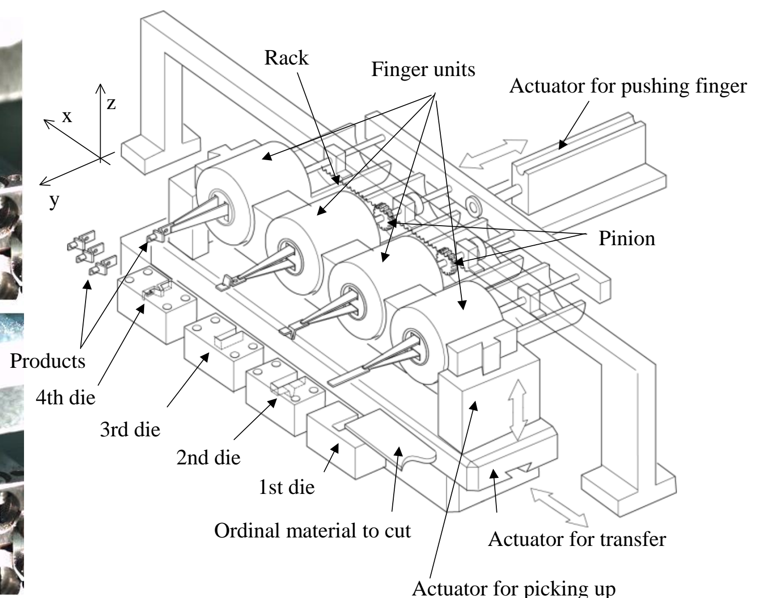

Fig. 12 Practical system set-up of transfer hand for in-lined press

3rd and 4th dies. Then two of the fingers have pinions behind each finger to rotate the materials. If we can set each position of the stopper as shown in Fig. 8, the finger is also selected as no rotating motion when the stopper is set on 0 degree position. Therefore, we can use same system for four fingers and it brings extensibility and flexibility to the transfer hand system such as installing more press machines or changing the dies and products for micro press.

5. Summary

In this study, we had the basic study for establishing the micro transfer press system. This system includes multi-in-lined press machines and multi-transfer systems with synchronizing reciprocation to press motion.

This study is summarized as follows:

1) A sensor system for transfer hand to detect the state of the grasped small materials is proposed. Strain gauge type and electric conductivity type were selected as the sensor and we had a series of experiments to evaluate these sensors. Strain gauge type sensors can detect the grasping position within 0.5mm. Electric contact detection type has an advantage in stability.

2) A test bench to move the material in reverse or half rotate for value added press machining is developed. Rack-pinion, slip clutch and rotation stopper mechanism realized this motion. The transfer experiments were performed to evaluate micro transfer system. Not less than 99% of micro transfer was achieved by this system without the mistake.

ACKNOWLEDGEMENT

This study was supported by A-STEP (Adaptable and Seamless Technology transfer Program through target-drive R&D) of Japan Science and Technology Agency, AS2211699B.

REFERENCES

1. M. Tanaka: "Development of desktop machining micro factory", RIKEN Review, No. 34, April, (2001), pp.46 -49.
2. N. Kawahara, T. Suto, et al.: "Microfactories", Micros ystem Technologies, Vol. 3, 2, (1997), pp.37-41.
3. Y. Okazaki, N. Mishima, and K. Ashida: "Microfactory-Concept, History, and Developments", J. Manufacturing Science and Engineering, Vol. 126, 11, (2004), pp.837-844.
4. Sol-Kil Oh, Hye-Jin Lee, et al.: "Reserch on the Micro Pattern forming of Spiral Grooves in a Dynamic Thrust Bearing", World Academy of Science, Engineering and Technology, Vol. 56, (2009), pp.622-625.
5. Hye-Jin Lee, Jung-Han Song, et al.: "Desktop Micro Forming System for Micro Pattern on the Metal Substrate", International Federation for Information Processing 2010, pp.301-308.
6. W. Presz, B. Andersen, and T. Wanheim, "Piezoelectri c Driven Micro-press for Microforming", Journal of A chievements in Materials and Manufacturing Engineeri ng, Vol. 18, 1-2, (2006), pp.411-414.
7. M. Broomfield, T. Mori, et al.: "Micro-Hole Multi-Poi nt Punching System Using Punch and Die Made by E DM", Journal of Solid Mechanics and Materials Engin eering, Vol. 3, 4, (2009), pp.710-720.
8. N.A. Palam, M. Arentoft, and R.S. Eriksen, "Productio n Equipment and Processes for Bulk Formed Micro C omponents", American Institute of Physics Conference Proceedings, Vol. 907, (2007), pp. 463-468.
9. M. Yang, K. Manabe, and K. Ito, "Micro Press Formi ng and Assembling of Micro Parts in a Progressive D ie", Journal of Mechanical Science and Technology, V ol. 21, (2007), 1452-1455.
10. M. Arentoft, R.S. Eriksen, et al.: "Towards the First Generation Micro Bulk Forming System", CIRP Annal s – Manufacturing Technology, Vol. 60, (2011), 335-3 38.
11. S. Nakano, K. Ashida, et al.: "On-demand MEMS factory system consists of metal forming and aerosol deposition", Proc. of the 24th International Japan-Korea Seminar on Ceramics, pp.735-738.
12. A. Razali, Y. Qin, et al.: "Investigation of Feeding De vices and Development of Design Considerations for a New Feeding for Micro-Sheet-Forming", The 6th Intern ational Conference on Manufacturing Research, 9, (20 08).
13. J. Jionghua, S. Jianjun: "Press Tonnage Signal Decomposition and Validation Analysis for Transfer or Progressive Die Processes", J. Manufacturing Science and Engneering, Vol. 127, 2, (2005), pp.231-235.

Micro-milling with Active Piezoelectric Stage Error Compensator

Hendra Prima Syahputra[1], Hyeon Mo Yang[1], Byeong Mook Chung[1], Tae Jo Ko[1,#], and Jong Kweon Park[2]

1 School of Mechanical Engineering, Yeungnam University, 214-1, Dae-dong, Gyeongsan-si, Gyeongsangbuk-do, South Korea, 712-749
2 Division of Nano-Mechanical Systems, Korea Institute of Machinery and Materials, Daejon, South Korea, 305-343
Corresponding Author / E-mail: tjko@yu.ac,kr, TEL: +82-53-810-3836, FAX: +82-53-810-4627

KEYWORDS : Micro-milling, Error compensation, Positioning performance, Linear stage, Piezoelectric actuators.

An active error compensation for positioning system in micro-milling application was designed. The focus was on improving the positioning performance of micro-milling machine. A high-precision piezoelectric stage was added to standard micro-milling machine which perform as error compensator. The control method used in the system was active error compensation type, where the error from linear stage cancelled by piezoelectric stage motion. Positioning experiments showed an improvement of machine accuracy and ensured by machining results. Therefore, this technique can be implemented for high-precision positioning in manufacturing and machining systems.

1. Introduction

The need for high-precision parts has recently become an important concern in the manufacturing industry. Such a machine is required to provide versatility, speed and workspace as well as high precision positioning [1]. This requirement impacts on machine tool design by improving machining performance, especially in terms of accuracy and precision. For such high-precision machines, drive systems with sub-micrometer accuracy over a travel range of several hundred millimeters are necessary [2].

The ball-screw is currently the most frequently used in feed drives of the machine tools [3]. Together with rotary motors it forms a linear stage system which has high load capacity and simple configuration for long stroke application. Linear stages positioning accuracy depends on a number of factors, for instance their control electronics, motors, mechanical parts, and transmission configuration. For these reason, linear stages have several limitations such as: transmission errors, dead zone, backlash, elasticity, large inertia and wear [4]. This deficiency will greatly impact the on micro-milling machining results.

Positioning systems based on piezoelectric materials have received increased attention recently in many high-precision applications [1]. They have advantages that include: unlimited resolution, large force, fast expansion and no magnetic effects [5]. These characteristics make piezoelectric actuators a good choice for precision actuator. The disadvantages of piezoelectric actuators are their short travel range, hysteresis and creep. Hysteresis and creep are undesirable characteristics which lead to large errors when a piezoelectric actuator is used in positioning application [6].

The main goal of micro-milling with active piezoelectric stage error compensator in this work was to obtain overall system that has the travel range of linear stage and the accuracy of piezoelectric actuators which leads to improvements in machining results. The control method proposed in this paper applies the concept of active error compensator, where the error from linear stage cancelled by piezoelectric actuators stage in synchronous motion. To analyze the positioning performance, experiments were carried out for linear motion, circular motion, and micro-machining to map the overall performance of the system.

2. The Experimental Setup

2.1 Design of Piezoelectric Stage for Error Compensation

Although piezoelectric devices can provide large output forces, the typical 15 μm displacement of stack-type actuator is not sufficient for most general engineering applications, for which much larger movement ranges (0.05-0.5 mm or more) are typically required. In most cases, therefore, the use of a flexure-hinge mechanical displacement amplifier is the most

appropriate approach to magnifying the output displacement of the piezoelectric actuators [7]. A piezoelectric stage with flexure-hinge-type lever mechanisms was designed to increase the error compensation range. Simulation results for the piezoelectric stage deformation are shown in Fig. 1 and Fig. 2.

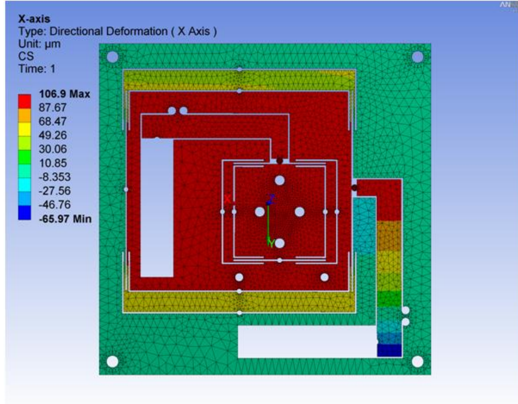

Fig. 1 Piezoelectric stage simulation for *x*-axis deformation

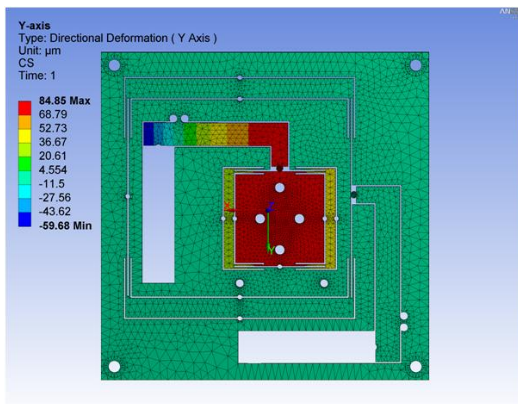

Fig. 2 Piezoelectric stage simulation for *y*-axis deformation

Piezoelectric actuators used in the stage were PI-830.20 made by Physik Instrumente. They had a travel range of 30 µm and a 1000 N pushing force with a voltage range of 0 to 100 V. With the help of the lever mechanism, simulation shows the maximum travel ranges of the piezoelectric stage become 106.90 µm and 84.85 µm for the *x*- and *y*- axes, respectively.

The open-loop relation between given voltage and displacement was tested by measuring the piezoelectric stage displacement using capacitive displacement sensor. The results are shown in Fig. 3.

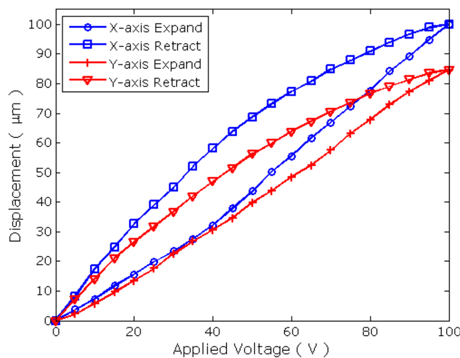

Fig. 3 Measured result of relation between applied voltage and piezoelectric stage displacement

The measurement shows that hysteresis phenomena occur in both of piezoelectric actuator. The overall displacement also lower compared to simulation results because of the preload force added to the piezoelectric actuators. The frequency response was performed to analyze the piezoelectric stage respond at various frequencies. The test was done by using dynamic signal analyzer with amplitude 0 to 85 Volt started from 0 to 3000 Hz. The results are shown on Fig. 4.

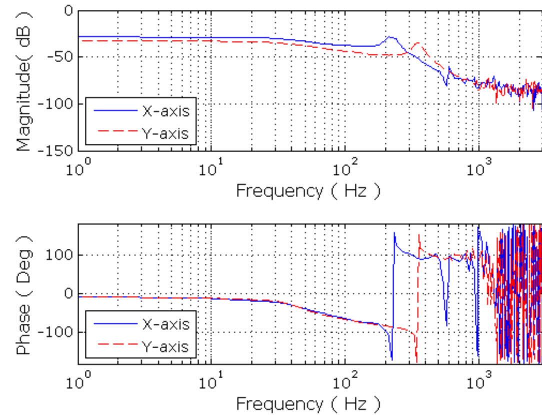

Fig. 4 Piezoelectric stage frequency response

2.2 The Developed System

A standard 3-axis milling machine was modified by stacking the piezoelectric stage on top of the *x*-*y* (horizontal) working table. The linear stages used 50000 pulse/rev step motor, 8 mm ball screw lead and 0.1 µm linear encoder feedbacks. The piezoelectric stage used 0.05 µm resolution linear encoders as a feedback for each *x*- and *y*-axis. A 2-D grid encoder with 0.1 µm resolution monitored the positioning error of the overall system. The sensor arrangements are shown in Fig. 5.

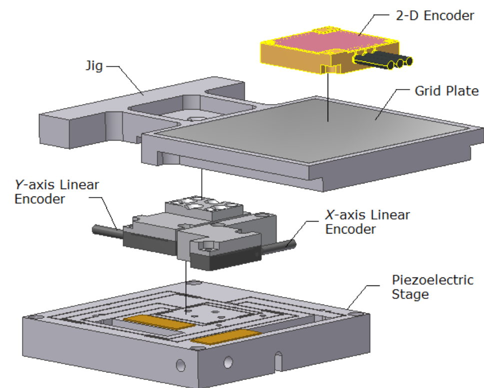

Fig. 5 Sensor arrangements

The controller used for the system was DeltaTau UMAC DSP. The active error compensation algorithm was downloaded to the controller. Position commands were generated on the controller with program code and sent to the actuators. All the actuators were tuned by integrated tuning software from the controller. The piezoelectric amplifier magnified command voltage by 10 times before passing it to

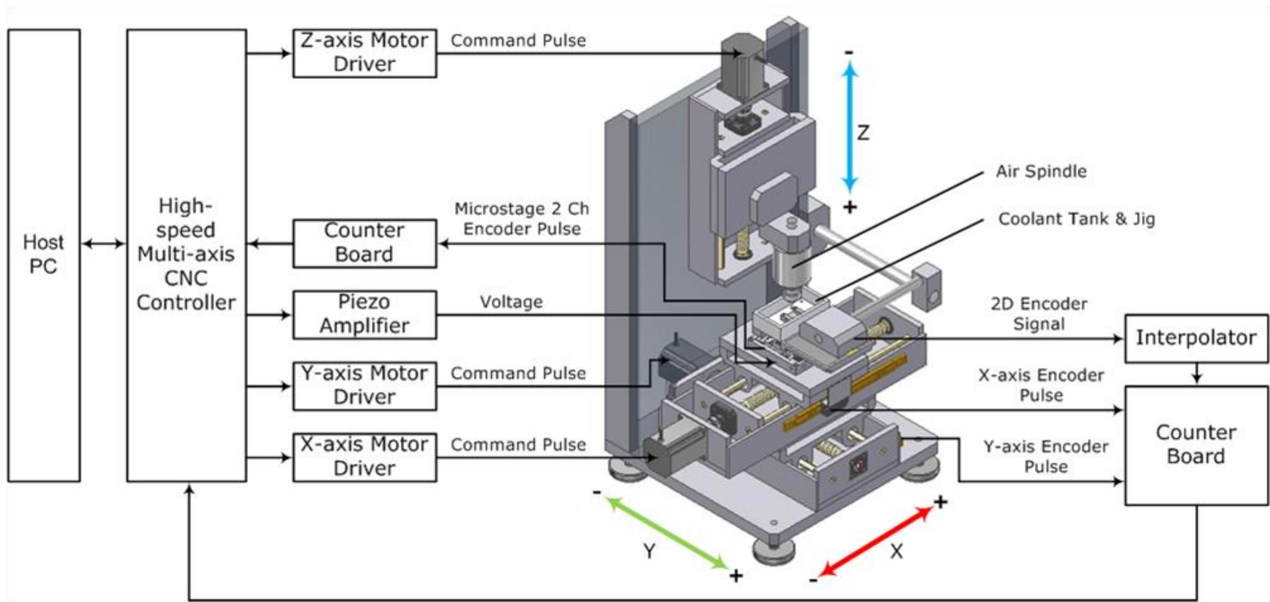

Fig. 6 Complete experimental setup

the piezoelectric actuator. The spindle used for the micro-milling was NSK Nakanishi air spindle attached to the *z*-axis (vertical). Complete experimental setup is shown in Fig. 6.

3. Control Strategy

The control strategy used in the system was active error compensation type, where an error from linear stage cancelled by the piezoelectric stage motion. The concept is to have compensation action by the piezoelectric stage simultaneously with the movement of linear stage.

For the control law in the piezoelectric stage, a PI (proportional-integral) controller was applied (Fig. 7.). The parameter used in the controller was obtained by experiment and was tuned to compensate the nonlinearities characteristics of piezoelectric actuators. The performance was tested by step response analysis detected by linear encoders (Fig. 8.). The initial position of *x*- and *y*-axis in the piezoelectric stage should be shifted approximately 50 µm from the resting position in order to have compensation capability in both forward and backward direction.

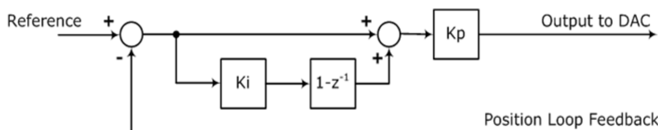

Fig. 7 Piezoelectric stage control block diagram

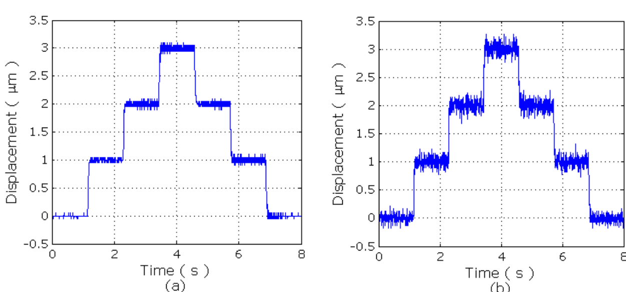

Fig. 8 Piezoelectric actuator step response; a) *x*-axis direction; b) *y*-axis direction

The piezoelectric stage works as an error compensator for the linear stage which made the command for the piezoelectric stage is a deviation from commanded position and actual position of linear stage. The linear stage was controlled by PID (proportional-integral-derivative) controller, and the resulting control block diagram for the overall system is shown in Fig. 9.

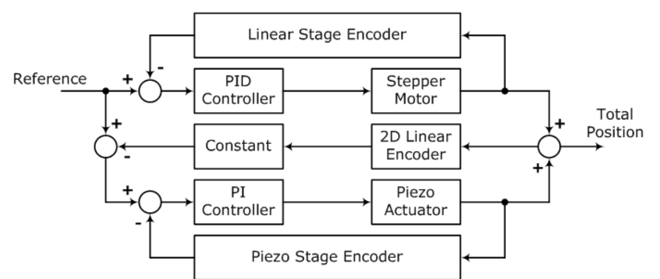

Fig. 9 Overall system control block diagram

4. Experiments on the Milling Machine

4.1 Linear Trajectory Motion Test

To perform the positioning experiment for linear trajectory, commanded trajectory for 1 mm back-and-forth was sent to linear stage with 500 µm/s constant speed and 1 s delay before reversing direction. The linear trajectory motion experiment for *x*- and *y*-axis was performed separately. For each *x*- and *y*-axis, we compared the results of motion positioning error with

and without error compensation. The results for linear stage motion without error compensation are shown in Fig. 10, Fig. 11, Fig. 12, and Fig. 13.

The graph shows us the magnitude of error along the *y*-axis was greater than along *x*-axis because in the milling machine the *x*-axis was stacked on top of the *y*-axis, which meant the *y*-axis experienced a larger load than the *x*-axis. The maximum positioning error in the *x*-axis was 25.56 µm, with 11.92 µm error average. For the *y*-axis the maximum positioning error was 30.06 µm, with 13.92 µm error average. However, these errors were still within the compensation range of the piezoelectric stage. The positive and negative signs of the error magnitude indicate the error direction. The most important concept is that the magnitude of error at any given time will affect the accuracy of a target point that needs to be achieved.

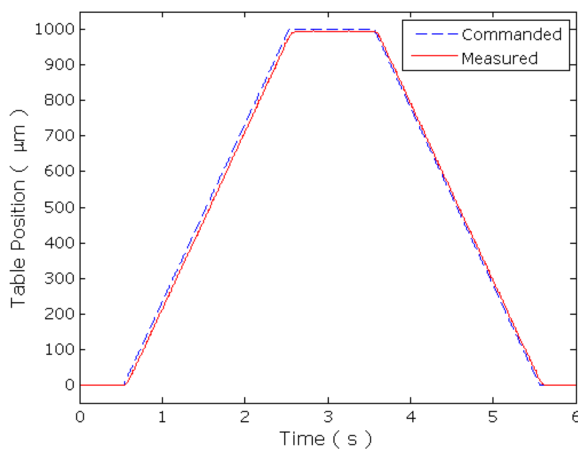

Fig. 10 *X*-axis linear trajectory motion commanded and measured position without error compensation

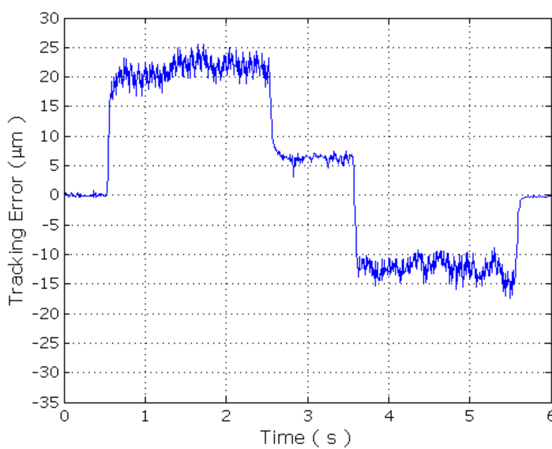

Fig. 11 *X*-axis linear trajectory motion error map without error compensation

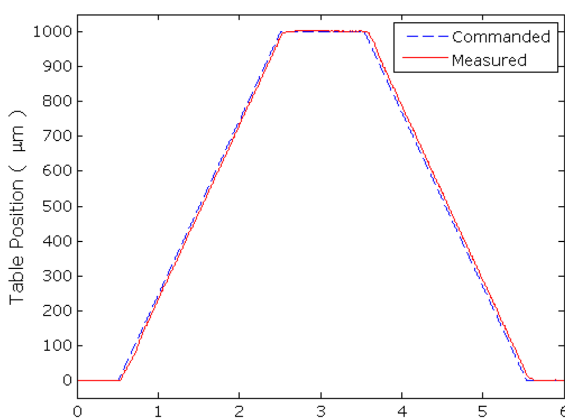

Fig. 12 *Y*-axis linear trajectory motion commanded and measured position without error compensation

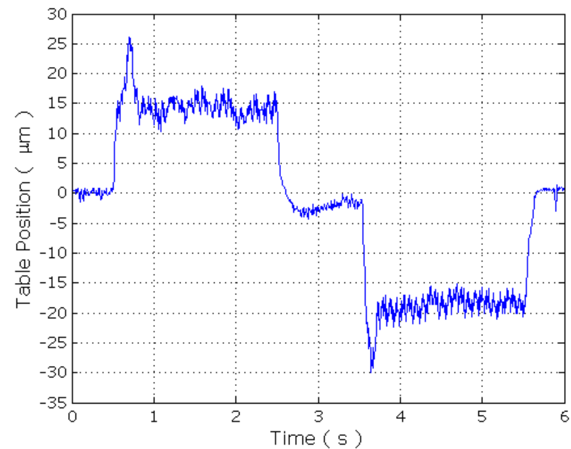

Fig. 13 *Y*-axis linear trajectory motion error map without error compensation

The analysis of linear trajectory motion without error compensation confirmed that the errors generated from the linear stages were still in the compensation range of the piezoelectric stage. For this reason we performed a linear trajectory motion experiment with error compensation. The results are shown in Fig. 14, Fig. 15, Fig. 16 and Fig. 17.

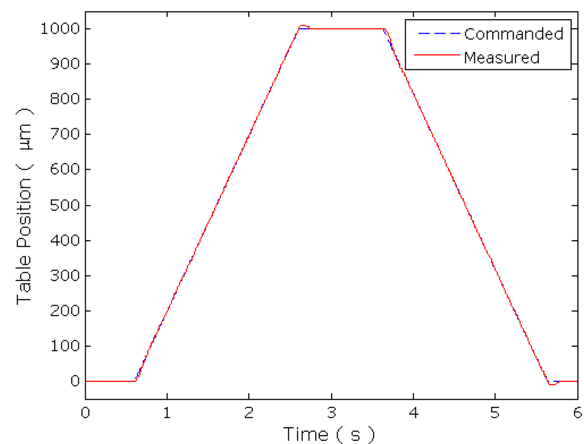

Fig. 14 *X*-axis linear trajectory motion commanded and measured position with error compensation

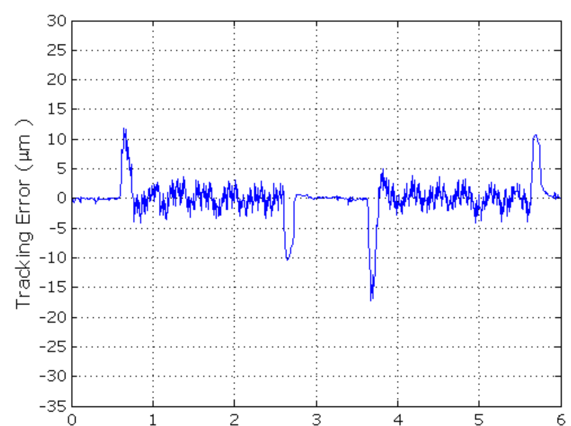

2

Fig. 15 *X*-axis linear trajectory motion error map with error compensation

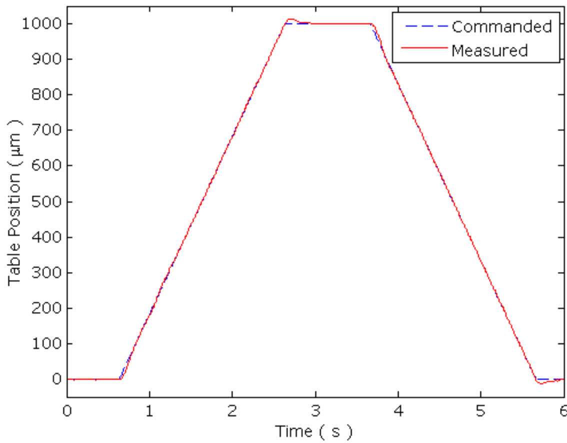

Fig. 16 *Y*-axis linear trajectory motion commanded and measured position with error compensation

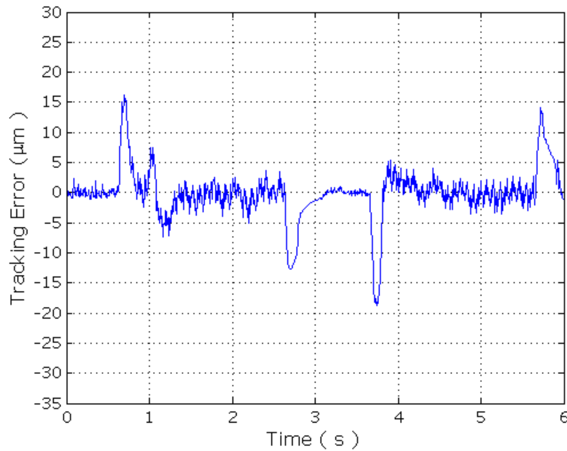

Fig. 17 *Y*-axis linear trajectory error map with error compensation

The graphs show error reduction in the *x*- and *y*-axis for linear trajectory motion, although there were still some error peaks, in particular at the beginning of motion and when the motor reversed direction. Both conditions are times when the linear stage brings out the largest error because of the inertia of the system. The *x*-axis maximum positioning error with error compensation was 17.11 μm, with 1.61 μm error average. For the *y*-axis the maximum positioning error was 18.79 μm, with 2.26 μm error average. This result indicated accuracy improvement by using piezoelectric stage as error compensator.

The performance of the error compensation system was defined largely by the relationship between the linear stage and the piezoelectric stage. Piezoelectric stage responses also affect the overall performance of the system. The ability of the piezoelectric stage to respond error generation in the linear stage will determine the performance of the system.

4.2 Circular Motion Test

During milling processes, circular motion also plays an important rule. Circular motion requires collaboration between two or even more axis. In our system we used *x*- and *y*-axes to generate circular motion in *x*-*y* plane. The interpolation command generated in the controller was to generate a circular motion with radius 1 mm at 500 μm/s constant speed. Experimental results for circular motion with and without error compensation are shown on the next figures:

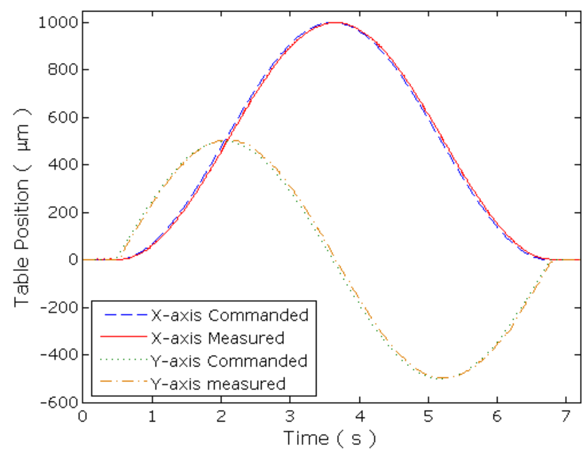

Fig. 18 *X*- and *y*-axes circular motion commanded and measured position without error compensation

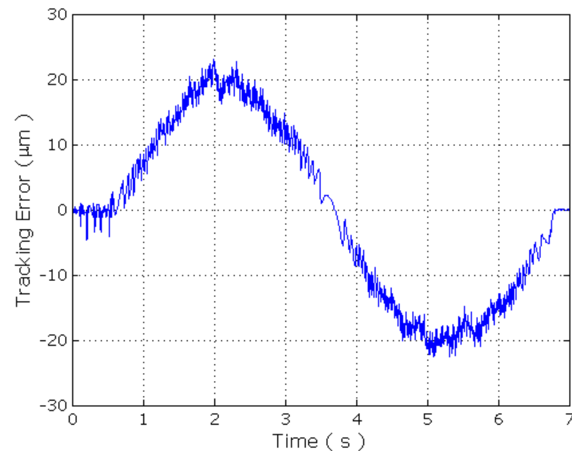

Fig. 19 *X*-axis circular motion error map without error compensation

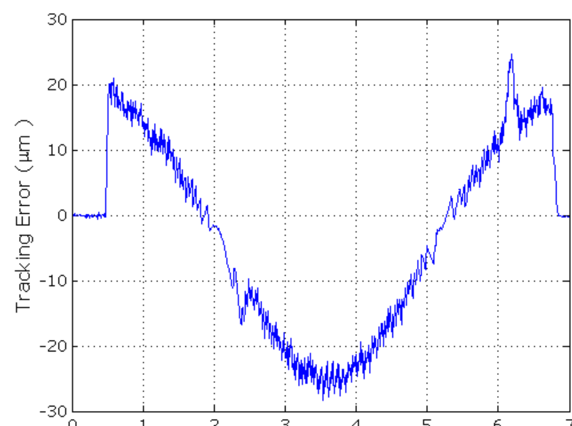

Fig. 20 *Y*-axis circular motion error map without error compensation

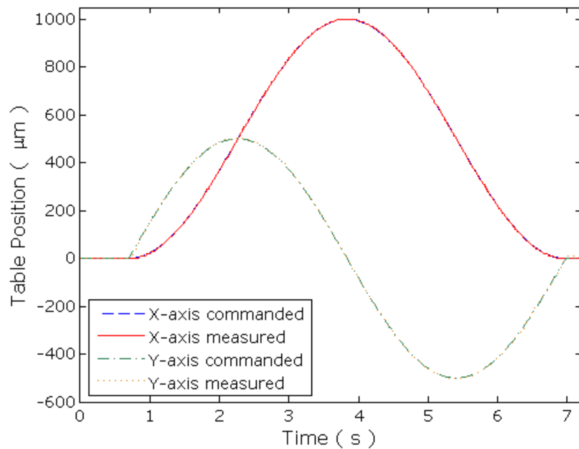

Fig. 21 *X*- and *y*-axes circular motion commanded and measured position with error compensation

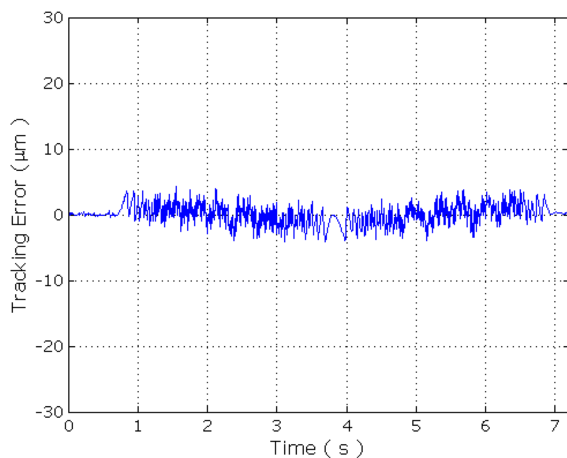

Fig. 22 *X*-axis circular motion error map with error compensation

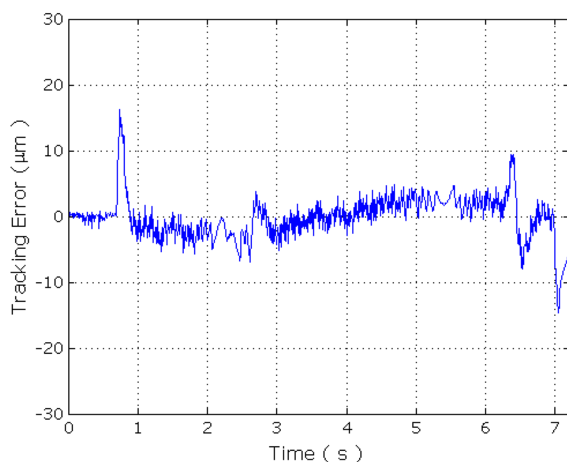

Fig. 23 *Y*-axis circular motion error map with error compensation

The maximum error on circular motion without error compensation for *x*-axis was 23.10 µm with 10.92 µm error average. For the *y*-axis the maximum error was 28.26 with 11.73 error average. By using active error compensation this error could be reduced with the maximum error in *x*-axis becoming 4.29 µm with 1.14 µm error average. For the *y*-axis the maximum error was reduced to 16.15 µm with 2.20 µm error average.

4.3 Machining Test

Amongst several mechanical-machining processes, micro-milling is the most flexible process and thus is able to generate a wide variety of complex micro-components and microstructures [8]. Experiment under real metal cutting was performed to evaluate the performance of the system. Method used on the experiment was to try the micro-milling machine ability to mill micro-pole structure. Micro-pole structures, such as column, rectangular pole and gear shaft, made by the micro-endmilling process, can be utilized in industry. Examples include electrode for electrical discharge machining and micro-mold for injection molding [9]. The objective was to fabricate 3 pieces of 5 µm height aluminium micro-poles with 100 µm, 50 µm and 25 µm diameters. The tool used in micro-milling process was 0.1 mm diameter micro-endmill rotated with 80000 RPM spindle speed. The neatness of the micro-poles indicates the accuracy of the micro-milling process. The results are shown in the following figures:

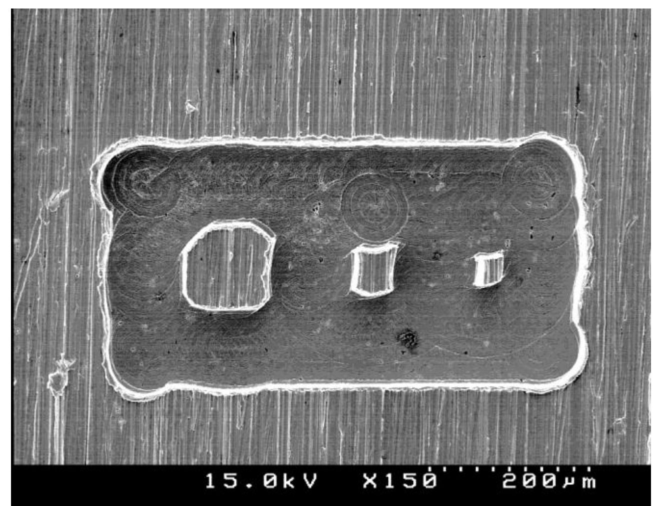

Fig. 24 Machining result without error compensation

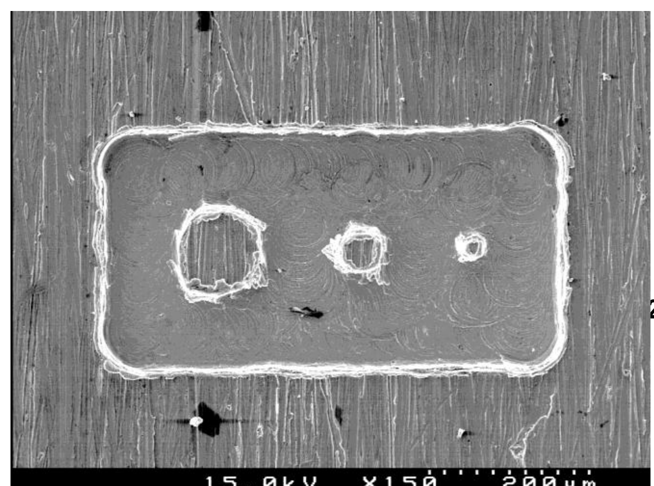

Fig. 25 Machining result with error compensation

As shown on the figures, the machining result with error compensation shows a better micro-poles structure. The sections of the micro-poles were more rounded by using active piezoelectric compensator. This result indicates the improvement of the micro-milling machine positioning ability by implementing active error compensation with piezoelectric stage.

5. Conclusions

In this study, an active piezoelectric stage error compensator mechanism for micro-milling application was designed and developed. The purpose was to improve the positioning performance of micro-milling machine. The control strategy used on the system was active error compensator type where errors from linear stage cancelled by piezoelectric stage motion.

Experiments for linear and circular motion were carried out. We evaluated the positioning performance by comparing the performance of linear stage motion without error compensation and the one with error compensation. In both cases there were significant improvements in machine accuracy by implementing active error compensation. The results were ensured by performing micro-milling on real metal cutting. Therefore, this technique can be applied to develop high-precision positioning in the manufacturing and machining systems.

ACKNOWLEDGEMENT

This work has been supported by Basic Science Research Program through the National Research Foundation of Korea (NRF) funded by the Ministry of Education, Science and Technology (MEST) (grant No. 2011-0013496).

REFERENCES

1. Elfizy, A.T., Bone, G.M., and Elbestawi, M.A., “Design and Control of a Dual-stage Feed Drive,” International Journal of Machine Tools & Manufacture,” Vol. 45, pp. 153-156, 2005.
2. Fujita, T., Matsubara, A., Kono, D., and Yamaji, I., “Dynamic Characteristics and Dual Control of a Ball Screw Drive with Integrated Piezoelectric Actuator,” Precision Engineering, Vol. 34, pp.34-42, 2010.
3. Altintas, Y., Verl, A., Brecher, C., Uriarte, L., and Pritschow, G., “Machine Tool Feed Drives,” Annals of the CIRP, Vol. 60, pp.779-796, 2011.
4. Pritschow, G., “A Comparison of Linear and Conventional Electromechanical Drives,” Annals of the CIRP, Vol. 47(2), pp.541-548, 1998.
5. Ni, J., Zhu, Z., “Design of Linear Piezomotor with Ultra-high Stiffness and Nanoprecision,” IEEE/ASME Transactions on Mechatronics, Vol. 5(4), pp.441-443, 2000.
6. Minase, J., Lu, T.-F, Cazzolato, B., and Grainger, S., “A review, Supported by Experimental Results, of Voltage, Charge and Capacitor Insertion Method for Driving Piezoelectric Actuators,” Precision Engineering, Vol.34, pp.672-700, 2010.
7. Xu, W., King, T., “Flexure Hinges for Piezoactuator Displacement Amplifiers: Flexibility, Accuracy and Stress Considerations,” Precision Engineering, Vol. 19, pp.4-10, 1996.
8. Huo, D., Cheng, K., and Wardle, F., “Design of a Five-axis Ultra-precision Micro-milling Machine-Ultramill. Part 1: Holistic Design Approach, Design Considerations and Specifications,” International Journal of Advanced Manufacturing Technology, Vol. 47, pp.867-877, 2010.
9. Je, T., Lee, J., Choi, D., Lee, E., Shin, B., and Whang, K., “A Study of The Micro Pole Structure Fabrication and Application Technology by Micro End-Milling Process,” Key Engineering Materials, Vol. 257-258, pp. 453-458, 2004.

Performance Evaluation of Scanning Electron Microscopes using Signal-to-Noise Ratio

Naresh Marturi[#] , Sounkalo Dembélé, and Nadine Piat
FEMTO-ST Institute, AS2M Department, UMR CNRS 6174 - UFC / ENSMM / UTBM, Besançon, France
Corresponding Author E-mail: naresh.marturi@femto-st.fr, TEL: +33-381 402 913, FAX: +33-381 402 809
KEYWORDS: Scanning Electron Microscopes, Image Signal-to-Noise ratio

Scanning Electron Microscope is becoming a vital imaging tool in desktop laboratories because of its high imaging capability. Through this work we evaluate the performance of two different SEMs consisting of a tungsten gun and a field effect gun, with respect to time and magnification by estimating their image signal-to-noise ratio. SNR is mainly applied to quantify the level of image noise over changes in the acquisition time and magnification rates. Majority of the existing methods to estimate this quantity are based on cross-correlation technique and requires two images of the same specimen area. In this paper we propose a simple and efficient technique to compute signal-to-noise ratio using median filters. Unlike other techniques the proposed method uses only a single image and can be used in real time applications. The derived results show the effectiveness of the developed algorithm.

NOMENCLATURE

FIB = Focused Ion Beam
SEM = Scanning Electron Microscope
TEM = Transmission Electron Microscope
GIS = Gas Injection System
SNR = Signal-to-Noise Ratio
FEG = Field Effect Gun
SE = Secondary Electron
BSE = Back Scattered Electron
ACF = Auto Correlation Function
I,S,N = Acquired, signal and noise images
STD = Standard deviation

1 Introduction

The control of machining provided by FIB facilitates a fast expansion of desktop laboratories dedicated to the preparation of S/TEM samples. These laboratories commonly include a FIB, a GIS, a robot manipulation system and a SEM. The FIB performs machining to obtain a very thin specimen transparent to electrons and the width varying between $500nm$ and $10nm$. It also enables cutting of samples before transferring them to the final support. The GIS performs the deposition or removal of matter by SEM electron beam or by FIB. The robotic system performs the lift-out i.e. picking up a sample from the primary matrix, transferring and placing on the final support. All these elements are positioned inside the SEM chamber that supplies adequate level of vacuum and cleanliness for the overall processing [1]. Besides sample preparation, a SEM based desktop laboratory can be used to perform dynamic analysis and characterization of samples to retrieve their structural, mechanical, electrical or optical properties. Both applications sample preparation and analysis require long operation times and also a change in SEM magnification to fit the accuracy of measurements as well as the field-of-view.

Moreover, SEM is a powerful imaging instrument used in a variety of applications mainly because of its capability in providing images with high resolution and magnification ranges. These images are produced by detecting and converting various signals emitted during the electron beam - specimen interaction [2]. They are used to provide a dynamic visual feedback and real-time monitoring of the working scene in order to perform the assembly/handling task [3].

However, to perform an autonomous micro-manipulation of a sample ($< 10\mu m$) using a SEM based desktop factory, the primary requirement is that the quality of acquired images is high enough (i.e. having less percentage of noise) to be exploitative. One main indicator of the acquired image quality is the SNR mainly because of its efficiency in quantifying the level of noise in an image.

SNR is a commonly used measure in the field of signal processing to estimate the strength of a signal with respect to the background noise. So far, two microscope images of the same specimen area have been used in many research works to compute the SNR based on cross-correlation technique [4, 5]. The primary disadvantage associated with the used methods is that they require two images to be perfectly aligned and in ad-

dition, requires long processing times which makes them difficult to use in real-time applications. Apart from that for SEM imaging, if a sample is scanned for too long by probe it may become contaminated and unusable. Thong [6] used a single image to compute the SNR based on the simple approximation and first-order extrapolation. Even though the results are good enough but the used method is highly dependent on the nature of images.

In this work, assuming the level of noise is high and presence of the image drift, we overcome the above difficulties by developing a simple and robust noise estimation method based on non-linear filtering and then computing the SNR using a single image. In turn, it is used to estimate the SEM's performance in real-time at varying time and magnification rates. This work is mainly aimed to evaluate various SEMs and to choose an available best configuration for the future vision based autonomous micro sample handling process. It is also used to quantify any SEM with respect to the noise.

This paper is organised as follows. The basic concepts of SEM imaging are described in Section 2. In Section 3 we present the related work regarding SNR computation along with the proposed method. Experiments with the system and results are shown in section 4 followed by the conclusion.

2 SEM Imaging

The two different SEMs used for this work are JEOL JSM 820 with a tungsten filament gun and Carl Zeiss Supra with a FEG. The important difference between them is the maximum possible resolution with a tungsten gun SEM is $10nm$ whereas for a FEG it is $1nm$. Conventionally, a SEM consists of an electron column equipped with an electron gun (to produce a continuous beam of electrons), a sample chamber with a positioning stage and different electron detectors for detecting various types of emitted electrons during probe-sample interaction. The apertures and coils present inside the column are responsible to reduce the generated beam diameter, accelerate and focus the beam on the supplied scanning surface of a specimen. The basic construction of the column is shown in the Figure 2.1.

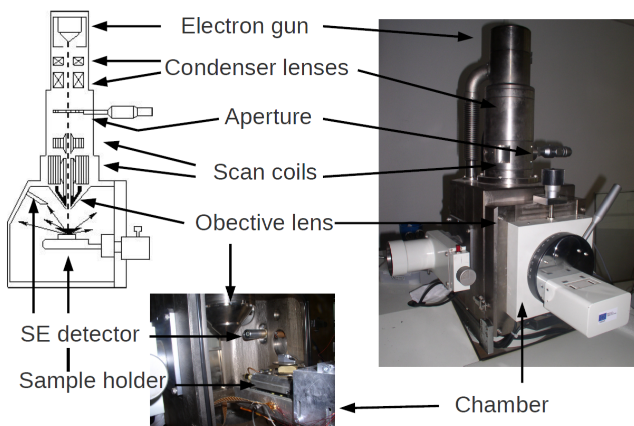

Figure 2.1: SEM electron column construction in reference with JEOL SEM

SEM images are formed by raster scanning the specimen area with produced electron beam and by recording the emitted electron information during this process. Later the gathered information is amplified and displayed on the monitor. SEM produces two dimensional gray scale images. The main advantage with a SEM is its ability in producing images with high depth-of-field and magnification. Typically, the magnification rates vary from 25× to 250,000×. The image resolution can be changed by changing the probe current and the acquisition time. In general, the common trade-off for image resolution in electron microscopy is the image SNR. The quality of the images produced can be expressed in terms of SNR. Operationally, high quality images can be acquired by increasing the beam current or by increasing the scanning time.

The images produced by a SEM are classified into different types based on the emitted electrons. Commonly used image types for most of the micro/nano applications are SE and BSE images. In this work, SE images have been used. Figure 2.2 shows a sample SE image of a standard gold on carbon sample. Normally the SE images are result of inelastic collisions and scattering of incident electrons with the electrons present on specimen surface. These images mainly provide the surface topographical information. More information about the other image types can be found in [2].

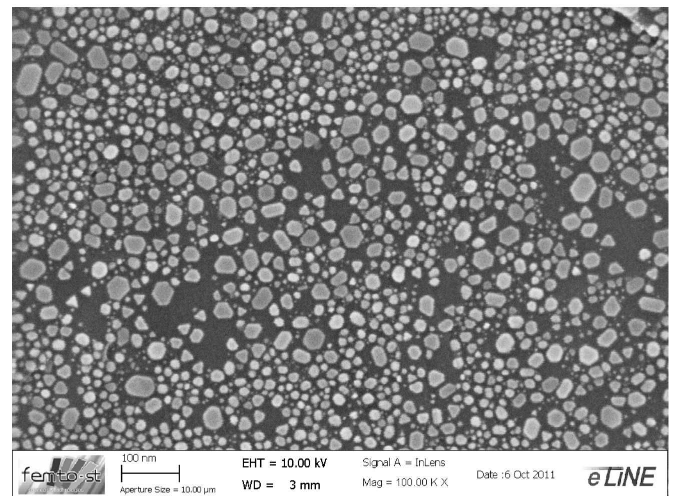

Figure 2.2: SE image of gold on carbon sample at 100k× magnification

However, SEM image acquisition is known to be affected by the addition of noise during beam production, its interaction with the sample and also by the presence of instabilities and non-linearities in the electron column during the scanning process [7]. At low scanning times the level of noise in the images is high in turn reducing the level of SNR. Moreover, noise can also be added by the charge-up of specimen surfaces due to continuous scanning by electron beam and also by mechanical vibrations. This work mainly focus on selecting the best possible quality images over time and magnifications based on the image SNR to estimate the variance of noise under the particular instrument in use.

3 SNR computation

SNR is one of the commonly used quantitative measures in the context of image quality as a measure of image noise. Many applications like image restoration, noise filtering algorithms use this parameter for estimating the noise variance [8]. Mainly with SEM SE imaging, the quantification of SNR is an important task where the images are possibly degraded by noise. SNR provides the level of original details present in the image in comparison with the level of noise. The higher the value of SNR the better the quality of acquired image. Following the

industry standards, SNR can be defined as

$$SNR \triangleq 10\log_{10}\frac{variance\{signal\}}{variance\{noise\}} \tag{3.1}$$

3.1 Related work

One of the most commonly used methods to compute SNR is by using image cross correlation technique [4]. However in order to use this method, two perfectly aligned microscopic images of the same specimen area are required. This approach assumes that the drift effects are negligible and only noise varies between images. Thong [6] proposed a single image SNR estimation method using the same technique by assuming that the noise in the image is additive white noise. Later, the ACF is computed for the corrupted image from which the noise and noise free peaks are estimated using interpolation. Figures 3.1a and 3.1b shows the ACF and 2 dimensional ACF curve taken along x-axis respectively for the sample image shown in Figure 2.2.

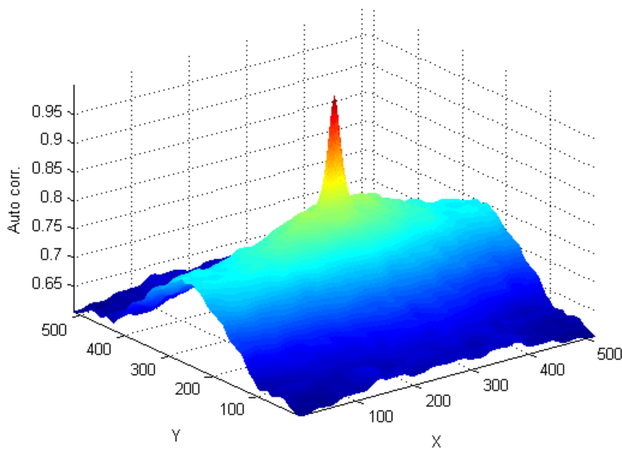

Figure 3.1a: ACF curve for the image shown in Figure 2.2

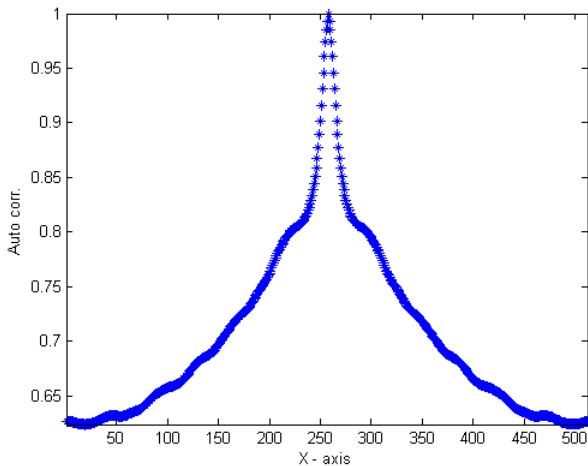

Figure 3.1b: ACF curve along x-axis

From the computed ACF, noise free peak is found using interpolation. Figure 3.2 shows the two peaks. The SNR is described as:

$$SNR = \frac{Noisefreepeak - (mean(pixels))^2}{Noisepeak - Noisefreepeak} \tag{3.2}$$

It is difficult to use the above method for online applications mainly because of the reason that the Overal computational time is more. Moreover, accuracy of the method is highly dependent on noise free peak estimation.

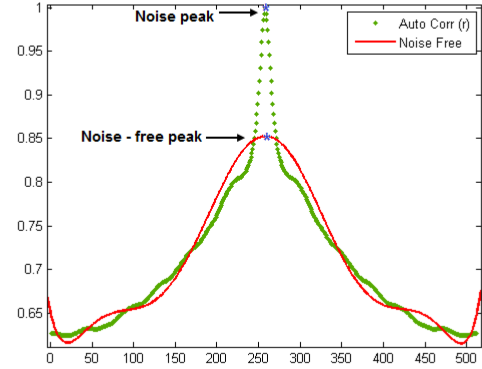

Figure 3.2: Estimated noise and noise free peaks

To overcome the drawback associated with the above method, a simple technique using single image to estimate the SNR for online applications is implemented based on noise filtering by convoluting the image with a nonlinear filter kernel. By comparing all the available nonlinear filter masks like Gaussian, median etc., median filtering seem to provide best performance in filtering the noise and preserving image details [9]. Even though Gaussian is good at filtering noise, it removed fine image details like sharp edges. The proposed method is explained below.

3.2 Proposed approach

Assuming the acquired image is corrupted by spatially uncorrelated additive Gaussian white noise [5, 6, 10] the image model is given by

$$I(x,y) = S(x,y) + N(x,y) \tag{3.3}$$

Each captured frame undergoes histogram equalisation as a step of normalising the intensity levels and enhancing the image contrast. This is an optional step as the software provided with modern SEMs includes this functionality directly while acquiring the images. The normalised image is then convoluted with a median filter of appropriate size in order to reduce the noise effects. In detail, each pixel in the image is replaced by the median value of its surrounding neighbourhood. The size of the filter is chosen by trial and error. Figures 3.3a and 3.3b shows the resulting filtered image, S and removed noise image, N respectively for Figure 2.2.

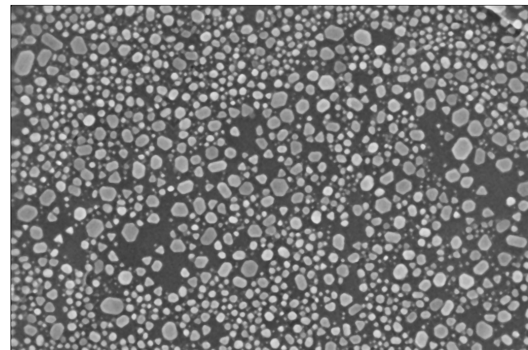

Figure 3.3a: Filtered image

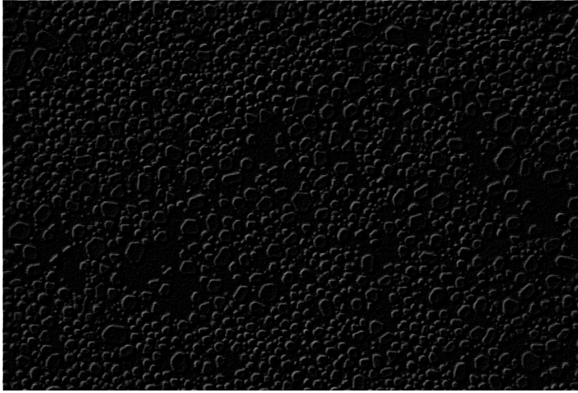

Figure 3.3b: Noise image

Using S, the noise can be formulated by subtracting S from I resulting in N. In turn both S and N are used in computing SNR. The final SNR following industry standards of $20\log_{10}$ can be defined as:

$$SNR = 20\log_{10}\frac{STD(S)}{STD(N)} \quad (3.4)$$

A specimen is positioned upon the positioning stage inside SEM vacuum chamber. A set of images are acquired from t_0 to t_f with a sampling time T for each magnification ranging from g_0 to g_f with a sampling step of G. The SNR quantification using the proposed approach is described in algorithm 3.2.

Algorithm 3.2 Algorithm for SNR quantification

1: **for** $g = g_0 \rightarrow g_f$ **do**
2: **for** $t = t_0 \rightarrow t_f$ **do**
3: Acquire image, I;
4: Normalise intensity levels;
5: Apply median filter to get S;
6: I-S to get N;
7: Compute SNR using 3.4;
8: **end for**
9: **end for**

The robustness of the proposed method is evaluated by corrupting a noise free image shown in Figure 3.4a with additive white Gaussian noise for which the SNR level is known prior to the addition. Later the SNR is computed from the corrupted image using proposed method and is compared with the original values in order to test its efficiency. Table 3.1 shows the original and obtained SNR values.

Figure 3.4a: Noise free image

Figure 3.4b: Image corrupted with Gaussian noise of 20dB

Table 3.1: **Original and obtained SNR values**

Original SNR (dB)	Obtained SNR (dB)
15	14.3743
16	15.2436
17	17.2480
18	18.1332
19	19.5319
20	20.0264
21	21.0056
22	21.8679
23	22.6670
24	23.7125
25	24.6833
26	25.2426
27	26.7032
28	27.9277
29	28.6508
30	29.4661

From the obtained results it is clear that the proposed method has a reliable performance in estimating the noise level from a given corrupted signal as well as in computing SNR values.

4 Evaluation and discussion

The performance of two different SEMs Jeol JSM 820 and Carl Zeiss Supra is evaluated using the proposed approach. It uses SE images of standard Gold on Carbon sample with low voltage resolution ($30nm - 500nm$) for Jeol SEM as it is an aged SEM and normal resolution ($5nm - 150nm$) for Carl Zeiss SEM.

The accelerating voltage used to accelerate the produced beam is 10kV and the magnifications used for this work are ranged from 10k× to 100k× with an increase of 10k. For each magnification 20 – 30 images are acquired with a sampling time of 30 seconds i.e. a single image is captured for every 30 seconds. Chosen image size for this work is 512 × 512. Once an image is acquired its SNR value is computed using algorithm 3.2.

The evaluation process is performed in two steps. The primary step is to estimate the SEM performance with increase in time. Tables 4.1 and 4.2 summarises the obtained SNR values (in dB) for different magnifications with increase in time (30 seconds for each count) for tungsten gun SEM (Jeol) and FEG SEM (Carl Zeiss Supra). Sample plots comparing the SNR levels with both the SEMs at different magnifications are shown in the Figures 4.1 and 4.2.

Table 4.1: SNR values (in dB) for Jeol SEM

Magnification rates				
10000×	15000×	20000×	25000×	30000×
17.4536	18.9045	17.7562	20.8551	19.5582
17.4708	18.9635	17.8127	20.8353	19.6026
17.5719	18.9120	17.8672	20.7796	19.6623
17.5645	18.9678	18.9029	20.8866	19.6288
17.7280	18.9216	18.9257	20.9368	19.7071
17.7317	18.9774	18.9626	20.0229	19.7394
17.7580	18.9923	18.9819	20.1088	19.7572
17.7815	19.0035	18.0084	20.1029	19.8194
17.8303	19.0058	18.0263	20.2038	19.8408
17.8454	19.0827	18.0523	20.2695	19.8644
17.8698	19.0426	18.0831	20.2787	19.8408
17.9208	19.1212	18.1636	20.3237	19.8904
18.0420	19.1128	18.2382	20.3480	19.8707
17.9926	19.1868	18.2554	20.3478	19.9000
18.0404	19.1412	19.2752	20.3786	20.9191
18.0637	19.1544	19.2871	20.3900	20.9219
18.1012	19.1549	19.2466	20.3842	20.9297
18.1205	19.1755	19.3011	20.3497	20.9101
18.1626	19.1797	19.3197	20.3293	20.9209
18.1596	19.1864	19.3117	20.3190	20.8867

Table 4.2: SNR values (in dB) for Carl Zeiss SEM

Magnification rates				
60000×	70000×	80000×	90000×	100000×
17.3942	16.9059	15.4394	16.2897	16.6367
17.8734	16.9669	15.5451	16.4657	16.9874
18.2265	17.1716	15.5451	16.4657	17.2667
18.6786	17.1716	15.8911	16.8509	17.4951
18.7267	17.6672	15.9604	16.9306	17.6999
18.9605	17.8276	16.0912	17.1262	17.8748
19.1688	17.9797	16.2547	17.3217	18.0521
19.2134	18.0416	16.3372	17.4020	18.2933
19.3825	18.1382	16.4224	17.4020	18.4179
19.2693	18.2387	16.4833	17.8535	18.5065
19.5012	18.3103	16.6785	17.9680	18.4610
19.8314	18.4442	16.7113	18.1125	18.5710
20.0031	18.4381	16.9536	18.2303	18.7546
19.8055	18.7222	16.9712	18.3546	18.7331
20.6075	18.6924	17.0032	18.4183	18.8932
20.8755	18.7884	17.0457	18.6238	18.9844
20.8318	18.8678	17.1389	18.6963	19.0937
20.8405	18.9278	17.1812	18.8157	19.0546
21.0915	19.0026	17.4818	18.9375	19.2215
20.9610	19.4176	17.4339	19.0563	19.3941

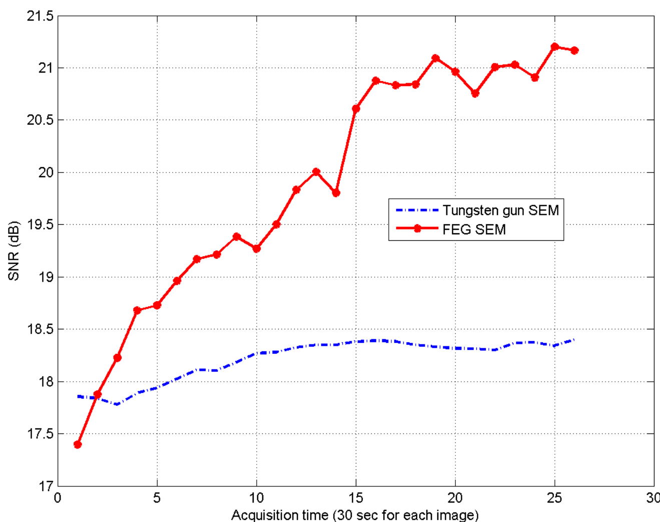

Figure 4.1: Acquisition time vs. SNR at 40,000 × magnifications

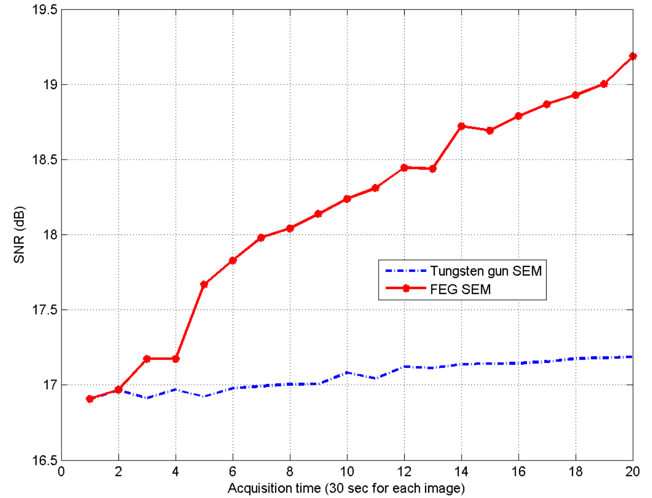

Figure 4.2: Acquisition time vs. SNR at 70,000 × magnifications

After evaluating the two SEMs, it is observed that the level of SNR is increased with increase in time. And also it is clear from the Figures 4.1 and 4.2 that the SNR level is weak for Jeol SEM in comparison with Zeiss SEM. However, in every case the SNR level is high enough (>15dB) to make the images exploitable. Next, the SEMs performance is evaluated with increase in magnifications and the results are summarised in Figures 4.3 and 4.4 for Jeol and Carl Zeiss SEMs respectively.

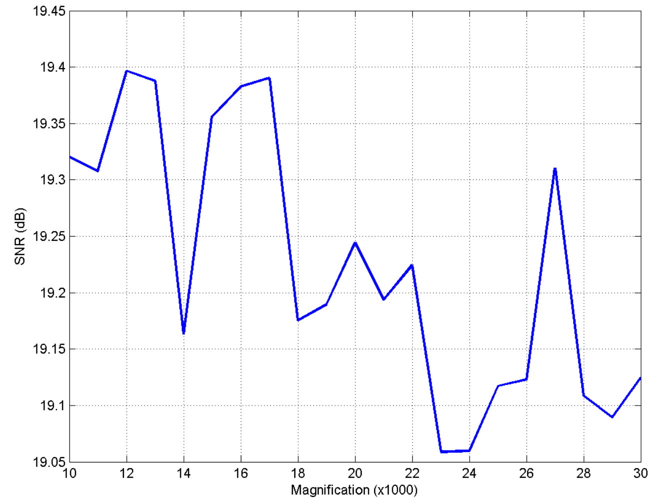

Figure 4.3: Magnification vs. SNR for Jeol SEM

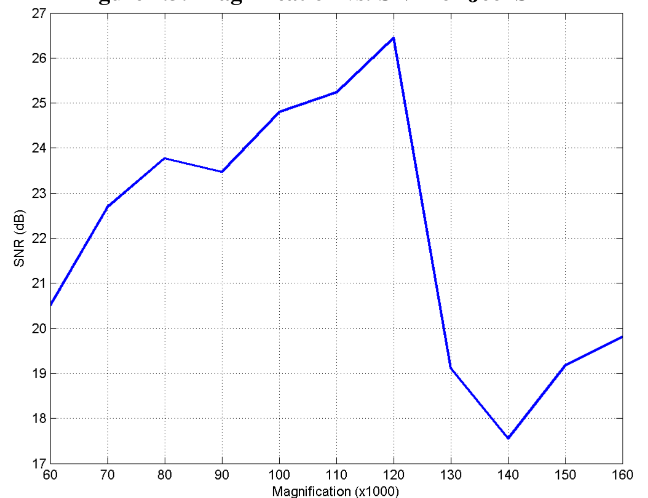

Figure 4.4: Magnification vs. SNR for Carl Zeiss SEM

The results obtained shows that, unlike with time the level of SNR decreases with increase in magnification rates. From figure 4.3 we can say that this rate of decrease is comparatively negligible for Jeol SEM.

5 Conclusion

In this paper, we evaluate the performance of two different SEMs with respect to time and magnification using image SNR. After evaluation it is clear that the FEG SEM (Carl Zeiss) shows better performance or imaging abilities in comparison with the SEM containing a tungsten gun (Jeol). The results obtained show that the level of SNR increases with respect to time for both the SEMs, but the rate of increase is more for the FEG SEM than the tungsten gun SEM.

To compute image SNR a new, simple and fast method based on median filtering has been proposed. It overcomes the difficulties associated with various other SNR computation algorithms by using only a single image. As the time taken for overall process is very less the proposed method can be used with real time applications. The obtained results show the effectiveness of the proposed algorithm.

ACKNOWLEDGEMENT

This work is conducted with financial support from the project “Caractérisation multiphysique de nano-objets et manipulation robotisée sous environnement MEB (NANOROBUST ANR-11-NANO-006)” funded by the Agence Nationale de la Recherche.

REFERENCES

[1] J. Dai, S. Tee, C. Tay, Z. Song, S. Ansari, E. Er, and S. Redkar, “Development of a rapid and automated tem sample preparation method in semiconductor failure analysis and the study of the relevant tem artifact,” *Microelectronics journal*, vol. 32, no. 3, pp. 221–226, 2001.

[2] J. Goldstein, D. Newbury, D. Joy, C. Lyman, P. Echlin, E. Lifshin, L. Sawyer, and J. Michael, *Scanning electron microscopy and X-ray microanalysis*, vol. 1. Springer Us, 2003.

[3] T. Sievers and S. Fatikow, “Visual servoing of a mobile microrobot inside a scanning electron microscope,” in *Intelligent Robots and Systems, 2005.(IROS 2005). 2005 IEEE/RSJ International Conference on*, pp. 1350–1354, IEEE, 2005.

[4] J. Frank and L. Al-Ali, “Signal-to-noise ratio of electron micrographs obtained by cross correlation,” *Nature*, vol. 256, pp. 376–379, 1975.

[5] K. S. Sim, M. E. Nia, and C. P. Tso, “Image noise cross-correlation for signal-to-noise ratio estimation in scanning electron microscope images,” *Scanning*, vol. 33, no. 2, pp. 82–93, 2011.

[6] J. Thong, K. Sim, and J. Phang, “Single-image signal-to-noise ratio estimation,” *Scanning*, vol. 23, no. 5, pp. 328–336, 2001.

[7] M. Abed, D. Sounkalo, P. Nadine, A. Claire, and M. Naresh, “Toward fast calibration of the global drift in scanning electron microscopes with respect to time and magnification,” *International Journal of Optomechatronics*, vol. 6, no. 1, pp. 1–16, 2012.

[8] T. Bose, F. Meyer, and M. Chen, *Digital signal and image processing*. J. Wiley, 2004.

[9] R. Gonzalez and R.E.Woods, *Digital Image Processing*. Pearson Prentice Hall Press, New Jersey, 3 ed., 2008.

[10] N. Kamel and S. Kafa, “Image snr estimation using the autoregressive modeling,” in *International Conference on Intelligent and Advanced Systems (ICIAS), 2010*, pp. 1–5, IEEE, june 2010.

An in-situ manufacturing module for fabricating, adjusting and regenerating the micro grinding tool with Ni-diamond composites

Jung-Chou Hung[1*], Da-Yu Lin[1], Hung-Yi Chen[1], Hai-Ping Tsui[1] and Yan-Cherng Lin[2]

1 Regional R&D Services Department, Metal Industries Research & Development Centre, Taichung, Taiwan
2 Graduate School of Vehicle & Mechatronic Industry, Nan Kai University of Technology, Nantou, Taiwan
Corresponding Author / E-mail: jchung@mail.mirdc.org.tw, TEL: +886-4-23502169, FAX: +886-4-23501174

KEYWORDS : In-situ manufacturing module, Electro co-deposition, Ni-diamond composites, Micro grinding tool, Regenerating process.

This research presents an in-situ manufacturing module could be added upon suitable machine to produce a micro grinding tool, so as to reach multi-function as miniaturization, modularization, high accuracy, low cost and in-situ adjustment. The manufacturing system included five working stations as electro co-deposition, water cleaning, acid pickling, electrolytic machining and regenerating process. A micro cylindrical tool was machined by WEDG, and which tool was deposited with the Ni-diamond composites to be a micro grinding tool by electro co-deposition. The in-situ adjusting or regenerating process could be carried out immediately if the tool size of which want be changed or is over setting value. The module was designed to reach miniaturization via circulating channel and reducing volume of working fluid. The module includes a plurality of stations to be arranged side by side and all of which has some portions being arranged forming a row to reach multi-workability. The experimental result shows the design characteristic of the module can be executed successfully to produce a micro grinding tool more flexible.

1. Introduction

Micromachining techniques are widely needed day by day with the progress of industry, such as micro-channel of biochip, micro-holes of fiber optic connector, optical lenses and micro-mold. The facilities and expenses conventional micromachining processes, such as electro beam machining, laser beam machining, Laser machining, LIGA process et al [1-5], are costly but the surface machining in a highly quality is not easy to reach the goal. Therefore, how to reach the process in low-cost, high accuracy and high quality is very important. Micro electrical discharge machining (MEDM) is a kind of process which could reach the high accuracy. However, micro-EDM suffers from the defect of poor surface quality because the recast layer formed on the machined surface is covered with discharge craters and micro-cracks. These defects affect the diameter of the micro-hole and undermine the precision of the geometric shape. These machining shape accuracy and surface roughness are not easily to be improved. However, conventional grinding methods have difficulty in extending the tools into the micro-hole to perform precision grinding. In order to overcome these issues, previous studies [11, 12] have studied the surface roughness of micro-holes using micro- EDM combined with fluid grinding particles. A grinding tool combined with complex procedures has been proposed for improving machining accuracy and surface roughness after MEDM process in previous study [8], although changing the every procedure is still inconvenient.

For this reason, in order to achieve in-situ manufacturing, this study presents the manufacturing module was designed to satisfy could be added upon suitable machine to in-situ produce a micro grinding tool as shown in fig. 1, so as to reach multi-function as miniaturization, modularization, high accuracy, low cost and in-situ adjustment are addressed.

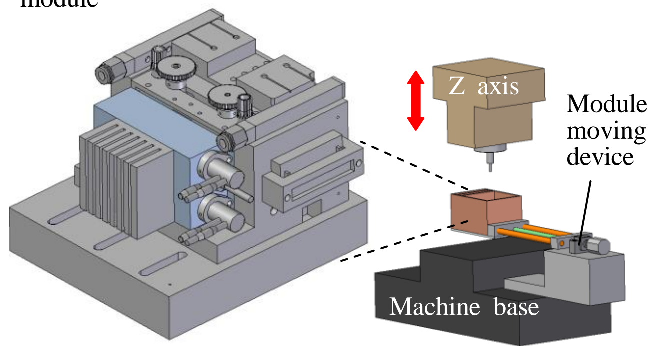

Fig.1 The in-situ manufacturing module could be added upon suitable machine

2. The design of module system

2.1 The design of electro co-deposition unit

2.1.1 Circulating channel type

Figure 2 presents the single-cycle channel design in electro co-deposition unit. The concept of circulating channel type is adopted. It makes most of the channels to hide inside the body, but some portions are adopted in open channel. Therefore it makes electrolyte flow inside the circulating channel. It forced the electrolyte to only flow in circulative way into the channel. The suitable diameter of the channel outlet for the electrolyte can be gushed out, which is the best dimension design to fit the electro co-deposition unit, that the efficiencies of fluid driver and electro co-deposition are enhanced. This circulating channel type design is different from any square or circle open-type tank [7]. The quantity and its flow directions of electro co-deposition electrolyte cannot be controlled in open-type tank. Those would cause a lot of shortcomings as lavish of electro-deposition electrolyte, enormous volume, deposition is not equally divided, et al. Thus the shortcoming of the open groove has been improved by this circulating-channel type design.

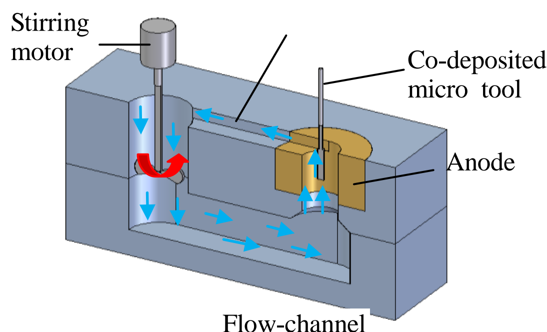

Fig. 2 The single-cycle channel type

The above designs are based on single-cycle channel. In order to increase the particle density and uniformity of micro grinding tool, another design is adopted by twin-cycle channel. The particle density and uniformity are also elevated while twin-cycle channel is adopted as shown in fig. 3 [8].

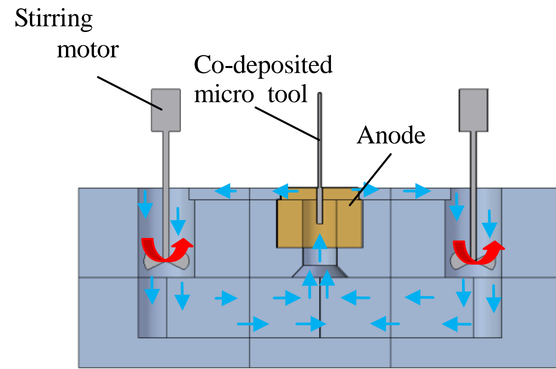

Fig. 3 The twin-cycle channel type

2.1.2 Electrode unit

When electro co-deposition procedure of grinding tool is produced, the adhesion force condition and equalization of grinding grains are affected by the shape and dimension of electrode. The adhesion quantity of grinding grains would be increased when grinding tool is much closer to the electrode, but it would also cause unqualified influence for too close to it. Therefore the adhesion quantity and equalization of grinding grains on grinding tool were reached by positive ring electrode and optimal design [8]. This positive ring is placed on gushing extremity. The grinding tool is extended inside the center of positive ring to carry out electro-deposition.

2.1.3 Temperature control unit

To heat the electrolyte equally, this temperature control unit is different from traditional method which used heater immerse into the electrolyte directly. In this heated design, the heater and thermo sensor are embedded the metallic tank body as shown in fig. 4. The whole inside tank wall can heat the electrolyte up equally.

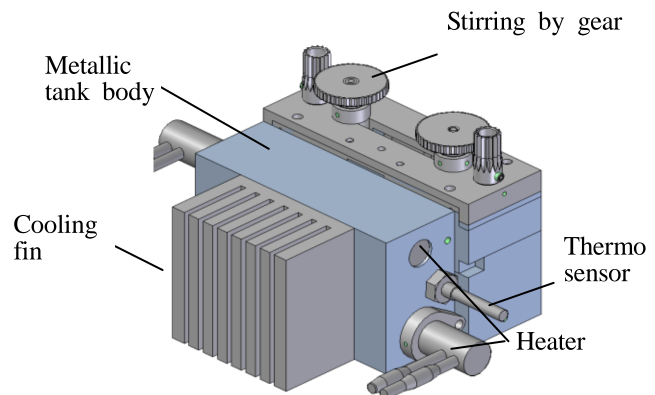

Fig.4 The temperature control unit

2.2 All the manufacturing procedures layout

The manufacturing system included five working stations as electro co-deposition, water cleaning, acid pickling, electrolytic machining and regenerating process as shown in fig. 5. The main design concept is that tool inlet points were arranged as an alignment to enhance the precision.

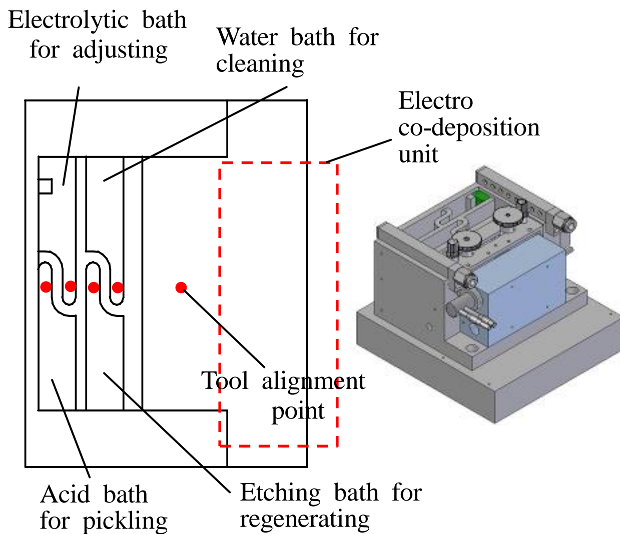

Fig. 5 All the manufacturing procedures layout

3 Results and discussion

3.1 In-situ manufacturing module assembly

Figure 6 shows the entity picture of manufacturing module. After all modules are integrated, and make it possess the function of grinding tool making/adjusting/regeneration, with the characteristic of miniaturization, simple structure, less solution, low-cost, high deposition uniformity and easy maintenance etc.

The electro deposition module includes a circulation flow tank, fluid drive unit, the electrode unit and temperature control unit. The circulation flow channel tank is made up of the stainless steel with thermal conductivity and corrosion resistance. The fluid drive unit is assembly by the motor, gear, blades. The temperature control unit is composed of heating rods, cooling fin and the temperature sensor. In addition, fig. 7 shows the situation of the liquid pours out from the positive ring outlet and flow into channel with suitable height and width.

Adjusting/ regeneration module is made of plastic materials in order to achieve the insulating effect of the machine. When manufacturing the plastic module, the milling process is used on the plastic material to form the electrolytic bath, acid bath, water bath and etching bath for adjusting/ regenerating module.

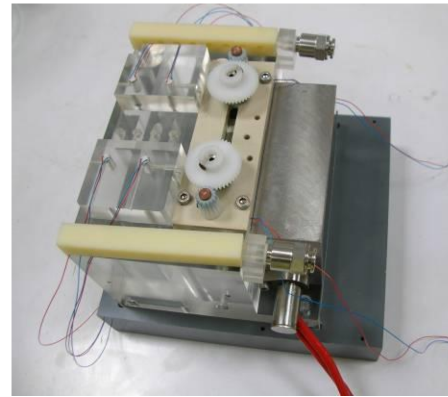

Fig.6 The entity picture of the manufacturing module

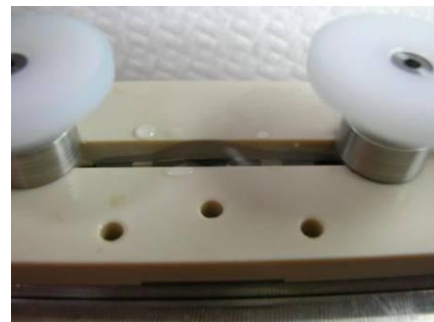

Fig.7 The liquid pours out the outlet of positive ring

3.2 Electro co-deposition situation of the grinding tools

The WEDG process is utilized to manufacture the original tool diameter of 0.1mm as shown in fig. 8. The nickel-base mixed grinding particle of 2μm diamond is utilized to carry out electro co-deposition on grinding tool for 5 min, 10 min, 15 min and 20 min. Deposited tool diameter dimensions respectively are 0.12 mm, 0.132 mm, 0.15 mm and 0.163 mm as shown in fig. 9. Figure 10 shows the SEM image comparison before and after co-deposition.

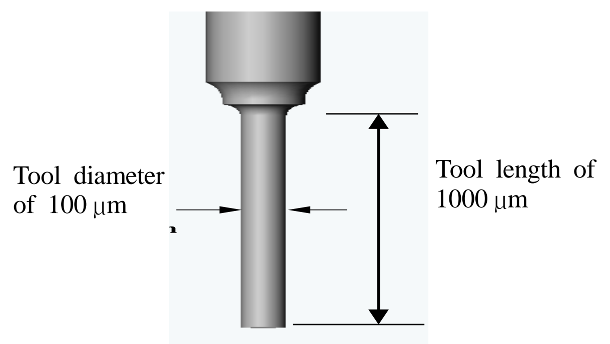

Fig. 8 Schematic diagram of a tungsten carbide micro-tool by WEDG

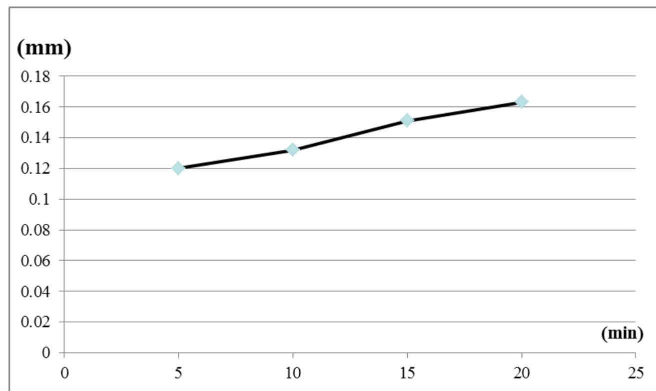

Fig. 9 A contrast of coating layer thickness increases with co-deposition time.

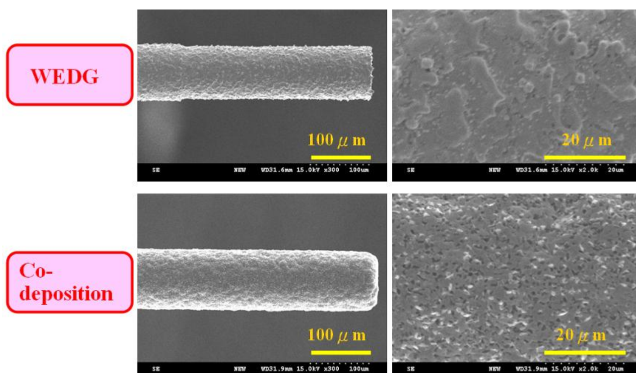

Fig.10 The SEM image comparison before and after co-deposition

3.3 The reproducibility of grinding tool

In order to achieve the high accuracy to effective apply for process, the reproducibility must be tested to know. Four grinding tools are co-deposited in 5 minutes to make sure the diameter reproducibility. The diameters of grinding tool are about 128 μm as shown in fig. 11.

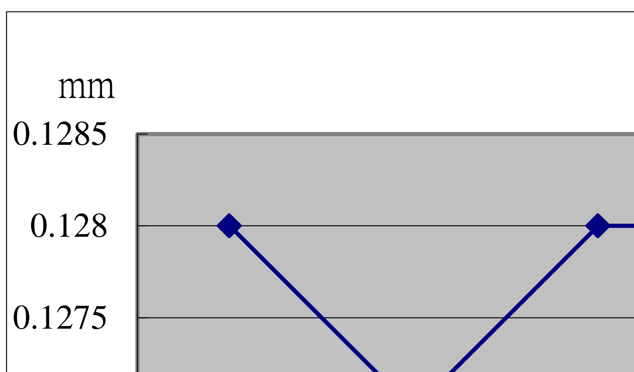

Fig. 11 The reproducibility of grinding tools by co-deposition

4. Conclusions

The major conclusions drawn from this study are summarized in the following.

1) In-situ manufacturing module could be added upon suitable machine to produce a micro grinding tool, so as to reach multi-function as miniaturization, modularization, high accuracy, low cost and in-situ adjustment as well as to enhance machining accuracy.
2) The in-situ adjusting or regenerating process could be carried out immediately if the tool size of which want be changed or is over setting value.
3) The experimental result shows the design characteristic of the module can be executed successfully to produce a micro grinding tool more flexible.

REFERENCES

1. Wang, A. C., Yan, B. H., Li, X. T. and Huang, F. Y., “Use of micro ultrasonic vibration lapping to enhance the precision of microholes drilled by micro electro-discharge machining,” International Journal of Machine Tools and Manufacture, Vol. 42, pp. 915-923, 2002.
2. Ehrfeld, W. and Lehr, H., “Deep X-Ray Lithography for the production of three-dimensional microstructures from metals, polymers and ceramics,” Radiation physics and chemistry, Vol. 45, pp. 349-365, 1995.
3. Choi, S. S., Jung, M. Y., Kim, D. W., Yakshin, M. A., Park, J. Y. and Kuk, Y., “Frabrication and microelectron gun arrays using laser micromachining,” Microelectronic Engineering, Vol. 41/42, pp. 167-170, 1998.
4. Huang, H., Zhang, H., Zhou, L. and Zheng, H. Y., “Ultrasonic vibration assisted electro-discharge machining of microholes in Nitinol,” Journal of Micromechanics and Microengineering, Vol. 13, pp. 693-700, 2003.
5. Kupka, R. K., Bouamrance, F., Cremers, C. and S. Megtert, “Microfabrication: LIGA-X and applications,” Applied Surface Science, Vol. 164, pp. 97-110, 2000.
6. Hung, J. C., Yan, B. H., Liu, H. S. and Chow, H. M., “Micro-hole machining using micro-EDM combined with electropolishing,” Journal of Micromechanics and Microengineering, Vol. 16, pp. 1480-1486, 2006.
7. Chen, S. T., Lai, Y. C. and Liu, C. C., “Fabrication of a miniature diamond grinding tool using a hybrid process of micro-EDM and co-deposition,” Journal of Micromechanics and Microengineering, Vol. 18, No. 5, pp. 55005-55012, 2008.
8. Hung, J. C., Wu, W. C., Yan, B. H., Huang, F. Y. and Wu, K. L., “Fabrication of a micro-tool in micro-EDM combined with co-deposited Ni-SiC composites for micro-hole machining,” Journal of Micromechanics and Microengineering, Vol. 17, pp. 763-774, 2007.

Comparison of Five Low Cost Manipulators for Microfactories

Niko Siltala[1, #] , Asser Vuola[1] , Timo Prusi[1] , Riku Heikkilä[1] and Reijo Tuokko[1]
1 Department of Production Engineering, Tampere University of Technology, Tampere, Finland
Corresponding Author E-mail: niko.siltala@tut.fi, TEL: +358-40-536-6017, FAX: +358-3-3115-2793
KEYWORDS: microfactory, manipulators, robots

This paper presents and compares characteristics of five low cost manipulators for microfactories. Four of the manipulators are self designed and implemented prototypes. The fifth one is a commercially available product. They all are fitting in the TUT microfactory concept developed at Tampere University of Technology. The main focus is on construction, performance, accuracies, and costs of these manipulators. The characteristics and issues of each of the manipulators are compared, discussed and finally summarised.

NOMENCLATURE

CAD = Computer Aided Design
DOF = Degrees of Freedom
TCP = Tool Centre Point
TUT = Tampere University of Technology

1 Introduction

The concept of microfactories origins back to beginning of 90's in Japan [1] and has been ever since researched in various places globally [2]. The main characteristics and benefits are in the savings of energy, material and space. These are achieved through smaller sized machinery, which is closer the size range of the part billets and final products. Machinery should be preferably in portable range, so that a human can handle the modules easily without any lifting aid.

Almost any application for microfactories require some kind of part transfer or manipulation operation. In many cases some kind of manipulator with two to four or more degrees of freedom (DOF) would be perfect for the job. Generic type, reusable manipulators as reconfigurable modules would be perfect and covering large proportion of the tasks. However, as example the required accuracy, range of motion and payload vary case by case and set boundaries for implementation.

The TUT microfactory concept is developed at department of Production Engineering at Tampere University of Technology. It has been introduced at 2005 and details of the concept can be found from [3, 4, 5]. The main characteristics of this microfactory concept are: modularity, well defined interfaces, construction kit type of structure, reusable and self-contained modules, and easy reconfiguration.

The difference compared to many other microfactory concepts are mainly in self-containing approach and seek for lower cost solutions. In many other approaches the modules might have large control cabinets under the desk to make system live. In our case all controllers, amplifiers, etc. are included inside the module. The strive for lower cost reflects on focusing not the most accurate and demanding tasks, but to find optimum solution for miniaturising manufacturing and assembly tasks. There exist a vast amount of tasks, which do not require that high accuracy, but which could benefit greatly from small size machinery.

We have identified that the manipulator is a key component as it can be used flexibly for various handling and manipulation operations needed in most of (micro)assembly and (micro)manufacturing tasks. Therefore this paper compiles together and compares some of the TUT microfactory manipulator implementations and summarise the findings of these different cases.

The paper is organised as follows: After the introduction the research method is defined. This is followed by representing and characterising the modules used in this comparison. The results are presented and key figures are summarised on a table. The results are analysed, discussed and finally concluded.

2 Method

This paper compares and evaluates the characteristics of different manipulators used in our TUT microfactory concept. The characteristics considered here include: performance mainly velocity and acceleration; payload; accuracy (i.e. construction, feedback configuration and resolution); mechanical construction of the manipulator; work envelope of the manipulator and its workspace; and of course the costs.

The manipulators included to the study base on existence in our laboratory and that they all are integrated as modules to TUT microfactory concept. They all are dedicated for pick-and-place type of operation or processing a stationary product with a moving tool fixed in the manipulator.

There does exist other similar or even smaller in size manipulators and robots as Prusi et.al. describes in [6]. Ones not included into this comparison, but which should be mentioned at this context are Parvus[7] and APIS[8] manipulators from IWF, TU Braunschweig. These are comparable or even beyond by size, construction, and accuracy with the ones discussed in this paper.

3 Special Microfactory Issues

In our experience, micro and desktop size devices demonstrate special types of issues comparing to larger scale machinery [**Vai olisko tähän joku hyvä REF???**]. The issues are related to the smaller size of components, and the constructional and design changes, which therefore are needed. Downscaling of existing macro solutions is not possible or at least are not providing the optimum solutions; cabling and tubing create issues; relative accuracies are getting into high demand class, even if absolute accuracy requirement is kept the same as in macro.

Small size components are difficult to handle and they are usually costly. Reduced size of components shows smaller performance, like force or torque, which is making it also necessary to completely rethink the application from a new perspective. Only this way it is possible to manage with the components available and not to over size and over design the application. The system is possible to be kept lightweight and high performing with new, innovative design choices.

Cabling is getting difficult as relative size of cabling is increasing. Also small wire diameter together with small connectors and junctions are causing issues at connectivity and in signal quality. Therefore new solutions like flat cables and/or serial buses are used.

The accuracy issues are arisen from the fact that the manufacturing tolerances are getting closer to the range of the feature size of the component itself. Maintaining the same relative accuracy requirement level as in macro domain is getting very hard or even impossible to keep. This sets also requirements on system, machine or end-product design, as larger relative tolerances should be allowed. **Tarkista väitteet ja kirjaa ne oikein!**

4 Devices

Four of the compared devices are self made and focus of this comparison. The fifth is a commercial minirobot provided as reference. The devices are introduced following in chronological order of appearance. Labels for each manipulator are set in titles, and these are used later as reference.

4.1 Manipulator A: H-Portal

The three DOF manipulator together with its screwing application is presented in [9]. It is a belt driven, parallel kinematic manipulator. The belt is a loop forming a H-pattern, which provides the slide movements in XY-plane. The belt goes through pinion of both motors and some pulleys, establishing a the H-pattern. It is firmly attached to the moving slide from one side. The position of the slide is determined by driving the combination of both motors into specific positions. Z is a ball screw driven and motor is located into the moving body. A pneumatic cylinder is used to provide a constant Z directional force while screwing operation is performed. At the same time it provides fast movements for the Z axis.

The Fig. 4.1 shows in addition to the manipulator the manual screwdriver integrated to the manipulator and its controller. The black cylinders on top are the motors and gears for the XY movement and the box between motors is the controller for electrically driven screwdriver.

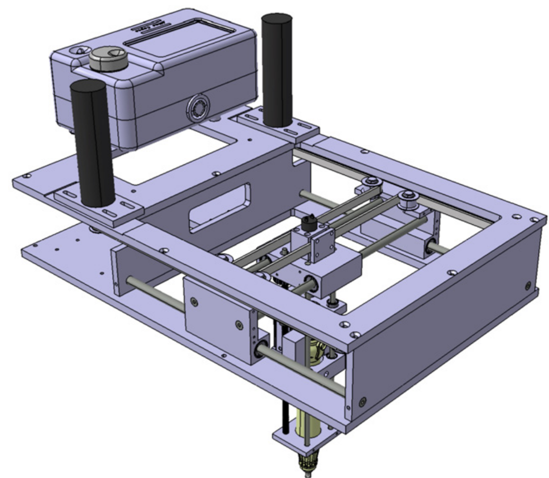

Figure 4.1: 3D CAD illustration of the H-Portal manipulator with screwdriver

The main design drivers have been reduction of the mass of the moving body and reduction of the wiring to the moving parts. Thus, the motors for X and Y axes are located out of moving body. The belt driven parallel H-structure construction itself has been also the interest for the development.

The measured accuracy of the manipulator at XY plane is at worst case 201 μm [9]. The measurement was made with laser interferometers. The sources of position error are: elasticity and flexibility of the belt, transmission and gear backlash, guides, and encoder resolution. Encoder with 512 pulses per revolution (p/rev) is placed at the end of the motor. After quadrature count and gears

it represents resolution of 0,9 μm at linear axis. The second component of the position error is transmission, gear backlash (10,4 μm) and guides. Use of combination of two motors determining the position doubles the error for an axis. The position error caused from encoder and transmission is calculated to be around 22,6 μm ($= 2 \times$ (resolution + gear backlash)). However, the main component of the error is the elasticity and flexibility of the belt, which causes around ten times more error than all the other components together.

4.2 Manipulator B: H-Scara

The good experiences gathered from the H-Portal led us to develop a magnitude more complex construction - a H-Scara manipulator as shown as CAD model in Fig. 4.2 and a photo of the final module in Fig. 4.3. The ability to access workspace of parallel cells has been the main design driver. Manipulator is a dual parallel kinematic manipulator, which is composed from two parallel kinematic structures mounted on series [10, 11]. The first part is a H-belt driven structure mounted on the back wall providing motion at XZ plane. The second kinematic structure - parallel scara - is mounted in series to the slide of the H-structure. The second part is providing movement at XY plane - a bit like the human arms when keeping hands together and moving only your shoulders. The fourth DOF is the W in the end tip of the parallel scara. It has unlimited rotation, standard gripper interface with four pass through service ports, each of which can be either electrical or pneumatic.

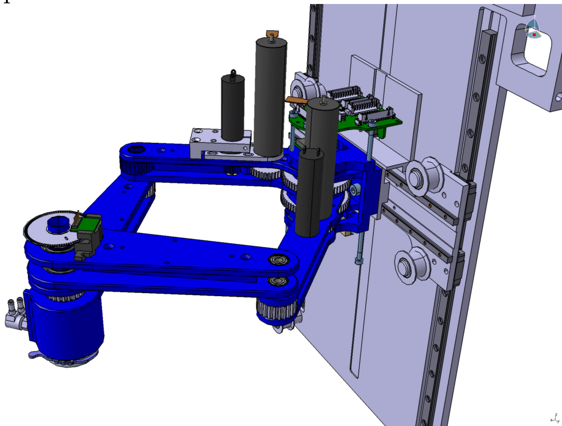

Figure 4.2: Illustration of the H-Scara manipulator [10]

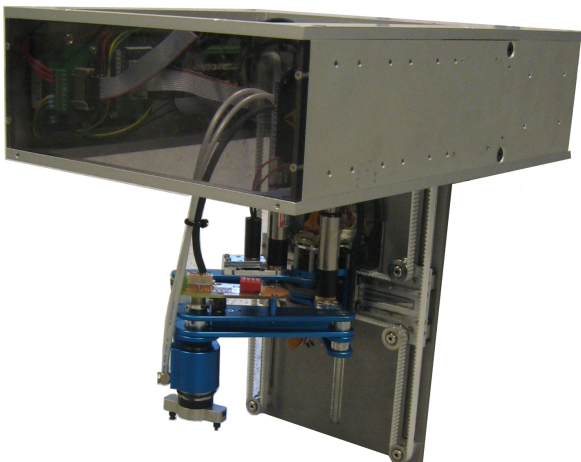

Figure 4.3: Photo of the H-Scara manipulator module [6]

The workspace of the scara structure is limited on large arc and two smaller ones making together a pattern which is a bit like a side profile of an open umbrella. The entire workspace of the manipulator is illustrated on Fig. 4.4.

All drives and wirings are integrated into the single manipulator module. Because of this, the only connections to the module are power supply, fieldbus communication and pressured air. The controls (position, numerical and logic) are located on different physical module.

The manipulator, its kinematics and controls, its development steps and challenges are discussed more deeply in [10, 11, 12]. The entire case application for this robot cell is presented in [12].

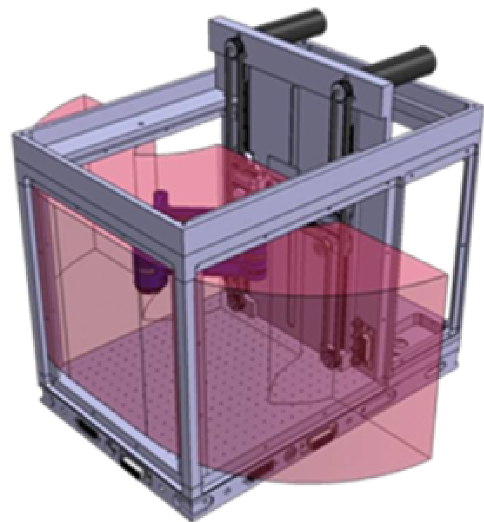

Figure 4.4: Workspace of H-Scara manipulator. Illustrated is also the base module on which the manipulator module is located. [10]

The H-structure is working reliably and is fairly accurate. The position accuracy has been increased comparing to H-Portal (A) by using external linear encoders. These encoders, with resolution of 1 μm, are used for direct position feedback of X and Z axes. The velocity feedback for the servo loop is received still from the encoder at the end of motor. The resolution of the motor encoder is 512 p/rev = 0,9 μm, which is on range of the linear encoder. But, on the other hand the gear backlash is 9,9 μm. Which makes it necessary to use external encoders. W axis has been working quite well, even though the accuracy of the axis is not very high, due to the low resolution of the used sensor. It has only 500 p/rev leading to angular resolution of 0,18°.

The main issues with this delicate manipulator has been mainly related to the parallel scara structure. More specific these are the feedback and backlash of shoulder angles, cabling, and the Z directional stiffness of the manipulator. The gear system has significant backlash. We have accurate encoder to directly measure the exact shoulder angle (0,005° = <14,1 μm), but the backlash from gearing makes the control unstable. The control situation could be improved by having additional encoder at the axis of the drive motor and use same configuration as we have in case of XZ axes. However this would not improve the

overall accuracy of the manipulator as the huge backlash in gearing remains. There has been many thoughts and attempts of pretensioning the manipulator to eliminate the backlash. None of them has fully solved the issue.

A lot of wires need to be delivered to the moving parts. First from frame to slide of H-structure and then to the end tip of parallel scara. Cabling with small and slender wires is not an easy task. Reliability and quality issues are constantly present, which are realised by broken and cut wires, and noise or malfunction in encoder signals.

The stiffness of the scara falls short and originates from the mechanical construction. Especially the distance between bearings on joint axis and construction of links causes the lost of stiffness. This will become an issue in many assembly cases, when pressing force is needed. This issue is solved in the next generation model of the manipulator (D) discussed in Ch. 4.4.

Considering the manipulator B, we should only focus on XZ part, because the design and implementation issues in XY part reduce the manipulator performance and accuracy too much. The accuracy of the manipulator is not measured, but some approximation can be made from configuration, construction and resolution. This is done here considering separately each section of the mechanics. The accuracy estimate for XZ (H-structure part) is under ± 10 μm. This originates from resolution of linear encoder, backlash in gearing, guides, and controls. The XZ part demonstrates high performance and high accuracy, but with high price. The play of XY (scara part) is so large that accuracy is not even estimated here. Accuracy of W is determined by encoder resolution and accumulated angle errors from XY, because W is affected by inaccuracies in XY position. Gear backlash is negligible in this case. The W error is around or more than 0,2°.

4.3 Manipulator C: Low Cost Cartesian

For a case demonstration [12] we needed an additional cell for glue dispensing. The main objective was to design low cost solution of a manipulator. Sub-objectives or design restrictions were: the use of linear motors [13], reduce wiring to minimum, and traditional cartesian construction. This determines the design of our low cost cartesian manipulator. More information about the cell and application can be found from [12].

The manipulator has three DOF and it follows schema of traditional cartesian manipulator. XY movements are made with linear motors, with configuration of having one motor responsible for each axis. The Z axis is based on a ball screw driven by a rotational motor. Model of the manipulator is illustrated in Fig. 4.5. The largest possible work envelope is (width × depth × height) 130×140×73, but the application instrumentation limits it smaller to size of 120×102×50. The speciality in this case has been that the position feedback is collected from the HALL-sensors used for motor commutation. This reduces the amount of components in and wiring to the moving parts. The resolution and accuracy is not therefore very high, but it is sufficient for many applications.

The dynamics of the manipulator are quite high or at least reasonable. It is simple, robust and parts are limited to minimum.

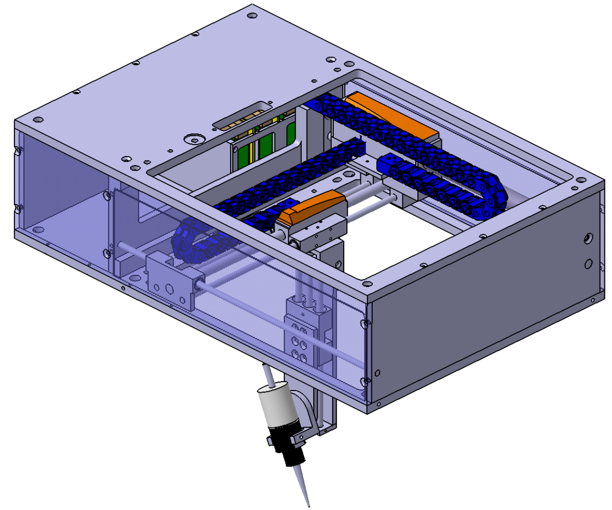

Figure 4.5: Illustration of the Low Cost Cartesian manipulator.

Issues with Low Cost Cartesian manipulator are mainly from mechanical stiffness, guiding and bearings, and in controls. The selected guides are not stiff enough and represents significant source of position error. Situation could be improved just by selecting one size larger guides. This is partially due to the fact that the final application and all its requirements were not known during the time of design. For example the mass of dispenser that is located at the end of a long beam increases torsion around X and Y axes.

In case of controls, the linear motors and the drives used, set some limitations for the position control. Because velocity control mode was not available option for the motors, it is impossible to have trajectories or interpolated movements implemented with the manipulator. Currently it makes only point to point movements.

The accuracy of the two motors making XY movements are 220/400 μm and the repeatability respectively 40/60 μm [13]. The overall accuracy of the manipulator is not measured, but should be worse than motor accuracy because of position error from guides.

4.4 Manipulator D: Parallel Scara

This shows the next iteration of parallel scara construction after implementing the H-Scara (B) (See Ch. 4.2). Main differences are in use of the direct drive technology, stiffer construction of the arm structure, and simplified construction as we focus only to the parallel scara structure. [14, 10] The construction is similar to the arms of H-Scara, but this has currently three DOF implemented with three axes. There is a ball screw driven axis providing the Z movement. The parallel scara structure is mounted on the slide of Z axis. The scara provides movement in XY-plane (See Fig. 4.7). The XY workspace of robot is presented in [14]. The hole matrix at front in Fig. 4.7 represents more or less the largest rectangular workspace of the scara.

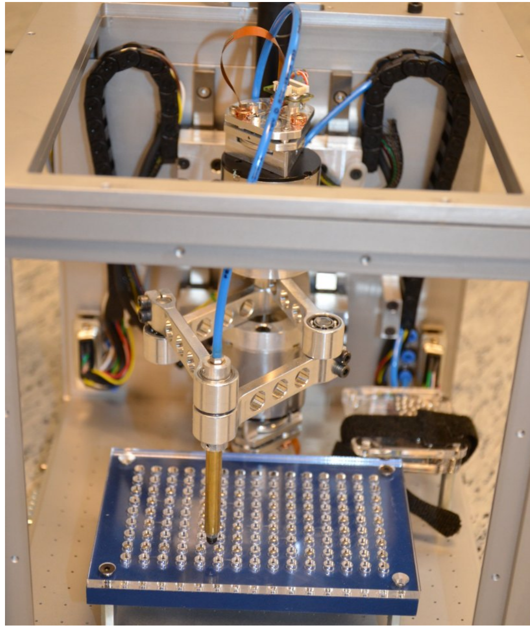

Figure 4.6: The Parallel Scara manipulator

The stiffness and rigidity of the arms are substantially improved in this version of the parallel scara manipulator compared to the previous one. On the other hand new issues arise at dynamics and control side. The absence of gear removed completely the backlash, but as a consequence the stiffness at control is significantly reduced. Tuning is getting difficult as the inertia of arm structure varies greatly depending on the distance between TCP and shoulder joints of arms (i.e. axis of motors).

The accuracy of the manipulator is measured with optical coordinate measuring machine (CMM) [14]. The measured worst case accuracy of the manipulator is 300 μm. The unreliable edge areas are excluded from error i.e. places where the links are getting almost overlapped. The encoder has resolution of 0,005° leading to less than 9,9 μm resolution, because the position resolution is function of arm angles. The scara is most accurate when the arm angle is around 90° and worst at arm angles close to 0° or 180°.

4.5 Manipulator E: Pocket Delta

PocketDelta 100 is last on the list as it is not made by ourself, but a commercial robot from Asyril[15] (developed at CSEM [16]). It has been introduced to public at 2005 [17] and acquired to TUT at the end of 2006. Therefore it is older than ourself developed manipulators. However, it is by size fitting nicely to our concept and it is mounted on our interface adapter plate thus included for comparison. This particular manipulator is one of the first prototype devices CSEM delivered, and it differs from the current ones of Asyril. However, the performance figures are according the latest models from Asyril.

The pocket delta manipulator is three DOF delta kinematic manipulator and has option for W rotational axis. The moving mass has been reduced to minimum; TCP is moving on cylindrical workspace (ϕD100 $\times$ 30 mm) with help of lightweight bars driven by three motors. The motors are mounted on top part of the frame, 120° angle between each other. The manipulator has position accuracy of $\pm$2,5 μm [15]. This is most sensitive to payload changes of these five, as the whole weight is hold directly by the actuator torque. There is not mechanical construction bearing the weight. For the same reason, the performance is dropping quicker when payload is increased.

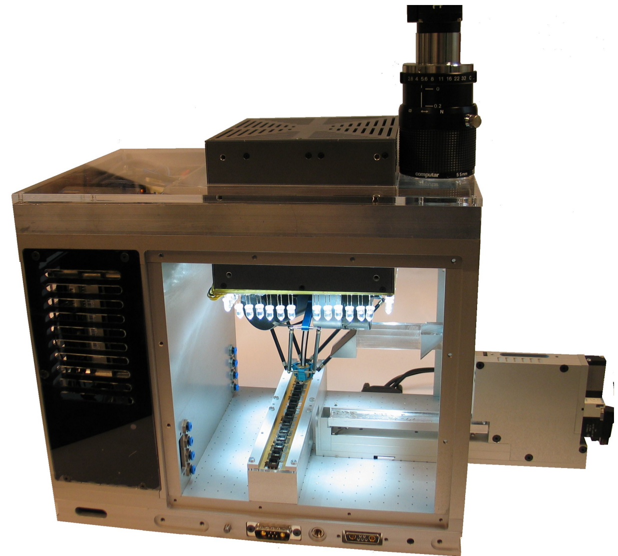

Figure 4.7: Asyril's Pocket delta manipulator mounted on TUT microfactory

5 Results

This chapter compiles together the results from different manipulators. The key performance indicators for manipulators are performance, accuracy, payload, module size, and its workspace. Also investment cost plays an important role. The construction of the manipulator affects indirectly to all of the mentioned key performance indicators. The facts from manipulators are collected together in Table 5.1.

5.1 Construction

The detailed construction of each manipulator is presented together with the presentation of each manipulator. At the same time specialities associated to the choice of construction are presented.

5.2 Module Size and Workspace

The module size includes the space a manipulator consumes in minimum when in operational configuration. In most of the cases the interface of TUT microfactory concept determines the occupation in XY plane (i.e. width and length). The actual real occupation of the manipulator is generally much smaller. Occupation at Z dimension varies more between manipulators. Workspace is the volume the manipulator is capable to reach of for an operation. In this comparison, workspace is usually below the size of module, except in case of B.

5.3 Payload

The payload of the manipulator can carry. This includes also the weight of the gripper and possible gripper exchange interfaces. The payloads are estimated with spring scale and visual observation, when bending starts. **Täytyy tehdä mittaustarviot!**

5.4 Performance

Performance includes the maximum velocity and acceleration of the manipulator. These are based on realised figures on controllers. Not the calculated maximum values, which are some times considerably higher.

5.5 Accuracy

Encoder resolution, linear resolution in operation plane, and overall accuracy are reported for each robot. The accuracy of some axis is not measured or not known. The latter considers mainly Z-axes, as our interest has been on the manipulator design and its accuracy.

5.6 Costs

The costs for manipulators A..D are component acquiring costs (list prices) for a single piece of prototype device without value added tax. Shown prices include only manipulator and its control related costs like mechanical construction; bearings and guides; motors, gears and amplifiers; I/O interfaces; and controllers. The work and company profits are all excluded, thus the E is not directly comparable with these ones.

Table 5.1: Comparison of characteristics

Characteristic\ Device name	H-Portal	H-Scara	LC Cartes.	ParallelScara	Pocket Delta
Device label / reference	**A [9]**	**B [12]**	**C [12, 13]**	**D [14]**	**E [15]**
Axis Denote	**XY/Z**	**XZ/XY/W**	**XY/Z**	**XY/Z**	**XYZ**
Kinematic construction	**belt H-structure/ screw**	**belt H-structure/ parallel kinematic scara arms/ rotation**	**cartesian/ screw**	**parallel kinematic scara arms/ screw**	**delta kinematics**
Module size (W×L×H) [mm]	**200×300×270**	**200×300×275**	**200×300×204**	**200×300×215**	**153×153×191**
Workspace [mm]	**101×123×46**	**525×130×150 Rec ?×?**	**120×102×50**	**224×112×50 Rec 100×72**	**ϕD100×30**
Payload [g]	**<100?**	**<50?**	**<50?**	**<200?**	**<40**
Velo$_{Max}$ [m/s]	**0,7/0,013**	**0,63/0,2/ (3,1rev/s)**	**1,0/0,24**	**1,0**	**na**
Acc$_{Max}$ [m/s^2]	**2,8/0,032**	**3,1/1,0/ (9,4rev/s^2)**	**20/2,4**	**0,030**	**na**
Encoder Resolution [μm]	**0,9/0,03**	**1/0,005deg/ 0,18deg**	**6/0,12**	**0,005deg/na**	**na**
Resolution [μm]	**0,9/0,03**	**1/<14,1/ 0,18deg**	**≈40/??**	**<9,9/na**	**≪ ±2,5**
Accuracy [μm]	**201/na**	**≈<20/na/ ≈>0,19deg**	**≈>400/na**	**300/na**	**±2,5**
Component costs [EUR]	**5100**	**11000**	**4400**	**5600**	**≈15k..20k(***

Notes: ≈ = estimated values.
na = not available.
(* = Acquiring price.

6 Discussion

6.1 Construction

Design and construction of the manipulator plays the main role for determining the rest of the manipulator characteristics. The design and construction are actually predetermining the success or failure of the following parameters. Use of rigid, stable and lightweight construction; use of backlash free gears and mechanics; direct and accurate feedback; and simplicity are all coming back to the initial constructional decisions. Therefore the construction of the manipulator is most important part to be designed well and wisely.

6.2 Module Size and Workspace

From the user perspective this is reduced more or less to a boolean value. In order to meet the size requirements, the workspace must be larger than the application requirements and module itself needs to fit on space available.

Modular solution like TUT microfactory concept improves the reuse and reconfiguration - sustainability. The manipulator and controller module can be quickly and easily exchanged, and taken to other use at different application with minimum effort.

6.3 Payload

Payload is one key term from application requirements. It shows great difference between different constructions and designs. Usually the performance of the manipulator is starting to get reduced immediately when the payload is increased. Carried weight affect to the fastest possible movements (more precise to maximum accelerations and decelerations). This will be easily visible in case of manipulator E as the whole payload is hanging directly from the torque of actuators.

6.4 Performance

Performance is always a trade-off between speed and accuracy, at least on some level. When building a low-cost device, normally neither is at excellent level (or at least both at the same time), but even though solution is sufficient for many applications. If both properties are required at excellent level, the costs of the device increase exponentially. Thus keeping a balance of speed, accuracy and costs, a trade-off is needed between these three properties. This means that the user requirements must be appropriately defined in advance, so that the application does not get over specified or over costly for a specific purpose.

This is also visible at our case. The cost of manipulator C has been reduced for example by leaving out additional position sensors. It has high velocity and acceleration, but on the other hand accuracy is poor. On the other hand, the expenses are almost tripled from C to B, where the manipulator represent better feedback and accuracy properties (considering only results of XZ part).

6.5 Accuracy

Accuracy of the manipulator mainly originates from rigid and stiff mechanical construction of the manipulator; accurate and allowance free (i.e. backlash free) mechanics specifically gears, gearboxes and belts; and from high resolution encoders. In high accuracy applications, the thermal stability arises as well a meaningful component for the accuracy.

The gears and gearboxes are the main sources of backlash. The allowance happens in all other joints and bearings as well. The use of backlash free gears like harmonic drives improves the situation, but with a penalty of high cost. An other option is to leave out the gear completely i.e. direct drive solution, but in this case the available torque remains easily very small or the actuator size is increased drastically. The belts and other flexible structures are causing deflections and elasticity, which represent large proportion of the position error. This effect may be slightly reduced by pre-tensioning the belts. The belt construction should be avoided for the high precision application, at least without use of additional, direct position feedback.

Use of high resolution encoders measuring position directly from the mechanical body improves the accuracy (like the H-structure (B) or arms of scara of manipulator (B&D)). Use of double sensors improves the situation. The manipulator B also demonstrates the issues with backlash and having the feedback measurement on the "other side" of the gear (Scara of the manipulator B), because of non-availability of small sized encoders for used motors. This demonstrates that the control and feedback loops need to be well designed and implemented for stable and optimal solution. The optimum situation would be when velocity control loop is closed by encoder at the end of the motor offering direct measurement of the motor angle. The direct position sensor (e.g. linear encoder) provides feedback for the position control loop. The backlash from the gear gets eliminated from the measurements with this arrangement and controls can be provided with more exact information.

The mechanical rigidity of links and their stiff and stable construction is one key for high accuracy solution. The same implies also to the design of the joints. By selecting wrong construction the end result may be spoiled. On the other hand selecting wisely, the construction is giving good performance and other parts of construction can be improved by e.g. reducing weight.

6.6 Costs

The complexity of manipulator, high performance and high accuracy are all directly visible at the costs. The price gets increased by adding components and especially if the component needs to be a high precision one.

7 Conclusion

The manipulator or other parts for microfactories bear always the balance between the performance, accuracy and costs. Therefore it is important to specify and select appropriate level, and not more, for the components for your application needs. Not all applications require the most accurate or highest performance machinery, which directly affects positively to the cost of the machine.

The paper compare some manipulator solutions which fits into the TUT microfactory environment. The comparison shows that construction and design has large effect on the final result, especially on accuracy, performance and costs. The construction of the manipulator predefines indirectly all the following properties, thus increasing its importance. Additional encoders are needed for high accuracy applications to compensate errors appearing different parts of the axis and to optimise configuration of different control loops.

ACKNOWLEDGEMENT

This work around TUT microfactory and presented devices has been done in series of projects including .., Desk, Mz-DTF, DeskConcept and AC-Desk [5]. These all are funded by *TEKES - the Finnish Funding Agency for Technology and Innovation* and several participating companies.

REFERENCES

[1] Y. Okazaki, N. Mishima, and K. Ashida, “Microfactory and micro machine tools,” in *Proc. of Korean-Japan Conference on Positioning Technology, Daejeon, Korea*, pp. 150–155, 2002.

[2] Y. Okazaki, N. Mishima, and K. Ashida, “Microfactory - concept, history, and developments,” *Journal of Manufacturing Science and Engineering*, vol. 126, no. 4, p. 837, 2004.

[3] R. Heikkilä, E. Järvenpää, and R. Tuokko, “Advances in the tut microfactory concept development,” *International Journal of Automation Technology*, vol. 4, no. 2, pp. 117–126, 2010.

[4] N. Siltala, R. Heikkilä, A. Vuola, and R. Tuokko, “Architectures and interfaces for a micro factory concept,” in *5th IFIP WG 5.5, International Precision Assembly Seminar, IPAS 2010* (S. Ratcev, ed.), vol. 315/2010, pp. 293–300, Ifip International Federation For Information Processing, 2010.

[5] R. Heikkilä, “Tut microfactory web pages.” http://www.tut.fi/microfactory/, 2012. Online, Accessed 7.5.2012.

[6] T. Prusi, A. Vuola, N. Siltala, R. Heikkilä, and R. Tuokko, “Robots for micro and desktop factories : Examples and experiences examples of micro and desktop scale robots,” in *Proceedings of the joint conference of the 41st International Symposium on Robotics, ISR 2010, and 6th German Conference on Robotics, ROBOTIK 2010*, pp. 1088–1094, 2010.

[7] A. Burisch, J. Wrege, A. Raatz, J. Hesselbach, and R. Degen, “Parvus - miniaturised robot for improved flexibility in micro production,” *Assembly Automation*, vol. 27, no. 1, pp. 65–73, 2007.

[8] G. Borchert, A. Burisch, and A. Raatz, “Apis - a miniaturized robot for precision assembly with low-cost piezoelectric motors,” in *Proc. of 7th Int. Workshop on Microfactories (IWMF2010)*, pp. 5–10, Oct 2010.

[9] A. Vuola, R. Heikkilä, T. Prusi, M. Remes, P. Rokka, N. Siltala, and R. Tuokko, “Miniaturization of flexible screwing cell,” in *5th IFIP WG 5.5, International Precision Assembly Seminar, IPAS 2010* (S. Ratcev, ed.), vol. 315/2010, pp. 309–316, Ifip International Federation For Information Processing, 2010.

[10] A. Vuola, N. Siltala, R. Heikkilä, and R. Tuokko, “Micro h-scara robot: Findings and results,” in *Proceedings of 7th International Workshop on Microfactories (IWMF 2010), Daejeon, Korea*, p. 5, Oct 2010.

[11] N. Siltala, A. Vuola, R. Heikkilä, and R. Tuokko, “A h-scara mini robot - a dual parallel kinematics mini manipulator,” in *Proceedings of the joint conference of the 41st International Symposium on Robotics, ISR 2010, and 6th German Conference on Robotics, ROBOTIK 2010*, pp. 1218–1224, 2010.

[12] N. Siltala, T. Prusi, A. Vuola, R. Heikkilä, and R. Tuokko, “Modular microfactory system for gas sensor assembly,” in *Proceedings of International Symposium on Assembly and Manufacturing (ISAM2011)*, p. 6, IEEE, May 2011.

[13] Faulhaber, “Product info and datasheets of linear dc-motors.” http://www.faulhaber.com/n428412/n.html, 2012. Online, Accessed 7.5.2012.

[14] A. Vuola and R. Tuokko, “Accuracy measurements of miniature robot using optical cmm,” in *Precision Assembly Technologies and Systems - 6th IFIP WG 5.5 International Precision Assembly Seminar, IPAS 2012* (S. Ratchev, ed.), vol. 371, pp. 126–133, Springer Boston, 2012.

[15] Asyril, “Pocket delta datasheet.” http://www.asyril.ch/media/PDF/PocketDelta_E.pdf, 2012. Online, Accessed 4.5.2012.

[16] S. Perroud, A. Codourey, and Y. Mussard, “Pocket-delta: a miniature robot for micro-assembly,” in *Proceedings of 5th International Workshop on Microfactories (IWMF 2006)*, Oct 2006.

[17] E. Schmid and A. Codourey, “Csem develops the world’s smallest delta robot.” Press Release. http://www.csem.ch/docs/Show.aspx/8733/docname/CP05-PocketDelta_EN.pdf, 2005. Online, Accessed 4.5.2012.

Process Design for Automated Surface Inspection in Micro Cold Forming

Bernd Scholz-Reiter[1], Daniel Rippel[1,#], Daniel Weimer[1], Janet Jacobi[1], Michael Lütjen[1] and Hendrik Thamer[1]

1 Intelligent Production Systems, BIBA – Bremer Institut für Produktion und Logistik GmbH at the University of Bremen, Bremen, Germany
Corresponding Author / E-mail: rip@biba.uni-bremen.de, TEL: +49-421-218-50137, FAX: +49-421-218-50003

KEYWORDS : Micro Process Design, Process Integration, Optical Quality Management, Micro Production

With a decreasing product size, the complexity of components and production processes increases. At a certain level of miniaturization, the application of common production techniques is not feasible anymore. In order to ensure a profitable micro manufacturing in spite of these production restrictions, three main challenges are detected and discussed in this paper. First, as common production techniques are reaching their limits, new specialized manufacturing techniques are necessary. Therefore, the Collaboration Research Centre 747 is investigating specific cold forming techniques. Second, due to the lack of standardized techniques and interfaces, a detailed planning of the overall production process chain, covering handling, production and appropriate quality assurance processes becomes increasingly important. Finally, despite high process uncertainties, micro components require very small manufacturing tolerances. Thus, micro processes require strict quality assurance mechanisms. This article presents a method for the visual quality measurement of metallic micro components and their integration into the design of process chains.

1. Introduction

Micro system technology is one of the most important cross-sectional technologies and the trend of miniaturization will continue the next decades [11]. Although industries demand constantly miniaturized products, common production techniques reach their limits with a decreasing size of the processed products. These limits are implied by physical constraints of the used materials, tools and production processes. In order to produce miniaturized products, the size of product components and pre-products has to be adapted. Thereby, material properties do not scale appropriately for very small components. For instance, characteristics like yield-stress, maximum elongation and hardness of metal sheets in a deep drawing production process are not affected, while reducing the sheets thickness. Consequently, the production process results in a hardly predictable number of sub-standard commodities. In comparison to chip manufacturing and the use of lithographic technologies such as LIGA-processes, mechanical micro manufacturing is not yet very advanced. Therefore, the development of micro manufacturing technologies and micro production concepts is still an active field of research. The most challenging issue in the development of high performance micro processes is the balance of accuracy and efficiency [15].

In micro production, precise manufacturing is decisive for the product quality. Vollertsen et al. (2004) define a micro component as follows: at least two of its geometrical dimensions are smaller than one millimeter [23]. In production, geometrical structure deviations below one micrometer are a common goal setting. To ensure these high quality requirements, quality tests are indispensable. Up to now, standardized methods and instruments for automated quality inspections are missing [9]. In general, there is a lack of knowledge about the behaviour of micro production processes and the relationships between their parameters. In addition, micro production processes are highly sensitive to changes in the production process parameters. Therefore, actual quality management techniques are insufficient. As a result, adequate processes and tools are necessary, which ensure high quality production while satisfying the required small tolerances. In conclusion, the use of common downscaled production processes is not any longer able to satisfy customer needs. Therefore, manufactures and researchers have to focus on the development of micro products and production processes, which enable a profitable and reliable middle and high volume production.

This article presents a quality-measurement technique,

which is designed to satisfy the high requirements of micro production. Therefore, the second section characterizes the application field of micro cold forming. It presents common problems as well as technologies which are specifically designed for this area. Section 3 describes a quality-measurement system for an automatic surface inspection of micro metal components. The fourth section discusses the integration of this system into higher level process chains.

2. Micro Cold Forming for Metallic Micro Components

The Collaborative Research Centre 747 "Micro Cold Forming – Processes, Characterisation, Optimisation" (CRC 747) is motivated by the requirement to produce tiny, lightweight, and cost effective high-precision components and products that provide a wide range of functionality. For instance, today, micro-vents in a car's anti-lock braking system nearly have the size of a ball pen. In future, the size of these components is required to be reduced to the size of a match stick. The CRC 747 focuses on the provision of processes and methods for the systematic design of reliable micro cold forming processes for metallic micro components. The CRC regards the entire process chain from material development and analysis, over quality management to production planning. Therefore, it investigates and develops processes and techniques that can be applied in micro cold forming.

2.1 Size-Effects

At first sight, the development of a micro production process, under the assumption of a well-known macro process, seems to be a simple task: If the process, including all process properties, is scaled down, then the product will be as well. Although this is theoretically true, the downscaling of all dimensions and forces, relevant to the production process is not possible. For instance, it would have to include the downscaling of natural constants, such as the density of materials, or the gravity force. The deviations of process parameters, which occur, while scaling down geometrical dimensions, are called size-effects [28], [4]. As a result, a direct downscaling of traditional macro metal-forming processes to the micro-level is not applicable [8]. Vollertsen et al. (2008) distinguish between three main categories of size effects: density, shape and micro structure [21]. An overview of the size-effect categories is given in Fig. 1.

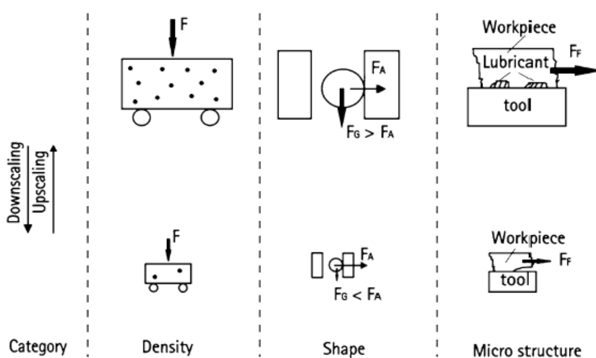

Fig. 1 Schematic representation of the three main groups of size effects: F force, F_A adhesion force, F_f friction force and F_G gravity force [21]

Density effects occur, when the density of materials remains constant, while downsizing. For example, material defects are widely distributed in larger scaled materials, averaging their impact on the materials quality. In contrast, in small-scaled materials, local defects can have a high impact on the quality depending on their location in the sample.

Shape effects occur due to the fact that holding the shape constant during downscaling, leads to a change in the relation of the surface to volume ratio. Hence, surface effects become more important, especially if only a fraction of the surface is involved in the process.

The last category, the *microstructure effects,* combine all effects that occur, due to the simultaneous downscaling of all structural values is physically or practically impossible. For example, it could be that lubrication cannot be used on a micro part, because the surface structure does not allow the creation of lubrication pockets and the frictional resistance increases with the downscaling.

In general, the impact of size-effects on manufacturing, handling and quality-measurement technologies has to be regarded. On the one hand, classical technologies can be rendered inappropriate, e.g. because of the increase of adhesive forces due to shape effects. On the other hand, size effects also provide the opportunity for new technologies like the laser-based free form heading process developed as a part of the CRC 747 [5], [24], [25].

2.2 Size-Effect related Manufacturing Techniques

The aim of the CRC 747 is the development of processes and methods for the manufacturing of metallic micro components by means of micro cold forming techniques. This paragraph presents two of these techniques exemplarily.

2.2.1 Laser-Based Accumulation

Several forming processes such as micro rotary swaging require a preliminary accumulation of material. A common technique to obtain an accumulation is an upsetting process. In order to achieve a high amount of formable material, high upsetting ratios are desired. Commonly applied multi-stage processes lead to an upsetting ratio up to 2.3 [5]. Nevertheless, the application of multi-stage processes in micro production is not feasible, due to imprecisions of handling devices and the diminishing correlation between the product's internal microstructure and its size.

Therefore, the CRC 747 developed a single-stage

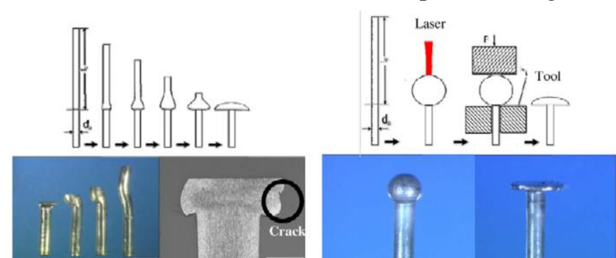

Fig. 2 Conventional (left) and laser-based (right) free form heading processes [25]

accumulation technique for the application in micro production. The laser-based micro upsetting process is able to benefit from the size-effects and thereby provides a new accumulation technique, which is capable to substitute the critical mechanical process. Due to the fact that, with increasing miniaturization, the surface tension exceeds the gravitation force, a melted material accumulation forms a droplet shaped pre-form for consecutive calibrating processes (Fig. 2) [25]. Even more, the laser-based free-form heading process improves an upset ratio up to 45 which is about 20 times higher than in macro-scale [24]. Hence, a laser-based accumulation process leads to a robust and efficient free-form heading process and opens possibilities to process more complex geometries as well as to control the material microstructure.

2.2.2 Micro Deep Drawing

A special technique in the cold forming domain is micro deep drawing. Micro deep drawing is defined as the forming of a sheet metal part using pressure, for example by means of a stamp. Using this technique, micro components with a diameter of one millimeter or smaller can be produced in a very high manufacturing frequency. Furthermore, the application of deep drawing in micro-scale allows a lubricant-free production process. This leads to a decreasing amount of detrimental effects on the environment and facilitates the

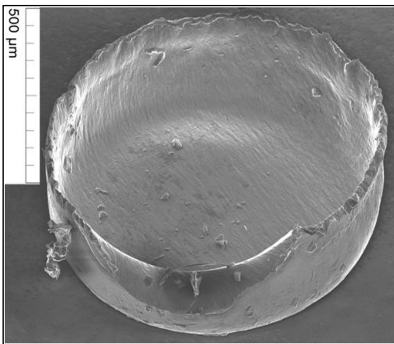

Fig. 3 Micro cup produced by micro deep drawing [26]

cleaning of the parts [6]. In this paper the focus is set to micro cups, as shown is Fig. 3.

The diameter of the a micro cup is 1 millimeter with a sheet thickness of about 20 microns [22]. For producing micro components with this technique a micro deep drawing machine was developed (Fig. 4). The MDM is able to produce more than 1000 micro parts per minute [18]. In comparison to macro deep-drawing, there are still small crinkles on the flange of the micro part. The drawing velocity of the micro cup is 1.0 mm/s. The realization of large production requires an automated measurement system, which is able to identify surface defects. Afterwards, a machine vision system is necessary to detect the surface imperfections and to classify the defect.

2.3 Measurement Uncertainty

Exact knowledge about geometry, forces, surface roughness and flow characteristics is required to guarantee high quality (micro) products. The generation of a quality

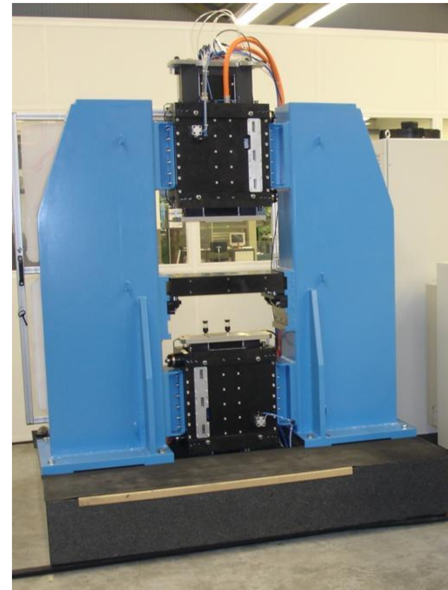

Fig. 4 Micro Deep Drawing Machine (MDM) [18]

control concept that integrates all of these aspects is a challenge and probably the reason, why quality control in micro-technology has not been completely established yet [9]. The major quality characteristics consist of dimension and surface properties. The impact of calibration uncertainty, uncertainty of the repeated measurement, uncertainty from variations of work piece features and the absolute value of the systematic measurement error have to be considered within the field of measurement uncertainty.

Micro manufacturing processes are characterized by high process variability and increased significance of measurement uncertainty [1]. For example, the assumption that measurement devices are 10 times more precise than given tolerance intervals is hardly satisfiable in micro manufacturing. The measured data is always a result of a superposition of process variation and measurement variation. Hence, dimensional metrology is based on imprecise information, so that a probability distribution is induced. The superposition of process and measurement variation renders the micro process control and therefore it needs defined rules and guidelines.

The relationship between tolerances, processing capability and metrology methods is challenging in micro technology. Significantly small tolerances are a result of absolute small

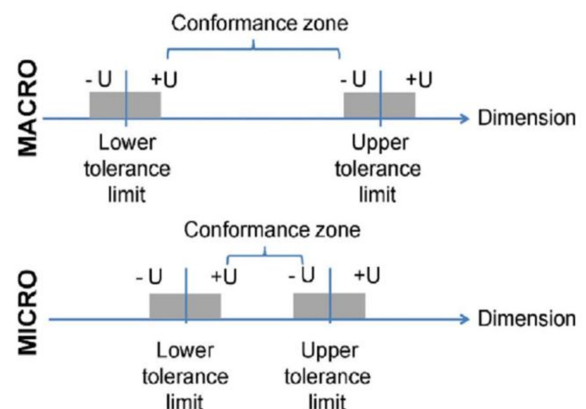

Fig. 5 Illustration of relationship between tolerance and measurement uncertainty [20]

part dimensions in micro forming. In order to verify tolerances, which are necessary to ensure product functionality, the measurement needs to be sufficiently exact. In general, measurement uncertainty becomes larger; the tolerance conformance zone for process variations becomes smaller. The reduction of the conformance zone in the micro dimension due to an existing and constant measurement uncertainty is shown in Fig. 5.

3. Surface Inspection for Logistic Quality Control

Due to the arbitrary shape, size and orientation of surface imperfections as well as the size of micro parts, automated surface inspection in the micro domain is a very challenging task. In a first step, suitable metrology technologies have to be selected. Measurement techniques successfully applied in the micro domain are confocal laser microscopy, digital holography and low-coherence interferometry [2]. Each technique is able to generate 2D and 3D form and surface information. To fulfill the strict requirements with respect to measurement accuracy, the focus in this paper is set to confocal laser microscopy.

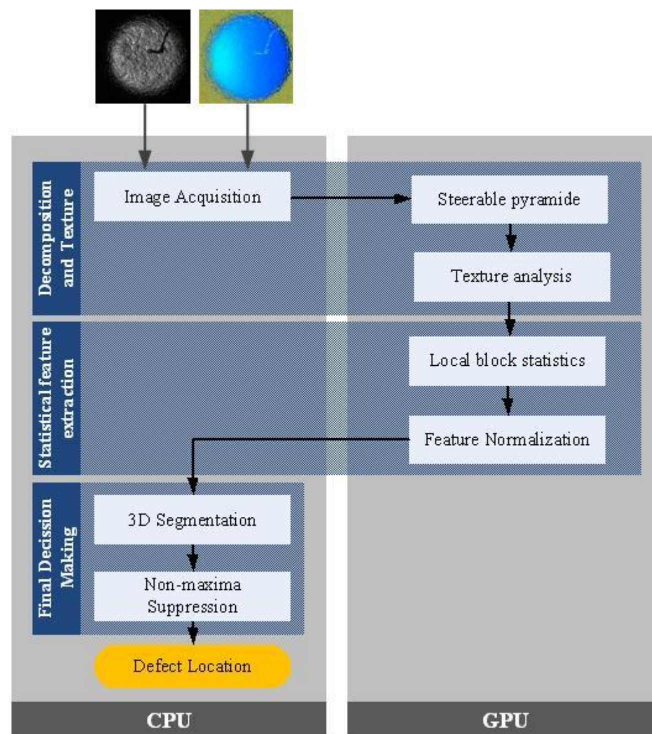

Fig. 6 Service Inspection Framework

In a second step, a reliable, fast and accurate surface inspection method is required, based on image processing techniques. The structure of the Surface Inspection Framework (SIF) is shown in Fig. 6. In the first stage of the framework, the 2D input image is decomposed in a number of images defined by specified orientations and resolutions. They are generated using the steerable pyramid technique introduced by Simoncelli [19]. The decomposition in orientation sub-images enables the framework to find defects with arbitrary orientation, even in very noisy and strong textured images. To find defects of arbitrary size and shape, each orientation sub-image is decomposed in different resolution images. The resolution decomposition is realized by applying Gaussian low pass filters and reducing the image size by a factor of two in width and height, compared to the previous stage. Coarse structures remain in the sub images with smaller resolution, whereas fine structures are in the upper resolution domain. As a reasonable tradeoff between computation time and accuracy we choose 4 scales for decomposition. The orientation decomposition is calculated in 30° steps starting from 0° up to 150 degrees. Negative angles are treated as their positive counterparts and therefore not focused. This gives $6\times4=24$ sub-images for each input image. On each sub-image, the local binary pattern (LBP) operator is applied [7]. This operator represents each pixel of the input image as variation in texture by applying local pixel thresholding. The result is a number for each pixel between $[0, 255]$, where zero denotes no change and 255 maximum change in texture.

After that each LBP sub-image is divided into overlapping blocks with a size of $32px\times32px$ with half block size of overlap. In each block several statistics are calculated like mean, median, maximum, minimum and standard deviation. Finally, all statistic block representations are merged using a non-maxima suppression technique. The final results show the most probable defect regions for each block-statistic separately.

A very important aspect in surface inspection is real-time behavior. Therefore, each input image will be acquired by the CPU and copied to GPU global memory by using the GPU library NVIDIA CUDA. A GPU consists of hundreds of cores and massively parallel block processing is possible. This technique shows great potential for accelerating runtime intensive algorithms (e.g. [27]).

4. Integration of the Automated Surface Inspection in Micro Process Chains

Due to the high customization of production, handling and quality measurement techniques, interdependencies between the different process types have to be regarded in micro production. The lack of standardized interfaces in the area of micro production requires a very precise design of the overall processes. Thereby, specific requirements and characteristics of products, production and handling devices as well as of quality-management systems need to be integrated and aligned within and between different processes and operations. It is necessary, to describe these process and to combine them into process chains to enable a comprehensive planning [13].

4.1 Simultaneous Engineering of Micro Process Chains

Process chains include all processes that have an impact on the product quality, including parameters of material, tools, and associated product components. Various scientific research has already be done on the topic of micro production processes ([23], [10], [3], etc.) .

In general, process chains in micro production subsume different production, handling and quality-management processes. Each process consists of elemental operations. For example, a quality-management process can consist of a combination of handling and measurement operations all conducted at a single workstation (e.g. [16]). Planning of the micro production process chains is proposed to be performed

jointly with the product design, due to the dependencies between distinct processes and the small tolerances in micro production, [14], [13]. This approach is called Simultaneous Engineering. In general, "Simultaneous Engineering describes an approach, in which the different phases of new product development, from the first basic idea to the moment when the new product finally goes into production, are carried out in parallel." [17]. Thereby, all characteristics and demands regarding the products complete life-cycle can be taken into account early. In particular, the lack of standardized tools and interfaces between processes require several changes in the production process or even the development of new tools and processes. The application of Simultaneous Engineering techniques enables an early determination of problems, which could occur during later stages of the production planning [12]. As a consequence, the overall costs of the product development are reduced, since changes in the product structure or in the production process can be communicated and applied at early stages. The use of process chains for the description of a production process enables the involved designers to itemize the complex correlations in a production process into a temporal and logical sequence of necessary production steps.

The planning of micro production processes can be divided into two major phases: First, the definition of the process chain. Second, the determination and configuration of relevant processes parameters [14]. On the one hand, both phases depend on the product to manufacture. On the other hand, available production, handling and quality measurement technologies can require specific properties from the product.

The first phase describes the modeling of required processes and operations. Thereby, production, handling and quality-management processes are defined with reference to the necessary manufacturing steps. Each process has specific requirements and characteristics, based on technological and logistic parameters. Examples for logistic parameters are the number of parts processed per minute or the costs that occur during processing. Technological parameters depend on the type of the process and highly depend on the resources involved. For example, handling devices can require specific shapes, while they apply a certain amount of pressure on the product. Quality-management processes usually require a very precise positioning of the micro products, which has to be provided by the according handling devices.

During the second phase, technologies and resources are assigned to each process and operation. The parameters are aligned according to the resources available. As a consequence the modeled process chain is configured by adjusting parameters and resources with respect to the product's and the processes' mutual requirements. Thereby, inconsistencies, e.g. unrealizable operations or inadequate tools, can be determined early in the planning stage.

4.2 Quality-Management Process

In general, the automated surface inspection uses visual image recognition to determine errors on the provided micro product. The corresponding quality-management process starts with the reception of the micro product at the surface-inspection-workstation. First, the product has to be positioned, in order to guarantee the required quality of the image. The second operation is the actual surface inspection. Thereby, the images of the micro product are taken. Subsequently, the image is evaluated using specific algorithms described previously. The surface inspection algorithm provides detailed information on the existence and type of errors detected on the product. If the product passed the surface inspection, it is forwarded to succeeding production processes. If it fails the quality test, the product is rejected. In addition, a validation of the used tools and materials in the preceding production process can be triggered if necessary. Fig. 7 provides an overview of the complete process.

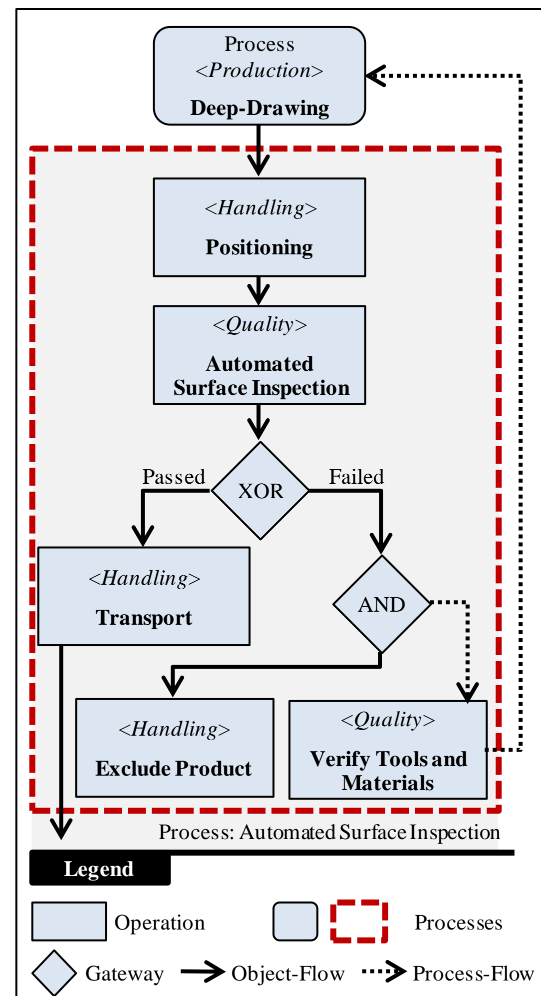

Fig. 7 Process: Automated Surface Inspection

4.3 Parameters of the Quality-Management Process

Due to the high number of manufactured parts and the relatively long time it takes to obtain and analyze the images, only a small set of samples can be analyzed using the automated surface inspection. Actually, the sample size is determined using a fuzzy-controller, based on the results of past quality-measurements [16]. As a result, the automated surface inspection process receives charges of products as input. The positioning-operation is required to separate single samples from the charge and to place it accurately with respect to the position, required by the image-taking device, e.g. the

confocal laser microscope. To achieve a high accuracy of error detection, the images have to provide a predetermined resolution. In addition, the processing time of the handling operation may not be longer than the processing time of the automated surface inspection operation. Fig. 8 depicts a simplified example of relevant parameters and their relations.

During the configuration of this process, each parameter is selected according to available technologies (e.g. the confocal laser microscope as image-taking device or vacuum-pipettes for the separation). The other way around, by referring to in-

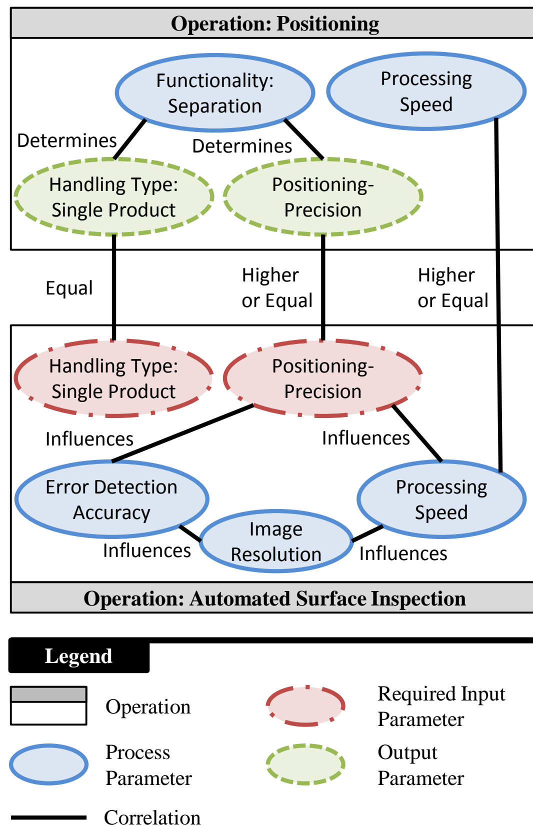

Fig. 8 Example for Operation-Parameters and their correlations

or output parameters, devices can be obtained or developed according to the processes demands.

5. Conclusion and Outlook

In general, the development and application of micro production processes requires the consideration of a variety of technical and logistic parameters. In particular, size-effects and high requirements on accuracy and processing times contribute important impact factors for the quality of micro products. The automated surface inspection presented in this article provides a non-tactile technology, which satisfies these requirements. Nevertheless, the integration of such technologies into the general process design of micro process chains requires the consideration of additional parameters, implied by preceding and succeeding processes, as well as implied by the work piece itself.

In future work, the Simultaneous Engineering approach will be applied on more complex micro products. Currently, the CRC 747 is working on a micro valve, which consists of four micro parts manufactured using specifically developed micro cold forming processes. Due to the unknown correlations between the individually production processes, current work on the Simultaneous Engineering approach focuses on the cause-effect-relationships among the whole process chain. Due to the high number of interacting factors, slight parameter changes in early production steps may cause unpredictable parameter changes in later steps. In order to detect crucial product deviations in early production steps, the embedding of quality inspection is an important task for process chain design. Currently, the SIF will be developed for the inspection of basic metallic micro components. In future research, the framework will be extended for more complex micro structures too.

ACKNOWLEDGEMENT

This research is funded by the German Research Foundation (DFG) as a part of the subprojects C4 “Simultaneous Engineering” and B5 “Reliable Processes” of the Collaborative Research Centre 747 “Micro Cold Forming - Processes, Characterisation, Optimisation” (CRC 747).

REFERENCES

1. Fleischer, J., Lanza, G., and Schlipf, M., "Statistical quality control in micro-manufacturing through multivariate μ-EWMA chart," CIRP Annals - Manufacturing Technology, Vol. 57, pp. 521-524, 2008.
2. Hansen, H. N., Carneiro, K., Haitjema, H., and De Chiffre, L., "Dimensional Micro and Nano Technology," Annals of the CIRP, Vol. 55, No. 2, pp. 721-734, 2006.
3. Hu, Z., Walther, R., and Vollertsen, F., "Umformwerkzeuge beim Mikrotiefziehen – Einfluss der geometrischen Abweichungen der Werkzeuge auf die Stempelkraft beim Mikrotiefziehen," Werkstattstechnik online, Vol. 11, No. 11, pp. 814-819 2009.
4. Lai, X., Peng, L., Hu, P., Lan, S., and Ni, J., "behavior modelling in micro/meso-scale forming process with considering size/scale effects," Computational Materials Science, Vol. 209, pp. 4949-4953, 2008.
5. Lange, K., "Umformtechnik. Band 2: Massivumformung". Berlin, Heidelberg: Springer Verlag, 1988.
6. Moumi, E., Kuhfuß, B., and V., P., "Potenzial der Trockenbearbeitung beim Mikrorundkneten " in: Kraft, O., Haug, A., Vollertsen, F., and Büttgenbach, S., (Eds.), Kolloquium Mikroproduktion und Abschlusskolloquium SFB 499, Karlsruhe, 2011.
7. Ojala, T., Pietikäinen, M., and Mäenpää, T., "Multiresolution Gray-Scale and Rotation Invariant Texture Classification with Local Binary Patterns," IEEE Transactions on Pattern Analysis and Machine Intelligence, Vol. 24, No. 7, pp. 971-987, 2002.
8. Pawelski, O., "Ways and limits of the theory of similarity in application to problems of physics and metal forming," Journal of Materials Processing Technology, Vol. 34, No. 1-4, pp. 19–30, 1992.
9. Pfeifer, T., Driessen, S., and Dussler, G., "Process observation for the assembly of hybrid micro systems,"

Microsystems Technologies Vol. 10, pp. 211-218, 2004.

10. Piotrowska, I., Brandt, C., Karimi, H. R., and Maaß, P., "Mathematical model of micro turning process," International Journal of Advanced Manufacturing Technology, Vol. 45, No. 1, pp. 33-40, 2009.
11. Reimer, H., "BMBF: Die Hightech-Strategie für Deutschland," Datenschutz und Datensicherheit - DuD, pp. 665-666, 2006.
12. Reinhart, G. and Meis, J. F., "Requirements Management as a Success Factor for Simultaneous Engineering - Enabling Manufacturing Competitiveness and Economic Sustainability," in: ElMaraghy, H. A., (Ed.), Enabling Manufacturing Competitiveness and Economic Sustainability, Berlin, Heidelberg: Springer Verlag, pp. 221-226, 2012.
13. Scholz-Reiter, B., Brenner, N., and Kirchheim, A., "Integrated Micro Process Chains," in: Vellespir, B. and Thècle, A., (Eds.), Advances in Production Management Systems, Berlin, Heidelberg: Springer Verlag, pp. 27-32, 2010.
14. Scholz-Reiter, B., Lütjen, M., and Brenner, N., "Technologieinduzierte Wirkungszusammenhänge in der Mikroproduktion - Entwicklung eines Modellierungskonzepts," in: Schenk, M., (Ed.), 22. HAB-Forschungsseminar „Digital Engineering - Herausforderung für die Arbeits- und Betriebsorganisation“, Magdeburg: GITO Verlag, pp. 81-102, 2009.
15. Scholz-Reiter, B., Lütjen, M., and Heger, J., "Integrated simulation method for investment decisions of micro production systems," Microsystem Technologies, Vol. 14, pp. 2001-2005, 2008.
16. Scholz-Reiter, B., Lütjen, M., Lappe, D., Thamer, H., and Brenner, N., "Logistische Qualitätslenkung in der Mikrokaltumformung - Einsatz von Fuzzy-Regelung zur Optimierung von Stichprobenintervallen," Industrie Management, Vol. 26, No. 4, pp. 13-16, 2010.
17. Schroeder, R. G. and Flynn, B. B., "High Performance Manufacturing: Global Perspectives". New York: John Wiley & Sons, 2002.
18. Schulze Niehoff, H., "Entwicklung einer hochdynamischen, zweifachwirkenden Mikroumformpresse," in: Strahltechnik, Vol. 33. Bremen: BIAS Verlag, 2008.
19. Simoncelli, E. P. and Freeman, W. T., "The Steerable Pyramid: A Flexible Architecture for Multi-Scale Derivative Computation," in International Conference on Image Processing, 1995, p. International Conference on Image Processing.
20. Tosello, G. and Gasparin, S., " Applications of dimensional micro metrology to the product and process quality control in manufacturing of precision polymer micro components," CIRP Annals - Manufacturing Technology, Vol. 58, pp. 467-472, 2009.
21. Vollertsen, F., "Categories of size effects," Production Engineering, Vol. 2, No. 4, pp. 377-383, 2008.
22. Vollertsen, F., Hu, Z., Schulze Niehoff, H., and Theiler, C., "State of the art in micro forming and investigations in micro deep drawing," Journal of Materials Processing Technology, Vol. 151, pp. 70-79, 2004.
23. Vollertsen, F., Schulze Niehoff, H., and Hu, Z., "State of the art in micro forming," in 1st International Conference on New Forming Technology, China, 2004, pp. 17-28.
24. Vollertsen, F. and Walther, R., "Energy balance in laser-form heading,". CIRP Annals - Manufacturing Technology Vol. 57, pp. 291–294, 2008
25. Walther, R., "An enhanced model for energy balance in laser based free form heading," Journal of Micromechanics and Microengineering, Vol. 19, pp. 1-6, 2009.
26. Wang, N., von Kopylow, C., and Falldorf, C., "Rapid optical inspection of micro deep drawing parts by means of digital holography," Production Engineering, Vol. 6, No. 1, pp. 47-53, 2012.
27. Weimer, D., Koehler, S., Hellert, C., Doll, K., Brunsmann, U., and Krzikalla, R., "GPU Architecture for Stationary Multisensor Pedestrian Detection at Smart Intersections," in Proceedings of the IEEE Intelligent Vehicle Symposium, 2011, pp. 89-94.
28. Zhang, K. and Kun, L., "Classification of size effects and similarity evaluating method in micro forming," Journal of Materials Processing Technology, Vol. 209, pp. 4949-4953, 2009.

A Flexible Laser Micro-Machining Platform

Jorma Vihinen#, Jyrki Latokartano and Tero Kumpulainen
Department of Production Engineering, Tampere University of Technology, Tampere, Finland
Corresponding Author / E-mail: jorma.vihinen@tut.fi, TEL: +358-40-5567874, FAX: +358-3-31152753

KEYWORDS : Laser, micro-machining, platform, sensor integration

Micro-machining is one of the fastest growing areas in laser processing technology. Laser pulse frequency and average power have increased substantially in recent years, this generally means higher processing efficiency. In many cases beam manipulation has become a bottleneck in laser micro-machining. The accurate and fast motion components and sensors required are expensive compared even to lasers. Tampere University of Technology has been developing a laser micro-machining platform which enables fast replacement of laser sources and additional equipment. The platform includes a system which enables corrections of some errors caused by the fixtures and topology of the material surface. The laser processing results can be analyzed without removing pieces from the fixtures. This paper presents the components used, the system architecture and some results of tested applications.

1. Introduction

Laser micro-machining is one of the fastest growing areas in laser processing technology [1]. The accurate and fast motion components and sensors required are expensive compared even to lasers. Laser pulse frequency and average power have increased substantially in recent years, this generally means higher processing efficiency [2, 3]. Beam manipulation has become a bottleneck in micro-machining.

Development of galvonometer scanners, acousto-optic deflector, rotating mirrors and combinations of the afore-mentioned devices can respond to the laser properties, which are capable of over hundred meter per second process speed [4, 5]. The situation changes when the beam diameter should be some micrometers on the target. In this case microscope optics are still used. Use of microscope optics means that the beam needs to be manipulated using traditional mechanical solutions.

Different materials and processes (e.g. ablation, engraving, drilling, welding) require slightly different types of lasers. The wavelength, frequency, pulse energy and pulse duration are examples of varied parameters. Well-equipped research laboratories have good movement equipment, and lasers available. They can combine equipment in the best possible way. Unfortunately this is not the case in most of the research laboratories. Many research laboratories are trying to respond to the needs of the industry and research partners with limited resources.

When resources are limited, equipment flexibility is important. Tampere University of Technology has been developing a laser micro-machining platform which enables fast replacement of laser sources and additional equipment. The platform includes a system which enables corrections of some errors caused by the fixtures and topology of the material surface. The laser processing results can also be analyzed without removing pieces from the fixtures. The basis of the TUT Microlaser Platform is accurate axes, with well known behavior. The whole system is accurately measured and all of the error sources are defined (e.g. temperature, vibration).

The behavior of the laser equipment (e.g. beam pointing accuracy, thermal lens effects) has to be taken into account to estimate the accuracy of the whole system. Quality assessments of the laser process are more important when using flexible platforms than when using fixed setups. This is due to the larger number of variable parameters in flexible platforms.

This paper presents the system architecture and components used in the platform, some results of application tests are also presented. The structure of this paper is as follows: Chapter 2 introduces the basic devices. Chapter 3 defines the system architecture which was developed and used in this application. Chapter 4 describes the implementation. Chapter 5 represents the results and the final chapter 6 lists some future improvements and concludes this paper.

2. Environment

A three-axis micro-machining station made by Singulase Ltd (Figure 1) was purchased in 2005. The processing equipment was a picosecond laser made by Corelase Ltd (Figure 2). The workstation is located in a temperature and humidity controlled cleanroom. The original workstation was equipped also with a microscope and triangular distance sensor. The main features of the devices are described in table 1.

Figure 1. LD-10 laser micro-machining station.

Figure 2. X-Lase, picosecond pulsed fibre laser, laser head inside the workstation.

Table 1. Specification of the workstation and picosecond pulsed fibre laser

Workstation:	**LD10**
Speed	2000 mm/s
Accuracy x/y directions	+/- 5µm
Accuracy z direction	+/-10µm
Laser:	**Xlase**
Wave length	~ 1060nm
Pulse length	<30ps
Repetition rates	0.25...10MHz
Laser beam quality	<1.5M2

The micro-machining workstation was designed to be used only with the Xlase laser. The features of new lasers and demands on the processes required the development of new solutions to face the challenges. Many lasers, especially femtosecond lasers require more space than the originally used laser. The only solution for new lasers was to locate the laser outside the cabin and guide the beam to the optics inside the cabin (direct optics or galvo scanner). This is a very traditional way to solve the situation (figure 3).

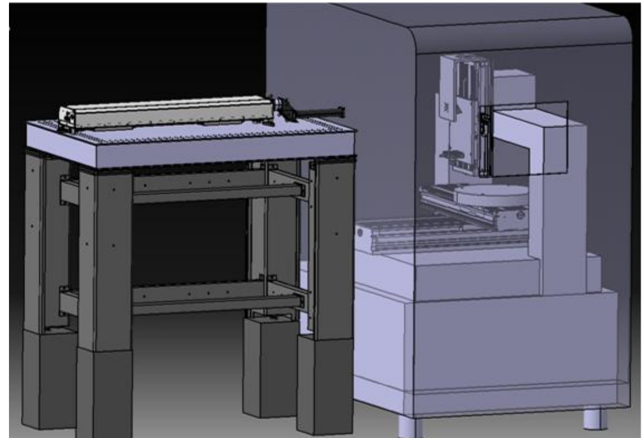

Figure 3. Laser outside the micro-machining station.

Another challenge came from the process side. There was increasing needs for measuring the sample surface more precisely and also to follow the surface in a controlled way. One solution was to use a precise height sensor, because compensations are related in many cases to the height of the track.

The sensor requirements were manifold. It needed to measure the distance between the laser and the working plane exactly. The thickness of thin transparent materials should be possible to measure. The sampling frequency of the sensor should be in a reasonable range etc. To meet these requirements a Keyence LT-9010M confocal sensor (Figure 4, Table 2) was chosen because of its usability.

Figure 4. LT-9010M confocal sensor and LT-9501 controller.

Table 2. Specification of the confocal sensor

Manufacturer and model	Keyence LT-9010M
Measurement range	±0.3mm
Light source	670 nm semiconductor laser
Spot diameter	Ø 2 µm
Resolution	0.01µm
Scan width/interval	0 to 1100 µm
Microscope field of view	1.3 x 1.05 mm

3. System Architecture

The general rule in designing system architecture is to keep things as simple as possible. Previously tested programs are used as much as possible. Applications integrative program is an independent program that can be deployed when needed. Almost all of the functions can be done without the plug-in software. The Etel NC-terminal software can take care of the linear drives. The independent Keyence controller can be used for height measurements. IDS software can be used for analyzing the microscope pictures. MountainsMap measurement data analysis software is also a separate software, which can be utilized when needed.

The main target for the custom made software is to connect different data sources. In the Z-axis correction function, the software communicates with the Keyence sensor and the Etel EDI-library. The software transfers the measured points to the Etel Dsmax controller via EDI –library using API when the NC controller requires them. The measured points are stored to the variables used in the NC code. A block diagram of the software and the hardware modules can be seen in figure 5.

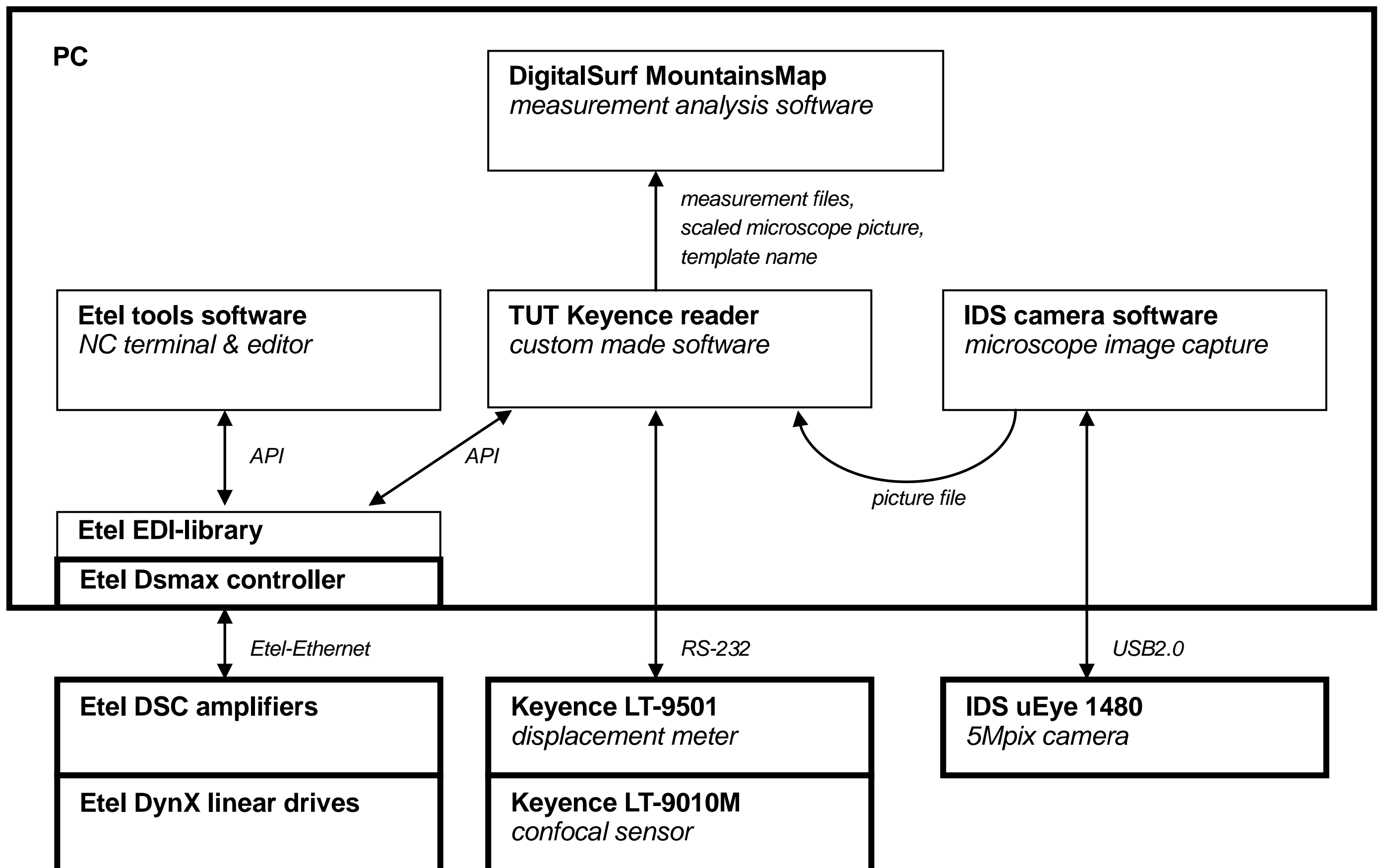

Figure 5. Block diagram of software and hardware modules

4. Implementation

Safety related issues and overall reliabilty were the most important things in the implementation. The system was divided into several communication parts: linear drives, confocal sensor, microscope, and measurement analysis software.

The main aim was to integrate the confocal sensor measurements with the tool path height variations. This is used when the samples are quite planar. The requirements for the system in tool path heigth measurement are as follows:

- Z-axis correction before laser processing
- Measurement request signaled by NC-variable
- Displacement type measurements (one point at a time)
- Results are stored into the NC-variables
- The NC-program follows measured points

An additional objective was to use the measurement data for surface topography analysis. A measurement report with microscope pictures should also be generated automatically. The used report software is DigitalSurf MountainsMap. The requirement for the sensor and the system is as follows:

- Quality assurance measurement
- Profile type measurements (one line at a time)
- Reader program sends commands to numerical control to reach a new position (for surfaces)
- Stores the measurement data in a data file

The TUT Keyence Reader is a custom software for reading the data from the sensor and from the NC controller. The normal procedure is as follows:

1. Move the axes to the start point (using the control window (figure 6) or the terminal of the controller)
2. Adjust the setting parameters for the sensor (figure 7)
3. Start the measurement
4. The results can be followed visually from the graph window or numerically from the log window (figure 8)
5. Save the data
6. Analyse the data with the MountainsMap software

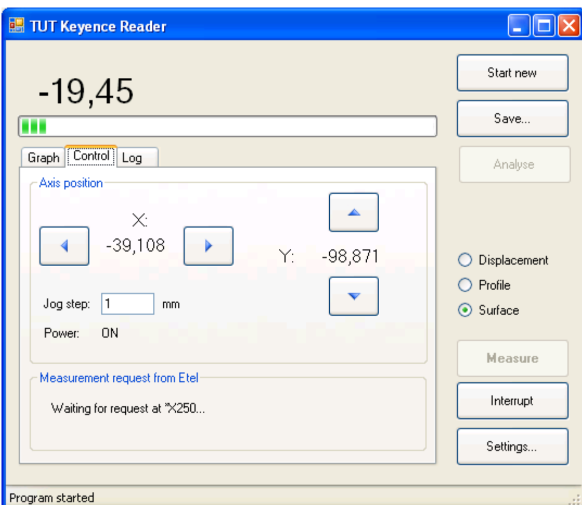

Figure 6. The control view

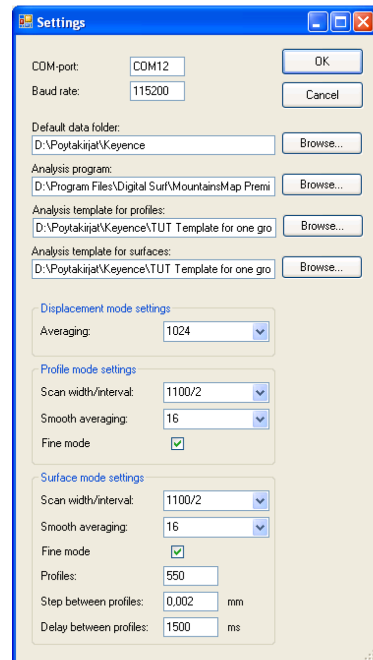

Figure 7. The sensor setting view.

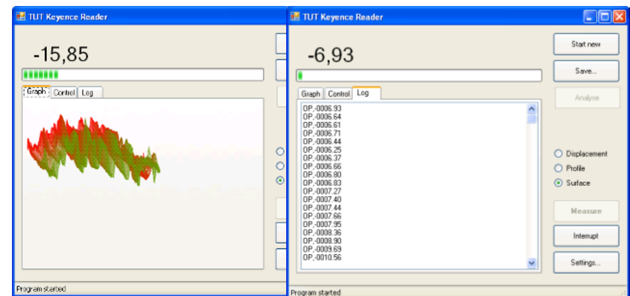

Figure 8. The graph view, b. the log view

The analysis software can use different templates which are defined in the settings window. As a result a report is automatically generated(Figure 9).

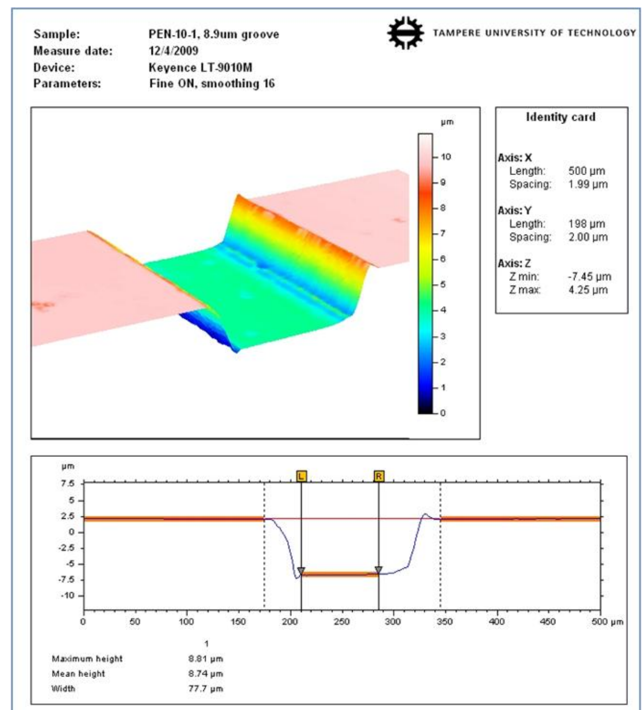

Figure 9. A report from the Keyence sensor

5. Results

The improvements achieved are evaluated through examples. Major changes in the platform setup were the changing of the laser and the changing of optics from direct optics to a galvo scanner and vice versa (figure 10). Laser changes from beam to beam are done in less than 8 hours. This means that an old laser is changed to a new one. This time includes also all optical changes. Also, the laser focal plane is calibrated to a known level in relation to the microscope and confocal sensor.

Figure 10. Picosecond laser setup change to a femtosecond laser setup at the workstation.

One major target of the new platform was the surface tracking system. Surface following with the confocal sensor is done offline. The path is measured first and then the measured heights are moved (automatically) to the NC program. The LD-10 work station can follow a measured surface up to a 600 mm/s feedrate on the X-axis when the measured points have 2 mm interval (figure 11). The real position differs from the measured curve by about 1 µm at the end of a 20 mm long path. The stage can follow a measured path up to 600 mm/s with ±1 µm accuracy.

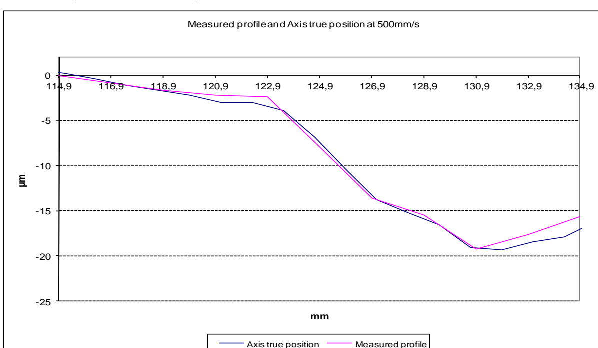

Figure 11. Measured profile and real axis position 600mm/s

The beginning of the profile follows the measured curve nicely. During the last 4 mm, the real curve differs from the measured z-profile by about 1 µm. Figure 12 shows a groove manufactured with the Xlase laser using microscope optics (depth of focus around 1 µm) in sapphire. The quality of the groove (width around 3 µm) is quite even, though the sample was curved can been seen in figure 13.

Figure 12. Groove at beginning, 20 mm, 40 mm, speed 100mm/s.

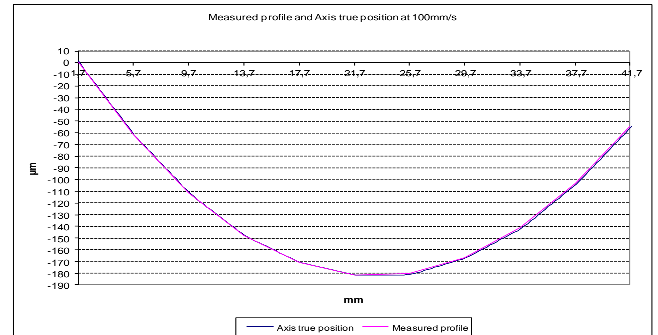

Figure 13. Measured profile and Real axis position 100mm/s.

Basic laser processing tests are dramatically accelerated through the use of the confocal sensor. In the old system the specimen had to be taken out of the fixture and go to a separate measuring device to see the results. Based on these results, the processing parameters were changed as needed. This was an iterative procedure which normally took several days. With the new setup it is possiple to machine, measure and machine the samples again if needed. After each measurement the data analysis is possible (figure 14).

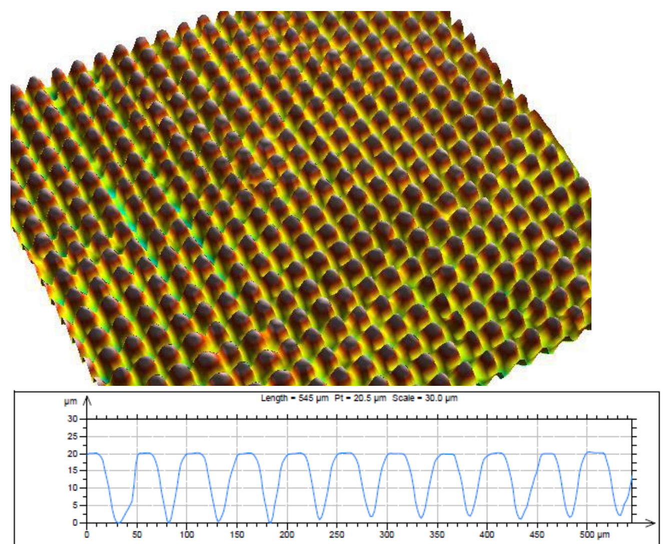

Figure 14. Measurement data is moved to MountainsMap-program and the height of the grooves are analysed.

6. Discussion and Conclusion

The paper presents a method for diversifying a laser micro-machining platform. High speed and accuracy in the process is a challenge to achieve in laser micro-machining. This requires a good knowledge of the properties of the movement equipment, therefore it is often appropriate to use expensive and precise movement equipment as efficiently as possible. Process equipment such as lasers can easily be changed if the platform is well designed. Sensor data can be used e.g. for controlling, quality assurance and reporting. With simple plug-in software the workstation availability can be improved considerably.

Future actions for improving the laser micro-manufacturing platform are: impromevent of surface tracking system; development of reporting system. The surface tracking system will be developed towards online control. A confocal or triangular sensor measures the surface before the microscope lens and the piezo actuator adjusts the focus height according to the sensor information. Further research will be published during the autumn in ICALEO and LANE conferences. The reporting system based on DigitalSurf MountainsMap software will be diversified.

ACKNOWLEDGEMENT

The authors thank Dr. Jouni Hölsä for implementing most of the hardware installation and also the software development. Part of this effort was made in the IiLase-project funded by Tekes and within the LIFT project which has received funding from the European Community's Seventh Framework Program FP7-NMP-2008-4.0.4 under grant agreement n° CP-IP 228587-1.

REFERENCES

1. “Annual Review an Forecast”, Laser Focus World, Volume 48, Issue 01, 2012
2. Russbueldt, P., Mans, T., Hoffmann, H.D. & Poprawe, R. 2010, "Status quo and outlook of power scaling of ultrafast lasers", 29th International Congress on Applications of Lasers and Electro-Optics, ICALEO 2010 - Congress Proceedings, pp. 1226.
3. Tünnermann, A., Nolte, S. & Limpert, J. 2010, "Femtosecond vs. Picosecond Laser Material Processing", *Laser Techn.J.,* vol. 7, no. 1, pp. 34-38..
4. Brüning, S., Henning, G.., 2012, “3D-Micro-Structuring of Embossing Cylinders with Ultrashort Pulse Lasers”, AKL - International Laser Technology Congress Proceedings, 9-11.5.2012 Aachen
5. Eifel, S., 2012, “Process Development for High-Power Laser Ablation”, AKL - International Laser Technology Congress Proceedings, 9-11.5.2012 Aachen